EARTH-REFERENCED AIRCRAFT NAVIGATION AND SURVEILLANCE ANALYSIS

Michael Geyer

Frederick de Wit

Navigation

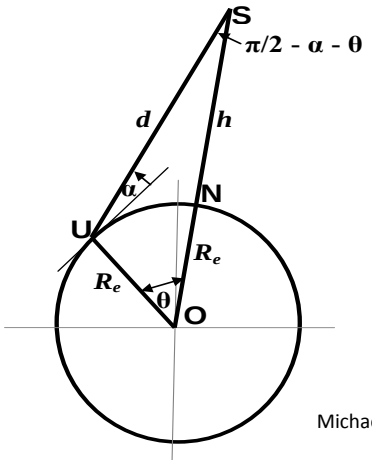

Michael Gever

Vertical Plane Model

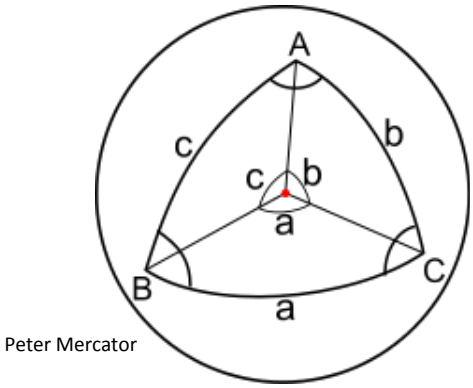

Peter Mercator

Spherical Surface Model

Federico Rostagno

Surveillance

Project Memorandum — June 2016

DOT-VNTSC-FAA-16-12

Prepared for:
Federal Aviation Administration
Wake Turbulence Research Office

U.S. Department of Transportation
Research and Innovative Technology Administration
John A. Volpe National Transportation Systems Center

FOREWORD

This document addresses a basic function of aircraft (and other vehicle) surveillance and navigation systems analyses — quantifying the geometric relationship of two or more locations relative to each other and to the earth. Here, geometry means distances and angles, including their projections in a defined coordinate frame. Applications that fit well with these methods include (a) planning a vehicle's route; (b) determining the coverage region of a radar or radio installation; and (c) calculating a vehicle's latitude and longitude from measurements (e.g., of slant- and spherical-ranges or range differences, azimuth and elevation angles, and altitudes).

The approach advocated is that the three-dimensional problems inherent in navigation/surveillance analyses should, to the extent possible, be re-cast as a sequence of sub-problems:

- **Vertical-Plane Formulation** (two-dimensional (2D) problem illustrated in top right panel on cover) — Considers the vertical plane containing two problem-specific locations and the center of a spherical earth, and utilizes plane trigonometry as the primary analysis method. This formulation provides closed-form solutions.
- **Spherical-Surface Formulation** (2D problem illustrated in bottom left panel on cover) — Considers two or three problem-specific locations on the surface of a spherical earth; utilizes spherical trigonometry as the primary analysis method. This formulation provides closed-form solutions.
- **Three-Dimensional Vector Formulation** — Utilizes 3D Cartesian vector framework; best-suited to situations involving four or more problem-specific points and slant-range or slant-range difference measurements; provides closed-form solutions.
- **Non-Linear Least-Squares (NLLS) Formulation** — Employed for the most complex situations, and does not require many of the idealizations necessary for simpler approaches. Provides estimates of the accuracy of its solutions. Drawback is that it requires numerical methods, consequently solution properties are not evident.

These techniques are applied, in the context of a spherical earth, to a series of increasing complex situations, starting with two problem-specific points (e.g., a route's origin and destination) and extending to three or more points (e.g., an aircraft and multiple surveillance/navigation stations). Closed-form solutions are presented for measurements involving virtually every combination of ranges, pseudo ranges, azimuth/elevation angles and altitude.

The Gauss-Newton NLLS methodology is employed to address the most complex situations. These include circumstances where there are more measurements than unknowns and/or the measurement 'equations' cannot be inverted analytically[*] (including those for an ellipsoidal-shaped earth) and/or are not analytic expressions (e.g., involve empirical data).

[*] The term 'analytic' is used for expressions that are described by mathematical symbols, typically from algebra, trigonometry and calculus. 'Inverting' refers to solving such expressions for a set of desired unknown variables.

TABLE OF CONTENTS

LIST OF FIGURES

LIST OF TABLES

1. INTRODUCTION

1.1 Overview of Analysis Methodologies and Their Applications

This document addresses a fundamental function in surveillance and navigation analysis — quantifying the geometry of two or more locations relative to each other and to the earth. Here, 'geometry' refers to: (a) points (idealized locations); (b) paths between points; and (c) distances and angles involving paths. Points represent locations of either vehicles, route origins/destinations/waypoints and navigation/surveillance sensors. Paths are trajectories followed by vehicles or sensor signals. Distances are the lengths of paths that are either straight lines or follow the earth's surface. Angles between paths may be measured in horizontal or vertical planes.

1.1.1 Trigonometric and Vector Analysis Methodologies (Chapters 3 – 5)

The approach that may first come to mind when addressing an analysis situation is to treat it as a three-dimensional problem, and to employ vector analysis. Vector analysis a modern technique (it was not well formulated until approximately 1900) and is often useful. However, a classical approach (with roots dating to approximately 500 AD) is recommended as the first option. Thus, to the extent possible, three-dimensional problems should be re-cast as two separate two-dimensional problems, each of which can be addressed by a branch of trigonometry:

- **Vertical Plane Formulation** (Chapter 3)[*] — This formulation considers the vertical plane containing two problem-specific locations and the center of the earth. Problem-specific locations are unconstrained vertically, except that at least one altitude must be known. Plane trigonometry is the natural analysis tool when altitudes, elevation angles and slant-ranges are involved. Conversely, latitude and longitude coordinates are not utilized.
- **Spherical Surface Formulation** (Chapter 4) — This formulation —sometimes called great-circle navigation — considers two or more problem-specific locations on the surface of a spherical earth. Spherical trigonometry is the natural analysis tool when the earth's curvature must be considered explicitly. Latitudes and longitudes, as well as spherical-ranges (distances along the earth's surface) and azimuth angles with respect to north or between two paths, are inherent to this formulation. A limitation is that altitudes cannot be accounted for.

These two-dimensional analyses can generally be performed in the above sequence, with the result that most limitations of each analysis method are overcome. Section 1.2 provides an overview of this process. (For historical and practical reasons, in this document when there are

[*] Organizational terminology: X designates a Chapter; X.Y designates a Section (of a Chapter); X.Y.Z designates a Subsection (of a Section).

two problem-specific locations, they are often labeled **U** [user]) and **S** [satellite] [*]. These are only labels, and do not restrict application of the analysis.)

Some problems/situations are better suited to vector analysis than to trigonometric analysis, and important methodologies are based on vector analysis. Thus, it is addressed as well:

- **Vector Analysis Formulation** (Chapter 5) — The 3D-vector approach is preferable in situations that involve: (1) three or more problem-specific points that must be considered simultaneously (rather than sequentially, which allows one vertical plane to be considered at one time); and/or (2) only slant-range-type measurements (true slant-ranges, slant-range differences and/or altitude).

Limitations of the vector formulation are that (1) the earth's curvature is not handled well, and (2) insight into a problem can be hindered by the vector notation. Ultimately, the two methodologies are complementary: some situations can be addressed by both; some only by the combined trigonometric formulations; and some only by the vector formulation.

1.1.2 Applications of Trigonometric and Vector Methods (Chapters 6 – 7)

Chapters 6 and 7 apply the analysis methodologies described in Chapter 3-5 to situations involving three or more problem-specific points (e.g., an aircraft and two, three or four sensors). The following two significant restrictions are imposed:

(1) the number of measurements and unknown quantities are equal

(2) the earth is modeled as a sphere.

These restrictions enable closed-form solutions to be found. The primary value of a closed-form solution is that its properties — such as existence (e.g., What ranges of measured quantities do / do not result in a solution?) and uniqueness (e.g., Are there multiple solutions? Can the correct solution be determined?) — can be examined. It is also beneficial to have a comprehensible set of expressions for a solution.

Chapter 6 addresses scenarios involving sensors that measure slant- or spherical-range and azimuth angles (with aircraft altitude always known).

Chapter 7 addresses systems that measure slant- or spherical-range differences (a capability enabled by 20th century technologies). Often, these problems require consideration of all measurements simultaneously, and the vector methodology plays a more prominent role than the trigonometry-based methodology; however, both are used.

[*] Historical: these notes were begun for a project involving satellites. Practical: the Microsoft Word Equation Editor v3.1 does not have a global change capability.

1.1.3 Gauss-Newton NLLS Methodology and Applications (Chapter 8)

Chapter 8 eliminates restrictions (1) and (2) in the previous subsection. It first describes the Gauss-Newton Non-Linear Least-Squares (NLLS) method, which addresses situations that: (a) may involve more measurements than unknown variables, and (b) do not necessarily have invertible (or even analytic) measurement equations. This generality enables the calculation of numerical solutions for situations involving non-ideal sensors, an ellipsoidal earth, and/or other analytically intractable aspects. However, a drawback of the NLLS technique is that its solution properties cannot be readily characterized. The NLLS methodology is applied to a series of problems that, for various reasons, cannot be addressed by the trigonometric or vector methods.

1.2 Summary of Trigonometric Methodology

1.2.1 Vertical Plane Formulation

Figure 1 depicts a vertical-plane involving: an earth-based user **U**; a satellite **S** above a spherical earth; the satellite nadir (or sub-point) **N**; and the center of the earth **O**. Points **U** and **S** (or **N**) are problem-specific; **O** is not. All four locations are in the plane of the paper. Points **O**, **N** and **S** form a straight line. These points have no special relationship with the earth's spin axis. Since a 'snapshot' analysis is involved, no assumptions are made regarding the satellite's trajectory.

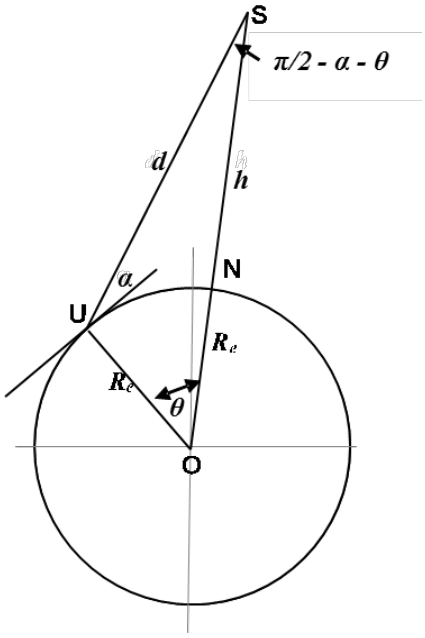

Figure 1 Vertical Plane Bisecting a Spherical Earth and Containing Points **U**, **O**, **N** and **S**

In Figure 1, three linear distances are of interest:

- R_e Earth radius (length of **OU** and **ON**)
- h Satellite altitude above the earth (length of **NS**)
- d User-satellite slant-range (length of **US**).

And two angles are of interest:

- α Satellite elevation angle relative to the user's horizon (may be positive or negative)
- θ Geocentric angle between the user and satellite nadir (is always positive).

The earth radius R_e is always assumed to be known.

There are four variables associated with this formulation: h, d, α and θ. If any two are known, the remaining two can be found. Thus, there are six possible groupings. Subsection 3.2.2 shows how to relax the restriction of **U** being on the earth's surface, to its having a known altitude. Chapter 3 details the full set of 12 possible equations for this formulation.

Of these four variables, the geocentric angle θ (which is equivalent to distance along the earth's surface, or spherical-range) is also a variable in the spherical surface formulation. It serves as the link for relating the two formulations — i.e., for transferring a solution to the vertical plane formulation into the spherical surface formulation (Subsection 4.1.3 elaborates on this topic). The other three variables (h, d and α) are related to the altitude of **S** above the earth's surface and have no role in the spherical surface formulation.

1.2.2 Spherical Surface Formulation

The spherical surface formulation is an application of spherical trigonometry. This formulation is almost perfectly matched to marine surface navigation, and was developed by the ancients partly for that purpose. It can be used for many aviation navigation and surveillance situations by combining it with the vertical plane formulation.

The left-hand side of Figure 2 depicts the earth's familiar latitude/longitude grid. The right-hand side shows two problem-specific points **U** and **S** on the surface and the seven variables involved in a two-location problem on a sphere:

- the latitude/longitude, respectively, of **U** (L_U, λ_U) and of **S** (L_S, λ_S)
- the geocentric angle θ between **U** and **S**, and
- the azimuth angles $\psi_{S/U}$ and $\psi_{U/S}$ of the great circle* arc connecting **U** and **S**.

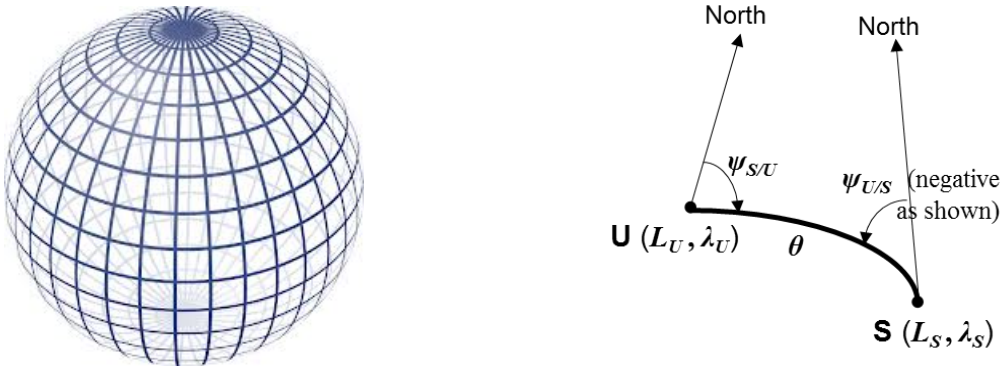

Figure 2 Spherical Surface Containing Points **U** and **S**

Generally, four of these variables must be known; from those, the other three can be computed. Even this simple problem involves 35 possible groupings of known / unknown variables. By taking advantage of symmetries, the situation can be described by 16 unique problems (Sub-section 4.1.8) —still a significant number. Thus, in contrast with the exhaustive approach taken for the vertical plane formulation, a more selective approach is adopted for the spherical-earth

* A great circle results when a sphere is sliced exactly in half. An arc from great circle (also called an orthodrome) is the path having the shortest length between two points along the surface of a sphere.

formulation: equations are presented only for the variable groupings of highest interest.

"Geodesy is the science concerned with the exact positioning of points on the surface of the Earth" (Ref. 1). In geodesy, analyses involving two groupings of known/unknown variables occur so frequently that they have been named:

- **Direct** (or *first*) problem* of geodesy: (a) Given the coordinates (L_U, λ_U) of **U**, the geocentric angle θ between **U** and **S**, and azimuth angle $\psi_{S/U}$ of a great circle path starting at **U** and ending at **S**; (b) Find the coordinates (L_S, λ_S) of the end point **S** and the path azimuth angle at the end point $\psi_{U/S}$.
- **Indirect** (or *second*, or *inverse*) problem of geodesy: (a) Given the coordinates (L_U, λ_U) and (L_S, λ_S) of points **U** and **S**, respectively; (b) Find the geocentric angle θ connecting **U** and **S**, and the azimuth angles (from north), $\psi_{S/U}$ and $\psi_{U/S}$, of the path at each end.

In both Chapter 4 (spherical surface formulation) and Chapter 5 (vector formulation), solution equations are provided for the Direct and Indirect problems of geodesy, and variations thereon that have relevant applications. Many of the problems addressed in Chapter 6 use the Direct or Indirect problem as a step in the solution algorithm.

1.3 Applicability and Limitations of Methodologies

With a few exceptions, the methodologies presented herein generally reflects conditions and assumptions appropriate to aircraft navigation and surveillance, including:

- **Earth Curvature Considered** — With the exception of aircraft on the surface of an airport, the curvature of the earth is a fundamental aspect of aircraft navigation and surveillance analysis and cannot be neglected.
- **Three-Dimensions Frequently Must Be Considered** — Some essential operations, such as aircraft approach, require that lateral/longitudinal position and altitude all be considered, necessitating a three-dimensional analysis methodology.
- **Horizontal Position and Altitude Are Decoupled at Long Ranges** — Generally, scenarios requiring simultaneous consideration of three dimensions involve aircraft-sensor ranges of less than 250 miles, the maximum visible distance of aircraft at 40,000 feet of altitude.
- **Altitude Measurement Are Always Available** — Virtually all aircraft provide baro-metric altitude information that can be adjusted to the elevation above sea level.

The analysis also embodies the following assumptions/limitations:

- **Static Scenarios** — Scenarios analyzed are 'snapshots' — i.e., motion of an aircraft is not explicitly involved. Sequence of locations are considered, but the notions of velocity or time as mechanisms for relating those locations are not utilized.
- **Straight-Line / Great-Circle Vehicle Paths** — When a spherical-earth model is

* Note the academic/mathematical use of the word "problem" in the narrow sense of specific groupings of known and unknown variables. This document also uses "problem" in the broader sense of a situation to be analyzed.

used, vehicle 'horizontal' (latitude/longitude) trajectories are always great circles. That is, they lie in a vertical plane that contains the center of a spherical earth. Vertical trajectories may be constant altitude or a geometric straight line.

- **Geometrically Simple Radio Wave Propagation Paths**— Radio waves follow paths that result in the shortest transmission time between a transmitter and receiver. When the intervening media can be treated as free space, a geometric straight-line path model is used. When the density of the atmosphere must be considered, a 4/3^{rds} earth path model is used. When the conductivity of the earth must be considered, great circle paths are assumed.
- **Terrain/Obstacles Ignored** — Except for the earth itself, obstacles such as hills/ mountains or man-made structures that could block the signal path between two locations (e.g., a sensor and a vehicle) are not addressed.

One might ask: Why emphasize a spherical earth model, when an ellipsoidal model is more accurate? The rationale is:

- **Insight/Confidence** — When the number of measurements is equal to the number of unknown quantities, a spherical earth-model often has a closed-form solution that is understandable. Conversely, an ellipsoidal model never has a closed form solution; the analyst must initialize, utilize and trust a numerical solution. In such a situation, a method for checking the numerical solution is necessary.
- **Ellipticity Error Often Acceptable** — While an ellipsoidal model more accurately describes the earth's shape, the earth is '99.7% round' (the ratio of the polar to equatorial radii). The ellipticity error resulting from employing the spherical-approximation is acceptably small for some applications.
- **Initialize Iterative Solution Process, When Needed** — The spherical-earth approximation provides excellent initial values for iterative solution processes that are required to eliminate the above assumptions/limitations.

Engineering analyses methods have been characterized thusly: "There are exact solutions to approximate problems, and approximate solutions to exact problems. But there are no exact solutions to exact problems".[*] The techniques described in Chapters 3–7, based on the spherical earth approximation, are exact solutions to approximate problems. The spherical-earth approximation is often made in authoritative documents that address similar applications (e.g., Refs. 1, 2 and 3). When an ellipsoidal-earth model is required and iterative numerical technique must be employed (Chapter 8), the spherical-earth approximation provides excellent initial values for the iteration process.

1.4 Document Outline

Chapter 1 (this one) describes the basic problems to be addressed, and outlines the recommended methodology for their solution. Chapter 2 is mathematical in nature, and is included to make this

[*] Conveyed by Prof. Donald Catlin (Univ. of Mass. Amherst, Mathematics Dept.), who attributed it to Prof. Lotfi Zadeh (Univ. of Calif. Berkley, Electrical Engineering Dept.).

document more self-contained.

Chapters 3 through 8 address mathematical solution techniques that are matched to the nature of the problem at hand – e.g., geometry and number and types of measurements. These are synopsized in Section 1.1. Table 1 is a high-level roadmap of location of the topics addressed.

Table 1 Topic Locations by Geometric Factors

Dimension / Shape	Two Dimensions	Three Dimensions
Spherical Earth	▪ Plane Trigonometry (problem limited to a vertical plane) – Chapter 3 ▪ Spherical Trigonometry (problem limited to the surface of a sphere) – Chapter 4 (2 points) and Chapter 6 (3 points)	▪ Vector Analysis – Chapter 5 ▪ Plane & Spherical Trigonometry combined – Chapter 6 ▪ Non-Linear Least Squares – Chapter 8
Ellipsoidal Earth	▪ Vincenty's Algorithm (2 points on an ellipsoid) – Subsection 2.2.3 ▪ Non-Linear Least Squares (>2 points on an ellipsoid) – Chapter 8	▪ Vector Analysis – Section 9.3 ▪ 'Bancroft' sections in Chapter 7 ▪ Non-Linear Least Squares – Chapter 8

To illustrate application of the analysis techniques described herein, example applications are presented at the ends of several chapters that address:

- Air Traffic Control (ATC) radar coverage (Example 1)
- Precision approach procedure design (Example 2)
- Satellite visibility of/from the Earth (Example 3)
- Great-circle flight path between Boston and Tokyo (Example 4)
- ATC radar display coordinate transformations (Example 5)
- Single VOR/DME station RNAV fix (Example 6)
- Ground path length ellipticity error for selected airport pairs (Example 7)
- Simplified navigation system that measures slant-ranges in two dimensions (Examples 8)
- Simplified navigation system that measure slant-range difference in two dimensions (Examples 9)
- Aircraft latitude/longitude determination from measurements of the pseudo spherical-ranges to three stations in a single Loran chain (Example 10);
- Aircraft latitude/longitude determination from measurements of the pseudo spherical-ranges involving four stations from two Loran chains (Example 11)
- A Wide Area Multilateration (WAM) surveillance system using measurements of slant-range differences and altitude for an aircraft (Example 12)
- Aircraft latitude/longitude determination from measurements of the pseudo spherical-range to five stations (Example 13)
- Aircraft latitude/longitude determination from measurements of the azimuth angles to two ground-based transmitters (Example 14).

Relevant specialized topics are presented in an Appendix (Chapter 9).

2. MATHEMATICS AND PHYSICS BASICS

2.1 Exact and Approximate Solutions to Common Equations

2.1.1 Law of Sines for Plane Triangles

For future reference, the law of sines applied to the plane triangle **UOS** in Figure 1 yields

$$\frac{\sin(\theta)}{d} = \frac{\sin(\frac{1}{2}\pi + \alpha)}{R_e + h} = \frac{\sin(\frac{1}{2}\pi - \alpha - \theta)}{R_e} \qquad \text{Eq 1}$$

Using the properties of trigonometric functions, Eq 1 reduces to

$$\frac{\sin(\theta)}{d} = \frac{\cos(\alpha)}{R_e + h} = \frac{\cos(\alpha + \theta)}{R_e} \qquad \text{Eq 2}$$

In Eq 2, the left-center equality,

$$(R_e + h)\sin(\theta) = d\cos(\alpha) \qquad \text{Eq 3}$$

relates all five quantities of interest in a simple way.

The left-right equality in Eq 2 is equivalent to

$$R_e \sin(\theta) = d\cos(\alpha + \theta) \qquad \text{Eq 4}$$

This expression relates one side variable, d, and the two angle variables, α and θ.

Similarly, the center-right equality in Eq 1 is equivalent to

$$R_e \cos(\alpha) = (R_e + h)\cos(\alpha + \theta) \qquad \text{Eq 5}$$

This expression relates one side variable, h, and the two angle variables, α and θ.

2.1.2 Law of Cosines for Plane Triangles

For future reference, the law of cosines is applied to the plane triangle **UOS** in Figure 1. When the angle at **O** is used as the angle of interest, the result is

$$d^2 = R_e^2 + (R_e + h)^2 - 2R_e(R_e + h)\cos(\theta) \qquad \text{Eq 6}$$

When the law of cosines is applied using the angle at **U**, the result is

$$(R_e + h)^2 = R_e^2 + d^2 - 2R_e\, d\cos(\tfrac{1}{2}\pi + \alpha) \qquad \text{Eq 7}$$

Each of these equations relates variables for two sides, d and h, and one angle — θ in Eq 6, and α in Eq 7.

2.1.3 Law of Tangents for Plane Triangles

The law of tangents for a plane triangle having sides a and b (respectively) with opposite angles A and B is

$$\frac{a-b}{a+b} = \frac{\tan(\frac{1}{2}(A-B))}{\tan(\frac{1}{2}(A+B))} \qquad \text{Eq 8}$$

The law of tangents can be used to find angles A and B simultaneously from their opposite sides, a and b, and the angle, C, enclosed by a and b. Thus

$$\begin{aligned} A - B &= 2\arctan\left[\frac{a-b}{a+b}\tan(\tfrac{1}{2}(\pi - C))\right] \\ A + B &= \pi - C \end{aligned} \qquad \text{Eq 9}$$

It follows that

$$\begin{aligned} A &= \tfrac{1}{2}(\pi - C) + \arctan\left[\frac{a-b}{a+b}\cot(\tfrac{1}{2}C)\right] \\ B &= \tfrac{1}{2}(\pi - C) - \arctan\left[\frac{a-b}{a+b}\cot(\tfrac{1}{2}C)\right] \end{aligned} \qquad \text{Eq 10}$$

The law of tangents (like the law of sines) can be used to find one side of a triangle from a linear equation, given another side and both opposite angles. Both denominators in Eq 8 must be positive. Thus $A > B$ if and only if $a > b$. So, if the sides of a plane triangle are ordered based on length, their opposite angles must have the same order based on magnitude, and vice versa.

2.1.4 Quadratic Algebraic Equation

In some instances, a quadratic equation similar to the following must be solved

$$Ax^2 + Bx + C = 0 \qquad \text{Eq 11}$$

The algebraic solution is

$$x = \frac{-B \pm \sqrt{B^2 - 4AC}}{2A} \qquad \text{Eq 12}$$

Generally, we cannot have imaginary roots, so $B^2 > 4AC$ when A and C have the same sign. In many instances, the positive root is sought. In these situations:

$$\begin{aligned} x &= \frac{-B + \sqrt{B^2 - 4AC}}{2A} = \frac{B}{2A}\left(-1 + \sqrt{1 - D}\right) \quad , \quad D \equiv \frac{4AC}{B^2} \quad , \quad |D| < 1 \\ x &= -\frac{B}{2A}\left(\frac{1}{2}D + \frac{1}{8}D^2 + \frac{1}{16}D^3 + \frac{5}{128}D^4 + \frac{7}{256}D^5 + \frac{21}{1024}D^6 + \frac{33}{2048}D^7 + \cdots\right) \\ x &\to -\frac{BD}{4A} = -\frac{C}{B} \quad \text{as} \quad D \to 0 \end{aligned} \qquad \text{Eq 13}$$

2.1.5 Computational Precision

To retain measurement precision, geodetic navigation and surveillance calculations typically require a minimum of ten decimal places (although they may not be needed in all applications). The reasons are that: (1) the earth radius and related quantities are known to an accuracy of one foot, or eight decimal places (Section 2.2); and (2) locations of interest on the earth's surface are often stated to hundredths of a foot, or ten decimal places (typical FAA and Coast Guard data).

If the analyst determines that calculations should be capable of replicating specified locations in the presence of computational effects (typically when using automation equipment), floating-point double-precision arithmetic is a minimum requirement. The IEEE 64-bit float pointing format "gives 15–17 significant decimal digits precision" (Ref. 4). Moreover, awareness of potential precision issues remains the analyst's responsibility.

2.1.6 Inverse Trigonometric Functions

Intrinsic to navigation analysis is the calculation of angles using inverse trigonometric functions. In performing such calculations, two concerns must be borne in mind: (1) numerical ill-conditioning and (2) ambiguous/extraneous solutions. Numerical ill-conditioning typically occurs when sine or cosine function values are close to ±1. Ambiguous/extraneous solutions occur when multiple angles satisfy a mathematical equation, and are a concern when the approximate value of the correct angle is not known. The equations in the following chapters attempt to address these concerns, but every situation cannot be anticipated.

Numerical Ill-Conditioning — Both the sine and cosine functions have angular arguments for which, simultaneously, the function's (a) value is ±1, and (b) derivative is zero. In such situations, relatively large changes in the angular argument can result in small changes in the function value, which may be subject to truncation or round off. Thus, computing an angle using the inverse of a trigonometric function often requires care and/or increased precision.

Table 2 illustrates numerical ill-conditioning for geocentric angle θ computed from the arc cosine function. For illustrative purposes, five decimal digits are used for angles in radians and their trigonometric function values (linear distances are regarded as comments). Here the minimum detectable cosine function change corresponds a linear distance greater than 10.3 NM. For most applications, use of double precision will alleviate problems of this nature, but use of single precision (which typically is accurate to seven decimal places) typically will not.

Table 2 Behavior of Trigonometric Functions for Small Geocentric Angles θ

θ (rad)	$R_e\theta$ (NM)	$R_e\theta$ (feet)	cos(θ)	1-cos(θ)	sin(θ)	sin(θ) / 1-cos(θ)
0.00000	0.000	0	1.00000	0.00000	0.00000	—
0.00001	0.034	209	1.00000	0.00000	0.00001	2.00 E+05
0.00003	0.103	627	1.00000	0.00000	0.00003	6.67 E+04
0.00010	0.344	2,090	1.00000	0.00000	0.00010	2.00 E+04
0.00030	1.031	6,270	1.00000	0.00000	0.00030	6.67 E+03
0.00100	3.438	20,900	1.00000	0.00000	0.00100	2.00 E+03
0.00300	10.313	62,700	1.00000	0.00000	0.00300	6.67 E+02
0.01000	34.378	209,000	0.99995	0.00005	0.01000	2.00 E+02
0.03000	103.134	627,000	0.99955	0.00045	0.03000	6.67 E+01
0.10000	343.780	2,090,000	0.99500	0.00500	0.09983	2.00 E+01

When hand calculations were the norm, a remedy to such situations was to employ the sine or tangent function, rather than the cosine function, when small angles are to be found. Unlike the cosine function, the sine and tangent functions increase monotonically from a zero value for a zero angle. In Table 2, the last column (calculated using double precision) indicates that for an angle of 0.000,01 rad, the sine function has a five decimal place precision advantage over the cosine function.

A method for recasting an ill-conditioned expression for $\cos(\theta)$, which dates to the middle of the first millennium, is illustrated in Eq 14.

$$\begin{aligned} &\textit{Given} \quad \cos(\theta) = f(\textit{other variables}) = 1-\varepsilon(\textit{other variables}) \\ &\textit{Invoke} \quad \cos(\theta) \equiv 1-2\sin^2\left(\frac{\theta}{2}\right) \\ &\textit{Thus} \quad \sin\left(\frac{\theta}{2}\right) = \frac{1}{\sqrt{2}}\sqrt{1-f} = \sqrt{\frac{\varepsilon}{2}} \\ &\textit{So} \quad \theta = 2\arcsin\left(\sqrt{\frac{\varepsilon}{2}}\right) \end{aligned} \qquad \text{Eq 14}$$

An example application of Eq 14 is finding the shortest side θ_A of a right spherical triangle, given the hypotenuse θ_H and the other side θ_B which have similar magnitudes. Spherical trigonometry, addressed in Section 4.1, provides the spherical equivalent of Pythagoras' theorem, $\cos(\theta_H) = \cos(\theta_A)\cos(\theta_B)$. Using $\cos(\theta_B) - \cos(\theta_C) = 2\sin\left[\frac{1}{2}(\theta_C + \theta_B)\right]\sin\left[\frac{1}{2}(\theta_C - \theta_B)\right]$, an identity from plane trigonometry, it follows that

$$\theta_A = \arccos\left(\frac{\cos(\theta_H)}{\cos(\theta_B)}\right) = 2\arcsin\left(\sqrt{\frac{\sin\left[\frac{1}{2}(\theta_H + \theta_B)\right]\sin\left[\frac{1}{2}(\theta_H - \theta_B)\right]}{\cos(\theta_B)}}\right) \qquad \text{Eq 15}$$

$$= 2 \arcsin\left(\frac{\sqrt{\sin\left[\frac{1}{2}(\theta_H + \theta_B)\right]}\sqrt{\sin\left[\frac{1}{2}(\theta_H - \theta_B)\right]}}{\sqrt{\cos(\theta_B)}}\right)$$

Ambiguous/Extraneous Solutions — Trigonometric functions are periodic. Consequently, inverse trigonometric functions can result in multiple angles. (Figure 3 illustrates the principal values for the arccos and arcsin.) Herein, the term 'ambiguous' refers to situations where more than one solution to a mathematical equation satisfies the physical problem posed, whereas 'extraneous' solutions satisfy the mathematical equation but not the physical problem. To limit the frequency of such situations, when selecting an equation, the analyst should consider the expected range of values for the angle involved — e.g.,

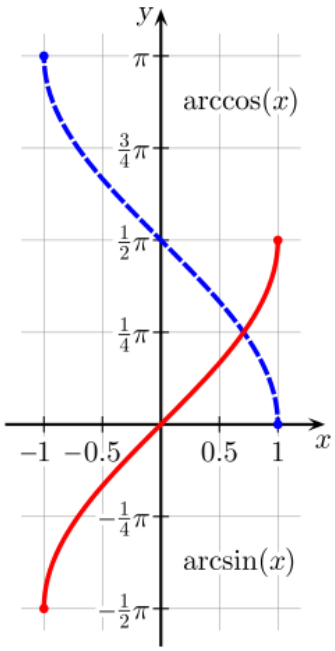

Figure 3 Principal Values of arcsin and arccos Functions

- Elevation Angles — Elevation angles α vary between -π/2 and π/2, so the arc sine and arc tangent functions, which result in unique angles in [-π/2, π/2] are preferred.
- Geocentric Angles — Geocentric angles θ vary between 0 and π, so the arc cosine or half-angle arc sine formulas are preferred, since both yield unique angles in [0,π]
- Azimuth Angles — Azimuth angles ψ vary between –π and π, so the four-quadrant (two argument) arc tangent function is preferred.

Unfortunately, some physical situations are inherently ambiguous. When such a situation occurs and the correct solution cannot be determined by inspection, the approach taken herein is make the ambiguity explicit by using the principal value of the arc function involved and introducing additional notation such as '±'. When the principal value is to be used, the 'a' in arc is capitalized. Such situations occur, e.g., in Subsections 3.3.1 and 3.4.4. In the former, the quantity 'arccos$[u\cos(\alpha)]$' is to be found, where $u > 0$. Since the correct resulting angle may be positive or negative when $\alpha > 0$, for clarity, the quantity is written as '$\pm$Arccos$[u\cos(\alpha)]$'.

2.1.7 Power Series Expansions for arcsin, arccos and arctan

In the analysis that follows, a common situation is the need to compute the inverse of a trigonometric function for an argument such that the resulting angle will be close to 0 — e.g., $\theta = \arcsin(x)$, $\theta = \arccos(1 - x)$ or $\theta = \arctan(x)$, where x is close to 0.

First, it is known that (Ref. 5)

$$\arcsin(x) = x + \frac{1}{6}x^3 + \frac{3}{40}x^5 + \frac{5}{112}x^7 + \frac{35}{1152}x^9 + \frac{63}{2816}x^{11} + \cdots \quad \text{Eq 16}$$

A Taylor series expansion of $\arccos(1-x)$ is not available, due to its lacking a derivative at $x = 0$. However, a more general power series (often called a Frobenius expansion) is available; thus, utilizing Eq 14 and Eq 16:

$$\begin{aligned} \arccos(1-x) &= 2\arcsin\left(\sqrt{\tfrac{1}{2}x}\right) \\ &= \sqrt{2x}\left(1 + \frac{1}{12}x + \frac{3}{160}x^2 + \frac{5}{896}x^3 + \frac{35}{18432}x^4 + \frac{63}{90112}x^5 + \cdots\right) \end{aligned} \quad \text{Eq 17}$$

Lastly, from Ref. 5:

$$\arctan(x) = x - \frac{1}{3}x^3 + \frac{1}{5}x^5 - \frac{1}{7}x^7 + \frac{1}{9}x^9 - \frac{1}{11}x^{11} \pm \cdots \quad \text{Eq 18}$$

2.1.8 Single-Variable Numerical Root Finding Methods

Introduction — When it's necessary to find an unknown scalar quantity, the preferred situation is to have (or develop) an equation whereby all known quantities are on one side and the unknown quantity is isolated on the opposite side (sometimes call 'inverting' the original equation). However, situations inevitably arise whereby the available expressions cannot be manipulated to isolate the unknown quantity (sometimes called 'intractable'). This is particularly true when three-dimensions are involved and/or an ellipsoidal model of the earth is employed. In such situations, recourse is often made to numerical root finding techniques.

The most widely-known scalar root-finding technique is "Newton's" or the "Newton-Raphson" method (Ref. 6). Newton's method performs well for most functions, but has the disadvantage that it requires the derivative of the expression with respect to the variable whose value is sought. Often the derivative is difficult or impossible to find analytically. Thus, in applied work, interest is frequently focused on derivative-free root-finding techniques. Such techniques were first investigated by the ancients, including the Babylonians and Egyptians.

Secant Method — The secant method is among the simplest and oldest root-finding algorithms. Assume that we seek a value of *x* that satisfies $f(x) = 0$ and that two initial or previous estimates for *x* are available, x_{n-1} and x_n. The expression for the next estimate, x_{n+1}, then is

$$x_{n+1} = x_n - f(x_n)\frac{x_n - x_{n-1}}{f(x_n) - f(x_{n-1})} = \frac{x_{n-1}f(x_n) - x_n f(x_{n-1})}{f(x_n) - f(x_{n-1})} \quad \text{Eq 19}$$

The secant method is a finite difference version of Newton's method; in effect, it uses the previous two points to estimate the function's derivative. The points x_{n-1} and x_n that are used to generate x_{n+1} maybe, but are not required to be, on opposite sides of the root sought.

Example of Secant Method — An example of the secant method is determining the square root of 2 — i.e., finding the root of $f(x) = x^2 - 2$. Table 3 shows the results of applying Newton's method and the secant method, beginning from similar points.

Table 3 Comparison of Newton's and Secant Methods for Finding the Square Root of 2

Iteration, *n*	Newton's Method		Secant Method	
	Variable, x_n	Function, $f(x_n)$	Variable, x_n	Function, $f(x_n)$
1	1.0000000000	-1.0000000000	1.0000000000	-1.0000000000
2	1.5000000000	0.2500000000	1.5000000000	0.2500000000
3	1.4166666667	0.0069444444	1.4000000000	-0.0400000000
4	1.4142156863	0.0000060073	1.4137931034	-0.0011890606
5	1.4142135624	0.0000000000	1.4142156863	0.0000060073
6	—	—	1.4142135621	-0.0000000009
7	—	—	1.4142135624	0.0000000000

Discussion — After initialization, both Newton's and the secant method converge in one step if the function *f* is linear over the interval between the initial value(s) and the root. Generally, convergence is governed by the first and second derivatives of *f*. Functions that have a constant or continuously increasing (or decreasing) derivative are most amenable to a numerical root finder. For such functions, Newton's method convergence is order 2 (i.e., the error for iteration *n* is proportional to the square of the error for iteration *n*-1); the secant method convergence is order 1.6 (termed 'superlinear'). If one weights function and derivative evaluations equally, the secant method can be faster than Newton's method.

Guaranteed Convergence Methods — While effective for favorable initial conditions, convergence is not guaranteed for either Newton's or the secant method. If not chosen close enough to the root sought, the initial point(s) can result in a derivative (or numerical approximation thereof) which is much smaller in absolute value and/or of opposite sign than the derivative at the solution. That, in turn, can cause the next estimate, x_{n+1}, to be far from the root sought (divergence).

The two methods described immediately below guarantee convergence, provided that the initial estimates x_1 and x_2 are on opposite sides of the root sought and that there is only one root between x_1 and x_2. These conditions are often satisfied in navigation problems. The cost of this robustness generally is speed of convergence. Neither method converges as rapidly as Newton's or the secant method for well-chosen initial point(s). Two examples are provided below.

False Position (*Regula Falsi*) — The method of false position uses almost the same expression as the secant method to find the next estimate, x_{n+1}, for the root sought. The difference is that the

initial two estimates, now labeled x_1 and x_1', are required to be on opposite sides of the root sought. Moreover, at each subsequent iteration, the two points used to compute x_{n+1} (i.e., x_n and x_n' in Eq 20) are required to be on opposite sides of the root. The weakness of the false position method is that convergence can be very slow when *f* is highly nonlinear, because the actual function and assumed linear function behaviors are widely different.

$$x_{n+1} = \frac{x_n' f(x_n) - x_n f(x_n')}{f(x_n) - f(x_n')} \quad , \quad x_{n+1}' = x_n \text{ or } x_n' \quad \text{such that} \quad f(x_{n+1}) f(x_{n+1}') < 0 \qquad \text{Eq 20}$$

Interval Bisection — Interval bisection is among the oldest root finding techniques. Like the method of false position, the initial two estimates, x_1 and x_1', are required to be on opposite sides of the root sought. Then, at each iteration, x_{n+1} is set to the mean of x_n and x_n' (Eq 21). As for the method of false position, x_{n+1}' is set to either x_n or x_n', whichever is on the side opposite x_{n+1} of the root. Except for its sign, the interval bisection method does not take account of the value of the function *f*. This is a drawback when *f* is almost linear. However, it is an advantage when *f* is highly nonlinear, since it is better to assume nothing about a function's behavior than to make an incorrect assumption.

$$x_{n+1} = 0.5\,(x_n + x_n') \quad , \quad x_{n+1}' = x_n \text{ or } x_n' \quad \text{such that} \quad f(x_{n+1}) f(x_{n+1}') < 0 \qquad \text{Eq 21}$$

These two methods can be used separately or in combination, either as the first root finding technique employed or as an alternative when the secant method fails.

Example of Guaranteed Convergence Methods (Poor Initial Values) — The function selected is specified in Eq 22 and illustrated in Figure 4. It is representative of functions often encountered in navigation analysis. Although highly nonlinear, it is ordinary in many aspects. It's monotonically increasing, as is its derivative. The initial two points are on opposite sides of the root sought (at π/4 = 0.785398…), but are intentionally selected not to be close to the root.

$$f(x) = \frac{1}{\cos^2(x)} - 2 \qquad x_1 = 0 \qquad x_1' = 1.5 \qquad \text{Eq 22}$$

Three guaranteed-convergence root finding algorithms are employed for Eq 22: interval bisection, false position, and alternating between the two. The stopping criterion is $|f(x_n)| < 10^{-10}$. The iteration numbers *n* that satisfy the stopping criterion are (and an opinion): interval bisection, *n* = 37 (acceptable); false position, *n* = 1,696 (not acceptable); and alternating, *n* = 20 (preferred).

The excessive number of iterations required by the false position method is due to its primary limitation: one of the two points used to compute x_{n+1} (Eq 20) may remain fixed ('pinned') at one of the initial values. In this case, $x_n' = x_1' = 1.5$ for $n = 2,3,4,$ ... while x_n increases

gradually from slightly greater than zero to the root sought.

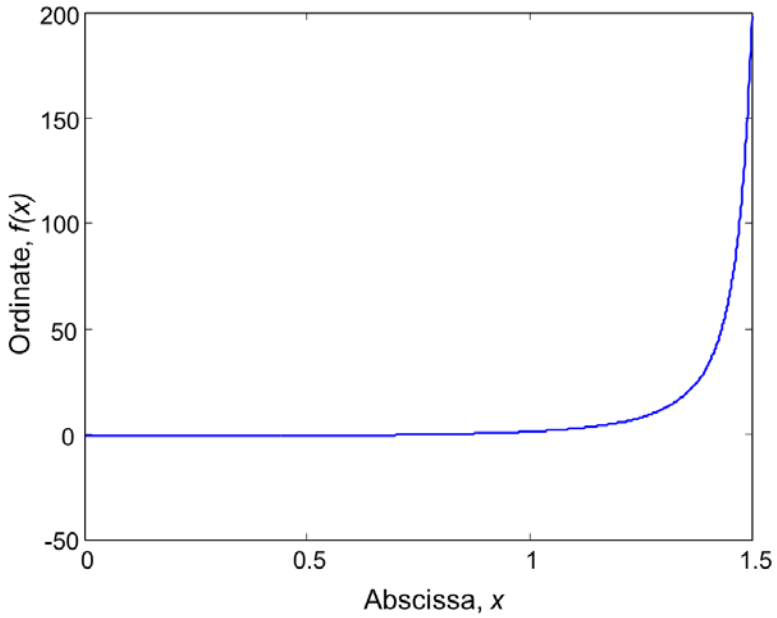

Figure 4 Example Function for Numerical Root Finding Techniques

The secant method diverges for this example. The values computed for x_3 and x_4 are the same as x_2 and x_3 for the false position method. However, for the secant method, the computed value for x_5 is 44.26…, which is well outside the initial interval. One might posit that the very slow convergence of the false position method for this example is the 'cost' of using a linear method that guarantees convergence in a situation where the secant method diverges.

Role of Initial Values — The initial values are an integral part of a root-finding problem. 'Good' initial values result in a situation whereby the function is almost linear for the interval containing the root sought and the initial values. Then the secant method can be used and convergence is rapid. Conversely, for 'poor' initial values, the function is highly nonlinear over that interval. Then a guaranteed-convergence algorithm is needed and convergence is slower. Conceptually, one may regard alternating between the interval bisection and false position methods as using the interval bisection method to improve the initial estimates for the false position method.

Example of Guaranteed Convergence Methods (Good Initial Values) — If the example of Eq 22 is modified by choosing $x_1' = 1$ rather than 1.5 (without changing anything else), then the problem is transformed from one that is highly nonlinear to one that is almost linear. The iteration numbers *n* that satisfy the stopping criterion are: interval bisection, *n* = 37; false position, *n* = 29; and alternating between the two, *n* = 16. For this modified example, the secant method converges and satisfies the stopping criterion when *n* = 11.

Summary: Guaranteed Convergence Methods — Convergence of the false position method is highly sensitive to the initial values used, while convergence of the interval bisection method is completely insensitive to the initial values. Alternating between the two methods is often more efficient than using either exclusively, for both 'good' and 'poor' initial conditions. Other techniques for combining the interval bisection and false position methods may also be used.

2.2 Shape of the Earth

2.2.1 WGS-84 Ellipsoid Parameters

While use of a spherical earth model is basic to much of the analysis herein, the most-accepted model for the shape of the earth is an oblate spheroid (ellipse rotated about its minor axis). The term 'ellipticity error' is used for differences between distances or angles found using a spherical earth model and the same quantities found using an ellipsoidal model.

The World Geodetic Survey 1984 (WGS-84) model parameter are the ellipsoid's semi-major axis, *a*, and the flattening *f*. Their numerical values are

- $a = 6{,}378{,}137$ m (WGS-84)
- $f = 1 / 298.257{,}223{,}563$ (WGS-84)

Eq 23

Flattening of the ellipsoid is defined by Eq 24, where b is the semi-minor axis.

$$f = \frac{a - b}{a} \qquad \text{Eq 24}$$

In computations, the square of the eccentricity e^2 is frequently used in lieu of the flattening.

$$e^2 = \frac{a^2 - b^2}{a^2} = 2f - f^2 = f(2 - f) \qquad \text{Eq 25}$$

Although the earth's shape is not a sphere, it is nearly so. A useful 'rule of thumb' is that the ellipticity error in the computed length of a path is 0.3%. The basis of this estimate is that the earth's flattening is approximately 0.003353, or 0.34%. Subsection 4.8.7 contains examples of the ellipticity error in computing the ranges between selected airports.

In the U.S., the foot is the most common unit of distance. As a result of the International Yard and Pound Agreement of July 1959, the international foot is defined to be exactly 0.3048 meter. Thus

- $a = 20{,}925{,}646.3$ ft (WGS-84)
- $b = (1 - f)a = 6{,}356{,}752.3$ m = 20,855,486.6 ft (WGS-84)
- $e^2 = 0.006{,}694{,}379{,}990{,}14$ (WGS-84)

Eq 26

In marine and aviation applications, the nautical mile (NM) is usually used as the unit of

distance. The international nautical mile was defined by the First International Extraordinary Hydrographic Conference in Monaco (1929) as exactly 1,852 meters. This definition was adopted by the United States in 1954. The international nautical mile definition, combined with the definition for the foot cited above, result in there being 6,076.1155 feet in one nautical mile.

2.2.2 Radii of Curvature in the Meridian and the Prime Vertical

To approximate the ellipsoidal earth at a location on its surface by a sphere, two radii of curvature (RoCs) are commonly defined — the RoC in the meridian (north-south orientation), R_{ns}, and the RoC in the prime vertical (east-west orientation), R_{ew} (Ref. 7). These RoCs lie in orthogonal planes that include the normal (perpendicular line) to the surface of the ellipse. Their values are a function of the geodetic latitude L of the location involved — see Appendix (Section 9.3). Their analytic expressions are shown in Eq 27 and they are plotted in Figure 5.

$$R_{ns} = \frac{a(1-e^2)}{[1-e^2\sin^2(L)]^{3/2}} = \frac{a^2b^2}{[a^2\cos^2(L)+b^2\sin^2(L)]^{3/2}}$$
$$R_{ew} = \frac{a}{[1-e^2\sin^2(L)]^{1/2}} = \frac{a^2}{[a^2\cos^2(L)+b^2\sin^2(L)]^{1/2}} \qquad \text{Eq 27}$$

The R_{ns} RoC in Eq 27 can vary more widely than the rule of thumb for ellipticity error. Figure 5 shows that while R_{ew} does change by about 0.34% between the Equator and a Pole, R_{ns} changes by slightly over 1%. Excursions of the radius of curvature from a reasonable average value will usually be greater, on a percentage basis, than the ellipticity error in a path length.

The RoC in an arbitrary vertical plane that includes the normal to the ellipse and makes azimuth angle ψ with north is given by (Ref. 7):

$$\frac{1}{R_\psi} \equiv \frac{\cos^2(\psi)}{R_{ns}} + \frac{\sin^2(\psi)}{R_{ew}} \qquad \text{Eq 28}$$

The average of R_ψ over $0 \le \psi \le 2\pi$ (at a given latitude) is the Gaussian radius of curvature R_G

$$R_G \equiv \sqrt{R_{ns}R_{ew}} = \frac{a(1-f)}{1-e^2\sin^2(L)} \qquad \text{Eq 29}$$

In some applications, a global approximation to R_e (independent of latitude) may be sufficient. One such approximation is the arithmetic mean of the three semi-axes of the ellipsoid

$$R_{e,mean} \equiv \tfrac{1}{3}(a+a+b) = \left(1-\tfrac{1}{3}f\right)a \qquad \text{Eq 30}$$

Thus

- $R_{e,mean}$ = 6,371,008.8 m = 20,902,259.7 ft (WGS-84) Eq 31

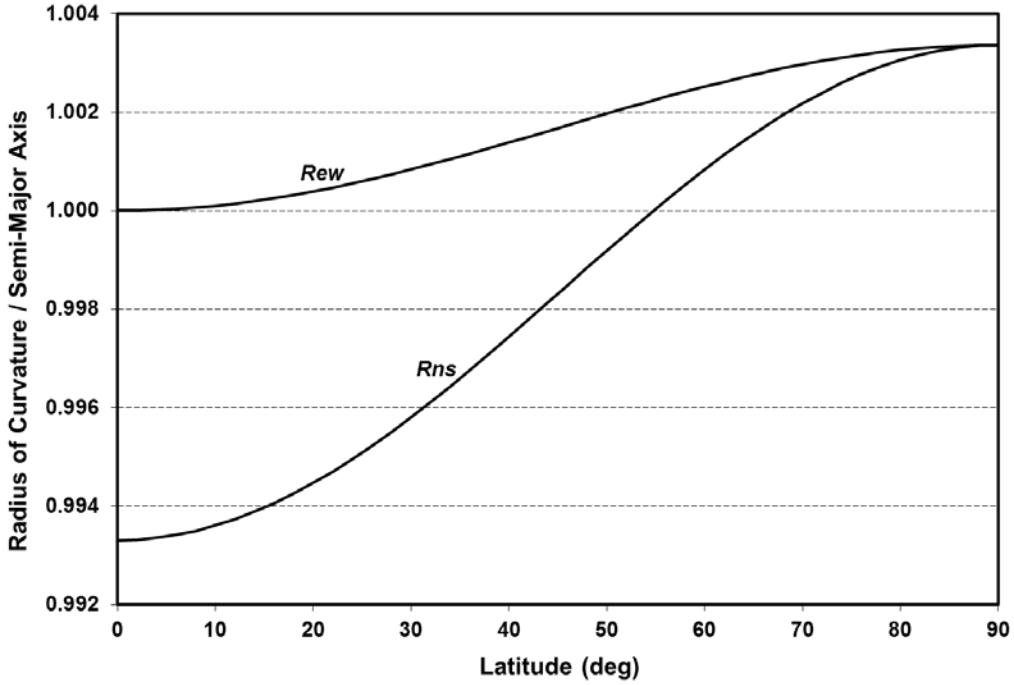

Figure 5 Ellipsoidal Earth's Radii of Curvature, Normalized to the Semi-Major Axis

When analyzing procedures for the FAA and other U.S. Government agencies with an aviation mission, the value of R_e to be used is defined in Ref. 2:

- $R_{e,TERPS} = 20{,}890{,}537$ ft (U.S. TERPS) Eq 32

An earth-centered, earth-fixed (ECEF) Cartesian coordinate frame for an ellipsoidal model of the earth is defined in the Appendix (Section 9.3).

2.2.3 Methods for Addressing an Ellipsoidal Earth

During approximately the past half-century, there has been a resurgence of interest in ellipsoidal earth models. Reasons for this interest include: (1) wide availability of machine-based computational capabilities, (2) deployment of accurate long-range radionavigation systems, and (3) development of long-range weapons systems. Much of the recent work derives from two volumes by Helmert* which were published in the 1880s (Ref. 8) and translated into English (Ref. 9) in the 1960s.

Andoyer-Lambert Formula — The Andoyer-Lambert formula results from expansion of the geodesic (shortest) arc between two points on a reference ellipsoid to first-order in the flattening (Ref. 10). This approximation was widely used in conjunction with both the Loran-C (Ref. 11) and Omega (Ref. 12) radionavigation systems. Accuracy for the Andoyer-Lambert formula is

* Friedrich Robert Helmert (July 31, 1843 – June 15, 1917) was born in Freiberg, Kingdom of Saxony (now Germany). According to Wikipedia, his texts "laid the foundations of modern geodesy".

10 m for distances up to 6,000 miles (Ref. 11).

Sodano's Method — In a series of papers published between 1958 and 1968, Sodano* described approximate solutions to the Direct and Indirect problems of geodesy based on expansion of the arc length between two points to higher orders in the eccentricity (Refs. 13, 14 and 15). Quoting Ref. 13: "The accuracy of geodetic distances computed through the e^2, e^4, e^6 order for very long geodesics is within a few meters, centimeters and tenth of millimeters respectively. Azimuths are good to tenth, thousandths and hundreds thousandths of a second. Further improvement of results occurs for shorter lines".

Vincenty's Method — During the early 1970s, Vincenty† revisited the issue of geodesics on an ellipsoid. He developed and programmed a version of earlier algorithms (including Helmert's) for a calculator. To accommodate the available computing technology, Vincenty's primary concern was minimizing the program's memory consumption. Accordingly, he developed iterative algorithms for both the Direct and Indirect problems of geodesy (Ref. 16).

Due to its ease of coding, Vincenty's algorithms are now the most widely used method for computing geodesics on an ellipsoidal earth. Their accuracy is quoted as less than one millimeter, which has been independently validated by comparison with numerical integration of the differential equations governing geodesic arcs on an ellipsoid (Ref. 17).

2.2.4 Surface Area of a Spherical Earth Visible to a Satellite

If the earth is modeled as a sphere with radius R_e, its surface area is $4\pi R_e^2$. The surface area enclosed by a circle on the surface of that sphere is

$$A = 2\pi (R_e)^2 [1 - \cos(\theta)] \qquad \text{Eq 33}$$

Here θ is the half-angle of the cone, with apex at the center of the spherical earth, whose intersection with the surface forms the circle under discussion. In Figure 1, the cone would be formed by rotating line **OU** about line **ON**. Thus A is the area of the earth visible to satellite **S** at altitude h when the user's elevation angle α or larger. An expression for the cone angle θ as a function of the satellite altitude h and user's elevation angle α is provided subsequently (Eq 40).

* Emanuel Sodano worked at the U.S. Army Map Service and the Army Geodesy, Intelligence and Mapping Research and Development Agency.
† Thaddeus Vincenty worked at the U.S. Defense Mapping Agency Aerospace Center, Geodetic Survey Squadron, Warren Air Force Base, in Wyoming.

3. TWO-POINT / VERTICAL-PLANE FORMULATION

3.1 Mathematical Problem and Solution Taxonomy

3.1.1 Mathematical Formulation

In mathematical terms, the objective of this chapter is to analyze a plane triangle similar to **UOS** in Figure 1. A plane triangle is fully described by its three sides and three interior angles (or quantities having a one-to-one relationship with these six quantities). However, since the interior angles of a plane triangle (quantified in radians) must sum to π, interest can be limited to two interior angles (or their one-to-one equivalents). Thus, in Figure 1, any three of the five quantities R_e, h, d, α and θ can be selected independently (noting that at least one quantity must be a side), and the other two quantities will be (almost) uniquely determined. In this analysis,

- The angle having its vertex at the satellite **S** has a secondary role and is treated as a dependent variable.
- The earth's radius R_e is assumed to be a known parameter, rather than a variable.

Consequently, the purpose of this chapter is to provide solutions for any one of the four variables (h, d, α, θ) as a function of any two of the remaining variables (and the known parameter R_e). When a known user altitude h_U is introduced in Section 3.2, h is a surrogate for $h_S - h_S$. However there is no change in the number of known/unknown quantities or to the solution methodology.

3.1.2 Taxonomy of Solution Approaches

Calculating any one variable (of four possible) as a function of any two (of three possible) other variables results in a total of 12 equations. These equations are addressed in the following sections of this chapter and are described Table 4. In the fourth column of the table, the classic trigonometric terminology for 'solving a triangle' is utilized — e.g., SAS denotes two sides and the included angle (Ref. 18).

Two complications can arise when 'solving a triangle'. One is that — due to measurement errors or other reasons — the values for the independent variables are not consistent with a valid triangle. For example: in an ASA situation, the two known angles may sum to π or greater; in an SSS situation, one side may be longer than the sum of the other two. A second complication can occur when the three quantities available are consistent with a valid triangle; they may in fact be consistent with two triangles (ambiguous solution). This can only occur for the SSA taxonomy category, and only when the available angle is adjacent to the longer of the two available sides. Sections 3.2 through 3.6 address these complications.

Table 4 Taxonomy for the Vertical Plane Triangle **OUS** in Figure 1

Independent Variables*	Dependent Variable	Subsection	Triangle Taxonomy†	Solution Guaranteed?	Solution Unique?	Solution Method
h & α	θ	3.3.1‡	SSA	No	No	Law of Sines
h & d	θ	3.3.3	SSS	No	Yes	Law of Cosines
d & α	θ	3.3.4‡	SAS	Yes	Yes	Law of Sines
h & θ	α	3.4.1‡	SAS	Yes	Yes	Law of Sines
h & d	α	3.4.3	SSS	No	Yes	Law of Cosines
d & θ	α	3.4.4	SSA	No	No	Law of Sines
h & θ	d	3.5.1	SAS	Yes	Yes	Law of Cosines
h & α	d	3.5.2	SSA	No	No	Law of Cosines
θ & α	d	3.5.3	ASA	No	Yes	Law of Sines
d & θ	h	3.6.1	SSA	No	No	Law of Cosines
d & α	h	3.6.2	SAS	Yes	Yes	Law of Cosines
θ & α	h	3.6.3‡	ASA	No	Yes	Law of Sines

* Side **OU**, length R_e, is always known.

† SAS = side-angle-side; ASA = angle-side-angle; SSS = side-side-side; SSA = side-side-angle.

‡ The following subsection contains an alternative solution method for the same set of variables.

There are often alternatives to solution approaches based on the law of cosines and of sines. Four are presented herein — three based on the law of tangents and one on the quadratic equation.

3.1.3 Detailed Geometry

Figure 6 is a more detailed depiction of the vertical-plane problem geometry shown in Figure 1. For each of vertex of triangle **OUS**, a line is constructed that intersects the opposite side (or an extension thereof) in a right angle. (Similar lines are created in some proofs of the law of sines and law of cosines.) The intersection points are labeled **A**, **B** and **C**. Because triangle **OUS** is oblique, intersections points **B** and **C** are outside the perimeter of **OUS**. Each constructed line results in the creation of two right triangles (for example, line **OC** creates right triangles **OCU** and **OCS**). Thus its length can be found from each of the two right triangles. Because the angles at **B** or **C** are constructed as right angles, it follows that $\angle BSU = \alpha$ and $\angle COU = \alpha$. Figure 6 also introduces the chord **UN**, which relates to the half-angle $\frac{1}{2}\theta$. Color-coded distances (violet) and angles (blue) associated with these lines and points are also shown.

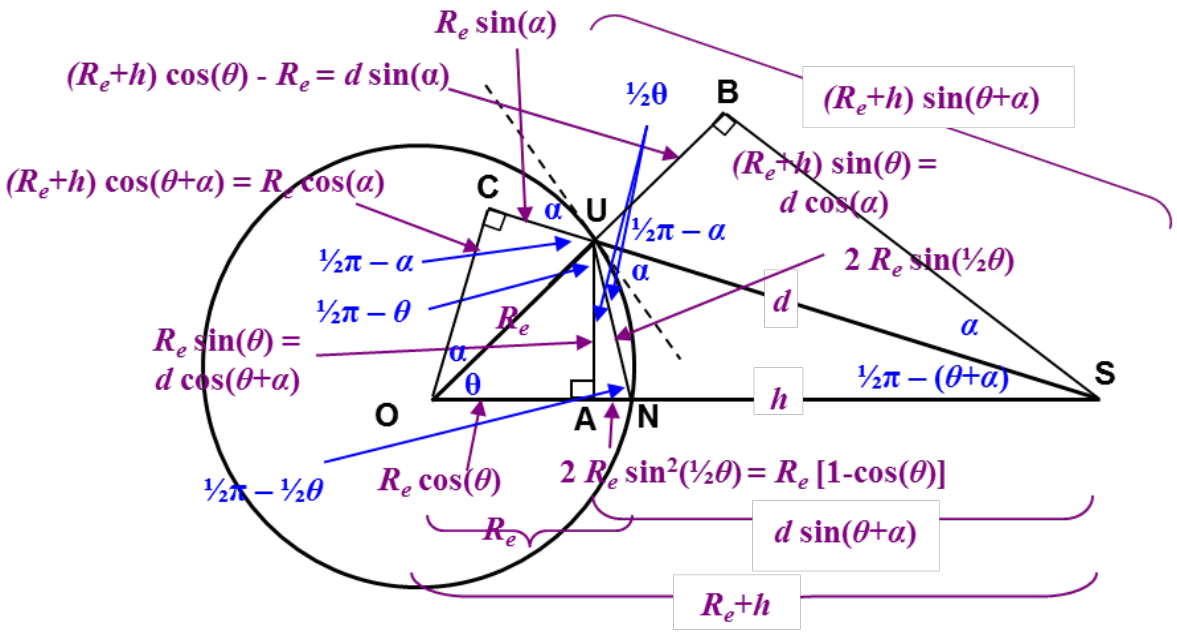

Figure 6 Detailed Geometry for Vertical Plane Formulation

3.2 Accounting for Known User Altitude

3.2.1 Need to Account for User Altitude

The equations in Section 3.3 through 3.6 — which address the vertical plane containing the User's location **U**, the Satellite's location **S** and the earth's surface center **O** (Figure 1) — can be developed assuming that **U** is on the earth's surface. The equations that result are sufficient when **S** represents an actual, earth-orbiting satellite, as their minimum satellite altitudes are hundreds of miles. Moreover, in situations involving satellites, if more accuracy is needed, one is generally free to re-define the earth's radius to include the elevation of **U** above, say, sea level.

However, the 'vertical situation' is very different when **S** represents an airplane. At most, aircraft are only a few miles above the earth's surface. Additionally, absent a compelling reason to do otherwise, in aviation, the earth's radius corresponds to sea level (this information is provided by a baro-altimeter – see Subsection 9.1.1) and should not be redefined. Thus, for aviation, the altitude of **U**, while known, must be explicitly accounted for.

Subsection 3.2.2 shows how to modify the equations in Section 2.1 to account of a non-zero, known user elevation/altitude, and Subsection 3.2.3 shows how to select the user altitude to ensure an unblocked line-of-sight to a satellite at a given distance or altitude (which is not guaranteed by the equations in Section 3.3 through 3.6).

3.2.2 Method of Accounting for Known User Altitude

In many situations, there is no concern about the line-of-sight (LOS) between the 'User' **U** (generally a sensor) and the 'Satellite' (actual satellite or aircraft) **S** being blocked by the earth's curvature. This is the situation depicted in Figure 1. A method for determining the minimum elevation angle for which there is no LOS blockage is shown in Subsection 3.2.3.

When the user altitude h_U is known, the equations presented in Subsections 2.1.1 and 2.1.2 can be used with these substitutions to account for a non-zero user altitude:

- $R_e \rightarrow R_e + h_U$, and
- $h \rightarrow h_S - h_U$ (where h_S is the satellite altitude)

Eq 34

3.2.3 Conditions for Unblocked Line-of-Sight (LOS)

The expressions developed in Sections 3.3 through 3.6 require that **OUS** be a valid geometric triangle, including one of its degenerate forms. However, they do not require that the LOS between **U** and **S** be unblocked by the earth. The possibility that a signal (or flight) path is physically blocked must be checked separately, using the expressions in this subsection.

Conditions for which the LOS between two points is unblocked by the earth can be determined with the aid of Figure 7, which shows the LOS connecting the User **U** and Satellite **S** having a point of tangency **T** with the earth's surface. Eq 35 applies to a situation where the user altitude h_U and satellite altitude h_S are known and the geocentric angle θ is be selected to ensure LOS visibility. Altitudes h_U and h_S can be traded off to avoid blockage. If the largest value θ is selected consistent with LOS visibility, the variables d, α_U and α_S, can be found from Eq 36.

$$\theta_U = \arccos\left(\frac{R_e}{R_e + h_U}\right) = 2\arcsin\left(\sqrt{\frac{h_U}{2(R_e + h_U)}}\right)$$

$$\theta_S = \arccos\left(\frac{R_e}{R_e + h_S}\right) = 2\arcsin\left(\sqrt{\frac{h_S}{2(R_e + h_S)}}\right)$$

$\theta \leq \theta_U + \theta_S$ for LOS visibility, when h_U and h_S are fixed

Eq 35

For $\theta = \theta_U + \theta_S$

$$d = R_e \tan(\theta_U) + R_e \tan(\theta_S)$$

$$\alpha_U = -\arccos\left(\frac{R_e}{R_e + h_U}\right) = -2\arcsin\left(\sqrt{\frac{h_U}{2(R_e + h_U)}}\right)$$

$$\alpha_S = -\arccos\left(\frac{R_e}{R_e + h_S}\right) = -2\arcsin\left(\sqrt{\frac{h_S}{2(R_e + h_S)}}\right)$$

Eq 36

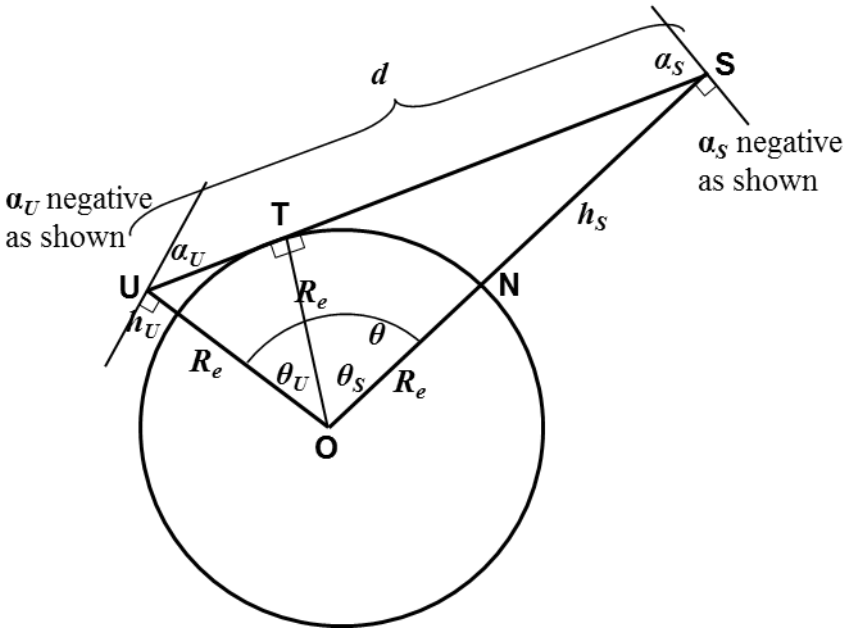

Figure 7 Geometry for LOS Signal Path Tangent to the Earth's Surface

A slightly different situation is the siting a radar at **U** to provide visibility of an aircraft at **S**. Here h_S (minimum required coverage altitude) and $\theta = \theta_U + \theta_S$ (distance between the location where the radar is to be installed and the outer boundary of the coverage region) are known. Then the radar elevation h_U is found using Eq 37. If the minimum altitude h_U is selected consistent with LOS visibility, then d, α_U and α_S, can be found from Eq 36.

$$\theta_S = \arccos\left(\frac{R_e}{R_e + h_S}\right) = \arccos\left(1 - \frac{h_S}{R_e + h_S}\right) = 2\arcsin\left(\sqrt{\frac{h_S}{2(R_e + h_S)}}\right)$$

$$\theta_U = \theta - \theta_S$$

$$h_U \geq \left(\frac{1}{\cos\theta_U} - 1\right) R_e = \frac{2\sin^2\left(\frac{1}{2}\theta_U\right)}{\cos(\theta_U)} R_e \quad \text{for LOS visibility}$$

Eq 37

In addition to the above geometric considerations, the analyst should be aware that radar signal propagation paths, such as **US** in Figure 7, may be subject to bending caused by changes in atmospheric density with altitude. A simple, commonly used method for modeling this phenomenon is discussed in Subsection 3.7.1.

3.3 Computing Geocentric Angle

3.3.1 Satellite Altitude and Elevation Angle Known – Basic Method

In this subsection, the independent variables are the satellite altitude h_S and the elevation angle α. The dependent variable is the geocentric angle θ. The same pair of independent

variables is considered in Subsection 3.5.2, in conjunction with determining the slant-range d. In terms of the classic taxonomy for triangles, this is an SSA (side-side-angle) situation.

Manipulating Eq 5 and using the substitutions of Eq 34 yields the formal solution

$$\theta = -\alpha + \arccos\left(\frac{R_e + h_U}{R_e + h_S}\cos(\alpha)\right) \qquad \text{Eq 38}$$

Due to the possibility of unsolvable formulations and multiple solutions, it is desirable to consider three cases.

Constraints on Solution Existence — There are two constraints in generating a usable solution from Eq 38.

- First, assume that $\alpha \geq 0$. Since $\theta \geq 0$, $(R_e + h_S)\cos(\theta + \alpha) = (R_e + h_U)\cos(\alpha)$. Thus, $h_S \geq h_U$.
- Second, assume that $\alpha < 0$. Then $(R_e + h_S)\cos(|\alpha| - \theta) = (R_e + h_U)\cos(|\alpha|)$. It follows that $(R_e + h_S) \geq (R_e + h_U)\cos(\alpha)$.

These constraints have geometric interpretations. The elevation angle α describes an inclined line having one end that terminates at **U**, while the satellite altitude h_S describes a circle concentric with the earth's center **O**. For a solution to exist, these loci must intersect. When $\alpha \leq 0$, $(R_e + h_U)\cos(\alpha)$ is the shortest distance between the center of the earth **O** and locus of points with constant depression angle $|\alpha|$. This occurs when the triangle **OUS** has a right angle at **S**; then $\alpha = -\theta$. These constraints to not prevent the line **US** from penetrating the earth.

In summary, for a solution to exist:

$$\begin{gathered} h_S > h_U \quad \text{when} \quad \alpha \geq 0 \\ h_S \geq (R_e + h_U)\cos(\alpha) - R_e \quad \text{when} \quad \alpha < 0 \end{gathered} \qquad \text{Eq 39}$$

Let Arccos and Arcsin denote the principal values of the arccos and arcsin functions, respectively (Subsection 2.1.6). Then the solution in Eq 38 can be decomposed as follows.

Case: $\boldsymbol{\alpha \geq 0}$: This condition eliminates one of the ambiguous solutions that can occur in an SSA situation. (When $\alpha \geq 0$ necessarily $h_S > h_U$.) When it's satisfied, the unique solution to Eq 38 is

$$\begin{aligned} \theta &= -\alpha + \text{Arccos}\left(\frac{R_e + h_U}{R_e + h_S}\cos(\alpha)\right) \\ &= -\alpha + 2\,\text{Arcsin}\left(\sqrt{\frac{(R_e + h_U)\sin^2\left(\frac{1}{2}\alpha\right) + \frac{1}{2}(h_S - h_U)}{R_e + h_S}}\right) \end{aligned} \qquad \text{Eq 40}$$

Referring to Figure 6, the first line of Eq 40 can also be derived from the right triangle **AUS**,

where the length of the adjacent side is $(R_e + h)\sin(\theta)$ and the length of the hypotenuse is $(R_e + h)\sin(\theta) / \cos(\alpha)$. Since the argument of the Arccos function is smaller than $\cos(\alpha)$, it yields an angle that is larger than α. Thus $\theta > 0$.

The two lines of Eq 40 are analytically equivalent. The first is more revealing geometrically, and likely better-conditioned numerically when α is close to ½π, which can occur in satellite applications. The second line is better-conditioned numerically when α is small, which occurs often in aviation applications. This case is the most common in aviation and is the only case relevant to satellite analysis.

Case: $\boldsymbol{\alpha < 0}$ & $\boldsymbol{(R_e + h_U)\cos(\alpha) - R_e \le h_S \le h_U}$: When both of these conditions are satisfied, the ambiguous solution for θ is

$$\theta = -\alpha \pm \text{Arccos}\left(\frac{R_e + h_U}{R_e + h_S}\cos(\alpha)\right)$$
$$= -\alpha \pm 2\,\text{Arcsin}\left(\sqrt{\frac{(R_e + h_U)\sin^2\left(\frac{1}{2}\alpha\right) + \frac{1}{2}(h_S - h_U)}{R_e + h_S}}\right) \quad \text{Eq 41}$$

The $\pm$ sign ambiguity in Eq 41 cannot be resolved without additional information, except for two special cases: $\alpha = -\frac{1}{2}\pi$ and $(R_e + h_S) = (R_e + h_U)\cos(\theta)$. Since the argument of the Arccos function is equal to or larger than $\cos(\alpha)$, it yields an angle that is, at most, equal to $|\alpha|$. Thus $0 \le \theta \le 2|\alpha|$. The '$-$' applies when the geocentric angle satisfies $\theta \le |\alpha|$ and the '$+$' sign applies when $\theta \ge |\alpha|$. Therefore, approximate knowledge of θ may resolve the ambiguity.

Case: $\boldsymbol{\alpha < 0}$ & $\boldsymbol{h_U \le h_S}$: The condition $h_U \le h_S$ eliminates the possibility of an ambiguous solution in an SSA situation. When both of these conditions are satisfied, the unique solution for θ is given by Eq 40. The difference in usage is that here $\alpha < 0$. This solution necessarily satisfies $\theta \ge 2|\alpha|$.

Special-case checks/examples for Eq 40 include:

- If the elevation angle is $\alpha = 0$ (i.e., triangle **OUS** has a right angle at **U**), then by substituting this value, the first line of Eq 40 reduces to
$$\theta = \text{Arccos}\left(\frac{R_e + h_U}{R_e + h_S}\right)$$
- If the satellite altitude and elevation angle satisfy $h_S = (R_e + h_U)\cos(\alpha) - R_e$, where necessarily $\alpha < 0$ (i.e., triangle **OUS** has a right angle at **S**), then by eliminating h_S the first line of Eq 41 reduces to
$$\theta = -\alpha$$
- If the user and satellite altitudes are equal, $h_U = h_S$ (i.e., **OUS** is an isosceles triangle with sides **OU** and **OS** equal), then by eliminating h_S the first line of Eq 41 reduces to

$$\theta = -2\alpha \quad , \quad \theta = 0$$

The first solution is consistent with **OUS** being an isosceles triangle. The second solution corresponds to the pathological situation where **U** and **S** merge.

- If the elevation angle is $\alpha = \frac{1}{2}\pi$ (i.e., **S** is directly above **U**), then by substituting this value the first line of Eq 40 reduces to 0.

$$\theta = 0$$

3.3.2 Satellite Altitude and Elevation Angle Known – Alternative Method

An alternative expression for the geocentric angle can be found by starting with Eq 7 (which involves d, h and α). Then, using Eq 4 to introduce θ and eliminate d, and using the substitutions of Eq 34, results in:

$$\left[\frac{R_e + h_S}{\cos(\alpha)}\right]^2 \sin^2(\theta) + [2(R_e + h_U)(R_e + h_S)\tan(\alpha)]\sin(\theta) + [(h_U)^2 - (h_S)^2 + 2R_e(h_U - h_S)] = 0 \qquad \text{Eq 42}$$

This is a quadratic equation in $\sin(\theta)$. Its solution is given by

$$\theta = \arcsin(x) \quad \text{where} \quad x = \frac{-B \pm \sqrt{B^2 - 4AC}}{2A}$$
$$A = \left[\frac{R_e + h_S}{\cos(\alpha)}\right]^2 \quad , \quad B = 2(R_e + h_U)(R_e + h_S)\tan(\alpha) \qquad \text{Eq 43}$$
$$C = (h_U)^2 - (h_S)^2 + 2R_e(h_U - h_S) = (h_U - h_S)(2R_e + h_U + h_S)$$

The correct value for x must satisfy $0 \le x \le 1$. Thus when $\alpha > 0$, use of the '+' sign before the radical appears to be correct.

Special-case checks/examples for Eq 43 include:

- If the elevation angle is $\alpha = 0$ (i.e., triangle **OUS** has a right angle at **U**), then by substituting this value, the expression for $\sin(\theta)$ reduces to

$$\sin^2(\theta) = \frac{(h_S)^2 - (h_U)^2 + 2R_e(h_S - h_U)}{(R_e + h_S)^2} = \frac{(R_e + h_S)^2 - (R_e + h_U)^2}{(R_e + h_S)^2}$$

- If the user and satellite altitudes are equal, $h_U = h_S$ (i.e., triangle **OUS** is isosceles with **OU** and **OS** equal), then by substituting these values, the expression for $\sin(\theta)$ reduces to

$$\sin(\theta) = -2\sin(\alpha)\cos(\alpha) = -\sin(2\alpha) \quad \text{so} \quad \theta = -2\alpha$$

3.3.3 Satellite Altitude and Slant-Range Known

In this subsection, the independent variables are the satellite altitude h_S and the slant-range d. The dependent variable is the geocentric angle θ. The same pair of independent variables is

considered in Subsection 3.4.2, in conjunction with determining the elevation angle α. In terms of the classic taxonomy for triangles, this is an SSS (side-side-side) situation.

From Eq 6, and using the substitutions of Eq 34, the geocentric angle θ is given by

$$\begin{aligned}\theta &= \arccos\left(1 - \frac{(d - h_S + h_U)(d + h_S - h_U)}{2(R_e + h_U)(R_e + h_S)}\right) \\ &= 2\arcsin\left(\frac{1}{2}\sqrt{\frac{(d - h_S + h_U)(d + h_S - h_U)}{(R_e + h_U)(R_e + h_S)}}\right) \\ \theta &\approx \frac{1}{R_e}\sqrt{d^2 - (h_S - h_U)^2} \quad \text{for} \quad h_U, h_S \ll R_e \\ &\approx \frac{d}{R_e}\left(1 - \frac{1}{2}\left(\frac{h_S - h_U}{d}\right)^2\right) \quad \text{for} \quad |h_S - h_U| \ll d\end{aligned} \qquad \text{Eq 44}$$

Using Figure 6, the first line of Eq 44 can also be derived by applying Pythagoras's theorem to right triangle **UAS**, having hypotenuse d and sides $R_e\sin(\theta)$ and $h + R_e[1 - \cos(\theta)]$. The first two lines of Eq 44 are analytically equivalent. The first is more revealing geometrically and is better-conditioned numerically when the fraction involved is close to 1 (which can occur in situations involving satellites). The second line is better-conditioned numerically when the fraction is much smaller than 1, which is usually the case in aviation applications.

The slant-range d describes a circle about **U**, while the satellite altitude h_S describes a circle about the earth's center **O**. If d and h_S include errors, their associated loci may not intersect. In that case, Eq 44 will not yield a solution for θ. From both geometry and analysis, it is evident that the requirement for the existence of a solution is that d and h_S satisfy $d \geq |h_S - h_U|$. When a solution exists, it is unique.

Analytically, the condition $d \geq |h_S - h_U|$ ensures that the numerator of the fraction on the right-hand side of Eq 44 is positive; otherwise the argument of the arccos function would not be valid. Additionally, for the arccos argument to be valid, that fraction must be less than or equal to 2. In order for **OUS** to be a proper triangle, it must be true that $d \leq (R_e + h_U) + (R_e + h_S)$. Substituting this bound into the fraction yields

$$\frac{(d - h_S + h_U)(d + h_S - h_U)}{2(R_e + h_U)(R_e + h_S)} \leq \frac{(2R_e + 2h_U)(2R_e + 2h_S)}{2(R_e + h_U)(R_e + h_S)} = 2$$

A common aviation application of Eq 44 is — assuming that the aircraft altitude h_S is known — converting a measured slant-range d to a geocentric angle θ (which is generally more useful in geodetic navigation/surveillance calculations). In radar processing, this conversion is termed the 'slant-range correction'.

Special-case checks/examples for Eq 44 include:

- If the satellite altitude and slant-range satisfy $d^2 = (R_e + h_S)^2 - (R_e + h_U)^2$ (i.e., triangle **OUS** has a right angle at **U**), then by eliminating d, the first line of Eq 44 reduces to

$$\theta = \arccos\left(\frac{R_e + h_U}{R_e + h_S}\right)$$

- If the satellite altitude and slant-range satisfy $d^2 = (R_e + h_U)^2 - (R_e + h_S)^2$ (i.e., triangle **OUS** has a right angle at **S**), then by eliminating d, the first line of Eq 44 reduces to

$$\theta = \arccos\left(\frac{R_e + h_S}{R_e + h_U}\right)$$

- If the user and satellite altitudes are equal, $h_S = h_U$ (i.e., **OUS** is an isosceles triangle with sides **OU** and **OS** equal), then by eliminating h_S, the second line of Eq 44 reduces to

$$\theta = 2\arcsin\left(\frac{\frac{1}{2}d}{R_e + h_U}\right)$$

3.3.4 Elevation Angle and Slant-Range Known – Basic Method

In this subsection, the independent variables are the elevation angle α and the slant-range d. The dependent variable is the geocentric angle θ. The same pair of independent variables is considered in Subsection 3.6.2, in conjunction with determining the satellite altitude h_S. In terms of the classic taxonomy for triangles, this is an SAS (side-angle-side) situation.

Eq 4 can be written

$$R_e \sin(\theta) = d\ \cos(\alpha)\cos(\theta) - d\ \sin(\alpha)\sin(\theta) \qquad \text{Eq 45}$$

Thus, using the substitutions of Eq 34, the result is

$$\begin{aligned}\theta &= \arctan\left(\frac{d\ \cos(\alpha)}{(R_e + h_U) + d\ \sin(\alpha)}\right) \\ &= \frac{\pi}{2} - \arctan\left(\tan(\alpha) + \frac{R_e + h_U}{d\ \cos(\alpha)}\right)\end{aligned} \qquad \text{Eq 46}$$

The right-hand side of the first line in Eq 46 can also be derived from right triangle **OBS** in Figure 6, and is more revealing geometrically. The second line is simply an alternative form, as the arc tangent function is not ill-conditioned for any value of its argument. No combination of values for the elevation angle α and slant-range d can be specified for which Eq 46 does not yield a valid solution for the geocentric angle θ.

Special-case checks/examples for Eq 46 include:

- If the elevation angle is $\alpha = 0$ (i.e., triangle **OUS** has a right angle at **U**), then by substituting this value, the first line of Eq 46 reduces to

$$\theta = \arctan\left(\frac{d}{R_e + h_U}\right)$$

- If the elevation angle and slant-range satisfy $d = (R_e + h_U)\cos\left(\frac{1}{2}\pi + \alpha\right)$ (i.e., triangle **OUS** has a right angle at **S** and $\alpha < 0$), then by eliminating d, the first line of Eq 46 reduces to

$$\theta = -\alpha$$

- If the elevation angle and slant-range satisfy $d = 2(R_e + h_U)\sin(-\alpha), \alpha < 0$ (i.e., are consistent with **OUS** being an isosceles triangle with sides **OU** and **OS** equal), then by eliminating d, the first line of Eq 46 reduces to

$$\theta = -2\alpha$$

- If the elevation angle is $\alpha = \frac{1}{2}\pi$ (i.e., **S** is directly above **U**) or is $\alpha = -\frac{1}{2}\pi$ (i.e., **S** is directly beneath **U**), then by substituting these values, the first line of Eq 46 reduces to

$$\theta = 0$$

- If the slant-range is $d = 0$ (i.e., **S** and **U** merge), then by substituting this value, the first line of Eq 46 reduces to

$$\theta = 0$$

3.3.5 Elevation Angle and Slant-Range Known – Alternative Method

The law of tangents (Eq 8) applied to triangle **OUS** (Figure 1), specifically to sides **OU** and **US** and their opposite angles, and using the substitutions of Eq 34, yields

$$\theta = \tfrac{1}{4}\pi - \tfrac{1}{2}\alpha - \arctan\left(\frac{R_e + h_U - d}{R_e + h_U + d}\tan\left(\tfrac{1}{4}\pi - \tfrac{1}{2}\alpha\right)\right) \qquad \text{Eq 47}$$

Special-case checks/examples for Eq 47 are:

- If the elevation angle is $\alpha = 0$ (i.e., triangle **OUS** has a right angle at **U**), then by substituting this value, Eq 47 reduces to

$$\theta = \tfrac{1}{4}\pi - \arctan\left(\frac{R_e + h_U - d}{R_e + h_U + d}\right)$$

  If, additionally, $d = R_e + h_U$ (i.e., **OUS** is an isosceles right triangle), then the immediately previous expression reduces to $\theta = \frac{1}{4}\pi$.

- If the elevation angle is $\alpha = \frac{1}{2}\pi$ (i.e., **S** is directly above **U**), then by substituting these values, Eq 47 reduces to

$$\theta = 0$$

- If the elevation angle approaches its minimum possible value, $\alpha \to -\frac{1}{2}\pi$ (i.e., **S** approaches a location directly below **U**), then Eq 47 reduces to

$$\theta \to 0$$

3.4 Computing Elevation Angle

3.4.1 Satellite Altitude and Geocentric Angle Known – Basic Method

In this subsection, the independent variables are the satellite altitude h_S and the geocentric angle θ. The dependent variable is the elevation angle α. The same pair of independent variables is considered in Subsection 3.5.1, in conjunction with determining the slant-range d. In terms of the classic taxonomy for triangles, this is an SAS (side-angle-side) situation.

Manipulating Eq 5 and using the substitutions of Eq 34 yields

$$\begin{aligned}\tan(\alpha) &= \frac{(R_e + h_S)\cos(\theta) - (R_e + h_U)}{(R_e + h_S)\sin(\theta)} \\ &= \cot(\theta) - \frac{R_e + h_U}{(R_e + h_S)\sin(\theta)} \\ &= -\frac{(R_e + h_U)}{(R_e + h_S)}\tan(\tfrac{1}{2}\theta) + \frac{(h_S - h_U)}{(R_e + h_S)}\cot(\theta)\end{aligned} \qquad \text{Eq 48}$$

The expression on the first line of Eq 48 can also be derived from right triangle **UBS** in Figure 6. The three lines of Eq 48 are analytically equivalent. The first is more revealing geometrically. The second line is better suited to satellite applications where $R_e < h_S$. Then the second term on the right-hand side can be regarded as a parallax correction. The third line is better-conditioned numerically when $h_U \ll R_e$ and $d \ll R_e$, which is generally the case in aviation applications. No combination of values for the satellite altitude h_S and geocentric angle θ can be specified for which Eq 48 does not yield a valid solution for the elevation angle α.

Special-case checks/examples for Eq 48 are:

- If the satellite altitude and geocentric angle satisfy $(R_e + h_U) = (R_e + h_S)\cos(\theta)$ (i.e., triangle **OUS** has a right angle at **U**), then by eliminating h_S, the first line of Eq 48 reduces to
$$\tan(\alpha) = 0 \quad \text{so} \quad \alpha = 0$$
- If the satellite altitude and geocentric angle satisfy $(R_e + h_U)\cos(\theta) = (R_e + h_S)$ (i.e., triangle **OUS** has a right angle at **S**), then by eliminating h_S, the first line of Eq 48 reduces to
$$\tan(\alpha) = -\tan(\theta) \quad \text{so} \quad \alpha = -\theta$$
- If the user and satellite altitudes are equal, $h_U = h_S$ (i.e., **OUS** is an isosceles triangle with sides **OU** and **OS** equal), then by eliminating h_S, the first line of Eq 48 reduces to
$$\tan(\alpha) = -\tan\left(\tfrac{1}{2}\theta\right) \quad \text{so} \quad \alpha = -\tfrac{1}{2}\theta \quad \text{for} \quad \theta \neq 0$$
- If the elevation angle is $\alpha = 0$ (i.e., triangle **OUS** has a right angle at **U**), then by substituting this value, the first line of Eq 48 reduces to

$$h_S = \frac{R_e + h_U}{\cos(\theta)} - R_e \quad \text{for} \quad \theta \neq 0$$

3.4.2 Satellite Altitude and Geocentric Angle Known – Alternative Method

The law of tangents (Eq 8) applied to triangle **OUS** (Figure 1), specifically to sides **OU** and **OS** and their opposite angles, and using the substitutions of Eq 34, yields

$$\alpha = -\tfrac{1}{2}\theta + \arctan\left(\frac{h_S - h_U}{(2R_e + h_S + h_U)\tan\left(\tfrac{1}{2}\theta\right)}\right) \qquad \text{Eq 49}$$

Special-case checks/examples for Eq 49 are:

- If the user and satellite altitudes are equal, $h_U = h_S$ (i.e., **OUS** is an isosceles triangle with sides **OU** and **OS** equal), then by substituting for h_S, Eq 49 reduces to
$$\alpha = -\tfrac{1}{2}\theta \quad \text{for} \quad \theta \neq 0$$
- If the elevation angle is $\alpha = 0$ (i.e., triangle **OUS** has a right angle at **U**), then by substituting for α, Eq 49 reduces to
$$\tan\left(\tfrac{1}{2}\theta\right) = \sqrt{\frac{h_S - h_U}{2R_e + h_S + h_U}}$$
- If the elevation angle and geocentric angle satisfy $\alpha = -\theta$ (which is consistent with triangle **OUS** having a right angle at **S**), then by substituting for α, Eq 49 reduces to
$$\tan\left(\tfrac{1}{2}\theta\right) = \sqrt{\frac{h_U - h_S}{2R_e + h_S + h_U}}$$

3.4.3 Satellite Altitude and Slant-Range Known

In this subsection, the independent variables are the satellite altitude h_S and the slant-range d. The dependent variable is the elevation angle α. The same pair of independent variables is considered in Subsection 3.3.3, in conjunction with determining the geocentric angle θ. In terms of the classic taxonomy for triangles, this is an SSS (side-side-side) situation.

Manipulating Eq 7 and using the substitutions of Eq 34 yields

$$\begin{aligned}\sin(\alpha) &= \frac{(h_S - h_U)^2 + 2(R_e + h_U)(h_S - h_U) - d^2}{2(R_e + h_U)d} \\ &= \frac{1}{d}\left[(h_S - h_U) - \frac{(d - h_S + h_U)(d + h_S - h_U)}{2(R_e + h_U)}\right]\end{aligned} \qquad \text{Eq 50}$$

Using Figure 6, the first line of Eq 50 can also be derived by applying Pythagoras's theorem to the right triangle **OBS**, with the length of the hypotenuse being $(R_e + h)$ and the lengths of the

sides being $(R_e + d\sin(\alpha))$ and $d\cos(\alpha)$. The two lines of Eq 50 are analytically equivalent. The first is more revealing geometrically and is better-conditioned numerically when the fraction involved is close to 1 (which can occur in situations involving satellites). The second line is better-conditioned numerically when the fraction is much smaller than 1, which is generally the case in aviation applications.

As noted in Subsection 3.3.3, when the available values for slant-range d and satellite altitude h_S have errors, it is possible to formulate a mathematically infeasible problem. The requirement on d and h_S for mathematical feasibility is that $d \geq |h_S - h_U|$. When a solution exists, it is unique.

To partially validate the geometric analysis analytically, note that if $d = h_S - h_U > 0$, then the first line of Eq 50 reduces to $\sin(\alpha) = 1$. Similarly, if $d = h_U - h_S > 0$, then the first line of Eq 50 reduces to $\sin(\alpha) = -1$. Thus the limiting values for d correspond to the limiting values for α. Moreover, assume that $h_S > h_U$ and let $d = h_S - h_U + \varepsilon$, where ε can be positive or negative. Then, to first order in ε, the first line of Eq 50 reduces to

$$\sin(\alpha) = 1 - \left(\frac{1}{h_S - h_U} + \frac{1}{R_e + h_U}\right)\varepsilon + O(\varepsilon^2) + \cdots$$

Thus when $\varepsilon \geq 0$ (i.e., $d \geq h_S - h_U$) the arcsin function has a valid argument, and when $\varepsilon < 0$ (i.e., $d < h_S - h_U$) the arcsin function does not have a valid argument. A similar analysis can be done for the situation where $h_U > h_S$.

On the second line of Eq 50, the term in large brackets is the height of the satellite above the tangent plane at the user's location. It can be interpreted as the satellite altitude relative to the user altitude, minus a term which corrects for the earth's curvature.

Special-case checks/examples for Eq 50 are:

- If the satellite altitude and slant-range satisfy $(R_e + h_S)^2 = (R_e + h_U)^2 + d^2$ (i.e., triangle **OUS** has a right angle at **U**), then by eliminating d, the first line of Eq 50 reduces to
$$\sin(\alpha) = 0 \quad \text{so} \quad \alpha = 0$$
- If the elevation angle $\alpha = 0$ (i.e., triangle **OUS** has a right angle at **U**), then by substituting this value, the first line of Eq 50 reduces to
$$d^2 = (R_e + h_S)^2 - (R_e + h_U)^2$$
- If the user and satellite altitudes are equal, $h_U = h_S$ (i.e., **OUS** is an isosceles triangle with sides **OU** and **OS** equal), then by eliminating h_S, the first line of Eq 50 reduces to
$$\sin(\alpha) = -\frac{\frac{1}{2}d}{R_e + h_S} = -\sin\left(\tfrac{1}{2}\theta\right) \quad \text{so} \quad \alpha = -\tfrac{1}{2}\theta$$

3.4.4 Geocentric Angle and Slant-Range Known

In this subsection, the independent variables are the geocentric angle θ and the slant-range d. The dependent variable is the elevation angle α. The same pair of independent variables is considered in Subsection 3.6.1, in conjunction with determining the satellite altitude h_S. In terms of the classic taxonomy for triangles, this is an SSA (side- side-angle) situation.

Manipulating Eq 4 and using the substitutions of Eq 34 yields the formal solution

$$\alpha = -\theta + \arccos\left(\frac{R_e + h_U}{d}\sin(\theta)\right) \qquad \text{Eq 51}$$

The permissible range for elevation angles is $-\frac{1}{2}\pi \leq \alpha \leq \frac{1}{2}\pi$. Thus the arccos function can yield two possible values that result in permissible values for α (i.e., ambiguous solutions can occur). For clarity, the solution to Eq 51 is decomposed into two cases.

Case: $\boldsymbol{d \leq (R_e + h_U)}$: In Eq 51, let the principal value (Subsection 2.1.6) of the result of the arccos function be $\frac{1}{2}\pi - \theta'$. Satisfaction of this condition on d (which virtually always applies in aviation applications) results in $\theta' \geq \theta$, so the two possible values for α, $\alpha = -\theta \pm \left(\frac{1}{2}\pi - \theta'\right)$ can both be valid. Thus, the ambiguous solutions to Eq 51 can be written

$$\alpha = -\theta \pm \text{Arccos}\left(\frac{R_e + h_U}{d}\sin(\theta)\right) \qquad \text{Eq 52}$$

This ambiguity cannot be resolved with the information available.

Case: $\boldsymbol{d > (R_e + h_U)}$: In Eq 51, again denote the principal value of the result of the arccos function as $\frac{1}{2}\pi - \theta'$. Satisfaction of this condition (which in practice only applies to satellite applications) results in $\theta' < \theta$, so of the two possible values for α, $\alpha = -\theta \pm \left(\frac{1}{2}\pi - \theta'\right)$, the '–' value is not valid. Thus, the unique solution to Eq 51 can be written:

$$\alpha = -\theta + \text{Arccos}\left(\frac{R_e + h_U}{d}\sin(\theta)\right) \qquad \text{Eq 53}$$

Geometrically, Eq 53 can also be derived from right triangle **AUS** in Figure 6.

Due measurement or other errors, it is possible that Eq 52 or Eq 53 will not have a solution for the available values for d and θ. The analytic requirement for a solution to exist is that $d \geq (R_e + h_U)\sin(\theta)$. The geometric interpretation of this condition is that d must be at least equal to the minimum distance between **U** and the locus for constant θ.

Special-case checks/examples for Eq 52/Eq 53 are:

- If the slant-range and geocentric angle satisfy $d = (R_e + h_U)\tan(\theta)$ (which is consistent with triangle **OUS** having a right angle at **U**), then by eliminating d, Eq 52 reduces to the ambiguous solutions

$$\alpha = 0 \quad , \quad \alpha = -2\theta$$

The first solution is also consistent with triangle **OUS** having a right angle at **U**. Concerning the second solution: If the geocentric angle θ and the computed elevation angle $\alpha = -2\theta$ are substituted in Eq 61, the result is $d = (R_e + h_U)\tan(\theta)$. Thus, it also a valid solution to Eq 52.

- If the slant-range and geocentric angle satisfy $d = 2(R_e + h_U)\sin(\frac{1}{2}\theta)$ (which is consistent with **OUS** being an isosceles triangle with sides **OU** and **OS** equal), then by eliminating d, Eq 52 reduces to the ambiguous solutions

$$\alpha = -\frac{1}{2}\theta \quad , \quad \alpha = -\frac{3}{2}\theta$$

The first solution is also consistent with **OUS** being an isosceles triangle. Concerning the second solution: If the geocentric angle θ and the computed elevation angle $\alpha = -\frac{3}{2}\theta$ are substituted in Eq 61, the result is $d = 2(R_e + h_U)\sin(\frac{1}{2}\theta)$. Thus, it also a valid solution to Eq 52. Because $-\frac{1}{2}\pi \leq \alpha$, the second solution is only valid when $\theta \leq \frac{1}{3}\pi$.

- If the slant-range and geocentric angle satisfy $d = (R_e + h_U)\sin(\theta)$ (i.e., triangle **OUS** has a right angle at **S**), then by eliminating d, Eq 52 reduces to the unique solution

$$\alpha = -\theta$$

- If the slant-range satisfies $d = (R_e + h_U)$ (i.e., **OUS** is an isosceles triangle with sides **OU** and **US** equal), then by eliminating d, Eq 52 reduces to the ambiguous solutions

$$\alpha = -\frac{1}{2}\pi \quad , \quad \alpha = \frac{1}{2}\pi - 2\theta$$

The first solution is the pathological case where **O** and **S** merge. The second solution describes a possible satellite scenario, and includes the limiting situations where the satellite is directly above the user ($\alpha = \frac{1}{2}\pi$, $\theta = 0$) and is on the user's horizon ($\alpha = 0$, $\theta = \frac{1}{4}\pi$).

- If the geocentric angle is $\theta = 0$ (i.e., **S** is above or below **U**), then by substituting this value, Eq 52 reduces to the ambiguous solutions

$$\alpha = -\frac{1}{2}\pi \quad , \quad \alpha = \frac{1}{2}\pi$$

3.5 Computing Slant-Range

3.5.1 Satellite Altitude and Geocentric Angle Known

In this subsection, the independent variables are the satellite altitude h_S and the geocentric angle θ. The dependent variable is the slant-range d. The same pair of independent variables is considered in Subsection 3.4.1, in conjunction with determining the elevation angle α. In terms of the classic taxonomy for triangles, this is an SAS (side-angle-side) situation.

Using the substitutions of Eq 34, Eq 6 can be expressed as

$$d = \sqrt{(h_S - h_U)^2 + 2(R_e + h_U)(R_e + h_S)[1 - \cos(\theta)]} \qquad \text{Eq 54}$$

$$= 2R_e \sin\left(\tfrac{1}{2}\theta\right) \sqrt{\left(1+\frac{h_U}{R_e}\right)\left(1+\frac{h_S}{R_e}\right)+\left(\frac{h_S-h_U}{2R_e \sin\left(\frac{1}{2}\theta\right)}\right)^2} \quad , \quad \theta \neq 0$$

$$d \approx R_e\theta + \tfrac{1}{2}(h_U+h_S)\theta + \frac{h_U\, h_S}{2R_e}\theta + \frac{(h_S-h_U)^2}{2R_e\theta} \quad , \quad 0 < \theta \ll 1 \;\&\; h_U, h_S \ll R_e$$

The first line of Eq 54 can also be derived by applying Pythagoras's theorem to right triangle **AUS** in Figure 6. As would be expected from this formulation, this expression is symmetric in h_U and h_S. The second line is analytically equivalent to the first, but numerically better-conditioned when $\theta \ll 1$ and $h_U, h_S \ll R_e$, which is typically the case in aviation applications (at the surface of the earth, $\theta = 1$ corresponds to spherical distance of $s \approx 3{,}438$ NM). No combination of values for the satellite altitude h_S and geocentric angle θ can be specified for which Eq 54 does not yield a valid solution for the slant-range d.

Special-case checks/examples for Eq 54 include:

- If the geocentric angle is $\theta = 0$ (i.e. **U** and **S** lie along the same radial), then the first line of Eq 54 reduces to
$$d = |h_S - h_U|$$
- If the satellite altitude and geocentric angle satisfy $h_S = (R_e + h_U) / \cos(\theta) - R_e$ (which is consistent with triangle **OUS** having a right angle at **U**), then by eliminating h_S, the first line of Eq 54 reduces to
$$d = (R_e + h_U)\tan(\theta)$$
- If the satellite altitude and geocentric angle satisfy $h_S = (R_e + h_U)\cos(\theta) - R_e$ (i.e., triangle **OUS** has a right angle at **S**), then by eliminating h_S, the first line of Eq 54 reduces to
$$d = (R_e + h_U)\sin(\theta)$$
- If the user and satellite altitudes are equal, $h_U = h_S$ (i.e., **OUS** is an isosceles triangle with sides **OU** and **OS** equal), then by eliminating h_S, the second line of Eq 54 reduces to
$$2(R_e + h_U)\sin\left(\tfrac{1}{2}\theta\right)$$

3.5.2 Satellite Altitude and Elevation Angle Known

In this subsection, the independent variables are the satellite altitude h_S and the elevation angle α. The dependent variable is the slant-range d. The same pair of independent variables is considered in Subsection 3.3.1, in conjunction with determining the geocentric angle θ. In terms of the classic taxonomy for triangles, this is an SSA (side-side-angle) situation.

Eq 7 can be expressed, after applying the substitutions of Eq 34, as

$$d^2 + [2(R_e + h_U)\sin(\alpha)]d + [(h_U^2 - h_S^2) + 2R_e(h_U - h_S)] = 0 \qquad \text{Eq 55}$$

The formal solution of Eq 55 is

$$d = -(R_e + h_U)\sin(\alpha) \pm \sqrt{(R_e + h_U)^2 \sin^2(\alpha) + (h_S^2 - h_U^2) + 2R_e(h_S - h_U)} \qquad \text{Eq 56}$$

Due to the sign ambiguity in Eq 56 and the possibility of infeasible problem formulations, it is advantageous to address this situation in terms of cases. When interpreting the expressions below, note that the quantity under the radical in Eq 56 can be written in two alternative forms

$$(R_e + h_U)^2 \sin^2(\alpha) + (h_U - h_S)(2R_e + h_S + h_U) = (R_e + h_S)^2 - (R_e + h_U)^2 \cos^2(\alpha)$$

Conditions for Solution Existence — Conditions for the existence of a solution are discussed in Subsection 3.3.1 and summarized by Eq 39, which is repeated here.

$$\begin{gathered} h_S > h_U \quad \text{when} \quad \alpha \geq 0 \\ h_S \geq (R_e + h_U)\cos(\alpha) - R_e \quad \text{when} \quad \alpha < 0 \end{gathered} \qquad \text{Eq 57}$$

Case: $\boldsymbol{\alpha \geq 0}$: The condition $\alpha \geq 0$ eliminates one of the ambiguous solutions that can occur in an SSA situation. Also, when $\alpha \geq 0$, necessarily $h_S > h_U$. In this situation, the unique solution to Eq 56 can be written

$$\begin{gathered} d = -(R_e + h_U)\sin(\alpha) + \sqrt{(R_e + h_U)^2 \sin^2(\alpha) + (h_S^2 - h_U^2) + 2R_e(h_S - h_U)} \\ d = (R_e + h_U)\sin(\alpha)\left(\frac{x}{2} - \frac{x^2}{8} + \frac{x^3}{16} \pm \cdots\right), x \equiv \frac{(h_S - h_U)(h_S + h_U + 2R_e)}{(R_e + h_U)^2 \sin^2(\alpha)}, \alpha > 0 \\ d \approx \frac{h_S - h_U}{\sin(\alpha)} \quad \text{for} \quad h_U, h_S \ll R_e \;\; \& \;\; \alpha > 0 \end{gathered} \qquad \text{Eq 58}$$

Referring to Figure 6, the first line of Eq 58 can be interpreted as length(**CS**)-length (**CU**), where length(**CS**) is found by Pythagoras's theorem applied to right triangle **OCS** having **OS** is its hypotenuse.

Case: $\boldsymbol{\alpha < 0}$ & $\boldsymbol{(R_e + h_U)\cos(\alpha) - R_e \leq h_S \leq h_U}$: When both of these conditions are satisfied, the ambiguous solution is

$$d = -(R_e + h_U)\sin(\alpha) \pm \sqrt{(R_e + h_U)^2 \sin^2(\alpha) + (h_S^2 - h_U^2) + 2R_e(h_S - h_U)} \qquad \text{Eq 59}$$

The $\pm$ sign ambiguity in Eq 59 cannot be resolved without additional information, except extreme case of $\alpha = -\frac{1}{2}\pi$. The '$-$' applies when the geocentric angle satisfies $\theta \leq |\alpha|$ and the '$+$' sign applies when $\theta \geq |\alpha|$.

Case: $\boldsymbol{\alpha < 0}$ & $\boldsymbol{h_U \leq h_S}$: The condition $h_U \leq h_S$ eliminates one of the ambiguous solutions that can occur in an SSA situation. When these conditions are satisfied, the unique solution is

$$d = -(R_e + h_U)\sin(\alpha) + \sqrt{(R_e + h_U)^2 \sin^2(\alpha) + (h_S^2 - h_U^2) + 2R_e(h_S - h_U)} \qquad \text{Eq 60}$$

This is the same expression as the first line of Eq 58; however, here $\alpha < 0$.

Special-case checks/examples include:

- If the elevation angle is $\alpha = 0$ (i.e., triangle **OUS** has a right angle at **U**) and the satellite altitude satisfies $h_S > h_U$, then by substituting for α, the first line of Eq 58 reduces to
$$d = \sqrt{(R_e + h_S)^2 - (R_e + h_U)^2}$$
- If the elevation angle is $\alpha = \frac{1}{2}\pi$ (i.e., **S** is directly above **U**) and the satellite altitude satisfies $h_S > h_U$, then by substituting for α, the first line of Eq 58 reduces to
$$d = h_S - h_U$$
- If the elevation angle is $\alpha = -\frac{1}{2}\pi$ (i.e., **S** is directly beneath **U**) and the satellite altitude satisfies $h_S < h_U$, then by substituting for α, Eq 59 reduces to
$$d = h_U - h_S$$
- If the user and satellite altitudes are equal, $h_U = h_S$ (i.e., **OUS** is an isosceles triangle with sides **OU** and **OS** equal), then the elevation angle must satisfy $\alpha < 0$ and, by eliminating h_S, Eq 60 reduces to
$$d = 2(R_e + h_U)\sin(|\alpha|) = 2(R_e + h_U)\sin\left(\tfrac{1}{2}\theta\right)$$
- If the satellite altitude and elevation angle satisfy $h_S = (R_e + h_U)\cos(\alpha) - R_e$ (i.e., triangle **OUS** has a right angle at **S**), the elevation angle necessarily satisfies $\alpha < 0$. Then by eliminating h_S, Eq 59 reduces to
$$d = (R_e + h_U)\sin(|\alpha|)$$
- If the elevation angle is $\alpha = \frac{1}{6}\pi$, the user altitude is $h_U = 0$ and the satellite altitude is $h_S = 3R_e$ (i.e., an approximation to a GPS user's situation), then, by substituting these values, the first line of Eq 58 reduces to $d = 3.4R_e$

3.5.3 Geocentric Angle and Elevation Angle Known

In this subsection, the independent variables are the geocentric angle θ and the elevation angle α. The dependent variable is the slant-range d. The same pair of independent variables is considered in Subsection 3.6.3, in conjunction with determining the satellite altitude h_S. In terms of the classic taxonomy for triangles, this is an ASA (angle-side-angle) situation.

Eq 5 can be written, after applying the substitutions of Eq 34, as

$$d = \frac{\sin(\theta)}{\cos(\alpha + \theta)}(R_e + h_U) \qquad \text{Eq 61}$$

Eq 61 is a manipulation of the two expressions for the length of **AU** in Figure 6. A valid solution for d only exists if $\alpha + \theta < \frac{1}{2}\pi$ (because the three angles of a plane triangle must sum to π). However, due to errors, the available values for α and θ may sum to $\frac{1}{2}\pi$ (whereby the loci of

constant elevation angle and constant geocentric angle are parallel) or a larger number (whereby the loci diverge). When a solution exists, it is unique.

Special-case checks/examples for Eq 61 include:

- If the elevation angle is $\alpha = 0$ (i.e., triangle **OUS** has a right angle at **U**), then by substituting this value, Eq 61 reduces to
$$d = (R_e + h_U)\tan(\theta)$$
- If the elevation angle and geocentric angle satisfy $\alpha = -\theta$ (i.e., triangle **OUS** has a right angle at **S**), then by eliminating α, Eq 61 reduces to
$$d = (R_e + h_U)\sin(\theta)$$
- If the elevation angle and geocentric angle satisfy $\alpha = -\frac{1}{2}\theta$ (i.e., **OUS** is an isosceles triangle with sides **OU** and **OS** equal), then by eliminating α, Eq 61 reduces to
$$d = 2(R_e + h_U)\sin\left(\tfrac{1}{2}\theta\right)$$

3.6 Computing Satellite Altitude

3.6.1 Slant-Range and Geocentric Angle Known

In this subsection, the independent variables are the slant-range d and the geocentric angle θ. The dependent variable is the satellite altitude h_S. The same pair of independent variables is considered in Subsection 3.4.4, in conjunction with determining the elevation angle α. In terms of the classic taxonomy for triangles, this is an SSA (side-side-angle) situation.

Eq 6 can be written as a quadratic equation in $R_e + h$. Applying the substitutions of Eq 34 yields the formal solution

$$h_S = (R_e + h_U)\cos(\theta) - R_e \pm \sqrt{d^2 - (R_e + h_U)^2[1 - \cos^2(\theta)]} \qquad \text{Eq 62}$$

For a valid solution to exist, the expression under the radical in Eq 62 must be non-negative; thus, validity requires that $d \geq (R_e + h_U)\sin(\theta)$. Because an ambiguous solution is possible, for clarity, the solution description is decomposed into two cases. Note that, if $d = (R_e + h_U)$, then '–' solution in Eq 62 reduces to $R_e + h_S = 0$.

Case: $\boldsymbol{d \leq (R_e + h_U)}$: Satisfaction of this condition on d (which virtually always applies in aviation applications) ensures, in Eq 62, that $(h_S + R_e) \geq 0$ for both the '+' and '–' signs and any value of θ. Thus, the ambiguous solutions to Eq 62 can be written

$$\begin{aligned} h_S &= (R_e + h_U)\cos(\theta) - R_e \pm \sqrt{d^2 - (R_e + h_U)^2\sin^2(\theta)} \\ &= h_U - 2(R_e + h_U)\sin^2(\tfrac{1}{2}\theta) \pm \sqrt{d - (R_e + h_U)\sin(\theta)}\sqrt{d + (R_e + h_U)\sin(\theta)} \end{aligned} \qquad \text{Eq 63}$$

The two lines of Eq 63 are analytically equivalent. However, the second line is numerically

better-conditioned when θ is small, as is often the case in aviation applications. The choice between the '+' and '–' signs cannot be resolved from the information available.

Case: $d > (R_e + h_U)$: Satisfaction of this condition (which in practice only applies to satellite applications) ensures, in Eq 62, that, for the '–' sign and any value of θ, $R_e + h_S < 0$, and thus is invalid. Therefore, the unique solution to Eq 62 can be written:

$$h_S = (R_e + h_U)\cos(\theta) - R_e + \sqrt{d^2 - (R_e + h_U)^2 \sin^2(\theta)} \qquad \text{Eq 64}$$

Referring to Figure 6, Eq 64 can be interpreted as length(**AS**)-length(**AN**), where length(**AS**) is found by Pythagoras's theorem applied to right triangle **AUS**. Another interpretation is that h_S is the projection of $R_e + h_U$ onto **OS**, with R_e then subtracted, followed by an adjustment for the length of d in excess of the minimum distance between **U** and **OS**. The solutions in Eq 63 and Eq 64 both require that $(h_S + R_e) \geq 0$, which is equivalent to requiring that **OUS** form at least a degenerate form of a triangle.

Special-case checks/examples for Eq 63/Eq 64 include:

- If the geocentric angle satisfies $\theta = 0$ (i.e., **S** is above or below **U**), then by substituting this value, Eq 63 reduces to
$$h_S = h_U \pm d$$
- If the slant-range and geocentric angle satisfy $d = (R_e + h_U)\sin(\theta)$ (which is consistent with triangle **OUS** having a right angle at **S**), then by eliminating d, the first line of in the first line of Eq 63 the expression under the radical is zero and the unique solution is
$$h_S = (R_e + h_U)\cos(\theta) - R_e$$
This solution is consistent with triangle **OUS** having a right angle at **S**.
- If the slant-range and geocentric angle satisfy $d = (R_e + h_U)\tan(\theta)$ (which is consistent with triangle **OUS** having a right angle at **U**), then by eliminating d, the first line of Eq 63 reduces to the ambiguous solutions
$$h_S = -R_e + \frac{(R_e + h_U)}{\cos(\theta)} \quad , \quad h_S = -R_e + \frac{(R_e + h_U)}{\cos(\theta)}\cos(2\theta)$$
The first solution is consistent with triangle **OUS** having a right angle at **U**. Concerning the second solution: If the geocentric angle θ and the computed satellite altitude h_S are substituted in Eq 54, the result is $d = (R_e + h_U)\tan(\theta)$. Thus, it is also a valid solution to Eq 63.
- If the slant-range and geocentric angle satisfy $d = 2(R_e + h_U)\sin(\frac{1}{2}\theta)$ (which is consistent with **OUS** being an isosceles triangle with sides **OU** and **OS** equal), then by eliminating d, the first line of Eq 63 reduces to the ambiguous solutions
$$h_S = h_U \quad , \quad h_S = h_U - 4(R_e + h_U)\sin^2(\tfrac{1}{2}\theta)$$
The first solution is consistent with **OUS** being an isosceles triangle. Concerning the second solution: If the geocentric angle θ and the computed satellite altitude h_S are substituted in Eq 54, the result is $d = 2(R_e + h_U)\sin(\frac{1}{2}\theta)$. Thus, it is also a valid

solution to Eq 63.

3.6.2 Slant-Range and Elevation Angle Known

In this subsection, the independent variables are the slant-range d and the elevation angle α. The dependent variable is the satellite altitude h_S. The same pair of independent variables is considered in Subsection 3.3.4, in conjunction with determining the geocentric angle θ. In terms of the classic taxonomy for triangles, this is an SAS (side-angle-side) situation.

Rearranging Eq 7 and using the substitutions of Eq 34 yields

$$h_S = -R_e + \sqrt{(R_e + h_U)^2 + d^2 + 2(R_e + h_U)\, d \sin(\alpha)}$$

$$h_S = h_U + (R_e + h_U)\left(\frac{x}{2} - \frac{x^2}{8} + \frac{x^3}{16} \pm \cdots\right) \quad \text{for} \quad x \equiv \frac{2d\sin(\alpha)}{R_e + h_U} + \frac{d^2}{(R_e + h_U)^2} \qquad \text{Eq 65}$$

$$h_S \approx h_U + d\sin(\alpha) \quad \text{for} \quad d \ll R_e + h_U$$

Referring to Figure 6, the first line in Eq 65 can be interpreted as length(**OS**)-length(**ON**), where length(**OS**) is found by Pythagoras's theorem applied to right triangle **OBS**. The first two lines of Eq 65 are analytically equivalent. The first is more revealing geometrically. The second line is better-conditioned numerically when $h_U \ll R_e$ and $d \ll R_e$, which is generally the case in aviation applications. The quantity under the radical on first line of Eq 65 is guaranteed to be non-negative. Thus, no combination of values for the slant-range d and elevation angle α can be specified for which Eq 65 does not yield a valid solution for the satellite altitude h_S.

Special-case checks/examples for Eq 65 are:

- If the elevation angle is $\alpha = 0$ (i.e., triangle **OUS** has a right angle at **U**), then by substituting this value, the first line of Eq 65 reduces to
$$h_S = -R_e + \sqrt{(R_e + h_U)^2 + d^2}$$
- If the slant-range and elevation angle satisfy $d = (R_e + h_U)\sin(-\alpha)$ where $\alpha < 0$ (i.e., triangle **OUS** has a right angle at **S**), then by eliminating d, the first line of Eq 65 reduces to
$$h_S = -R_e + (R_e + h_U)\cos(-\alpha)$$
- If the slant-range and elevation angle satisfy $d = 2(R_e + h_U)\sin(-\alpha)$ where $\alpha < 0$ (i.e., are consistent with **OUS** being an isosceles triangle with sides **OU** and **OS** equal), then the first line of Eq 65 reduces to
$$h_S = h_U$$
- If the elevation angle is $\alpha = \frac{1}{2}\pi$ (i.e., **S** is directly above **U**), then the first line of Eq 65 reduces to
$$h_S = h_U + d$$
- If the elevation angle is $\alpha = -\frac{1}{2}\pi$ (i.e., **S** is directly beneath **U**), then the first line of Eq

65 reduces to

$$h_S = h_U - d$$

3.6.3 Elevation Angle and Geocentric Angle Known – Basic Method

In this subsection, the independent variables are the elevation angle α and the geocentric angle θ. The dependent variable is the satellite altitude h_S. The same pair of independent variables is considered in Subsection 3.5.3, in conjunction with determining the slant-range d. In terms of the classic taxonomy for triangles, this is an ASA (angle-side-angle) situation.

Manipulating Eq 5 and using the substitutions of Eq 34 yields

$$h_S = \frac{\cos(\alpha)}{\cos(\alpha+\theta)}(R_e + h_U) - R_e = h_U + \left(\frac{\cos(\alpha)}{\cos(\alpha+\theta)} - 1\right)(R_e + h_U)$$
$$= h_U + 2\frac{\sin(\alpha + \frac{1}{2}\theta)\sin(\frac{1}{2}\theta)}{\cos(\alpha+\theta)}(R_e + h_U) \qquad \text{Eq 66}$$
$$h_S \approx h_U + \theta\left(\alpha + \tfrac{1}{2}\theta\right)R_e \quad \text{for} \quad \alpha \ll 1\,, \theta \ll 1\,, h_U \ll R_e$$

Eq 66 can also be derived by manipulating the two expressions for the length of **OC** in Figure 6. The first two lines of Eq 66 are analytically equivalent. The first is more revealing geometrically. The second line is better-conditioned numerically when $h_U \ll R_e$ and both angles are small, which is generally the case in aviation applications.

A valid solution for h_S only exists if $\alpha + \theta < \frac{1}{2}\pi$ (because the angles of a plane triangle must sum to π). However, due errors, the available values for α and θ may sum to $\frac{1}{2}\pi$ (whereby the loci of constant elevation angle and constant geocentric angle are parallel) or a larger number (whereby the two loci diverge). When a solution exists, it is unique.

Special-case checks/examples for Eq 66 include:

- If the elevation angle is $\alpha = 0$ (i.e., triangle **OUS** has a right angle at **U**), then the first line of Eq 66 reduces to
$$h_S = \frac{R_e + h_U}{\cos(\theta)} - R_e$$
- If the elevation angle and geocentric angle satisfy $\alpha = -\theta$ (i.e., are consistent with triangle **OUS** having a right angle at **S**), then the first line of Eq 66 reduces to
$$h_S = (R_e + h_U)\cos(\theta) - R_e$$
- If the elevation angle and geocentric angle satisfy $\alpha = -\frac{1}{2}\theta$ (i.e., are consistent with **OUS** being an isosceles triangle with sides **OU** and **OS** equal), then the first two lines of Eq 66 reduce to
$$h_S = h_U$$

3.6.4 Elevation Angle and Geocentric Angle Known – Alternative Method

The law of tangents (Eq 8) applied to triangle **OUS** (Figure 1), specifically to sides **OU** and **OS** and their opposite angles, and using the substitutions of Eq 34, yields

$$h_S = \frac{h_U + (2R_e + h_U)\tan\left(\alpha + \frac{1}{2}\theta\right)\tan\left(\frac{1}{2}\theta\right)}{1 - \tan\left(\alpha + \frac{1}{2}\theta\right)\tan\left(\frac{1}{2}\theta\right)} = \frac{(2R_e + h_U) + h_U\cot\left(\alpha + \frac{1}{2}\theta\right)\cot\left(\frac{1}{2}\theta\right)}{\cot\left(\alpha + \frac{1}{2}\theta\right)\cot\left(\frac{1}{2}\theta\right) - 1} \qquad \text{Eq 67}$$

$$h_S \approx h_U + \theta\left(\alpha + \frac{1}{2}\theta\right)R_e \quad \text{for} \quad \alpha \ll 1\,, \theta \ll 1\,, h_U \ll R_e$$

Special-case checks/examples for Eq 67 are:

- If the elevation angle is $\alpha = 0$ (i.e., triangle **OUS** has a right angle at **U**), then the first line of Eq 67 reduces to

$$h_S = \frac{R_e + h_U}{\cos(\theta)} - R_e$$

- If the elevation angle and geocentric angle satisfy $\alpha = -\frac{1}{2}\theta$ (i.e., are consistent with **OUS** being an isosceles triangle with sides **OU** and **OS** equal), then the first line of Eq 67 reduces to

$$h_S = h_U$$

- If the elevation angle and geocentric angle satisfy $\alpha = -\theta$ (i.e., are consistent with triangle **OUS** having a right angle at **S**), then the first line of Eq 67 reduces to

$$h_S = (R_e + h_U)\cos(\theta) - R_e$$

3.7 Example Applications

Three example applications are presented in this section, with the intent of providing a sense of how the mathematical equations presented earlier in this chapter relate to real problems. The examples are intended to illustrate that it is necessary to understand the application in order to utilize the equations properly and to interpret the results. Also, these examples suggest that, while providing useful information, the equations in this chapter cannot answer some relevant question. For that reason, the same examples are re-visited at the end of Chapter 4.

3.7.1 Example 1: En Route Radar Coverage

Application Context — A frequent surveillance engineering task is predicting a radar installation's 'coverage'. There are two common formulations: Calculate either the minimum visible aircraft (a) Elevation MSL for a known ground range (geocentric angle) from the radar; or (b) Ground range (geocentric angle) from the radar, for a known elevation MSL. For either case, the issues to be considered, and the approach taken herein, are:

- **Terrain Effects** — As stated in Chapter 1, blockage of electromagnetic waves by hills/mountains/structures is not addressed herein. These effects would be included in a

more thorough analysis, and are particularly important in mountainous areas. However, terrain effects are handled numerically, rather than by an analytic model, and are thus outside the scope of this document. The earth surrounding the radar is assumed to be smooth, although not necessarily at sea level.

- **Propagation Model** — As stated in Chapter 1, real sensors may not have the straight line propagation paths. Relevant to radars: electromagnetic waves behave according to Snell's Law and refract towards the vertical as the atmospheric density increases with decreased altitude. Refraction effects are most pronounced for long, predominantly horizontal paths within the earth's atmosphere (such as occur for an en route radar). A widely used model that approximates the effects of refraction and is compatible with the equations developed earlier in this chapter is the 'four-thirds earth' model (Refs. 19 and 20). According to Ref. 19: "The 4/3 Earth radius rule of thumb is an average for the Earth's atmosphere assuming it is reasonably homogenized, absent of temperature inversion layers or unusual meteorological conditions." Ref. 20 is an in-depth treatment of radar signal refraction.
- **Radar Antenna Height** — Three values are used for the height of the radar antenna phase center above the surrounding terrain, h_U: 50 ft, representative of the antenna height for a radar mounted on a tower; 500 ft, representative of the antenna height for a radar on a hill top; and 5,000 ft, representative of the antenna height for a radar on a mountain top.

Based on these considerations, the two known/independent variables are taken to be:

(1) The satellite/aircraft elevation angle α (provided it is equal to or greater than the minimum value for the associated antenna height h_U); and

(2) Either

(a) The geocentric angle θ between the radar and a target aircraft (so the unknown/ dependent variable is the aircraft altitude h_S above the terrain) — governed by Eq 66; or

(b) The aircraft altitude h_S (so the unknown/dependent variable is the geocentric angle θ) — governed by Eq 40.

Associating **U** with the radar antenna location (because its elevation is known) and **S** with aircraft locations, the resulting equations are shown in Eq 68 below. The first line is derived from Eq 66, with substitutions to account for the four-thirds earth model. Similarly, the second line, is derived from the second line of Eq 40. Also included is the equation for the geocentric angle θ_U between the radar and the location **T** where the signal path (for elevation angle α_{min}) is tangent to the earth (Figure 7). In Eq 68: Arcsin and Arccos yield the smallest non-negative angle solution for arcsin and arccos, respectively; and on the second line, the '+' is correct except when $\alpha < 0$ and the aircraft is between the radar **U** and the radial passing through the point of tangency **T**.

$$h_S = h_U + \left(\frac{\cos(\alpha)}{\cos(\alpha + \frac{3}{4}\theta)} - 1\right)\left(\tfrac{4}{3}R_e + h_U\right) \quad , \quad \alpha \geq \alpha_{min}$$

$$\theta = -\frac{4}{3}\alpha \pm \frac{8}{3}\,\text{Arcsin}\left(\sqrt{\frac{\left(\tfrac{4}{3}R_e + h_U\right)\sin^2\left(\tfrac{1}{2}\alpha\right) + \tfrac{1}{2}(h_S - h_U)}{\tfrac{4}{3}R_e + h_S}}\right) \quad , \quad \alpha \geq \alpha_{min} \qquad \text{Eq 68}$$

$$\alpha_{min} = -\text{Arccos}\left(\frac{\frac{4}{3}R_e}{\frac{4}{3}R_e + h_S}\right) = -2\,\text{Arcsin}\left(\sqrt{\frac{h_U}{2\left(\frac{4}{3}R_e + h_S\right)}}\right)$$

$$\theta_U = -\frac{4}{3}\alpha_{min}$$

The results of exercising the first line of Eq 68 are shown in Figure 8. The maximum range depicted, 250 NM, is the specified value for current en route ATC radars (e.g., ARSR-4 and ATCBI-6). Curves are shown that correspond to three radar elevations above mean sea level (MSL) when $\alpha = \alpha_{min}$, the theoretical minimum elevation angle for which targets are visible (blue) and for $\alpha = \alpha_{min}$+1 deg larger than the minimum elevation angle (violet). Aircraft whose range / altitude combinations are above a given curve are visible to the radar; otherwise they are said to be 'below the radar horizon'. If the visibility of aircraft relative to terrain (rather than mean sea level) is needed, the elevation of the terrain is subtracted from the MSL values in Figure 8.

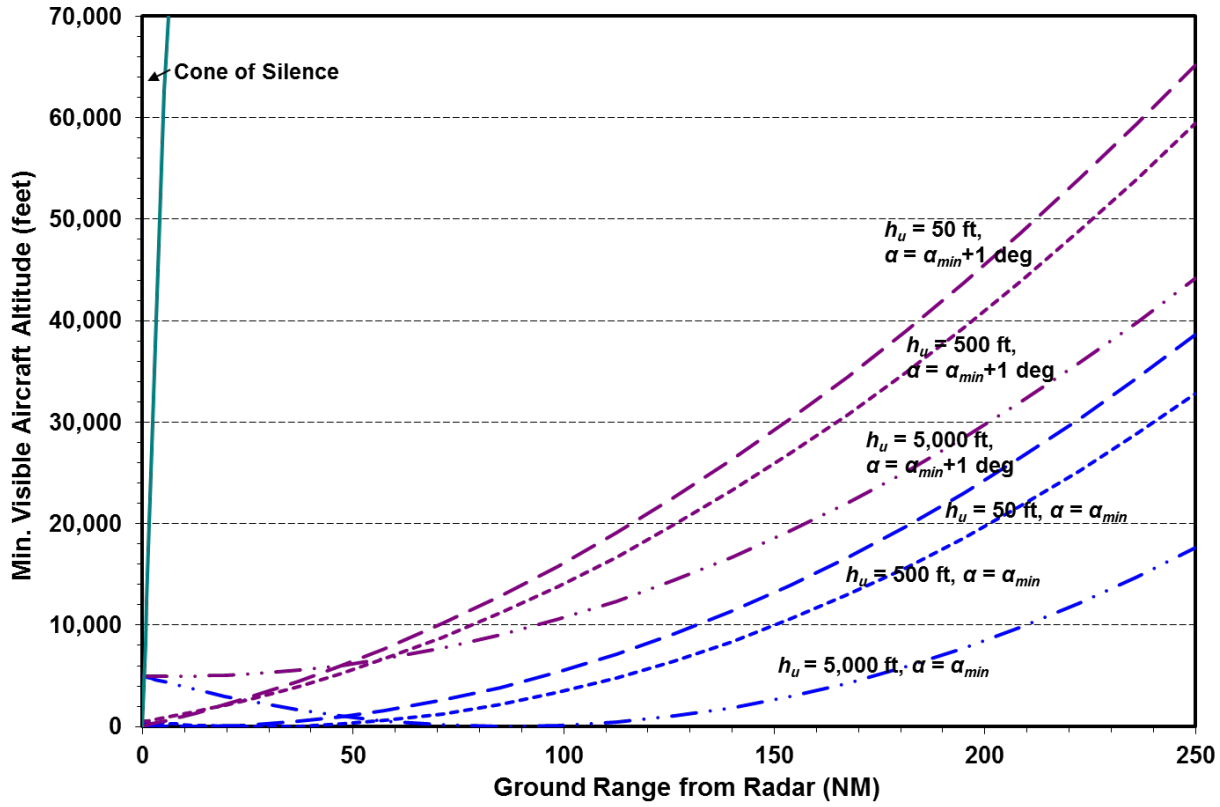

Figure 8 Minimum Visible Altitude vs. Range for Three Radar Antenna Altitudes

Sensitivity to radar antenna elevation — Increasing the height of the radar's antenna decreases the minimum altitude at which aircraft are visible. In this example, at the maximum radar range, raising the antenna from 50 feet to 5,000 feet decreases the visible aircraft altitude by almost 21,000 feet — i.e., the ratio is greater than 4:1. The reason can be appreciated by examining

Figure 7. Line **US** acts like a lever arm with its fulcrum at **T**. Raising **U** lowers **S**, and since **T** is generally closer to **U** than **S**, the change in the elevation of **S** is greater than it is in **U**.

Sensitivity to antenna boresight angle — Increasing the elevation angle of a radar antenna above the minimum required to avoid blockage of the signal by the earth has a significant coverage penalty. At the radar's maximum range, a 1 degree increase in elevation angle corresponds to an increase in the minimum altitude at which targets are visible by approximately

$$\Delta\alpha\, d \approx (1 \text{ deg})(\pi \text{ rad}/180 \text{ deg})(250 \text{ NM})(6{,}076 \text{ ft/NM}) \approx 26{,}500 \text{ feet} \qquad \text{Eq 69}$$

The resulting decrease in surveillance coverage is more than is gained by raising the radar elevation to 5,000 feet. Thus, aligning (often called 'bore sighting') the antenna is an important aspect of a radar installation.

Cone of Silence — 'Visibility' is necessary for an aircraft to be detected by a radar. But it is not sufficient. Energy transmitted by the radar must reach the aircraft; then, energy scattered (primary radar) or transmitted (secondary radar) by the aircraft must return to the radar at a detectable level. When a radar performs well for most targets (the case here) and a target is visible, the determining factor for detectability is the antenna pattern. ATC radar antennas are designed to have their gain concentrated near the horizon, where most aircraft are. Conversely, ATC radar antenna are not designed to detect aircraft almost directly above them (the 'cone of silence').

A 'rule of thumb' for detecting a target by an ATC radar is that the target range be at least twice its height above the radar antenna — e.g., an aircraft at 10,000 ft above the antenna would not be detected when less than 20,000 ft or 3.3 NM from the radar (Ref. 21). Figure 8 includes the predicted cone of silence for an ATC radar antenna on the surface; larger antenna elevation values will result in slightly smaller cones of silence. Generally, the cone of silence is an issue to be aware of, but is not a major concern.

Targets 'Below' the Radar — While the cone of silence is a concern for aircraft nearly above a radar, when a radar antenna is installed significantly higher than the local terrain level, a similar issue arises for aircraft close to but at lower altitudes than the antenna. Figure 9 depicts the vertical plane (analogous to Figure 1) containing the radar antenna and the signal paths (for a $4/3^{rds}$ earth model) that are unblocked by the earth for antenna heights of 50 ft, 500 ft and 5,000 ft above the earth. (Data for these curves are the same as data for Figure 8.) The points of tangency **T** with the earth's surface for these signal paths are 8.7, 27.5 and 86.9 NM from the radar **U**. Aircraft located between **U** and **T** and vertically below the paths that are tangent to the earth's surface are visible to the radar (i.e., the propagation paths between those aircraft and the antenna are unblocked). Whether the radar can detect them is primarily an issue of the antenna

vertical pattern. Some radars are designed with a 'look down' mode to detect such aircraft. Thus, Figure 8 and Figure 9 may understate coverage for such targets.

Earth Model — For either the standard-size or 4/3^{rds} earth model, the minimum visible aircraft altitudes are small at short ranges, and model differences are not important. However, the minimum visible altitudes for the separate models, and their differences, are substantial at longer ranges. For example, at a ground range of 250 NM, the predicted visible aircraft altitude for a 4/3^{rds} earth model is less than that for a normal-size earth by between 13.4 kft (for a radar antenna elevation of 50 ft) and 9.4 kft (for a radar antenna elevation of 5,000 ft).

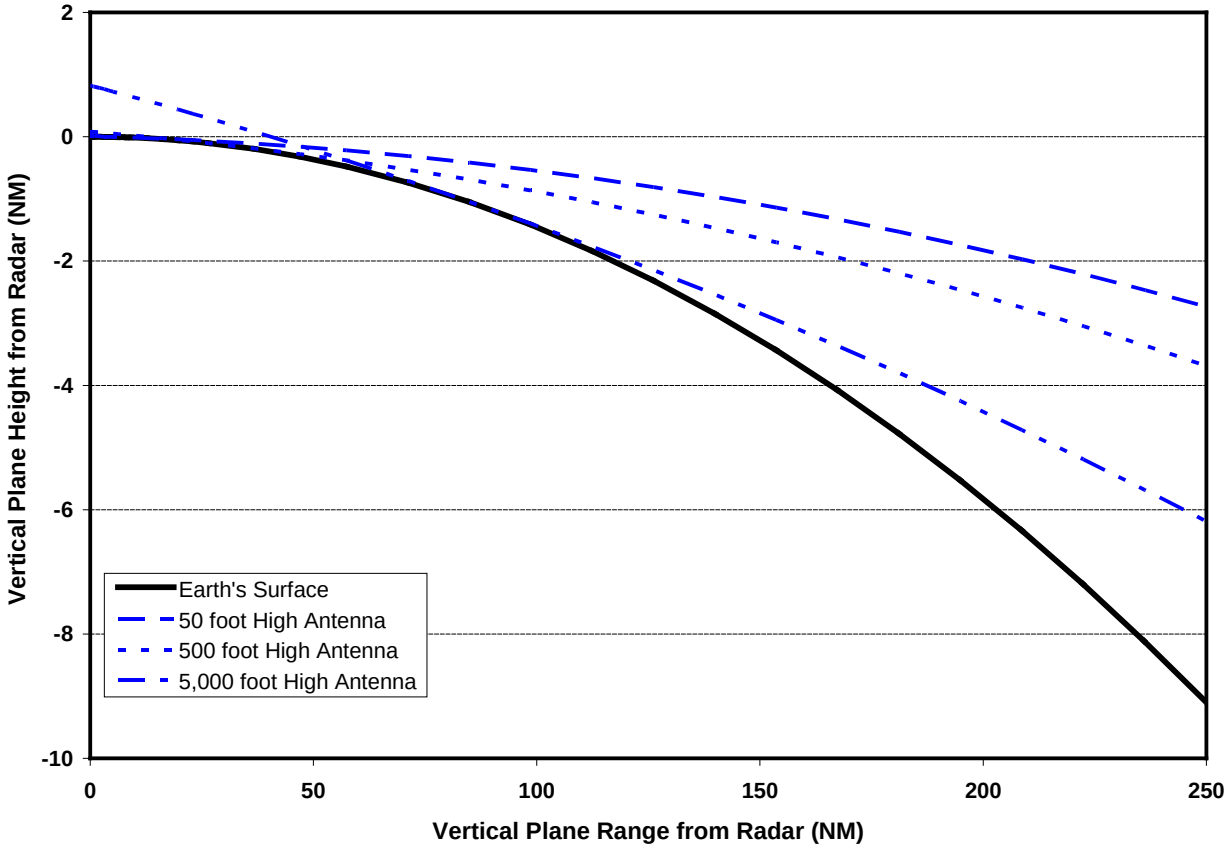

Figure 9 Radar Minimum Visible Altitude vs. Horizontal Range

3.7.2 Example 2: Aircraft Precision Approach Procedure

Design of a Precision Instrument Approach Procedure (IAP) is a straightforward application of the analyses in this chapter. The RNAV (GPS) LPV approach to Kansas City International Airport (MCI) runway 19L is selected as an example. The approach plate is shown as Figure 10.

The first consideration is that, since the navigation fixes on the approach plate quantify vertical height in terms of altitude MSL, the same quantity must be used for procedure design. Second, the user location **U** is chosen as the point where aircraft crosses the runway threshold. The

elevation above MSL of **U** is the sum of the elevation of the runway threshold (THRE = 978 ft) and the threshold crossing height (TCH = 59 ft); thus, $h_U = h_T = 1{,}037$ ft (where *T* denotes threshold).

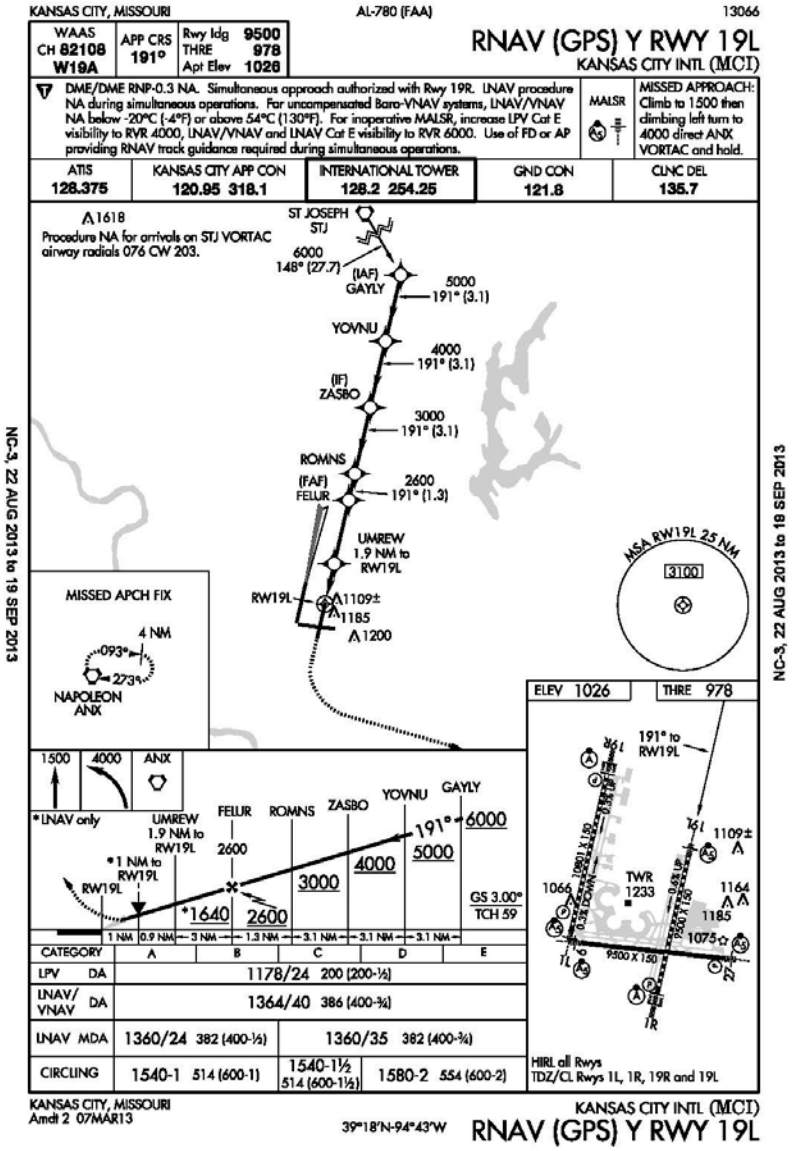

Figure 10 Approach Plate: RNAV (GPS) Y for MCI Runway 19L

In terms of the four variables defined in Subsection 3.1.1, the elevation angle α is set equal to the specified glide path (GP) angle — i.e., $\alpha = 3.00$ deg — and is one independent variable. The second independent variable describes movement along the approach route. Either θ or $h_S = h_A$ (*A* denoting aircraft) could be used; in this example, θ is selected because it has fewer drawbacks. While its published precision (0.1 NM) is less than desired, the limits of its precision are known. Conversely, only lower bounds for h_A are specified on the approach plate; the amount that each is below the glide path angle is not known. (A reason for selecting this example is that

there are six positions along the approach route where the minimum altitude MSL is stated.)

For this set of variables — α and θ known, and h_A unknown — Subsection 3.6.3 provides the solution (Eq 66). Evaluating this equation, repeated here as Eq 70, using the TERPS value for R_e (Eq 32), yields Table 5.

$$h_A = -R_e + \frac{\cos(\alpha)}{\cos(\alpha + \theta)}(R_e + h_T) \qquad \text{Eq 70}$$

Table 5 Specified and Computed Fix Altitudes for MCI Runway 19L LPV Approach

Fix Name	UMREW	FELUR	REMNS	ZASBO	YOVNU	GAYLY
Dist. from Threshold, NM (Figure 10)	1.9	4.9	6.2	9.3	12.4	15.5
Chart Min. Altitude, ft MSL (Figure 10)	1,640	2,600	3,000	4,000	5,000	6,000
Computed GP Altitude, ft MSL (Eq 70)	1,645	2,619	3,046	4,075	5,122	6,187

The computed values in the last row of Table 5 are slightly larger than the published minimum altitudes in Figure 10. Since published minimum altitudes are usually rounded down to the largest multiple of one hundred feet, it is reasonable to conclude that the IAP design process described in the subsection closely replicates FAA process.

3.7.3 Example 3: Satellite Visibility of/from Earth

A question that is readily addressed using the equations in this chapter is: What fraction of the earth's surface can see (and be seen by) a satellite at altitude h_S? Clearly, h_S is one independent variable in such an analysis. The other independent variable is taken to be the minimum elevation angle α (often called the mask angle in this context) at which the satellite provides a usable signal. The quality of signals received at low elevation angles can be degraded due to multipath and attenuation by the atmosphere; and terrain blockage is an issue at low elevation angles. The dependent variable is taken to be θ, the geocentric angle between the satellite nadir **N** and the user **U**. For this set of variables, Subsection 3.3.1 provides the solution approach.

An issue is whether to use a normal-size or 4/3rds earth model. Here, normal-size is selected, because (unlike radar signals) satellite signals are outside of the earth's atmosphere over most of their propagation path. The earth's atmosphere extends to an altitude of approximately 5 NM, while satellite altitudes are at least several hundred nautical miles. The basic equation to be evaluated is thus taken from Eq 40. To visualize the impact of satellite altitude on visibility, a modified version of Eq 33 is used to generate Figure 11.

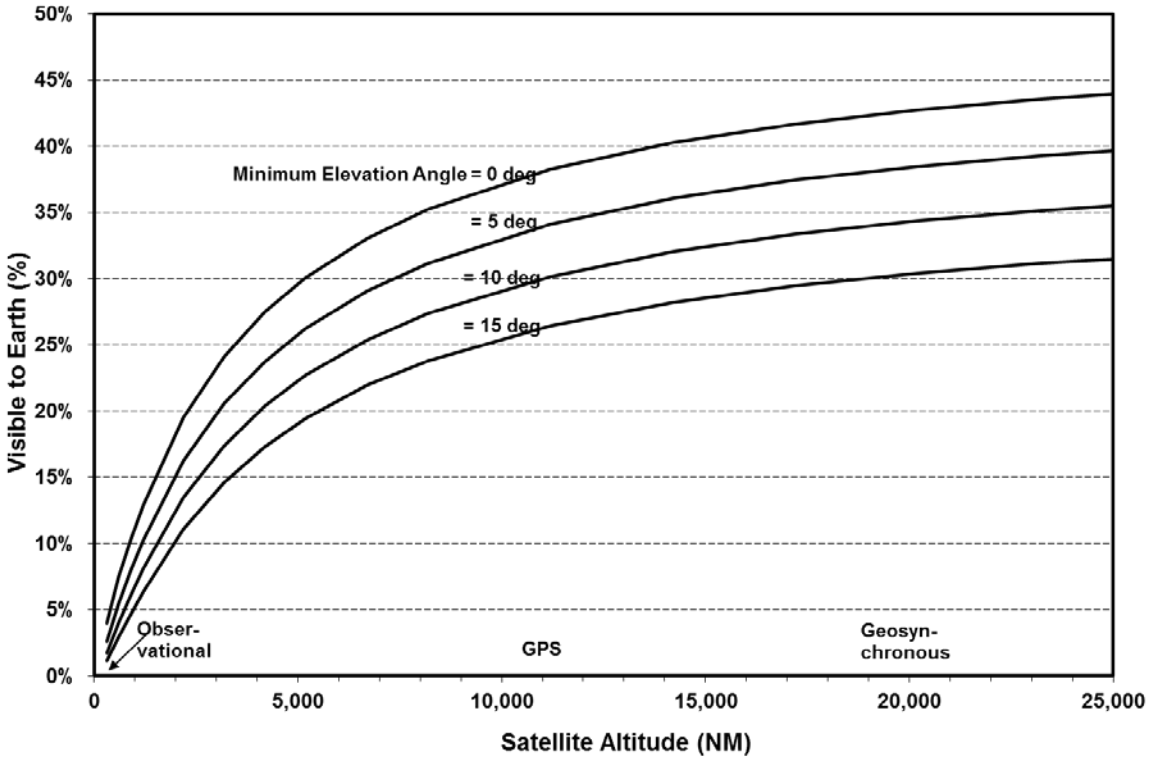

Figure 11 Fraction of Earth Visible vs. Satellite Altitude

4. TWO-POINT / SPHERICAL-SURFACE FORMULATION

4.1 Basics of Spherical Trigonometry

4.1.1 Basic Definitions

Spherical trigonometry deals with relationships among the sides and angles of spherical triangles. Spherical triangles are defined by three vertices (points **A**, **B** and **C** in Figure 12) on the surface of a sphere and three arcs of great circles (**a**, **b** and **c** in Figure 12), termed sides, connecting the vertices. The angles at the vertices are *A*, *B* and *C*, and the lengths of the sides are quantified by their corresponding geocentric angles (*a*, *b* and *c*). In this document, the sphere always represents the earth.

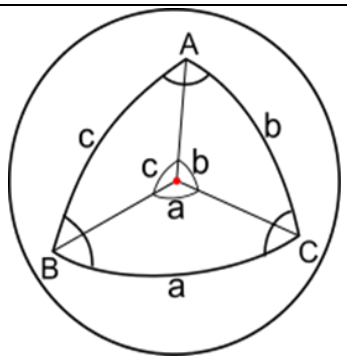

Figure 12 Example Spherical Triangle

Spherical trigonometry originated over 2,000 years ago, largely motivated by maritime navigation and understanding the relationship of the earth to the 'heavenly bodies'. Early contributors were from Greece, Persia and Arabia. The subject was completed by Europeans in the 18th and 19th centuries. Until the 1950s, spherical trigonometry was a standard part of the mathematics curriculum in U.S. high schools (Refs. 22 and 23).

4.1.2 Application to Navigation and Surveillance

In this document, a distinction is made between 'mathematical' and 'navigation' spherical triangles. The three vertices of a 'mathematical' spherical triangle can be arbitrarily located on the surface of a sphere — i.e., all three points can be problem-specific. The sides and interior angles are all positive in the range $(0, \pi)$. A 'mathematical' spherical triangle does not have an defined relationship with the sphere's latitude/longitude grid.

In contrast, 'navigation' spherical triangles involve only two problem-specific locations, typically labeled **U** and **S** in this chapter. The third vertex is chosen as the North Pole **P***[*], enabling **U** and **S** to be related to the latitude/longitude grid. (In many texts, 'navigation' triangles are called 'polar' triangles.) Six triangle parts (requiring seven navigation variables) define a 'navigation' spherical triangle (Figure 13):

[*] While the North Pole is used in deriving navigation equations, the resulting expressions are valid for points in the southern hemisphere as well.

(a) Angular lengths of sides **PU** and **PS** — complements of the latitudes of points **U** and **S**, respectively;

(b) Angle at **P** — the difference in the longitude of the points **U** and **S**;

(c) Angular length of side **US** — the geocentric angle between points **U** and **S**; and

(d) Angles at **U** and **S** — the azimuth angles of the leg joining **U** and **S** with respect to north.

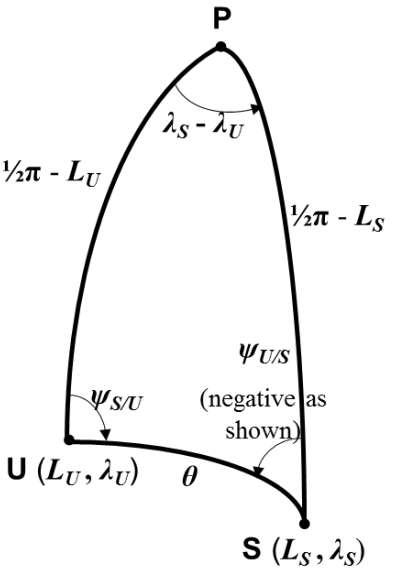

Figure 13 Navigation Spherical Triangle

This chapter is devoted to problems involving two-points on the surface of a sphere. These can be solved using navigation spherical triangles. Chapter 6 addresses situations involving three problem-specific points.

4.1.3 Applicability to Two-2D Problem Formulation

A drawback of spherical trigonometry is that it not suited to problems involving locations above the earth's surface — i.e., it does not 'handle' altitude. However, the vertical plane defined by two vertices of a spherical triangle and the center of the sphere conform to the assumptions employed in Chapter 3. Points directly above the two vertices lie in that plane as well. Thus, for situations involving two problem-specific points, plane and spherical trigonometry are complementary techniques that can be employed for their analysis. Moreover, situations involving three problem-specific points can be analyzed in the same way, so long as the altitude components can be handled in a pairwise manner. Often, problems involving an aircraft and two navigation or surveillance sensors satisfy this condition.

4.1.4 General Characteristics of Spherical Triangles

The interior angles of a spherical triangle do not necessarily sum to π, and right triangles do not play as prominent a role as they do in plane trigonometry; interest is largely focused on oblique triangles. Although Figure 12 and Figure 13 depicts all angles and sides as acute, angles and sides of mathematical spherical triangles lie in the range $(0, \pi)$. Angles in navigation analysis have a wider range of values: latitude varies over $[-\pi/2, \pi/2]$, longitude varies over $(-\pi, \pi]$, geocentric angles vary over $(0, \pi)$ and azimuths vary over $(-\pi, \pi]$. Thus, preferable: latitudes are found with the arc sine or arc tangent function; longitudes with the two-argument arc tangent; geocentric angles with the arc cosine; and azimuths with the two-argument arc tangent. Difference between two longitudes or two azimuth angles may need to be adjusted by $\pm 2\pi$, so that the magnitude of the difference is less than or equal to π.

Two points on a sphere are diametrically opposite (antipodal) if the straight line connecting them

passes through the center of the sphere. Mathematically, **U** and **S** are antipodal when $L_S = -L_U$ and $\lambda_S = \lambda_U \pm \pi$. If that is the case, the geocentric angle between **U** and **S** is π, and an infinite number of great circle paths connect **U** and **S**. Many spherical trigonometry equations, and particularly those for azimuth angles, are indeterminate for antipodal points.

The expressions developed in this chapter are based on triangle **UPS** Figure 13 — specifically, **U** is west of **S**. The positive interior angles of mathematical triangle **UPS** are: $\lambda_S - \lambda_U$, $\psi_{S/U}$, and $2\pi - \psi_{U/S}$ If, in fact, **S** is west of **U**, the expressions derived remain correct. It is apparent (and shown in Subsection 4.6.2) that if $0 < \psi_{S/U} < \pi$ then $-\pi < \psi_{U/S} < 0$, and vice versa.

4.1.5 Resources on the Web

The internet has many useful resources concerning spherical trigonometry. Examples, in approximate decreasing order of their complexity, are:

- I. Todhunter, *Spherical Trigonometry*, 5th Edition (Ref. 24) — Written by a British academic. Considered to be the definitive work on the subject, and readily understood as well. Later editions were published but are not available without charge.
- W.M. Smart and R.M. Green, *Spherical Astronomy* (Ref. 25) — Also written by a British academics. Chapter 1 is devoted to spherical trigonometry. It has equations and their derivations (including more complex and useful ones).
- Wikipedia, *Spherical Trigonometry* (Ref. 26) — A fine collection of equations and background information.
- Wolfram MathWorld (Ref. 27) — Another good collection of equations
- Ed Williams' Aviation Formulary (Ref. 28) — A website with equations similar to those in this chapter, without derivations. Also offers an Excel spreadsheet with formulas as macros.
- Spherical Trigonometry (Ref. 29) — An easily understood, unintimidating introduction to the topic.

4.1.6 Key Formulas/Identities

The key formulas/identities for oblique spherical triangles are presented below. These formulas presume the existence of a solution — i.e., that the known angles and sides correspond to an actual triangle. Some formulas do not have a solution if that is not the case.

In general, the labeling of the angles and sides of a spherical triangle is arbitrary. Thus, referring to Figure 12, cyclic substitutions — i.e., $A \rightarrow B$, $a \rightarrow b$, etc. — can be made to derive alternate versions of each identity. In addition to the formulas displayed below, there is a rich set of other identities that can be found in the literature.

Law of Cosines for Sides (also simply called Law of Cosines):

$$\cos(a) = \cos(b)\cos(c) + \sin(b)\sin(c)\cos(A) \qquad \text{Eq 71}$$

The right-hand side contains two sides (here, *b* and *c*) and their included angle (*A*). The left-hand side contains the third side (*a*), which is opposite to the included angle. This is the most used identity (or law) of spherical trigonometry.

Primary applications: (1) finding the third side of a triangle, given two sides and their included angle; and (2) finding any angle of a triangle (using cyclic substitution), given three sides.

The right-hand side of Eq 71 is similar to the expression for $\cos(b \pm c)$, except that another factor, whose absolute value is no greater than unity, is present. It follows that the right-hand side must have absolute value no greater than unity, regardless of the values of the three variables.

Law of Cosines for Angles (also called Supplemental Law of Cosines):

$$\cos(A) = -\cos(B)\cos(C) + \sin(B)\sin(C)\cos(a) \qquad \text{Eq 72}$$

The right-hand side contains two angles (here, *B* and *C*) and their included side (*a*). The left-hand side contains the third angle (*A*), which is opposite to the included side. The right-hand side must have absolute value no greater than unity, regardless of the values of the three variables.

Primary applications: (1) finding the third angle of a triangle, given the other two angles and their included side; and (2) finding any side of a triangle (by cyclic substitution) from all three angles.

Law of Sines:

$$\frac{\sin(a)}{\sin(A)} = \frac{\sin(b)}{\sin(B)} \qquad \text{Eq 73}$$

Primary application: Considering two angles and their opposite sides, and given three of these parts, find the remaining part. It is possible to select values for three of the parts such that a solution for the fourth part does not exist.

When a solution does exist, the ambiguity of the arc sine function must be considered. From Ref. 24, Article 83: “the point may be sometimes settled by observing that the greater angle of a triangle is opposite to the greater side.” Article 86 addresses this topic further. For angle *B* unknown, it states “if a lies between b and $\pi - b$, there will be one solution; if a does not lie between b and $\pi - b$, either there are two solutions or there is no solution”. The cases of $a = b$ and $a = \pi - b$ are addressed separately.

Analog of Law of Cosines for Sides (also called the Five-Part Rule):

$$\sin(a)\cos(B) = \cos(b)\sin(c) - \sin(b)\cos(c)\cos(A)$$
$$\sin(a)\cos(C) = \cos(c)\sin(b) - \sin(c)\cos(b)\cos(A) \qquad \text{Eq 74}$$

These equations can also be written as

$$\sin(opposite\ side\ a)\cos(adj\ ang\ X) = \cos(side\ x)\sin(side\ y) - \sin(side\ x)\cos(side\ y)\cos(included\ angle\ A)$$

For the formulas herein, the right-hand sides of both lines of Eq 74 have the same two sides and included angle (and almost identical functions) as the right-hand side of the law of cosines for sides (Eq 71). However, whereas the law of cosines for sides has the opposite side on the left-hand side, the analogue law has the opposite side and an adjacent angle.

Primary application: This law is not often used; herein, it's employed in situations where two sides and the included angle are known, and it is desired to unambiguously find the two adjacent angles directly from the known quantities — e.g., see Subsection 4.2.2.

Four-Part Cotangent Formula:

$$\begin{aligned} \cos(a)\cos(B) &= \sin(a)\cot(c) - \sin(B)\cot(C) \qquad (cBaC) \\ \cos(a)\cos(C) &= \sin(a)\cot(b) - \sin(C)\cot(B) \qquad (BaCb) \end{aligned} \qquad \text{Eq 75}$$

These equations can also be written as

$$\cos(inner\ side)\cos(inner\ angle) = \sin(inner\ side)\cot(outer\ side) - \sin(inner\ angle)\cot(outer\ angle)$$

The six elements (or parts) of a triangle may be written in cyclic order as (*aCbAcB*). The four-part cotangent formula relates two sides and two angles constituting four consecutive elements. The outer side and angle (i.e., at the ends of such a sequence) each appears once in Eq 75, as the argument of a cotangent function, whereas the inner parts appear twice.

Primary applications: (1) Given two angles (here, *B* and *C*) and their included side (*a*), find the adjacent sides (*b* and *c*). (2) Given two sides (*c* and *a*, or *a* and *b*) and their included angle (*B* or *C*), find the adjacent angles (*C* and *B*).

For same three known quantities as the two cosine laws (Eq 71 and Eq 72), the four-part cotangent formula provides solutions for the adjacent quantities that the cosine laws do not. However, application (2) can also be accomplished by a combination of the law of cosines (Eq 71) and the analogue law (Eq 74).

Napier's Analogies[*]:

$$\begin{aligned} \tan\left[\tfrac{1}{2}(A+B)\right] &= \frac{\cos\left[\tfrac{1}{2}(a-b)\right]}{\cos\left[\tfrac{1}{2}(a+b)\right]}\cot\left[\tfrac{1}{2}C\right] \qquad \tan\left[\tfrac{1}{2}(a+b)\right] = \frac{\cos\left[\tfrac{1}{2}(A-B)\right]}{\cos\left[\tfrac{1}{2}(A+B)\right]}\tan\left[\tfrac{1}{2}c\right] \\ \tan\left[\tfrac{1}{2}(A-B)\right] &= \frac{\sin\left[\tfrac{1}{2}(a-b)\right]}{\sin\left[\tfrac{1}{2}(a+b)\right]}\cot\left[\tfrac{1}{2}C\right] \qquad \tan\left[\tfrac{1}{2}(a-b)\right] = \frac{\sin\left[\tfrac{1}{2}(A-B)\right]}{\sin\left[\tfrac{1}{2}(A+B)\right]}\tan\left[\tfrac{1}{2}c\right] \end{aligned} \qquad \text{Eq 76}$$

[*] In mathematics, the term 'analogies' was historically used for proportions.

For each equation, either: (a) the right-hand side contains two sides and their included angle, and the left-hand side contains the opposite two angles; or (b) the right-hand side contains two angles and their included side, and the left-hand side contains the opposite two sides.

Primary applications (1): Given two sides (here, *a* and *b*) and their opposite angles (*A* and *B*), find the remaining side (*c*) and remaining angle (*C*). (2) By combining two equations: (a) given two sides and the included angle, find the opposite two angles, or (b) given two angles and the included side, find the opposite two sides.

Considering the lower left-hand equation, $\tan\left[\frac{1}{2}(A-B)\right]$ and $\sin\left[\frac{1}{2}(a-b)\right]$ must have the same sign. Thus, $A > B$ if and only if $a > b$. It follows that, if the sides of a spherical triangle are ordered based on length, their opposite angles must have the same order based on magnitude, and vice versa. The lower right-hand equation leads to the same result.

The Law of Tangents for spherical triangles is the ratio of the lower to the upper equations on either side of Eq 76. It is not used herein.

Delambre's Analogies:

$$\frac{\cos\left[\frac{1}{2}(A+B)\right]}{\cos\left[\frac{1}{2}(a+b)\right]} = \frac{\sin\left[\frac{1}{2}C\right]}{\cos\left[\frac{1}{2}c\right]} \qquad \frac{\cos\left[\frac{1}{2}(A-B)\right]}{\sin\left[\frac{1}{2}(a+b)\right]} = \frac{\sin\left[\frac{1}{2}C\right]}{\sin\left[\frac{1}{2}c\right]}$$

$$\frac{\sin\left[\frac{1}{2}(A+B)\right]}{\cos\left[\frac{1}{2}(a-b)\right]} = \frac{\cos\left[\frac{1}{2}C\right]}{\cos\left[\frac{1}{2}c\right]} \qquad \frac{\sin\left[\frac{1}{2}(A-B)\right]}{\sin\left[\frac{1}{2}(a-b)\right]} = \frac{\cos\left[\frac{1}{2}C\right]}{\sin\left[\frac{1}{2}c\right]} \qquad \text{Eq 77}$$

For each equation: the left-hand side contains two angles and their their opposites sides, and the right-hand side contains the remaining angle and its opposite side. Angles are always in the numerator, and sides in the denominator. Napier's Analogies are ratios of Delambre's Analogies.

Primary application: Checking a solution for a triangle (as each expression contains all six parts of a spherical triangle).

Same Affection for Sums/Difference of Opposite Sides/Angles:

The sides and angles of a 'mathematical' spherical triangle all lie in (0, π). Thus $½(A+B)$ and $½(a+b)$ must as well. Considering the upper left-hand equation in Eq 77, it follows that these two sums are less-than/equal-to/greater-than $½\pi$ synchronously (Ref. 24). Also, $½(A-B)$ and $½(a-b)$ both lie in $(-½\pi, ½\pi)$. Considering the lower right-hand equation in Eq 77, it follows that these differences are less-than/equal-to/greater-than zero simultaneously. Ref. 24 terms this characteristic as 'having the same affection'.

Solving for Angles and Sides:

When solving for angles and sides using the above formulas, one must be aware of the possibility of multiple angle solutions to inverse trigonometric functions (Subsection 2.1.6). In the realm of 'mathematical' spherical triangles, where angles and sides are in the range $(0, \pi)$, the arc sine function (often arising from use of the law of sines) is the primary source of concern, as two angles in the range $(0, \pi)$ can have the same sine value. (However, some physical problems have two possible solutions — i.e., one solution is ambiguous [not extraneous] and additional information must be used to select the correct physical solution.) In the following text, an attempt is made to avoid these situations, or at least to point them out when they do occur.

4.1.7 Taxonomy of Mathematical Spherical Triangle Problems

A spherical triangle is fully defined by its six parts. The case of five known parts is trivial, requiring only a single application of either cosine law or the sine law. For four known parts, there is one non-trivial case. For three known parts there are six cases. Each of the seven cases is illustrated in Figure 14 and enumerated below (Ref. 26), along with a solution approach. For some cases, others solutions exist.

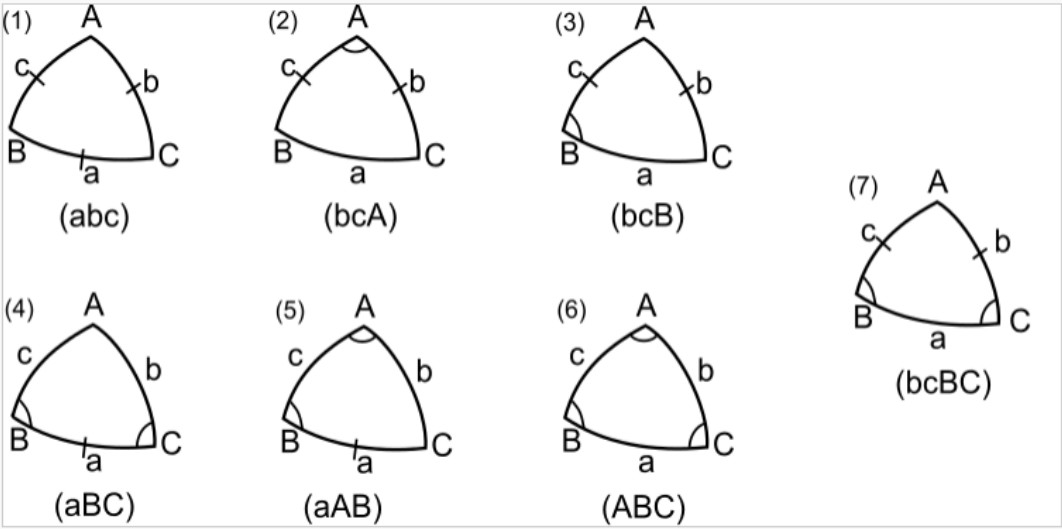

Figure 14 Taxonomy of Mathematical Spherical Triangle Problems

Mathematical spherical triangle taxonomy:

(1) Three sides known; SSS (side-side-side) case — Eq 71, three times

(2) Two sides and the included angle known; SAS (side-angle-side) case — Eq 71 for *a*, Eq 73 and/or Eq 74 for *B* and *C*

(3) Two sides and a non-included angle known; SSA (side-side-angle) case — Eq 73 for *C*, then follow case 7

(4) Two angles and the included side known; ASA (angle-side-angle) case — Eq 72 for *A*, then Eq 73 or Eq 75 *b* and *c*

(5) Two angles and a non-included side known; AAS (angle-angle-side) case — Eq 73 for *b*, then follow case 7

(6) Three angles known; AAA (angle-angle-angle) case — Eq 72, three times

(7) Two sides and their opposite angles known; AASS (angle-angle-side-side) case — Eq 76 for *A* and *a*.

4.1.8 Taxonomy of Navigation Spherical Surface Problems

The spherical surface formulation introduced in Section 1.2.2 involves seven variables. For a full solution to a situation, four variables must be known; from these, the remaining three can be found. Thus, 35 mathematical problems and 105 solution equations can be posed. However, the spherical surface situation is symmetric in **U** and **S**; interchanging **U** and **S** only changes the notation, but does not change the underlying problem. Of the 35 possible problems, three are self-symmetric and 16 have symmetric versions — see Table 6.

Table 6 Taxonomy of Spherical Surface Navigation Problems

Prob #	Known Quantities							Problem Structure				Comment
	L_U	λ_U	$\psi_{S/U}$	L_S	λ_S	$\psi_{U/S}$	θ	SP[1]	SS[2]	No λ[3]	Case[4]	
1	X	X		X	X				X		2	Section 4.2
2	X	X	X	X				X			3	Section 4.6
3	X	X		X		X		X			3	Similar to #2
4	X	X		X			X	X			1	
5	X	X	X		X			X			4	Section 4.5
6	X	X			X	X		X			5	
7	X	X			X		X	X			3	
8	X	X	X			X		X			5	
9	X	X	X				X	X			2	Section 4.3
10	X	X				X	X	X			3	Section 4.4
11	X		X	X		X			X	X	7	Over-specified
12	X		X	X			X	X		X	1, 2, +	Over-specified
13	X		X		X	X		X			5	Similar to #8
14	X		X		X		X	X			2	Similar to #9
15	X				X	X	X	X			3	
16	X		X			X	X	X		X	2, 4, +	Over-specified
17		X	X		X	X			X		6	
18		X	X		X		X	X			5	
19		X	X			X	X	X			4	Subsection 4.2.3

[1] Symmetric Problem exists

[2] This problem is Self-Symmetric

[3] Insufficient information to determine longitude

[4] Spherical Triangle Case (Subsection 4.1.7)

As noted in Table 6 (column labeled 'No λ'), 3 of 19 problems summarized (and 5 of the full 35) do not involve either longitude being known. Thus the solution can only yield a longitude difference rather than an actual longitude. Table 6 also references the corresponding spherical triangle case (Subsection 4.1.7) and the cases that are addressed in the remainder of this chapter. All seven spherical triangle cases presented in Subsection 4.1.7 occur in Table 6

4.2 The Indirect Problem of Geodesy

The Indirect problem of geodesy (introduced in Sub-section 1.2.2) is illustrated in Figure 15 (also see Figure **13**). The known elements (and their values) of triangle **PUS** are sides **PU** ($½\pi - L_U$) and **PS** ($½\pi - L_S$) and the included angle at **P** ($\lambda_S - \lambda_U$). In terms of the taxonomy of spherical triangles of Subsection 4.1.7, this problem falls under Case (2) – a SAS (side-angle-side) situation.

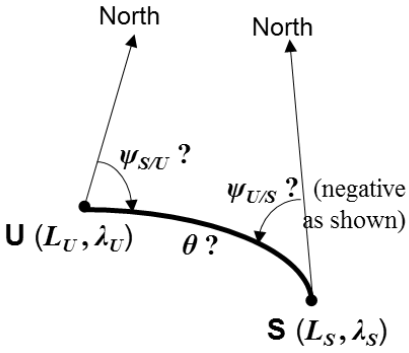

Figure 15 Indirect Problem of Geodesy

4.2.1 Computing the Geocentric Angle

Finding the geocentric angle between two locations on the spherical earth is fundamental navigation task. Referring to Figure 13, the angular distance between **U** and **S** is readily derived from the law of cosines for sides (Eq 71), with the length θ of the great circle are connecting **U** and **S** as the unknown quantity

$$\cos(\theta) = \cos(L_U)\cos(L_S)\cos(\lambda_U - \lambda_S) + \sin(L_U)\sin(L_S) \qquad \text{Eq 78}$$

The right-hand side of Eq 78 evaluates to a value in [-1, 1]; thus θ can be found uniquely in [0, π]. As 'sanity' checks, this expression reduces to $\theta = |L_S - L_U|$ when $\lambda_S = \lambda_U$, and to $\theta = |\lambda_S - \lambda_U|$ when $L_S = L_U = 0$.

Forms of Eq 78 (e.g., involving logarithms) were utilized for centuries using paper-and-pencil and rudimentary tables. However, great circle routes only became practical with the introduction of steam power. During this era, since Eq 78 is ill-conditioned for small values of θ, alternatives were sought. Thus, a modification was formulated utilizing the versine (Latin: *sinus versus*, or flipped sine) – see Figure 16 (Ref. 30).

$$\text{vers}(\theta) \equiv 1 - \cos(\theta) = 2\sin^2\left(\tfrac{1}{2}\theta\right) \qquad \text{Eq 79}$$

In early terminology, the ordinary sine function was called *sinus rectus*, or vertical sine. Tables for the versine or haversine (half

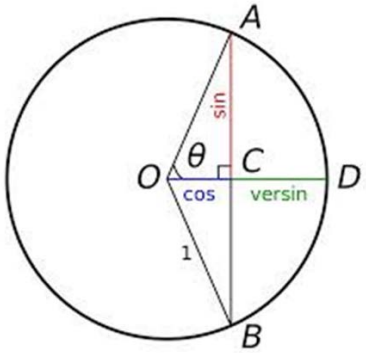

Figure 16 Sine, Cosine and Versine, and the Unit Circle

of versine) date to the third century BC.

Using the haversine function, the geocentric angle θ between known locations **U** and **S** can be found from the historically significant 'haversine formula' (Ref. 31)

$$\text{hav}(\theta) = \text{hav}(L_S - L_U) + \cos(L_S)\cos(L_S)\,\text{hav}(\lambda_S - \lambda_U) \qquad \text{Eq 80}$$

Without explicitly utilizing the versine or haversine functions (which are less needed today, due to the availability of computers), an analytically equivalent version of the haversine formula is

$$\sin\left(\tfrac{1}{2}\theta\right) = \sqrt{\sin^2\left(\tfrac{1}{2}(L_S - L_U)\right) + \cos(L_S)\cos(L_U)\sin^2\left(\tfrac{1}{2}(\lambda_S - \lambda_U)\right)} \qquad \text{Eq 81}$$

The right-hand side of Eq 81 evaluates to a value in [0, 1], so θ can then be found uniquely in [0, π]. Latitude and longitude differences only involve the sine function. This expression reduces to $\theta = |L_S - L_U|$ when $\lambda_S = \lambda_U$, and to $\sin\left(\tfrac{1}{2}\theta\right) = \cos(L_U)\left|\sin\left(\tfrac{1}{2}(\lambda_S - \lambda_U)\right)\right|$ when $L_S = L_U$.

A drawback of Eq 81 (although of far less concern than the problem it solves) is that it's ill-conditioned for geocentric angles near π. One solution is to use the original equation (Eq 78) in these situations. Another is to use the following:

$$\cos\left(\tfrac{1}{2}\theta\right) = \sqrt{\cos^2\left(\tfrac{1}{2}(L_S - L_U)\right) - \cos(L_S)\cos(L_U)\sin^2\left(\tfrac{1}{2}(\lambda_S - \lambda_U)\right)} \qquad \text{Eq 82}$$

The previous two equations can be combined to create a form that is monotonically increasing for $0 < \theta < \pi$ and thus not ill-conditioned for any value of θ when finding an inverse

$$\tan\left(\tfrac{1}{2}\theta\right) = \frac{\sqrt{\sin^2\left(\tfrac{1}{2}(L_S - L_U)\right) + \cos(L_S)\cos(L_U)\sin^2\left(\tfrac{1}{2}(\lambda_S - \lambda_U)\right)}}{\sqrt{\cos^2\left(\tfrac{1}{2}(L_S - L_U)\right) - \cos(L_S)\cos(L_U)\sin^2\left(\tfrac{1}{2}(\lambda_S - \lambda_U)\right)}} \qquad \text{Eq 83}$$

Remarks: (a) All of the equations for θ in this subsection are unchanged if **U** and **S** are inter-changed. (b) When the three points **P**, **U** and **S** are aligned (so the triangle **PUS** is degenerate), the equations remain valid. (c) An expression for $\tan(\theta)$, vice that for $\tan(\tfrac{1}{2}\theta)$ in Eq 83, can also be derived; see the following two subsections and Section 5.2 (Eq 143).

4.2.2 Computing the Azimuth Angles of the Connecting Arc

Having solved for the geocentric angle, the remaining goal of the Indirect problem of geodesy is finding the azimuth angles at **U** and **S** of the great circle arc connecting these two points. This determination is slightly complicated by the fact that azimuth angles can vary over the range [-π, π], so that a two-argument arc tangent function should be used.

First, the spherical trigonometry law of sines (Eq 73), applied to the angles at **P** and at **U**, yields

$$\sin(\psi_{S/U}) = \frac{\cos(L_S)\sin(\lambda_S - \lambda_U)}{\sin(\theta)} \qquad \text{Eq 84}$$

Second, the analogue to the law of cosines for sides (Eq 74) yields

$$\cos(\psi_{S/U}) = \frac{\sin(L_S)\cos(L_U) - \cos(L_S)\sin(L_U)\cos(\lambda_S - \lambda_U)}{\sin(\theta)} \qquad \text{Eq 85}$$

Combining Eq 84 and Eq 85 yields

$$\tan(\psi_{S/U}) = \frac{\cos(L_S)\sin(\lambda_S - \lambda_U)}{\sin(L_S)\cos(L_U) - \cos(L_S)\sin(L_U)\cos(\lambda_S - \lambda_U)} \qquad \text{Eq 86}$$

While Eq 84 and Eq 85 depend upon the geocentric angle θ (which is not a 'given' for the Indirect problem), the solution (Eq 86) for $\psi_{S/U}$ only depends upon the latitudes and longitudes of the great circle arc end points, which are 'givens'. Thus, the solution for $\psi_{S/U}$ does not chain from the solution for θ.

The spherical trigonometry methodology employed is symmetric with respect to **U** and **S**, so

$$\tan(\psi_{U/S}) = \frac{\cos(L_U)\sin(\lambda_U - \lambda_S)}{\sin(L_U)\cos(L_S) - \cos(L_U)\sin(L_S)\cos(\lambda_U - \lambda_S)} \qquad \text{Eq 87}$$

As mentioned previously, in navigation analyses it is useful to employ azimuth angles in the range [-π, π], where negative values denote angles west of north. In some texts, the azimuth angle at **S** is taken to be the angle the path would take if it were to continue — i.e., implicitly or explicitly, point **U** is taken as the origin and **S** as the destination of a trajectory. However, herein, the two points are on an equal basis and the azimuth angle at the second point is that for the great circle path toward the first point. Eq 86 and Eq 87 reflect this point of view.

Remarks:

- When the three points **P**, **U** and **S** are aligned (so the triangle **PUS** is degenerate), the equations in this subsection remain valid.
- If Eq 84 and Eq 85 are squared and added, the result is .

$$\sin(\theta) = \sqrt{[\cos(L_S)\sin(\lambda_S - \lambda_U)]^2 + [\cos(L_U)\sin(L_S) - \sin(L_U)\cos(L_S)\cos(\lambda_S - \lambda_U)]^2} \qquad \text{Eq 88}$$

This expression for the geocentric angle does not have the historical significance of Eq 78 or Eq 80 in Subsection 4.2.1, but is now used in software routines, often in conjunction with Eq 78 to form $\tan(\theta)$. It is derived using vector analysis in Section 5.2 (Eq 142).

4.2.3 Alternate Solution Using Napier's Analogies

Referring to Figure 13 (with **P**=*C*, **S**=*B* and **U**=*A*), Napier's Analogies yields

$$\tan\left[\tfrac{1}{2}\left(\psi_{S/U}-\psi_{U/S}\right)\right]=\frac{\cos\left[\tfrac{1}{2}(L_U-L_S)\right]}{\sin\left[\tfrac{1}{2}(L_U+L_S)\right]}\cot\left[\tfrac{1}{2}(\lambda_S-\lambda_U)\right]$$
$$\tan\left[\tfrac{1}{2}\left(\psi_{S/U}+\psi_{U/S}\right)\right]=\frac{\sin\left[\tfrac{1}{2}(L_U-L_S)\right]}{\cos\left[\tfrac{1}{2}(L_U+L_S)\right]}\cot\left[\tfrac{1}{2}(\lambda_S-\lambda_U)\right] \qquad \text{Eq 89}$$

Because the left-hand side of Eq 89 uses half-angle formulas, the sum and difference of $\psi_{U/S}$ and $\psi_{S/U}$ can be found uniquely in the range $(-\pi,\pi)$. Since $\psi_{U/S}$ and $\psi_{S/U}$ have opposite signs, the result of the arc tangent function will be correct for the sum but the difference may require adjustment by 2π.

Special cases: When $L_S = L_U$, the second line of Eq 89 yields $\psi_{S/U} = -\psi_{U/S}$ and the first line yields $\tan\left[\psi_{S/U}\right] = \cot[½(\lambda_S - \lambda_U)] \,/\, \sin[L_U]$. When $L_S = -L_U$, the first line of Eq 89 yields $\psi_{S/U} - \psi_{U/S} = \pi$ and the second line yields $\tan\left[\psi_{S/U}\right] = -\tan[½(\lambda_S - \lambda_U)] \,/\, \sin[L_U]$.

The remaining two Napier's Analogies yield the following espressions for the geocentric angle, which requiring chaining.

$$\tan\left[\tfrac{1}{2}\theta\right]=\frac{\cos\left[\tfrac{1}{2}\left(\psi_{S/U}-\psi_{U/S}\right)\right]}{\cos\left[\tfrac{1}{2}\left(\psi_{S/U}+\psi_{U/S}\right)\right]}\cot\left[\tfrac{1}{2}(L_U+L_S)\right]$$
$$\tan\left[\tfrac{1}{2}\theta\right]=\frac{\sin\left[\tfrac{1}{2}\left(\psi_{S/U}-\psi_{U/S}\right)\right]}{\sin\left[\tfrac{1}{2}\left(\psi_{S/U}+\psi_{U/S}\right)\right]}\tan\left[\tfrac{1}{2}(L_U-L_S)\right] \qquad \text{Eq 90}$$

Eq 89 and Eq 90, in reverse order, can also be used to solve what may be termed the complement of the Indirect problem of geodesy (Table 6, Row 19): Given the geocentric angle θ between points **U** and **S** and the path azimuth angles $\psi_{U/S}$ and $\psi_{S/U}$ at both points, what are the latitudes and the longitude differences for the points?

4.3 The Direct Problem of Geodesy

The Direct problem of geodesy, introduced in Subsection 1.2.2, is illustrated in Figure 17 (also see Figure 13). The known elements (values) of triangle **PUS** are side **PU** (½π - L_U) and side **US** (θ), and their included angle at **U** ($\psi_{S/U}$). In the taxonomy of Subsection 4.1.7, this problem falls under case (2) – a SAS (side-angle-side) situation.

The coordinates L_U and λ_U and the azimuth angle $\psi_{S/U}$

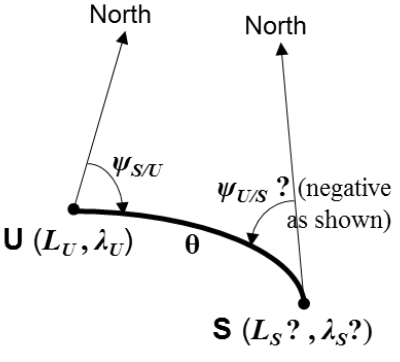

Figure 17 Direct Problem of Geodesy

define a great circle. The Direct problem is the determination of the coordinates of **S** which is a given distance θ from **U**.along that great circle Related problems are addressed in Sections 4.4, 4.5 and 4.6.

4.3.1 Computing the Satellite Latitude

Applying the spherical law of cosines for sides, where the unknown is the side **PS**, yields

$$\sin(L_S) = \sin(L_U)\cos(\theta) + \cos(L_U)\sin(\theta)\cos(\psi_{S/U}) \quad \text{Eq 91}$$

Latitude angles are restricted to the range [-π/2, π/2], so the principal value of the arc sine function always yields the correct solution to Eq 91. As checks: when $\psi_{S/U} = 0$, $L_S = L_U + \theta$; when $\psi_{S/U} = \pi$, $L_S = L_U - \theta$; and when $\psi_{S/U} = ½\pi$, $L_S = \arcsin[\sin(L_U)\cos(\theta)]$. Alternatives to Eq 91 for finding L_S are presented in Subsections 4.3.2 and 4.3.3.

4.3.2 Computing the Satellite Longitude

Finding the satellite longitude λ_S is more complex, as longitude angles are in the range [-π, π]. First, apply the spherical law of sines to the angels at **P** and **U**

$$\sin(\lambda_S - \lambda_U) = \frac{\sin(\psi_{S/U})\sin(\theta)}{\cos(L_S)} \quad \text{Eq 92}$$

Then apply the analogue to the law of cosines for sides

$$\cos(\lambda_S - \lambda_U) = \frac{\cos(L_U)\cos(\theta) - \sin(L_U)\sin(\theta)\cos(\psi_{S/U})}{\cos(L_S)} \quad \text{Eq 93}$$

Thus the satellite longitude can be found from

$$\tan(\lambda_S - \lambda_U) = \frac{\sin(\psi_{S/U})\sin(\theta)}{\cos(L_U)\cos(\theta) - \sin(L_U)\sin(\theta)\cos(\psi_{S/U})} \quad \text{Eq 94}$$

The right-hand side of the above equation only depends upon ‘given’ quantities for the Direct problem, and not on the solution for L_S. By employing a two-argument arc tangent function, the solution will yield a value of $\lambda_S - \lambda_U$ in the range [-π, π]. If this is added to a value of λ_U (also in the range [-π, π]), the result will be in the range [-2π, 2π]. Adjustments of ±2π must then be made to obtain a value of λ_S in the range (-π, π].

Two checks on Eq 94, assuming that $L_U = 0$ are: (1) if $\psi_{S/U} = 0$, then $\lambda_S = \lambda_U$; (2) if $\psi_{S/U} = \pm ½\pi$, then $\lambda_S = \lambda_U \pm \theta$.

Remarks:

- If Eq 92 and Eq 93 are squared and added, the result is .

$$\cos(L_S) = \sqrt{\left[\sin(\psi_{S/U})\sin(\theta)\right]^2 + \left[\cos(L_U)\cos(\theta) - \sin(L_U)\sin(\theta)\cos(\psi_{S/U})\right]^2} \qquad \text{Eq 95}$$

This expression for the satellite latitude is not well known, but may have a numerical advantage over Eq 91 when L_S is near a pole.

4.3.3 Computing the Path Azimuth at the Satellite

After L_S and λ_S have been found, the Direct problem solution can be completed by finding the azimuth of the great circle arc at the satellite's location, $\psi_{U/S}$, using Eq 87. An alternative approach that does not chain solutions is to first apply the law of sines,

$$\sin(\psi_{U/S}) = -\frac{\sin(\psi_{S/U})\cos(L_U)}{\cos(L_S)} \qquad \text{Eq 96}$$

A minus sign is present in Eq 96 because, for triangle **PUS**, the interior angle at **S** is $2\pi - \psi_{U/S}$. Subsection 4.6.2 elaborates on this topic.

Then apply the analogue to the law of cosines for sides

$$\cos(\psi_{U/S}) = \frac{\sin(L_U)\sin(\theta) - \cos(L_U)\cos(\theta)\cos(\psi_{S/U})}{\cos(L_S)} \qquad \text{Eq 97}$$

Thus

$$\tan(\psi_{U/S}) = \frac{-\cos(L_U)\sin(\psi_{S/U})}{\sin(L_U)\sin(\theta) - \cos(L_U)\cos(\theta)\cos(\psi_{S/U})} \qquad \text{Eq 98}$$

Remarks:

- Once L_S and λ_S have been found, $\psi_{U/S}$ may also be computed using Eq 87.
- If Eq 96 and Eq 97 are squared and added, an alternative expression to Eq 95 results:

$$\cos(L_S) = \sqrt{\left[\cos(L_U)\sin(\psi_{S/U})\right]^2 + \left[\sin(L_U)\sin(\theta) - \cos(L_U)\cos(\theta)\cos(\psi_{S/U})\right]^2} \qquad \text{Eq 99}$$

4.3.4 Alternate Solution Using Napier's Analogies

Referring to Figure 13 (with **P**=*B*, **S**=*A* and **U**=*C*), the two expressions on left-hand of Eq 76 (Napier's Analogies) yield

$$\tan\left[\tfrac{1}{2}(\lambda_S - \lambda_U - \psi_{U/S})\right] = \frac{\cos\left[\tfrac{1}{2}(\tfrac{1}{2}\pi - L_U - \theta)\right]}{\cos\left[\tfrac{1}{2}(\tfrac{1}{2}\pi - L_U + \theta)\right]}\cot\left[\tfrac{1}{2}\psi_{S/U}\right]$$

$$\tan\left[\tfrac{1}{2}(\lambda_U - \lambda_S - \psi_{U/S})\right] = \frac{\sin\left[\tfrac{1}{2}(\tfrac{1}{2}\pi - L_U - \theta)\right]}{\sin\left[\tfrac{1}{2}(\tfrac{1}{2}\pi - L_U + \theta)\right]}\cot\left[\tfrac{1}{2}\psi_{S/U}\right] \qquad \text{Eq 100}$$

Because both $\psi_{U/S}$ and $\lambda_S - \lambda_U$ lie in $(-\pi, \pi]$, both angles can be found uniquely by using other than the principal value of the arc tangent function. Using these results, either of the two right-hand expressions in Eq 76 yield the satellite latitude L_S

$$\tan\left[\frac{1}{2}\left(\frac{1}{2}\pi - L_S\right)\right] = \frac{\cos\left[\frac{1}{2}\left(\lambda_S - \lambda_U - \psi_{U/S}\right)\right]}{\cos\left[\frac{1}{2}\left(\lambda_U - \lambda_S - \psi_{U/S}\right)\right]} \tan\left[\frac{1}{2}\left(\frac{1}{2}\pi - L_U + \theta\right)\right]$$

$$\tan\left[\frac{1}{2}\left(\frac{1}{2}\pi - L_S\right)\right] = \frac{\sin\left[\frac{1}{2}\left(\lambda_S - \lambda_U - \psi_{U/S}\right)\right]}{\sin\left[\frac{1}{2}\left(\lambda_U - \lambda_S - \psi_{U/S}\right)\right]} \tan\left[\frac{1}{2}\left(\frac{1}{2}\pi - L_U - \theta\right)\right] \qquad \text{Eq 101}$$

Eq 100 and Eq 101 (in reverse order) can also be used to solve what may be termed the complement of the Direct problem of geodesy (Table 6, Row 5); also see Section 4.5.

- Given the latitude of point **S**, the longitude difference $\lambda_S - \lambda_U$ between points **U** and **S** the azimuth angle $\psi_{U/S}$ from **S** to **U**
- What is the latitude L_U of point **U**, the geocentric angle θ between **U** to **S** and the azimuth angle $\psi_{S/U}$ from **U** to **S**?

4.3.5 Remarks

Two applications of the equations in this section to 'real world' problems are

- Finding intermediate points on the trajectory from **U** to **S** (using Eq 91 and Eq 94) by replacing θ by $\mu\theta$, where $0 < \mu < 1$. A similar functionality that applies to the vector approach is described in Subsection 5.3.2.
- Determining the latitude and longitude of aircraft **S** using range/bearing measurements from a VOR/DME ground station **U** at a known location (Subsection 4.8.6).

For future reference, using Eq 91-Eq 93, Eq 95 and Eq 98, if $\theta = ½\pi$, then

$$\sin(L_S) = \cos(L_U)\cos\left(\psi_{S/U}\right) \qquad \cos(L_S) = \sqrt{\sin^2(\psi_{S/U}) + \sin^2(L_U)\cos^2(\psi_{S/U})}$$

$$\sin(\lambda_S - \lambda_U) = \frac{\sin(\psi_{S/U})}{\cos(L_S)} \qquad \cos(\lambda_S - \lambda_U) = -\frac{\sin(L_U)\cos(\psi_{S/U})}{\cos(L_S)}$$

$$\sin(\lambda_S) = \frac{\sin(\psi_{S/U})\cos(\lambda_U) - \sin(L_U)\cos(\psi_{S/U})\sin(\lambda_U)}{\sqrt{\sin^2(\psi_{S/U}) + \sin^2(L_U)\cos^2(\psi_{S/U})}}$$

$$\cos(\lambda_S) = -\frac{\sin(\psi_{S/U})\sin(\lambda_U) + \sin(L_U)\cos(\psi_{S/U})\cos(\lambda_U)}{\sqrt{\sin^2(\psi_{S/U}) + \sin^2(L_U)\cos^2(\psi_{S/U})}} \qquad \text{Eq 102}$$

$$\tan\left(\psi_{U/S}\right) = -\cot(L_U)\sin(\psi_{S/U})$$

4.4 A Modified Direct Problem: Path Azimuth at Satellite Known

In this modification to the Direct problem of geodesy (Section 4.3), the azimuth angle $\psi_{U/S}$ of the path at the satellite **S** toward the user **U** is known, while the azimuth angle $\psi_{S/U}$ of the path at **U** toward **S** is unknown (the opposite of the assumptions for these quantities in unmodified problem). In the taxonomy of spherical triangles in Subsection 4.1.7, this problem falls under case (3) – a SSA (side-side-angle) situation. In terms of the navigation triangle **UPS**, the known elements (values) are sides **UP** ($½\pi - L_U$) and **US** (θ) and angle **USP** ($2\pi - \psi_{U/S}$).

4.4.1 Computing the Satellite Longitude

The approach begins by applying the law of sines to triangle **UPS**

$$\sin(\lambda_S - \lambda_U) = -\frac{\sin(\theta)\sin(\psi_{U/S})}{\cos(L_U)} \qquad \text{Eq 103}$$

A minus sign is present on the right-hand side of Eq 103 because the interior angle of triangle **PUS** at **S** is $2\pi - \psi_{U/S}$ (Figure 13). In computing λ_S from Eq 103, two solutions are possible. One solution satisfies $|\lambda_S - \lambda_U| \leq \pi/2$, and the other satisfies $\pi/2 \leq |\lambda_S - \lambda_U| \leq \pi$. Except near the poles, the incorrect solution will typically require that the distance between **U** and **S** be much further than the correct solution, and often is not consistent with the sensors' ranges; thus, the correct solution can usually be deduced. It may be necessary to adjust λ_S to lie in (-π, π].

4.4.2 Computing the Satellite Latitude

The satellite latitude L_S is found from Napier's Analogies (Eq 76), using the solutions for λ_S obtained from Eq 103

$$\tan\left[\tfrac{1}{2}\left(\tfrac{\pi}{2} - L_S\right)\right] = \frac{\cos\left[\tfrac{1}{2}\left(\psi_{U/S} + \lambda_S - \lambda_U\right)\right]}{\cos\left[\tfrac{1}{2}\left(\psi_{U/S} - \lambda_S + \lambda_U\right)\right]} \tan\left[\tfrac{1}{2}\left(\tfrac{\pi}{2} - L_U + \theta\right)\right]$$

$$\tan\left[\tfrac{1}{2}\left(\tfrac{\pi}{2} - L_S\right)\right] = \frac{\sin\left[\tfrac{1}{2}\left(\psi_{U/S} + \lambda_S - \lambda_U\right)\right]}{\sin\left[\tfrac{1}{2}\left(\psi_{U/S} - \lambda_S + \lambda_U\right)\right]} \tan\left[\tfrac{1}{2}\left(\tfrac{\pi}{2} - L_U - \theta\right)\right] \qquad \text{Eq 104}$$

The two expressions in Eq 104 are mathematically equivalent, but one may be preferred numerically in some situations.

4.4.3 Computing the Azimuth of the Connecting Arc at the User

There are multiple ways to find the azimuth angle $\psi_{S/U}$. Napier's Analogies (Eq 76) is used because it raises the possibility of using the four-quadrant arc tangent function.

$$\tan\left[\frac{1}{2}\psi_{S/U}\right] = \frac{\cos\left[\frac{1}{2}\left(\theta - \frac{\pi}{2} + L_U\right)\right]}{\cos\left[\frac{1}{2}\left(\theta + \frac{\pi}{2} - L_U\right)\right]} \tan\left[\frac{1}{2}\left(\lambda_S - \lambda_U + \psi_{U/S}\right)\right]$$

$$\tan\left[\frac{1}{2}\psi_{S/U}\right] = \frac{\sin\left[\frac{1}{2}\left(\theta - \frac{\pi}{2} + L_U\right)\right]}{\sin\left[\frac{1}{2}\left(\theta + \frac{\pi}{2} - L_U\right)\right]} \tan\left[\frac{1}{2}\left(\lambda_S - \lambda_U - \psi_{U/S}\right)\right] \quad \text{Eq 105}$$

4.5 A Modified Direct Problem: Satellite Longitude Known

For this modification to the Direct problem of geodesy (Section 4.3), the longitude of satellite **S**, λ_S, is known, and the geocentric angle, θ, between the user **U** and satellite **S** is unknown. These are the reverse of the assumptions for these quantities in the Direct problem. In taxonomy of spherical triangles in Subsection 4.1.7, this problem falls under case (4) – an ASA (angle-side-angle) situation. The known elements (values) are angles **UPS** ($\lambda_S - \lambda_U$) and **SUP** ($\psi_{S/U}$) and their included side **UP** (½π - L_U). Subsection 4.3.4 addesses this problem using Napier's Analogies; a different approach is used here.

In the development below, it is assumed that $\lambda_S \neq \lambda_U$, because when $\lambda_S = \lambda_U$ there is either no solution ($\psi_{S/U} \neq 0$ and $\psi_{S/U} \neq \pi$) or an infinite number of solutions. With this assumption, the problem is well-posed, since every non-meridian great circle crosses every line of longitude exactly once.

4.5.1 Computing the Satellite Latitude

The latitude L_S is found from the four-part cotangent formula (Eq 75)

$$\tan(L_S) = \frac{\sin(L_U)\cos(\lambda_S - \lambda_U) + \sin(\lambda_S - \lambda_U)\cot(\psi_{S/U})}{\cos(L_U)} \quad \text{Eq 106}$$

When using the arc tangent function, L_S can be unambiguously found in (-π/2, π/2).

4.5.2 Computing the Geocentric Angle

The geocentric angle θ is found from the four-part cotangent formula (Eq 75)

$$\cot(\theta) = \frac{\sin(L_U)\cos(\psi_{S/U}) + \sin(\psi_{S/U})\cot(\lambda_S - \lambda_U)}{\cos(L_U)} \quad \text{Eq 107}$$

When using the arc cotangent function, θ can be unambiguously found in (0, π).

4.5.3 Computing the Azimuth of the Connecting Arc at the Satellite

The azimuth angle $\psi_{U/S}$ is found without chaining from the law of cosines for angles (Eq 72)

$$\cos(\psi_{U/S}) = \sin(\psi_{S/U})\sin(\lambda_S - \lambda_U)\sin(L_U) - \cos(\psi_{S/U})\cos(\lambda_S - \lambda_U) \quad \text{Eq 108}$$

Using the arc cosine function, $\psi_{U/S}$ can be found uniquely in either [0, π] or [-π, 0], whichever of the two ranges does not contain $\psi_{S/U}$ (see Eq 110 and associated discussion). Using chaining, $\psi_{U/S}$ can also be found unambiguously from the four-quadrant arc tangent function.

$$\tan(\psi_{U/S}) = \frac{\cos(L_U)\sin(\lambda_S - \lambda_U)}{\sin(\theta)\left[\sin(\psi_{S/U})\sin(\lambda_S - \lambda_U)\ \sin(L_U) - \cos(\psi_{S/U})\cos(\lambda_S - \lambda_U)\right]} \quad \text{Eq 109}$$

4.6 The Hybrid Problem of Geodesy

4.6.1 Problem Characterization

For this modification to the Direct problem of geodesy (Section 4.3), the latitude L_S of satellite **S** is known, and the geocentric angle θ between the user **U** and satellite **S** is unknown. These are the reverse of the assumptions for these quantities in the Direct problem. In the taxonomy of mathematical spherical triangle problems (Subsection 4.1.7), this situation falls under case (3) – a SSA (side-side-angle) situation. Referring to Figure 13,the known elements (values) are sides **PU** ($½\pi - L_U$) and **PS** ($½\pi - L_S$) and angle **PUS** ($\psi_{S/U}$). The user's longitude λ_U is not used in solving the mathematical triangle, but is used in situating that triangle on the earth's surface.

This problem, which has been termed the Hybrid problem of geodesy, may not have a solution. The reason is that, except a meridian, every great circle has a maximum latitude L_{max} and minimum latitude $-L_{max}$. If the $|L_{max}|$ associated with a specified L_U and $\psi_{S/U}$ is less than the specified $|L_S|$, then a solution does not exist.

Conversely, if the $|L_{max}|$ associated with a specified L_U and $\psi_{S/U}$ is larger than the specified $|L_S|$, then two solutions exist. Solutions pairs are symmetric in longitude about λ_{max}, the longitude corresponding to L_{max}. For convenience, assume that $L_U > 0$:

- **When $0 < \psi_{S/U} < \frac{1}{2}\pi$**: If $L_U < L_S < L_{max}$, there is a solution pair with both satisfying $0 < \lambda_S - \lambda_U < \pi$; if $L_U = L_S$, there is one solution satisfying $0 < \lambda_S - \lambda_U < \pi$ (**U** is the other 'solution' in the pair); if $-L_U < L_S < L_U$, there is a solution pair with one satisfying $0 < \lambda_S - \lambda_U < \pi$ and one satisfying $-\pi < \lambda_S - \lambda_U < 0$; if $-L_{max} < L_S < -L_U$, there is a solution pair with both satisfying $-\pi < \lambda_S - \lambda_U < 0$.
- **When $\frac{1}{2}\pi < \psi_{S/U} < \pi$**: If $L_U < L_S < L_{max}$, there is a solution pair with both satisfying $-\pi < \lambda_S - \lambda_U < 0$; if $L_U = L_S$, there is one solution satisfying $-\pi < \lambda_S - \lambda_U < 0$ (**U** is the other 'solution' in the pair); if $-L_U < L_S < L_U$, there is a solution pair with one satisfying $0 < \lambda_S - \lambda_U < \pi$ and one satisfying $-\pi < \lambda_S - \lambda_U < 0$; if $-L_{max} < L_S < -L_U$, there is a solution pair with both satisfying $0 < \lambda_S - \lambda_U < \pi$.

4.6.2 Computing the Azimuth of the Connecting Arc at the Satellite

The solution approach begins by applying the law of sines to find $\psi_{U/S}$

$$\sin(\psi_{U/S}) = -\frac{\cos(L_U)\sin(\psi_{S/U})}{\cos(L_S)} \qquad \text{Eq 110}$$

As in Eq 103, a minus sign is present on the right-hand side of Eq 110. Thus, Eq 110 requires that if $0 < \psi_{S/U} < \pi$ then $-\pi < \psi_{U/S} < 0$, and vice versa.

The absolute value computed for the right-hand side of Eq 110 can be: (a) greater than unity (in which case there is no solution, as $|L_S| > L_{max}$); (b) equal to unity (in which case there is one solution, as $|L_S| = L_{max}$); and (c) less than unity (in which case there usually two solutions, as $|L_S| < L_{max}$). If (c) is true, label the two possible solutions $\psi_{U/S,1}$ and $\psi_{U/S,2}$ and proceed. If (b) is true, proceed assuming $\psi_{U/S,1} = \psi_{U/S,2}$ (also, refer to Section 4.7).

4.6.3 Computing the Satellite Longitude

For the two solutions for $\psi_{S/U,i}$ found in Eq 110, the corresponding longitudes $\lambda_{S,i}$ are found using Napier's Analogies (Eq 76) applied to triangle **PUS**.

$$\tan\left[\tfrac{1}{2}(\lambda_{S,i} - \lambda_U)\right] = \frac{\cos\left[\tfrac{1}{2}(L_U - L_S)\right]}{\sin\left[\tfrac{1}{2}(L_U + L_S)\right]}\cot\left[\tfrac{1}{2}(\psi_{S/U} - \psi_{U/S,i})\right]$$

$$\tan\left[\tfrac{1}{2}(\lambda_{S,i} - \lambda_U)\right] = \frac{\sin\left[\tfrac{1}{2}(L_U - L_S)\right]}{\cos\left[\tfrac{1}{2}(L_U + L_S)\right]}\cot\left[\tfrac{1}{2}(\psi_{S/U} + \psi_{U/S,i})\right] \qquad \text{Eq 111}$$

Because a half-angle formula is used on the left-hand side of Eq 111, given a value for $\psi_{U/S,i}$, each solution for $\lambda_{S,i}$ can be unambiguously found in the range $(\lambda_U, \lambda_U \pm \pi)$. Selecting between the two expressions in Eq 111 can be based on numerical behavior. Limiting cases are:

- **North-South Path** — For both expressions, the cotangent function fails on a perfect north-south route ($\psi_{S/U} = 0$ or $\psi_{S/U} = \pi$). By inspection, in this situation $\lambda_S = \lambda_U$; handling it as a special-case is one way to address it.
- **'East-West' Path** — When $L_S = L_U$, then $\psi_{U/S} = -\psi_{S/U}$ and the second expression in Eq 111 reduces to the indeterminate form $0 \times \infty$. However, the first expression yields the correction solution: $\tan\left[\frac{1}{2}(\lambda_S - \lambda_U)\right] = \cot\left[\psi_{S/U}\right]/\sin[L_U]$. (The last expression reduces to the indeterminate form $0 \times \infty$ at the equator, as there is not a unique solution then.)

4.6.4 Computing the Geocentric Angle

The geocentric angle θ is found from 'the other half' of Napier's Analogies (Eq 76), again using the solutions for $\psi_{S/U}$ found using Eq 110.

$$\tan\left[\tfrac{1}{2}\theta_i\right] = \frac{\cos\left[\tfrac{1}{2}\left(\psi_{S/U} - \psi_{U/S,i}\right)\right]}{\cos\left[\tfrac{1}{2}\left(\psi_{S/U} + \psi_{U/S,i}\right)\right]} \cot\left[\tfrac{1}{2}(L_U + L_S)\right]$$

$$\tan\left[\tfrac{1}{2}\theta_i\right] = \frac{\sin\left[\tfrac{1}{2}\left(\psi_{S/U} - \psi_{U/S,i}\right)\right]}{\sin\left[\tfrac{1}{2}\left(\psi_{S/U} + \psi_{U/S,i}\right)\right]} \tan\left[\tfrac{1}{2}(L_U - L_S)\right] \qquad \text{Eq 112}$$

The choice between the two expressions in Eq 112 can be based on the numerical behavior and avoidance of singularities. Limiting cases are:

- **North-South Path** —If $\psi_{S/U} = 0$ then $\psi_{U/S} = \pi$, and vice versa. In both cases, the fraction in the first expression reduces to the indeterminate form 0/0. However, for either direction of travel, the second expression yields the correction solution, $\theta = |L_U - L_S|$.
- **'East-West' Path** — When $L_S = L_U$, then $\psi_{U/S} = -\psi_{S/U}$ and the second expression reduces to the indeterminate form 0/0. However, the first expression yields the correction solution (Subsection 4.2.3), $\tan\left[\tfrac{1}{2}\theta_i\right] = \cos\left[\psi_{S/U}\right]\cot[L_U]$. (This expression reduces to the indeterminate form $0 \times \infty$ at the equator, because there is not a unique solution in that situation.)

4.6.5 Remarks

- Unlike the solution for the Direct problem of geodesy (Section 4.3), the solution sequence here involves chaining (which is typical of SSA problems). Thus, $\psi_{U/S}$ must be found, even if it is not needed.
- One way this problem could arise in aviation is using a sextant to measure latitude ('shoot' the North Star) and using a VOR to measure $\psi_{S/U}$.
- While the topic of lines (or surfaces) of position is deferred to Chapter 6, it's clear that for this set of known quantities, the geometry favors (approximately) north-south routes. On (approximately) east-west routes, the latitude and bearing information are close to being redundant while there is little information about change in east-west location.
- With minimal modifications, the analysis of this section applies to the problem where $\psi_{U/S}$ is known, rather than $\psi_{S/U}$. The only explicit change in the above equations is that Eq 110 is modified to place $\psi_{S/U}$ on the left-hand side.

4.7 Vertices of a Great Circle

4.7.1 Clairaut's Equation

A special case of Clairaut's equation* applies to great circles (i.e., encircling the earth), and can be simply derived by applying the law of sines to 'mathematical' triangle **UPS**. The result is:

$$\cos(L_U)\sin\left(\psi_{S/U}\right) = -\cos(L_S)\sin\left(\psi_{U/S}\right) \qquad \text{Eq 113}$$

The minus sign occurs in Eq 114 because the interior angle at **S** is $2\pi - \psi_{U/S}$ and

* Alexis Claude de Clairaut (or Clairault) (1713 –1765) was a prominent French mathematician, astronomer and geophysicist.

$\sin(2\pi - \psi_{U/S}) = -\sin(\psi_{U/S})$. So at all points on a great circle, when moving in one direction:

$$\cos(L)\sin(\psi) = C \quad , \quad C \text{ a constant} \qquad \text{Eq 114}$$

Clearly, $|C| \leq 1$; C is positive for eastward routes and negative for westward routes. Satisfying Eq 114 is a necessary, but not sufficient, condition for the path to be a great circle — e.g., a counterexample is a constant-latitude route.

4.7.2 Great Circle Vertex Latitude

A common application of Eq 114 is finding the northern-most and southern-most latitudes of a full great circle — termed 'vertices' in Ref. 1. At a vertex, $\sin(\psi) = \pm 1$, so if the latitude L_U and azimuth $\psi_{S/U}$ of one point on a great circle are known:

$$\cos(L_{max}) = \cos(L_U)\left|\sin\left(\psi_{S/U}\right)\right| = |C| \qquad \text{Eq 115}$$

The great circle lies in a plane containing the center of the earth **O**. L_{max} is the angle between the great circle plane and the equatorial plane (and $|C|$ is the cosine of that angle). The latitude of the Southern Hemisphere vertex is $-L_{max}$.

If two points **U** (L_U, λ_U) and **S** (L_S, λ_S) on a great circle are known, the Indirect problem of geodesy can be used to find $\psi_{S/U}$; then Eq 115 can be used to find L_{max}. An alternative is to use the Indirect problem to find the geocentric angle θ_{US} between **U** and **S**; then $\psi_{S/U}$ can be found in terms of θ_{US} using Eq 84 and the result substituted into Eq 115:

$$\cos(L_{max}) = \left|\frac{\cos(L_U)\cos(L_S)\sin(\lambda_S - \lambda_U)}{\sin(\theta_{US})}\right| \qquad \text{Eq 116}$$

With L_{max}, the geocentric angle θ_{UV} between **U** and the vertex **V** can be found from the law of cosines applied to triangle **UPV** with a right-angle at **V** (where L_U may be positive or negative)

$$\cos(\theta_{UV}) = \frac{\sin(L_U)}{\sin(L_{max})} \qquad \text{Eq 117}$$

4.7.3 Great Circle Azimuth Angles

At the two points displaced in longitude by ±π/2 from a vertex, the great circle crosses the equator. There $\sin(\psi) = C$, so $|\psi| = \frac{1}{2}\pi \pm L_{max}$. For an eastward route, ψ satisfies $\frac{1}{2}\pi - L_{max} \leq \psi \leq \frac{1}{2}\pi + L_{max}$; for a westward route, $-\frac{1}{2}\pi - L_{max} \leq \psi \leq -\frac{1}{2}\pi + L_{max}$.

4.7.4 Great Circle Vertex Longitude

The longitude λ_{max} corresponding to L_{max} can be found unambiguously using equations from

Section 4.6. At vertex **V**, the path azimuth ψ is $\pm\pi/2$. If **V** is thought of as **S**, the sign of what would be $\psi_{U/S}$ is the opposite of the sign of $\psi_{S/U}$. Thus from Eq 111:

$$\tan\left[\tfrac{1}{2}(\lambda_{max}-\lambda_U)\right]=\frac{\cos\left[\tfrac{1}{2}(L_U-L_{max})\right]}{\sin\left[\tfrac{1}{2}(L_U+L_{max})\right]}\cot\left[\tfrac{1}{2}\left(\psi_{S/U}+\mathrm{sgn}(\psi_{S/U})\tfrac{1}{2}\pi\right)\right]$$

$$\tan\left[\tfrac{1}{2}(\lambda_{max}-\lambda_U)\right]=\frac{\sin\left[\tfrac{1}{2}(L_U-L_{max})\right]}{\cos\left[\tfrac{1}{2}(L_U+L_{max})\right]}\cot\left[\tfrac{1}{2}\left(\psi_{S/U}-\mathrm{sgn}(\psi_{S/U})\tfrac{1}{2}\pi\right)\right] \qquad \text{Eq 118}$$

The longitude of the Southern Hemisphere vertex is $\lambda_{max}\pm\pi$. An expression for λ_{max} that does not involve chaining from the solution for L_{max} is derived by vector analysis in Chapter 5 (Eq 156).

Using geocentric angle θ_{UV}, an alternative but ambiguous expression for λ_{max} can found using the law of sines

$$\sin(\lambda_{max}-\lambda_U)=\frac{\sin(\theta_{UV})}{\cos(L_U)} \qquad \text{Eq 119}$$

4.7.5 Conditions for a Path Containing a Vertex

As stated in Section 4.6, not all great circle paths connecting points **U** and **S** pass through the vertex at (L_{max},λ_{max}) or its Southern Hemisphere counterpart. To pass through a vertex, the route between **U** and **S** must have enough of a change in longitude to bend towards, and away from, a pole. The path between **U** and **S** will pass through (L_{max},λ_{max}) if the absolute values of the azimuth angles at **U** and **S** are both less than 90 deg:

$$|\psi_{S/U}|<\tfrac{1}{2}\pi \quad \text{and} \quad |\psi_{U/S}|<\tfrac{1}{2}\pi \qquad \text{Eq 120}$$

In this situation, the great circle route connecting **U** and **S** will pass closer to the North Pole than either end point, **U** or **S**.

The great circle route connecting **U** and **S** will pass closer to the South Pole than either **U** or **S** if the absolute values of both azimuth angles are obtuse

$$|\psi_{S/U}|>\tfrac{1}{2}\pi \quad \text{and} \quad |\psi_{U/S}|>\tfrac{1}{2}\pi \qquad \text{Eq 121}$$

4.8 Example Applications

The example applications presented at the end of Chapter 3 are extended in the first three (of the seven) subsections below. These demonstrate the capabilities of spherical trigonometry to provide more complete solutions to problems. Then, four examples are added — flight route planning, display of radar measurements, determining an aircraft's coordinates from a single VOR/DME station and the error in modeling the ellipsoidal earth as a sphere.

4.8.1 Example 1, Continued: En Route Radar Coverage

Predictions of radar visibility of aircraft as a function of the aircraft's range and altitude, introduced in Subsection 3.7.1, are useful. However, for a specific radar installation, a more valuable analysis product is a depiction of the radar's altitude coverage overlaid on a map. As an example, the ARSR-4/ATCBI-6 installation at North Truro, MA (FAA symbol: QEA) is selected. Associating **U** with the radar location, its coordinates are L_U = 42.034531 deg and λ_U = -70.054272 deg, and its antenna elevation is h_U = 224 ft MSL. Assumming that the terrain elevation in the coverage area is 0 ft MSL, which is correct for the nearby ocean and optimistic (i.e., terrain blocking is not considered) for the nearby land.

Associating **S** with the aircraft location,the sequence of calculations is:

- Using Eq 68 (third line), the radar's minimum usable elevation angle is found to be $\alpha_{\min} = -0.230$ deg
- Aircraft altitudes h_S of 3,000 ft, 10,000 ft and 25,000 ft MSL are selected for the contours to be depicted.
- Using Eq 68 (second line), the geocentric angles θ corresponding to the selected altitudes are found. The associated ground ranges $R_e\,\theta$ are 85.7 NM, 141.2 NM and 212.6 NM, respectively.
- Using Eq 68 (first line), the minimum visible aircraft altitude at the radar's maximum ground range of 250 NM is found to be h_S = 35,590 ft.
- A set of equally spaced azimuth angles $\psi_{S/U}$ are selected for the radials from the radar **U** to each point **S** on a coverage contour
- For the geocentric angle θ corresponding to each contour, and for each azimuth angle $\psi_{S/U}$, the latitude/longitude (L_S, λ_S) of the corresponding point **S** on the contour are found from Eq 91 and Eq 94.

The result of performing the above steps for the North Truro radar system is shown in Figure 18. (An alternative method for finding coverage contours is described in Subsection 4.8.3. The method described immediately above can be adapted to situations where terrain blocking must be considered, while the method of Subsection 4.8.3 cannot, but is more efficient.)

Significance of contours: (a) Inside a contour, aircraft having altitudes equal to or greater than the contour value are visible to the radar; and (b) Outside the contour, aircraft having altitudes less than the contour value are not visible to the radar. The contours in Figure 18 appear as circles, but that is not true in every case. When terrain is not accounted for, the contours appear smooth, but their shape depends upon the map projection employed. When a terrain blocking is accounted for, the contours are irregular/jagged.

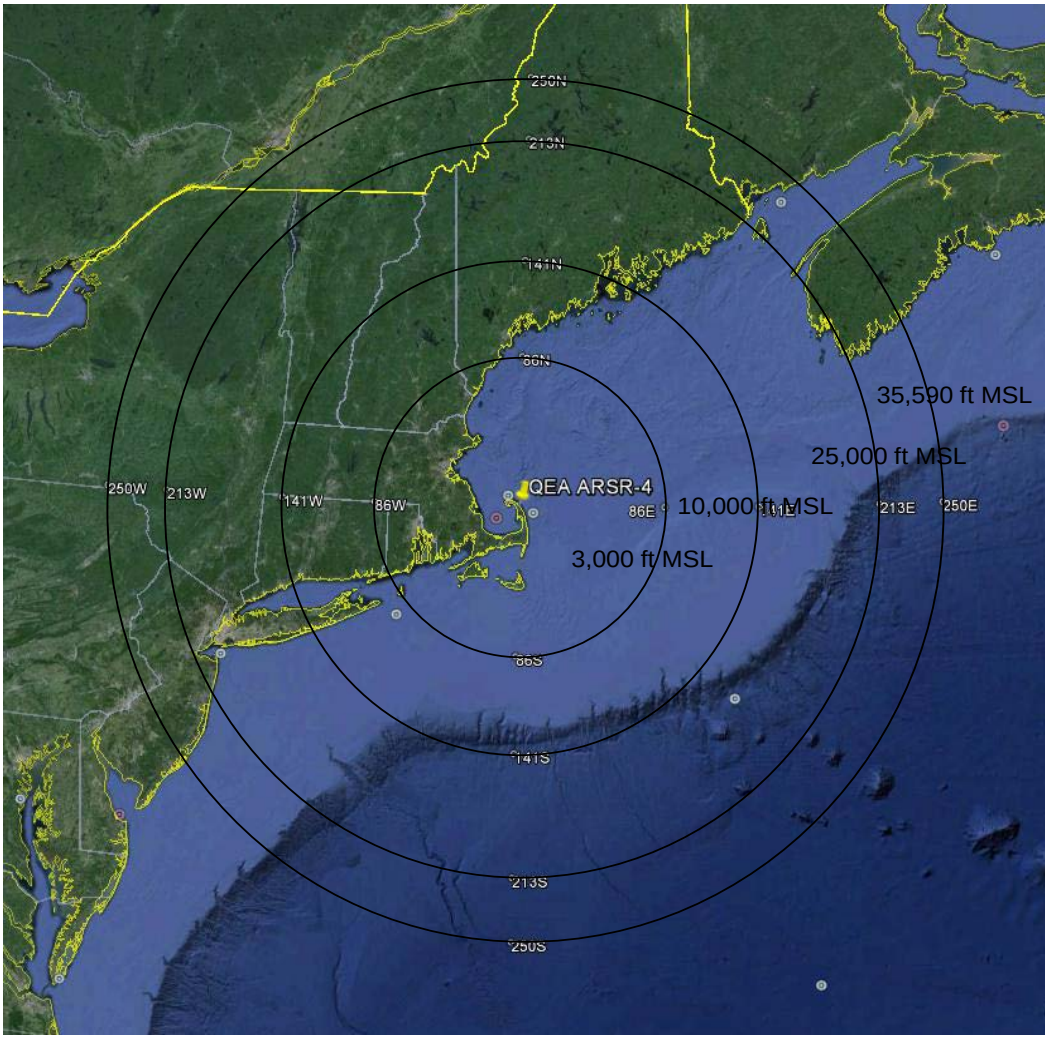

Figure 18 Aircraft Altitude Visibility Contours for the North Truro, MA, Radar System

Consistency Check — The primary purposes of QEA are (1) surveillance of higher altitude airspace, for use by ARTCC controllers; and (2) surveillance of much of the New England off shore airspace, for use by the Department of Defense (DoD). A third purpose is backup surveillance of the Boston TRACON airspace; horizontally, this airspace is a circle centered on Logan Airport with a radius of 60 NM. Boston TRACON controllers have stated that they consider QEA coverage to extend upward from an altitude of 3,000 ft MSL. Figure 18 is consistent with that statement.

Cone of Silence — As discussed in Subsection 3.7.1, ATC radars usually have a cone of silence directly above the antenna; aircraft within this (relatively small) cone may not be detectable. Following the usual practice, contours for QEA's cone of silence are not shown in Figure 18.

The U.S. has an extensive ATC radar infrastructure. Generally, one radar station's cone of silence will be within the coverage area of one or more other radars. In the case of QEA, the

Boston ARTCC also receives feeds from: the Nantucket, MA, terminal radar (46.5 NM from QEA, at essentially sea level), which covers QEA's cone of silence down to approximately 500 ft MSL; and the Cummington, MA, en route radar (132.1 NM from QEA, at an elevation of 2,000 ft MSL) which covers QEA's cone of silence down to approximately 5,000 ft MSL.

4.8.2 Example 2, Continued: Aircraft Precision Approach Procedure

Subsection 3.7.2 illustrates computation of the flight profile (altitude vs. distance from threshold) for an aircraft precision approach procedure. However, for the procedure to be used operationally, the coordinates of the fixes are needed by ATC personnel. Computing them is a straightforward application of spherical geometry.

The sequence of calculations is as follows:

- Using the FAA's National Flight Data Center (NFDC, Ref. 32) or the AirNav (Ref. 33) websites, the latitudes and longitudes of the ends of KMCI runway 19L / 1R are obtained.
- Associating **U** with the 1R end and **S** with the 19L end of the runway, the azimuth of the approach course in the direction away the 19R end is computed, using Eq 86, to be $\psi_{S/U}$ = 12.89 deg
- Associating **U** with the 19R end of the runway and **S** with the fix locations, the coordinates of the fixes are found using Eq 91 and Eq 94.

The results of carrying out steps 1-3 are shown in Table 7.

Table 7 Computed Fix Coordinates for MCI Runway 19L LPV Approach

Fix Name	UMREW	FELUR	REMNS	ZASBO	YOVNU	GAYLY
Range from Threshold, NM	1.9	4.9	6.2	9.3	12.4	15.5
Latitude, deg	39.337737	39.386470	39.407586	39.457940	39.508292	39.558642
Longitude, deg	-94.692345	-94.677907	-94.671645	-94.656696	-94.641725	-94.626732

4.8.3 Example 3, Continued: Satellite Visibility of/from Earth

Extending the analysis in Subsection 3.7.3 to calculating the latitude/longitude coordinates of the perimeter of the footprint of a geostationary satellite is an example of the application of the topics in this chapter. Geostationary satellites are approximated as having circular orbits and being positioned above the earth's equator. Their altitudes are selected so that their orbital speed matches the earth's rotation rate. Thus, from the earth, they appear to be stationary.

The Wide Area Augmentation System (WAAS) satellites (which augment the Global Positioning System (GPS)) are chosen for this example. The FAA currently operates three geostationary WAAS satellites (Ref. 34) in order to satisfy the requirements of demanding civil aviation operations — e.g., precision approaches similar to ILS Category I.

This analysis is done in two distinct steps. The first step (discussed in Subsection 3.7.3) is to find the geocentric angle θ from the nadir **N** (of satellite **S**) to user **U** on the perimeter of the foot-print. The parameters used in this calculation are:

- Satellite altitude $h_S = 35{,}786{,}000$ m $= 19{,}323$ NM
- Mask angle $\alpha = 5$ deg
- Radius of the earth $R_e = 6{,}378{,}137$ m $= 3{,}444$ NM (Eq 23)

Substituting these values into Eq 40 yields θ = 76.3 deg. Thus the a user **U** on the earth's surface can be up to 76.3 deg (in terms of the geocentric angle) away from the satellite nadir **N** and WAAS satellite will be visible. Since geostationary satellites are directly above the equator, the maximum user latitudes with visibility are ±76.3 deg if the user is at the same longitude as the satellite. Similarly, if the user is on the equator, the longitude extremes at which the satellite is visible are ±76.3 deg from the satellite longitude.

The second step of the analysis is obtaining the latitude/longitude coordinates (L_U, λ_U) of an arbitrary point **U** on the perimeter of the visible region. This step can be done in at least two ways. One way, described in Subsection 4.8.1, utilizes Eq 91 and Eq 94 (with subscript U replaced by N, and subscript S replaced by U).

An alternative method for finding the coordinates of coverage perimeter locations employs a modified version of Eq 81. Taking the coordinates of the satellite nadir to be (L_N, λ_N), where $L_N = 0$, for a given (or assumed) user latitude L_U, the corresponding user longitude λ_U given by

$$\lambda_U = \lambda_N \pm 2 \arcsin\left(\sqrt{\frac{\sin^2\left(\frac{1}{2}\theta\right) - \sin^2\left(\frac{1}{2}(L_U)\right)}{\cos(L_U)}}\right) \qquad \text{Eq 122}$$

Using Eq 122 and a set values is assumed for L_U in the interval [-θ, θ], the corresponding two sets of values for λ_U are computed (which are symmetrically located about λ_N).

The WAAS satellite labels and longitudes are: AMR, -98 deg; CRE, -107.3 deg; and CRW, -133 deg. After the calculations of Eq 122 are carried out, the results are depicted in Figure 19. For context, the locations of a few airports are also shown in Figure 19. Ref. 34 has a page, "WAAS GEO Footprint", which contains a figure that is similar to Figure 19.

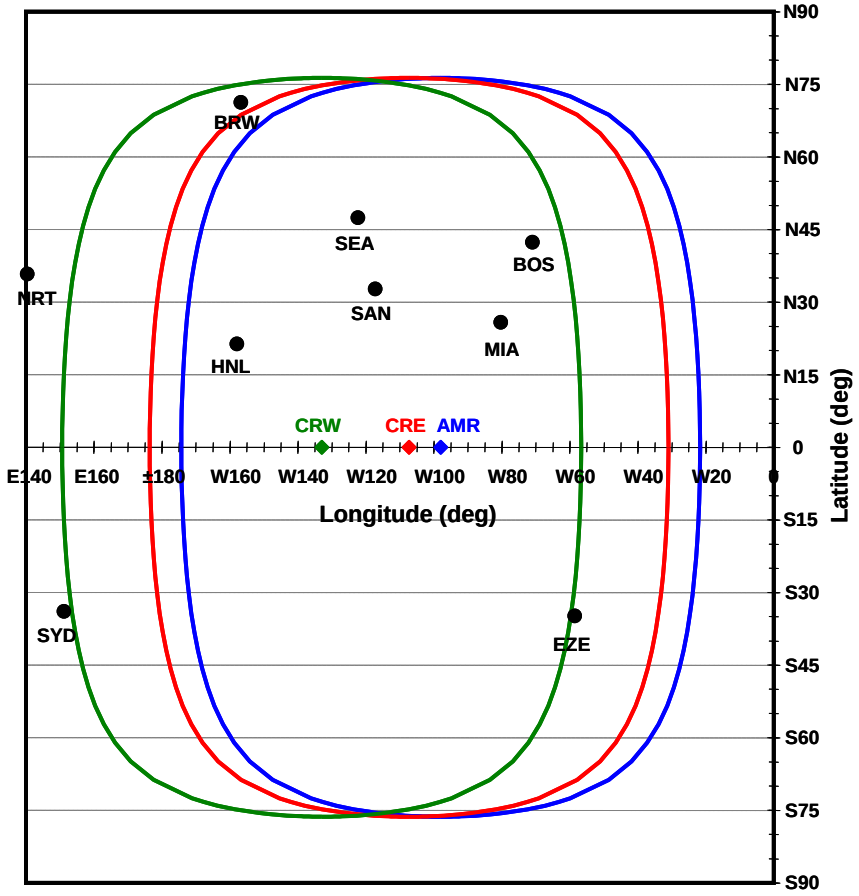

Figure 19 WAAS Satellite Visibility Contours for 5 deg Mask Angle

4.8.4 Example 4: Great Circle Flight Route

For many reasons — e.g., siting of ground-based communications, navigation and surveillance equipment; estimation of fuel consumption; positioning of search and rescue assets; and analysis of flight routes — there is a need to calculate path distances between any two locations on the earth. Such calculations are a straightforward application of the equations presented earlier in this chapter. The basic approach is: (a) solve the Indirect problem of geodesy (Section 4.2), so that geocentric angle (i.e., path length) and the azimuth angles of the path end points are known; then (b) divide the path into equal-length segments and solve the Direct problem of geodesy (Section 4.3) for each segment, starting at one end of the path and progressing to the other.

The result of carrying out these steps for the route between the Boston Logan (BOS) and Tokyo Narita (NRT) airports is shown in Figure 20. This figure employs Cartesian coordinates to display longitude on the abscissa (which is effectively a Mercator scaling) versus latitude on the ordinate utilizing equal map distances for equal angles (which is not Mercator scaling). In addition to showing the great circle flight path for a spherical earth model (green curve), Figure 20 also shows the shortest path for an ellipsoidal earth model using Vincenty's algorithm

(Subsection 2.2.3). On this graphic, the separation between the curves is not perceptible. The largest separation occurs at the highest latitude, where the ellipsoidal-earth path latitude is 0.06 deg greater than the great circle/spherical earth path.

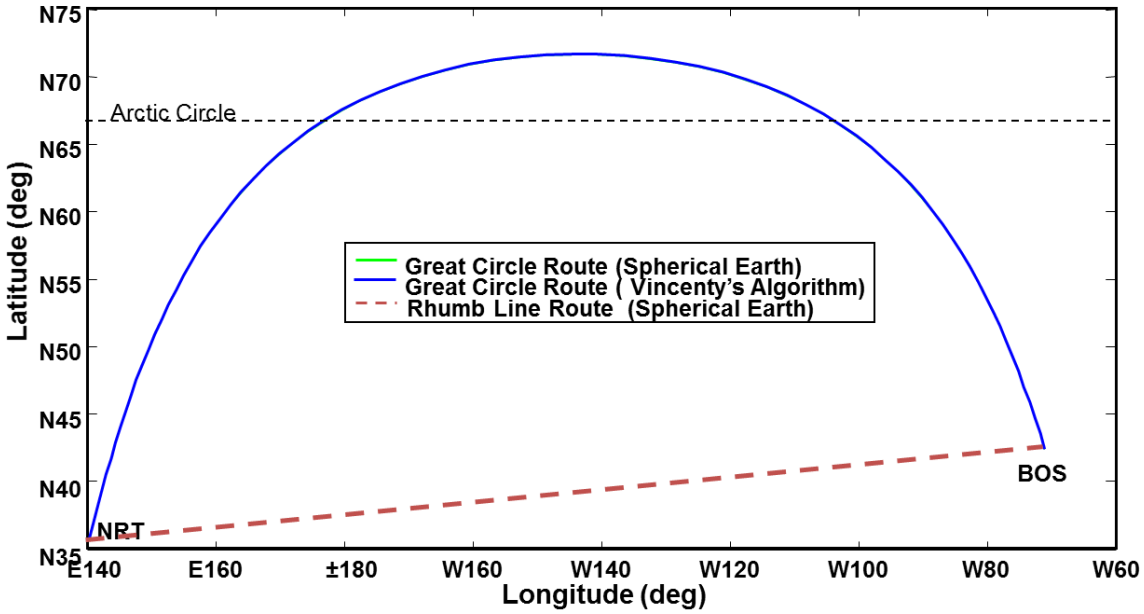

Figure 20 Mercator-Like View of BOS-NRT Great Circle and Rhumb Line Routes

For the great circle/spherical earth route; the azimuth angle at BOS is 334.8 (-25.2) deg, the azimuth angle at NRT is 22.8 deg, and the geocentric angle is θ = 1.689 rad, or 53.8% of π rad (π rad being the longest possible great circle route). The computed distance (using the earth radius defined in Eq 31) is 5,810.4 NM, while the distance computed using Vincenty's algorithm is 5,823.5 NM. The ellipticity error for the spherical-earth path length is 0.2%.

The trajectory's northern-most latitude is N71.7 deg (Eq 116), which occurs at a longitude of W143.42 deg. Equations from Section 4.6 predict that the trajectory crosses the Arctic Circle (N67 deg latitude) at longitudes of W104.7 deg and E177.9 deg. The trajectory is within the Arctic Circle for 29.2% of its length, although in Figure 20 it appears to be a larger fraction because the convergence of longitude lines at the Pole is not depicted.

Figure 20 also shows the course from BOS to NRT for the rhumb line (constant azimuth angle) method historically used for marine navigation (Section 9.3). The azimuth angle for a rhumb line from BOS to NRT is 266.7 (-93.3) deg. The rhumb line path is 19% or 1,106.7 NM longer than the great circle route calculated using Vincenty's algorithm.

Figure 21 depicts a polar view of the great circle and rhumb line routes. For this perspective, (a) the great circle route is almost a straight line while the rhumb line route is circular, and (b) the difference in the lengths of the paths is obvious.

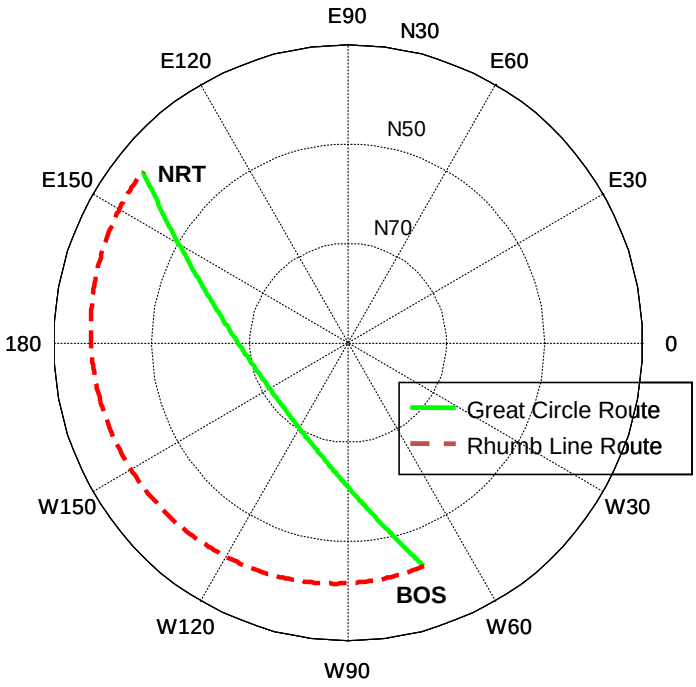

Figure 21 Polar View of BOS-NRT Great Circle and Rhumb Line Routes

Contrasting Figure 20 and Figure 21 illustrates value of matching the charting technique to the method for defining a route. Figure 20 is similar to a Mercator projection*, with both having the property that rhumb lines are straight; and Figure 21 similar to a gnomonic projection†, which has the property that great circles are depicted as straight lines. Mercator projections were preferred for maritime navigation before the equivalent of autopilots were available, while gnomonic projections are preferred for aircraft navigation.

The BOS-NRT city pair has all three factors that favor great circle navigation over rhumb line navigation: widely separated origin and destination, approximately co-latitude origin and destination, and the end points are at mid-latitudes. A contrasting route is Boston (BOS) - Buenos Aires (EZE). It has a roughly similar length, but is oriented north-south. For BOS-EZE the rhumb line path is 0.007% (0.3 NM) longer than the great circle path.

4.8.5 Example 5: Radar Display Coordinate Transformations

In this subsection, an ATC radar is associated with the user **U** and an aircraft under surveillance with the satellite **S**. The radar's installation information will include:

* For a true Mercator projection, the displayed linear distance between equal latitude angular increments as well as between equal longitude angular increments increases towards the poles.

† For a true gnomonic projection, the displayed linear distance between equal latitude increments increases toward the equator.

L_U – Radar latitude
λ_U – Radar longitude
h_U – Radar antenna elevation above sea level

For each scan (antenna revolution), a secondary surveillance radar provides three quantities concerning an aircraft:

$\psi_{S/U}$ – Aircraft azimuth relative to North (determined from the antenna direction)
d – Slant-range between the aircraft and the radar (determined from interrogation-reply time)
h_S – Aircraft barometric elevation above sea level (reported by the aircraft transponder).

Some long-range radars may correct for propagation phenomena (e.g., refraction), but those capabilities are not addressed here.

The first goal in ATC radar display is to accurately depict the horizontal separation between aircraft pairs. When two aircraft are only separated vertically (i.e., are at the same latitude and longitude) then their screen icons should overlay each other — or at least be close in comparison to the minimum allowable separation. Figure 22 illustrates the effect of directly displaying the slant-range of two aircraft that are only separated vertically (although it exaggerates the effect). Without altitude or elevation angle information, this may be the best that can be done. Partly for this reason, aircraft operating in busy airspace are required to have a Mode C capable transponder.

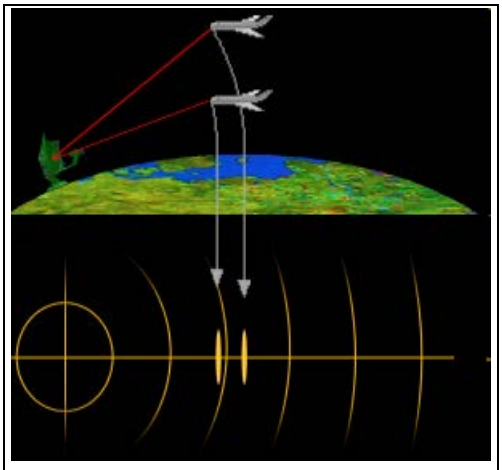

Figure 22 Effect of Displaying a Target's Slant-Range

Generally, the display processing methodology depends upon the radar's maximum range. Two situations are addressed.

Tangent Plane Display — This method displays targets on a plane that is tangent to the earth at the radar's latitude/longitude and sea level. Locations on the plane can be computed in Cartesian (east/north) or polar (range/azimuth) coordinates. The steps in the calculation are:

- The aircraft elevation angle, α, is found using Eq 50, repeated here:

$$\sin(\alpha) = \frac{(h_S - h_U)^2 + 2(R_e + h_U)(h_S - h_U) - d^2}{2(R_e + h_U)\,d} \qquad \text{Eq 123}$$

- The aircraft range along the tangent plane, Rng_{TP} , is found (sometimes called the slant-range correction)

$$Rng_{TP} = d\cos(\alpha) \qquad \text{Eq 124}$$

- If needed, *TPRng* can be resolved into east and north components

$$East_{TP} = Rng_{TP} \sin(\psi_{S/U})$$
$$North_{TP} = Rng_{TP} \cos(\psi_{S/U}) \qquad \text{Eq 125}$$

This method accounts for the difference between slant-range and ground range, but does not account for the curvature of the earth. Figure 23 shows the slant-range correction error (difference in computed Rng_{TP} values for two aircraft at the same latitude/longitude but different altitudes) for ranges/altitudes characteristic of a terminal area radar.

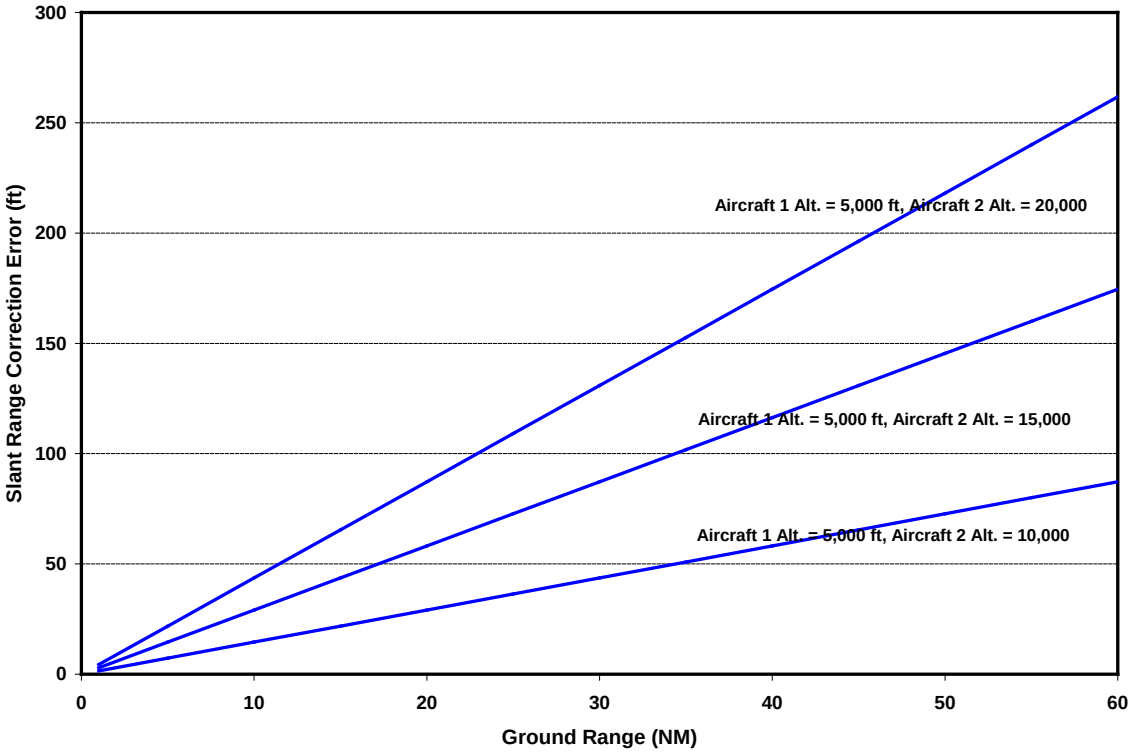

Figure 23 Slant-Range Correction Error for Tangent Plane Terminal Radar Display

The maximum slant-range correction error is approximately 260 ft. This may be contrasted with the difference in the slant-ranges, 644 ft, and the nominal terminal area separation standard of 3 NM. Thus the display processing removes more than half of the error that would occur with display of measured ranges, but there remains a residual error of 1.5% of the separation standard.

Latitude/Longitude Display — Because errors for a tangent plane display increase with the ranges and altitude differences of aircraft targets, en route radars use a more accurate method that fully accounts for the earth's curvature.

- The aircraft's geocentric angle relative to the radar is found using Eq 44
- The aircraft's latitude/longitude are found from Eq 91 and Eq 94
- The aircraft's latitude and longitude are converted to the coordinates of a map projection (e.g., Lambert conformal conic) for display to a controller.

En route radar coverage area will include multiple airports, including possibly several major ones. It's advantageous to display targets relative to the airport locations.

4.8.6 Example 6: Single-Station VOR / DME RNAV Fix

A single VOR/DME station **S** provides an aircraft **A** with its azimuth angle $\psi_{A/S}$ (VOR function) and slant-range distance d_{SA} (DME function) relative to the station. For area navigation (RNAV), it may be necessary to use those measurements to determine the aircraft's latitude and longitude **A** (L_A, λ_A). The aircraft's altitude h_A is assumed known, as are the station coordinates (L_S, λ_S) and DME antenna altitude h_S.

The first step is to convert the measured slant-range d_{SA} to the geocentric angle θ_{SA} (sometimes called the slant-range correction). This is accomplished by utilizing Eq 44, except that subscript U is replaced by S, and subscript S is replaced by A. The Direct problem of geodesy is then applicable (Section 4.3). The aircraft's latitude and longitude are found from Eq 91 and Eq 94, with the same subscript substitutions applied. Finally, if desired, the azimuth angle of the station relative to the aircraft may found from Eq 98 (again, with the same subscript substitutions).

Remarks:

- While the terminology and notation are different, the processing steps in this subsection are identical to those used for an en route radar latitude/longitude display in Subsection 4.8.5.
- While the slant-range correction of is usually considered a necessary step in en route radar processing, it is often not performed in navigation applications. The distances involved are generally shorter, and the measurements are generally less accurate (particularly the VOR measurement of $\psi_{A/S}$). Thus, for RNAV, the approximation $\theta_{SA} \approx d_{SA}/R_e$ (in lieu of Eq 44) may be sufficient.
- If the station only provides a range (DME) measurement, but the azimuth angle from the aircraft to the station, $\psi_{S/A}$, can be measured, then the expressions in Section 4.4 can be used to find the aircraft latitude/longitude and the aircraft azimuth from the station.

4.8.7 Example 7: Path-Length Ellipticity Error for Selected Airport Pairs

To provide an indication of the accuracy of the spherical earth approximation, a set of fourteen airports were selected. These airports are intended to be representative of current aviation activity. However, in terms of frequency of operations, they over-emphasize longer routes (and some are too long for commercial transport aircraft at this time). The result is a total of 91 possible paths between airport pairs. For each pair, estimates of the length of the paths are computed for:

a) WGS-84 ellipsoidal earth model utilizing Vincenty's algorithm cited in Subsection 2.2.3 (which is treated as a 'black box'), and

b) Spherical approximation of the earth utilizing the radius in Eq 31 and the expressions in Eq 143, Eq 144 and Eq 145.

The fourteen airports are partitioned into two groups of seven each — CONUS (Table 8) and International (Table 9). The CONUS group spans the CONUS land area and includes paths of various lengths and orientations. The International group, which includes airports in Alaska and Hawaii, has airport pairs with greater separation and paths that cross the equator. The longest path is HNL-JNB (10,365 NM), which is not feasible with current commercial aircraft. As a point of interest, the longest scheduled commercial flight route was 8,285 NM, between Newark and Singapore; it is no longer in operation, reportedly for business reasons.

Table 8 CONUS Airports Used in Ellipticity Error Analysis

Airport Name (IATA Code)	Lat. (deg)	Lon. (deg)	Major City Served
Gen. Edward L. Logan International (BOS)	42.3629722	-71.0064167	Boston, MA
Ronald Reagan Washington National (DCA)	38.8522	-77.0378	Washington, DC
O'Hare International (ORD)	41.9786	-87.9047	Chicago, IL
Miami International (MIA)	25.7933	-80.2906	Miami, FL
San Diego International (SAN)	32.7336	-117.1897	San Diego, CA
Dallas/Fort Worth International (DFW)	32.8969	-97.0381	Dallas/Fort Worth, TX
Seattle–Tacoma International (SEA)	47.4489	-122.3094	Seattle, WA

Table 9 International Airports Used in Ellipticity Error Analysis

Airport Name (IATA Code)	Lat. (deg)	Lon. (deg)	Major City Served
Wiley Post–Will Rogers Memorial (BRW)	71.2848889	-156.7685833	Barrow, Alaska
Honolulu International (HNL)	21.318681	-157.9224287	Honolulu, Hawaii
London Heathrow (LHR)	51.4775	-0.4614	London, England
Narita International (NRT)	35.7647	140.3864	Tokyo, Japan
Ministro Pistarini International (EZE)	-34.8222	-58.5358	Buenos Aires, Argentina
Oliver Reginald Tambo International (JNB)	-26.1392	28.246	Johannesburg, South Africa
Sydney (SYD)	-33.946111	151.177222	Sydney, Australia

Figure 24 is a histogram of the path length differences for the 91 paths analyzed using the methods labeled a) and b) above (a positive error corresponds to the spherical earth path being longer than the ellipsoidal earth path).

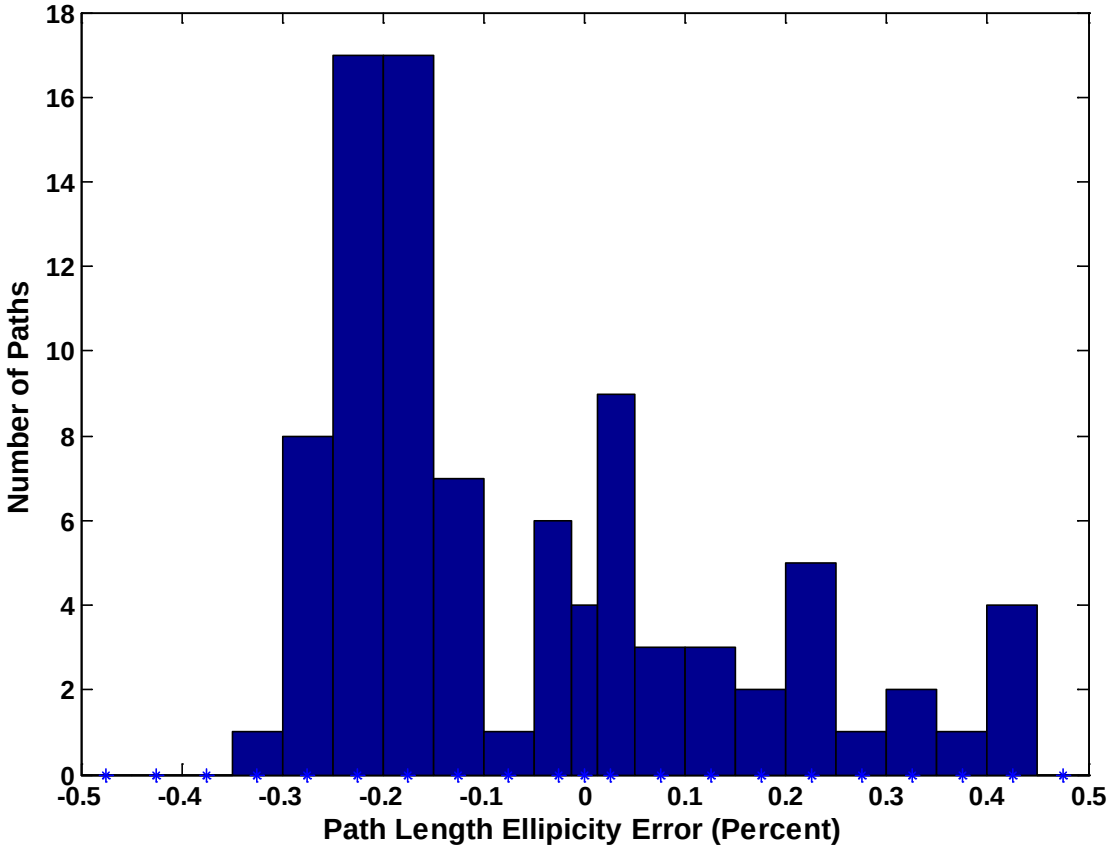

Figure 24 Histogram of Path Length Ellipticity Errors for 91 Airport Pairs

- For all 91 paths: the average of the absolute value of the relative path length ellipticity errors is 0.17%; the maximum is 0.43% (NRT-SYD); the minimum is 0.005% (DCA-SYD). Over 90% (83 of 91) of the paths have path length ellipticity errors whose absolute values less than the 'rule of thumb' of 0.3%. At the path end points, the average absolute azimuth error is 0.10 deg, and the maximum is 1.87 deg (HNL-JNB).
- For the 21 paths within CONUS: the average of the absolute value of the relative path length ellipticity errors is 0.18%; the maximum is 0.27% (BOS-SEA); the minimum is 0.02% (ORD-DFW). At the path end points, the average absolute azimuth error is 0.07 deg, and the maximum is 0.12 deg (ORD-DFW).

5. TWO-POINT / 3D-VECTOR FORMULATION

Many of the expressions derived in Chapter 4 using spherical trigonometry can also be developed using vectors and matrices. In utilizing this approach, one: (a) forms the relevant vectors/matrices, generally by assigning values to individual elements (which often involves computing trigonometric functions); (b) manipulates the vectors/matrices as entities, typically utilizing vector/matrix addition and multiplication, vector dot and cross products, etc., but not involving calculation of trigonometric functions; and (c) computes the desired scalar quantites, often utilizing inverse trigonometric functions. The purposes of this chapter are to demonstrate this approach in detail and to show that the results are identical to those found using spherical trigonometry.

Section 5.1 provides definitions of the vectors and coordinate frames needed to analyze the geometry of two points (user **U** and satellite **S**) relative to a spherical earth. Section 5.2 addresses the Indirect problem of geodesy, and provides vector versions of the key equations derived in Section 4.2 using spherical trigonometry. Section 5.3 returns to the Indirect problem, and demonstrates that for some combinations of known and unknown variables, vector analysis provides an alternative method of deriving other solutions found in Chapter 4. Section 5.4 addresses the Direct problem of geodesy, and shows that the equations in Section 4.3 can be found by vector/matrix analysis as well. Section addresses the intersection of two small circles on the earth's surface, a classic celestial navigation problem and an application of the Indirect and Direct problems of geodesy. Lastly, Section 5.5 demonstrates that vector analysis provides an alternative method of deriving certain expressions found in Chapter 3.

An advantage of the vector/matrix technique is ease of coding. Once the vector/matrix elements have been assigned, the calculations can largely utilize general- and special-purpose software packages. Matlab's Mapping Toolbox is an example; Ref. 35 has another. A disadvantage of the vector/matrix technique is that it can obscure geometric aspects of the problem being addressed.

5.1 Vector and Coordinate Frame Definitions

5.1.1 Earth-Centered Earth-Fixed (ECEF) Coordinate Frame

The coordinates of two locations of interest on the earth's surface are:

- User position: latitude L_U, longitude λ_U and altitude h_U
- Satellite position: latitude L_S, longitude λ_S and altitude h_S

Define the earth-centered earth-fixed (ECEF) coordinate frame **e** by (see Figure 25, where the figure's φ denotes latitude):

- x-axis: lies in the plane of the equator and points toward Greenwich meridian
- y-axis: completes the right-hand orthogonal system
- z-axis: lies along the earth's spin axis.

The location of the user and satellite in the *e*-frame are, respectively

$$\underline{\mathbf{r}}^{\mathbf{e}}_{\mathbf{0U}} = \begin{bmatrix} \underline{\mathrm{r}}^{\mathrm{e}}_{\mathrm{OU},x} \\ \underline{\mathrm{r}}^{\mathrm{e}}_{\mathrm{OU},y} \\ \underline{\mathrm{r}}^{\mathrm{e}}_{\mathrm{OU},z} \end{bmatrix} = \underline{\mathbf{1}}^{\mathbf{e}}_{\mathbf{0U}} (R_e + h_U) = \begin{bmatrix} \underline{1}^{\mathrm{e}}_{\mathrm{OU},x} \\ \underline{1}^{\mathrm{e}}_{\mathrm{OU},y} \\ \underline{1}^{\mathrm{e}}_{\mathrm{OU},z} \end{bmatrix} (R_e + h_U) = \begin{bmatrix} \cos(L_U)\cos(\lambda_U) \\ \cos(L_U)\sin(\lambda_U) \\ \sin(L_U) \end{bmatrix} (R_e + h_U)$$

$$\underline{\mathbf{r}}^{\mathbf{e}}_{\mathbf{0S}} = \begin{bmatrix} \underline{\mathrm{r}}^{\mathrm{e}}_{\mathrm{OS},x} \\ \underline{\mathrm{r}}^{\mathrm{e}}_{\mathrm{OS},y} \\ \underline{\mathrm{r}}^{\mathrm{e}}_{\mathrm{OS},z} \end{bmatrix} = \underline{\mathbf{1}}^{\mathbf{e}}_{\mathbf{0S}} (R_e + h_S) = \begin{bmatrix} \underline{1}^{\mathrm{e}}_{\mathrm{OS},x} \\ \underline{1}^{\mathrm{e}}_{\mathrm{OS},y} \\ \underline{1}^{\mathrm{e}}_{\mathrm{OS},z} \end{bmatrix} (R_e + h_S) = \begin{bmatrix} \cos(L_S)\cos(\lambda_S) \\ \cos(L_S)\sin(\lambda_S) \\ \sin(L_S) \end{bmatrix} (R_e + h_S)$$

Eq 126

Here $\underline{\mathbf{1}}^{\mathbf{e}}_{\mathbf{0U}}$ and $\underline{\mathbf{1}}^{\mathbf{e}}_{\mathbf{0S}}$ are unit vectors associated with $\underline{\mathbf{r}}^{\mathbf{e}}_{\mathbf{0U}}$ and $\underline{\mathbf{r}}^{\mathbf{e}}_{\mathbf{0S}}$, respectively. Note that the *e*-frame, as are all frames used herein, is right-handed — e.g., $\underline{1}^{\mathrm{e}}_{\mathrm{OU},x} \times \underline{1}^{\mathrm{e}}_{\mathrm{OU},y} = \underline{1}^{\mathrm{e}}_{\mathrm{OU},z}$.

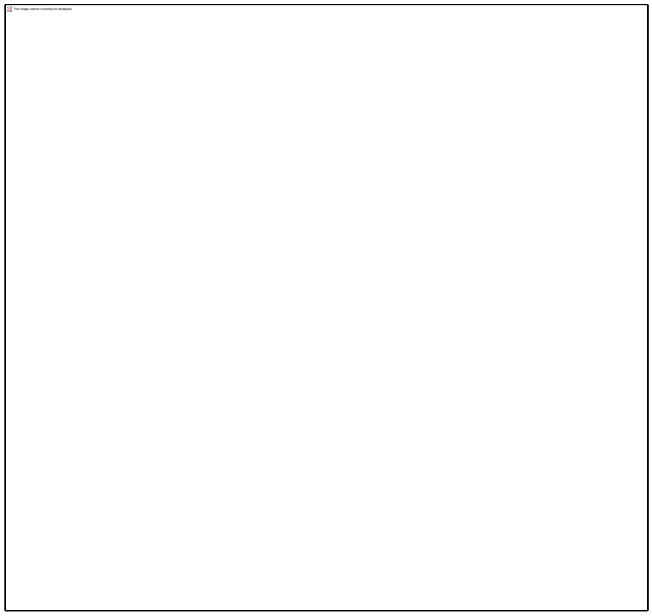

Figure 25 Vector Technique Coordinate Frames of Interest (φ = Latitude)

Given $\underline{\mathbf{r}}^{\mathbf{e}}_{\mathbf{0U}}$, the user's latitude, longitude and altitude can be found (respectively) from

$$L_U = \arctan\left(\frac{\underline{\mathrm{r}}^{\mathrm{e}}_{\mathrm{OU},z}}{\sqrt{\left(\underline{\mathrm{r}}^{\mathrm{e}}_{\mathrm{OU},x}\right)^2 + \left(\underline{\mathrm{r}}^{\mathrm{e}}_{\mathrm{OU},y}\right)^2}} \right) = \arcsin\left(\frac{\underline{\mathrm{r}}^{\mathrm{e}}_{\mathrm{OU},z}}{R_e + h_U} \right)$$

$$\lambda_U = \arctan\left(\underline{\mathrm{r}}^{\mathrm{e}}_{\mathrm{OU},y}, \underline{\mathrm{r}}^{\mathrm{e}}_{\mathrm{OU},x}\right)$$

$$h_U = \sqrt{\left(\underline{\mathrm{r}}^{\mathrm{e}}_{\mathrm{OU},x}\right)^2 + \left(\underline{\mathrm{r}}^{\mathrm{e}}_{\mathrm{OU},y}\right)^2 + \left(\underline{\mathrm{r}}^{\mathrm{e}}_{\mathrm{OU},z}\right)^2} - R_e$$

Eq 127

Similarly, given $\underline{\mathbf{r}}^{\mathbf{e}}_{\mathbf{0S}}$, the satellite's latitude, longitude and altitude can be found from

$$L_S = \arctan\left(\frac{\underline{\mathrm{r}}^{\mathrm{e}}_{\mathrm{os},z}}{\sqrt{\left(\underline{\mathrm{r}}^{\mathrm{e}}_{\mathrm{os},x}\right)^2 + \left(\underline{\mathrm{r}}^{\mathrm{e}}_{\mathrm{os},y}\right)^2}}\right) = \arcsin\left(\frac{\underline{\mathrm{r}}^{\mathrm{e}}_{\mathrm{os},z}}{R_e + h_S}\right)$$

$$\lambda_S = \arctan\left(\underline{\mathrm{r}}^{\mathrm{e}}_{\mathrm{os},y}, \underline{\mathrm{r}}^{\mathrm{e}}_{\mathrm{os},x}\right) \qquad \text{Eq 128}$$

$$h_S = \sqrt{\left(\underline{\mathrm{r}}^{\mathrm{e}}_{\mathrm{os},x}\right)^2 + \left(\underline{\mathrm{r}}^{\mathrm{e}}_{\mathrm{os},y}\right)^2 + \left(\underline{\mathrm{r}}^{\mathrm{e}}_{\mathrm{os},z}\right)^2} - R_e$$

5.1.2 Local-Level Coordinate Frame at User's Position

Define a local-level coordinate frame *u* that is parallel to a plane tangent to the earth at the user's position having coordinate axes:

- *e*-axis point east
- *n*-axis points north
- *u*-axis points up (away from earth's center).

The direction cosine matrix (DCM) which rotates the *e*-frame into the *u*-frame (e.g., Eq 134) is

$$\mathbf{C}^{\mathbf{u}}_{\mathbf{e}} = \mathbf{T}\,\mathbf{T}_2(-L_U)\,\mathbf{T}_3(\lambda_U) \qquad \text{Eq 129}$$

Here $\mathbf{T}_i(\xi)$ denotes the rotation matrix about axis *i* by angle ξ and and $\mathbf{T}$ denotes an axis-permutation matrix

$$\mathbf{T}_1(\xi) = \begin{bmatrix} 1 & 0 & 0 \\ 0 & \cos(\xi) & \sin(\xi) \\ 0 & -\sin(\xi) & \cos(\xi) \end{bmatrix} \qquad \mathbf{T}_2(\xi) = \begin{bmatrix} \cos(\xi) & 0 & -\sin(\xi) \\ 0 & 1 & 0 \\ \sin(\xi) & 0 & \cos(\xi) \end{bmatrix}$$

$$\mathbf{T}_3(\xi) = \begin{bmatrix} \cos(\xi) & \sin(\xi) & 0 \\ -\sin(\xi) & \cos(\xi) & 0 \\ 0 & 0 & 1 \end{bmatrix} \qquad \mathbf{T} = \begin{bmatrix} 0 & 1 & 0 \\ 0 & 0 & 1 \\ 1 & 0 & 0 \end{bmatrix} \qquad \text{Eq 130}$$

Thus $\mathbf{C}^{\mathbf{u}}_{\mathbf{e}}$ is given by

$$\mathbf{C}^{\mathbf{u}}_{\mathbf{e}} = \begin{bmatrix} -\sin(\lambda_U) & \cos(\lambda_U) & 0 \\ -\sin(L_U)\cos(\lambda_U) & -\sin(L_U)\sin(\lambda_U) & \cos(L_U) \\ \cos(L_U)\cos(\lambda_U) & \cos(L_U)\sin(\lambda_U) & \sin(L_U) \end{bmatrix} \qquad \text{Eq 131}$$

Clearly, L_U and λ_U can be found from $\mathbf{C}^{\mathbf{u}}_{\mathbf{e}}$ as well as from $\underline{\mathbf{r}}^{\mathbf{e}}_{\mathbf{OU}}$ — e.g., by

$$L_U = \arctan\left(\frac{\mathbf{C}^{\mathbf{u}}_{\mathbf{e}}(3,3)}{\mathbf{C}^{\mathbf{u}}_{\mathbf{e}}(2,3)}\right) \qquad \lambda_U = \arctan\left(\frac{-\mathbf{C}^{\mathbf{u}}_{\mathbf{e}}(1,1)}{\mathbf{C}^{\mathbf{u}}_{\mathbf{e}}(1,2)}\right) \qquad \text{Eq 132}$$

As is the case for any DCM, $\mathbf{C}^{\mathbf{u}}_{\mathbf{e}}$ is orthonormal; thus

$$\mathbf{C}^{\mathbf{e}}_{\mathbf{u}} = (\mathbf{C}^{\mathbf{u}}_{\mathbf{e}})^{-1} = (\mathbf{C}^{\mathbf{u}}_{\mathbf{e}})^T \qquad \text{Eq 133}$$

5.1.3 User and Satellite Positions in User's Local-Level Frame

Using the DCM $\mathbf{C_e^u}$, the positions of the user and satellite in the *u*-frame are, respectively

$$\underline{\mathbf{r}}_{\mathbf{OU}}^{\mathbf{u}} = \begin{bmatrix} \underline{r}_{OU,e}^{u} \\ \underline{r}_{OU,n}^{u} \\ \underline{r}_{OU,u}^{u} \end{bmatrix} = \mathbf{C_e^u}\, \underline{\mathbf{r}}_{\mathbf{OU}}^{\mathbf{e}} = \mathbf{C_e^u} \begin{bmatrix} \underline{r}_{OU,x}^{e} \\ \underline{r}_{OU,y}^{e} \\ \underline{r}_{OU,z}^{e} \end{bmatrix} = \begin{bmatrix} 0 \\ 0 \\ 1 \end{bmatrix} (R_e + h_U) \qquad \text{Eq 134}$$

and

$$\underline{\mathbf{r}}_{\mathbf{OS}}^{\mathbf{u}} = \begin{bmatrix} \underline{r}_{OS,e}^{u} \\ \underline{r}_{OS,n}^{u} \\ \underline{r}_{OS,u}^{u} \end{bmatrix} = \mathbf{C_e^u}\, \underline{\mathbf{r}}_{\mathbf{OS}}^{\mathbf{e}} = \mathbf{C_e^u} \begin{bmatrix} \underline{r}_{OS,x}^{e} \\ \underline{r}_{OS,y}^{e} \\ \underline{r}_{OS,z}^{e} \end{bmatrix}$$

$$= \begin{bmatrix} \cos(L_S)\sin(\lambda_S - \lambda_U) \\ -\cos(L_S)\sin(L_U)\cos(\lambda_S - \lambda_U) + \sin(L_S)\cos(L_U) \\ \cos(L_S)\cos(L_U)\cos(\lambda_S - \lambda_U) + \sin(L_S)\sin(L_U) \end{bmatrix} (R_e + h_S) \qquad \text{Eq 135}$$

Thus, using Eq 134 and Eq 135, the vector from **U** to **S** is $\underline{\mathbf{r}}_{\mathbf{US}}^{\mathbf{u}} = \underline{\mathbf{r}}_{\mathbf{OS}}^{\mathbf{u}} - \underline{\mathbf{r}}_{\mathbf{OU}}^{\mathbf{u}}$, is

$$\underline{\mathbf{r}}_{\mathbf{US}}^{\mathbf{u}} = \underline{\mathbf{r}}_{\mathbf{OS}}^{\mathbf{u}} - \underline{\mathbf{r}}_{\mathbf{OU}}^{\mathbf{u}} = [\underline{r}_{US,e}^{u} \quad \underline{r}_{US,n}^{u} \quad \underline{r}_{US,u}^{u}]^T$$

$$= \begin{bmatrix} (R_e + h_S)\cos(L_S)\sin(\lambda_S - \lambda_U) \\ (R_e + h_S)[-\cos(L_S)\sin(L_U)\cos(\lambda_S - \lambda_U) + \sin(L_S)\cos(L_U)] \\ (R_e + h_S)[\cos(L_S)\cos(L_U)\cos(\lambda_S - \lambda_U) + \sin(L_S)\sin(L_U)] - (R_e + h_U) \end{bmatrix} \qquad \text{Eq 136}$$

The horizontal and vertical components of $\underline{\mathbf{r}}_{\mathbf{US}}^{\mathbf{u}}$ can be expressed as

$$\underline{r}_{US,horiz}^{u} = \sqrt{\left(\underline{r}_{US,e}^{u}\right)^2 + \left(\underline{r}_{US,n}^{u}\right)^2} = (R_e + h_S)\sin(\theta)$$
$$\underline{r}_{US,vert}^{u} = \underline{r}_{US,u}^{u} = (R_e + h_S)\cos(\theta) - (R_e + h_U) \qquad \text{Eq 137}$$

Here, θ is the geocentric angle between vectors $\underline{\mathbf{r}}_{\mathbf{OU}}$ and $\underline{\mathbf{r}}_{\mathbf{OS}}$. The far right-hand sides of both lines of Eq 137 can be found from Figure 1 by inspection. Expressions for $\cos(\theta)$ and $\sin(\theta)$ in terms of (L_U, λ_U) and (L_S, λ_S) are given below, in Eq 141 and Eq 142, respectively. Agreement of those expressions with the elements of $\underline{\mathbf{r}}_{\mathbf{US}}^{\mathbf{u}}$ in Eq 136 can be readily verified.

Two angles associated with $\underline{\mathbf{r}}_{\mathbf{US}}^{\mathbf{u}}$ are of interest

- $\psi_{S/U}$ – The azimuth angle of the horizontal component of $\underline{\mathbf{r}}_{\mathbf{US}}^{\mathbf{u}}$, measured clockwise from north
- α – The elevation angle of $\underline{\mathbf{r}}_{\mathbf{US}}^{\mathbf{u}}$, measured from the horizontal plane

$$\psi_{S/U} = \arctan\left(\underline{r}_{US,e}^{u}, \underline{r}_{US,n}^{u}\right) \qquad \text{Eq 138}$$

$$\alpha = \arctan\left(\frac{\underline{\mathrm{r}}^{\mathrm{u}}_{\mathrm{US},u}}{\sqrt{\left(\underline{\mathrm{r}}^{\mathrm{u}}_{\mathrm{US},e}\right)^2 + \left(\underline{\mathrm{r}}^{\mathrm{u}}_{\mathrm{US},n}\right)^2}}\right) \quad \text{Eq 139}$$

The two-argument arc tangent function is used in Eq 138.

The Euclidean length d of $\underline{\mathbf{r}}^{\mathbf{u}}_{\mathbf{US}}$ is also of interest, and is given by

$$d = \left\|\underline{\mathbf{r}}^{\mathbf{u}}_{\mathbf{US}}\right\| = \sqrt{\left(\underline{\mathrm{r}}^{\mathrm{u}}_{\mathrm{US},e}\right)^2 + \left(\underline{\mathrm{r}}^{\mathrm{u}}_{\mathrm{US},n}\right)^2 + \left(\underline{\mathrm{r}}^{\mathrm{u}}_{\mathrm{US},u}\right)^2} \quad \text{Eq 140}$$

5.2 The Indirect Problem of Geodesy

5.2.1 Computing the Geocentric Angle

The vectors $\underline{\mathbf{r}}^{\mathbf{e}}_{\mathbf{OU}}$ and $\underline{\mathbf{r}}^{\mathbf{e}}_{\mathbf{OS}}$ meet at the earth's center, in geocentric angle θ. The dot product of these vectors, normalized by the product of their lengths, yields

$$\begin{aligned}\cos(\theta) = \underline{\mathbf{1}}^{\mathbf{e}}_{\mathbf{OU}} \bullet \underline{\mathbf{1}}^{\mathbf{e}}_{\mathbf{OS}} &= \frac{\underline{\mathrm{r}}^{\mathrm{e}}_{\mathrm{OU},x}\,\underline{\mathrm{r}}^{\mathrm{e}}_{\mathrm{OS},x} + \underline{\mathrm{r}}^{\mathrm{e}}_{\mathrm{OU},y}\,\underline{\mathrm{r}}^{\mathrm{e}}_{\mathrm{OS},y} + \underline{\mathrm{r}}^{\mathrm{e}}_{\mathrm{OU},z}\,\underline{\mathrm{r}}^{\mathrm{e}}_{\mathrm{OS},z}}{\sqrt{\left(\underline{\mathrm{r}}^{\mathrm{e}}_{\mathrm{OU},x}\right)^2 + \left(\underline{\mathrm{r}}^{\mathrm{e}}_{\mathrm{OU},y}\right)^2 + \left(\underline{\mathrm{r}}^{\mathrm{e}}_{\mathrm{OU},z}\right)^2}\sqrt{\left(\underline{\mathrm{r}}^{\mathrm{e}}_{\mathrm{OS},x}\right)^2 + \left(\underline{\mathrm{r}}^{\mathrm{e}}_{\mathrm{OS},y}\right)^2 + \left(\underline{\mathrm{r}}^{\mathrm{e}}_{\mathrm{OS},z}\right)^2}} \\ &= \cos(L_S)\cos(L_U)\cos(\lambda_S - \lambda_U) + \sin(L_S)\sin(L_U)\end{aligned} \quad \text{Eq 141}$$

Eq 141 demonstrates that if one forms either vector expression indicated on the first line, the result will be the same as if one performed the scalar operations indicated on the second line, which is identical to the equation for $\cos(\theta)$ found by spherical trigonometry (Eq 78).

The cross product of vectors $\underline{\mathbf{1}}^{\mathbf{e}}_{\mathbf{OU}}$ and $\underline{\mathbf{1}}^{\mathbf{e}}_{\mathbf{OS}}$ (see Eq 153 for the components of $\underline{\mathbf{1}}^{\mathbf{e}}_{\mathbf{OU}} \times \underline{\mathbf{1}}^{\mathbf{e}}_{\mathbf{OS}}$) yields another expression for the geocentric angle:

$$\begin{aligned}\sin(\theta) &= \left\|\underline{\mathbf{1}}^{\mathbf{e}}_{\mathbf{OU}} \times \underline{\mathbf{1}}^{\mathbf{e}}_{\mathbf{OS}}\right\| \\ &= \sqrt{[\cos(L_S)\sin(\lambda_S - \lambda_U)]^2 + [\cos(L_U)\sin(L_S) - \sin(L_U)\cos(L_S)\cos(\lambda_S - \lambda_U)]^2}\end{aligned} \quad \text{Eq 142}$$

This expression for $\sin(\theta)$ on the second line is identical to Eq 88, which is derived by spherical trigonometry. If used to find θ in the range $[0, \pi]$, Eq 142, yields ambiguous solutions. Also, precision issues may occur near $\theta = ½\pi$. As 'sanity' checks: when $\lambda_S = \lambda_U$, Eq 142 reduces to $\sin(\theta) = |\sin(L_S - L_U)|$; when $L_S = L_U = 0$, Eq 142 reduces to $\sin(\theta) = |\sin(\lambda_S - \lambda_U)|$.

Utilizing Eq 141 and Eq 142, a third expression (Eq 143) for the geocentric angle θ in terms of **U** and **S** follows. Generalization of the expression on the second line to an ellipsoidal-shaped earth has been termed the Vincenty formula.

$$\tan(\theta) = \frac{\left\|\underline{\mathbf{1}}^{\mathbf{e}}_{\mathbf{OU}} \times \underline{\mathbf{1}}^{\mathbf{e}}_{\mathbf{OS}}\right\|}{\underline{\mathbf{1}}^{\mathbf{e}}_{\mathbf{OU}} \bullet \underline{\mathbf{1}}^{\mathbf{e}}_{\mathbf{OS}}} = \frac{\left\|\underline{\mathbf{r}}^{\mathbf{e}}_{\mathbf{OU}} \times \underline{\mathbf{r}}^{\mathbf{e}}_{\mathbf{OS}}\right\|}{\underline{\mathbf{r}}^{\mathbf{e}}_{\mathbf{OU}} \bullet \underline{\mathbf{r}}^{\mathbf{e}}_{\mathbf{OS}}}$$
$$= \frac{\sqrt{[\cos(L_S)\sin(\lambda_S - \lambda_U)]^2 + [\cos(L_U)\sin(L_S) - \sin(L_U)\cos(L_S)\cos(\lambda_S - \lambda_U)]^2}}{\cos(L_S)\cos(L_U)\cos(\lambda_S - \lambda_U) + \sin(L_S)\sin(L_U)} \qquad \text{Eq 143}$$

In using Eq 143, the two-argument arc tangent function should be employed, to avoid issues when θ is near ½π. The result will be unambiguous for $0 \leq \theta \leq \pi$.

5.2.2 Computing the Path Azimuth Angles

By substituting two elements of $\underline{\mathbf{r}}^{\mathbf{u}}_{\mathbf{US}}$ from Eq 136 into Eq 138, $\psi_{S/U}$ is found to be equal to

$$\psi_{S/U} = \arctan\left(\underline{\mathrm{r}}^{\mathrm{u}}_{\mathrm{US},e}, \underline{\mathrm{r}}^{\mathrm{u}}_{\mathrm{US},n}\right)$$
$$= \arctan\left(\frac{\cos(L_S)\sin(\lambda_S - \lambda_U)}{\cos(L_U)\sin(L_S) - \sin(L_U)\cos(L_S)\cos(\lambda_S - \lambda_U)}\right) \qquad \text{Eq 144}$$

Eq 144 demonstrates that if $\psi_{S/U}$ is computed using the arc tangent function with elements of $\underline{\mathbf{r}}^{\mathbf{u}}_{\mathbf{US}}$ as arguments, the result will be identical to that found by spherical trigonometry (Eq 86).

The labeling of the points **U** and **S** in Eq 144 can be reversed, yielding

$$\psi_{U/S} = \arctan\left(\underline{\mathrm{r}}^{\mathrm{s}}_{\mathrm{SU},e}, \underline{\mathrm{r}}^{\mathrm{s}}_{\mathrm{SU},n}\right)$$
$$= \arctan\left(\frac{\cos(L_U)\sin(\lambda_U - \lambda_S)}{\cos(L_S)\sin(L_U) - \sin(L_S)\cos(L_U)\cos(\lambda_U - \lambda_S)}\right) \qquad \text{Eq 145}$$

While the arguments on right-hand sides of Eq 144 and Eq 145 are shown as ratios, the azimuth angles should be computed using the two-argument arc tangent function.

In Eq 145, vector $\underline{\mathbf{r}}^{\mathbf{s}}_{\mathbf{SU}}$ is found from

$$\underline{\mathbf{r}}^{\mathbf{s}}_{\mathbf{SU}} = \underline{\mathbf{r}}^{\mathbf{s}}_{\mathbf{OU}} - \underline{\mathbf{r}}^{\mathbf{s}}_{\mathbf{OS}} = \mathbf{C}^{\mathbf{s}}_{\mathbf{e}}\left(\underline{\mathbf{r}}^{\mathbf{e}}_{\mathbf{OU}} - \underline{\mathbf{r}}^{\mathbf{e}}_{\mathbf{OS}}\right) \qquad \text{Eq 146}$$

Here $\underline{\mathbf{r}}^{\mathbf{e}}_{\mathbf{OU}}$ and $\underline{\mathbf{r}}^{\mathbf{e}}_{\mathbf{OS}}$ are given by Eq 126; interpreting Eq 131, $\mathbf{C}^{\mathbf{s}}_{\mathbf{e}}$ is given by

$$\mathbf{C}^{\mathbf{s}}_{\mathbf{e}} = \begin{bmatrix} -\sin(\lambda_S) & \cos(\lambda_S) & 0 \\ -\sin(L_S)\cos(\lambda_S) & -\sin(L_S)\sin(\lambda_S) & \cos(L_S) \\ \cos(L_S)\cos(\lambda_S) & \cos(L_S)\sin(\lambda_S) & \sin(L_S) \end{bmatrix} \qquad \text{Eq 147}$$

5.3 Corollaries of the Indirect Problem Solution

5.3.1 Locations Along the Straight-Line between **U** and **S**

Route planning generally requires selecting a set of intermediate points along a planned route from **U** to **S**. One option is to select a set of equally-spaced points along the straight-line

connecting **U** and **S**. (If $h_U = h_S = 0$, then the straight line path is a chord corresponding to great circle arc.) A way to do this is to choose points along the vector $\underline{\mathbf{r}}^{\mathbf{e}}_{\mathbf{US}}$, then find their associated latitudes, longitudes and altitudes. Accordingly, let $\mu, 0 \le \mu \le 1$, be the fractional distance of point **X** from **U** to **S** along the vector $\underline{\mathbf{r}}^{\mathbf{e}}_{\mathbf{US}}$. Thus,

$$\underline{\mathbf{r}}^{\mathbf{e}}_{\mathbf{OX}} = \underline{\mathbf{r}}^{\mathbf{e}}_{\mathbf{OU}} + \mu\underline{\mathbf{r}}^{\mathbf{e}}_{\mathbf{US}} = \underline{\mathbf{r}}^{\mathbf{e}}_{\mathbf{OU}} + \mu\left(\underline{\mathbf{r}}^{\mathbf{e}}_{\mathbf{OS}} - \underline{\mathbf{r}}^{\mathbf{e}}_{\mathbf{OU}}\right) = (1-\mu)\underline{\mathbf{r}}^{\mathbf{e}}_{\mathbf{OU}} + \mu\underline{\mathbf{r}}^{\mathbf{e}}_{\mathbf{OS}} \quad \text{Eq 148}$$

Then, as in Eq 127 and Eq 128

$$L_X = \arctan\left(\frac{\underline{\mathrm{r}}^{\mathrm{e}}_{\mathrm{OX},z}}{\sqrt{\left(\underline{\mathrm{r}}^{\mathrm{e}}_{\mathrm{OX},x}\right)^2 + \left(\underline{\mathrm{r}}^{\mathrm{e}}_{\mathrm{OX},y}\right)^2}}\right)$$

$$\lambda_X = \arctan\left(\underline{\mathrm{r}}^{\mathrm{e}}_{\mathrm{OX},y}, \underline{\mathrm{r}}^{\mathrm{e}}_{\mathrm{OX},x}\right) \quad \text{Eq 149}$$

$$h_X = \sqrt{\left(\underline{\mathrm{r}}^{\mathrm{e}}_{\mathrm{OX},x}\right)^2 + \left(\underline{\mathrm{r}}^{\mathrm{e}}_{\mathrm{OX},y}\right)^2 + \left(\underline{\mathrm{r}}^{\mathrm{e}}_{\mathrm{OX},z}\right)^2} - R_e$$

Equally-spaced points along the straight line $\underline{\mathbf{r}}^{\mathbf{e}}_{\mathbf{US}}$ will not correspond to equally-spaced points along the great circle arc connecting **U** and **S**.

5.3.2 Locations Along the Great Circle Arc Connecting **U** and **S**

It is sometimes desirable to find the coordinates of an arbitrary point along the arc of the great circle between **U** and **S**. One situation is planning a long-distance flight, where (a) the straight line between **U** and **S** is almost entirely beneath the earth's surface, and (b) the aircraft altitude is never more than about 0.2% of the earth's radius.

Toward that end, let $\mu, 0 \le \mu \le 1$, be the fractional distance of point **X** from **U** to **S** along the great circle arc of length θ between the subpoints of **U** and **S**. The unit vector $\underline{\mathbf{1}}^{\mathbf{e}}_{\mathbf{OX}}$ can be expressed as

$$\underline{\mathbf{1}}^{\mathbf{e}}_{\mathbf{OX}} = \frac{\sin[(1-\mu)\theta]}{\sin(\theta)}\underline{\mathbf{1}}^{\mathbf{e}}_{\mathbf{OU}} + \frac{\sin(\mu\theta)}{\sin(\theta)}\underline{\mathbf{1}}^{\mathbf{e}}_{\mathbf{OS}} \quad \text{Eq 150}$$

Vector $\underline{\mathbf{1}}^{\mathbf{e}}_{\mathbf{OX}}$ lies in the plane defined by $\underline{\mathbf{1}}^{\mathbf{e}}_{\mathbf{OU}}$ and $\underline{\mathbf{1}}^{\mathbf{e}}_{\mathbf{OS}}$ and satisfies the following necessary and sufficient conditions for its claimed attributes

$$\underline{\mathbf{1}}^{\mathbf{e}}_{\mathbf{OX}} \bullet \underline{\mathbf{1}}^{\mathbf{e}}_{\mathbf{OU}} = \frac{\sin[(1-\mu)\theta]}{\sin(\theta)} + \frac{\sin(\mu\theta)}{\sin(\theta)}\cos(\theta) = \cos(\mu\theta)$$

$$\underline{\mathbf{1}}^{\mathbf{e}}_{\mathbf{OX}} \bullet \underline{\mathbf{1}}^{\mathbf{e}}_{\mathbf{OS}} = \frac{\sin[(1-\mu)\theta]}{\sin(\theta)}\cos(\theta) + \frac{\sin(\mu\theta)}{\sin(\theta)} = \cos[(1-\mu)\theta] \quad \text{Eq 151}$$

$$\underline{\mathbf{1}}^{\mathbf{e}}_{\mathbf{OX}} \bullet \underline{\mathbf{1}}^{\mathbf{e}}_{\mathbf{OX}} = \frac{\sin[(1-\mu)\theta]}{\sin(\theta)}\underline{\mathbf{1}}^{\mathbf{e}}_{\mathbf{OX}} \bullet \underline{\mathbf{1}}^{\mathbf{e}}_{\mathbf{OU}} + \frac{\sin(\mu\theta)}{\sin(\theta)}\underline{\mathbf{1}}^{\mathbf{e}}_{\mathbf{OX}} \bullet \underline{\mathbf{1}}^{\mathbf{e}}_{\mathbf{OS}} = 1$$

The components of $\underline{\mathbf{1}}^{\mathbf{e}}_{\mathbf{OX}}$ are given by

$$\underline{\mathbf{1}}^{\mathbf{e}}_{\mathbf{OX}} = \begin{bmatrix} \underline{1}^{\mathrm{e}}_{\mathrm{OX},x} \\ \underline{1}^{\mathrm{e}}_{\mathrm{OX},y} \\ \underline{1}^{\mathrm{e}}_{\mathrm{OX},z} \end{bmatrix} = \frac{1}{\sin(\theta)} \begin{bmatrix} \sin[(1-\mu)\theta]\, \underline{1}^{\mathrm{e}}_{\mathrm{OU},x} + \sin(\mu\theta)\underline{1}^{\mathrm{e}}_{\mathrm{OS},x} \\ \sin[(1-\mu)\theta]\, \underline{1}^{\mathrm{e}}_{\mathrm{OU},y} + \sin(\mu\theta)\underline{1}^{\mathrm{e}}_{\mathrm{OS},y} \\ \sin[(1-\mu)\theta]\, \underline{1}^{\mathrm{e}}_{\mathrm{OU},z} + \sin(\mu\theta)\underline{1}^{\mathrm{e}}_{\mathrm{OS},z} \end{bmatrix} \qquad \text{Eq 152}$$

Expressions similar to those in Eq 149 can be used to find the coordinates L_X and λ_X. These equations (Eq 152 and Eq 149) provide essentially the same functionality for the vector technique that can be achieved with spherical trigonometry using Eq 91 and Eq 94.

5.3.3 Vertices of a Great Circle

The vertices (northern- and southern-most latitudes) of a great circle are readily found by vector analysis. The cross product of unit vectors $\underline{\mathbf{1}}^{\mathbf{e}}_{\mathbf{OU}}$ and $\underline{\mathbf{1}}^{\mathbf{e}}_{\mathbf{OS}}$ (Eq 126) is normal to the plane of the great circle containing **U** and **S**. In this subsection, it is assumed that **U** is west of **S**, so that $\underline{\mathbf{1}}_{\mathbf{OU}} \times \underline{\mathbf{1}}_{\mathbf{OS}}$ points toward the northern hemisphere.

$$\underline{\mathbf{1}}^{\mathbf{e}}_{\mathbf{OU}} \times \underline{\mathbf{1}}^{\mathbf{e}}_{\mathbf{OS}} = \begin{bmatrix} \left(\underline{\mathbf{1}}^{\mathbf{e}}_{\mathbf{OU}} \times \underline{\mathbf{1}}^{\mathbf{e}}_{\mathbf{OS}}\right)_x \\ \left(\underline{\mathbf{1}}^{\mathbf{e}}_{\mathbf{OU}} \times \underline{\mathbf{1}}^{\mathbf{e}}_{\mathbf{OS}}\right)_y \\ \left(\underline{\mathbf{1}}^{\mathbf{e}}_{\mathbf{OU}} \times \underline{\mathbf{1}}^{\mathbf{e}}_{\mathbf{OS}}\right)_z \end{bmatrix} = \begin{bmatrix} \underline{1}^{\mathrm{e}}_{\mathrm{OU},y}\, \underline{1}^{\mathrm{e}}_{\mathrm{OS},z} - \underline{1}^{\mathrm{e}}_{\mathrm{OU},z}\, \underline{1}^{\mathrm{e}}_{\mathrm{OS},y} \\ \underline{1}^{\mathrm{e}}_{\mathrm{OU},z}\, \underline{1}^{\mathrm{e}}_{\mathrm{OS},x} - \underline{1}^{\mathrm{e}}_{\mathrm{OU},x}\, \underline{1}^{\mathrm{e}}_{\mathrm{OS},z} \\ \underline{1}^{\mathrm{e}}_{\mathrm{OU},x}\, \underline{1}^{\mathrm{e}}_{\mathrm{OS},y} - \underline{1}^{\mathrm{e}}_{\mathrm{OU},y}\, \underline{1}^{\mathrm{e}}_{\mathrm{OS},x} \end{bmatrix}$$

$$= \begin{bmatrix} \cos(L_U)\sin(L_S)\sin(\lambda_U) - \sin(L_U)\cos(L_S)\sin(\lambda_S) \\ \sin(L_U)\cos(L_S)\cos(\lambda_S) - \cos(L_U)\sin(L_S)\cos(\lambda_U) \\ \cos(L_U)\cos(L_S)\sin(\lambda_S - \lambda_U) \end{bmatrix} \qquad \text{Eq 153}$$

When $\underline{\mathbf{1}}^{\mathbf{e}}_{\mathbf{OU}} \times \underline{\mathbf{1}}^{\mathbf{e}}_{\mathbf{OS}}$ is normalized to unit length, its *z*-component is equal to the cosine of the latitude of the highest (and lowest) point on the great circle that includes the route in question (projection of a unit vector onto the earth's spin axis). Thus, using Eq 142

$$\cos(L_{max}) = \frac{\left(\underline{\mathbf{1}}^{\mathbf{e}}_{\mathbf{OU}} \times \underline{\mathbf{1}}^{\mathbf{e}}_{\mathbf{OS}}\right)_z}{\left\|\underline{\mathbf{1}}^{\mathbf{e}}_{\mathbf{OU}} \times \underline{\mathbf{1}}^{\mathbf{e}}_{\mathbf{OS}}\right\|} = \frac{\cos(L_U)\cos(L_S)\,|\sin(\lambda_S - \lambda_U)|}{\sin(\theta_{US})}$$

$$= \frac{\cos(L_U)\cos(L_S)\,|\sin(\lambda_S - \lambda_U)|}{\sqrt{[\cos(L_S)\sin(\lambda_S - \lambda_U)]^2 + [\cos(L_U)\sin(L_S) - \sin(L_U)\cos(L_S)\cos(\lambda_S - \lambda_U)]^2}} \qquad \text{Eq 154}$$

Clearly, $L_{min} = -L_{max}$. Eq 154 is identical to Eq 116, demonstrating that manipulating the components of $\underline{\mathbf{1}}^{\mathbf{e}}_{\mathbf{OU}}$ and $\underline{\mathbf{1}}^{\mathbf{e}}_{\mathbf{OS}}$ yields the same result that Clairaut's equation does. An alternative expression for L_{max} is

$$\cot(L_{max}) = \frac{\left(\underline{\mathbf{1}}^{\mathbf{e}}_{\mathbf{OU}} \times \underline{\mathbf{1}}^{\mathbf{e}}_{\mathbf{OS}}\right)_z}{\sqrt{\left(\underline{\mathbf{1}}^{\mathbf{e}}_{\mathbf{OU}} \times \underline{\mathbf{1}}^{\mathbf{e}}_{\mathbf{OS}}\right)_x^2 + \left(\underline{\mathbf{1}}^{\mathbf{e}}_{\mathbf{OU}} \times \underline{\mathbf{1}}^{\mathbf{e}}_{\mathbf{OS}}\right)_y^2}} \qquad \text{Eq 155}$$

The longitude where the highest/lowest latitudes are achieved can be found from the *x*- and *y*-

components of vector $\underline{\mathbf{1}}^{\mathbf{e}}_{\mathbf{0U}}$ x $\underline{\mathbf{1}}^{\mathbf{e}}_{\mathbf{0S}}$ (from Eq 153) using the two-argument arc tangent function.

$$\lambda_{max} = \arctan\left(\frac{-\left(\underline{\mathbf{1}}^{\mathbf{e}}_{\mathbf{0U}} \times \underline{\mathbf{1}}^{\mathbf{e}}_{\mathbf{0S}}\right)_y}{-\left(\underline{\mathbf{1}}^{\mathbf{e}}_{\mathbf{0U}} \times \underline{\mathbf{1}}^{\mathbf{e}}_{\mathbf{0S}}\right)_x}\right) = \arctan\left(\frac{\cos(L_U)\sin(L_S)\cos(\lambda_U) - \sin(L_U)\cos(L_S)\cos(\lambda_S)}{\sin(L_U)\cos(L_S)\sin(\lambda_S) - \cos(L_U)\sin(L_S)\sin(\lambda_U)}\right) \quad \text{Eq 156}$$

Criteria for when a route will include a vertex are given in Section 4.7.

Rather than requiring two points, the coordinates of the vertices of a great circle can be expressed in terms of the latitude L_U and longitude λ_U of a single point and the path azimuth $\psi_{S/U}$ at that point. Substituting from Eq 102 into Eq 154 and Eq 156 yields

$$\cos(L_{max}) = \cos(L_U)\left|\sin(\psi_{S/U})\right|$$
$$\tan(\lambda_{max}) = \frac{\sin(L_U)\left[\sin(\lambda_U)\tan(\psi_{S/U}) + \sin(L_U)\cos(\lambda_U)\right] + \cos^2(L_U)\cos(\lambda_U)}{\sin(L_U)\left[\cos(\lambda_U)\tan(\psi_{S/U}) - \sin(L_U)\sin(\lambda_U)\right] - \cos^2(L_U)\sin(\lambda_U)} \quad \text{Eq 157}$$

The first line of Eq 157 is the same as Eq 115. Since point **U** is arbitrary, it is effectively Clairaut's equation. When $\psi_{S/U}$ is close to $\pm$½π, it is advantageous to multiply the numerator and denominator of the second line by $\cos(\psi_{S/U})$, to eliminate use of $\tan(\psi_{S/U})$.

5.3.4 Locus of Points on a Great Circle

From Eq 126, any point **X** on the earth's surface has the *e*-frame coordinates $\underline{\mathbf{r}}^{\mathbf{e}}_{\mathbf{0X}}$ given by

$$\underline{\mathbf{r}}^{\mathbf{e}}_{\mathbf{0X}} = \begin{bmatrix} \underline{\mathrm{r}}^{\mathrm{e}}_{\mathrm{0X},x} \\ \underline{\mathrm{r}}^{\mathrm{e}}_{\mathrm{0X},y} \\ \underline{\mathrm{r}}^{\mathrm{e}}_{\mathrm{0X},z} \end{bmatrix} = \underline{\mathbf{1}}^{\mathbf{e}}_{\mathbf{0X}} R_e = \begin{bmatrix} \underline{1}^{\mathrm{e}}_{\mathrm{0X},x} \\ \underline{1}^{\mathrm{e}}_{\mathrm{0X},y} \\ \underline{1}^{\mathrm{e}}_{\mathrm{0X},z} \end{bmatrix} R_e = \begin{bmatrix} \cos(L_X)\cos(\lambda_X) \\ \cos(L_X)\sin(\lambda_X) \\ \sin(L_X) \end{bmatrix} R_e \quad \text{Eq 158}$$

Here L_X and λ_X are the latitude and longitude of **X**, respectively. In order for **X** to be on the great circle containing **U** and **S**, the vector $\underline{\mathbf{r}}^{\mathbf{e}}_{\mathbf{0X}}$ must be orthogonal to the vector $\underline{\mathbf{1}}^{\mathbf{e}}_{\mathbf{0U}} \times \underline{\mathbf{1}}^{\mathbf{e}}_{\mathbf{0S}}$ — that is, the dot product of these two vectors must be zero. One can then solve for L_X in terms of λ_X and the coordinates of **U** and **S**. The result is

$$L_X = -\arctan\left(\frac{\left(\underline{\mathbf{1}}^{\mathbf{e}}_{\mathbf{0U}} \times \underline{\mathbf{1}}^{\mathbf{e}}_{\mathbf{0S}}\right)_x \cos(\lambda_X) + \left(\underline{\mathbf{1}}^{\mathbf{e}}_{\mathbf{0U}} \times \underline{\mathbf{1}}^{\mathbf{e}}_{\mathbf{0S}}\right)_y \sin(\lambda_X)}{\left(\underline{\mathbf{1}}^{\mathbf{e}}_{\mathbf{0U}} \times \underline{\mathbf{1}}^{\mathbf{e}}_{\mathbf{0S}}\right)_z}\right) \quad \text{Eq 159}$$

Solving for λ_X in terms of L_X and the coordinates of **U** and **S** is more complicated. While every great circle crosses every line of longitude exactly once, a great circle may cross a line of latitude zero, one or two times. Section 4.6 addresses this issue using spherical trigonometry.

5.4 The Direct Problem of Geodesy

The Direct problem of geodesy (addressed using spherical trigonometry in Section 4.3) is concerned with two points, **U** and **S**, on the earth's surface. The known quantities are: the latitude/longitude of **U**, (L_U, λ_U); the geocentric angle, θ, between **U** and **S**; and the azimuth of **S** relative to **U**, $\psi_{S/U}$. The quantities to be found are: the latitude/longitude of **S**, (L_S, λ_S); and the azimuth of **U** relative to **S**, $\psi_{U/S}$. Two solution methods are presented — a method utilizing Direction Cosine Matrices (DCMs) which yields all three unknown quantities and a method based on the vector from **U** to **S** which only yields the coordinates (L_S, λ_S).

5.4.1 Full Solution Using Direction Cosine Matrices

Subsection 5.1.2 derives the DCM $\mathbf{C}_{\mathbf{e}}^{\mathbf{u}}$ which rotates the ECEF *e*-frame to a north-pointing *u*-frame that is parallel to a plane tangent to the earth at the user's location ('local-level'). Since interest is focused on a great circle path from **U** having azimuth angle $\psi_{S/U}$, it is useful to rotate the *u*-frame counter clockwise about its vertical axis by $½\pi - \psi_{S/U}$. The resulting u'-frame, which is an example of a 'wander azimuth' frame, has axes: e' (rotated from east, so that its azimuth angle is $\psi_{S/U}$), n' (rotated from north by the same amount as the e′ axis), and *u* (points up). Using Eq 129, the DCM $\mathbf{C}_{\mathbf{e}}^{\mathbf{u}'}$ is given by

$$\mathbf{C}_{\mathbf{e}}^{\mathbf{u}'} = \mathbf{T}_3(½\pi - \psi_{S/U})\,\mathbf{C}_{\mathbf{e}}^{\mathbf{u}} = \mathbf{T}_3(½\pi - \psi_{S/U})\mathbf{T}\,\mathbf{T}_2(-L_U)\,\mathbf{T}_3(\lambda_U) \qquad \text{Eq 160}$$

Upon carrying out the indicated multiplications, the elements of $\mathbf{C}_{\mathbf{e}}^{\mathbf{u}'}$ are given by

$$\begin{aligned}
\mathbf{C}_{\mathbf{e}}^{\mathbf{u}'}(1,1) &= -\sin(\lambda_U)\sin(\psi_{S/U}) - \sin(L_U)\cos(\lambda_U)\cos(\psi_{S/U}) \\
\mathbf{C}_{\mathbf{e}}^{\mathbf{u}'}(1,2) &= \cos(\lambda_U)\sin(\psi_{S/U}) - \sin(L_U)\sin(\lambda_U)\cos(\psi_{S/U}) \\
\mathbf{C}_{\mathbf{e}}^{\mathbf{u}'}(1,3) &= \cos(L_U)\cos(\psi_{S/U}) \\
\mathbf{C}_{\mathbf{e}}^{\mathbf{u}'}(2,1) &= \sin(\lambda_U)\cos(\psi_{S/U}) - \sin(L_U)\cos(\lambda_U)\sin(\psi_{S/U}) \\
\mathbf{C}_{\mathbf{e}}^{\mathbf{u}'}(2,2) &= \cos(\lambda_U)\cos(\psi_{S/U}) - \sin(L_U)\sin(\lambda_U)\sin(\psi_{S/U}) \\
\mathbf{C}_{\mathbf{e}}^{\mathbf{u}'}(2,3) &= \cos(L_U)\sin(\psi_{S/U}) \\
\mathbf{C}_{\mathbf{e}}^{\mathbf{u}'}(3,1) &= \cos(L_U)\cos(\lambda_U) \\
\mathbf{C}_{\mathbf{e}}^{\mathbf{u}'}(3,2) &= \cos(L_U)\sin(\lambda_U) \\
\mathbf{C}_{\mathbf{e}}^{\mathbf{u}'}(3,3) &= \sin(L_U)
\end{aligned} \qquad \text{Eq 161}$$

It follows from Eq 161 that

$$L_U = \arcsin\left(\mathbf{C}_{\mathbf{e}}^{\mathbf{u}'}(3,3)\right) \qquad \lambda_U = \arctan\left(\frac{\mathbf{C}_{\mathbf{e}}^{\mathbf{u}'}(3,2)}{\mathbf{C}_{\mathbf{e}}^{\mathbf{u}'}(3,1)}\right) \qquad \psi_{S/U} = \arctan\left(\frac{\mathbf{C}_{\mathbf{e}}^{\mathbf{u}'}(2,3)}{\mathbf{C}_{\mathbf{e}}^{\mathbf{u}'}(1,3)}\right) \qquad \text{Eq 162}$$

The DCM $\mathbf{C}_{\mathbf{e}}^{\mathbf{s}'}$ that rotates the *e*-frame to a plane that is parallel to a plane tangent to the earth at

S with its first axis aligned with the direction of rotation is given by

$$\mathbf{C}_{\mathbf{e}}^{\mathbf{s}'} = \mathbf{T}_2(\theta)\,\mathbf{C}_{\mathbf{e}}^{\mathbf{u}'} = \mathbf{T}_2(\theta)\,\mathbf{T}_3(½\pi - \psi_{S/U})\,\mathbf{T}\,\mathbf{T}_2(-L_U)\,\mathbf{T}_3(\lambda_U) \qquad \text{Eq 163}$$

The DCM $\mathbf{C}_{\mathbf{e}}^{\mathbf{s}'}$ can also be written in a form similar to Eq 160:

$$\mathbf{C}_{\mathbf{e}}^{\mathbf{s}'} = \mathbf{T}_3(½\pi - \psi_{U/S} - \pi)\,\mathbf{T}\,\mathbf{T}_2(-L_S)\,\mathbf{T}_3(\lambda_S) \qquad \text{Eq 164}$$

Equating these two forms for $\mathbf{C}_{\mathbf{e}}^{\mathbf{s}'}$, carrying out the multiplications indicated in Eq 163 and using the equivalent of Eq 162 results in:

$$L_S = \arcsin\left(\mathbf{C}_{\mathbf{e}}^{\mathbf{s}'}(3,3)\right) = \arcsin\left(\sin(L_U)\cos(\theta) + \cos(L_U)\sin(\theta)\cos\left(\psi_{S/U}\right)\right)$$

$$\lambda_S = \arctan\left(\frac{\mathbf{C}_{\mathbf{e}}^{\mathbf{s}'}(3,2)}{\mathbf{C}_{\mathbf{e}}^{\mathbf{s}'}(3,1)}\right)$$

$$= \arctan\left(\frac{\cos(L_U)\sin(\lambda_U)\cos(\theta) + \left[\cos(\lambda_U)\sin\left(\psi_{S/U}\right) - \sin(L_U)\sin(\lambda_U)\cos\left(\psi_{S/U}\right)\right]\sin(\theta)}{\cos(L_U)\cos(\lambda_U)\cos(\theta) - \left[\sin(\lambda_U)\sin\left(\psi_{S/U}\right) + \sin(L_U)\cos(\lambda_U)\cos\left(\psi_{S/U}\right)\right]\sin(\theta)}\right) \qquad \text{Eq 165}$$

$$\psi_{U/S} = \arctan\left(\frac{-\mathbf{C}_{\mathbf{e}}^{\mathbf{s}'}(2,3)}{-\mathbf{C}_{\mathbf{e}}^{\mathbf{s}'}(1,3)}\right) = \arctan\left(\frac{-\cos(L_U)\sin\left(\psi_{S/U}\right)}{\sin(L_U)\sin(\theta) - \cos(L_U)\cos(\theta)\cos\left(\psi_{S/U}\right)}\right)$$

When using Eq 165 to compute numerical values for L_S, λ_S and $\psi_{U/S}$, the elements of $\mathbf{C}_{\mathbf{e}}^{\mathbf{s}'}$ are taken from Eq 163. A two-argument arc tangent function is used for finding λ_S and $\psi_{U/S}$.

The expressions for L_S and $\psi_{U/S}$ that are right-most on the first and third lines of Eq 165 are identical to those derived using spherical trigonometry (Eq 91 and Eq 98, respectively). The expression for λ_S that is right-most on the second line is different from that derived using spherical trigonometry (Eq 94); however, the expressions can be shown to be equivalent using trigonometric identities.

5.4.2 Position Solution Using Vector **US**

A simpler but less rigourous approach to finding L_S and λ_S is to form $\underline{\mathbf{r}}_{\mathbf{OS}}^{\mathbf{e}}$ and utilize its components. Given L_U, λ_U, θ and $\psi_{S/U}$, one can form right triangle **OUS** with right angle at **U**, sides **OU** (length R_e) and **US** (length d), and hypotenuse **OS** (length $R_e + h_S$). Thus

$$d = R_e \tan(\theta)$$
$$R_e + h_S = \frac{R_e}{\cos(\theta)} \qquad \text{Eq 166}$$

Then $\underline{\mathbf{r}}_{\mathbf{US}}^{\mathbf{u}}$ is given by

$$\underline{\mathbf{r}}^{\mathbf{u}}_{\mathbf{US}} = \begin{bmatrix} \underline{\mathrm{r}}^{\mathrm{u}}_{\mathrm{US},e} \\ \underline{\mathrm{r}}^{\mathrm{u}}_{\mathrm{US},n} \\ \underline{\mathrm{r}}^{\mathrm{u}}_{\mathrm{US},u} \end{bmatrix} = \begin{bmatrix} \tan(\theta)\sin(\psi_{S/U}) \\ \tan(\theta)\cos(\psi_{S/U}) \\ 0 \end{bmatrix} R_e \qquad \text{Eq 167}$$

Utilizing Eq 126 and Eq 131 yields

$$\underline{\mathbf{r}}^{\mathbf{e}}_{\mathbf{OS}} = \underline{\mathbf{r}}^{\mathbf{e}}_{\mathbf{OU}} + \underline{\mathbf{r}}^{\mathbf{e}}_{\mathbf{US}} = \underline{\mathbf{r}}^{\mathbf{e}}_{\mathbf{OU}} + \mathbf{C}^{\mathbf{e}}_{\mathbf{u}}\,\underline{\mathbf{r}}^{\mathbf{u}}_{\mathbf{US}} = \underline{\mathbf{r}}^{\mathbf{e}}_{\mathbf{OU}} + (\mathbf{C}^{\mathbf{u}}_{\mathbf{e}})^T\,\underline{\mathbf{r}}^{\mathbf{u}}_{\mathbf{US}} = [\underline{\mathrm{r}}^{\mathrm{e}}_{\mathrm{OS},x} \quad \underline{\mathrm{r}}^{\mathrm{e}}_{\mathrm{OS},y} \quad \underline{\mathrm{r}}^{\mathrm{e}}_{\mathrm{OS},z}]^T$$

$$= \begin{bmatrix} \cos(L_U)\cos(\lambda_U) - \sin(\lambda_U)\tan(\theta)\sin(\psi_{S/U}) - \sin(L_U)\cos(\lambda_U)\tan(\theta)\cos(\psi_{S/U}) \\ \cos(L_U)\sin(\lambda_U) + \cos(\lambda_U)\tan(\theta)\sin(\psi_{S/U}) - \sin(L_U)\sin(\lambda_U)\tan(\theta)\cos(\psi_{S/U}) \\ \sin(L_U) + \cos(L_U)\tan(\theta)\cos(\psi_{S/U}) \end{bmatrix} R_e \qquad \text{Eq 168}$$

The magnitude of $\underline{\mathbf{r}}^{\mathbf{e}}_{\mathbf{OS}}$ is $R_e/\cos(\theta)$. Thus, from Eq 128 and Eq 168, L_S and λ_S are given by

$$L_S = \arcsin\left(\frac{\underline{\mathrm{r}}^{\mathrm{e}}_{\mathrm{OS},z}}{R_e/\cos(\theta)}\right) = \arcsin\big(\sin(L_U)\cos(\theta) + \cos(L_U)\sin(\theta)\cos(\psi_{S/U})\big)$$

$$\lambda_S = \arctan\big(\underline{\mathrm{r}}^{\mathrm{e}}_{\mathrm{OS},y}\,,\underline{\mathrm{r}}^{\mathrm{e}}_{\mathrm{OS},x}\big) \qquad \text{Eq 169}$$

$$= \arctan\left(\frac{\cos(L_U)\sin(\lambda_U)\cos(\theta) + \big[\cos(\lambda_U)\sin(\psi_{S/U}) - \sin(L_U)\sin(\lambda_U)\cos(\psi_{S/U})\big]\sin(\theta)}{\cos(L_U)\cos(\lambda_U)\cos(\theta) - \big[\sin(\lambda_U)\sin(\psi_{S/U}) + \sin(L_U)\cos(\lambda_U)\cos(\psi_{S/U})\big]\sin(\theta)}\right)$$

The geometric rationale for Eq 169 requires that $\theta < ½\pi$. However, the expressions are in fact identical to those in Eq 165 and are valid for $\theta \leq \pi$. Development of an expression for $\psi_{U/S}$ that does not involve chaining from the solutions for L_S and λ_S (as, e.g., Eq 145 does) does not appear to be possible using this approach.

5.5 Satellite Elevation Angle and Slant-Range

Sections 5.2 through 5.4 address the Direct and Indirect problems of geodesy, and show that, for two points on the surface of a spherical earth, the vector method can be used to perform essentially the same calculations as spherical trigonometry. However, Sections 5.2 through 5.4 do not address the quantities h_U, h_S, d or α — all of which are related to the height of the aircraft/satellite above the earth's surface. The two subsections immediately below show that if h_U, h_S and θ are known, then d and α can be found by the vector method. The expressions that are derived are identical to those found in Chapter 3 using the coordinate-free method.

Assuming h_U to be known, the four other possible equations associated with an aircraft or satellite above the earth when the geocentric angle θ is known — finding h_S or d from α and θ, and finding h_S or α from d and θ — are not pursued. For these variable combinations, the solutions for the unknown variables involve manipulation of the scalar components of $\underline{\mathbf{r}}^{\mathbf{u}}_{\mathbf{US}}$. That being the case, one may as well utilize the scalar equations in Chapter 3.

5.5.1 Solution for Elevation Angle from Altitude and Geocentric Angle

As shown in Eq 139 the satellite elevation angle can be found from the components of $\underline{\mathbf{r}}^{\mathbf{u}}_{\mathbf{US}}$. Using Eq 137, Eq 139 can be expanded as

$$\tan(\alpha) = \frac{(R_e + h_S)\cos(\theta) - (R_e + h_U)}{(R_e + h_S)\sin(\theta)} = \cot(\theta) - \frac{R_e + h_U}{(R_e + h_S)\sin(\theta)} \qquad \text{Eq 170}$$

The expressions in Eq 170 is identical to those in Eq 48, demonstrating that manipulating the components of $\underline{\mathbf{r}}^{\mathbf{u}}_{\mathbf{US}}$ can yield the same value for α as the scalar methodology used in Chapter 3.

5.5.2 Solution for Slant-Range from Altitude and Geocentric Angle

The user-satellite slant-range can be found by substituting both lines of Eq 137 into Eq 140, yielding:

$$d = 2R_e \sin\left(\tfrac{1}{2}\theta\right) \sqrt{\left(1 + \frac{h_U}{R_e}\right)\left(1 + \frac{h_S}{R_e}\right) + \left(\frac{h_S - h_U}{2R_e \sin\left(\frac{1}{2}\theta\right)}\right)^2} \quad , \quad \theta \neq 0 \qquad \text{Eq 171}$$

Eq 171 is identical to the second line of Eq 54. This demonstrates that applying Pythagoras's theorem to the components of $\underline{\mathbf{r}}^{\mathbf{u}}_{\mathbf{US}}$ (Eq 140) yields the same value for d as the scalar methodology used in Chapter 3.

5.6 Intersections Involving Two Great and/or Small Circles

This section addresses the intersection of two circles on a sphere: two great circles (Subsection 5.6.1), two small circles (Subsection 5.6.2) and a small circle with a great circle (Subsection 5.6.3). Small circles on the surface of a sphere are simply circles that are not great circles. Since there are three locations involved — the centers of the circles and intersection sought — the topic of this section contradicts the portion of the chapter title referring to 'two points'. This section draws upon material addressing both the Indirect (Section 5.3) and the Direct (Section 5.4) problems of geodesy.

5.6.1 Intersection of Two Great Circles

As noted in Subsection 5.3.3, a great circle can be characterized by a unit vector which is normal to the plane containing the great circle. When two points, **U** (L_U, λ_U) and **S** (L_S, λ_S), on great circle are known, the unit vector is given by (from Eq 153 and Eq 142)

$$\underline{\mathbf{1}}^{\mathbf{e}}_{\mathbf{GC}} = \frac{1}{\sin(\theta_{US})} \begin{bmatrix} \cos(L_U)\sin(L_S)\sin(\lambda_U) - \sin(L_U)\cos(L_S)\sin(\lambda_S) \\ \sin(L_U)\cos(L_S)\cos(\lambda_S) - \cos(L_U)\sin(L_S)\cos(\lambda_U) \\ \cos(L_U)\cos(L_S)\sin(\lambda_S - \lambda_U) \end{bmatrix} \qquad \text{Eq 172}$$

Alternatively, when one point **U** (L_U, λ_U) and the great circle's azimuth angle $\psi_{S/U}$ at **U** are

known, the normal can be found by assuming that $\theta_{US} = ½\pi$ and utilizing Eq 102

$$\underline{\mathbf{1}}^{\mathbf{e}}_{\mathbf{GC}} = \begin{bmatrix} \cos^2(L_U)\sin(\lambda_U)\cos(\psi_{S/U}) - \sin(L_U)\left[\sin(\psi_{S/U})\cos(\lambda_U) - \sin(L_U)\cos(\psi_{S/U})\sin(\lambda_U)\right] \\ -\cos^2(L_U)\cos(\lambda_U)\cos(\psi_{S/U}) - \sin(L_U)\left[\sin(\psi_{S/U})\sin(\lambda_U) + \sin(L_U)\cos(\psi_{S/U})\cos(\lambda_U)\right] \\ \cos(L_U)\sin(\psi_{S/U}) \end{bmatrix} \quad \text{Eq 173}$$

If two great circles are of interest, let the single known point on each have latitude L_i, longitude λ_i, and azimuth ψ_i, where $i = 1,2$. Thus, the unit normal vectors are given by

$$\underline{\mathbf{1}}^{\mathbf{e}}_i = \begin{bmatrix} \cos^2(L_i)\sin(\lambda_i)\cos(\psi_i) - \sin(L_i)\left[\sin(\psi_i)\cos(\lambda_i) - \sin(L_i)\cos(\psi_i)\sin(\lambda_i)\right] \\ -\cos^2(L_i)\cos(\lambda_i)\cos(\psi_i) - \sin(L_i)\left[\sin(\psi_i)\sin(\lambda_i) + \sin(L_i)\cos(\psi_i)\cos(\lambda_i)\right] \\ \cos(L_i)\sin(\psi_i) \end{bmatrix} \quad \text{Eq 174}$$

The cross product $\underline{\mathbf{1}}^{\mathbf{e}}_1 \times \underline{\mathbf{1}}^{\mathbf{e}}_2$ lies in the planes of both great circles. Thus the cross product and its negation point toward the intersections of the two great circles at $(L_{int+}, \lambda_{int+})$ and $(L_{int-}, \lambda_{int-})$.

$$L_{int\pm} = \pm \arctan\left(\frac{\left(\underline{\mathbf{1}}^{\mathbf{e}}_1 \times \underline{\mathbf{1}}^{\mathbf{e}}_2\right)_z}{\sqrt{\left(\underline{\mathbf{1}}^{\mathbf{e}}_1 \times \underline{\mathbf{1}}^{\mathbf{e}}_2\right)_x^2 + \left(\underline{\mathbf{1}}^{\mathbf{e}}_1 \times \underline{\mathbf{1}}^{\mathbf{e}}_2\right)_y^2}}\right)$$

$$\lambda_{int\pm} = \arctan\left(\frac{\pm\left(\underline{\mathbf{1}}^{\mathbf{e}}_1 \times \underline{\mathbf{1}}^{\mathbf{e}}_2\right)_y}{\pm\left(\underline{\mathbf{1}}^{\mathbf{e}}_1 \times \underline{\mathbf{1}}^{\mathbf{e}}_2\right)_x}\right) \quad \text{Eq 175}$$

In Eq 175, the plus or minus sign must be used consistently. The first line can be evaluated using the one-argument arc tangent function, while the two-argument arc tangent function should be used for the second line. The intersection of two great circles is addressed using spherical trigonometry in Section 6.3.

Great circles can be used to represent azimuth measurement of sensors, such as a radar or VOR. This representation overstates the actual coverage of physically realizable sensors, which generally extends from the sensor antenna in arc of a great circle with a length of at most a few degrees. Thus, the model can result in mathematical intersections (Eq 175) that are not 'physically real' which must be rejected.

5.6.2 Intersection of Two Small Circles

Let the centers (and known coordinates) of the small circles on the earth's surface be **U** (L_U, λ_U) and **S** (L_S, λ_S). The known geocentric angles (similar to radii) of the circles about **U** and **S** are θ_{UA} and θ_{SA}, respectively, where **A** denotes an aircraft with unknown coordinates (L_A, λ_A). (When celestial sightings are involved, the error incurred by assuming that aircraft **A** is on the earth's surface is less than that incurred by assuming that the earth is a sphere.)

The first step is to utilize the Indirect problem of geodesy (Section 5.2) to find the geocentric angle θ_{US} between **U** and **S** and the azimuth angle $\psi_{S/U}$ of **S** at **U**. The mathematical issues of existence and uniqueness must then be considered. If either of the following conditions are true, an intersection does not exist:

$$\theta_{UA} + \theta_{SA} < \theta_{US} \qquad |\theta_{UA} - \theta_{SA}| > \theta_{US} \qquad \text{Eq 176}$$

When a solution does exist, there may be one intersection (which is located along the great circle connecting **U** and **S** and for which one expression in Eq 176 would become an equality) or two intersections (which are equal distance from the great circle connecting **U** and **S**). The general case is two intersections.

Assuming a solution exists, it is useful, as in Subsection 5.4.1, to consider the local level *u*-frame after being rotated counter clockwise about its vertical axis by $½\pi - \psi_{S/U}$, resulting in the wander azimuth *u'*-frame. The DCM $\mathbf{C}_{\mathbf{e}}^{\mathbf{u}'}$ is given by Eq 160 and Eq 161. Utilizing Eq 134 and Eq 135 (the latter in conjunction with Eq 78, Eq 84 and Eq 85), the vectors $\underline{\mathbf{r}}_{\mathbf{OU}}^{\mathbf{u}'}$ and $\underline{\mathbf{r}}_{\mathbf{OS}}^{\mathbf{u}'}$ are

$$\underline{\mathbf{r}}_{\mathbf{OU}}^{\mathbf{u}'} = \mathbf{T}_3(½\pi - \psi_{S/U})\,\underline{\mathbf{r}}_{\mathbf{OU}}^{\mathbf{u}} = \begin{bmatrix}0\\0\\1\end{bmatrix} R_e$$
$$\underline{\mathbf{r}}_{\mathbf{OS}}^{\mathbf{u}'} = \mathbf{T}_3(½\pi - \psi_{S/U})\,\underline{\mathbf{r}}_{\mathbf{OS}}^{\mathbf{u}} = \begin{bmatrix}\sin(\theta_{US})\\0\\\cos(\theta_{US})\end{bmatrix} R_e \qquad \text{Eq 177}$$

Let the components of $\underline{\mathbf{r}}_{\mathbf{OA}}^{\mathbf{u}'}$ be given by $\underline{\mathbf{r}}_{\mathbf{OA}}^{\mathbf{u}'} = \begin{bmatrix}\underline{\mathrm{r}}_{\mathrm{OA},e'}^{\mathrm{u}'} & \underline{\mathrm{r}}_{\mathrm{OA},n'}^{\mathrm{u}'} & \underline{\mathrm{r}}_{\mathrm{OA},u}^{\mathrm{u}'}\end{bmatrix}^T$. Because its length is constrained to be R_e, only two components of $\underline{\mathbf{r}}_{\mathbf{OA}}^{\mathbf{u}'}$ are independent. Knowledge of the small circle geocentric angles yields

$$\underline{\mathbf{r}}_{\mathbf{OU}}^{\mathbf{u}'} \bullet \underline{\mathbf{r}}_{\mathbf{OA}}^{\mathbf{u}'} = R_e\,\underline{\mathrm{r}}_{\mathrm{OA},u}^{\mathrm{u}'} = R_e^2\cos(\theta_{UA})$$
$$\underline{\mathbf{r}}_{\mathbf{OS}}^{\mathbf{u}'} \bullet \underline{\mathbf{r}}_{\mathbf{OA}}^{\mathbf{u}'} = R_e\left[\underline{\mathrm{r}}_{\mathrm{OA},e'}^{\mathrm{u}'}\sin(\theta_{US}) + \underline{\mathrm{r}}_{\mathrm{OA},u}^{\mathrm{u}'}\cos(\theta_{US})\right] = R_e^2\cos(\theta_{SA}) \qquad \text{Eq 178}$$

Thus, the two intersections are given by

$$\underline{\mathbf{r}}_{\mathbf{OA}\pm}^{\mathbf{u}'} = \begin{bmatrix}\underline{\mathrm{r}}_{\mathrm{OA},e'}^{\mathrm{u}'}\\ \underline{\mathrm{r}}_{\mathrm{OA},n'\pm}^{\mathrm{u}'}\\ \underline{\mathrm{r}}_{\mathrm{OA},u}^{\mathrm{u}'}\end{bmatrix} = \begin{bmatrix}\dfrac{\cos(\theta_{SA}) - \cos(\theta_{UA})\cos(\theta_{US})}{\sin(\theta_{US})}\\ \pm\sqrt{1 - \cos^2(\theta_{UA}) - \left(\dfrac{\cos(\theta_{SA}) - \cos(\theta_{UA})\cos(\theta_{US})}{\sin(\theta_{US})}\right)^2}\\ \cos(\theta_{UA})\end{bmatrix} R_e \qquad \text{Eq 179}$$

The *e*-frame components of $\underline{\mathbf{r}}_{\mathbf{OA}\pm}$ are found, using Eq 160 and Eq 161, by

$$\underline{\mathbf{r}}^{\mathbf{e}}_{\mathbf{OA}\pm} = \begin{bmatrix} \underline{r}^{e}_{OA,x\pm} \\ \underline{r}^{e}_{OA,y\pm} \\ \underline{r}^{e}_{OA,z\pm} \end{bmatrix} = \mathbf{C}^{\mathbf{e}}_{\mathbf{u}'}\, \underline{\mathbf{r}}^{\mathbf{u}'}_{\mathbf{OA}\pm} = \left(\mathbf{C}^{\mathbf{u}'}_{\mathbf{e}}\right)^{T} \underline{\mathbf{r}}^{\mathbf{u}'}_{\mathbf{OA}\pm} \qquad \text{Eq 180}$$

Finally, the two possible latitudes and longitudes of **A** are found by

$$L_{A\pm} = \arctan\left(\frac{\underline{r}^{e}_{OA,z\pm}}{\sqrt{\left(\underline{r}^{e}_{OA,x\pm}\right)^2 + \left(\underline{r}^{e}_{OA,y\pm}\right)^2}}\right) = \arcsin\left(\frac{\underline{r}^{e}_{OU,z\pm}}{R_e}\right) \qquad \text{Eq 181}$$

$$\lambda_{A\pm} = \arctan\left(\underline{r}^{e}_{OA,y\pm}, \underline{r}^{e}_{OA,x\pm}\right)$$

In Eq 179-Eq 181, the plus or minus sign must be used consistently. The first line of Eq 181 can be evaluated using the one-argument arc tangent function, while the two-argument arc tangent function should be used for the second line.

Remarks:

- Because the elevation angle of a star, at a known time, defines a small circle on the earth, finding the intersection two small circles is a fundamental task of celestial navigation. Historically, converting a sextant measurement of a star's elevation angle to a small circle, called sight reduction, was a challenging task — see Chapter 20 of Ref. 1. The intersection of small circles was then usually found graphically, resulting in a fix with accuracy of approximately 1 NM. Today the computational process is automated; the U.S. Navy's STELLA (System To Estimate Latitude and Longitude Astronomically) program performs both sight reduction and intersection determination.
- Finding a vehicle location from two range type measurements is one the simplest non-trivial real-world navigation problems, yet it involves many of the issues present in more complex problems — e.g., solution existence/uniqueness and accuracy sensitivity to vehicle location. The closely related problems of finding the intersection of two DME or radar slant-ranges (the topic of Section 6.4) and finding the location of a vehicle on a hypothetical two-dimensional plane (Example 8, addressed in Subsections 7.12.1 and 8.5.1) involve and expand upon these issues.
- The ambiguity in Eq 179-Eq 181 cannot be resolved from the available measurements. However, in applications, additional information is often available — see Subsection 6.1.3, particularly item (2). In this situation, the two solutions are symmetric about the station baseline/extensions. Unless the vehicle is moving parallel to the baseline, both solutions will move with a component either toward or away from the baseline. The vehicle's actual direction of motion, sensed by an on-board compass, can be used to select the correct solution.

5.6.3 Intersection of a Small Circle and a Great Circle

A great circle can be defined either by two points (e.g., Eq 172) or by one point and the path azimuth at that point (e.g., Eq 173). However, neither of these formulations is involved in the

solution process described in this subsection. Thus, let the unit vector that is normal to the plane of the great circle in the ECEF frame **e** which points toward the northern hemisphere be $\underline{\mathbf{1}}^{\mathbf{e}}_{\mathbf{G}}$.

$$\underline{\mathbf{1}}^{\mathbf{e}}_{\mathbf{G}} = \begin{bmatrix} \underline{1}^{\mathrm{e}}_{\mathrm{G},x} \\ \underline{1}^{\mathrm{e}}_{\mathrm{G},y} \\ \underline{1}^{\mathrm{e}}_{\mathrm{G},z} \end{bmatrix} \qquad \text{Eq 182}$$

Let the center (and known coordinates) of the small circle be **C** (L_C, λ_C). The geocentric angle of the small circle about **C**, $\theta_{CA} \geq 0$, is also known. (The case of $\theta_{CA} = 0$ is addressed in the Remarks below.) Here, **A** denotes an aircraft with the unknown coordinates sought, (L_A, λ_A). The unit vector $\underline{\mathbf{1}}^{\mathbf{e}}_{\mathbf{OC}}$ from the earth's center **O** toward **C** is (Eq 126)

$$\underline{\mathbf{1}}^{\mathbf{e}}_{\mathbf{OC}} = \begin{bmatrix} \underline{1}^{\mathrm{e}}_{\mathrm{OC},x} \\ \underline{1}^{\mathrm{e}}_{\mathrm{OC},y} \\ \underline{1}^{\mathrm{e}}_{\mathrm{OC},z} \end{bmatrix} = \begin{bmatrix} \cos(L_C)\cos(\lambda_C) \\ \cos(L_C)\sin(\lambda_C) \\ \sin(L_C) \end{bmatrix} \qquad \text{Eq 183}$$

A solution (i.e., intersection) to this problem does not exist if

$$\theta_{CG} = \arccos\left(\underline{\mathbf{1}}^{\mathbf{e}}_{\mathbf{OC}} \bullet \underline{\mathbf{1}}^{\mathbf{e}}_{\mathbf{G}}\right) < \tfrac{1}{2}\pi - \theta_{CA} \qquad \text{Eq 184}$$

When a solution does exist, there may be one intersection (for which the expression in Eq 184 becomes an equality) or two intersections. The general case is two intersections.

Assuming that a solution exists, define the point **S** by the unit vector

$$\underline{\mathbf{1}}^{\mathbf{e}}_{\mathbf{OS}} = \frac{1}{\sin(\theta_{CG})}\left(\underline{\mathbf{1}}^{\mathbf{e}}_{\mathbf{G}} \times \underline{\mathbf{1}}^{\mathbf{e}}_{\mathbf{OC}}\right) = \begin{bmatrix} \underline{1}^{\mathrm{e}}_{\mathrm{OS},x} \\ \underline{1}^{\mathrm{e}}_{\mathrm{OS},y} \\ \underline{1}^{\mathrm{e}}_{\mathrm{OS},z} \end{bmatrix} \qquad \text{Eq 185}$$

Vector $\underline{\mathbf{1}}^{\mathbf{e}}_{\mathbf{OS}}$ is orthogonal to the plane containing $\underline{\mathbf{1}}^{\mathbf{e}}_{\mathbf{G}}$ and $\underline{\mathbf{1}}^{\mathbf{e}}_{\mathbf{OC}}$ and is in the plane containing the great circle. Then define the the point **U** on the great circle by its unit vector $\underline{\mathbf{1}}^{\mathbf{e}}_{\mathbf{OU}}$

$$\underline{\mathbf{1}}^{\mathbf{e}}_{\mathbf{OU}} = \underline{\mathbf{1}}^{\mathbf{e}}_{\mathbf{OS}} \times \underline{\mathbf{1}}^{\mathbf{e}}_{\mathbf{G}} = \begin{bmatrix} \underline{1}^{\mathrm{e}}_{\mathrm{OU},x} \\ \underline{1}^{\mathrm{e}}_{\mathrm{OU},y} \\ \underline{1}^{\mathrm{e}}_{\mathrm{OU},z} \end{bmatrix} \qquad \text{Eq 186}$$

Points **S** and **U** are orthogonal by construction. Point **U** is the location on the great circle nearest to **C**; its latitude L_U and longitude λ_U are given by Eq 127. The path azimuth $\psi_{S/U}$ at **U** can be found from Clairaut's equation (Eq 154 and Eq 157)

$$\sin(\psi_{S/U}) = \frac{\cos(L_{max})}{\cos(L_U)} = \frac{\underline{1}^{\mathrm{e}}_{\mathrm{G},z}}{\cos(L_U)} \qquad \text{Eq 187}$$

When L_U, λ_U and $\psi_{S/U}$ are known, the DCM $\mathbf{C}^{\mathbf{u}'}_{\mathbf{e}}$ for the wander azimuth, local level u'-frame

(Eq 160 and Eq 161) is fully specified. In the u'-frame, the known coordinates of **C** are given by

$$\underline{\mathbf{1}}_{\mathbf{OC}}^{\mathbf{u}'} = \begin{bmatrix} \underline{\mathrm{r}}_{\mathrm{OC},e'}^{\mathrm{u}'} \\ \underline{\mathrm{r}}_{\mathrm{OC},n'}^{\mathrm{u}'} \\ \underline{\mathrm{r}}_{\mathrm{OC},u}^{\mathrm{u}'} \end{bmatrix} = \begin{bmatrix} 0 \\ \sin\left(\frac{1}{2}\pi - \theta_{CG}\right) \\ \cos\left(\frac{1}{2}\pi - \theta_{CG}\right) \end{bmatrix} = \begin{bmatrix} 0 \\ \cos(\theta_{CG}) \\ \sin(\theta_{CG}) \end{bmatrix} \quad \text{Eq 188}$$

Let the components of $\underline{\mathbf{1}}_{\mathbf{OA}}^{\mathbf{u}'}$ be given by

$$\underline{\mathbf{1}}_{\mathbf{OA}}^{\mathbf{u}'} = \begin{bmatrix} \underline{1}_{\mathrm{OA},e'}^{\mathrm{u}'} \\ \underline{1}_{\mathrm{OA},n'}^{\mathrm{u}'} \\ \underline{1}_{\mathrm{OA},u}^{\mathrm{u}'} \end{bmatrix} = \begin{bmatrix} \underline{1}_{\mathrm{OA},e'}^{\mathrm{u}'} \\ 0 \\ \underline{1}_{\mathrm{OA},u}^{\mathrm{u}'} \end{bmatrix} \quad \text{Eq 189}$$

Because its length is constrained, only one component of $\underline{\mathbf{1}}_{\mathbf{OA}}^{\mathbf{u}'}$ can be independently chosen or determined. The inner product of $\underline{\mathbf{1}}_{\mathbf{OC}}^{\mathbf{u}'}$ and $\underline{\mathbf{1}}_{\mathbf{OA}}^{\mathbf{u}'}$ yields

$$\underline{\mathbf{1}}_{\mathbf{OU}}^{\mathbf{u}'} \bullet \underline{\mathbf{1}}_{\mathbf{OA}}^{\mathbf{u}'} = \underline{1}_{\mathrm{OA},u}^{\mathrm{u}'} \sin(\theta_{CG}) = \cos(\theta_{CA}) \quad \text{Eq 190}$$

Thus, the two intersections are given by

$$\underline{\mathbf{1}}_{\mathbf{OA}\pm}^{\mathbf{u}'} = \begin{bmatrix} \underline{1}_{\mathrm{OA},e'\pm}^{\mathrm{u}'} \\ \underline{1}_{\mathrm{OA},n'}^{\mathrm{u}'} \\ \underline{1}_{\mathrm{OA},u}^{\mathrm{u}'} \end{bmatrix} = \begin{bmatrix} \pm\sqrt{1 - \left(\frac{\cos(\theta_{CA})}{\sin(\theta_{CG})}\right)^2} \\ 0 \\ \frac{\cos(\theta_{CA})}{\sin(\theta_{CG})} \end{bmatrix} \quad \text{Eq 191}$$

The e-frame components of $\underline{\mathbf{r}}_{\mathbf{OA}\pm}$ are found, using Eq 160 and Eq 161, by

$$\underline{\mathbf{1}}_{\mathbf{OA}\pm}^{\mathbf{e}} = \begin{bmatrix} \underline{1}_{\mathrm{OA},x\pm}^{\mathrm{e}} \\ \underline{1}_{\mathrm{OA},y\pm}^{\mathrm{e}} \\ \underline{1}_{\mathrm{OA},z\pm}^{\mathrm{e}} \end{bmatrix} = \mathbf{C}_{\mathbf{u}'}^{\mathbf{e}} \, \underline{\mathbf{1}}_{\mathbf{OA}\pm}^{\mathbf{u}'} = \left(\mathbf{C}_{\mathbf{e}}^{\mathbf{u}'}\right)^T \underline{\mathbf{1}}_{\mathbf{OA}\pm}^{\mathbf{u}'} \quad \text{Eq 192}$$

Finally, the two possible latitudes and longitudes of **A** are found by

$$L_{A\pm} = \arctan\left(\frac{\underline{1}_{\mathrm{OA},z\pm}^{\mathrm{e}}}{\sqrt{\left(\underline{1}_{\mathrm{OA},x\pm}^{\mathrm{e}}\right)^2 + \left(\underline{1}_{\mathrm{OA},y\pm}^{\mathrm{e}}\right)^2}}\right) = \arcsin\left(\underline{1}_{\mathrm{OU},z\pm}^{\mathrm{e}}\right)$$
$$\lambda_{A\pm} = \arctan\left(\underline{1}_{\mathrm{OA},y\pm}^{\mathrm{e}}, \underline{1}_{\mathrm{OA},x\pm}^{\mathrm{e}}\right) \quad \text{Eq 193}$$

In Eq 191-Eq 193, the plus or minus sign must be used consistently. The first line of Eq 193 can be evaluated using the one-argument arc tangent function, while the two-argument arc tangent function should be used for the second line.

Remarks:

- Finding the intersection of a great circle and small circle is similar to the problem addressed in Section 6.5 using spherical trigonometry.
- The limiting case of a small circle is a point. Thus, point **U** is the location on the great circle with unit normal $\underline{\mathbf{1}}_{\mathbf{G}}^{\mathbf{e}}$ that is closest to point **C**.
- The solution ambiguity in Eq 191-Eq 193 cannot be resolved from the mathematical model employed. However, if the great circle is a representation of a sensor measurement of azimuth, it may be possible to simply discard one solution. Moreover, if that is not the case and the vehicle is in motion, the two solutions will both move toward or away from **U** in unison. In that case, an on-board compass may be used to determine the correct solution.

6. AIRCRAFT POSITION FROM TWO RANGE AND/OR AZIMUTH MEASUREMENTS (TRIGONOMETRIC FORMULATIONS)

6.1 General Considerations

6.1.1 Problems Addressed

This chapter combines the formulations of Chapter 3 (involving plane trigonometry applied to a vertical-plane) and Chapter 4 (involving spherical trigonometry applied to the earth's surface). Whereas both of those formulations are limited to two problem-specific points, usually labeled **U** and **S**, this chapter addresses situations involving three problem-specific points embedded in three dimensions. Relevant applications include aircraft navigation (specifically, Area Navigation, or RNAV) and aircraft surveillance (including sensor fusion).

For this methodology, typically, one point corresponds to the aircraft (having an unknown latitude/longitude but known altitude), and the other two points correspond to sensor stations having known locations and altitudes. Each sensor station provides a scalar measurement that describes a geometric Surface-Of-Position (SOP) on which the aircraft lies. The solution for the aircraft position is the intersection of three SOPs. When attention is limited to the earth's surface, 3D SOPs reduce to 2D Lines-Of-Position (LOPs).* Analytically, the three points form a mathematical spherical triangle which can be solved using spherical trigonometry.

Before circa 1950 (when synchronization of ground stations, and thus pseudorange measurements, became possible – see Chapter 7), the most common sensor systems measured

(a) Slant-range d_{AS} – line-of-sight distance between a sensor station **S** and aircraft **A**
(b) Spherical-range $s_{AS} = R_e\,\theta_{AS}$ – distance along the earth's surface between a sensor's and the aircraft's ground subpoints
(c) Azimuth $\psi_{A/S}$ – angle of the great circle path from the sensor station to the aircraft
(d) Azimuth $\psi_{S/A}$ – angle of the great circle path from the aircraft to the sensor station
(e) Altitude h_A – height of the aircraft above the mean sea level.

Slant-range measurements provide an SOP in the form of a sphere centered on the station. Spherical-range measurements provide an SOP in the form of a cone with apex at the earth's center and axis intersecting a known point on the surface. Azimuth measurements provide an SOP in the form of a vertical plane that passes through the sensor, the aircraft and the earth's center (i.e., a great circle). A barometric altimeter provides an SOP in the form of a sphere concentric with the earth.

* LOPs were first formulated by Capt. Thomas Hubbard Sumner, a U.S. Navy officer, in 1837, while commanding a sailing ship in heavy gales near the Irish coast. Sumner was born in Boston in 1807, and graduated from Harvard Univ. Two U.S. Navy survey ships have been named the *USS Sumner*. Some texts refer to LOPs as 'Sumner lines'.

The most common civil aviation slant-range and azimuth sensors are

- Slant-range between aircraft and station
  - Navigation: Distance Measuring Equipment (DME)
  - Surveillance: Secondary Surveillance Radar (SSR)
- Spherical-range between aircraft and station
  - Navigation: Star fix
- Azimuth angle from the station to the aircraft
  - Navigation: VHF Omnidirectional Range (VOR)
  - Navigation: Instrument Landing System (ILS) Localizer
  - Surveillance: Secondary Surveillance Radar (SSR)
- Azimuth angle from the aircraft to the station
  - Navigation: Non-Directional Beacon (NDB)
  - Navigation: Aircraft-based radar

This chapter addresses calculation of aircraft latitude/longitude from measurements of altitude in combination with those for slant-range and/or azimuth. In Sections 6.4 and 6.5, the slant-range measurements are converted to spherical-ranges at the start of each calculation; thus the material can be utilized for spherical-range measurements as well.

This chapter does not consider errors in the computed coordinates that result from measurement errors. That topic is addressed in Chapter 8. Also, there are several iterative methods for computing latitude and longitude from measurements of slant-range and/or azimuth on an ellipsoidal earth (e.g., Refs. 12 and 36). Those calculations can be initialized using solutions found using the approaches described in this chapter.

6.1.2 Geometric Concerns (Solution Existence/Uniqueness)

The geometric relationship of two sensors and an aircraft is an important aspect of these analyses. Situations where the aircraft is directly above a ground station are excluded for several reasons: ground station antenna patterns are generally not designed to irradiate directly above the station; and the azimuth angle to an aircraft is undefined when an aircraft is above an azimuth determination station. Moreover, when an aircraft is directly above a ground station, that situation intrinsically constitutes a fix.

Restricting attention to the surface of the earth, when two measurements are available, several unfavorable geometries can occur. Figure 26 depicts examples involving aircraft **A** and stations **U** and **S**. Panel (a): Due to measurement errors, it is possible that the measurements are inconsistent and a solution does not exist. Panel (b): When the SOPs for two sensors overlap, only a partial position solution exists. Panel (c): When the two SOPs are tangent, measurement errors can cause the computed position error to increase significantly along the direction of the two LOPs. Panel (d): Multiple solutions occur when the LOPs intersect at more than one point.

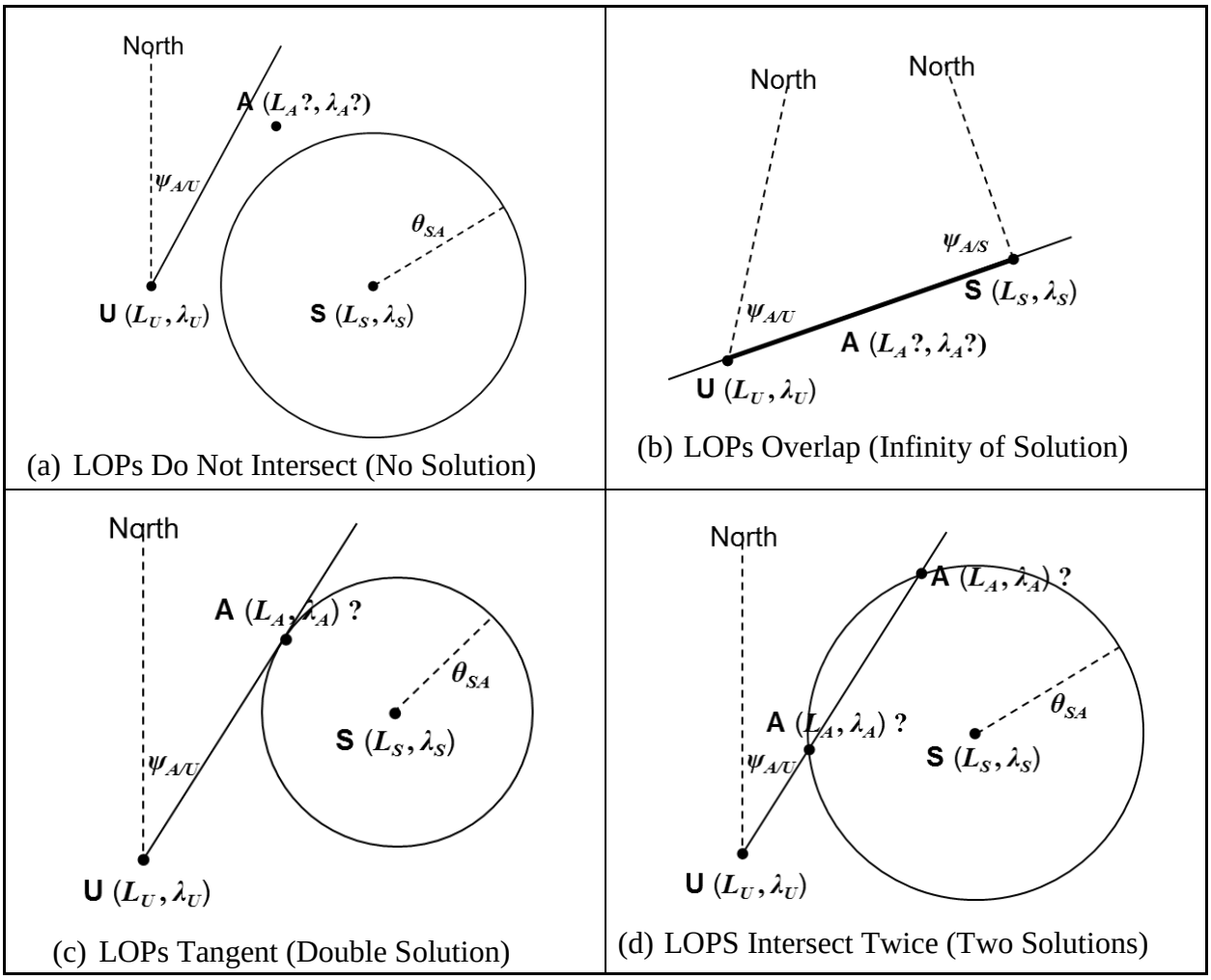

(a) LOPs Do Not Intersect (No Solution)

(b) LOPs Overlap (Infinity of Solution)

(c) LOPs Tangent (Double Solution)

(d) LOPS Intersect Twice (Two Solutions)

Figure 26 Possible Geometric Relationships involving an Aircraft and Two Ground Stations

6.1.3 Resolution of Multiple Solutions

Of the complications considered in Subsection 6.1.2, the one with the greatest need for the navigator's or analyst's involvement is the existence of a few (usually two) potential solutions. Multiple solutions arise in two ways:

- Ambiguous — Two or more aircraft locations can result in the same set of measurements, as in Figure 26(d); the correct solution cannot be determined without additional (sometimes called 'side') informaton.
- Extraneous — Additional solutions are introduced by analytic manipulations, but do not satisfy the measurement equations, and thus can be eliminated mathematically. These occur most often with pseudo range measurements — see Chapter 7.

While unresolvable mathematically, ambiguous solutions can often be resolved operationally. There are three general sources of information to do so:

(1) Prior position information — Often, based on dead reckoning from either the departure location or a previous fix, a vehicle's crew will be able to determine which

of two (or a few) position solutions are corect.

(2) Direction of vehicle motion — Usually, the track of a vehicle following a constant heading will correlate well with one ambiguous solution while it does not correlate with others. Examples are specific to the types of the sensors involved, and individual sections of this document address these situations.

(3) Additional 'position' sensors — There may be information available from other 'position' sensors, even approximate, which can be used to resolve solution ambiguities. Crude azimuth sensors (e.g., on-board radio direction-finding equipment) can be valuable in this regard.

6.1.4 Rationale for Two-Station Area Navigation (RNAV)

None of the geometric issues illustrated in Figure 26 arises when the slant-range and azimuth sensors are collocated. Since radars and combined VOR/DME stations are prevalent in the NAS, the question naturally arises: Why not only use a single radar or VOR/DME station to determine a vehicle's latitude and longitude? There are several reasons to utilize navigation fixes from geographically separate stations:

- Accuracy: When an aircraft is more than a few of miles from a radar or VOR/DME station, the range measurement is more accurate than the azimuth measurement. Moreover, the difference increases with distance from the station. Thus, for accuracy, utilizing two stations is generally preferable
- Contingency/backup: When one of the functions of a VOR/DME station is out of service, utilizing a second station may allow a flight to continue when otherwise it could not. More broadly, RNAV using VOR/DME stations is likely to become the backup to GPS for en route and terminal area navigation.
- Advanced avionics: Aircraft with advanced navigation systems (navigation radios and flight computers) are capable of utilizing measurements from multiple stations, whereas older and/or less sophisticated avionics cannot.

Standards for aircraft RNAV systems based on DME/DME measurements, but permitting VOR measurements, are presented in Ref. 37. Items (1) and (2) pertain to SSR surveillance as well. The FAA is now incorporating 'sensor fusion' into its Automation (surveillance processing) systems to take advantage of these benefits.

6.1.5 Chapter Overview

Following this introductory section, Section 6.2 analyzes the problem of a great circle and a point that is not necessarily on the great circle. The next three sections address situations involving two stations providing slant-range and/or azimuth measurements which are used (with aircraft altimeter information) to determine the aircraft location: Section 6.3, azimuth/ azimuth; Section 6.4, range/range; and Section 6.5, range/azimuth. Lastly, Section 6.6 addresses using a range measurement to crosscheck the altitude of an aircraft flying an approach procedure.

The solutions in Sections 6.3 - 6.5 follow a common pattern: (a) When a slant-range measurement d is involved, Eq 44 is used to obtain the corresponding geocentric angle θ. This reduces the problem to one of spherical trigonometry. (b) The parameters for the baseline joining the sensor stations are found as solutions to the Indirect problem of geodesy (Section 4.2). (c) The possibility that the problem is ill-posed is investigated (e.g., Figure 26(a)). (d) The case (Subsection 4.1.7) of the mathematical spherical triangle comprised of the two stations and the aircraft is identified, and the corresponding solution is found. (d) Parameters for the mathematical triangle are used to determine the aircraft latitude/longitude coordinates.

6.2 Relationship between a Point and a Great Circle Path

6.2.1 Problem Statement

Often there is a need to find the relationship between a discrete point on the earth's surface and a great circle path. A possible scenario is shown in Figure 27: A vessel **V** intends to transit a great circle path from location **U** [coordinates (L_U, λ_U)] to location **S** [coordinates (L_S, λ_S)], beginning with departure azimuth $\psi_{S/U}$. While in en route, the navigator determines that the actual vessel location is **V** (L_V, λ_V), which may not be on the intended path. The navigator wants to find relevant quantities such as how far off-course the vessel is in both distance and azimuth angle.

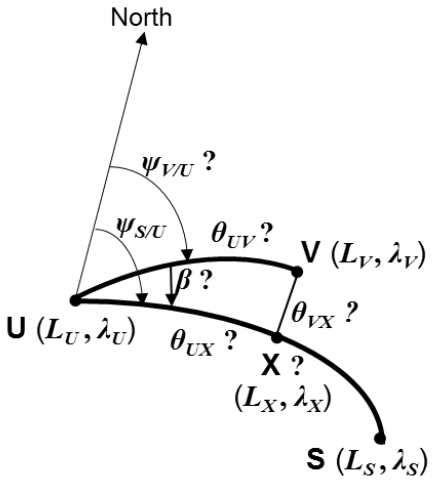

Figure 27 Vessel **V** and Intended Great Circle Path **US**

For such a scenario, the coordinates of **U**, **V** and **S** are all known. Thus, for triangle **UVS**, the side lengths and side azimuth angles can all be found as solutions to the Indirect problem of geodesy (Section 4.2). Given those calculations, in terms of the classic 'solving a triangle' taxonomy, this is an SSS (side-side-side) situation. However, it does not have infeasible formulations or ambiguous solutions, as occur in Section 6.4 for a 'pure' SSS situation.

In addition to the sides of **UVS**, the quantities of interest can include the coordinates of the nearest point **X** (L_X, λ_X) on the intended path, the distance θ_{VX} from the vessel to the nearest point on the intended path, the projection of the distance traveled onto the intended path θ_{UX} and the off-path angle β.

6.2.2 Problem Solution

Solution to this problem is a five-step process. The first step is to apply the Indirect problem of

geodesy (Section 4.2) to the great circle path **UV**, finding the azimuth angle $\psi_{V/U}$ and the distance θ_{UV}. The fact that the vessel's actual track over the earth may not have been the great circle path **UV** is not relevant – only the end points are.

Because (a) the great circle through **U** and **S** encircles the earth and the vehicle may have traveled 'in the wrong direction', and (b) azimuth (bearing) angles can vary over (–π, π], the angle β between **US** and **UV** is computed in the range [0, π] using

$$\beta = \min\left\{ \left|\psi_{S/U} - \psi_{V/U}\right|, \left|\psi_{S/U} - \psi_{V/U} + 2\pi\right|, \left|\psi_{S/U} - \psi_{V/U} - 2\pi\right| \right\} \quad \text{Eq 194}$$

When $\beta = 0$, the vessel is on the intended path.

The third step addresses the mathematical spherical triangle **UVX**, where the angle at **X** is a right-angle. The law of sines (Eq 73) yields the off-course distance θ_{VX} in the range [0, π/2]

$$\theta_{VX} = \text{Arcsin}[\sin(\theta_{UV})\sin(\beta)] \quad \text{Eq 195}$$

While Eq 195 has two mathematical solutions, the smaller of the two positive angles will be correct in all but the most extreme circumstances.

Again considering triangle **UVX**, the projection of the distance traveled onto the intended path θ_{UX} is found from the law of cosines for sides (Eq 71) and Eq 15

$$\theta_{UX} = \arccos\left(\frac{\cos(\theta_{UV})}{\cos(\theta_{VX})}\right) = 2\arcsin\left(\sqrt{\frac{\sin\left[\frac{1}{2}(\theta_{UV}+\theta_{VX})\right]\sin\left[\frac{1}{2}(\theta_{UV}-\theta_{VX})\right]}{\cos(\theta_{VX})}}\right) \quad \text{Eq 196}$$

Finally, the coordinates (L_X, λ_X) are found as a solution to the Direct problem of geodesy (Section 4.3) based on knowledge of (L_U, λ_U), θ_{UX} and $\psi_{S/U}$.

6.3 Solution for Two Azimuth Measurements

In this section, the assumption is that the latitude/longitude coordinates of stations **U** (L_U, λ_U) and **S** (L_S, λ_S) are known, as are their azimuth (or bearing) angles, $\psi_{A/U}$ and $\psi_{A/S}$, to a third (aircraft) location **A**. The solution for the coordinates of **A** and related parameters follows the pattern described in Subsection 6.1.5. The approach is based on the mathematical spherical triangle **USA**. In terms of the classic 'solving a triangle' taxonomy, this is an ASA (angle-side-angle) situation.

6.3.1 Step 1: Find the Parameters of the Path Connecting the Stations

This step is a straightforward application of the Indirect problem of geodesy. Section 4.2 is used

to find the following parameters of the great circle arc between the stations at **U** and **S**:

- Parameters related to the geocentric angle θ_{US} — specifically its cosine (from Eq 78) and sine (from Eq 88) functions
- The azimuth angles $\psi_{S/U}$ and $\psi_{U/S}$ (from Eq 86 and Eq 87, respectively).

6.3.2 Step 2: Determine If the Problem Is Well-Posed

The problem must be physically and mathematically well posed. In terms of a spherical earth, the two radials define two great circles which intersect at two antipodal points. The interior angles of triangle **USA** at **U** and **S**, both in the interval (0, π), are given by the following equations.

$$\beta_U = \min\left\{ \left|\psi_{S/U} - \psi_{A/U}\right|,\ \left|\psi_{S/U} - \psi_{A/U} + 2\pi\right|,\ \left|\psi_{S/U} - \psi_{A/U} - 2\pi\right| \right\}$$
$$\beta_S = \min\left\{ \left|\psi_{U/S} - \psi_{A/S}\right|,\ \left|\psi_{U/S} - \psi_{A/S} + 2\pi\right|,\ \left|\psi_{U/S} - \psi_{A/S} - 2\pi\right| \right\} \qquad \text{Eq 197}$$

For the two radials to intersect, both of the following must be true:

- Solution Existence: The radials must point to the same side of the station baseline **US**. The analyst must determine which one of the following conditions is true, or there is no solution:

  $\psi_{A/U} = \psi_{S/U} + \beta_U \qquad \psi_{A/S} = \psi_{U/S} - \beta_S$ When **A** south of **US** baseline*

  $\psi_{A/U} = \psi_{S/U} - \beta_U \qquad \psi_{A/S} = \psi_{U/S} + \beta_S$ When **A** north of **US** baseline*

  *Assuming **U** is west of **S**

- Solution Existence: It must be the case that $0 < \beta_U + \beta_S < \pi$. Otherwise, the two intersections will either be equidistant (both at a geocentric angle of π/2 from the midpoint of the station baseline) or the closer intersection will be on the opposite side of the station baseline of that intended.

A cannot be found uniquely if it is on the station baseline **US** or its extensions, as the radials then do not have a unique intersection. If both $\beta_U = 0$ and $\beta_S = 0$, then **A** is on the baseline between the stations; if $\beta_U = 0$ and $\beta_S = \pi$ then **A** is on the baseline extension closer to **S**; if $\beta_U = \pi$ and $\beta_S = 0$, then **A** is on the baseline extension closer to **U**.

6.3.3 Step 3: Find the Aircraft Location Coordinates

The unknown geocentric angles θ_{UA} and θ_{SA} can be found from the four-part cotangent formula (Eq 75)

$$\cot(\theta_{UA}) = \frac{\cos(\theta_{US})\cos(\beta_U) + \sin(\beta_U)\cot(\beta_S)}{\sin(\theta_{US})}$$
$$\cot(\theta_{SA}) = \frac{\cos(\theta_{US})\cos(\beta_S) + \sin(\beta_S)\cot(\beta_U)}{\sin(\theta_{US})} \qquad \text{Eq 198}$$

In computing θ_{UA} and θ_{SA} from Eq 198 using the arc cotangent function, the angles can be

unambiguously found in (0, π). Only one of the two angles is needed to find L_A and λ_A. The distances to the stations θ_{UA} and θ_{SA} can provide information about the strength and visibility of the stations' signals at the aircraft, as well as the distance-to-fly in some situations.

With θ_{UA} or θ_{SA} known, the latitude/longitude of **A** can be found from either the spherical triangle **PUA** or from triangle **PSA**. This is an application of the Direct problem of geodesy (Section 4.3). The latitude can be found from either of these equations

$$\sin(L_A) = \sin(L_U)\cos(\theta_{UA}) + \cos(L_U)\sin(\theta_{UA})\cos(\psi_{A/U})$$
$$\sin(L_A) = \sin(L_S)\cos(\theta_{SA}) + \cos(L_S)\sin(\theta_{SA})\cos(\psi_{A/S}) \qquad \text{Eq 199}$$

And the longitude can be found from either of these equations

$$\tan(\lambda_A - \lambda_U) = \frac{\sin(\psi_{A/U})\sin(\theta_{UA})}{\cos(L_U)\cos(\theta_{UA}) - \sin(L_U)\sin(\theta_{UA})\cos(\psi_{A/U})}$$
$$\tan(\lambda_A - \lambda_S) = \frac{\sin(\psi_{A/S})\sin(\theta_{SA})}{\cos(L_S)\cos(\theta_{SA}) - \sin(L_S)\sin(\theta_{SA})\cos(\psi_{A/S})} \qquad \text{Eq 200}$$

By employing the two-argument arc tangent function, Eq 200 will yield values of $\lambda_A - \lambda_U$ and $\lambda_A - \lambda_S$ in the range [-π, π].

6.3.4 Extensions, Alternatives and Remarks

Analysis Extensions — Additional quantities can be computed which are of interest in some applications. The angle of intersection of the two radials at **A** is given by the law of cosines for angles (Eq 72)

$$\cos(\beta_A) = -\cos(\beta_U)\cos(\beta_S) + \sin(\beta_U)\sin(\beta_S)\cos(\theta_{US}) \qquad \text{Eq 201}$$

When using the arc cosine function in Eq 201, β_A from can be unambiguously found in [0, π]. The crossing angle of the radials β_A provides information about the accuracy of the solutions for L_A and λ_A. Some sources suggest that a fix should only be used when $30° \leq \beta_A \leq 150°$. This would exclude locations near the baseline and its extensions and at large distances from both stations.

Also, it may be of interest to know the azimuths of the paths to **U** and **S** from **A**.

$$\tan(\psi_{U/A}) = \frac{-\sin(\psi_{A/U})\cos(L_U)}{\sin(L_U)\sin(\theta_{UA}) - \cos(L_U)\cos(\theta_{UA})\cos(\psi_{A/U})}$$
$$\tan(\psi_{S/A}) = \frac{-\sin(\psi_{A/S})\cos(L_S)}{\sin(L_S)\sin(\theta_{SA}) - \cos(L_S)\cos(\theta_{SA})\cos(\psi_{A/S})} \qquad \text{Eq 202}$$

By employing the two-argument arc tangent function, Eq 202 will yield values of $\psi_{U/A}$ and $\psi_{S/A}$

in the range [-π, π]. The azimuth angles $\psi_{U/A}$ and $\psi_{S/A}$ may be useful for steering and/or cross-checking the aircraft's direction finding equipment.

Analysis Alternatives — Other equations can be used in lieu of Eq 198. One option is to use Napier's Analogies (Eq 76). A disadvantage is that both θ_{UA} and θ_{SA} must be found.

$$\tan\left[\tfrac{1}{2}(\theta_{SA}+\theta_{UA})\right]=\frac{\cos\left[\tfrac{1}{2}(\beta_U-\beta_S)\right]}{\cos\left[\tfrac{1}{2}(\beta_U+\beta_S)\right]}\tan\left[\tfrac{1}{2}\theta_{US}\right]$$
$$\tan\left[\tfrac{1}{2}(\theta_{SA}-\theta_{UA})\right]=\frac{\sin\left[\tfrac{1}{2}(\beta_U-\beta_S)\right]}{\sin\left[\tfrac{1}{2}(\beta_U+\beta_S)\right]}\tan\left[\tfrac{1}{2}\theta_{US}\right] \qquad \text{Eq 203}$$

Another option is to use (a) Eq 201 to find β_A, then (b) Eq 72 and Eq 73 respectively to find the cosine and sine of θ_{UA} and/or θ_{SA}. The latter are the quantities needed in Eq 199 and Eq 200.

Remarks

- Solving the two-bearing (e.g., VOR-VOR cross-fix) problem can be done using only spherical trigonometry, and does not require aircraft altitude.
- A complete solution involves a total of 15 navigation variables (latitudes, longitudes, azimuth angles and geocentric angles). Of these, 6 are known at the start of the calculation.
- Mathematically, the sensor cross-fix problem (e.g., VORs or radars) addressed in this section is identical to finding the intersection of two great circles which is addressed in Subsection 5.6.1.

A problem closely-related to the subject of this section is determining an aircraft's position from the coordinates of two stations **U** and **S** and measurements of the angles $\psi_{U/A}$ and $\psi_{S/A}$ from the aircraft to those stations. In aviation or marine applications, the stations would often be non-directional beacons or commercial broadcast transmitters. The information available for this related problem is insufficient for the direct use of spherical trigonometry. For triangle **USA**, only the side θ_{US} and the opposite angle β_A are known. A viable solution approach is described in Chapter 8, Subsection 8.5.8.

6.4 Solution for Two Slant-Range Measurements

Here, the assumption is that the latitude/longitude/altitudes of stations **U** (L_U, λ_U, h_U) and **S** (L_S, λ_S, h_S) are known, as are the slant-ranges, d_{UA} and d_{SA}, to the aircraft location **A**, about which only its altitude h_A is known. The solution approach is based on the mathematical spherical triangle **USA**. Following a preliminary step (Subsection 6.4.1), the solution for the latitude and longitude of **A** and related parameters is a four-step process, like that in Section 6.3. In terms of the classic 'solving a triangle' taxonomy, this is an SSS (side-side-side) situation.

6.4.1 Step 0: Convert Slant-Ranges to Spherical-Ranges/Geocentric Angles

Accurate calculation of geocentric angles θ_{SA} and θ_{UA} takes account of the altitude/elevation of the aircraft and ground station above sea level. This is done using Eq 44, applied separately to each aircraft-station pair. Once the angles θ_{SA} and θ_{UA} are found, the problem reduces to one of pure spherical trigonometry (and can also by solved using vector analysis, as in Section 5.5).

6.4.2 Step 1: Solve the Navigation Spherical Triangle for the Two Stations

This is an application of the Indirect problem of geodesy. The approach in Section 4.2 is employed to find the geocentric angle θ_{US} between the stations **U** and **S** (Eq 81) and the azimuth angles $\psi_{S/U}$ and $\psi_{U/S}$ (Eq 86 and Eq 87) of the path (baseline) joining the stations.

6.4.3 Step 2: Determine if the Problem is Well-Posed

The problem must be mathematically well posed for a solution to exist. Ranges (geocentric angles) from two stations define small circles on the surface which can intersect at zero, one or two points. If either of the following conditions is true, then the problem is ill posed and does not have a valid solution.

- If $\theta_{UA} + \theta_{SA} < \theta_{US}$, then the circle radii are too small (relative to the distance between their centers) to intersect.
- If $|\theta_{UA} - \theta_{SA}| > \theta_{US}$, then one circle encloses the other and they do not intersect.

If either $\theta_{UA} + \theta_{SA} = \theta_{US}$ or $|\theta_{UA} - \theta_{SA}| = \theta_{US}$, then the circles are tangent and there is only one solution, which lies on the baseline connecting **U** and **S**, or its extension as a great circle. Otherwise, there are two solutions, located symmetrically relative to the baseline **US**. Additional information must be used to choose between the two solutions (see Subsection 6.4.6).

There is no partial solution case for this sensor combination. However, the single-solution case involves high sensitivity to measurement errors for the direction orthogonal to the baseline.

6.4.4 Step 3: Solve the Mathematical Spherical Triangle **USA**

The third step is to solve the mathematical spherical triangle (Subsection 4.1.2) **USA**. This situation falls under Case (1) in the taxonomy of Subsection 4.1.7 — all three sides are known. Denote the (positive) interior angles of **USA** by β_U, β_S and β_A. They can be found by applying the law of cosines (Eq 71) three times:

$$\cos(\beta_U) = \frac{\cos(\theta_{SA}) - \cos(\theta_{US})\cos(\theta_{UA})}{\sin(\theta_{US})\sin(\theta_{UA})} \qquad \text{Eq 204}$$

$$\cos(\beta_S) = \frac{\cos(\theta_{UA}) - \cos(\theta_{US})\cos(\theta_{SA})}{\sin(\theta_{US})\sin(\theta_{SA})}$$

$$\cos(\beta_A) = \frac{\cos(\theta_{US}) - \cos(\theta_{US})\cos(\theta_{SA})}{\sin(\theta_{UA})\sin(\theta_{SA})}$$

In computing β_U, β_S and β_A from Eq 204, by using the arc cosine function, the angles can be unambiguously found in (0, π). Also, β_U, β_S and β_A are found without chaining from one solution to another.

6.4.5 Step 4: Find the Coordinates/Path Azimuths for Aircraft **A**

With β_U and β_S known, azimuth angles $\psi_{A/U}$ and $\psi_{A/S}$ can be determined to within an ambiguity. The ambiguity arises because it is not known whether to add or subtract β_U from $\psi_{S/U}$ (or β_S from $\psi_{U/S}$, respectively) to form $\psi_{A/U}$ (or $\psi_{A/S}$). One and only one of the following alternatives is correct:

$\psi_{A/U} = \psi_{S/U} + \beta_U$	$\psi_{A/S} = \psi_{U/S} - \beta_S$	When **A** south of **US** baseline*
$\psi_{A/U} = \psi_{S/U} - \beta_U$	$\psi_{A/S} = \psi_{U/S} + \beta_S$	When **A** north of **US** baseline*

*Assuming **U** is west of **S**

The ambiguity may be resolvable from the azimuth angles $\psi_{A/U}$ and $\psi_{A/S}$ (because the navigator often knows, approximately, $\psi_{U/A}$ and/or $\psi_{S/A}$). Alternatively, two solutions can be found for the coordinates of **A** and the azimuths of the paths from **A**, and the ambiguity resolved subsequently. In either case, the calculations set forth in Subsection 6.3.3 are performed last — specifically, Eq 199 for the aircraft' latitude L_A, Eq 200 for the aircraft's longitude λ_A, and Eq 202 for the azimuth angles $\psi_{U/A}$ and $\psi_{S/A}$ of the stations relative to the aircraft.

6.4.6 Remarks

This section could also be entitled 'Position Solution for Two Spherical-Range (or Geocentric Angle) Measurements', since the first step in the solution is to convert the convert the slant-ranges to geocentric angles. After the stations and aircraft altitudes have been removed, the aircraft latitude and longitude can also be found using vectors and matrices (see Section 5.5).

Concerning resolution of the two-solution ambiguity:

- Resolving the ambiguity only requires knowing which side of the station baseline (including its extensions) the vehicle is on. Often, based on dead reckoning from either the departure location or a previous fix, the vehicle's crew will be able to make such a determination.
- Motion of a vehicle along a line of azimuth (heading) may be used to resolve the ambiguity. Because the ambiguous solutions are symmetric about the baseline, the

motion of the correct solution will correlate with heading while motion of the incorrect solution will not.

- If either station provides azimuth (in addition to range) information, or navigation information from a third station is available, that may be used to resolve the ambiguity.

To elaborate and provide context:

- The angle from the aircraft to the stations, β_A, provides information about the accuracy of the solutions for L_A and λ_A. Some have recommended that the fix only be accepted when $30° \leq \beta_A \leq 150°$. This would exclude locations near the baseline between stations (including its extensions) and at large distances from both stations.
- The solution presented above involves a total of 21 navigation variables (latitudes, longitudes, altitudes, azimuth angles, geocentric angles and slant-ranges). Of these, 9 are known at the start of the calculation.
- The solution involves calculating parameters that may not be needed in all situations.

6.5 Solution for a Slant-Range and an Azimuth Measurement

Here, the a priori known quantities are: the coordinates of DME station **D** (L_D, λ_D, h_D) and VOR station **V** (L_V, λ_V). The measured quantities are: the slant-range d_{DA} between the aircraft **A** and station **D**; the azimuth angle $\psi_{A/V}$ of **A** from **V**; and the aircraft altitude h_A. The quantities sought are the coordinates of **A** (L_A, λ_A) and the parameters for paths **AD** and **AV**. The solution approach is based on the mathematical spherical triangle **DVA**. In terms of the classic 'solving a triangle' taxonomy, this is an SSA (side-side-angle) situation.

6.5.1 Step 0: Convert Slant-Range to a Geocentric Angle

Convert the slant-range d_{DA} to the geocentric angle θ_{DA} using Eq 44, in the same manner as discussed in Subsection 6.4.1.

6.5.2 Step 1: Solve the Navigation Spherical Triangle **PDV**

Apply the Indirect problem of geodesy (Section 4.2) to find the geocentric angle θ_{DV} between stations **D** and **V** (Eq 81) and the azimuth angles $\psi_{D/V}$ and $\psi_{V/D}$ (Eq 86 and Eq 87) for the baseline joining the stations.

6.5.3 Step 2: Determine if the Problem is Well-Posed

In determining if the problem is well-posed, the first consideration is the magnitude of the measured geocentric angle between the aircraft **A** and station **D**, θ_{DA}, relative to the known geocentric angle between the stations **D** and **V**, θ_{DV}. There are three cases:

- Interior: If $\theta_{DV} < \theta_{DA}$, then **V** is within the perimeter of the circle of possible aircraft locations centered on **D**; there is one and only one intersection/solution

- Perimeter: If $\theta_{DV} = \theta_{DA}$, then **V** is on the perimeter of the circle centered on **D**; there can be zero or one solution
- Exterior: If $\theta_{DA} < \theta_{DV}$, then **V** is outside the perimeter of the circle centered on **D**; there can be zero, one or two solutions.

To further explore the scenario geometry, define the angle at **V**, β_V, between the great circle arcs to the aircraft **A** and the DME station **D**, in the range $0 \le \beta_V \le \pi$, by

$$\beta_V = \min\left\{ \left|\psi_{A/V} - \psi_{D/V}\right|, \left|\psi_{A/V} - \psi_{D/V} + 2\pi\right|, \left|\psi_{A/V} - \psi_{D/V} - 2\pi\right| \right\} \quad \text{Eq 205}$$

For the Perimeter case ($\theta_{DA} = \theta_{DV}$), there is a valid solution only if $0 \le \beta_V \le \frac{1}{2}\pi$. Otherwise, the problem is ill-posed and no solution exists.

For the Exterior case ($\theta_{DA} < \theta_{DV}$), define the critical value for β_V, $0 \le \beta_{V,crit} < \frac{1}{2}\pi$, by

$$\beta_{V,crit} = \arcsin\left(\frac{\sin(\theta_{DA})}{\sin(\theta_{DV})}\right) \quad \text{Eq 206}$$

Eq 206 is the law of sines applied to triangle **DVA** when β_A is a right angle. Three situations can occur: (a) when $\beta_{V,crit} < \beta_V$, the problem is ill-posed and there is no solution; (b) when $\beta_{V,crit} = \beta_V$, there is a single solution; and (c) when $\beta_V < \beta_{V,crit}$ there are two possible solutions.

There is no partial solution case for this sensor combination. However, the single-solution case involves high sensitivity to measurement errors for the direction along the radial from **V**.

6.5.4 Step 3: Solve the Mathematical Spherical Triangle **DVA**

When at least one solution exists, the third step is to solve the mathematical spherical triangle (Subsection 4.1.2) **DVA**. This problem falls under Case (3) in the taxonomy of Subsection 4.1.7 — two sides, θ_{DV} and θ_{DA}, and an adjacent (not included) angle β_V are known.

First, the interior angle at **A**, β_A, is found using the law of sines

$$\beta_A = \arcsin\left(\frac{\sin(\beta_V)\sin(\theta_{DV})}{\sin(\theta_{DA})}\right) \quad \text{Eq 207}$$

Consistent with Subsection 6.5.3, for a well-posed problem the quantity within the large parentheses in Eq 207 will have a value in [0, 1]. Thus two angles will be found in [0, π] except when the right-hand side is unity, in which situation β_A = π/2 and $\beta_V = \beta_{V,crit}$. For the Interior case, the value for β_A in [0, π/2) is correct, and the value in (π/2, π] is extraneous (a mathematical artifact which is discarded). For the Exterior case, either value for β_A may be correct (the situation is ambiguous); these values are labeled $\beta_{A,1}$ and $\beta_{A,2}$, and both are retained. The value of β_A is indicative of the solution accuracy (Subsection 6.5.6).

The angles $\beta_{D,1}$ and $\beta_{D,2}$ corresponding to angles $\beta_{A,1}$ and $\beta_{A,2}$ are found using either of the following expressions from Napier's Analogies (Eq 76)

$$\tan\tfrac{1}{2}\beta_{D,i} = \frac{\cos\frac{1}{2}(\theta_{DV}-\theta_{DA})}{\cos\frac{1}{2}(\theta_{DV}+\theta_{DA})}\cot\tfrac{1}{2}(\beta_{A,i}+\beta_V) = \frac{\sin\frac{1}{2}(\theta_{DV}-\theta_{DA})}{\sin\frac{1}{2}(\theta_{DV}+\theta_{DA})}\cot\tfrac{1}{2}(\beta_{A,i}-\beta_V) \quad \text{Eq 208}$$

The discussion in Subsection 4.1.6 concerning sums and differences of sides and angles having the 'same affection' is relevant here. As a consequence, both expressions on the right-hand side of Eq 208 are positive. Thus, in computing $\beta_{D,i}$ (i = 1, 2) from either line using the arc tangent function, each solution can be unambiguously found in (0, π). The second line is preferred, as it cannot be indeterminate. There is a small possibility that first line can, by the two sums of angles equaling π/2, resulting in the trigonometric functions of the sums both equaling zero.

The distance $\theta_{VA,i}$ can be found from either of the following expressions. As is the case for Eq 208, both expressions on the right-hand side of Eq 209 are positive. Thus, in computing $\theta_{VA,i}$ (i = 1, 2) from either line using the arc tangent function, each solution can be unambiguously found in (0, π). The first line is usually preferred, as it cannot be indeterminate. There is a possibility that second line can, by the two differences equaling 0, resulting in the trigonometric functions equaling zero.

$$\tan\tfrac{1}{2}\theta_{VA,i} = \frac{\cos\frac{1}{2}(\beta_{A,i}+\beta_V)}{\cos\frac{1}{2}(\beta_{A,i}-\beta_V)}\tan\tfrac{1}{2}(\theta_{DV}+\theta_{DA}) = \frac{\sin\frac{1}{2}(\beta_{A,i}+\beta_V)}{\sin\frac{1}{2}(\beta_{A,i}-\beta_V)}\tan\tfrac{1}{2}(\theta_{DV}-\theta_{DA}) \quad \text{Eq 209}$$

6.5.5 Step 4: Find the Coordinates/Path Azimuths for **X**

One and only one of the following conditions is true:

- $\psi_{A/D} = \psi_{V/D} + \beta_D$ and $\psi_{A/V} = \psi_{D/V} - \beta_V$
- $\psi_{A/D} = \psi_{V/D} - \beta_D$ and $\psi_{A/V} = \psi_{D/V} + \beta_V$.

Since both $\psi_{A/V}$ and $\psi_{D/V}$ are now known, the correct line can be selected, yielding $\psi_{A/D}$. Then the calculations set forth in Subsection 6.3.3 involving spherical triangles **PDA** and **PVA** can be performed — specifically, Eq 199 for the aircraft' latitude L_A, Eq 200 for the aircraft's longitude λ_A, and Eq 202 for the azimuth angles $\psi_{D/A}$ and $\psi_{V/A}$ of the stations relative to the aircraft.

6.5.6 Remarks

Concerning resolution of the two-solution ambiguity:

- The ambiguity can often be resolved from knowledge of the station locations and the approximate route from the departure point. Using dead reckoning, the vehicle operator may know the approximate distance to the VOR station.
- If the DME station provides azimuth (in addition to range) information, that may be used to resolve the ambiguity.

To elaborate and provide context:

- The angle from the aircraft to the stations, β_A, provides information about the accuracy of the solutions for L_A and λ_A. Some have recommended that the fix only be accepted when $0° \leq \beta_A \leq 60°$ or $120° \leq \beta_A \leq 180°$. This would exclude locations where the lines-of-sight to the stations are close to being orthogonal.
- The solution presented above involves a total of 18 navigation variables (latitudes, longitudes, altitudes, azimuth angles, geocentric angles and slant-ranges). Of these, 8 are known at the start of the calculation.
- The solution involves calculating parameters that may not be needed in all situations.
- The aircraft-DME station geocentric angle can be approximated — e.g., by $d_{DA} \,/\, R_e$ — but Eq 44 provides a more accurate solution.
- The solution method described in this section uses Napier's Analogies. An alternative solution method can be based on the equations in Section 6.2.

6.6 Check of Continuous Descent Approach Altitude

6.6.1 Application Context

FAA Advisory Circular AC 120-108 (Ref. 38) recommends and provides guidance for employing the Continuous Descent Final Approach (CDFA) technique, as an alternative to the traditional step down technique, for conducting a Non-Precision Approach (NPA) procedure:[*]

- "The goal of implementing CDFA is to incorporate the safety benefits derived from flying a continuous descent in a stabilized manner as a standard practice on an NPA.
- "CDFA starts from an altitude/height at or above the Final Approach Fix (FAF) and proceeds to an altitude/height approximately 50 feet (15 meters) above the landing runway threshold or to a point where the flare maneuver should begin for the type of aircraft being flown."

Simultaneous with publication of AC 120-108, the FAA began including CDFA Vertical Descent Angles (VDAs) on approach plates for NPAs. Figure 28, depicting part of the approach plate for the LOC IAP to runway 35 at Norwood Memorial Airport (KOWD), is an example.[†]

[*] CDFAs were not prohibited prior to publication of AC 120-108. However, the FAA did not recommend them nor provide information concerning their use. Some air carriers required utilization of CDFAs and supplied their flight crews with supplementary information on company-provided approach plates.

[†] Effective dates: May 1, 2014 – May 29, 2014

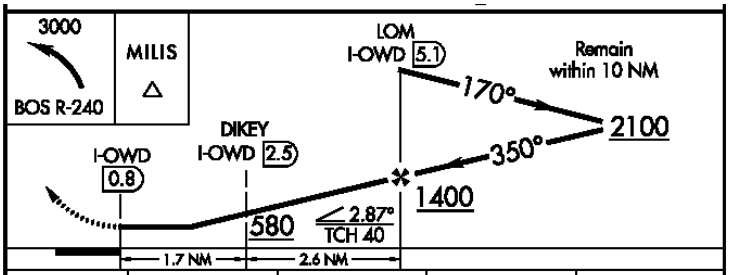

CATEGORY	A	B	C	D
S-35	580-¾ 531 (600-¾)		580-1½ 531 (600-1½)	580-1¾ 531 (600-1¾)
CIRCLING	600-1 551 (600-1)		700-1¾ 651 (700-1¾)	700-2 651 (700-2)
DIKEY FIX MINIMUMS				
S-35	500-¾ 451 (500-¾)		500-1¼ 451 (500-1¼)	500-1½ 451 (500-1½)
CIRCLING	600-1 551 (600-1)		700-1¾ 651 (700-1¾)	700-2 651 (700-2)

NORWOOD, MASSACHUSETTS

Figure 28 Portion of LOC IAP to KOWD Runway 35

When executing a CDFA in accordance with the LOC IAP to runway 35 at KOWD, upon passing the FAF (as determined either by a marker beacon receiver or a DME interrogator) at or above 1,400 ft MSL, the aircraft would descend to 580 ft MSL by following a CDFA with a VDA of 2.87 deg. Upon reaching 580 ft MSL, the aircraft should not descend further unless/until the fix DIKEY is identified utilizing a DME interrogator. If/when that occurs, the aircraft would be permitted to descend to 500 ft MSL — but no lower. If the airport environment is identified at that point, a visual landing could be performed; if not, a missed approach is required.

6.6.2 Altitude vs. DME Information for the Pilot

Employing the CDFA technique does not require additional equipment on the aircraft or on the ground — i.e., other than that required for the step down technique. Specifically, the avionics required for VNAV guidance specified in Advisory Circulars AC 90-105 (Ref. 39) and AC 20-138C (Ref. 40) are not required. However, if available, use of VNAV is recommended.

If VNAV avionics are not available, the pilot calculates a planned descent rate utilizing a table in AC 120-108, based on the charted VDA and planned ground speed. When executing a CDFA without VNAV, instrumentation errors in measuring airspeed and descent rate, variability in the headwind, the lack of a guidance display and other factors, will cause the aircraft's altitude flown to be less well controlled than it is for a VNAV operation. The contributions of some of error mechanisms accumulate, causing the difference between the altitude flown and the altitude desired to increase with time.

The safety aspect of an aircraft being at the incorrect altitude while performing a CDFA NPA is addressed by requiring the aircraft to remain above the Minimum Descent Altitude (MDA) along

the entire approach track. However, situational awareness is improved if the pilot has a readily available method for comparing the aircraft's measured altitude with the planned altitude on an almost continuous basis, particularly when VNAV is not used (Ref. 41). A technique adopted by some airlines has been to include a table of DME distance versus planned barometric altitude for each CDFA approach plate for an airport with a DME ground station. Generating such a table is the subject of this section. This analysis can also be used to determine the parameters of an approach fix defined by aircraft altitude or distance to a DME ground station.

Equations used to generate a table of DME distance versus planned barometric altitude must reflect the geometry of the DME ground station location relative to the approach ground track. Two types of DME stations are discussed:

- 'ILS DME' — The DME ground station antenna is located close to the centerline of a runway equipped with an ILS localizer* (regardless of whether an ILS glide slope subsystem is present). These DME stations are generally low-powered and are only approved for use as an aid for approaches to the associated runway. On approach plates and other FAA documentation, ILS DMEs are designed with an 'I-' prefix — e.g., I-OWD in Figure 28.
- 'Airport DME' — The DME ground station is generally on the airport but is not associated with a runway.† These DMEs generally have signal strength sufficient to serve aircraft approaching all runway ends as well as in the surrounding airspace within a radius of at least 50 NM.

6.6.3 'ILS DME' Scenario

This scenario involves a straight-in CDFA using the baro-altimeter system at descent angle α' to a runway with a DME ground station close to the runway centerline. Three locations, all on the same great circle, are involved. From the pilot's perspective, they are, in typical order of increasing distance: the aircraft, **A** (more precisely, its DME interrogator antenna); the runway threshold, **R** (more precisely, the threshold crossing location); and the DME ground station, **D** (more precisely, its antenna). In this analysis: h denotes altitude above MSL, θ denotes a geocentric angle and d denotes a slant-range.

The analysis is straightforward if the aircraft altitude h_A taken as the independent variable. From Section 9.2 (Eq 493) the geocentric angle θ_{RA} between the aircraft and the threshold (at altitude h_R) is

* For some runways, the 'ILS' DME ground station antenna is collocated (or nearly collocated) with a localizer antenna; it may serve one or both runway ends. In other situations, the DME ground station is between the ends of runway, with the antenna as close to the centerline as possible.

† The "Airport" DME ground station antenna should be either in front of or behind the aircraft throughout the descent portion of the approach procedure — i.e., until the Minimum Descent Altitude is reached.

$$\theta_{RA} = \frac{\log\left(\frac{R_e + h_A}{R_e + h_R}\right)}{\tan(\alpha')} \qquad \text{Eq 210}$$

The geocentric angle between the runway threshold and the DME θ_{RD} is known from the runway geometry. Reportedly, for some U.S. ILS DME installations, θ_{RD} should be set to zero, because the fixed DME ground station delay (which is transparent to the pilot) is adjusted so that the aircraft DME reads zero at the runway threshold. This is not the case for the procedure shown in Figure 28, nor for others examined at random.

Thus the geocentric angle between the aircraft and the DME ground station θ_{DA} is

$$\theta_{DA} = \theta_{RA} \pm \theta_{RD} \qquad \text{Eq 211}$$

The '+' sign applies if the DME is past the threshold and the '–' sign applies if the DME antenna is before the threshold.

Lastly, the slant-range between the aircraft and the DME ground station d_{DA} is found from Subsection 3.5.1 (Eq 54).

$$d_{DA} = 2R_e \sin\left(\tfrac{1}{2}\theta_{DA}\right) \sqrt{\left(1 + \frac{h_A}{R_e}\right)\left(1 + \frac{h_D}{R_e}\right) + \left(\frac{h_A - h_D}{2R_e \sin\left(\frac{1}{2}\theta_{DA}\right)}\right)^2} \quad , \quad \theta \neq 0 \qquad \text{Eq 212}$$

Remarks

- The solution for this scenario does not involve latitude or longitude coordinates — only altitudes and distances between the aircraft and destination runway.
- When generating a table for crosschecking aircraft altimeter readings against desired altitudes corresponding to DME readings, usually one would prefer to specify the slant-range d_{DA} as a 'round number' (e.g., 3.0 NM) and determine the associated desired altitude h_A. This is the inverse of the simpler solution approach described in this subsection. However, it can readily be achieved by 'wrapping an iteration method' around the equations of this subsection (Subsection 2.1.8).

6.6.4 'Airport DME' Scenario

The 'Airport DME' scenario is essentially a combination of: (1) the vertical plane situation addressed for 'ILS DME' scenario of (Subsection 6.6.3), and (2) the spherical earth's surface situation addressed in Section 6.5. Here, the locations of the aircraft, runway threshold and DME are not modeled as lying on the same great circle. Such geometries generally occur because the 'Airport DME' is not located close to the destination runway centerline

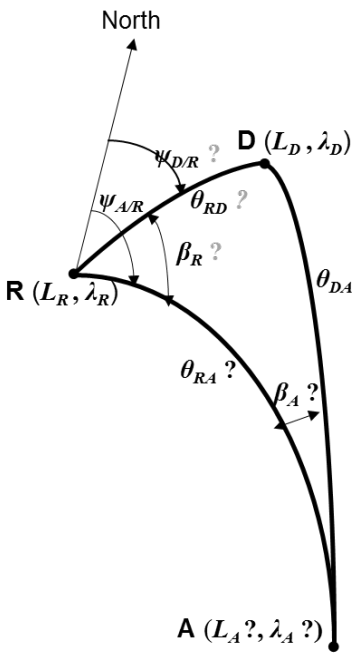

Figure 29 Airport DME CDA Scenario

The footprint on the earth's surface for this scenario is shown in Figure 29. The locations of the aircraft **A**, runway threshold **R** and DME ground station **D**, are shown. It is assumed that the coordinates of the threshold **R** (L_R, λ_R, h_R) and of the DME station **D** (L_D, λ_D, h_D) are known, as are the azimuth angle $\psi_{A/R}$ of the approach course. In terms of the classic 'solving a triangle' taxonomy, this is an SSA (side-side-angle) situation.

For this problem, the best choice for the independent variable is the geocentric angle between the aircraft and the DME antenna, θ_{DA}. When generating a table for operation use, one would generally prefer to perform altitude checks at defined DME slant-range readings, d_{DA}. Or, conversely, one could perform DME checks at defined altitude readings, h_A. Tables for either option can be generated by iterating on Steps A-2 to A-6 in the following procedure.

Initialization (executed once)

Step I-1: Apply the Indirect problem of geodesy to the path **RD** to find the geocentric angle θ_{RD} and azimuth angle $\psi_{D/R}$.

Step I-2: Compute the interior angle β_R between **RD** and **RA** (assuming the aircraft is on course) in the range [0, π] using Eq 213.

$$\beta_R = \min\left\{ \left|\psi_{A/R} - \psi_{D/R}\right|, \left|\psi_{A/R} - \psi_{D/R} + 2\pi\right|, \left|\psi_{A/R} - \psi_{D/R} - 2\pi\right| \right\} \qquad \text{Eq 213}$$

Find Slant-Range d_{DA} and Altitude h_A from Spherical Range θ_{DA} (executed at least once)

Step A-1: Select an initial value for θ_{DA}. This choice is not critical, as iterations are generally involved. A possible first choice is:

$$\theta_{DA} = k \frac{\text{specified } d_{DA}}{R_e} \quad , \quad k \approx 1 \qquad \text{Eq 214}$$

Step A-2: For triangle **RDA**, compute the interior angle β_A between **AR** and **AD** (assuming the aircraft is on course) using the law of sines.

$$\beta_A = \arcsin\left(\frac{\sin(\beta_R)\sin(\theta_{RD})}{\sin(\theta_{DA})}\right) \qquad \text{Eq 215}$$

When $\theta_{RD} < \theta_{DA}$, which is generally true when the DME is on the airport, then if the earth were flat, the only valid solution would be the acute angle which satisfies Eq 215. Since the approach region is small relative to the earth's surface, the acute angle will generally be correct as well. Angle β_A influences the accuracy of the crosscheck on aircraft altitude. In Subsection 6.5.6, it's noted some have recommended that a DME-VOR fix only be accepted when the equivalent angle satisfies $\beta \leq 60°$.

Step A-3: For spherical triangle **RDA**, the geocentric angle θ_{RA} in the interval [0, π) is found from Napier's Analogies using either of the following expressions. The choice can be based entirely on numerical considerations.

$$\tan\left(\tfrac{1}{2}\theta_{RA}\right) = \frac{\cos\left[\frac{1}{2}(\beta_R + \beta_A)\right]}{\cos\left[\frac{1}{2}(\beta_R - \beta_A)\right]}\tan\left[\tfrac{1}{2}(\theta_{DA} + \theta_{RD})\right]$$

$$\tan\left(\tfrac{1}{2}\theta_{RA}\right) = \frac{\sin\left[\frac{1}{2}(\beta_R + \beta_A)\right]}{\sin\left[\frac{1}{2}(\beta_R - \beta_A)\right]}\tan\left[\tfrac{1}{2}(\theta_{DA} - \theta_{RD})\right] \qquad \text{Eq 216}$$

Step A-5: For an aircraft flying a CDFA using the baro-altimeter, with descent angle α', the planned altitude h_A for the location involved is

$$h_A = (R_e + h_R)\exp[\theta_{RA}\tan(\alpha')] - R_e \qquad \text{Eq 217}$$

Step A-6: Eq 212 (repeated) is employed to find the aircraft-DME ground station slant-range d_{DA} for the location and planned altitude.

$$d_{DA} = 2R_e \sin\left(\tfrac{1}{2}\theta_{DA}\right)\sqrt{\left(1 + \frac{h_A}{R_e}\right)\left(1 + \frac{h_D}{R_e}\right) + \left(\frac{h_A - h_D}{2R_e\sin\left(\frac{1}{2}\theta_{DA}\right)}\right)^2} \quad , \quad \theta \neq 0 \qquad \text{Eq 218}$$

Iteration for Defined DME Slant-Range or Altitude

Given the computed values for d_{DA} and h_A, the value for θ_{DA} can be adjusted and Steps A-2 to A-6 repeated until a specified value for d_{DA} or for h_A is achieved (see Subsection 2.1.8). If an assumed aircraft location is to be designated as a fix, then the latitude and longitude coordinates of the fix (L_A, λ_A) are found as solutions to the Direct problem of geodesy (Section 4.3).

6.6.5 Remarks

For the Airport DME problem, in the majority of situations: (a) the aircraft-DME station distance d_{DA} is many times the aircraft altitude h_A; and (b) high computational accuracy is not needed, since measurement errors are present and the values presented to the pilot are rounded. In these situations, the aircraft-DME station geocentric angle θ_{DA}, computed using Eq 214 with $k = 1$, often results in sufficiently accurate values of the aircraft's altitude h_A and coordinates (L_A, λ_A) and the computed slant-range d_{DA} (Eq 218) is not be needed.

The location of the DME station in relation to the threshold should be approximately known to ensure that the correct solution to Eq 215 is used. The value of β_R is key — if $\beta_R > \frac{1}{2}\pi$ then the DME station is further than the runway threshold and the aircraft will not fly past the DME during the approach. However, if $\beta_R < \frac{1}{2}\pi$, Eq 215 may have two solutions when the aircraft nears the airport. These correspond to the DME being 'before' or 'behind' the aircraft. Usually, the aircraft will be abeam of the DME after reaching the Minimum Descent Altitude (MDA).

Although the case for doing so is not as strong as it is for an NPA, the technique in this section can also be used to crosscheck aircraft altitude during an ILS or LPV approach with glide path angle α. Detecting capture of a false glide slope signal is perhaps the most compelling such reason (Ref. 42). To do so, in place of Eq 217, the following (from Eq 66) would be used.

$$h_A = h_R + 2\frac{\sin(\alpha + \frac{1}{2}\theta_{RA})\sin(\frac{1}{2}\theta_{RA})}{\cos(\alpha + \theta_{RA})}(R_e + h_R) \qquad \text{Eq 219}$$

7. AIRCRAFT POSITION FROM PSEUDO RANGE MEASUREMENTS

7.1 Overview of Pseudo Ranges

7.1.1 Background

Pseudo ranges are measurements of the distance between an aircraft and a set of 'ground'* stations, with the provision that all measurements are offset (biased) by the same unknown amount. This situation generally occurs when: (a) there's a one-way transmission of energy, either from the aircraft to the stations (surveillance) or from the stations to the aircraft (navigation); and (b) the stations have synchronized clocks that measure the time(s) of transmission (navigation) or reception (surveillance), but the aircraft does not.† The pseudo range concept has been utilized for both slant-range and spherical-range propagation paths.

As any concept, pseudo range systems have advantages and disadvantages (Table 10). The most important advantage is that user equipage is significantly simpler/lower-cost than it would be for a system utilizing true ranges. Pseudo range systems became viable during the twentieth century, with development of technologies (e.g., atomic clocks) that can synchronize widely separated ground stations. It is currently the concept most often chosen for new systems.

Table 10 Pseudo Range Systems: Primary Advantages and Disadvantages

Advantages	Disadvantages
User Cost – User needs only a transmitter (surveillance) or a receiver (navigation)	Station Locations – Stations must essentially surround the service area
Accuracy – Avoids the 'turn-around' error of two-way ranging systems	Station Count – Requires one more station than a system based on true ranges
Antenna Size – Large antennas for measuring azimuth angles are not needed	Station Equipment Cost – Stations must have a synchronization method (often an atomic clock)

In terms of implementation and utilization, the two system types are as different as they are alike. Specifically, the effects of measurement geometry (station configurations and favorable aircraft locations) on true and pseudo range systems are quite different — see Section 8.5.

Systems that employ pseudo slant-ranges include aircraft Wide Area Multilateration (surveillance) and GPS (navigation). Low-frequency radionavigation systems provide pseudo spherical-range measurements by utilizing ground-wave propagation. Examples are/were: Decca, Loran-C

* In this terminology, navigation and surveillance satellites are 'ground' stations, as they are external to the aircraft of interest and their locations are assumed to be known.

† For navigation systems, all stations must transmit effectively simultaneously. Multiple methods have been employed to avoid mutual interference among such transmissions: use of the same frequency with known, short delays between station transmissions (Loran); use of different frequencies (Omega, Decca); and transmission at the same time and on the same frequency modulated by different pseudo random codes (GPS, Galileo).

and Omega. All U.S. pseudo spherical-range navigation systems have been decommissioned, but systems are in operation elsewhere in the world (Ref. 43).

7.1.2 Hyperbolic Lines-of-Position (LOPs) and Fix Geometry

One pseudo range station has no value. Measurements for a pair of pseudo range stations can be subtracted to obtain the difference of the true ranges from the stations to the aircraft (equivalent to a hyperboloid of revolution on which the aircraft is located). In a two-dimensional context, hyperbolic LOPs are shown in Figure 30(a).

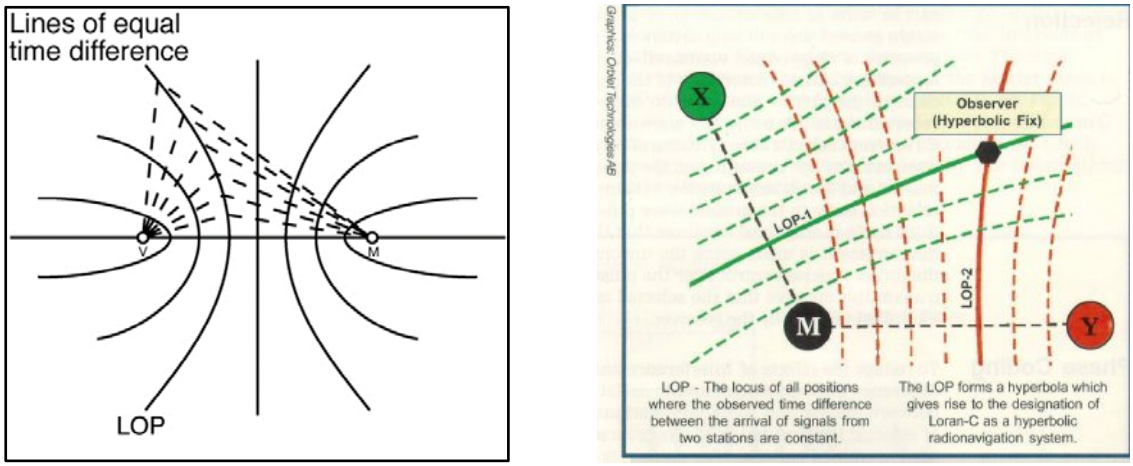

(a) Two-Station LOPs (b) Three Station Fix Geometry

Figure 30 Hyperbolic System Two-Dimensional Geometry

Pseudo range LOPs (hyperbolas) are different from LOPs for a true range-measuring sensor (concentric circles about the station) or those for an angle-measuring sensor (straight lines 'radiating' from the station). However, hyperbolic LOPs are closer in appearance to those for an angle-measuring sensor. LOPs for one angle station and a pair of pseudorange stations both: (a) emanate from the area when the station(s) are located and 'radiate' outward; and (b) diverge with distance from the station(s). A pseudo range station pair differs from a single-angle station in that its LOPs are curved, reducing its effective coverage area. Two pseudo range sensor pairs can be combined to obtain a position fix — e.g., Figure 30(b). For horizontal position determination, three stations are needed; one station being a member of two pairs. For accuracy, the LOP crossing angle should be between about 30 deg and 150 deg.

7.1.3 Role of the Common Range Bias

Prior to the advent of satellite systems, there was little need to determine the common bias in a set of pseudo range measurements. Early systems treated the bias as a nuisance parameter and formed pseudo range differences. These were often termed range-difference systems. Algorithms

published by Fang (Section 7.7, Ref. 44) for Cartesian coordinates, and by Razin (Section 7.10, Ref. 45) for a spherical earth, follow this practice. A general analysis of pseudo slant-range measurement processing can be found in Ref. 46.

With the advent of GPS, the range offset provided useful information, as GPS satellite transmission times are related to Coordinated Universal Time (UTC). Bancroft's algorithm (Ref. 47) and some variations on it solve for the aircraft position and common offset simultaneously. Section 8.4 contains a proof of the equivalence of the position solutions obtained with and without finding the common range offset.

7.1.4 Algorithm Taxonomy

When an aircraft and station altitudes are known, converting between slant- and spherical-ranges is straightforward in either direction — e.g., Eq 44 and Eq 54 and Subsection 3.2.2. Thus, except for details, only one algorithm is needed to compute an aircraft's latitude/longitude from either slant or spherical true range measurements. However, pseudo slant-ranges and pseudo spherical-ranges cannot be readily converted; separate algorithms are required.

More generally, separate algorithms are required for (a) different pseudo range measurement types (slant versus spherical); (b) different analysis frameworks (Cartesian versus spherical coordinates); (c) whether or not the common range bias is computed; and (d) whether or not altitude is included as a measurement. Table 11 contains a summary of available algorithms. Slant-range measurements are more naturally addressed using Cartesian coordinates, while spherical-range measurements are more naturally addressed using spherical coordinates. However, either framework can be used for either measurement type.

Table 11 Taxonomy for Range-Type Algorithms and Example Applications

Measurements / Dimensions	True Slant-Ranges	Pseudo Slant-Ranges	Pseudo Spherical-Ranges
Two (Plane or Sphere)	Section 7.3 Subsection 7.12.1	Section 7.7 Subsection 7.12.2	Section 7.10-7.11
	DME/DME approximation	Airport multilateration	Loran-C, Omega
Three (Physical Reality)	Section 7.3-7.4 Section 6.4*	Sections 7.2, 7.5-7.6; Sections 7.8-7.9	N/A
	DME/DME/Altimeter	GPS, WAM	

*The algorithm for true spherical-ranges is embedded in this description.

In addition to the algorithms of Fang, Razin and Bancroft — each of which applies to a homogeneous set of pseudo range measurements — this chapter contains extensions to combinations of pseudo and true slant-range measurements, to measurement of altitude and to multiple clock synchronization groups. Generally, a position determination algorithm for a set of

pseudo range measurements is readily simplified to true range measurements. The term 'Bancraft' is used herein for any algorithm involving (a) a Cartesian framework; (b) use of vectors; and (c) first finding an intermediate quantity such as a norm of the aircraft location vector, then its components. In contrast, 'traditional' solution methods utilize scalars and solve for the position components directly, usually in a specific sequence.

The algorithms presented in this chapter share several features with those presented in Chapter 6: (a) the earth is assumed to be a perfect sphere (except when the simpler plane/Flatland* assumption is used); (b) the number of measurements is the same as the number of unknown variables; and (c) the effects of possible measurement errors on the resulting position solutions are not considered. Chapter 8 relaxes all of these restrictions.

To simplify the exposition, the descriptions in this chapter assume a surveillance context. Thus, t_A denotes the unknown time of transmission by an aircraft and $t_i, i = 1,2,3,4$, denote the measured times of receiption of that transmission at four stations.

7.2 Bancroft Solution for Four Pseudo Slant-Ranges

7.2.1 Introduction

Context — While this document emphasizes navigation/surveillance with respect to a spherical earth, situations involving a Cartesian/rectangular coordinate framework are of interest (e.g., Chapter 5) for several reasons: (1) slant-range and pseudo slant-range measurements are more compatible with the rectangular framework than the spherical; (2) many analysts find the Cartesian framework more intuitive, so it can be used to gain insights into situations where a spherical framework may be more convenient for obtaining useful results; and (3) a Cartesian framework may be more convenient when the earth's ellipticity must be taken into account.

This section addresses position-finding from four pseudo slant-range (homogeneous) measurements. Bancroft's algorithm is extended situations involving only true slant-range measurements (including aircraft altitude), or a combination of pseudo and true slant-range measurements in Sections 7.3 to 7.5, respectively. Bancroft's algorithm can also be employed in situations involving multiple clock synchronization groups — e.g., see Section 7.6.

Spatial Coordinate Frame — The first step is the selection of an analysis origin. The analysis origin must be is different from the location of any station, and must satisfy other conditions discussed in Subsection 7.2.4. Bancroft's method can be viewed as a clever application of the cosine law of plane trigonometry. It involves a set of triangles each having vertices at the

* *Flatland: A Romance of Many Dimensions* is an 1884 satirical novella by the English schoolmaster Edwin Abbott Abbott. Here, 'Flatland' characterizes situations where both the aircraft and ground stations are restricted to a plane.

analysis origin (known), the station location (known) and the aircraft location (unknown). Thus the lengths of two sides of each triangle are known. The length of the side connecting the analysis origin and the aircraft is unknown, but that side is common to all triangles. Its length is found first. The aircraft coordinates then follow readily.

'Time' Coordinate — The offset common to all of a system's pseudo range measurements is inherently temporal, and arises because the aircraft transmissions are not synchronized with the ground station clocks. However, it sometimes convenient to treat the transmission time as a range offset (or bias). The two characterizations are related by the speed of propagation.

7.2.2 Problem Formulation

For many problems, the Earth-Centered, Earth-Fixed (ECEF, Subsection 5.1.1) *e*-frame is a good choice. For a spherical earth, in ECEF coordinates, the physical stations $\mathbf{S}_i$ are located at

$$\underline{\mathbf{r}}_i^{\mathbf{e}} = \begin{bmatrix} x_i^e \\ y_i^e \\ z_i^e \end{bmatrix} = \begin{bmatrix} \cos(L_i)\cos(\lambda_i) \\ \cos(L_i)\sin(\lambda_i) \\ \sin(L_i) \end{bmatrix} (R_e + h_i) \qquad i = 1,2,3,4 \qquad \text{Eq 220}$$

Here, L_i, λ_i and h_i denote the latitude, longitude and altitude (respectively) of station $\mathbf{S}_i$.

The (unknown) coordinates of the aircraft **A** are

$$\underline{\mathbf{r}}_A^{\mathbf{e}} = [x_A^e \quad y_A^e \quad z_A^e]^T \qquad \text{Eq 221}$$

For convenience, since quadratic quantities will be involved, use of the superscript *e* on $\underline{\mathbf{r}}_A^{\mathbf{e}}$ and $\underline{\mathbf{r}}_i^{\mathbf{e}}$ and their components is discontinued until the end of this section.

The aircraft-station pseudo range measurements satisfy equations of the form, for $i = 1,2,3,4$

$$\begin{gathered} (x_A - x_i)^2 + (y_A - y_i)^2 + (z_A - z_i)^2 = (ct_i - ct_A)^2 \\ [(x_A)^2 + (y_A)^2 + (z_A)^2 - (ct_A)^2] + [(x_i)^2 + (y_i)^2 + (z_i)^2 - (ct_i)^2] \\ = 2[x_i x_A + y_i y_A + z_i z_A - c^2 t_i t_A] \end{gathered} \qquad \text{Eq 222}$$

In vector-matrix notation, the equations of Eq 222 can be combined as

$$2\mathbf{B}\,\underline{\mathbf{s}}_A = \lambda \mathbf{1} + \mathbf{b} \qquad \text{Eq 223}$$

$$\underline{\mathbf{s}}_A = \begin{bmatrix} \mathbf{r}_A \\ ct_A \end{bmatrix} = [x_A \quad y_A \quad z_A \quad ct_A]^T$$

$$\lambda = \langle \underline{\mathbf{s}}_A, \underline{\mathbf{s}}_A \rangle = (x_A)^2 + (y_A)^2 + (z_A)^2 - (ct_A)^2$$

$$\mathbf{B} = \begin{bmatrix} x_1 & y_1 & z_1 & -ct_1 \\ x_2 & y_2 & z_2 & -ct_2 \\ x_3 & y_3 & z_3 & -ct_3 \\ x_4 & y_4 & z_4 & -ct_4 \end{bmatrix} \qquad \mathbf{b} = \begin{bmatrix} (x_1)^2 + (y_1)^2 + (z_1)^2 - (ct_1)^2 \\ (x_2)^2 + (y_2)^2 + (z_2)^2 - (ct_2)^2 \\ (x_3)^2 + (y_3)^2 + (z_3)^2 - (ct_3)^2 \\ (x_4)^2 + (y_4)^2 + (z_4)^2 - (ct_4)^2 \end{bmatrix} \qquad \mathbf{1} = \begin{bmatrix} 1 \\ 1 \\ 1 \\ 1 \end{bmatrix}$$

Eq 223 relates $\underline{\mathbf{s}}_A$ to its Lorentzian norm λ.

7.2.3 Problem Solution

Matrix **B** is nonsingular when (and only when) its rows are linearly independent. Assuming that to be true, the formal solution for $\underline{\mathbf{s}}_A$ is

$$\underline{\mathbf{s}}_A = \tfrac{1}{2}\lambda\mathbf{B}^{-1}\mathbf{1} + \tfrac{1}{2}\mathbf{B}^{-1}\mathbf{b} \qquad \text{Eq 224}$$

Eq 224 can be written as

$$\underline{\mathbf{s}}_A = \lambda\mathbf{u} + \mathbf{v} \qquad \text{Eq 225}$$

$$\mathbf{u} = \tfrac{1}{2}\mathbf{B}^{-1}\mathbf{1} = [u_x \quad u_y \quad u_z \quad u_t]^T$$
$$\mathbf{v} = \tfrac{1}{2}\mathbf{B}^{-1}\mathbf{b} = [v_x \quad v_y \quad v_z \quad v_t]^T$$

The Lorentzian norm λ of $\underline{\mathbf{s}}_A$ in Eq 225 can be found by (a) left-multiplying both sides of the equation by the diagonal matrix with diagonal elements (1,1,1,-1), then (b) left-multiplying both sides by the transpose of Eq 225. Upon collecting like terms, the result is

$$\alpha\lambda^2 + \beta\lambda + \gamma = 0 \qquad \text{Eq 226}$$

$$\alpha = \langle\mathbf{u},\mathbf{u}\rangle = u_x^2 + u_y^2 + u_z^2 - u_t^2$$
$$\beta = 2\langle\mathbf{u},\mathbf{v}\rangle - 1 = 2u_xv_x + 2u_yv_y + 2u_zv_z - 2u_tv_t - 1$$
$$\gamma = \langle\mathbf{v},\mathbf{v}\rangle = v_x^2 + v_y^2 + v_z^2 - v_t^2$$

Usually, Eq 226 has two distinct real roots

$$\lambda_+ = \frac{1}{2\alpha}\left(-\beta + \sqrt{\beta^2 - 4\alpha\gamma}\right)$$
$$\lambda_- = \frac{1}{2\alpha}\left(-\beta - \sqrt{\beta^2 - 4\alpha\gamma}\right) \qquad \text{Eq 227}$$

Thus there are two possible solutions for the aircraft state $\underline{\mathbf{s}}_A$

$$\underline{\mathbf{s}}_{A\pm} = \begin{bmatrix} x_{A\pm} \\ y_{A\pm} \\ z_{A\pm} \\ ct_{A\pm} \end{bmatrix} = \begin{bmatrix} \underline{\mathbf{r}}_{A\pm} \\ ct_{A\pm} \end{bmatrix} = \lambda_\pm\mathbf{u} + \mathbf{v} = \left(-\frac{\beta}{2\alpha}\mathbf{u} + \mathbf{v}\right) \pm \left(\frac{\sqrt{\beta^2 - 4\alpha\gamma}}{2\alpha}\mathbf{u}\right) \qquad \text{Eq 228}$$

One of the two solutions is correct; the other may be either ambiguous or extraneous. Depending upon the aircraft location, both can occur for pseudo range systems. Although unusual, situations can arise where there are not two distinct real roots to Eq 226 — see the following subsection.

The penultimate step is determining the two possible sets of aircraft latitude/longitude/altitude

coordinates. Reintroducing the superscript *e* to denote the coordinate frame, for a spherical earth, those quantities can be found from

$$L_{A\pm} = \arctan\left(\frac{z^e_{A\pm}}{\sqrt{\left(x^e_{A\pm}\right)^2 + \left(y^e_{A\pm}\right)^2}}\right)$$

$$\lambda_{A\pm} = \arctan\left(y^e_{A\pm}, x^e_{A\pm}\right) \qquad \text{Eq 229}$$

$$h_{A\pm} = \sqrt{\left(x^e_{A\pm}\right)^2 + \left(y^e_{A\pm}\right)^2 + \left(z^e_{A\pm}\right)^2} - R_e$$

In Eq 228 and Eq 229, a single sign, '+' or '–', must be used consistently.

The final step is selecting between the two candidate solutions. (The topic of selecting between multiple solutions is addressed in general terms in Subsection 6.1.3.) Mathematically, an extraneous solution arises from the squaring of the time differences in Eq 222, as squaring destroys the sign of the time differences $t_i - t_A$. When there is an extraneous solution, the solution for the aircraft time of transmission t_A can be used to detect it — the correct value for t_A must be less than $\min(t_1, t_2, t_3, t_4)$ and the extraneous value will be greater than $\max(t_1, t_2, t_3, t_4)$.

However, when an ambiguous solution occurs, the value for t_A will also be less than $\min(t_1, t_2, t_3, t_4)$. Generally, ambiguous solutions only occur when the aircraft is near an an extension of a baseline connecting two stations or between two extended baselines. (These areas are generally not within the service area where the system's use is intended.) When the aircraft is at a location where the system intended to be used, only detectable extraneous solutions occur (Ref. 48). Section 7.7 illustrates such situations in a two-dimensional context.

7.2.4 Remarks

Coordinate Frames — After a solution is found, the Cartesian coordinate frame employed for Bancroft's algorithm can be related to either a spherical or ellipsoidal earth model. Compatibility with an ellipsoidal earth is an advantage when the sensor-aircraft ranges are several hundred miles or more. However, if an ellipsoidal earth model is used, Eq 229 must be replaced by a slightly more complex set of expressions — see Section 9.3.

Invertibility of Matrix B — Invertibility of the 4x4 matrix **B** (Eq 223) is a requirement of Bancroft's Method. From the Matrix Inversion Lemma, it follows that the upper left-hand 3x3 submatrix must be invertible and that the (4,4) term cannot be zero. These mathematical requirements impose physical requirements — e.g.: (a) The spatial origin cannot lie along a baseline connecting any pair of stations (or its extensions past the stations); (b) Stations $\mathbf{S}_i$

(i=1,2,3) cannot lie in a straight line; (c) The aircraft cannot be on the extension of a straight line segment that passes through any three stations; (d) The time origin cannot coincide with the arrival of the signal at station $\mathbf{S}_4$. Aircraft-station geometry are explored further in Section 7.9.

Matrix **B** depends on measured times-of-arrival of signals at the pseudo slant-range stations. If a sequence of measurements are collected over time, matrix **B**, its inverse $\mathbf{B}^{-1}$, and vectors **u** and **v** must be recomputed for each measurement set.

Number and Types of Solutions — When pseudoranges are involved, each SOP is a hyper-boloid having two branches Solution possibilities for the quadratic equation of Eq 226 then are (bearing in mind that not all problems have all solution types):

(a) No real roots: Mathematically, $\beta^2 < 4\alpha\gamma$; geometrically, the SOPs do not intersect at a common point; this situation is often the result of measurement errors. It may be detectable from the measurements, as it is necessary that $|ct_i - ct_j| \leq \|\underline{\mathbf{r}}_i - \underline{\mathbf{r}}_j\|$ for every station pair, $\mathbf{S}_i$ and $\mathbf{S}_j$

(b) One real single root: Mathematically, $\alpha = 0$ (the quadratic equation is degenerately linear); geometrically, the SOPs only intersect at one common point; practically, this is a rare situation

(c) A real double root: Mathematically, $\beta^2 = 4\alpha\gamma$; geometrically, two or more of the SOPs are tangent and the other SOP passes through the point of tangency; practically, this is a rare situation

(d) Two real roots: Mathematically, $\beta^2 > 4\alpha\gamma$; physically, the three SOPs intersect at two distinct points; practically, this is the most common situation; one solution is correct and the other is either ambiguous or extraneous.

Relationship to Traditional Solutions — Bancroft's algorithm is readily programmed, but is not conducive to developing analytic expressions for the aircraft's position as a function of the measurements. Thus, when available, traditional solutions to problems involving real and pseudo slant-ranges (e.g., three of the four problem cases shown in Table 11) — which are equivalent to Bancroft's in terms of solution capability — remain valuable.

Other Comments

- Bancroft noted that his algorithm "performs better than an iterative solution in regions of poor GDoP". The Gauss-Newton iterative, linearized least-squares solution method is addressed in Chapter 8.
- Bancroft's solution has been extended to situations involving more measurements than unknown variables (Ref. 49). Those equations are not employed herein, as the linearized least squares method addressed in Chapter 8 is preferred (Ref. 50).
- Alternative solutions to the four-pseudo slant-range problem were published after Bancroft's paper (e.g., Ref. 51). One, based traditional scalar algebra, is presented in Section 7.9. These alternatives are not as easily generalizable as Bancroft's method.

7.3 Bancroft Solution for Three True Slant-Ranges

7.3.1 Problem Formulation

Bancroft's algorithm (Section 7.2) was derived as the solution for four pseudo slant-range measurements. Its simplification to three homogeneus true slant-range measurements is the topic of this section. Extensions to multiple measurement types are discussed in Sections 7.4 - 7.6.

Here, the slant-range measurements between the aircraft **A** and ground station $i = 1,2,3$ are

$$(x_A - x_i)^2 + (y_A - y_i)^2 + (z_A - z_i)^2 = (d_{iA})^2$$
$$[(x_A)^2 + (y_A)^2 + (z_A)^2] + [(x_i)^2 + (y_i)^2 + (z_i)^2 - (d_{iA})^2] = 2[x_i x_A + y_i y_A + z_i z_A] \quad \text{Eq 230}$$

A consequence of omitting the time component is that the Lorentzian norm is replaced by the Euclidean norm

$$\lambda = \langle \underline{\mathbf{r}}_A, \underline{\mathbf{r}}_A \rangle = (x_A)^2 + (y_A)^2 + (z_A)^2 \quad \text{Eq 231}$$

Also, matrix **B** and vectors **b** and **1** become

$$\mathbf{B} = \begin{bmatrix} x_1 & y_1 & z_1 \\ x_2 & y_2 & z_2 \\ x_3 & y_3 & z_3 \end{bmatrix} \qquad \mathbf{b} = \begin{bmatrix} (x_1)^2 + (y_1)^2 + (z_1)^2 - (d_{1A})^2 \\ (x_2)^2 + (y_2)^2 + (z_2)^2 - (d_{2A})^2 \\ (x_3)^2 + (y_3)^2 + (z_3)^2 - (d_{3A})^2 \end{bmatrix} \qquad \mathbf{1} = \begin{bmatrix} 1 \\ 1 \\ 1 \end{bmatrix} \quad \text{Eq 232}$$

With these definitions, Eq 223 becomes (with $\underline{\mathbf{s}}_A$ is replaced by $\underline{\mathbf{r}}_A$)

$$2\mathbf{B}\,\underline{\mathbf{r}}_A = \lambda \mathbf{1} + \mathbf{b} \quad \text{Eq 233}$$

7.3.2 Problem Solution

The solution proceeds as in Subsection 7.2.3, Eq 225 - Eq 228, using three-element vectors in place of four-element vectors (i.e., without involving transmission time).

$$\underline{\mathbf{r}}_A = \lambda \mathbf{u} + \mathbf{v} \quad \text{Eq 234}$$

$$\mathbf{u} = \tfrac{1}{2}\mathbf{B}^{-1}\mathbf{1} = [u_x \quad u_y \quad u_z]^T$$
$$\mathbf{v} = \tfrac{1}{2}\mathbf{B}^{-1}\mathbf{b} = [v_x \quad v_y \quad v_z]^T$$

The Euclidian norm λ of $\underline{\mathbf{r}}_A$ satisfies

$$\alpha\lambda^2 + \beta\lambda + \gamma = 0 \quad \text{Eq 235}$$

$$\alpha = \langle \mathbf{u}, \mathbf{u} \rangle = u_x^2 + u_y^2 + u_z^2$$
$$\beta = 2\langle \mathbf{u}, \mathbf{v} \rangle - 1 = 2u_x v_x + 2u_y v_y + 2u_z v_z - 1$$
$$\gamma = \langle \mathbf{v}, \mathbf{v} \rangle = v_x^2 + v_y^2 + v_z^2$$

Usually, Eq 235 has two distinct real roots

$$\lambda_{\pm} = \frac{1}{2\alpha}\left(-\beta \pm \sqrt{\beta^2 - 4\alpha\gamma}\right) \qquad \text{Eq 236}$$

Thus there are two possible solutions for the aircraft location $\underline{\mathbf{r}}_A$

$$\underline{\mathbf{r}}_{A\pm} = \begin{bmatrix} x_{A\pm} \\ y_{A\pm} \\ z_{A\pm} \end{bmatrix} = \lambda_{\pm}\mathbf{u} + \mathbf{v} = \left(-\frac{\beta}{2\alpha}\mathbf{u} + \mathbf{v}\right) \pm \left(\frac{\sqrt{\beta^2 - 4\alpha\gamma}}{2\alpha}\mathbf{u}\right) \qquad \text{Eq 237}$$

After reintroducing the superscript *e* to denote the coordinate frame, the aircraft latitude/longitude/ altitude are found from Eq 229.

7.3.3 Ambiguity Resolution / Sensor Plane of Symmetry

Assuming that the goal is to compute the aircraft's latitude, longitude and altitude (e.g., using Eq 229 or similar), processing of the slant-range measurements can be performed in any coordinate frame that subsequently can be related to the ECEF *e*-frame — typically by a translation and/or rotation. Thus, an analysis *a*-frame is considered which has its first two axes parallel to the plane defined by the three sensor locations. In this *a*-frame, the third coordinate of the sensors is the same, say z_S. Thus, in the *a*-frame, matrix **B** and vector **u** are

$$\mathbf{B^a} = \begin{bmatrix} x_1 & y_1 & z_S \\ x_2 & y_2 & z_S \\ x_3 & y_3 & z_S \end{bmatrix} \qquad \mathbf{u^a} = \tfrac{1}{2}(\mathbf{B^a})^{-1}\mathbf{1} = \frac{1}{2z_S}\begin{bmatrix} 0 \\ 0 \\ 1 \end{bmatrix} \qquad \text{Eq 238}$$

It is shown in Eq 228 that, in the coordinate frame used for analysis, the two solutions are the sum of a common vector plus equal and opposite vectors that are proportional to **u** (Table 12). Also, Eq 238 demonstrates that, for three slant-range measurements, the correct and ambiguous solutions are both perpendicular to the sensor plane (regardless of the frame used for analysis/ processing). It is clear physically that the two solutions must in fact be equi-distant from the sensor plane. Thus, for aircraft tracking using range sensors located on/near the ground, the ambiguous solution will be below the ground.

Table 12 Physical Significance of Vectors in Solution for Slant-Range Measurements

Vector	Description
$-\frac{\beta}{2\alpha}\mathbf{u} + \mathbf{v}$	Extends from the analysis origin to the location on the sensor plane that is closest to the aircraft
$\pm\frac{\sqrt{\beta^2 - 4\alpha\gamma}}{2\alpha}\mathbf{u}$	Extends perpendicular from the sensor plane to either the aircraft or the ambiguous solution for the aircraft position

7.3.4 Remarks

- When only slant-range measurements are involved, matrix **B** (Eq 232) is independent of the measurements. It is possible to compute its inverse, as well as vector **u** and scalar α once and store them for future use.
- A two-dimensional ('Flatland') application of a range-measuring system is presented in Example 8, in Subsections 7.12.1 and 8.5.1. The latter demonstrates the accuracy degradation when aircraft are near the baseline connecting the stations, or its extensions. Similarly, for a three-dimensional situation, accuracy of the distance from the sensor plane with be degraded for aircraft locations near the plane.
- For surveillance, three true range measurements can be accomplished using one transmit-receive station and two receive only stations, provided that the times of all transmissions and receiptions are measured using synchronized clocks.

7.4 Bancroft Solution for Two True Slant-Ranges and Altitude

Bancroft's algorithm can also be applied to situations involving two slant-range measurements and a measurement of aircraft altitude, because (for a spherical-earth model) an altitude measurement can be converted to a slant-range from the center of the earth.

When altitude is used as a measurement, one extra step is involved in the solution. For the Bancroft **B** matrix (e.g., Eq 232) to be inverted, the analysis origin must not be in the plane formed by the three stations — or, as here, the two physical stations and center of the earth. One possible analysis origin, in ECEF coordinates, is of the form

$$\underline{\mathbf{r}}_o^{\mathbf{e}} = \begin{bmatrix} x_o^e \\ y_o^e \\ z_o^e \end{bmatrix} = \begin{bmatrix} \cos(L_o)\cos(\lambda_o) \\ \cos(L_o)\sin(\lambda_o) \\ \sin(L_o) \end{bmatrix} kR_e \qquad \text{Eq 239}$$

Here L_o and λ_o are the latitude and longitude of an arbitrary point not on the baseline connecting the stations and k is a number slightly less than 1.

In ECEF coordinates, the physical stations locations are given by Eq 220, with *i*=1,2. The associated measurements equations are given by Eq 230, with *i*=1,2. The aircraft altitude h_A measurement equation is

$$(x_A)^2 + (y_A)^2 + (z_A)^2 = (R_e + h_A)^2 \qquad \text{Eq 240}$$

The altitude measurement 'station' is the earth's center, with ECEF coordinates given by:

$$\underline{\mathbf{r}}_3^{\mathbf{e}} = [0 \quad 0 \quad 0]^T \qquad \text{Eq 241}$$

Bancroft's algorithm is applied using offset station coordinates

$$\Delta\underline{\mathbf{r}}_i^{\mathbf{e}} = \underline{\mathbf{r}}_i^{\mathbf{e}} - \underline{\mathbf{r}}_o^{\mathbf{e}} = \begin{bmatrix} x_i^e \\ y_i^e \\ z_i^e \end{bmatrix} - \begin{bmatrix} x_o^e \\ y_o^e \\ z_o^e \end{bmatrix} = \begin{bmatrix} x_i^e - x_o^e \\ y_i^e - y_o^e \\ z_i^e - z_o^e \end{bmatrix} = \begin{bmatrix} \Delta x_i^e \\ \Delta y_i^e \\ \Delta z_i^e \end{bmatrix} \quad \text{Eq 242}$$

Matrix **B** and vector **b** are

$$\mathbf{B} = \begin{bmatrix} \Delta x_1 & \Delta y_1 & \Delta z_1 \\ \Delta x_2 & y\Delta_2 & \Delta z_2 \\ \Delta x_3 & \Delta y_3 & \Delta z_3 \end{bmatrix} \qquad \mathbf{b} = \begin{bmatrix} (\Delta x_1)^2 + (\Delta y_1)^2 + (\Delta z_1)^2 - (d_{1A})^2 \\ (\Delta x_2)^2 + (\Delta y_2)^2 + (\Delta z_2)^2 - (d_{2A})^2 \\ (\Delta x_3)^2 + (\Delta y_3)^2 + (\Delta z_3)^2 - (R_e + h_A)^2 \end{bmatrix} \quad \text{Eq 243}$$

For these definitions of **B** and **b**, the aircraft's location is found relative to the analysis origin

$$\Delta\underline{\mathbf{r}}_A^{\mathbf{e}} = [\Delta x_A^e \quad \Delta y_A^e \quad \Delta z_A^e]^T \quad \text{Eq 244}$$

from Eq 231 - Eq 237. The solution for $\Delta\underline{\mathbf{r}}_A^{\mathbf{e}}$ is then converted to ECEF coordinates using Eq 242, which is used to find the aircraft latitude and longitude using Eq 229.

Remarks

- The degradation in the accuracy of position estimates for aircraft near the baseline connecting the stations (and its extensions), which is cited in the previous section and described more fully in Subsection 8.5.1, is applicable here as well.
- For surveillance, two true range measurements can be accomplished using one transmit-receive station and one receive only station, provided that the times of all transmissions and receiptions are measured using synchronized clocks.
- The solution method described in this section is an alternative to that in Section 6.4.

7.5 Bancroft Solution for Pseudo Slant-Ranges and Altitude

7.5.1 Introduction

In terms of the subject system's functionality, this section best relates to Section 7.2. The two sections address the determination of an aircraft's location based at least in part on pseudo slant-ranges measured at a set of stations. While Section 7.2 assumes that only pseudo slant-range measurements are available, this section assumes that altitude is also available, and that a true slant-range may be as well. As often occurs when more than one measurement type is utilized, the resulting expressions are more complex than are expressions for a homogeneous set of measurements.

7.5.2 Problem Formulation: Three Pseudo Slant-Ranges and Altitude

The three physical ground stations have known coordinates latitude L_i, longitude λ_i, and altitude h_i, $i = 1,2,3$. In ECEF coordinates, their locations are

$$\underline{\mathbf{r}}_i^{\mathbf{e}} = \begin{bmatrix} x_i^e \\ y_i^e \\ z_i^e \end{bmatrix} = \begin{bmatrix} \cos(L_i)\cos(\lambda_i) \\ \cos(L_i)\sin(\lambda_i) \\ \sin(L_i) \end{bmatrix} (R_e + h_i) \qquad i = 1,2,3 \qquad \text{Eq 245}$$

As previously (Eq 221), the unknown ECEF coordinates of the aircraft are

$$\underline{\mathbf{r}}_A^{\mathbf{e}} = [x_A^e \quad y_A^e \quad z_A^e]^T \qquad \text{Eq 246}$$

For convenience, since quadratic quantities will be involved, use of the superscript **e** on $\underline{\mathbf{r}}_A^{\mathbf{e}}$ and $\underline{\mathbf{r}}_i^{\mathbf{e}}$ and their components is discontinued until the end of this section.

The aircraft-station pseudo slant-range measurements satisfy equations of the form

$$\begin{gathered} (x_A - x_i)^2 + (y_A - y_i)^2 + (z_A - z_i)^2 = (ct_i - ct_A)^2 \quad , \quad i = 1,2,3 \\ [(x_A)^2 + (y_A)^2 + (z_A)^2 - (ct_A)^2] + [(x_i)^2 + (y_i)^2 + (z_i)^2 - (ct_i)^2] \\ = 2[x_i x_A + y_i y_A + z_i z_A - c^2 t_i t_A] \quad , \quad i = 1,2,3 \end{gathered} \qquad \text{Eq 247}$$

The aircraft altitude h_A measurement equation is

$$(x_A)^2 + (y_A)^2 + (z_A)^2 = (R_e + h_A)^2 \qquad \text{Eq 248}$$

To formulate the vector-matrix equation to be solved, Eq 248 is substituted into Eq 247 as a constraint. The result can be written

$$2\mathbf{B}\,\underline{\mathbf{r}}_A = \mathbf{b} + (R_e + h_A)^2\mathbf{1} + 2c^2\mathbf{t}\,t_A - c^2\mathbf{1}(t_A)^2 \qquad \text{Eq 249}$$

$$\mathbf{B} = \begin{bmatrix} x_1 & y_1 & z_1 \\ x_2 & y_2 & z_2 \\ x_3 & y_3 & z_3 \end{bmatrix} \qquad \mathbf{b} = \begin{bmatrix} (x_1)^2 + (y_1)^2 + (z_1)^2 - (ct_1)^2 \\ (x_2)^2 + (y_2)^2 + (z_2)^2 - (ct_2)^2 \\ (x_3)^2 + (y_3)^2 + (z_3)^2 - (ct_3)^2 \end{bmatrix} \qquad \mathbf{1} = \begin{bmatrix} 1 \\ 1 \\ 1 \end{bmatrix} \qquad \mathbf{t} = \begin{bmatrix} t_1 \\ t_2 \\ t_3 \end{bmatrix}$$

7.5.3 Problem Solution: Three Pseudo Slant-Ranges and Altitude

Inverting matrix **B** and solving Eq 249 for $\underline{\mathbf{r}}_A$ yields

$$\underline{\mathbf{r}}_A = \mathbf{u} + \mathbf{v}\,t_A + \mathbf{w}\,(t_A)^2 \qquad \text{Eq 250}$$

$$\mathbf{u} = \tfrac{1}{2}\mathbf{B}^{-1}(\mathbf{b} + (R_e + h_A)^2\mathbf{1}) \qquad \mathbf{v} = c^2\mathbf{B}^{-1}\mathbf{t} \qquad \mathbf{w} = -\tfrac{1}{2}c^2\mathbf{B}^{-1}\mathbf{1}$$

Taking the Euclidian norm of $\underline{\mathbf{r}}_A$ in Eq 250 and using Eq 248 yields a quartic equation in t_A

$$a_4(t_A)^4 + a_3(t_A)^3 + a_2(t_A)^2 + a_1 t_A + a_0 = 0 \qquad \text{Eq 251}$$

$$a_4 = \mathbf{w}^T\mathbf{w} \qquad a_3 = 2\mathbf{v}^T\mathbf{w} \qquad a_2 = 2\mathbf{u}^T\mathbf{w} + \mathbf{v}^T\mathbf{v}$$
$$a_1 = 2\mathbf{u}^T\mathbf{v} \qquad a_0 = \mathbf{u}^T\mathbf{u} - (R_e + h_A)^2 \qquad —$$

When t_A is found as a root of Eq 251 (see Subsection 7.5.6 below), $\underline{\mathbf{r}}_A^{\mathbf{e}}$ follows from Eq 250. Then the aircraft latitude L_A and longitude λ_A are given by Eq 229.

7.5.4 Problem Formulation: Two Pseudo and One True Slant-Range Plus Altitude

Here again, the three physical ground stations have known latitude L_i, longitude λ_i, and altitude h_i, where i = 1, 2 or 3. In ECEF coordinates, their locations are given by Eq 245. The unknown ECEF coordinates of the aircraft are given by Eq 246. For convenience, use of the superscript **e** on $\underline{\mathbf{r}}_A^e$ and $\underline{\mathbf{r}}_i^e$ and their components is discontinued.

The aircraft-station pseudo slant-range measurements satisfy equations of the form

$$[(x_A)^2 + (y_A)^2 + (z_A)^2 - (ct_A)^2] + [(x_i)^2 + (y_i)^2 + (z_i)^2 - (ct_i)^2] = 2[x_i x_A + y_i y_A + z_i z_A - c^2 t_i t_A] \quad , \quad i = 1,2 \qquad \text{Eq 252}$$

The true slant-range measurement between the aircraft **A** and ground station 3 is

$$[(x_A)^2 + (y_A)^2 + (z_A)^2] + [(x_3)^2 + (y_3)^2 + (z_3)^2 - (d_{3A})^2] = 2[x_3 x_A + y_3 y_A + z_3 z_A] \qquad \text{Eq 253}$$

The aircraft altitude h_A measurement equation is

$$(x_A)^2 + (y_A)^2 + (z_A)^2 = (R_e + h_A)^2 \qquad \text{Eq 254}$$

In vector-matrix notation, Eq 252 - Eq 254 can be written as

$$2\mathbf{B}\,\underline{\mathbf{r}}_A = \mathbf{b}' + (R_e + h_A)^2\mathbf{1}_3 + 2c^2\mathbf{t}'\,t_A - c^2\mathbf{1}_2(t_A)^2 \qquad \text{Eq 255}$$

$$\mathbf{b}' = \begin{bmatrix} (x_1)^2 + (y_1)^2 + (z_1)^2 - (ct_1)^2 \\ (x_2)^2 + (y_2)^2 + (z_2)^2 - (ct_2)^2 \\ (x_3)^2 + (y_3)^2 + (z_3)^2 - (d_{3A})^2 \end{bmatrix} \qquad \mathbf{1}_3 = \begin{bmatrix} 1 \\ 1 \\ 1 \end{bmatrix} \qquad \mathbf{1}_2 = \begin{bmatrix} 1 \\ 1 \\ 0 \end{bmatrix} \qquad \mathbf{t}' = \begin{bmatrix} t_1 \\ t_2 \\ 0 \end{bmatrix}$$

Matrix **B** is given in Eq 249.

7.5.5 Problem Solution: Two Pseudo and One True Slant-Range Plus Altitude

Inverting matrix **B** and solving for $\underline{\mathbf{r}}_A$ yields

$$\underline{\mathbf{r}}_A = \mathbf{u}' + \mathbf{v}'\,t_A + \mathbf{w}'\,(t_A)^2 \qquad \text{Eq 256}$$

$$\mathbf{u}' = \tfrac{1}{2}\mathbf{B}^{-1}(\mathbf{b}' + (R_e + h_A)^2\mathbf{1}_3) \qquad \mathbf{v}' = c^2\mathbf{B}^{-1}\mathbf{t}' \qquad \mathbf{w}' = -\tfrac{1}{2}c^2\mathbf{B}^{-1}\mathbf{1}_2$$

Taking the Euclidian norm of $\underline{\mathbf{r}}_A$ in Eq 256 and using Eq 254 yields a quartic equation in t_A

$$a_4'(t_A)^4 + a_3'(t_A)^3 + a_2'(t_A)^2 + a_1' t_A + a_0' = 0 \qquad \text{Eq 257}$$

$$a_4' = (\mathbf{w}')^T\mathbf{w}' \qquad a_3' = 2(\mathbf{v}')^T\mathbf{w}' \qquad a_2' = 2(\mathbf{u}')^T\mathbf{w}' + (\mathbf{v}')^T\mathbf{v}'$$

$$a_1' = 2(\mathbf{u}')^T\mathbf{v}' \qquad a_0' = (\mathbf{u}')^T\mathbf{u}' - (R_e + h_A)^2 \qquad —$$

When t_A is found as a root of Eq 257, $\underline{\mathbf{r}}_A^e$ follows from Eq 256. Then the aircraft latitude L_A and longitude λ_A are given by Eq 229.

7.5.6 Remarks

- Algebraic methods for finding the roots of a quartic polynomial equation such as Eq 251 and Eq 257 has been known for approximately 500 years. Thus the two algorithms presented herein can be classified as non-iterative. The Matlab routine 'roots' implements one such method; in limited testing, it performed reliably (e.g., see Example 12, Subsection 7.12.5). During those tests, for aircraft locations in the service area, the correct root of Eq 251 was obvious from physical considerations.
- Three pseudo slant-ranges and an altitude measurement (Subsections 7.5.2 - 7.5.3) is conceptually the measurement set for Wide Area Multilateration aircraft surveillance.
- For surveillance, one true range and two pseudo range measurements (all slant-ranges) can be accomplished using a radar range subsystem and two receive-only 'multilateration' stations having clocks which are synchronized with each other but not with the radar. Not requiring that the radar and multilateration stations be synchronized simplifies their integration.
- Fang's algorithm (Section 7.7) considers three pseudo slant-range stations in a Cartesian plane. The simplicity of that situation provides insights into the three-station pseudo range problem which are less apparent in a spherical context. However, the behavior of the solutions are qualitatively similar.

7.6 Bancroft Solution for Two Pairs of Pseudo Slant-Ranges and Altitude

7.6.1 Introduction

In terms of the functionality of the system involved, this section is most closely related to Section 7.5. Each addresses the determination of an aircraft's location based on of time-difference-of-arrival measurements of slant-range signals for a set of ground stations, plus knowledge of the aircraft's altitude. However, whereas the preceding section assumes three ground stations with synchronized clocks, this section assumes two pairs of ground stations with the clocks for each pair being separately synchronized. This section is also related to Section 7.11, which addresses the determination of an aircraft's location based on time-difference-of-arrival measurements of spherical-range signals for two pairs of separately synchronized ground stations.

Unsynchronized slant-range differences can arise if one were to combine measurements from two separate navigation systems — e.g., GPS and Galileo. In the context of multilateration, it could arise as the result of a failure in the ground station synchronization network or intentionally, as an aspect of the system design. Loran-C 'cross-chaining' involves similar assumptions concerning station time synchronization.

7.6.2 Problem Formulation

One ground station pair is labeled **R** and **S**; the other is labeled **U** and **V**. The ground stations have the known locations latitude L_i, longitude λ_i, and altitude h_i, where i = R, S, U or V. In

ECEF coordinates, their locations are

$$\underline{\mathbf{r}}_i^{\mathbf{e}} = \begin{bmatrix} x_i^e \\ y_i^e \\ z_i^e \end{bmatrix} = \begin{bmatrix} \cos(L_i)\cos(\lambda_i) \\ \cos(L_i)\sin(\lambda_i) \\ \sin(L_i) \end{bmatrix} (R_e + h_i) \qquad i = R, S, U, V \qquad \text{Eq 258}$$

The altitude measurement 'station', labeled **H**, is the earth's center, with ECEF coordinates

$$\underline{\mathbf{r}}_H^{\mathbf{e}} = [0 \quad 0 \quad 0]^T \qquad \text{Eq 259}$$

The unknown ECEF coordinates of the aircraft labeled **A**, are

$$\underline{\mathbf{r}}_A^{\mathbf{e}} = [x_A^e \quad y_A^e \quad z_A^e]^T \qquad \text{Eq 260}$$

Since altitude will be utilized as a measurement — rather than as a constraint, as in Sections 7.4 and 7.5 — an analysis origin offset from the earth's center must be used. One possible origin, in ECEF coordinates, is of the form

$$\underline{\mathbf{r}}_o^{\mathbf{e}} = \begin{bmatrix} x_o^e \\ y_o^e \\ z_o^e \end{bmatrix} = \begin{bmatrix} \cos(L_o)\cos(\lambda_o) \\ \cos(L_o)\sin(\lambda_o) \\ \sin(L_o) \end{bmatrix} kR_e \qquad \text{Eq 261}$$

Here L_o and λ_o are the latitude and longitude of an arbitrary point not on either of the great circle arcs connecting the pairs of stations and *k* is a number slightly less than 1 — e.g., 0.97. Bancroft's algorithm is then applied using offset station coordinates

$$\Delta\underline{\mathbf{r}}_i^{\mathbf{e}} = \underline{\mathbf{r}}_i^{\mathbf{e}} - \underline{\mathbf{r}}_o^{\mathbf{e}} = \begin{bmatrix} x_i^e \\ y_i^e \\ z_i^e \end{bmatrix} - \begin{bmatrix} x_o^e \\ y_o^e \\ z_o^e \end{bmatrix} = \begin{bmatrix} x_i^e - x_o^e \\ y_i^e - y_o^e \\ z_i^e - z_o^e \end{bmatrix} = \begin{bmatrix} \Delta x_i^e \\ \Delta y_i^e \\ \Delta z_i^e \end{bmatrix} \qquad i = R, S, U, V, H \qquad \text{Eq 262}$$

Clearly, $\Delta\underline{\mathbf{r}}_H^{\mathbf{e}} = -\underline{\mathbf{r}}_o^{\mathbf{e}}$. The aircraft's location is first found relative to the analysis origin (Eq 244)

$$\Delta\underline{\mathbf{r}}_A^{\mathbf{e}} = \underline{\mathbf{r}}_A^{\mathbf{e}} - \underline{\mathbf{r}}_O^{\mathbf{e}} = [\Delta x_A^e \quad \Delta y_A^e \quad \Delta z_A^e]^T \qquad \text{Eq 263}$$

For convenience, since quadratic quantities will be involved, use of the superscript **e** on vectors and their components is discontinued until the end of this section.

For stations **R** and **S**, the aircraft-station pseudo slant-range measurements satisfy

$$\begin{aligned} &\left[(\Delta x_A)^2 + (\Delta y_A)^2 + (\Delta z_A)^2 - \left(ct_{A(RS)}\right)^2\right] + \left[(\Delta x_i)^2 + (\Delta y_i)^2 + (\Delta z_i)^2 - (ct_i)^2\right] \\ &\quad = 2\left[\Delta x_i \Delta x_A + \Delta y_i \Delta y_A + \Delta z_i \Delta z_A - c^2 t_i t_{A(RS)}\right] \quad , \quad i = R, S \end{aligned} \qquad \text{Eq 264}$$

Similarly, for stations **U** and **V**, the aircraft-station pseudo slant-range measurements satisfy

$$\begin{aligned} &\left[(\Delta x_A)^2 + (\Delta y_A)^2 + (\Delta z_A)^2 - \left(ct_{A(UV)}\right)^2\right] + \left[(\Delta x_i)^2 + (\Delta y_i)^2 + (\Delta z_i)^2 - (ct_i)^2\right] \\ &\quad = 2\left[\Delta x_i \Delta x_A + \Delta y_i \Delta y_A + \Delta z_i \Delta z_A - c^2 t_i t_{A(UV)}\right] \quad , \quad i = U, V \end{aligned} \qquad \text{Eq 265}$$

Here $t_{A(RS)}$ denotes the unknown time of transmission by the aircraft based on the clock for

stations **R** and **S**. Similarly $t_{A(UV)}$ denotes the unknown time of transmission by the aircraft based on the clock for stations **U** and **V**. Also, t_i the measured time of reception by ground station *i* based on its clock group.

The aircraft altitude h_A measurement equation is

$$\begin{gathered}(x_A)^2+(y_A)^2+(z_A)^2=(R_e+h_A)^2\\(\Delta x_A-\Delta x_H)^2+(\Delta y_A-\Delta y_H)^2+(\Delta z_A-\Delta z_H)^2=(R_e+h_A)^2\\[(\Delta x_A)^2+(\Delta y_A)^2+(\Delta z_A)^2]+[(\Delta x_H)^2+(\Delta y_H)^2+(\Delta z_H)^2-(R_e+h_A)^2]\\=2[\Delta x_H\Delta x_A+\Delta y_H\Delta y_A+\Delta z_H\Delta z_A]\end{gathered} \qquad \text{Eq 266}$$

7.6.3 Problem Solution

The solution approach is to: (1) consider station pair **R** and **S**, in conjunction with 'station' **H**, and find a relationship between the aircraft time of transmission $t_{A(RS)}$ and the squared distance between the analysis origin and the aircraft λ; (2) similarly, consider station pair **U** and **V** in conjunction with **H**, and find a relationship between $t_{A(UV)}$ and λ; and (3) consider both pairs of stations and find an additional relationship for $t_{A(RS)}$, $t_{A(UV)}$ and λ. All other results then follow.

Analysis of Stations R and S — First selecting stations **R** and **S** and the altitude measurement for analysis, Eq 264 and Eq 266 can be written as

$$2\mathbf{B}_{RS}\,\Delta\underline{\mathbf{r}}_A=\mathbf{b}_{RS}+\lambda\mathbf{1}_3+2c^2\mathbf{t}_{RS}\,t_{A(RS)}-c^2\mathbf{1}_2\left(t_{A(RS)}\right)^2 \qquad \text{Eq 267}$$

$$\mathbf{B}_{RS}=\begin{bmatrix}\Delta x_R & \Delta y_R & \Delta z_R\\ \Delta x_S & \Delta y_S & \Delta z_S\\ \Delta x_H & \Delta y_H & \Delta z_H\end{bmatrix}$$

$$\mathbf{b}_{RS}=\begin{bmatrix}(\Delta x_R)^2+(\Delta y_R)^2+(\Delta z_R)^2-(ct_R)^2\\ (\Delta x_S)^2+(\Delta y_S)^2+(\Delta z_S)^2-(ct_S)^2\\ (\Delta x_H)^2+(\Delta y_H)^2+(\Delta z_H)^2-(R_e+h_A)^2\end{bmatrix}$$

$$\lambda=(\Delta x_A)^2+(\Delta y_A)^2+(\Delta z_A)^2$$

$$\mathbf{1}_3=[1\quad 1\quad 1]^T \qquad \mathbf{1}_2=[1\quad 1\quad 0]^T \qquad \mathbf{t}_{RS}=[t_R\quad t_S\quad 0]^T$$

Inverting matrix $\mathbf{B}_{RS}$ yields

$$\Delta\underline{\mathbf{r}}_A=\mathbf{c}_{RS}+\mathbf{d}_{RS}\,\lambda+\mathbf{e}_{RS}\,t_{A(RS)}+\mathbf{f}_{RS}\left(t_{A(RS)}\right)^2 \qquad \text{Eq 268}$$

$$\mathbf{c}_{RS}=\tfrac{1}{2}\mathbf{B}_{RS}^{-1}\mathbf{b}_{RS} \qquad \mathbf{d}_{RS}=\tfrac{1}{2}\mathbf{B}_{RS}^{-1}\mathbf{1}_3$$

$$\mathbf{e}_{RS}=c^2\mathbf{B}_{RS}^{-1}\mathbf{t}_{RS} \qquad \mathbf{f}_{RS}=-\tfrac{1}{2}c^2\mathbf{B}_{RS}^{-1}\mathbf{1}_2$$

Taking the Euclidian norm of $\Delta\underline{\mathbf{r}}_A$ in Eq 268 and collecting terms yields

$$a_{RS,40}\left(t_{A(RS)}\right)^4 + a_{RS,30}\left(t_{A(RS)}\right)^3 + a_{RS,20}\left(t_{A(RS)}\right)^2 + a_{RS,10}\,t_{A(RS)} + a_{RS,00} + a_{RS,02}\lambda^2 + a_{RS,01}\lambda + a_{RS,21}\left(t_{A(RS)}\right)^2\lambda + a_{RS,11}\,t_{A(RS)}\lambda = 0 \quad \text{Eq 269}$$

$$a_{RS,40} = \mathbf{f}_{RS}^T\mathbf{f}_{RS} \qquad a_{RS,30} = 2\,\mathbf{e}_{RS}^T\mathbf{f}_{RS} \qquad a_{RS,20} = 2\,\mathbf{c}_{RS}^T\mathbf{f}_{RS} + \mathbf{e}_{RS}^T\mathbf{e}_{RS}$$

$$a_{RS,10} = 2\,\mathbf{c}_{RS}^T\mathbf{e}_{RS} \qquad a_{RS,00} = \mathbf{c}_{RS}^T\mathbf{c}_{RS} \qquad a_{RS,02} = \mathbf{d}_{RS}^T\mathbf{d}_{RS}$$

$$a_{RS,01} = 2\,\mathbf{c}_{RS}^T\mathbf{d}_{RS} - 1 \qquad a_{RS,21} = 2\,\mathbf{d}_{RS}^T\mathbf{f}_{RS} \qquad a_{RS,11} = 2\,\mathbf{d}_{RS}^T\mathbf{e}_{RS}$$

The above steps transform a situation (Eq 267) involving four unknown variables and three scalar equations into one involving: (a) one scalar polynomial equation (Eq 269) relating two unknown variables ($t_{A(RS)}$ and λ), and (b) a vector equation (Eq 268) for finding the unknown aircraft coordinates from $t_{A(RS)}$ and λ.

Analysis of Stations U and V — Analysis for stations **U** and **V** is identical (except for notation designating stations) to that for stations **R** and **S**. Thus Eq 265 and Eq 266 can be written as

$$2\,\mathbf{B}_{UV}\,\Delta\underline{\mathbf{r}}_A = \mathbf{b}_{UV} + \lambda\mathbf{1}_3 + 2c^2\mathbf{t}_{UV}\,t_{A(UV)} - c^2\mathbf{1}_2\left(t_{A(UV)}\right)^2 \quad \text{Eq 270}$$

$$\mathbf{B}_{UV} = \begin{bmatrix} \Delta x_U & \Delta y_U & \Delta z_U \\ \Delta x_V & \Delta y_V & \Delta z_V \\ \Delta x_H & \Delta y_H & \Delta z_H \end{bmatrix}$$

$$\mathbf{b}_{UV} = \begin{bmatrix} (\Delta x_U)^2 + (\Delta y_U)^2 + (\Delta z_U)^2 - (ct_U)^2 \\ (\Delta x_V)^2 + (\Delta y_V)^2 + (\Delta z_V)^2 - (ct_V)^2 \\ (\Delta x_H)^2 + (\Delta y_H)^2 + (\Delta z_H)^2 - (R_e + h_A)^2 \end{bmatrix}$$

$$\lambda = (\Delta x_A)^2 + (\Delta y_A)^2 + (\Delta z_A)^2$$

$$\mathbf{1}_3 = [1 \quad 1 \quad 1]^T \qquad \mathbf{1}_2 = [1 \quad 1 \quad 0]^T \qquad \mathbf{t}_{UV} = [t_U \quad t_V \quad 0]^T$$

Inverting matrix $\mathbf{B}_{UV}$ yields

$$\Delta\underline{\mathbf{r}}_A = \mathbf{c}_{UV} + \mathbf{d}_{UV}\,\lambda + \mathbf{e}_{UV}\,t_{A(UV)} + \mathbf{f}_{UV}\left(t_{A(UV)}\right)^2 \quad \text{Eq 271}$$

$$\mathbf{c}_{UV} = \tfrac{1}{2}\mathbf{B}_{UV}^{-1}\mathbf{b}_{UV} \qquad \mathbf{d}_{UV} = \tfrac{1}{2}\mathbf{B}_{UV}^{-1}\mathbf{1}_3$$

$$\mathbf{e}_{UV} = c^2\mathbf{B}_{UV}^{-1}\mathbf{t}_{UV} \qquad \mathbf{f}_{UV} = -\tfrac{1}{2}c^2\mathbf{B}_{UV}^{-1}\mathbf{1}_2$$

Taking the Euclidian norm of $\Delta\underline{\mathbf{r}}_A$ in Eq 271 and collecting terms yields

$$a_{UV,40}\left(t_{A(UV)}\right)^4 + a_{UV,30}\left(t_{A(UV)}\right)^3 + a_{UV,20}\left(t_{A(UV)}\right)^2 + a_{UV,10}\,t_{A(UV)} + a_{UV,00} + a_{UV,02}\lambda^2 + a_{UV,01}\lambda + a_{UV,21}\left(t_{A(UV)}\right)^2\lambda + a_{RS,11}\,t_{A(UV)}\lambda = 0 \quad \text{Eq 272}$$

$$a_{UV,40} = \mathbf{f}_{UV}^T\mathbf{f}_{UV} \qquad a_{UV,30} = 2\,\mathbf{e}_{UV}^T\mathbf{f}_{UV} \qquad a_{UV,20} = 2\,\mathbf{c}_{UV}^T\mathbf{f}_{UV} + \mathbf{e}_{UV}^T\mathbf{e}_{UV}$$

$$a_{UV,10} = 2\,\mathbf{c}_{UV}^T\mathbf{e}_{UV} \qquad a_{UV,00} = \mathbf{c}_{UV}^T\mathbf{c}_{UV} \qquad a_{UV,02} = \mathbf{d}_{UV}^T\mathbf{d}_{UV}$$

$$a_{UV,01} = 2\,\mathbf{c}_{UV}^T\mathbf{d}_{UV} - 1 \qquad a_{UV,21} = 2\,\mathbf{d}_{UV}^T\mathbf{f}_{UV} \qquad a_{UV,11} = 2\,\mathbf{d}_{UV}^T\mathbf{e}_{UV}$$

The result is a scalar polynomial equation relating the unknown variables $t_{A(UV)}$ and λ.

Combined Analysis of Both Station Pairs — Both Eq 269 and Eq 272 are relationships between an aircraft time-of-transmission, $t_{A(RS)}$ or $t_{A(UV)}$, and the square of the distance between the analysis origin and the aircraft λ. Thus a third relationship between these three quantities is needed. To that end, observe that the right-hand sides of Eq 268 and Eq 271 must be equal. Consequently, the norm of $\Delta\underline{\mathbf{r}}_A$, λ, is also given by the inner product of the two right-hand sides, which results in the following equation

$$\begin{aligned} &a_{220}\left(t_{A(RS)}\right)^2\left(t_{A(UV)}\right)^2 + a_{210}\left(t_{A(RS)}\right)^2\left(t_{A(UV)}\right) + a_{120}\left(t_{A(RS)}\right)\left(t_{A(UV)}\right)^2 \\ &\quad + a_{110}\left(t_{A(RS)}\right)\left(t_{A(UV)}\right) + a_{200}\left(t_{A(RS)}\right)^2 + a_{020}\left(t_{A(UV)}\right)^2 + a_{100}\left(t_{A(RS)}\right) \\ &\quad + a_{010}\left(t_{A(UV)}\right) + a_{201}\left(t_{A(RS)}\right)^2\lambda + a_{021}\left(t_{A(UV)}\right)^2\lambda + a_{101}\left(t_{A(RS)}\right)\lambda \\ &\quad + a_{011}\left(t_{A(UV)}\right)\lambda + a_{002}\lambda^2 + a_{001}\lambda + a_{000} = 0 \end{aligned} \qquad \text{Eq 273}$$

$$a_{220} = \mathbf{f}_{RS}^T\mathbf{f}_{UV} \qquad a_{210} = \mathbf{f}_{RS}^T\mathbf{e}_{UV} \qquad a_{120} = \mathbf{e}_{RS}^T\mathbf{f}_{UV}$$

$$a_{110} = \mathbf{e}_{RS}^T\mathbf{e}_{UV} \qquad a_{200} = \mathbf{f}_{RS}^T\mathbf{c}_{UV} \qquad a_{020} = \mathbf{c}_{RS}^T\mathbf{f}_{UV}$$

$$a_{100} = \mathbf{e}_{RS}^T\mathbf{c}_{UV} \qquad a_{010} = \mathbf{c}_{RS}^T\mathbf{e}_{UV} \qquad a_{201} = \mathbf{f}_{RS}^T\mathbf{d}_{UV}$$

$$a_{021} = \mathbf{c}_{RS}^T\mathbf{f}_{UV} \qquad a_{101} = \mathbf{e}_{RS}^T\mathbf{d}_{UV} \qquad a_{011} = \mathbf{d}_{RS}^T\mathbf{e}_{UV}$$

$$a_{002} = \mathbf{d}_{RS}^T\mathbf{d}_{UV} \qquad a_{001} = \mathbf{c}_{RS}^T\mathbf{d}_{UV} + \mathbf{d}_{RS}^T\mathbf{c}_{UV} - 1 \qquad a_{000} = \mathbf{c}_{RS}^T\mathbf{c}_{UV}$$

Solution from Three Analyses — The unknown variables λ, $t_{A(RS)}$ and $t_{A(UV)}$ are the solutions of the simultaneous equations Eq 269, Eq 272 and Eq 273. Then $t_{A(RS)}$ and λ are substituted into Eq 268 or ($t_{A(UV)}$ and λ are substituted into Eq 271) to find $\Delta\underline{\mathbf{r}}_{\boldsymbol{A}}$. Next, $\underline{\mathbf{r}}_A^{\mathbf{e}}$ is found from $\underline{\mathbf{r}}_A^{\mathbf{e}} = \Delta\underline{\mathbf{r}}_A + \underline{\mathbf{r}}_o^{\mathbf{e}}$. Finally, the aircraft latitude and longitude are found from Eq 229.

7.6.4 Remarks

- Simultaneous solution of equations Eq 269, Eq 272 and Eq 273 requires use of a numerical root-finding technique such Newton-Raphson. Since recourse must be made to a numerical method, the Gauss-Newton method addressed in Chapter 8 is a viable alternative to this approach.
- The problem addressed here illustrates the significantly greater degree of complexity involved where there are two clock synchronization groups. Section 7.11, which involves pseudo spherical-ranges, demonstrates the same behavior.

7.7 Traditional Solution for Three Pseudo Slant-Ranges in Flatland

7.7.1 Introduction

Flatland, two-dimensional plane, is a useful construct for developing an understanding of a three-dimensional situation. Moreover, Flatland can approximate three-dimensional situations involving limited geographical areas and vertical extent — e.g., the surface of an airport. Scenarios involving Flatland can be analyzed as special cases of the Bancroft/vector-norm method addressed earlier in this chapter. However, approaches involving direct solution for aircraft coordinates were developed prior Bancroft's work and remain useful. Solutions for traditional approaches are the same as those found using Bancroft's algorithm, but generally provide better insights and may require fewer manipulations.

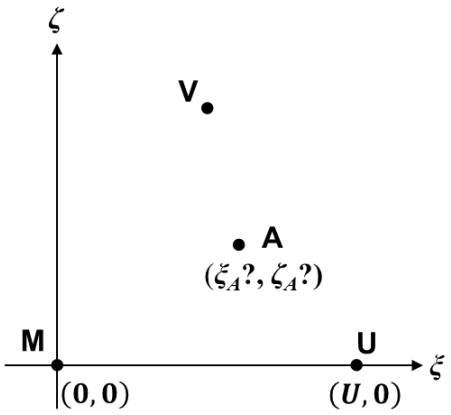

A relatively simple scenario involving two true range measurements in Flatland is addressed as Example 8 (Subsection 7.12.1). This section considers three pseudo slant-range measurements in Flatland, which requires more complex analysis.

Assume that an aircraft in Flatland is within the coverage region of a surveillance system that has three stations — **M**, **U** and **V** — with known coordinates (see figure). For this analysis, station **M** is at the origin and station **U** is on an axis. Station **V** is not necessarily on an axis. The Flatland plane is defined by the station locations.

The three stations have synchronized clocks (which are not synchronized with an aircraft clock), and each station measures the time-of-arrival of the same aircraft transmission at its location — t_M, t_U and t_V, respectively. The primary unknown variables are the aircraft coordinates ξ_A and ζ_A. The time of the aircraft's transmission t_A can also be found, but is often not needed.

The solution that follows utilizes the approach described in Ref. 44. The first step is to eliminate the common offset in t_M, t_U and t_V by forming the slant-range differences Δd_{MU} and Δd_{MV}, taking **M** as the common station and c as the propagation speed of electromagnetic waves

$$\Delta d_{MU} = c(t_M - t_U) \qquad \Delta d_{MV} = c(t_M - t_V) \qquad \text{Eq 274}$$

The measured range differences are equated to the modeled geometric range differences, treating ξ_A and ζ_A as unknown variables

$$\Delta d_{MU} = \sqrt{\xi_A^2 + \zeta_A^2} - \sqrt{(\xi_A - U)^2 + \zeta_A^2}$$
$$\Delta d_{MV} = \sqrt{\xi_A^2 + \zeta_A^2} - \sqrt{(\xi_A - V_\xi)^2 + (\zeta_A - V_\zeta)^2} \qquad \text{Eq 275}$$

In Eq 275: (a) each equation describes a hyperbola with the stations involved as foci, and (b) the left-hand side of each of equation can be either positive or negative. The solution is the intersection of specific branches of each hyperbola. Implicit in this formulation is that

$$|\Delta d_{MU}| \le U \qquad\qquad |\Delta d_{MV}| \le V \qquad\qquad \text{Eq 276}$$

After re-arranging, then squaring, each equation in Eq 275, the result is

$$\begin{aligned} U^2 - 2U\xi_A - \Delta d_{MU}^2 &= -2\,\Delta d_{MU}\sqrt{\xi_A^2 + \zeta_A^2} \\ V^2 - 2V_\xi\xi_A - 2V_\zeta\zeta_A - \Delta d_{MV}^2 &= -2\,\Delta d_{MV}\sqrt{\xi_A^2 + \zeta_A^2} \end{aligned} \qquad \text{Eq 277}$$

In Eq 277, $V^2 = V_\xi^2 + V_\zeta^2$. This pair of equations form the basis of the solution.

7.7.2 Solution General Case

This solution follows Ref. 44 by Fang. Dividing one line of Eq 277 by the other yields

$$\zeta_A = C_1\xi_A + C_0 \qquad \text{Eq 278}$$

$$C_1 = \frac{U\,\Delta d_{MV}}{V_\zeta\,\Delta d_{MU}} - \frac{V_\xi}{V_\zeta} \qquad V_\zeta \neq 0 \qquad \Delta d_{MU} \neq 0$$

$$C_0 = \frac{1}{2V_\zeta}\left[V^2 - \Delta d_{MV}^2 - \Delta d_{MU}\,\Delta d_{MV}\left(\left(\frac{U}{\Delta d_{MU}}\right)^2 - 1\right)\right] \qquad V_\zeta \neq 0 \qquad \Delta d_{MU} \neq 0$$

Condition $V_\zeta \neq 0$ requires that the three stations not form a straight line; its violation is addressed in Subsection 7.7.5. Condition $\Delta d_{MU} \neq 0$ requires that the aircraft not be on the perpendicular bisector of the baseline **MU**; its violation is addressed in Subsection 7.7.3.

Using Eq 278 to substitute for ζ_A in the first equation in Eq 277, then squaring and collecting like terms, yields:

$$E_2\xi_A^2 + E_1\xi_A + E_0 = 0 \qquad V_\zeta \neq 0 \qquad \Delta d_{MU} \neq 0 \qquad \text{Eq 279}$$

$$E_2 = C_1^2 - \left(\left(\frac{U}{\Delta d_{MU}}\right)^2 - 1\right) \qquad \Delta d_{MU} \neq 0$$

$$E_1 = 2C_1C_0 + U\left(\left(\frac{U}{\Delta d_{MU}}\right)^2 - 1\right) \qquad \Delta d_{MU} \neq 0$$

$$E_0 = C_0^2 - \frac{\Delta d_{MU}^2}{4}\left(\left(\frac{U}{\Delta d_{MU}}\right)^2 - 1\right)^2 \qquad \Delta d_{MU} \neq 0$$

Thus, the general solution of the ‘three station pseudo slant-range system in Flatland’ problem can be summarized as:

- Solve the quadratic equation that is first line of Eq 279 to obtain (generally) two candidate values for ξ_A
- Substitute the two candidate values for ξ_A into the first line of Eq 278 to find the corresponding values for ζ_A
- Attempt to determine which candidate solution pair (ξ_A, ζ_A) is correct by substituting each into Eq 275.

If needed, the aircraft time of transmission t_A can be found from

$$t_A = t_M - \frac{1}{c}\sqrt{\xi_A^2 + \zeta_A^2} \qquad \text{Eq 280}$$

The solution process (particularly dividing one line of Eq 277 by the other) can generate a second candidate solution that corresponds to pseudo slant-range differences of $-\Delta d_{MU}$ and $-\Delta d_{MV}$. (i.e., the negation of both measured slant-range differences). When this occurs, an extraneous solution is created, and can be detected by substituting both candidate solutions into the original equations to be solved (Eq 275). However, in other situations, two sets of aircraft locations can result in the same values for Δd_{MU} and Δd_{MV} — i.e., an ambiguous solution exists.

7.7.3 Solution Special Cases

Special case situations are addressed in this subsection. These are necessary for a complete analysis of the problem.

Aircraft Equidistant from Stations M and U — The general solution of Eq 278 and Eq 279 fails when $\Delta d_{MU} = 0$. When this occurs, Eq 277 reduces to

$$\xi_A = \tfrac{1}{2}U \qquad H_2\zeta_A^2 + H_1\zeta_A + H_0 = 0 \qquad \text{Eq 281}$$

$$H_2 = 4\Delta d_{MV}^2 - 4V_\zeta^2$$
$$H_1 = 4V_\zeta\left(V^2 - V_\xi U - \Delta d_{MV}^2\right)$$
$$H_0 = U^2\Delta d_{MV}^2 - \left(V^2 - V_\xi U - \Delta d_{MV}^2\right)^2$$

This is the most significant special case. It requires that measurements t_M and t_U be tested for equality, and when that condition is true, that Eq 281 be used rather than Eq 279 and Eq 278. An alternative method of addressing is $\Delta d_{MU} = 0$ is to redefine the coordinate axes so that the solution involves division by Δd_{MV} rather than Δd_{MU}.

Aircraft Equidistant from Station **M** and Stations **U** and **V** — When an aircraft is equidistant from both station pairs, **MU** and **MV**, the discriminant for the quadratic equation in ζ_A (Eq 281) is zero. Then the quadratic equation has a double root at:

$$\xi_A = \tfrac{1}{2}U \qquad \zeta_A = \frac{V^2 - UV_\xi}{2V_\zeta} = \tfrac{1}{2}V_\zeta + \frac{V_\xi}{2V_\zeta}\left(V_\xi - U\right) \qquad \text{Eq 282}$$

Aircraft at a Degenerate Point — When $H_2 = 0$ in Eq 281, the quadratic equation is degenerate; then there is a single root at:

$$\xi_A = \tfrac{1}{2}U \qquad \zeta_A = \frac{U^2 V_\zeta}{4V_\xi\left(U - V_\xi\right)} - \frac{V_\xi\left(U - V_\xi\right)}{4V_\zeta} \qquad \text{Eq 283}$$

The possible existence of a single-root requires that the quadratic equation in Eq 281 be tested for $H_2 = 0$ and that Eq 283 be utilized when the test is satisfied. The single-root case is discussed below (Eq 285), without requiring that $\Delta d_{MU} = 0$.

Aircraft on a Baseline Extension — When an aircraft is at a station or on a baseline extension, the slant-range difference for the two stations on the associated baseline is the same for any location and is equal in magnitude to the baseline length. For the station geometry shown above, assume that the aircraft is on the ξ-axis at or to the left of **M**. Then $\Delta d_{MU} = -U$, so the discriminant for Eq 279 is zero, indicating the occurrence of a double-root. Thus the aircraft position is

$$\xi_A = -\frac{C_0}{C_1} = \frac{V^2 - \Delta d_{MV}^2}{2\left(V_\xi + \Delta d_{MV}\right)} \qquad \zeta_A = 0 \qquad \text{Eq 284}$$

The expression for the location of the aircraft relative to the nearest station (i.e., ξ_A in Eq 284) does not depend upon the length of the baseline involved. This solution (Eq 284) is a simplification of the general solution; it need not be treated as a special case.

The solution in Eq 284 depends on both conditions $|\Delta d_{MU}| = U$ and $|\Delta d_{MV}| \leq V$ being valid. If either is violated, the solution will change in character — either it may not exist (the discriminant is negative) or the double root may divide into two single roots (the discriminant is positive). For this reason, locations on the baseline extensions (including at a station) are unstable. Also, while Eq 284 is derived for only one of six baseline extensions, by transforming the coordinate axes, it can be applied to any baseline extension.

Single Root – Degenerate Quadratic — While Eq 279 is generally a quadratic function of ξ_A, it reduces to a linear function of ξ_A when $E_2 = 0$. The condition $E_2 = 0$ is equivalent to

$$V^2 \Delta d_{MU}^2 + U^2 \Delta d_{MV}^2 - 2UV_\xi \Delta d_{MU} \Delta d_{MV} - U^2 V_\zeta^2 = 0 \qquad \text{Eq 285}$$

The loci of locations having a single-root solution can be found by substituting Eq 275 into Eq 285. The result is analytically intractable, as it involves all possible products of the three radicals in Eq 275; repeated isolating and squaring will yield in a 8th order polynomial. Alternatively, the expression can be readily solved numerically — e.g., using the methods of Subsection 2.1.8. The result of such a calculation, for stations that form an equilateral triangle with unit baselines, is

shown as the green curves in Figure 31. Geometrically, the single-solution case occurs when the hyperbolas corresponding to Δd_{MU} and Δd_{MV} have parallel asymptotes.

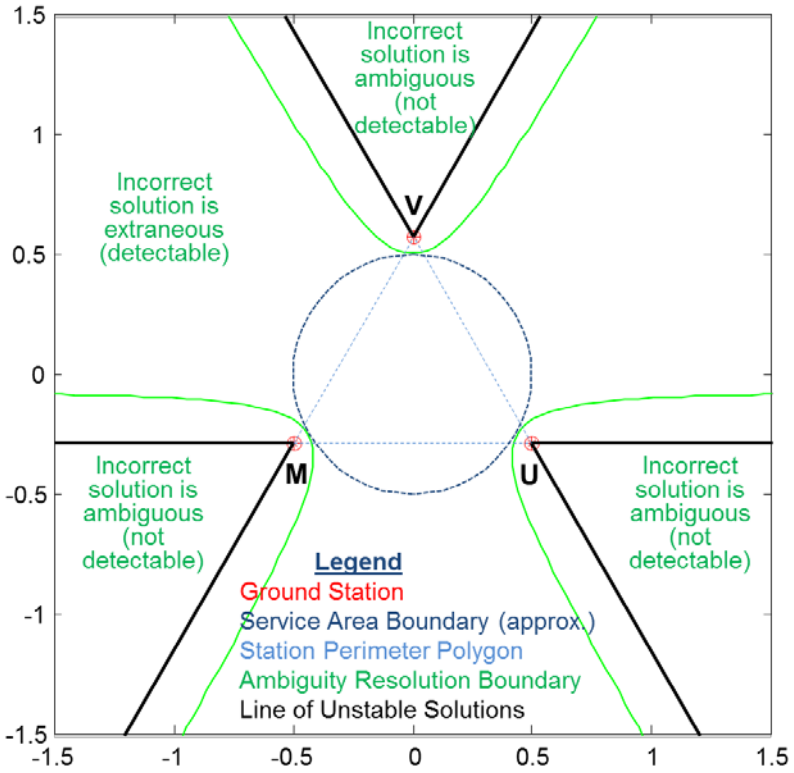

Figure 31 Solution Regions for Three Pseudo Slant-Range Stations in Flatland

7.7.4 Characterization of General Case Solutions

The loci of single-root solutions to Eq 281 (three green curves in Figure 31) partition the $\xi-\zeta$ plane into four regions. When there are two roots to Eq 279, both are located in the same region (Ref. 48). When the aircraft is near the boundary separating two regions, the incorrect solution is very distant from the correct solution.

Extraneous Solution: Roots from Different Branches — This situation occurs when the aircraft is in the 'extraneous (correct solution detectable)' area of the $\xi-\zeta$ plane in Figure 31. An algebraic indicator is that E in Eq 279 is negative. Geometrically, each solution is formed by the intersection of hyperbola branches which are distinct from those which form the other solution (Figure 32(a)). The filled circle corresponds to the correct slant-range differences, and the unfilled circle to their sign-reversed versions.

Ambiguous Solution: Roots from Same Branches — This situation occurs when the aircraft is in one of the three rounded-V-shaped 'ambiguous solution' areas in Figure 31. An algebraic indicator is that E in Eq 279 is positive. Both solutions are formed by intersections of the

branches of the hyperbolas which correspond to the correct slant-range differences (Figure 32(b)). The correct solution cannot be identified from the available information.

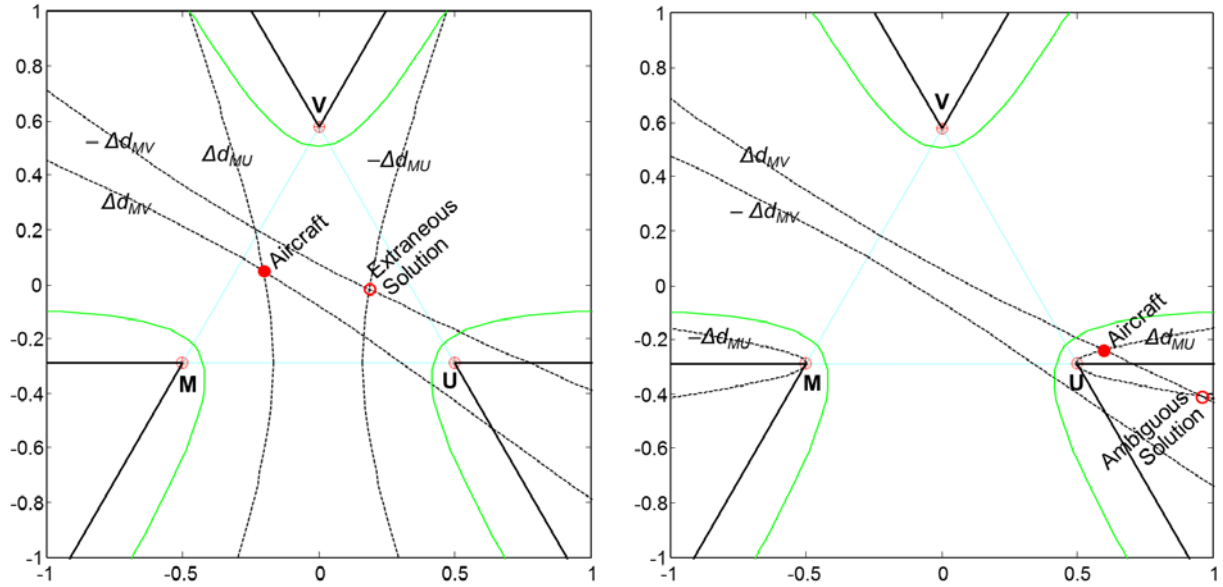

(a) Different Branches (Extraneous Soln.) (b) Same Branches (Ambiguous Soln.)

Figure 32 Types of Solutions for Three Pseudo Slant-Range Stations

For the square area shown in Figure 31 (3x3 BLUs), the 'extraneous (correct solution detectable)' region is 62.5% of the total area, and each of the three 'ambiguous (correct solution not detectable)' regions is 12.5%. If attention is limited to 1.5 x 1.5 BLUs (which better resembles a region of operational interest), the 'extraneous' region is 79.8% of the total and each of the three 'ambiguous' regions is 6.7%.

7.7.5 Stations Form a Straight Line

General Case — Arranging three pseudo-range stations in a straight line is not common, but may be an option in some situations — e.g., for a surveillance system monitoring off-shore flights that are nominally parallel to a coastline. When the stations form a line, the 'Flatland plane' can be defined by the stations and each aircraft, and need not be 'horizontal'. For this station arrangement (i.e., $V_\zeta = 0$ and $V = V_\xi$), the general case solution of Eq 278 - Eq 279 fails. However, the same solution process can be followed, starting from Eq 277, yielding

$$\xi_A = \frac{(V^2\Delta d_{MU} - U^2\Delta d_{MV}) + \Delta d_{MU}\,\Delta d_{MV}(\Delta d_{MU} - \Delta d_{MV})}{2(U\Delta d_{MV} - V\Delta d_{MU})}$$

$$\zeta_A = \pm\sqrt{\frac{\left(U^2 - 2U\xi_A - \Delta d_{MU}^2\right)^2}{4\Delta d_{MU}^2} - \xi_A^2} \qquad \Delta d_{MU} \neq 0$$

Eq 286

$$\zeta_A = \pm\sqrt{\frac{\left(V^2 - 2V\xi_A - \Delta d_{MV}^2\right)^2}{4\Delta d_{MV}^2} - \xi_A^2} \qquad \Delta d_{MV} \neq 0$$

The two solutions in Eq 286 are symmetric with respect to the line on which the stations are located, and the incorrect solution is ambiguous (rather than extraneous). Symmetric solutions are not unexpected for stations in a line; the same symmetry occurs for two slant-range measurements in Flatland (Subsection 7.12.1). This suggests that stations that 'almost' form a straight line will have ambiguous solutions that are 'almost' symmetric about that 'line'.

Aircraft Equidistant from Station M and Stations U and V — For this station arrangement, it is not possible for both Δd_{MU} and Δd_{MV} to be zero.

Aircraft on Baseline Extension — When an aircraft is on an extension of both baselines connecting stations **M**, **U** and **V**, then $\Delta d_{MU} = \pm U$ and $\Delta d_{MV} = \pm V$, with the same sign applying to both measurements. Thus, the expression for ξ_A in Eq 286 is singular and a solution does not exist. Recourse to Eq 277 yields $\zeta_A = 0$ from both expressions; there is no solution for ξ_A.

7.7.6 Remarks

Service Area — Navigation or surveillance systems are intended to provide service in a defined geographic area or volume. In a system's service area/volume, the measurement geometry (as well as the signal-to-noise ratio) must be satisfactory. For a three-station pseudorange system with equal baselines, the service area is approximately a circle with its center at the mid-point of the station locations and radius equal to one-half the baseline length (Figure 31). This region includes most of the area within triangle connecting the stations and part of the regions outside (but adjacent to) the baselines. Subsection 8.5.2 addresses service areas.

Contribution of Derivation — Fang's (Ref. 44) solution to the 'three pseudo slant-ranges in Flatland' problem has several advantages: (1) The coordinate system is sensor based; (2) it only requires finding the roots of a quadratic equation in one position coordinate; and (3) it provides insight into the effects of geometry on the solution. In contrast, Bancroft's algorithm employs vectors and involves the solution of a quadratic equation for the Lorentzian norm of the aircraft location, which itself is a quadratic quantity. Interestingly, the requirements for the coordinate frames for the two methods conflict. A third derivation takes a coordinate-free approach utilizing distances and angles (Ref. 52).

Key to Derivation — The key step in Fang's derivation is dividing the two equations in Eq 277. If, instead, one were to square the two equations separately to eliminate the radicals, the result would be two fourth-order polynomial equations. Geometrically, two families of hyperbolas, one

associated with each baseline, intersect at up to four points and thus can require a fourth-order polynomial for computing all the intersections. Fang's derivation takes advantage of the fact that the two slant-range differences have one station in common.

Two Pairs of Stations — One could define a hyperbolic system involving four stations comprised of two separately synchronized pairs of stations (similar to Loran-C cross-chaining). A derivation similar to the above would require two squaring operations to remove all radicals, which would result in a fourth-order polynomial.

Numerical Calculations — When numerical results are needed, Bancroft's algorithm may be preferable to implementing the method of this section. If vector-matrix software is available, the coding task is simpler and does not require that $\Delta d_{MU} = 0$ be treated as a special case.

Aircraft Latitude/Longitude Coordinates — If the Cartesian ξ–ζ frame origin and axes are known relative to the ECEF *e*-frame (Section 5.1), or if the station latitudes/longitudes/(altitudes) are known, then aircraft locations in the ξ–ζ frame can be converted to *e*-frame coordinates and thence to latitude/ longitude/(altitude) — see Subsection 7.8.2. Omitting/ignoring altitude implicitly assumes that the stations are on the surface of the earth.

Relationship to Classic Hyperbola Parameters — Figure 33 shows the classic form of a hyperbola which satisfies the equation

$$\frac{x^2}{a^2} - \frac{y^2}{b^2} = 1 \qquad \text{Eq 287}$$

This classic hyperbola can be related to the hyperbola described by the first line of Eq 275. Equating the distances between the vertices and the foci of the two hyperbolas, yields:

$$\begin{aligned} 2a &= |\Delta d_{MU}| \\ 2\sqrt{a^2 + b^2} &= U \end{aligned} \qquad \text{Eq 288}$$

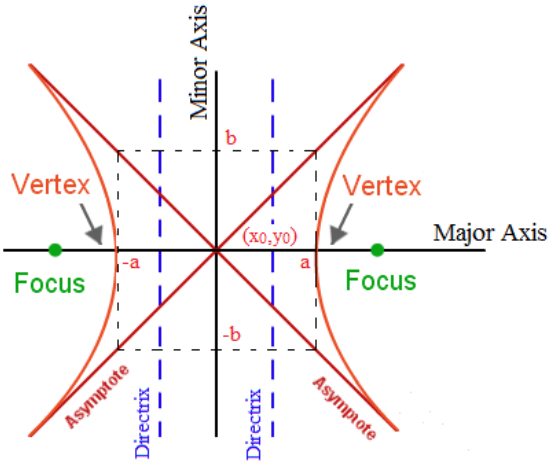

Figure 33 Classic Form for Hyperbola

Thus the tangent of the acute angle that an asymptote makes with the baseline is:

$$\frac{b}{a} = \sqrt{\left(\frac{U}{\Delta d_{MU}}\right)^2 - 1} \qquad \Delta d_{MU} \neq 0 \qquad \text{Eq 289}$$

The quantity under the radical in Eq 289 is fundamental to this formulation, and also appears in the expressions for C_0 (Eq 278) and E_2, E_1 and E_0 (Eq 279).

Application to Ellipsoid LOPs — Reference 44 points out that — with some sign reversals — the equations of this section would apply to measurements of the two sums of the slant-ranges for three ground stations to an aircraft. While not commonly implemented (e.g., by a multi-static radar involving one transmitter and two non-colocated receivers), it is a point worth noting.

Insight into More Complex Situations — The problem addressed in this section is a simpler version of the problem addressed in Section 7.10, which involves a spherical earth. Qualitatively, the solutions behave similarly.

7.8 Traditional Solution for Three Slant-Ranges

7.8.1 Cartesian Coordinate Solution

An aircraft's position can be found from three slant-range using Bancroft's vector norm (Section 7.3). However, a simpler approach, whereby the aircraft coordinates are found directly and in sequence, is readily developed using the station geometry employed in Section 7.7. Accordingly, consider the station arriangement shown on the right, where the three stations all lie in the ξ–ζ plane which is embedded in the three-dimensional the ξ–ζ–η space.

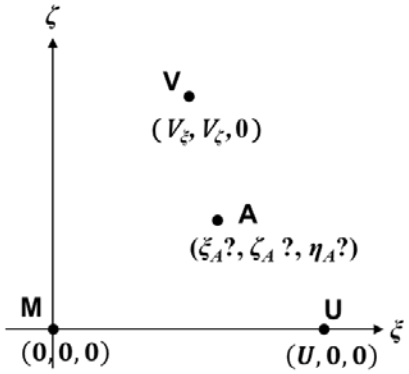

The three slant-range measurements – d_{iA} ($i = M, U, V$) – satisfy the equations

$$\begin{aligned} (\xi_A)^2 + (\zeta_A)^2 + (\eta_A)^2 &= (d_{MA})^2 \\ (\xi_A - U)^2 + (\zeta_A)^2 + (\eta_A)^2 &= (d_{UA})^2 \\ (\xi_A - V_\xi)^2 + (\zeta_A - V_\zeta)^2 + (\eta_A)^2 &= (d_{VA})^2 \end{aligned} \qquad \text{Eq 290}$$

Completing the squares and differencing first line with the second and third lines yields

$$\begin{aligned} -2U\xi_A + U^2 &= (d_{UA})^2 - (d_{MA})^2 \\ -2V_\xi \xi_A - 2V_\zeta \zeta_A + V^2 &= (d_{VA})^2 - (d_{MA})^2 \end{aligned} \qquad \text{Eq 291}$$

It follows that the aircraft position components (ξ_A,ζ_A,η_A) can be found in sequence by

$$\begin{aligned} \xi_A &= \frac{1}{2}U + \frac{(d_{MA})^2 - (d_{UA})^2}{2U} \\ \zeta_A &= -\frac{V_\xi}{V_\zeta}\xi_A + \frac{V^2}{2V_\zeta} + \frac{(d_{MA})^2 - (d_{VA})^2}{2V_\zeta} \\ \eta_{A\pm} &= \pm\sqrt{(d_{MA})^2 - (\xi_A)^2 - (\zeta_A)^2} \end{aligned} \qquad \text{Eq 292}$$

Remarks:

- The traditional solution approach discussed in this section involves significantly fewer computations than Bancroft's method (Section 7.3).
- The simplicity of this method is due to selection of the coordinate frame based on the station locations. However, that station-based frame is often not operationally useful. Calculation of aircraft latitude/longitude/altitude values is the subject of the following subsection.
- For this approach, the correct and ambiguous solutions (Eq 292) are symmetric about the plane containing the sensors. This behavior is also observed for the Bancroft approach in Subsection 7.3.3. For most aircraft application, the '–' solution can be rejected.

7.8.2 Aircraft Latitude/Longitude/Altitude

To convert the solution of Eq 292 to more useful geodetic quantities, assume that the latitudes L_i, longitudes λ_i and altitudes h_i of the stations are known ($i = M, U, V$). Then, for a spherical model of the earth, the ECEF *e*-frame station coordinates are (Section 5.1)

$$\underline{\mathbf{r}}^{\mathbf{e}}_{\mathbf{O}i} = \begin{bmatrix} x^e_{Oi} \\ y^e_{Oi} \\ z^e_{Oi} \end{bmatrix} = \begin{bmatrix} \cos(L_i)\cos(\lambda_i) \\ \cos(L_i)\sin(\lambda_i) \\ \sin(L_i) \end{bmatrix} (R_e + h_i) \qquad i = M, U, V \qquad \text{Eq 293}$$

Subscript O, denoting the center of the earth, is added to $\underline{\mathbf{r}}^{\mathbf{e}}_{\mathbf{O}i}$ and its components for emphasis, as two coordinate origins are involved. The *e*-frame unit vectors for the coordinate axis ξ–ζ–η are

$$\underline{\mathbf{1}}^{\mathbf{e}}_{\xi} = \begin{bmatrix} \underline{1}^{\mathrm{e}}_{\xi,x} \\ \underline{1}^{\mathrm{e}}_{\xi,y} \\ \underline{1}^{\mathrm{e}}_{\xi,z} \end{bmatrix} = \frac{\underline{\mathbf{r}}^{\mathbf{e}}_{\mathbf{O}U} - \underline{\mathbf{r}}^{\mathbf{e}}_{\mathbf{O}M}}{\left\| \underline{\mathbf{r}}^{\mathbf{e}}_{\mathbf{O}U} - \underline{\mathbf{r}}^{\mathbf{e}}_{\mathbf{O}M} \right\|}$$

$$\underline{\mathbf{1}}^{\mathbf{e}}_{\eta} = \begin{bmatrix} \underline{1}^{\mathrm{e}}_{\eta,x} \\ \underline{1}^{\mathrm{e}}_{\eta,y} \\ \underline{1}^{\mathrm{e}}_{\eta,z} \end{bmatrix} = \frac{\underline{\mathbf{1}}^{\mathbf{e}}_{\xi} \times \left(\underline{\mathbf{r}}^{\mathbf{e}}_{\mathbf{O}V} - \underline{\mathbf{r}}^{\mathbf{e}}_{\mathbf{O}M} \right)}{\left\| \underline{\mathbf{1}}^{\mathbf{e}}_{\xi} \times \left(\underline{\mathbf{r}}^{\mathbf{e}}_{\mathbf{O}V} - \underline{\mathbf{r}}^{\mathbf{e}}_{\mathbf{O}M} \right) \right\|} \qquad \text{Eq 294}$$

$$\underline{\mathbf{1}}^{\mathbf{e}}_{\zeta} = \begin{bmatrix} \underline{1}^{\mathrm{e}}_{\zeta,x} \\ \underline{1}^{\mathrm{e}}_{\zeta,y} \\ \underline{1}^{\mathrm{e}}_{\zeta,z} \end{bmatrix} = \underline{\mathbf{1}}^{\mathbf{e}}_{\eta} \times \underline{\mathbf{1}}^{\mathbf{e}}_{\xi}$$

The vector from the earth's center to the aircraft is the sum of the vectors $\underline{\mathbf{r}}^{\mathbf{e}}_{\mathbf{O}M}$ and $\underline{\mathbf{r}}^{\mathbf{e}}_{\mathbf{M}A\pm}$, the latter being $[\xi_A \quad \zeta_A \quad \eta_{A\pm}]^T$ after a coordinate transformation. Thus

$$\underline{\mathbf{r}}^{\mathbf{e}}_{\mathbf{O}A\pm} = \begin{bmatrix} x^e_{OA\pm} \\ y^e_{OA\pm} \\ z^e_{OA\pm} \end{bmatrix} = \begin{bmatrix} x^e_{OM} \\ y^e_{OM} \\ z^e_{OM} \end{bmatrix} + \begin{bmatrix} \underline{1}^{\mathrm{e}}_{\xi,x} & \underline{1}^{\mathrm{e}}_{\zeta,x} & \underline{1}^{\mathrm{e}}_{\eta,x} \\ \underline{1}^{\mathrm{e}}_{\xi,y} & \underline{1}^{\mathrm{e}}_{\zeta,y} & \underline{1}^{\mathrm{e}}_{\eta,y} \\ \underline{1}^{\mathrm{e}}_{\xi,z} & \underline{1}^{\mathrm{e}}_{\zeta,z} & \underline{1}^{\mathrm{e}}_{\eta,z} \end{bmatrix} \begin{bmatrix} \xi_A \\ \zeta_A \\ \eta_{A\pm} \end{bmatrix} \qquad \text{Eq 295}$$

It follows that

$$L_{A\pm} = \arctan\left(\frac{z^e_{OA\pm}}{\sqrt{\left(x^e_{OA\pm}\right)^2 + \left(y^e_{OA\pm}\right)^2}}\right)$$
$$\lambda_{A\pm} = \arctan\left(y^e_{OA\pm}, x^e_{OA\pm}\right)$$
$$h_{A\pm} = \sqrt{\left(x^e_{OA\pm}\right)^2 + \left(y^e_{OA\pm}\right)^2 + \left(z^e_{OA\pm}\right)^2} - R_e$$
Eq 296

For an ellipsoidal model of the earth, Eq 293 and Eq 296 must be modified (see Section 9.3).

7.9 Traditional Solution for Four Pseudo Slant-Ranges

7.9.1 Problem Formulation

The solution for three pseudo slant-range stations in Flatland — addressed in Section 7.8 and based on Ref. 44 — can be extended to four pseudo slant-range stations in a three-dimensional 'world'. The resulting solution is an alternative to using Bancroft's method (Section 7.2). Accordingly, and extending the notation of Section 7.8, consider a Cartesian coordinate frame with axes (ξ, ζ, η). The four stations and their known coordinates are: **M** (0,0,0), **U** $(U, 0,0)$, **V** $(V_\xi, V_\zeta, 0)$ and **W** (W_ξ, W_ζ, W_η). The aircraft and its unknown coordinates are denoted by **A** (ξ_A, ζ_A, η_A). The stations have synchronized clocks. Each station measures the time of arrival — denoted by in t_M, t_U, t_V and t_W, respectively — of the same aircraft transmission. The time of transmission is not known to the stations.

The first step is to eliminate the common clock offset included in t_M, t_U, t_V and t_W. The resulting slant-range differences Δd_{MU}, Δd_{MV} and Δd_{MW} are formed by taking **M** as the common station and c as the propagation speed of electromagnetic waves

$$\Delta d_{MU} = c(t_M - t_U) \qquad \Delta d_{MV} = c(t_M - t_V) \qquad \Delta d_{MW} = c(t_M - t_W) \qquad \text{Eq 297}$$

The scaled measured time differences are equated to the modeled geometric range differences, with the aircraft coordinates ξ_A, ζ_A and η_A as unknown variables

$$\Delta d_{MU} = \sqrt{\xi_A^2 + \zeta_A^2 + \eta_A^2} - \sqrt{\left(\xi_A - U\right)^2 + \zeta_A^2 + \eta_A^2}$$
$$\Delta d_{MV} = \sqrt{\xi_A^2 + \zeta_A^2 + \eta_A^2} - \sqrt{\left(\xi_A - V_\xi\right)^2 + \left(\zeta_A - V_\zeta\right)^2 + \eta_A^2} \qquad \text{Eq 298}$$
$$\Delta d_{MW} = \sqrt{\xi_A^2 + \zeta_A^2 + \eta_A^2} - \sqrt{\left(\xi_A - W_\xi\right)^2 + \left(\zeta_A - W_\zeta\right)^2 + \left(\eta_A - W_\eta\right)^2}$$

In Eq 298, each equation describes a hyperbola of revolution (also called a hyperboloid). The

two stations involved are the hyperpola foci and their connecting baseline forms the major axis, as well as the axis of revolution. The solution (aircraft position) is the intersection of specific branches of each hyperboloid. Implicit in this formulation is that

$$|\Delta d_{MU}| \le U \qquad |\Delta d_{MV}| \le V \qquad |\Delta d_{MW}| \le W \qquad \text{Eq 299}$$

After re-arranging, then squaring, each equation in Eq 298, the results are

$$\begin{aligned} U^2 - 2U\xi_A - \Delta d_{MU}^2 &= -2\,\Delta d_{MU}\sqrt{\xi_A^2 + \zeta_A^2 + \eta_A^2} \\ V^2 - 2V_\xi\xi_A - 2V_\zeta\zeta_A - \Delta d_{MV}^2 &= -2\,\Delta d_{MV}\sqrt{\xi_A^2 + \zeta_A^2 + \eta_A^2} \\ W^2 - 2W_\xi\xi_A - 2W_\zeta\zeta_A - 2W_\eta\eta_A - \Delta d_{MW}^2 &= -2\,\Delta d_{MW}\sqrt{\xi_A^2 + \zeta_A^2 + \eta_A^2} \end{aligned} \qquad \text{Eq 300}$$

In Eq 300, $V^2 = V_\xi^2 + V_\zeta^2$ and $W^2 = W_\xi^2 + W_\zeta^2 + W_\eta^2$.

7.9.2 Solution General Case

Referring to Eq 300, dividing the second line by the first and re-arranging yields

$$\zeta_A = C_1\xi_A + C_0 \qquad \text{Eq 301}$$

$$C_1 = \frac{U\,\Delta d_{MV}}{V_\zeta\,\Delta d_{MU}} - \frac{V_\xi}{V_\zeta} \qquad V_\zeta \ne 0 \qquad \Delta d_{MU} \ne 0$$

$$C_0 = \frac{1}{2V_\zeta}\left[V^2 - \Delta d_{MV}^2 - \Delta d_{MU}\Delta d_{MV}\left(\left(\frac{U}{\Delta d_{MU}}\right)^2 - 1\right)\right] \qquad V_\zeta \ne 0 \qquad \Delta d_{MU} \ne 0$$

Eq 301 is identical to Eq 278. Condition $V_\zeta \ne 0$ requires that stations **M**, **U** and **V** not form a straight line — see Subsections 7.9.5 and 7.9.6. Condition $\Delta d_{MU} \ne 0$ requires that the aircraft not be on the perpendicular bisector of the baseline **MU** — see Subsection 7.9.3.

In Eq 300, dividing third line by the first, using Eq 301 to eliminate ζ_A and re-arranging yields

$$\eta_A = D_1\xi_A + D_0 \qquad \text{Eq 302}$$

$$D_1 = \frac{U\,\Delta d_{MW}}{W_\eta\,\Delta d_{MU}} - \frac{W_\xi + W_\zeta C_1}{W_\eta} \qquad W_\eta \ne 0 \qquad \Delta d_{MU} \ne 0$$

$$D_0 = \frac{1}{2W_\eta}\left[W^2 - \Delta d_{MW}^2 - W_\zeta C_0 - \left(\left(\frac{U}{\Delta d_{MU}}\right)^2 - 1\right)\Delta d_{MU}\Delta d_{MW}\right]$$

Conditions $W_\eta \ne 0$ and $\Delta d_{MU} \ne 0$ apply to both lines of Eq 302. Condition $W_\eta \ne 0$ requires that station **W** not be in the plane formed by stations **M**, **U** and **V** — see Subsection 7.9.4.

Using Eq 301 and Eq 302 to substitute for ζ_A and η_A, respectively, in the first line in Eq 300, then

squaring and collecting like terms, yields:

$$E_2\xi_A^2 + E_1\xi_A + E_0 = 0 \qquad \text{Eq 303}$$

$$E_2 = 4\Delta d_{MU}^2(1 + C_1^2 + D_1^2) - 4U^2$$

$$E_1 = 4\Delta d_{MU}^2\left(2C_0C_1 + 2D_0D_1 + U\left(\left(\frac{U}{\Delta d_{MU}}\right)^2 - 1\right)\right)$$

$$E_0 = 4\Delta d_{MU}^2(C_0^2 + D_0^2) - (U^2 - \Delta d_{MU}^2)^2$$

The aircraft coordinates are found by substituting the two solutions to Eq 303 into Eq 301 and Eq 302, then determining which coordinate set is correct. The incorrect solution may be either extraneous (and detectable by substituting into Eq 298) or ambiguous (and not detectable without additional information). If needed, the aircraft time of transmission t_A can be found from

$$t_A = t_M - \frac{1}{c}\sqrt{\xi_A^2 + \zeta_A^2 + \eta_A^2} \qquad \text{Eq 304}$$

7.9.3 Solution Special Cases

Aircraft Equidistant from Stations M and U — The general solution of Eq 301 - Eq 303 fails when $\Delta d_{MU} = 0$. In this case, the first line of Eq 300 yields $\xi_A = \frac{1}{2}U$. Then, dividing the third line of Eq 300 by the second and re-arranging yields

$$\eta_A = F_1\zeta_A + F_0 \qquad \text{Eq 305}$$

$$F_1 = \frac{V_\zeta\Delta d_{MW} - W_\zeta\Delta d_{MV}}{W_\eta\Delta d_{MV}} = \frac{V_\zeta\Delta d_{MW}}{W_\eta\Delta d_{MV}} - \frac{W_\zeta}{W_\eta} \qquad \Delta d_{MV} \neq 0$$

$$F_0 = -\frac{\left(V^2 - V_\xi U - \Delta d_{MV}^2\right)\Delta d_{MW}}{2W_\eta\Delta d_{MV}} + \frac{W^2 - W_\xi U - \Delta d_{MW}^2}{2W_\eta} \qquad \Delta d_{MV} \neq 0$$

Using Eq 305 to substitute for η_A in the second line in Eq 300, then squaring and collecting like terms, yields:

$$G_2\zeta_A^2 + G_1\zeta_A + G_0 = 0 \qquad \text{Eq 306}$$

$$G_2 = 4\Delta d_{MV}^2(1 + F_1^2) - 4V_\zeta^2$$

$$G_1 = 8\Delta d_{MV}^2F_0F + 4V_\zeta\left(V^2 - V_\xi U - \Delta d_{MV}^2\right)$$

$$G_0 = 4\Delta d_{MV}^2\left(\frac{1}{4}U^2 + F_0^2\right) - \left(V^2 - V_\xi U - \Delta d_{MV}^2\right)^2$$

This case requires that measurements t_M and t_U be tested for equality. If that condition is true, then $\xi_A = \frac{1}{2}U$ and Eq 305 and Eq 306 are used rather than Eq 301 - Eq 303.

Aircraft Equidistant from Stations **M** and Stations **U** and **V** — The solution of Eq 305 and Eq 306 fails when both $\Delta d_{MU} = 0$ and $\Delta d_{MV} = 0$. In this 'double special case', the first and second lines of Eq 300 yield expressions identical to Eq 282

$$\xi_A = \tfrac{1}{2}U \qquad\qquad \zeta_A = \frac{V^2 - V_\xi U}{2V_\zeta} \qquad \text{Eq 307}$$

When this occurs, the third line of Eq 300 reduces to

$$H_2\eta_A^2 + H_1\eta_A + H_0 = 0 \qquad \text{Eq 308}$$

$$H_2 = 4\left(\Delta d_{MW}^2 - W_\eta^2\right)$$

$$H_1 = 4W_\eta\left(W^2 - W_\xi U - \frac{W_\zeta}{V_\zeta}\left(V^2 - V_\xi U\right) - \Delta d_{MW}^2\right)$$

$$H_0 = \Delta d_{MW}^2\left(U^2 + V^2\right) - \left(W^2 - W_\xi U - \frac{W_\zeta}{V_\zeta}\left(V^2 - V_\xi U\right) - \Delta d_{MW}^2\right)^2$$

This case requires that measurements t_M and t_V be tested for equality, after measurements t_M and t_U have been found to be equal. If $t_M = t_V$, then Eq 307 and Eq 308 are used rather than Eq 305 and Eq 306.

Aircraft Equidistant from Station **M** and Stations **U**, **V** and **W** — When all three range differences are zero — i.e., $\Delta d_{MU} = 0$, $\Delta d_{MV} = 0$ and $\Delta d_{MW} = 0$ — the values of ξ_A and ζ_A are given by Eq 307 and Eq 308 reduces to

$$\left[2W_\eta\eta_A - \left(W^2 - W_\xi U - W_\zeta V\right)\right]^2 = 0 \qquad \text{Eq 309}$$

Thus, there is a double root at

$$\xi_A = \tfrac{1}{2}U \qquad \zeta_A = \frac{V^2 - V_\xi U}{2V_\zeta} \qquad \eta_A = \frac{W^2 - W_\xi U - W_\zeta V}{2W_\eta} \qquad \text{Eq 310}$$

Single Root – Degenerate Quadratic — While Eq 303 is nominally a quadratic function of ξ_A, it reduces to a linear function when $E_2 = 0$. Similarly, Eq 306 is nominally a quadratic function of ζ_A but reduces to a linear function when $G_2 = 0$. Also, Eq 308 is nominally a quadratic function of η_A but reduces to a linear function when $H_2 = 0$. For the Flatland scenario addressed in Section 7.7, the locus of points where a governing quadratic equation degenerates to a linear function forms a boundary between an area where the incorrect solution is extraneous to an area where it is ambiguous. It is expected that a similar situation pertains to spatial volumes as well.

7.9.4 Stations in the Same Plane

General Case — Eq 300 is valid when the stations are in the same plane — i.e., $W_\eta = 0$. Thus, Eq 301, which is the result of dividing the first and second lines, remains correct. However, Eq 302, which is formed by dividing the second and third lines of Eq 300, is replaced by

$$\zeta_A = D_1'\xi_A + D_0' \qquad \text{Eq 311}$$

$$D_1' = \frac{U\,\Delta d_{MW}}{W_\zeta\,\Delta d_{MU}} - \frac{W_\xi}{W_\zeta} \qquad \Delta d_{MU} \neq 0$$

$$D_0' = \frac{W^2 - \Delta d_{MW}^2}{2W_\zeta} - \frac{(U^2 - \Delta d_{MU}^2)\Delta d_{MW}}{2W_\zeta \Delta d_{MU}} \qquad \Delta d_{MU} \neq 0$$

Upon solving Eq 301 and Eq 311 simultaneously for ξ_A and ζ_A, then substituting the result into the first line of Eq 300, the result is:

$$\xi_A = \frac{D_0' - C_0}{C_1 - D_1'} \qquad \zeta_A = \frac{C_1 D_0' - C_0 D_1'}{C_1 - D_1'} \qquad \Delta d_{MU} \neq 0$$

$$\eta_A = \pm\sqrt{\frac{\left(U^2 - 2U\xi_A - \Delta d_{MU}^2\right)^2}{4\,\Delta d_{MU}^2} - (\xi_A^2 + \zeta_A^2)} \qquad \Delta d_{MU} \neq 0 \qquad \text{Eq 312}$$

The two roots of Eq 312 are symmetric with respect to the plane containing the stations. The same symmetry occurs for three true slant-range measurements (Section 7.8). This suggests that stations which are 'almost' in the same plane will have correct and ambiguous solutions which are 'almost' symmetric about that 'plane'.

Aircraft Equidistant from Stations M and U — The solution of Eq 312 fails when $\Delta d_{MU} = 0$ (in which case, $\xi_A = \frac{1}{2}U$). When this occurs, dividing third line of Eq 300 by the second and re-arranging yields a closed-form solution for ζ_A. When the solutions for ξ_A and ζ_A are substituted into the second line of Eq 300, the result is

$$\xi_A = \tfrac{1}{2}U$$

$$\zeta_A = \frac{\left(W^2 - W_\xi U - \Delta d_{MW}^2\right)\Delta d_{MV} - \left(V^2 - V_\xi U - \Delta d_{MV}^2\right)\Delta d_{MW}}{2W_\zeta \Delta d_{MV} - 2V_\zeta \Delta d_{MW}} \qquad \text{Eq 313}$$

$$\eta_A = \pm\sqrt{\frac{\left(V^2 - V_\xi U - 2V_\zeta \zeta_A - \Delta d_{MV}^2\right)^2}{4\,\Delta d_{MV}^2} - (\xi_A^2 + \zeta_A^2)} \qquad \Delta d_{MV} \neq 0$$

Aircraft Equidistant from Station **M** and Stations **U** and **V** — The solution of Eq 313 fails when both $\Delta d_{MU} = 0$ and $\Delta d_{MV} = 0$. In this 'double special case', solving Eq 300 yields

$$\xi_A = \frac{1}{2}U \qquad \zeta_A = \frac{V^2 - V_\xi U}{2V_\zeta}$$

$$\eta_A = \pm\sqrt{\frac{\left(W^2 - 2W_\xi\xi_A - 2W_\zeta\zeta_A - \Delta d_{MW}^2\right)^2}{4\Delta d_{MW}^2} - (\xi_A^2 + \zeta_A^2)} \qquad \text{Eq 314}$$

Aircraft Equidistant from Station **M** and Stations **U**, **V** and **W** — The case of all three range differences being zero — i.e., $\Delta d_{MU} = 0$, $\Delta d_{MV} = 0$ and $\Delta d_{MW} = 0$ — cannot occur unless the perpendicular bisector of the line between stations **M** and **W** passes through the intersection of the perpendicular bisectors between **M** and **U** and between **M** and **V** at ξ_A and ζ_A given by Eq 314. This occurs when W_ξ and W_ζ satisfy

$$W_\xi U + W_\zeta\frac{V^2 - V_\xi U}{V_\zeta} = W^2 = W_\xi^2 + W_\zeta^2 \qquad \text{Eq 315}$$

One way that Eq 315 is satisfied is when the stations form a rectangle — i.e., $V_\xi = 0, V_\zeta = V, W_\xi = U, W_\zeta = V$. When all range differences are zero, a solution for η_A does not exist (all values of η_A result in the same range differences).

7.9.5 Stations in the Same Plane, Three Form a Line

General Case — For this configuration, the stations are located in the same plane — i.e., $W_\eta = 0$ — and stations **M**, **U** and **V** form a straight line — i.e., $V_\zeta = 0$, $V = V_\xi$. In this situation, the solution of Subsection 7.9.4 fails. However, Eq 300 can be solved for these conditions, yielding

$$\xi_A = \frac{(V^2 - \Delta d_{MV}^2)\Delta d_{MU} - (U^2 - \Delta d_{MU}^2)\Delta d_{MV}}{2V\Delta d_{MU} - 2U\Delta d_{MV}}$$

$$\zeta_A = \frac{\left(U\Delta d_{MW} - W_\xi\Delta d_{MU}\right)}{W_\zeta}\xi_A + \frac{(W^2 - \Delta d_{MW}^2)\Delta d_{MU} - (U^2 - \Delta d_{MU}^2)\Delta d_{MW}}{2W_\zeta}$$

$$\eta_A = \pm\sqrt{\frac{\left(U^2 - 2U\xi_A - \Delta d_{MU}^2\right)^2}{4\Delta d_{MU}^2} - (\xi_A^2 + \zeta_A^2)} \qquad \Delta d_{MU} \neq 0 \qquad \text{Eq 316}$$

$$\eta_A = \pm\sqrt{\frac{\left(V^2 - 2V\xi_A - \Delta d_{MV}^2\right)^2}{4\Delta d_{MV}^2} - (\xi_A^2 + \zeta_A^2)} \qquad \Delta d_{MV} \neq 0$$

Aircraft Equidistant from Station M and Stations U and V — For this station configuration, it is not possible for both Δd_{MU} and Δd_{MV} to be zero.

Aircraft on M-U-V Baseline Extension — When an aircraft is on an extension of the baseline containing stations **M**, **U** and **V**, then $\Delta d_{MU} = \pm U$ and $\Delta d_{MV} = \pm V$, with the same sign applying

to both measurements. Thus, the expression for ξ_A in Eq 316 is singular and a solution does not exist.

7.9.6 Four Stations Form a Straight Line

General Case — Arranging four pseudo-range stations in a straight line is not common, but may be considered in some situations. For that geometry: $V_\zeta = 0$, $V = V_\xi$, and $W_\zeta = W_\eta = 0$, $W = W_\xi$. The general case solution (Eq 301 - Eq 303) then fails. However, the same solution process can be followed, starting from Eq 300, yielding

$$\xi_A = \frac{(V^2\Delta d_{MU} - U^2\Delta d_{MV}) + \Delta d_{MU}\,\Delta d_{MV}(\Delta d_{MU} - \Delta d_{MV})}{2(U\Delta d_{MV} - V\Delta d_{MU})}$$
$$\zeta_A^2 + \eta_A^2 = \frac{\left(U^2 - 2U\xi_A - \Delta d_{MU}^2\right)^2}{4\,\Delta d_{MU}^2} - \xi_A^2 \qquad \text{Eq 317}$$

Using cyclical substitutions — i.e., $U \to V \to W$ — two other expressions for ξ_A and $\zeta_A^2 + \eta_A^2$ can be written, independently, for each line of Eq 317. These can be used as alternatives when 'divide by zero' situations occur, but otherwise result in the same values. However, on both ends of the extension of the baselines connecting station **M**, **U**, **V** and **W**, all expressions for ξ_A fail.

This equation (both lines) indicates that four stations located along a line can determine an aircraft's location parallel to that line and the distance to a circle centered on the line where the aircraft is located. However, this station configuration cannot determine the lateral distance from the line nor its vertical displacement from the line. Qualitatively, four pseudo slant-range stations in a line provide no more information than three stations do (Subsection 7.7.5).

7.9.7 Remarks

- Upon comparing the traditional solution approach in this section to Bancroft's method (Section 7.2), it is evident that:
  (a) The approaches are fundamentally consistent, in that each requires solution of a quadratic equation;
  (b) The traditional approach is algebraically tedious and requires handling some measurements as special cases, but can be implemented using scalar equations. Conversely, Bancroft's method is elegant and does not involve special cases, but requires use of vector/matrix calculations including inversion of a 4x4 matrix;
  (c) The traditional approach explicitly reveals the geometric issues associated with the station locations, while Bancroft's method contains these geometric issues in the requirement that a matrix be invertible.
- A method for determining the aircraft latitude, longitude and altitude from the Cartesian coordinates (ξ_A, ζ_A, η_A) is given in Subsection 7.8.2.
- Height Monitoring Units (HMUs), deployed by the FAA and several other nations, using

a set of multilateration stations to measure the altitude of overflying aircraft. HMU ground stations are 'almost' in a plane. Typically, four stations form a square 30 NM on a side, and a fifth station is located at the center of the square.

- With some sign reversals the equations of this section would apply to measurements of slant-range sums for one transmitter and three receive stations (Ref. 44).

7.10 Traditional Solution for Three Pseudo Spherical-Ranges

7.10.1 Problem Formulation

Pseudo spherical-ranges are the basis for several radionavigation systems, most prominently Loran-C and Omega. Spherical ranging systems are intended for use on or near the earth's surface; altitude has no role in their concepts or solutions.

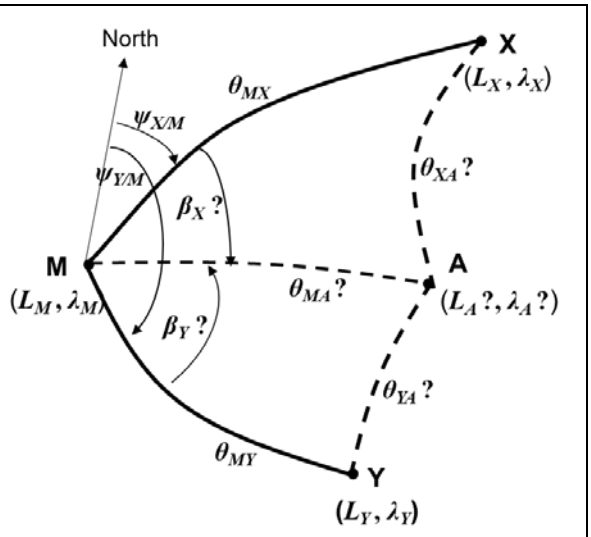

Figure 34 Scenario Involving Three Pseudo Spherical-Range Stations and Aircraft

Figure 34 illustrates a basic scenario using Loran-C station labels: **M** at latitude/longitude (L_M, λ_M) is the master station, and **X** (L_X, λ_X) and **Y** (L_Y, λ_Y) are secondary stations whose transmissions are synchronized with those from **M**. The coordinates of all stations are known. The assumption is that aircraft **A** is employing the system for navigation, and wishes to determine its latitude and longitude (L_A, λ_A).

Two time-difference-of-arrival (TDOA) measurements available from the station's transmissions; these are grouped as '**M** minus **X**' and '**M** and **Y**'. The TDOAs are equivalent to two spherical-range differences with constrained magnitudes:

$$\begin{aligned} \Delta\theta_{MXA} &= \theta_{MA} - \theta_{XA} & |\Delta\theta_{MXA}| &\le \theta_{MX} \\ \Delta\theta_{MYA} &= \theta_{MA} - \theta_{YA} & |\Delta\theta_{MYA}| &\le \theta_{MY} \end{aligned} \qquad \text{Eq 318}$$

7.10.2 Problem Solution

This solution follows Ref. 45 by Razin. Figure 34 depicts two mathematical spherical triangles **MXA** and **MYA** with common side **MA**. The goal in analyzing these triangles is to find θ_{MA} and either β_X or β_Y; having these quantities reduces the task to solution of the Direct problem of geodesy. As occurs for position determination based of three pseudo slant-range measurements in Flatland (Section 7.7), two solutions can occur.

Step 0: Solve the Indirect problem of geodesy (Section 4.2) for the paths **MX** and **MY**, yielding the geocentric angles θ_{MX} and θ_{MY} and the azimuth angles $\psi_{X/M}$ and $\psi_{Y/M}$.

Step 1: Form the difference of the azimuth angles $\psi_{X/M}$ and $\psi_{Y/M}$, yielding the angle β between great circle arcs **MX** and **MY** satisfying $0 < \beta \leq \pi$

$$\beta = \min\{|\psi_{Y/M} - \psi_{X/M}|, |\psi_{Y/M} - \psi_{X/M} + 2\pi|, |\psi_{Y/M} - \psi_{X/M} - 2\pi|\} \quad \text{Eq 319}$$

To establish the sign conventions, assume that the vehicle is within the V-shaped region with sides **MX** and **MY**. Then both β_X and β_Y are positive as shown. The following is always true:

$$\beta = \beta_X + \beta_Y \quad \text{Eq 320}$$

Step 2: Solve Eq 318 for θ_{XA} and θ_{YA}, then take the cosine of both sides, yielding:

$$\begin{aligned} \cos(\theta_{XA}) &= \cos(\theta_{MA})\cos(\Delta\theta_{MXA}) + \sin(\theta_{MA})\sin(\Delta\theta_{MXA}) \\ \cos(\theta_{YA}) &= \cos(\theta_{MA})\cos(\Delta\theta_{MYA}) + \sin(\theta_{MA})\sin(\Delta\theta_{MYA}) \end{aligned} \quad \text{Eq 321}$$

Step 3: Apply the spherical triangle law of cosines for sides (Eq 71) to **MXA** and **MYA**, yielding:

$$\begin{aligned} \cos(\theta_{XA}) &= \cos(\theta_{MA})\cos(\theta_{MX}) + \sin(\theta_{MA})\sin(\theta_{MX})\cos(\beta_X) \\ \cos(\theta_{YA}) &= \cos(\theta_{MA})\cos(\theta_{MY}) + \sin(\theta_{MA})\sin(\theta_{MY})\cos(\beta_Y) \end{aligned} \quad \text{Eq 322}$$

Step 4: The first and second lines, respectively, of Eq 321 and Eq 322 are equated, eliminating θ_{XA} and θ_{YA}. Then solving for θ_{MA} yields:

$$\begin{aligned} \tan(\theta_{MA}) &= \frac{\cos(\theta_{MX}) - \cos(\Delta\theta_{MXA})}{\sin(\Delta\theta_{MXA}) - \sin(\theta_{MX})\cos(\beta_X)} \\ \tan(\theta_{MA}) &= \frac{\cos(\theta_{MY}) - \cos(\Delta\theta_{MYA})}{\sin(\Delta\theta_{MYA}) - \sin(\theta_{MY})\cos(\beta_Y)} \end{aligned} \quad \text{Eq 323}$$

Step 5: Equate the two expressions for θ_{MA} in Eq 323 and eliminate β_Y using Eq 320, yielding:

$$\frac{\cos(\theta_{MX}) - \cos(\Delta\theta_{MXA})}{\sin(\Delta\theta_{MXA}) - \sin(\theta_{MX})\cos(\beta_X)} = \frac{\cos(\theta_{MY}) - \cos(\Delta\theta_{MYA})}{\sin(\Delta\theta_{MYA}) - \sin(\theta_{MY})\cos(\beta - \beta_X)} \quad \text{Eq 324}$$

Step 6: Re-write Eq 324 as:

$$\begin{aligned} B_c\cos(\beta_X) + B_s\sin(\beta_X) &= C \\ B_c &= \sin(\theta_{MX})[\cos(\theta_{MY}) - \cos(\Delta\theta_{MYA})] - \sin(\theta_{MY})[\cos(\theta_{MX}) - \cos(\Delta\theta_{MXA})]\cos(\beta) \\ B_s &= -\sin(\theta_{MY})[\cos(\theta_{MX}) - \cos(\Delta\theta_{MXA})]\sin(\beta) \\ C &= \sin(\Delta\theta_{MXA})[\cos(\theta_{MY}) - \cos(\Delta\theta_{MYA})] - \sin(\Delta\theta_{MYA})[\cos(\theta_{MX}) - \cos(\Delta\theta_{MXA})] \end{aligned} \quad \text{Eq 325}$$

Step 7: Re-write Eq 325 as:

$$B_m \cos\left(\beta_X - \gamma\right) = C$$
$$B_m = \sqrt{\left(B_c\right)^2 + \left(B_s\right)^2} \qquad \gamma = \arctan\ \left(B_s, B_c\right) \qquad \text{Eq 326}$$

The four-quadrant arc tangent function is used in Eq 326.

Step 8: Find β_X using Eq 327.

$$\beta_X = \arctan(B_s, B_c) \pm \text{Arccos}\left(\frac{C}{B_m}\right) \qquad \text{Eq 327}$$

In Eq 327, Arccos denotes the principal value of the arccos function — i.e., the value in the range [0, π]. Thus, in general, two solutions are possible.

Step 9: For both possible solutions, find θ_{MA} using the first line of Eq 323.

Step 10: For both possible solutions, find the aircraft's latitude and longitude (L_A, λ_A) as a solution to the Direct problem of geodesy, given the latitude/longitude (L_M, λ_M), the geocentric angle θ_{MA} and the azimuth angle $\psi_{A/M} = \psi_{X/M} + \beta_X$.

Step 11: For both possible solutions, the geocentric angles θ_{XA} and θ_{YA} are found from the aircraft and station latitudes and longitudes as solutions to the Indirect problem of geodesy.

Step 12: For both possible solutions, substitute the angles θ_{MA}, θ_{XA} and θ_{YA} in the right-hand side of Eq 318. Compare the resulting spherical-range difference to the measured values for these quantities. Discard a possible solution when agreement does not occur.

7.10.3 Types of Solutions

No Solution — Measurement errors can cause one of the inequalities in Eq 318 to be violated. That, in turn, can cause the argument of the arc cosine function in Eq 327 to be greater than one in magnitude, in which case a solution does not exist.

Double-Root Solution — If the aircraft is on a baseline extension, including at a station, then Eq 324 becomes indeterminate and the equations immediately before it must be used. For example, assume the aircraft is on the extension of **MX**, closer to **X**. Then $\theta_{MA} = \Delta\theta_{MXA}$, and equating the first two lines of Eq 321 and Eq 322 yields $\beta_X = 0$, hence $\beta_Y = \beta$. Thus, since $0 < \beta < \pi$, there is a single solution for θ_{MA} which is given by the second line of Eq 323.

Single Solution — In Eq 327, if B_m=C then the arccos term is zero and there is only one solution for β_X. The locus of latitudes/longitudes for which B_m=C can be found numerically.

Two Solutions: Ambiguous vs. Extraneous — In most instances, two candidate solutions are

found by the method described in Subsection 7.10.2. One is always correct. The other is either: (a) extraneous, corresponding to the negation of the measured spherical-range differences (thus will be detected in Step 12); or (b) ambiguous, also corresponding to the measured spherical-range differences, and thus not resolvable without additional information.

The intended service area for a pseudorange system is, approximately, the region within the perimeter of the polygon enclosing the stations (but not close to a station) and the border area outside the perimeter but near the bisector of the baseline joining the closest two stations. In the service area, one candidate solution is extraneous and corresponds to the '+' sign in Eq 327, while the correct solution corresponds to the '–' sign. Example 10 in Subsection 7.12.3 illustrates where both ambiguous and extraneous solutions occur.

7.10.4 Remarks

System Applications — The primary U.S. examples of long-range (over 1,000 NM) pseudo spherical-range systems are Loran-C and Omega. For their characteristics (ranges between stations and aircraft, radio wave propagation paths), steps in addition to those described in Subsection 7.10.2 were generally needed to achieve the systems' potential accuracies.

Accuracy Enhancements — Two areas have been addressed to improve the accuracy of low-frequency spherical-range difference systems:

- Earth Geometry — For distances of more than a few hundred miles, the ellipticity error incurred by using a spherical-earth model is usually unacceptably large. One approach is to employ approximations to an ellipsoid (Refs. 11-16 and 13-15) which are not amenable to closed-form solution. These can be utilized in an iterative solution technique that is initialized with the solution obtained from Razin's algorithm (see Chapter 8). A second approach is to tailor the spherical-earth model to the service area involved (Refs. 45 and 53).
- Radiowave Propagation — Low-frequency electromagnetic ground waves cannot be assumed to travel with constant speed, since their propagation depends upon the conductivity of the ground over which they travel. Modeling and measurements have both been used to address this issue. The resulting adjustments are easily incorporated in the pseudo spherical-range difference measurements.

Validation — Reference 53 contains the findings of a comparison, using Loran-C measurements, of Razin's algorithm and the semi-official, iterative algorithm published by the Radio Technical Commission for Maritime Services (RTCM) (Ref. 54). Differences between the computed latitude/longitude coordinates for the two algorithms are between 3 ft and 5 ft.

Similarity to Flatland Solution — Although the analysis formulations are different (rectangular versus spherical), the qualitative characteristics of the solutions for the Flatland/Fang and spherical-earth/Razin algorithms are qualitatively similar. Both have two solutions, with the

incorrect one being detectable in their useful service areas. Solutions for both are unstable along the extended baselines, and degraded in the V-shaped regions between two baselines.

7.11 Traditional Solution for Two Pairs of Pseudo Spherical-Ranges

7.11.1 Problem Formulation

This section addresses a problem close to the topic of the previous section: determining an aircraft's position from two spherical-range difference measurements. However, in this section, the measurements are obtained from four stations comprising two distinct pairs, rather than from three stations comprising two pairs having a common station (Figure 35). It is also close to the topic of Section □, which addresses two pairs of stations that measure pseudo slant-ranges.

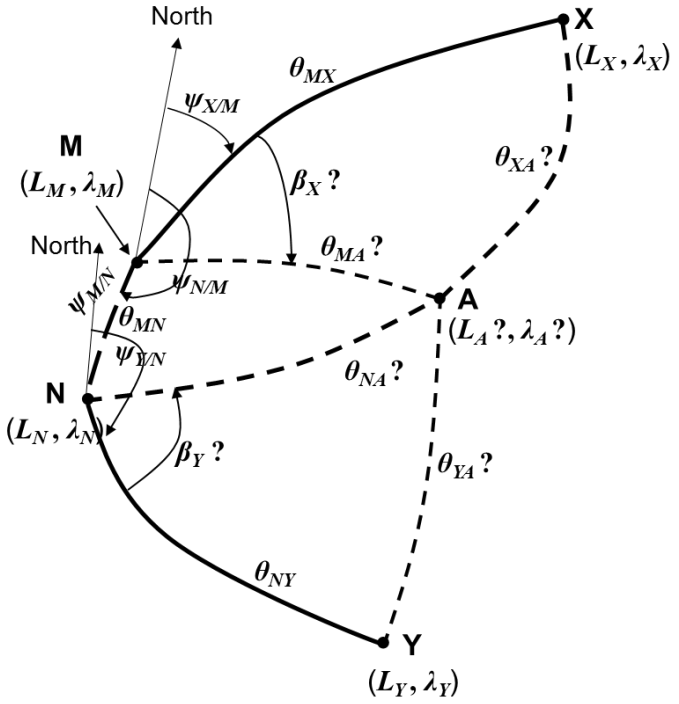

Figure 35 Pseudo Spherical-Range Scenario: Two Station Pairs and an Aircraft

In Figure 35, Loran-C-like station labels are used. Station **M** at latitude/ longitude (L_M, λ_M) is a master station, and station **X** (L_X, λ_X) is an associated secondary. Similarly, station **N** (L_N, λ_N) is the master for a second chain, and station **Y** (L_Y, λ_Y) is an associated secondary. The transmissions of each master-secondary pair are synchronized, but are asynchronous with those of the other pair.

The assumption is that aircraft **A** is employing this set of stations for navigation. The aircraft's first priority is to determine its latitude/longitude (L_A, λ_A) coordinates. A second priority is to determine the spherical-range to and azimuth angle toward each of the four stations.

Two time-difference-of-arrival (TDOA) measurements are available from the stations' transmissions; these follow the convention '**M** minus **X**' and '**N** minus **Y**'. These TDOAs are equivalent to two spherical-range differences. These are, with limitations on their magnitudes:

$$\begin{aligned} \Delta\theta_{MXA} &= \theta_{MA} - \theta_{XA} \qquad \left|\Delta\theta_{MXA}\right| \le \theta_{MX} \\ \Delta\theta_{NYA} &= \theta_{NA} - \theta_{YA} \qquad \left|\Delta\theta_{NYA}\right| \le \theta_{NY} \end{aligned} \qquad \text{Eq 328}$$

7.11.2 Problem Solution

Figure 35 depicts three mathematical spherical triangles: **MXA**, **NYA** and **MNA**. The goal in analyzing these triangles is to find values for the two spherical-range/bearing pairs θ_{MA} and β_X and θ_{NA} and β_Y. Knowing these quantities reduces the task of finding (L_A, λ_A) to a solution of the Direct problem of geodesy. As in other multi-dimensional problems, multiple solutions for (L_A, λ_A) may occur; when they do, the validity of each must be checked.

The immediate goal is to find β_X, as the quantities θ_{MA}, θ_{NA} and β_Y follow readily.

Step 0: Solve the Indirect problem of geodesy for three paths between stations:

- **MX** (master and associated secondary): Provides θ_{MX} and $\psi_{X/M}$
- **NY** (master and associated secondary): Provides θ_{NY} and $\psi_{Y/N}$
- **MN** (two master stations): Provides θ_{MN}, $\psi_{M/N}$ and $\psi_{N/M}$

Define the positive angles between the path **MN** and, respectively, the paths **MX** and **NY**

$$\begin{aligned} \psi_M &= \min\left\{ \left|\psi_{N/M} - \psi_{X/M}\right|, \left|\psi_{N/M} - \psi_{X/M} + 2\pi\right|, \left|\psi_{N/M} - \psi_{X/M} - 2\pi\right| \right\} \\ \psi_N &= \min\left\{ \left|\psi_{Y/N} - \psi_{M/N}\right|, \left|\psi_{Y/N} - \psi_{M/N} + 2\pi\right|, \left|\psi_{Y/N} - \psi_{M/N} - 2\pi\right| \right\} \end{aligned} \qquad \text{Eq 329}$$

Formally define β_X as the angle **XMA**, measured clockwise from **XM**. Similarly, define β_Y as the angle **YNA**, measured counter-clockwise from **YN**.

Step 1: Solve Eq 328 for θ_{XA} and θ_{YA}, then take the cosine of both sides, yielding:

$$\begin{aligned} \cos(\theta_{XA}) &= \cos(\theta_{MA})\cos(\Delta\theta_{MXA}) + \sin(\theta_{MA})\sin(\Delta\theta_{MXA}) \\ \cos(\theta_{YA}) &= \cos(\theta_{NA})\cos(\Delta\theta_{NYA}) + \sin(\theta_{NA})\sin(\Delta\theta_{NYA}) \end{aligned} \qquad \text{Eq 330}$$

Step 2: Apply the spherical law of cosines for sides to triangles **MXA** and **NYA**, yielding:

$$\begin{aligned} \cos(\theta_{XA}) &= \cos(\theta_{MA})\cos(\theta_{MX}) + \sin(\theta_{MA})\sin(\theta_{MX})\cos(\beta_X) \\ \cos(\theta_{YA}) &= \cos(\theta_{NA})\cos(\theta_{NY}) + \sin(\theta_{NA})\sin(\theta_{NY})\cos(\beta_Y) \end{aligned} \qquad \text{Eq 331}$$

Step 3: The first lines of Eq 330 and Eq 331 are equated, eliminating θ_{XA}. Then solving for the master station-aircraft distance yields θ_{MA} as a function of β_X and known quantities

$$\theta_{MA} = \arctan\left(\frac{\cos(\theta_{MX}) - \cos(\Delta\theta_{MXA})}{\sin(\Delta\theta_{MXA}) - \sin(\theta_{MX})\cos(\beta_X)}\right) \quad \text{Eq 332}$$

In Eq 332, the single-argument arc tangent function should be used.

Step 4: Consider spherical triangle **MNA**. The four-part cotangent formula yields an expression for β_Y as an explicit function of β_X and quantities that are either known or are functions of β_X:

$$\beta_Y = \psi_N - \arctan\left(\frac{\sin(\psi_M - \beta_X)}{\sin(\theta_{MN})\cot(\theta_{MA}) - \cos(\theta_{MN})\cos(\psi_M - \beta_X)}\right) \quad \text{Eq 333}$$

In Eq 333, the two-argument arc tangent function should be used.

Step 5: The second lines of Eq 330 and Eq 331 are equated, eliminating θ_{YA}. Then solving for the master station-aircraft distance yields θ_{NA} as a function of β_Y and known quantities

$$\theta_{NA} = \arctan\left(\frac{\cos(\theta_{NY}) - \cos(\Delta\theta_{NYA})}{\sin(\Delta\theta_{NYA}) - \sin(\theta_{NY})\cos(\beta_Y)}\right) \quad \text{Eq 334}$$

In Eq 334, the single-argument arc tangent function should be used.

Step 6: The value of β_X sought is a root of the following equation (application of the Law of Sines to spherical triangle **MNA**)

$$\frac{\sin(\psi_M - \beta_X)}{\sin(\theta_{NA})} = \frac{\sin(\psi_N - \beta_Y)}{\sin(\theta_{MA})} \quad \text{Eq 335}$$

By substituting and re-substituting Eq 332, Eq 333 and Eq 334 into Eq 335, the result would be an explicit function of β_X and known quantities. There is no point in doing so, however, since the expression would be too complex to be solved analytically for β_X. Instead, a root finding technique (Subsection 2.1.8) can used to find one or more values for β_X.

Step 7: For each candidate solution for β_X, find the corresponding value for θ_{MA} using Eq 332.

Step 8: For each candidate solution pair for bearing β_X and range θ_{MA}, find the aircraft's latitude and longitude (L_A, λ_A) as a solution to the Direct problem of geodesy.

Step 9: If multiple solutions to Eq 335 occur, for each solution set, find the geocentric angles θ_{XA} and θ_{YA} from the aircraft and station coordinates as solutions to the Indirect problem of geodesy.

Step 10: For each solution set, substitute the angles θ_{MA}, θ_{XA} and θ_{NA}, θ_{YA} in the right-hand side of Eq 328. Compare the resulting spherical-range difference to the measured values for these quantities. Discard a candidate solution when agreement does not occur.

7.11.3 Remarks

- An obvious application of this algorithm is to Loran-C 'cross-chaining' — finding position solutions using TDOA measurements from two separate chains. Loran-C cross-chaining can involve three stations, with one station being dual-rated. However, in terms of the position-solution algorithm, three-station cross-chaining is no different than three stations from a single chain. This section addresses the more-complex situation involving two pairs of stations, one pair from each chain.
- Sequences of equations other than those developed herein can be used derive a function of β_X (only) whose root is to be found. The solution sequence presented herein follows Razin (Ref. 45) and appears to yield satisfactory results (Subsection 7.12.4).

7.12 Example Applications

7.12.1 Example 8: Slant-Range Measurement System in Flatland

Problem Statement — This example considers the simplest application of Bancroft's algorithm — finding the intersections of two circles in a plane; it relates most closely to Section 7.3, which addresses a three-dimensional version. Stated as a navigation problem, an aviator in Flatland measures his/her slant-range to two stations — say, d_{1A} to station **S1** and d_{2A} to station **S2**, where both stations have known coordinates. This is a simplified version of computing a DME/DME fix.

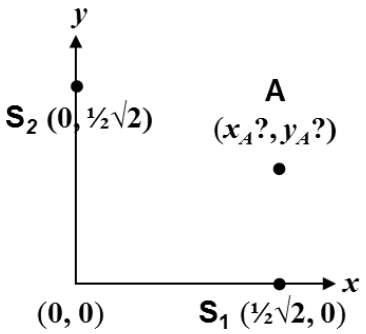

The first step is selecting the coordinate frame. Because Bancroft's algorithm involves calculating the inverse of a matrix based on station coordinates (e.g., **B** in Eq 232), the origin cannot be in-line with the two stations. A convenient choice is to place each station on one axis, equidistant from the origin (illustrated). A normalized distance scale is chosen such that the separation between the stations is one unit — i.e., distances are quantified in Base Line Units (BLUs).

Solution — Making the assignments indicated in Section 7.3 yields

$$\mathbf{B} = \begin{bmatrix} \frac{1}{2}\sqrt{2} & 0 \\ 0 & \frac{1}{2}\sqrt{2} \end{bmatrix} \qquad \mathbf{B}^{-1} = \begin{bmatrix} \sqrt{2} & 0 \\ 0 & \sqrt{2} \end{bmatrix}$$

$$\mathbf{b} = \begin{bmatrix} (x_1)^2 + (y_1)^2 - (d_{1A})^2 \\ (x_2)^2 + (y_2)^2 - (d_{2A})^2 \end{bmatrix} = \begin{bmatrix} \frac{1}{2} - d_{1A}^2 \\ \frac{1}{2} - d_{2A}^2 \end{bmatrix} \qquad \mathbf{1} = \begin{bmatrix} 1 \\ 1 \end{bmatrix} \qquad \text{Eq 336}$$

$$\mathbf{u} = \begin{bmatrix} u_x \\ u_y \end{bmatrix} = \tfrac{1}{2}\mathbf{B}^{-1}\,\mathbf{1} = \tfrac{1}{2}\sqrt{2}\begin{bmatrix} 1 \\ 1 \end{bmatrix}$$

$$\mathbf{v} = \begin{bmatrix} v_x \\ v_y \end{bmatrix} = \tfrac{1}{2}\mathbf{B}^{-1}\mathbf{b} = \tfrac{1}{2}\sqrt{2}\begin{bmatrix} \frac{1}{2} - d_{1A}^2 \\ \frac{1}{2} - d_{2A}^2 \end{bmatrix}$$

Therefore

$$\begin{gathered}\alpha\lambda^2+\beta\lambda+\gamma=0\\ \alpha=\langle\mathbf{u},\mathbf{u}\rangle=u_x^2+u_y^2\\ \beta=2\langle\mathbf{u},\mathbf{v}\rangle-1=2u_xv_x+2u_yv_y-1=-[d_{1A}^2+d_{2A}^2]\\ \gamma=\langle\mathbf{v},\mathbf{v}\rangle=v_x^2+v_y^2=\tfrac{1}{2}\left(\tfrac{1}{2}-d_{1A}^2\right)^2-\tfrac{1}{2}\left(\tfrac{1}{2}-d_{2A}^2\right)^2\\ Disc=\beta^2-4\alpha\gamma=[d_{1A}^2+d_{2A}^2]^2-2\left(\tfrac{1}{2}-d_{1A}^2\right)^2-2\left(\tfrac{1}{2}-d_{2A}^2\right)^2\\ =2[d_{1A}^2+d_{2A}^2]-[d_{1A}^2-d_{2A}^2]^2-1\end{gathered}$$ Eq 337

Thus

$$\begin{gathered}\lambda_\pm=\tfrac{1}{2}\left(d_{1A}^2+d_{2A}^2\pm\sqrt{2[d_{1A}^2+d_{2A}^2]-[d_{1A}^2-d_{2A}^2]^2-1}\right)\\ \begin{bmatrix}x_{A\pm}\\ y_{A\pm}\end{bmatrix}=\lambda_\pm\mathbf{u}+\mathbf{v}=\lambda_\pm\tfrac{1}{2}\sqrt{2}\begin{bmatrix}1\\1\end{bmatrix}+\tfrac{1}{2}\sqrt{2}\begin{bmatrix}\frac{1}{2}-d_{1A}^2\\ \frac{1}{2}-d_{2A}^2\end{bmatrix}\end{gathered}$$ Eq 338

Types of and Conditions on Solutions — Insight into the solution can be obtained by examining the sum and difference of the slant-ranges. Thus let

$$\begin{gathered}\Sigma d=d_{1A}+d_{2A}\qquad\Delta d=d_{1A}-d_{2A}\\ d_{1A}=\tfrac{1}{2}(\Sigma d+\Delta d)\qquad d_{2A}=\tfrac{1}{2}(\Sigma d-\Delta d)\end{gathered}$$ Eq 339

Upon substituting, the discriminant $Disc$ can be written as

$$Disc=\beta^2-4\alpha\gamma=[(\Sigma d)^2-1][1-(\Delta d)^2]$$ Eq 340

Four possible solution cases for the norm λ are enumerated in Subsection 7.2.4. It follows from Eq 337 that, since $\alpha=1$, a single real root cannot occur (Case (b)). Geometrically, this is because two circles in a plane must cross at two points (Case (d)), be tangent at a point (double root, Case (c)) or not cross (Case (a)).

Cases (a), (c) and (d) can all occur, depending upon the value of $Disc$. For a solution (i.e., real roots) to occur, both of the following conditions on the measurements must be true:

$$\Sigma d=d_{1A}+d_{2A}\geq 1\qquad|\Delta d|=|d_{1A}-d_{2A}|\leq 1$$ Eq 341

Since the two stations are separated by one BLU, Eq 341 ‘says’ that in the absence of measurement errors (a) the sum of the ranges to the stations must be at least equal to the separation between the stations, and (b) the absolute value of the difference between the ranges to the stations must be no more than the separation between the stations. Based on geometric reasoning, when Σd is unity, the aircraft must be on the baseline separating the stations, and when $|\Delta d|$ is

unity the aircraft must be on an extension of the baseline. Similar conditions are derived in Subsection 6.4.3 for the analogous problem involving a spherical earth.

Aircraft locations along the baseline connecting the stations and its extensions are unstable because small measurement errors can change the character of the solution — to a situation where a solution does not exist or to one where there are two separate candidate solutions.

It follows from Eq 338 and Eq 340 that

$$\lambda_{\pm} = \tfrac{1}{4}[(\Sigma d)^2 + (\Delta d)^2] \pm \tfrac{1}{2}\sqrt{[(\Sigma d)^2 - 1][1 - (\Delta d)^2]} \qquad \text{Eq 342}$$

Either solution to Eq 342 (and to Eq 338 as well) may be correct mathematically. Of course, only one solution is actually equal to the vehicle's true position — the other solution is ambiguous. Two slant-ranges do not provide enough information to make a determination.

'Natural' Coordinate System — While the (x, y) frame is compatible with Bancroft's algorithm, it is not the natural frame for this problem. Thus, consider the (ξ, ζ) frame (Figure 36) which is generated by rotating the (x, y) frame counter clockwise by 45 deg, then offsetting it by one-half a BLU to the right. The result is that (a) both stations lie on the ζ-axis, and (b) the ξ-axis is the perpendicular bisector of the baseline connecting the stations. The solutions for the aircraft location can be expressed in the (ξ, ζ) frame as:

$$\begin{bmatrix}\xi_A \\ \zeta_A\end{bmatrix} = \frac{1}{2}\begin{bmatrix}\pm\sqrt{2[d_{1A}^2 + d_{2A}^2] - [d_{1A}^2 - d_{2A}^2]^2 - 1} \\ d_{1A}^2 - d_{2A}^2\end{bmatrix} \qquad \text{Eq 343}$$

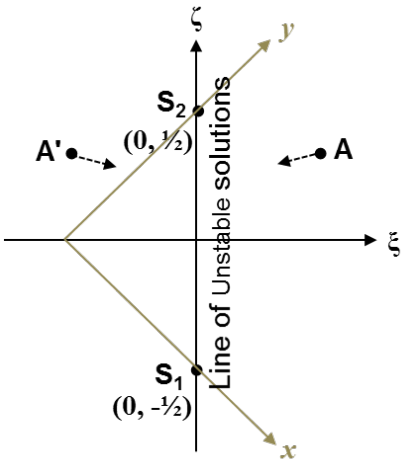

Figure 36 Two Slant-Range Stations and Aircraft in Flatland

This solution can also be written as

$$\begin{bmatrix}\xi_A \\ \zeta_A\end{bmatrix} = \frac{1}{2}\begin{bmatrix}\pm[(\Sigma d)^2 - 1][1 - (\Delta d)^2] \\ (\Sigma d)(\Delta d)\end{bmatrix} \qquad \text{Eq 344}$$

Let a breve diacritic mark above a normalized quantity denote its un-normalized version — e.g., $\breve{\xi} = B\xi$ and $\breve{\zeta} = B\zeta$, where B is the baseline length. The un-normalized version Eq 344 then is

$$\begin{bmatrix}\breve{\xi}_A \\ \breve{\zeta}_A\end{bmatrix} = \frac{1}{2B}\begin{bmatrix}\pm\left[\left(\Sigma\breve{d}\right)^2 - B^2\right]\left[B^2 - \left(\Delta\breve{d}\right)^2\right] \\ \left(\Sigma\breve{d}\right)\left(\Delta\breve{d}\right)\end{bmatrix} \qquad \text{Eq 345}$$

Geometry-Based Derivation — There is an older, more direct, geometry-based derivation of Eq 343. Referring to Figure 36, the two slant-ranges satisfy Pythagoras' theorem:

$$d_{1A}^2 = \xi_A^2 + \left(\zeta_A + \tfrac{1}{2}\right)^2$$
$$d_{1A}^2 = \xi_A^2 + \left(\zeta_A - \tfrac{1}{2}\right)^2 \qquad \text{Eq 346}$$

Completing the squares and subtracting the second equation from the first in Eq 346 yields the second line of Eq 343

$$\zeta_A = \tfrac{1}{2}(d_{1A}^2 - d_{2A}^2) \qquad \text{Eq 347}$$

Then, substituting for ζ_A in the first equation in Eq 346 yields the first line of Eq 343:

$$\xi_A = \pm\tfrac{1}{2}\sqrt{2[d_{1A}^2 + d_{2A}^2] - [d_{1A}^2 - d_{2A}^2]^2 - 1} \qquad \text{Eq 348}$$

Remarks

- In the absence of slant-range measurement errors that cause one or both of the inequalities of Eq 341 to be violated, there are no aircraft positions where either line in Eq 343 fails — i.e., the solution equations do not have any singularities.
- If the aircraft position is on the ζ-axis — either on the baseline connecting the stations or on an extension — the discriminant (Eq 340) is zero and Eq 337 has an unstable double root. This is slightly different than the situation for three pseudorange stations in a plane (Section 7.10); there, only positions on the baseline extensions are unstable.
- If the aircraft is not on the ζ-axis, then Eq 337 has two separate real roots that correspond to the actual and ambiguous aircraft locations.
- The correct and ambiguous solutions are symmetrically located with respect to the ζ-axis but cannot be distinguished based on two slant-range measurements. However, other information may be available (Subsection 6.1.3). Movement of the aircraft with a component toward or away from the ζ-axis (determined by, e.g., an on-board compass) is a method for determining the correct solution.
- The effect of measurement errors on the solution depends strongly on the location of the aircraft. This is the topic of Subsection 8.5.1.
- The two-ranging-stations-in-Flatland problem is a simplified version of the DME/DME/Altitude problem addressed in Section 6.4. Qualitatively, the solutions behave similarly.

7.12.2 Example 9: Three Pseudo Slant-Range Stations in Flatland

This subsection presents examples of results obtained using Fang's algorithm described in Section 7.7 for finding the two-dimensional position of an aircraft from three pseudo slant-range measurements. Figure 37 depicts three such stations, labeled **M**, **U** and **V**. The three green curves partition the space into four regions that contain both the correct and the incorrect (either ambiguous or extraneous) solutions — refer to Eq 285 and Figure 31.

The thicker, solid blue and red lines with filled symbols at their ends represent hypothetical

aircraft flight tracks. The thinner, dashed blue and red lines with unfilled symbols at their ends depict the incorrect solutions yielded by the algorithm for the hypothetical tracks of the same color. An asterisk marks the center of each hypothetical flight track.

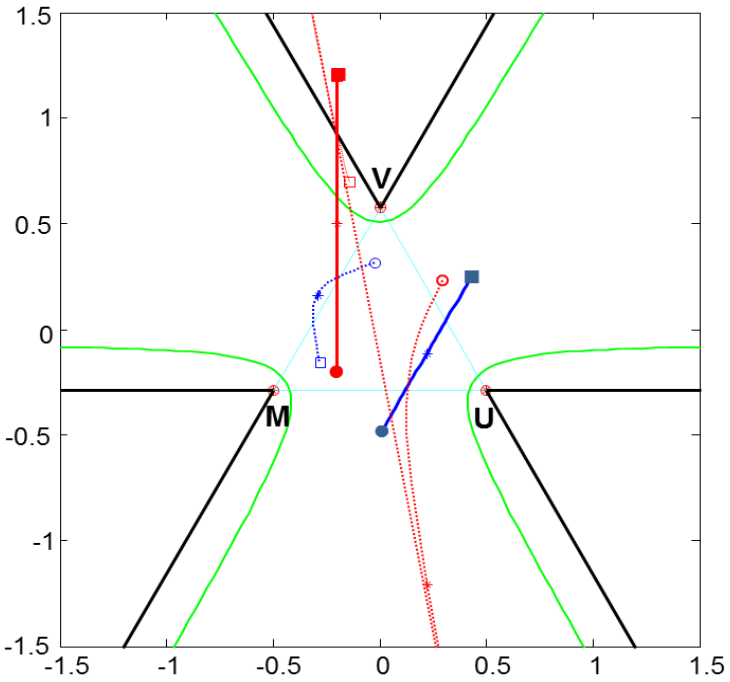

Figure 37 Three Pseudo Slant-Range Stations in Flatland and Two Aircraft Tracks

The solid blue track corresponding to the correct solution is well within the service area, as is its corresponding incorrect dashed blue track (which is in approximately the opposite direction, and is slightly curved). In the 'extraneous' region, the correct solution can be identified by inspection. For example, the filled blue circle is equidistant from **M** and **U** and furthest from **V**. In contrast, its counterpart, the unfilled blue circle, is equidistant from **M** and **U** and closest to **V** (i.e., the order is reversed). Similar statements can be made about every point in this region. The magnitudes of the slant-range differences are the same for the correct and incorrect solutions; however, their signs are reversed.

In contrast to the blue tracks, the red tracks corresponding to the incorrect solution transition from the 'extraneous' region to the 'ambiguous' region. Starting from the circle symbols the correct solution moves directly 'north' in a straight line, while the incorrect solution moves largely 'south' in a slightly curved path. As the aircraft approaches and crosses the transition between the regions, the incorrect solution moves at a high rate to the 'south' then reappears at the far 'north' and again moves at a high rate to the 'south'. As the aircraft moves away from the transition curve, the incorrect solution moves close to the correct solution.

7.12.3 Example 10: Three Pseudo Spherical-Range Stations

This subsection presents an example application of Razin's algorithm (Section 7.10) utilizing three pseudo spherical-range navigation stations in the U.S. Northeast Loran-C chain (Ref. 55). In Figure 38: **M** represents the master station at Seneca, NY; **W** represents the secondary station at Caribou, ME; and **X** represents the secondary station at Nantucket, MA. For a spherical-earth formulation, the baselines and their extensions for these stations are great circles.

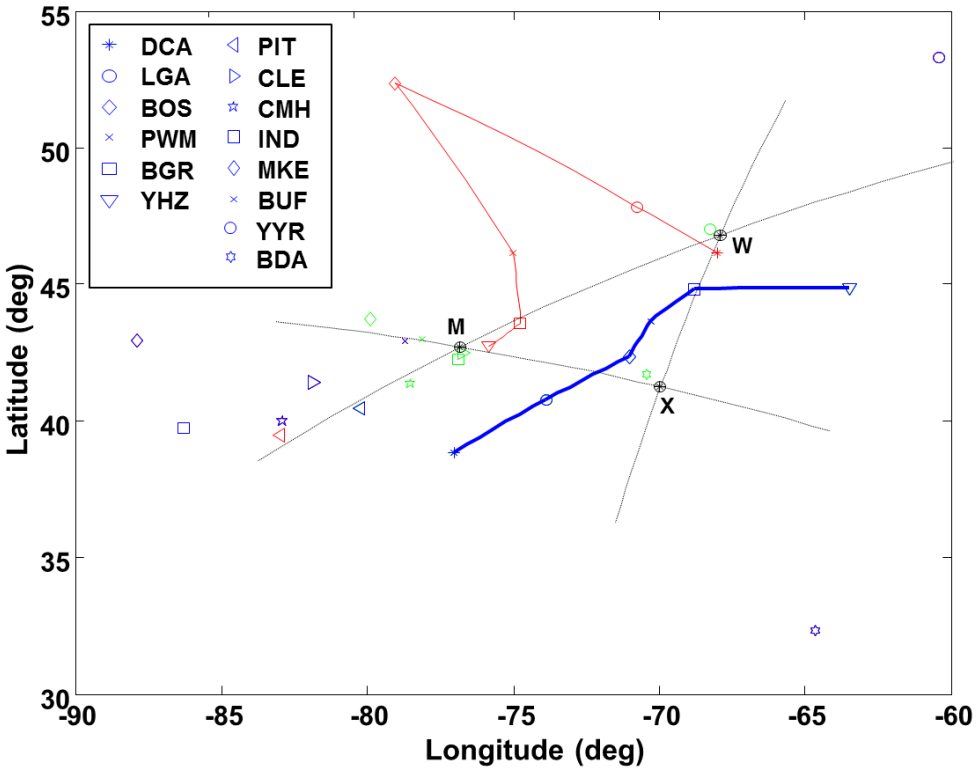

Figure 38 Position Solutions for Triad of Stations from the Northeast U.S. Loran-C Chain

Fourteen airport locations were selected, and spherical-range differences for the station pairs **M**-**W** and **M**-**X** were calculated using a spherical-earth model. The methodology of Section 7.10 was used to find solutions for the airport locations from the range differences. Green ('–' solution) and red ('+' solution) icons of the same shapes represent the algorithm's solutions for the same airport. Blue-colored symbols depict the actual airport locations, and overprint the correct solution (in all cases, they agree to machine precision).

Six airports are in the service area for these stations: Reagan National, VA (DCA); LaGuardia, NY (LGA); Boston, MA (BOS); Portland, ME (PWM); Bangor, ME (BGR); and Halifax, Nova Scotia (YHZ). A blue line represents a hypothetical flight path connecting these airports. A thinner red line connects the incorrect '+'solutions.

For airports in the service area, the incorrect solutions can be detected by inspection, as the range

differences for an extraneous solution will be negative versions of the range differences for the correct solution. For example, DCA is closest to station **M** and furthest from **W**; its extraneous version is closest to **W** and furthest from **M**. Another method for detecting the correct solution is to examine the flight path. In this case, the incorrect 'flight path' is, overall, in the opposite direction of the correct track.

Eight other airports are also depicted by blue symbols: Pittsburgh, PA (PIT); Cleveland, OH (CLE); Columbus, OH (CMH); Indianapolis, IN (IND); Milwaukee, WI (MKE); Buffalo, NY (BUF); Goose Bay, Labrador (YYR); and Bermuda (BDA). These airports are all outside the nominal service area for the stations, and are in or near the three regions bounded by baseline extensions. The incorrect solutions, which may be either the '–' or '+' solution of Eq 327, are all ambiguous — i.e., the range differences calculated from the correct and incorrect airport locations are identical.

This example is revisited in Subsection 8.5.4, which addresses the effect of mis-modeling the earth as a sphere (i.e., the ellipticity error), and presents a solution.

7.12.4 Example 11: Two Pairs of Pseudo Spherical-Range Stations

This subsection presents an example of the solution algorithm for two pairs of pseudo spherical-range navigation stations described in Section 7.11. Figure 39 depicts the master station at Seneca, NY for the U.S. Northeast Loran-C chain and a secondary station at Nantucket, MA. It also depicts the master station for the U.S. Great Lakes Loran-C chain at Dana, IN, and a secondary station at Malone, FL. (Loran station coordinates can be found in Ref. 53.)

Figure 39 also shows seven airports which represent possible locations of aircraft employing these stations for navigation: LaGuardia, NY (LGA); Elizabeth City, NC (ECG); Charleston, SC (CHS); Charleston, WV (CRW); Atlanta, GA (ATL); Nashville, TN (BNA); and St. Louis, MO (STL). All of the airports are within the expected service area for such a navigation system.

The solution algorithm presented in Section 7.11 is straightforward except for the process of finding values for β_X that are roots of Eq 335. Thus the primary issue explored is the behavior of Eq 335 as a function of β_X — i.e., with θ_{MA}, θ_{NA} and β_Y determined from β_X. (Here, β_X is the angle, measured clockwise, from (a) the baseline from Seneca to Nantucket to (b) a great circle path from Seneca to the aircraft.)

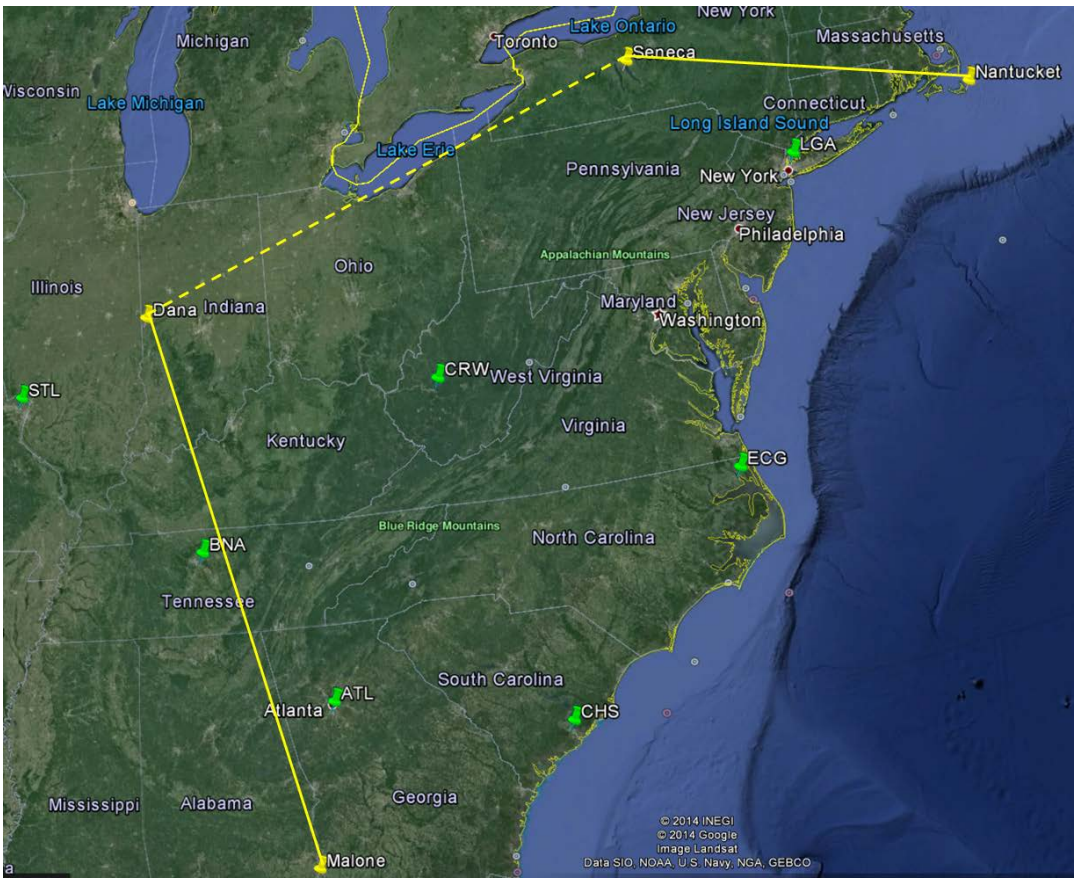

Figure 39 Two Pairs of Loran-C Stations and Seven Airport Locations

Figure 40 shows the difference between the left- and right-hand sides of Eq 335 as a function of assumed values for β_X in the range $(\psi_M - \pi) \leq \beta_X \leq \psi_M$. Each of the seven possible aircraft locations are considered for the half-sphere on the southeast side of the great circle path through Dana and Seneca. The curves for six of the seven airports (all except STL) have the same basic shape — a 'sideways S'. Most important is that each curve in Figure 40, including that for STL, has only one root, so ambiguous and extraneous solutions do not occur for locations in the area of interest. If the roots for β_X shown in Figure 40 are substituted into Steps 7-10 of the algorithm in Section 7.11, the original aircraft locations result.

A plot similar to Figure 40 was generated for the area on the northwest side of the great circle path through Dana and Seneca. Four of the airports of interest (LGA, ECG, CRW and BNA) had a single extraneous solution in this area. CHS and ATL did not have a second solution, and STL has two additional solutions. This example is re-visited in Subsection 8.5.5.

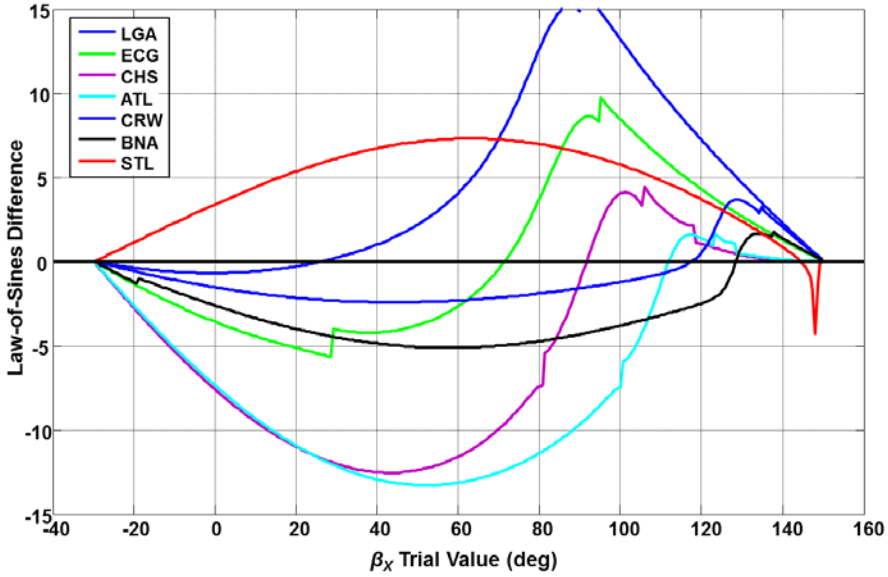

Figure 40 Example 11: Sensitivity of Law-of-Sines Difference to Trial Values of β_X

7.12.5 Example 12: Wide Area Multilateration (WAM)

As an example of the solution technique presented in Section 7.5, a WAM system is postulated which has ground stations at three airports: Boston, MA (BOS); Manchester, NH (MHT); and Hartford, CT (BDL) — see Figure 41. To investigate its performance in its intended service volume, an aircraft is assumed to over-fly five airports in the system's service area at an altitude of 25,000 ft: Westfield-Barnes Regional, MA (BAF); Dillant-Hopkins, Keene NH (EEN); Fitchburg Municipal, MA (FIT); Lawrence Municipal, MA (LWM); and Hanscom Field, Bedford MA (BED). To provide insight into the algorithm's behavior for poor measurement geometries, solutions are also computed for three locations outside the service volume and near extended baselines: Barnstable Municipal, MA (HYA); Stewart International, NY (SWF); and Portland International, ME (PWM).

Interest in the algorithm of Section 7.5 centers on the solution to Eq 251 for the aircraft time of transmission t_A. In this example, the times of reception at the ground stations t_i were shifted by the same amount, so that the earliest occurred at $t_i = 0$. As a result, the correct value for t_A must be negative. The four roots of Eq 251 were found using the Matlab routine 'roots'. These were multiplied by the speed of light, *c*, converting their units to nautical miles. Thus, the correct solution is the negative of the slant-range between the aircraft and the nearest ground station. Since the reception range of a WAM ground station is limited by line-of-sight considerations (Figure 8), ranges beyond a few hundred nautical miles are not feasible.

The calculated roots (potential values for t_A) are displayed in Table 13. Positive roots cannot be correct, nor can complex roots; only the two negative roots are possible solutions. For the five

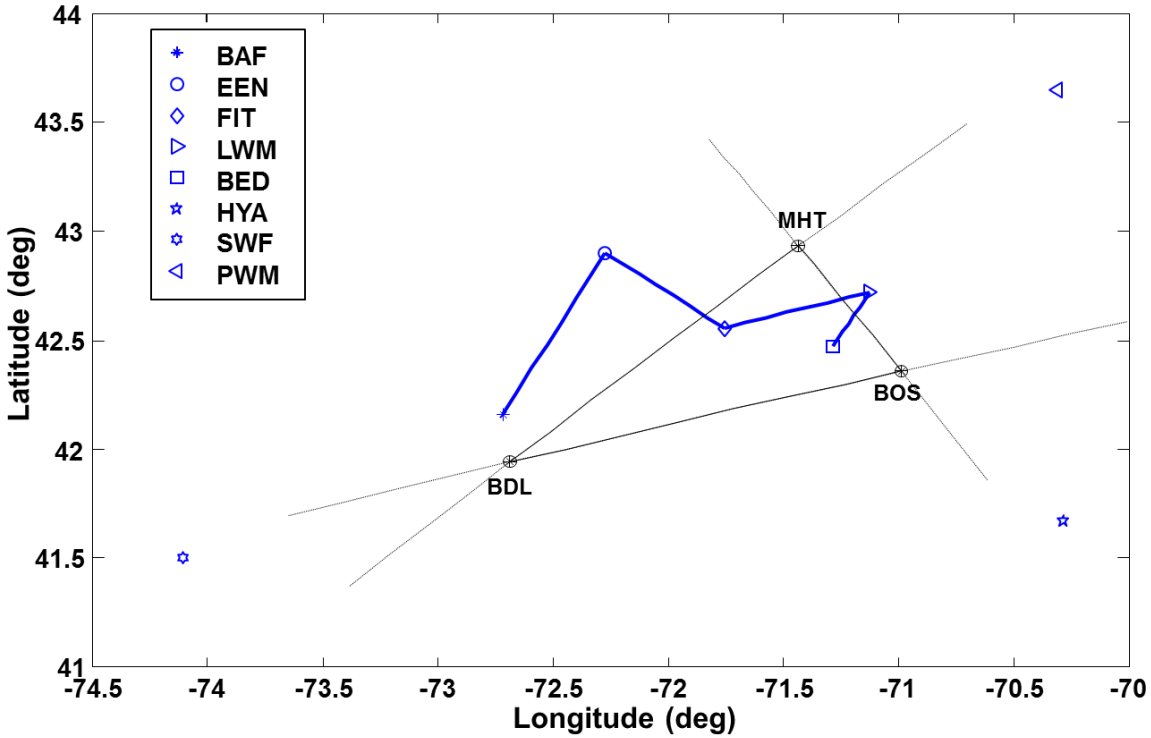

Figure 41 Hypothetical Three-Station WAM System and Flight Track

airports in the WAM system's service area, the negative root nearer to zero is the obvious correct choice. (The magnitude of other negative root is approximately an earth-radius.) In fact, the absolute values of the calculated correct roots are the slant-ranges used to generate the simulated measurements. For the three airports outside the service area, either negative root could be correct. Similar situations involving and ambiguous solutions occur in Examples 9 and 10.

Table 13 Roots for Aircraft Transmission Time, in NM, for Example 12

Aircraft	Root 1		Root 2		Root 3		Root 4	
Location	Real	Imag	Real	Imag	Real	Imag	Real	Imag
BAF	-4,002.6	0.0	-13.3	0.0	82.8	0.0	4,066.4	0.0
EEN	-4,748.8	0.0	-36.9	0.0	78.9	0.0	4,795.0	0.0
FIT	-6,361.5	0.0	-27.0	0.0	58.9	0.0	6,397.5	0.0
LWM	-4,022.4	0.0	-19.0	0.0	74.1	0.0	4,094.9	0.0
BED	-4,771.9	0.0	-15.1	0.0	86.0	0.0	4,812.5	0.0
HYA	-52.1	0.0	-29.5	0.0	106.1	-3,508.9	106.1	3,508.9
SWF	-68.7	0.0	-35.6	0.0	135.6	-1,072.8	135.6	1,072.8
PWM	-177.1	0.0	-65.3	0.0	211.6	-1,053.7	211.6	1,053.7

This example is re-visited in Subsection 8.5.6, where an ellipsoidal earth model is considered.

8. GAUSS-NEWTON NON-LINEAR LEAST-SQUARES (NLLS) METHOD

8.1 General NLLS Method

8.1.1 Background / Context

This final chapter is a fundamental departure from the previous chapters in several aspects. Situations addressed in Chapters 3-7 explicitly or implicitly assume that

- There are exactly as many measurements as there are unknown variables. There is no role for redundant measurements
- The measurements are described by equations that can be inverted to find the aircraft's coordinates (and/or other quantities of interest). There is no role for uninvertible expressions (often complex, involving recursion and/or tabular data).

One implication of the second limitation is that the problem's coordinate framework must be a spherical earth or a rectangular Cartesian system. An ellipsoidal earth framework does not provide for closed-form solutions. This chapter removes both of these restrictions, enabling more general situations to be addressed. It can be said that Chapters 3-7 provide analytic solutions to approximate problems, while this chapter provides numerical solutions to exact problems.

A drawback of the ability to address more general problems is that the techniques involved are iterative/numerical rather than analytic/closed-form. An important consequence is a loss of insight. For example, an iterative method does not reveal how many solutions may exist, or their nature (unique, extraneous, ambiguous, etc.). Moreover, iterative techniques require that an initial value be provided, which may be derived by an analytic method. Thus, there are useful roles for both closed-form and iterative techniques.

There are two basic alternatives for the coordinate system (framework) employed for the dependent navigation variables. When a spherical or ellipsoidal earth model is employed, the aircraft position variables are generally its latitude L_A and longitude λ_A, and possibly altitude h_A. When an earth-fixed rectangular coordinate system is used, the unknown aircraft position variables are usually its Cartesian components (x_A, y_A, z_A). Appendix Section 9.3 shows how to convert between these formulations for an ellipsoidal earth. When pseudorange measurements are involved, the time of transmission by the aircraft t_A (surveillance) or a set of ground station t_S (navigation) is also an unknown variable.

The coordinate system selection may be influenced by the measurements available. Analysis of a situation involving only slant-ranges (and/or slant-range differences) is often simpler using a rectangular Cartesian frame. Conversely, analysis of a situation involving only spherical-ranges (and/or their differences) and/or azimuth angles may be simpler using a spherical-earth frame.

However, either framework can be employed to analyze any measurement type.

In terms of mathematical methodologies, the Non-Linear Least Squares (NLLS) technique utilizes the linear algebra of vectors and matrices. The apparent contradiction in terminology (linear algebra used to solve a non-linear problem) arises because — rather than attack the non-linear problem directly — linear algebra is employed iteratively to solve a sequence of linear problems. In contrast, Chapters 3-4 and 6-7 solve multiple, non-linear scalar equations.

The NLLS methodology of this chapter applies to problems where the number of measurements n is equal to or exceeds the number of unknown variables p. The $n=p$ situation is often termed fully-determined; herein it is also referred to as the Newton situation. The $n>p$ situation is often termed over-determined; herein it is also referred to as the Gauss situation. The solution technique is independent of whether a Newton or Gauss situation is involved. However, the properties of the resulting solutions are different enough that a distinction is useful.

8.1.2 Problem Formulation

For specificity, in this section a spherical coordinate system is used for the unknown navigation variables. However, the basic technique also applies to a rectangular coordinate system. Thus the navigation variables are taken to be those immediately below, but other sets are possible.

$$\underline{\text{Example}}: \quad \mathbf{x} = [L_A \quad \lambda_A \quad h_A \quad t_X]^T \qquad \dim(\mathbf{x}) = p \qquad \text{Eq 349}$$

It is assumed that a set of measurements $\tilde{z}_i$ are available (combinations of slant-ranges, spherical-ranges, pseudo slant- and spherical-ranges, azimuth angles, etc.) which are of the form

$$\begin{aligned} \tilde{z}_i &= z_i + v_i \qquad i = 1, \cdots, n \\ z_i &= f_i(L_A, \lambda_A, h_A, t_X) = f_i(\mathbf{x}) \end{aligned} \qquad \text{Eq 350}$$

Here: (a) **x** denotes the vector of p unknown variables ($p=2, 3$ or 4 in this document); (b) n is the number of measurements (which must satisfy $n \geq p$); and (c) v_i is the measurement error that is usually present. When included, the time of transmission t_X may refer to either the aircraft (t_A, surveillance) or to a station (t_S, navigation).

The measurement errors are characterized by as having a zero-mean vector **v** and known covariance matrix **R**. Thus, all known biases have been removed from the measurements.

$$E(\mathbf{v}) = \mathbf{0} \qquad E(\mathbf{v}\mathbf{v}^T) = \mathbf{R} \qquad \text{Eq 351}$$

Eq 350 is termed the non-linear measurement model. Functions $f_i(L_A, \lambda_A, h_A, t_X)$ are known in the sense that they can be evaluated when the variables $(L_A, \lambda_A, h_A, t_X)$ are known. These functions need not be invertible; they can be combinations of analytic expressions, recursive

algorithms and tables. However, reasonably accurate analytic, differentiable approximations to $f_i(L_A, \lambda_A, h_A, t_X)$ must be known. For the range and angle measurements considered herein, plane and spherical geometry and trigonometry provide the required approximations.

8.1.3 Solution Approach

To find a solution, each unknown variable is expressed as the sum of an initial estimate for the iteration step involved, denoted here by an overbar, and a perturbation term, having **δ** as a prefix. For the first iteration step, the initial estimate must be provided (e.g., an approximate solution or previous position solution); for subsequent steps, the initial estimate is the updated value for the previous step. Thus,

$$\mathbf{x} = \bar{\mathbf{x}} + \boldsymbol{\delta}\mathbf{x} \qquad \text{Eq 352}$$

$$\bar{\mathbf{x}} = \begin{bmatrix} \bar{L}_A & \bar{\lambda}_A & \bar{h}_A & \bar{t}_X \end{bmatrix}^T \qquad \boldsymbol{\delta}\mathbf{x} = [\delta L_A \;\; \delta\lambda_A \;\; \delta h_A \;\; \delta t_X]^T$$

By linearizing the measurement functions $f_i(L_A, \lambda_A, h_A, t_X)$ — or analytic approximations thereto — about the initial values $\bar{\mathbf{x}}$, the scalar measurement $\tilde{z}_i$ can be replaced by the first-order (linearized) measurement

$$\begin{aligned} \delta z_i &\equiv \tilde{z}_i - f_i(\bar{L}_A, \bar{\lambda}_A, \bar{h}_A, \bar{t}_X) \\ &= \left.\frac{\partial f_i}{\partial L_A}\right|_{\bar{\mathbf{x}}} \delta L_A + \left.\frac{\partial f_i}{\partial \lambda_A}\right|_{\bar{\mathbf{x}}} \delta\lambda_A + \left.\frac{\partial f_i}{\partial h_A}\right|_{\bar{\mathbf{x}}} \delta h_A + \left.\frac{\partial f_i}{\partial t_X}\right|_{\bar{\mathbf{x}}} \delta t_X + v_i \end{aligned} \qquad \text{Eq 353}$$

In Eq 353, all partial derivatives are evaluated at the current estimate $\bar{\mathbf{x}}$ for the unknown variables. The quantity $\delta z_i = \tilde{z}_i - f_i(\bar{\mathbf{x}})$ is the measurement residual. An abnormally large residual can be the basis for rejecting a measurement as anomalous.

A quadratic scalar cost function *C* that quantifies the measurement residuals is chosen:

$$C = \boldsymbol{\delta}\mathbf{z}^T \mathbf{W}\, \boldsymbol{\delta}\mathbf{z} = (\mathbf{W}^{1/2}\boldsymbol{\delta}\mathbf{z})^T (\mathbf{W}^{1/2}\boldsymbol{\delta}\mathbf{z}) \qquad \text{Eq 354}$$

$$\boldsymbol{\delta}\mathbf{z} = \tilde{\mathbf{z}} - \mathbf{f}(\bar{\mathbf{x}}) = \tilde{\mathbf{z}} - \mathbf{f}(\bar{L}_A, \bar{\lambda}_A, \bar{h}_A, \bar{t}_X)$$

$$\boldsymbol{\delta}\mathbf{z} = [\delta z_1 \;\; \delta z_2 \cdots \delta z_n]^T \qquad \tilde{\mathbf{z}} = [\tilde{z}_1 \;\; \tilde{z}_2 \cdots \tilde{z}_n]^T \qquad \mathbf{f} = [f_1 \;\; f_2 \cdots f_n]^T$$

Here, $\mathbf{W} = \mathbf{W}^{1/2}\mathbf{W}^{1/2}$ is an analyst-defined positive semi-definite, symmetric matrix that weights the measurement equations. Common choices are: (1) $\mathbf{W} = \mathbf{I}$, the measurements are equally weighted; and (2) $\mathbf{W} = \mathbf{R}^{-1}$, the measurments are weighted by the inverse of the measurement error covariance matrix, to take account of unequal measurement accuracies and correlations between measurement pairs (Subsection 8.1.5).

The full set of equations for the linearized measurement model (Eq 353) can be written as

$$\begin{bmatrix} \delta z_1 \\ \vdots \\ \vdots \\ \delta z_n \end{bmatrix} = \begin{bmatrix} \frac{\partial f_1}{\partial L_A} & \frac{\partial f_1}{\partial \lambda_A} & \frac{\partial f_1}{\partial h_A} & \frac{\partial f_1}{\partial t_X} \\ \vdots & \vdots & \vdots & \vdots \\ \frac{\partial f_n}{\partial L_A} & \frac{\partial f_n}{\partial \lambda_A} & \frac{\partial f_n}{\partial h_A} & \frac{\partial f_n}{\partial t_X} \end{bmatrix} \begin{bmatrix} \delta L_A \\ \delta \lambda_A \\ \delta h_A \\ \delta t_X \end{bmatrix} + \begin{bmatrix} v_1 \\ \vdots \\ \vdots \\ v_n \end{bmatrix} \qquad \text{Eq 355}$$

Denoting the matrix of partial derivatives as **J** (for Jacobian*), Eq 355 can be written as the linearized matrix measurement model

$$\boldsymbol{\delta z = J\,\delta x + v}$$

$$\mathbf{J} = \begin{bmatrix} \frac{\partial f_1}{\partial L_A} & \frac{\partial f_1}{\partial \lambda_A} & \frac{\partial f_1}{\partial h_A} & \frac{\partial f_1}{\partial t_X} \\ \vdots & \vdots & \vdots & \vdots \\ \frac{\partial f_n}{\partial L_A} & \frac{\partial f_n}{\partial \lambda_A} & \frac{\partial f_n}{\partial h_A} & \frac{\partial f_n}{\partial t_X} \end{bmatrix} \qquad \mathbf{v} = \begin{bmatrix} v_1 \\ \vdots \\ \vdots \\ v_n \end{bmatrix} \qquad \text{Eq 356}$$

Informally, the estimation problem corresponding to Eq 356 is sometimes stated as: "find the value for **δx** that best satisfies"

$$\mathbf{J}\,\boldsymbol{\delta x} \approx \boldsymbol{\delta z} \qquad \text{Eq 357}$$

In general, matrix **J** is non-square and cannot be inverted.

8.1.4 Iterative Solution Process

Cost Function — The standard approach to addressing Eq 357 is to compute the value of **δx** that minimizes the weighted sum of the squared measurement residuals after being adjusted by based on a the linear model of Eq 356. Thus, denoting $\widehat{C}$ as the cost function after adjustment, **δx** is selected to minimize:

$$\begin{aligned} \min_{\boldsymbol{\delta x}} \widehat{C} &= (\boldsymbol{\delta z} - \mathbf{J}\,\boldsymbol{\delta x})^T \mathbf{W} (\boldsymbol{\delta z} - \mathbf{J}\,\boldsymbol{\delta x}) \\ &= \boldsymbol{\delta z}^T \mathbf{W} \boldsymbol{\delta z} - 2\boldsymbol{\delta x}^T \mathbf{J}^T \mathbf{W}\,\boldsymbol{\delta z} + \boldsymbol{\delta x}^T \mathbf{J}^T \mathbf{W}\,\mathbf{J}\,\boldsymbol{\delta x} \end{aligned} \qquad \text{Eq 358}$$

Normal Equations — Taking the derivative of the right-hand side of Eq 358 with respect to **δx** and setting the result equal to zero yields the well-known Normal Equation(s). Here, consistent with convention, $\boldsymbol{\delta \hat{x}}$ denotes the solution to the Normal Equations

$$\left(\mathbf{J}^T \mathbf{W}\,\mathbf{J}\right) \boldsymbol{\delta \hat{x}} = \mathbf{J}^T \mathbf{W}\,\boldsymbol{\delta z} \qquad \text{Eq 359}$$

General Estimator — The value for **δx** that minimizes $\widehat{C}$ in Eq 358 is

* Carl Gustav Jacob Jacobi (Dec. 10, 1804 – Feb. 18, 1851) was a German mathematician.

$$\boldsymbol{\delta\hat{x}} = \left(\mathbf{J}^T\mathbf{W}\,\mathbf{J}\right)^{-1}\mathbf{J}^T\mathbf{W}\,\boldsymbol{\delta z} = \mathbf{K}\,\boldsymbol{\delta z}$$
$$\mathbf{K} = \left(\mathbf{J}^T\mathbf{W}\,\mathbf{J}\right)^{-1}\mathbf{J}^T\mathbf{W} = \left[\left(\mathbf{W}^{½}\mathbf{J}\right)^T\left(\mathbf{W}^{½}\mathbf{J}\right)\right]^{-1}\left(\mathbf{W}^{½}\mathbf{J}\right)^T\mathbf{W}^{½} \qquad \text{Eq 360}$$

Matrix $\mathbf{K} = \left(\mathbf{J}^T\mathbf{W}\,\mathbf{J}\right)^{-1}\mathbf{J}^T\mathbf{W}$ is called the estimator matrix. Existence of the matrix inverse indicated in Eq 360 requires that $\mathbf{W}^{½}\,\mathbf{J}$ be of full rank, i.e., to have linearly independent columns. Thus **J** must have linearly independent columns. (That is, every unknown variable must affect the measurements, taken as a group, differently.)

Optimal Estimator — For the estimator in Eq 360, the variance of the estimation error, i.e., of the difference $\boldsymbol{\delta\hat{x}} - \boldsymbol{\delta x}$, is smallest when $\mathbf{W} = \mathbf{R}^{-1}$ (see Eq 365 and Eq 366). Thus, the optimal estimator is

$$\boldsymbol{\delta\hat{x}} = \left(\mathbf{J}^T\mathbf{R}^{-1}\mathbf{J}\right)^{-1}\mathbf{J}^T\mathbf{R}^{-1}\,\boldsymbol{\delta z} = \mathbf{K}\,\boldsymbol{\delta z}$$
$$\mathbf{K} = \left(\mathbf{J}^T\mathbf{R}^{-1}\mathbf{J}\right)^{-1}\mathbf{J}^T\mathbf{R}^{-1} \qquad \text{Eq 361}$$

Newton Estimator — For the situation where the number of measurements is the same as the number of unknown variables, Eq 360 and Eq 361 reduce to Eq 362 below, which is the Newton form of the estimator. In such situations, there is no role for a weighting matrix **W**.

$$\boldsymbol{\delta\hat{x}} = \mathbf{J}^{-1}\,\boldsymbol{\delta z} = \mathbf{K}\,\boldsymbol{\delta z} \qquad \dim(\mathbf{x}) = \dim(\mathbf{z})$$
$$\mathbf{K} = \mathbf{J}^{-1} \qquad \text{Eq 362}$$

It is possible to implement Eq 360 or Eq 361 for all situations where $n = \dim(\mathbf{z}) \geq p = \dim(\mathbf{x})$. Then when $n = p$, such an implementation will be algebraically equivalent to Eq 362. Thus, a least-squares approximation will not actually be involved; however, that would not necessarily be obvious to the analyst.

Update Estimate for Variables — Given the estimate for the perturbation, $\boldsymbol{\delta\hat{x}}$, the estimates of the unknown variables are updated in accordance with

$$\hat{\mathbf{x}} = \bar{\mathbf{x}} + \boldsymbol{\delta\hat{x}} \qquad \text{Eq 363}$$

$$\hat{L}_A = \bar{L}_A + \delta\hat{L}_A \qquad \hat{\lambda}_A = \bar{\lambda}_A + \delta\hat{\lambda}_A \qquad \hat{h}_A = \bar{h}_A + \delta\hat{h}_A \qquad \hat{t}_X = \bar{t}_X + \delta\hat{t}_X$$

Iteration Process Summary

0. The initial estimate for the independent variables, $\hat{\mathbf{x}}_0$, must be provided.

After completing an iteration (say, *k*), the process is repeated for iteration *k*+1:

1. Assign the updated values for the independent variables found in the previous step to $\bar{\mathbf{x}}_{k+1}$ —i.e., set $\bar{\mathbf{x}} \equiv \bar{\mathbf{x}}_{k+1} = \hat{\mathbf{x}}_k$.
2. Evaluate the measurement residual $\boldsymbol{\delta z}$ using $\bar{\mathbf{x}}$ (Eq 354)

3. Optional: Examine the components of $\boldsymbol{\delta z}$ and determine/reject outliers, if present
4. Optional/recommended: Compute the cost function *C* using $\boldsymbol{\delta z}$ (Eq 354)
5. Compute the Jacobian matrix $\mathbf{J}$ for $\bar{\mathbf{x}}$ (Eq 356)
6. Compute the estimated perturbation vector $\boldsymbol{\delta}\hat{\mathbf{x}} = \boldsymbol{\delta}\hat{\mathbf{x}}_{k+1}$ (Eq 360, Eq 361 or Eq 362)
7. Update the estimate of the variables sought $\hat{\mathbf{x}} = \hat{\mathbf{x}}_{k+1}$ (Eq 363)
8. Examine $\boldsymbol{\delta}\hat{\mathbf{x}}_{k+1} = \hat{\mathbf{x}}_{k+1} - \hat{\mathbf{x}}_k$, and possibly other quantities, and decide among:
   (1) Convergence to the correct solution is occurring and the iteration process should continue;
   (2) Convergence to the correct solution has occurred and the process should be stopped;
   (3) Convergence to an incorrect solution is occurring and the process should be stopped
   (4) Divergence is occurring and the process should be stopped.

Possibilities (3) and (4) are addressed in Subsection 8.1.7.

Computing Cost Function — While not required, it is recommended that the cost function (item 4) be computed during each interation. Since the measurement residuals are available (item 2) there is little added effort and the cost function provides information on the nature of the solution being computed. For a Newton estimator, the cost function 'should' converge to zero. If it does not, then there may be an inconsistency in the measurement equations (a solution may not exist) or the initial estimate may be 'too far' from the solution. For a Gauss estimator, one expects the statistics of the cost function to be related to the measurement errors.

Minimum Number of Iterations — If the measurement functions $\mathbf{f}(\mathbf{x})$ depend nonlinearly on the unknown variables (virtually always the case for navigation and surveillance applications), at least two iterations should be performed. The final iteration confirms that the changes in the values of the variables sought are negligible.

8.1.5 Solution Properties

Overview — Linear Least Squares (LLS), also called linear regression, is perhaps the most widely used statistical technique, and consequently has a rich literature. LLS characteristics/ properties, which apply to each iteration of the NLLS approach, are summarized first. Characteristics of the NLLS solution (i.e., upon convergence) are then provided.

Numerical Solution of the Normal Equation — The Normal Equation (Eq 359) has been called the defining equation of the Gauss-Newton technique (Ref. 56). One viewpoint is that the cost function of Eq 354 is simply a rationale for generating the Normal Equation. The iteration process described above can be performed without computing the value for a cost function.

Methods are available for solving the Normal Equation that are more numerically stable than computing the inverse of the matrix on the left-hand side of Eq 359. Perhaps the best approach is

to perform orthogonal decomposition on $\mathbf{W}^{½}\mathbf{J}$ (i.e., utilize the antecedent of Eq 359, similar to Eq 357). Some software packages have this capability.

General Estimator Error Covariance — If the expression in Eq 356 is substituted into Eq 360, the result is

$$\boldsymbol{\delta}\hat{\mathbf{x}} = \boldsymbol{\delta}\mathbf{x} + \left(\mathbf{J}^T\mathbf{W}\mathbf{J}\right)^{-1}\mathbf{J}^T\mathbf{W}\mathbf{v} \qquad \text{Eq 364}$$

Thus, in the context of the linearized measurement model, $\boldsymbol{\delta}\hat{\mathbf{x}}$ from Eq 360 is an unbiased estimate of $\boldsymbol{\delta}\mathbf{x}$ and is corrupted only by measurement errors. The covariance matrix of the estimation error for the general estimator is

$$E\left(\boldsymbol{\delta}\hat{\mathbf{x}} - \boldsymbol{\delta}\mathbf{x}\right)\left(\boldsymbol{\delta}\hat{\mathbf{x}} - \boldsymbol{\delta}\mathbf{x}\right)^T = \left(\mathbf{J}^T\mathbf{W}\mathbf{J}\right)^{-1}\mathbf{J}^T\mathbf{W}\mathbf{R}\mathbf{W}\mathbf{J}\left(\mathbf{J}^T\mathbf{W}\mathbf{J}\right)^{-1} \qquad \text{Eq 365}$$

Optimal Estimator Error Covariance — It can be shown (Ref. 57, Section 6.7) that, when the measurement error covariance matrix $\mathbf{R}$ is invertible, the estimation error covariance for the unknown variables (Eq 365) has a lower bound of $\left(\mathbf{J}^T\mathbf{R}^{-1}\mathbf{J}\right)^{-1}$ and this lower bound is achieved when and only when $\mathbf{W} = \mathbf{R}^{-1}$. Thus, when $\mathbf{R}^{-1}$ exists, the optimal estimator's error covariance matrix is

$$E\left(\boldsymbol{\delta}\hat{\mathbf{x}} - \boldsymbol{\delta}\mathbf{x}\right)\left(\boldsymbol{\delta}\hat{\mathbf{x}} - \boldsymbol{\delta}\mathbf{x}\right)^T = \left(\mathbf{J}^T\mathbf{R}^{-1}\mathbf{J}\right)^{-1} \qquad \text{Eq 366}$$

When $\mathbf{R}$ is not invertible, for some combinations of $\mathbf{J}$, $\mathbf{R}$, and $\mathbf{W}$ the right-hand side of Eq 365 reduces to an expression of the form $\left(\mathbf{J}^T\mathbf{Q}\mathbf{J}\right)^{-1}$ where $\mathbf{Q}$ is positive semi-definite. Subsection 8.4.4 provides an example.

Newton Estimator Error Covariance — If the number of measurements and unknown variables are equal, then $\mathbf{J}$ is square and must be invertible for a solution to exist. That being the case, the error covariance for estimator of Eq 362 becomes

$$E\left(\boldsymbol{\delta}\hat{\mathbf{x}} - \boldsymbol{\delta}\mathbf{x}\right)\left(\boldsymbol{\delta}\hat{\mathbf{x}} - \boldsymbol{\delta}\mathbf{x}\right)^T = \mathbf{J}^{-1}\mathbf{R}\mathbf{J}^{-T} = \left(\mathbf{J}^T\mathbf{R}^{-1}\mathbf{J}\right)^{-1} \qquad \dim(\mathbf{x}) = \dim(\mathbf{z}) \qquad \text{Eq 367}$$

Existence of the right-most expression in Eq 367, $\left(\mathbf{J}^T\mathbf{R}^{-1}\mathbf{J}\right)^{-1}$, requires that $\mathbf{R}$ be invertible. In such situations, the Newton estimator's error covariance has the same form as that for the optimal estimator when redundant measurements are available. In contrast, the directly-derived expression $\mathbf{J}^{-1}\mathbf{R}\mathbf{J}^{-T}$ does not require $\mathbf{R}$ to be invertible, and addresses situations involving both error-corrupted and perfect measurements.

Uncorrelated Similar Measurements — For situations where the measurement errors can be considered to be uncorrelated with a common variance σ^2_{meas} (typically a situation involving similar stations for a single system such as GPS), both Eq 366 and Eq 367 reduce to (where $\mathbf{I}_n$ is the nxn identity matrix)

$$E(\boldsymbol{\delta}\hat{\mathbf{x}} - \boldsymbol{\delta}\mathbf{x})(\boldsymbol{\delta}\hat{\mathbf{x}} - \boldsymbol{\delta}\mathbf{x})^T = \left(\mathbf{J}^T\mathbf{J}\right)^{-1}\sigma_{meas}^2 \qquad \mathbf{R} = \sigma_{meas}^2\,\mathbf{I}_n \qquad \text{Eq 368}$$

Linearized Model Residuals — During each iteration, after $\boldsymbol{\delta}\hat{\mathbf{x}}$ has been found from Eq 360 (the general estimator), the difference between $\tilde{\mathbf{z}}$ its updated residual value is

$$\tilde{\mathbf{z}} - [\mathbf{f}(\bar{\mathbf{x}}) + \mathbf{J}\,\boldsymbol{\delta}\hat{\mathbf{x}}] = [\tilde{\mathbf{z}} - \mathbf{f}(\bar{\mathbf{x}})] - \mathbf{J}\,\boldsymbol{\delta}\hat{\mathbf{x}} = \left[\mathbf{I}_n - \mathbf{J}\left(\mathbf{J}^T\mathbf{W}\,\mathbf{J}\right)^{-1}\mathbf{J}^T\mathbf{W}\right]\boldsymbol{\delta}\mathbf{z} \qquad \text{Eq 369}$$

Eq 369 provides an estimate for (but is not equal to) the residual measurement error for the non-linear model, $\tilde{\mathbf{z}} - \mathbf{f}(\hat{\mathbf{x}})$.

It is often expected that the updated residual measurement vector of Eq 369 will have components that are statistically similar, and tests have been developed for identifying 'large' residuals. Examination of residuals has been tailored for GPS, a system that usually provides more than the minimum required number of measurements needed for a fix.

Projection Matrix — The matrix **P** defined in Eq 370 — or when **W** is proportional to $\mathbf{I}_n$, by $\mathbf{P} \equiv \mathbf{J}\left(\mathbf{J}^T\mathbf{J}\right)^{-1}\mathbf{J}^T$ — is termed the projection matrix for the Jacobian matrix **J**.

$$\mathbf{P} \equiv \mathbf{J}\left(\mathbf{J}^T\mathbf{W}\mathbf{J}\right)^{-1}\mathbf{J}^T\mathbf{W} = \mathbf{J}\left[\left(\mathbf{W}^{½}\mathbf{J}\right)^T\left(\mathbf{W}^{½}\mathbf{J}\right)\right]^{-1}\left(\mathbf{W}^{½}\mathbf{J}\right)^T\mathbf{W}^{½} \qquad \text{Eq 370}$$

In Statistics, **P** is sometimes called the influence (or, informally, the hat) matrix. Matrix **P** projects the measurement residuals onto the column space of **J**. (This can be proved using singular value decomposition.) Thus, $\mathbf{I}_n$ **- P** projects onto the space which is orthogonal to the column space of **J**.

Formally, matrix **P** is idempotent, $\mathbf{P}\mathbf{P} = \mathbf{P}$, and satisfies $\mathbf{P}\mathbf{J} = \mathbf{J}$. Both are necessary conditions for **P** to be a projection matrix for **J**. Similarly, $\mathbf{I}_n$ **- P** is idempotent and satisfies $(\mathbf{I}_n - \mathbf{P})\mathbf{J} = \mathbf{0}$. Matrix $\mathbf{W}\mathbf{P} = (\mathbf{W}\mathbf{P})^T = \mathbf{P}^T\mathbf{W}$ is symmetric. It follows that $\mathbf{W}\mathbf{P} = \mathbf{W}\mathbf{P}\mathbf{P} = (\mathbf{W}\mathbf{P})^T\mathbf{P} = \mathbf{P}^T\mathbf{W}\mathbf{P}$ and $\mathbf{W}[\mathbf{I}-\mathbf{P}] = [\mathbf{I}-\mathbf{P}]^T\mathbf{W}[\mathbf{I}-\mathbf{P}]$ **P** is symmetric when **W** is proportional to **I**. When **J** is square and invertible, **P** becomes the identity matrix.

Estimator Matrix — The estimator matrix **K** (Eq 360, Eq 361 and Eq 362) always satisfies $\mathbf{K}\mathbf{J} = \mathbf{I}_p$ (where $\mathbf{I}_p$ is the $p \times p$ identity matrix). Thus **K** is one form of an inverse of **J** — the unique, true inverse when **J** is square, or a non-unique left-inverse when **J** is not square. This situation is consistent with $\boldsymbol{\delta}\hat{\mathbf{x}} = \mathbf{K}\,\boldsymbol{\delta}\mathbf{z}$ being a 'best solution' to Eq 357.

A physical interpretation of **K** is readily available for a system utilizing (a) a Cartesian coordinate formulation and (b) uncorrelated slant-range measurements. In that case (Subsection 8.4.3), the rows of **J** are unit vectors $\mathbf{u}_{iA}$ from each station **S***i* to the assumed location of the aircraft **A** (embedded in $\bar{\mathbf{x}}$). Thus **K** and $\boldsymbol{\delta}\hat{\mathbf{x}}$ can be thought of as the products of two factors

$$\boldsymbol{\delta\hat{\mathbf{x}}} = \left(\mathbf{J}^T\mathbf{J}\right)^{-1}\mathbf{J}^T\boldsymbol{\delta\mathbf{z}} = \left(\mathbf{J}^T\mathbf{J}\right)^{-1}\sum_i \delta z_i\,\mathbf{u}_{iA} \qquad \text{Eq 371}$$

On the right-hand side of Eq 371, the summation involves the station-aircraft unit vectors scaled by the associated measurement residuals δz_i (the differences between the measured ranges to the aircraft and the calculated ranges based on its assumed location $\bar{\mathbf{x}}$). The factor $\left(\mathbf{J}^T\mathbf{J}\right)^{-1}$ converts coordinatized range residuals into incremental position values. In effect, multiplication by $\left(\mathbf{J}^T\mathbf{J}\right)^{-1}$ removes the correlations in the components of $\mathbf{J}^T\boldsymbol{\delta\mathbf{z}}$.

Estimated Cost Function Reduction — Using $\mathbf{P}$, Eq 369 can be written

$$\tilde{\mathbf{z}} - [\mathbf{f}(\bar{\mathbf{x}}) + \mathbf{J}\,\boldsymbol{\delta\hat{\mathbf{x}}}] = [\tilde{\mathbf{z}} - \mathbf{f}(\bar{\mathbf{x}})] - \mathbf{J}\,\boldsymbol{\delta\hat{\mathbf{x}}} = [\mathbf{I} - \mathbf{P}]\boldsymbol{\delta\mathbf{z}} \qquad \text{Eq 372}$$

Thus, invoking $\mathbf{WP}=\mathbf{P}^T\mathbf{WP}$, $\widehat{C}$ in Eq 358 evaluates to

$$\begin{aligned}\widehat{C} &= \boldsymbol{\delta\mathbf{z}}^T[\mathbf{I} - \mathbf{P}]^T\mathbf{W}[\mathbf{I} - \mathbf{P}]\boldsymbol{\delta\mathbf{z}} \\ &= \boldsymbol{\delta\mathbf{z}}^T\mathbf{W}\boldsymbol{\delta\mathbf{z}} - (\mathbf{P}\,\boldsymbol{\delta\mathbf{z}})^T\mathbf{W}(\mathbf{P}\,\boldsymbol{\delta\mathbf{z}})\end{aligned} \qquad \text{Eq 373}$$

The second line of Eq 373 shows that $\widehat{C}$ is the difference between the weighted sum of the squared residuals before updating and the estimated amount, $(\mathbf{P}\,\boldsymbol{\delta\mathbf{z}})^T\mathbf{W}(\mathbf{P}\,\boldsymbol{\delta\mathbf{z}})$, that the residual would be reduced based on a linear model estimate $\boldsymbol{\delta\hat{\mathbf{x}}}$. The first line shows that $\widehat{C}$ must be non-negative (Ref. 57).

When the number of equations is equal to the number of unknowns, since $\mathbf{J}$ must be invertible in that situation, $\widehat{C}$ is equal to zero for each iteration. This is the multi-dimensional version of the characteristic behavior of the Newton-Raphson algorithm.

Equating the two lines of Eq 373 shows that pre-update and post-update residuals for the linear model are related by a version of Pythagoras's theorem. This relationship is well-known in statistics.

$$\boldsymbol{\delta\mathbf{z}}^T\mathbf{W}\boldsymbol{\delta\mathbf{z}} = (\mathbf{P}\,\boldsymbol{\delta\mathbf{z}})^T\mathbf{W}(\mathbf{P}\,\boldsymbol{\delta\mathbf{z}}) + \boldsymbol{\delta\mathbf{z}}^T[\mathbf{I} - \mathbf{P}]^T\mathbf{W}[\mathbf{I} - \mathbf{P}]\boldsymbol{\delta\mathbf{z}} \qquad \text{Eq 374}$$

Orthogonality of Estimate and Updated Residual — Using Eq 370 for $\mathbf{P}$ and Eq 360 for $\boldsymbol{\delta\hat{\mathbf{x}}}$ (and invoking $\mathbf{WP}=\mathbf{P}^T\mathbf{WP}$) yields

$$\begin{aligned}\mathbf{J}\,\boldsymbol{\delta\hat{\mathbf{x}}} &= \mathbf{P}\,\boldsymbol{\delta\mathbf{z}} \qquad & \boldsymbol{\delta\mathbf{z}} - \mathbf{J}\,\boldsymbol{\delta\hat{\mathbf{x}}} &= [\mathbf{I} - \mathbf{P}]\boldsymbol{\delta\mathbf{z}} \\ (\boldsymbol{\delta\mathbf{z}} - \mathbf{J}\,\boldsymbol{\delta\hat{\mathbf{x}}})^T\mathbf{W}\mathbf{J}\,\boldsymbol{\delta\hat{\mathbf{x}}} &= \boldsymbol{\delta\mathbf{z}}^T[\mathbf{I} - \mathbf{P}]^T\mathbf{W}\mathbf{P}\,\boldsymbol{\delta\mathbf{z}} = 0\end{aligned} \qquad \text{Eq 375}$$

The second line of Eq 375 is interpreted as stating that the vectors $\boldsymbol{\delta\mathbf{z}} - \mathbf{J}\,\boldsymbol{\delta\hat{\mathbf{x}}}$ and $\mathbf{J}\,\boldsymbol{\delta\hat{\mathbf{x}}}$ are orthogonal after each iteration. Thus, in the context of linear algebra, there no information remaining in $\boldsymbol{\delta\mathbf{z}}$ that can be used to improve the estimate $\boldsymbol{\delta\hat{\mathbf{x}}}$. When/if convergence is achieved and $\boldsymbol{\delta\hat{\mathbf{x}}} = \mathbf{0}$, the residual measurement error $\boldsymbol{\delta\mathbf{z}} = \tilde{\mathbf{z}} - \mathbf{f}(\bar{\mathbf{x}})$ is in the null space of $\mathbf{P}$, or

equivalently, orthogonal to the column space of **J**.

Using Eq 375, an alternate to Eq 373 for computing $\widehat{C}$ is

$$\widehat{C} = (\boldsymbol{\delta z} - \mathbf{J}\boldsymbol{\delta \hat{x}})^T \mathbf{W}\,\boldsymbol{\delta z} = \boldsymbol{\delta z}^T \mathbf{W}\boldsymbol{\delta z} - \boldsymbol{\delta \hat{x}}^T \mathbf{J}^T \mathbf{W}\boldsymbol{\delta z} \qquad \text{Eq 376}$$

Equivalence of NLLS to Newton and Gauss Solutions — Combining Eq 354, Eq 362 and Eq 363 for the Newton estimator yields

$$\hat{\mathbf{x}} = \overline{\mathbf{x}} + \mathbf{J}^{-1}[\tilde{\mathbf{z}} - \mathbf{f}(\overline{\mathbf{x}})] \qquad \dim(\mathbf{z}) = \dim(\mathbf{x}) \qquad \text{Eq 377}$$

Eq 377 is the multi-dimensional Newton-Raphson formula for solving $\tilde{\mathbf{z}} = \mathbf{f}(\mathbf{x})$ by iteration. It applies when the number of measurements is equal to the number of unknown variables — a common situation in navigation and surveillance applications.

Combining Eq 354, Eq 360 and Eq 363 for the general estimator yields

$$\hat{\mathbf{x}} = \overline{\mathbf{x}} + \left(\mathbf{J}^T\mathbf{W}\mathbf{J}\right)^{-1}\mathbf{J}^T\mathbf{W}[\tilde{\mathbf{z}} - \mathbf{f}(\overline{\mathbf{x}})] \qquad \dim(\mathbf{z}) > \dim(\mathbf{x}) \qquad \text{Eq 378}$$

Eq 378 is the Gauss-Newton formula for solving $\tilde{\mathbf{z}} \approx \mathbf{f}(\mathbf{x})$ by iteration, and applies when the number of measurements *n* exceeds the number of unknown variables *p*.

In contrast to Eq 377 and Eq 378, the solutions of Chapters 3-7 can be written $\mathbf{x} = \mathbf{f}^{-1}(\tilde{\mathbf{z}})$ in the vector/matrix notation employed in this chapter. In Chapters 3-7, by taking advantage of the structure of specific problems, the measurement equations can be inverted.

Measurement Residual at Convergence — Assuming that the iteration process described in Subsection 8.1.4 converges, the solution $\boldsymbol{\delta \hat{x}}$ to the Normal Equation Eq 359 becomes a *p*-length null vector. However, the associated conditions imposed on the measurement residual vector $\boldsymbol{\delta z}$ for the Newton and Gauss solutions are different.

Newton Solution — When the number of measurements *n* equals the number of unknown variables *p*, if the iterative solution process converges the residual measurement $\boldsymbol{\delta z}$ becomes a *p*-length null vector. Equivalently, the equation $\tilde{\mathbf{z}} = \mathbf{f}(\overline{\mathbf{x}})$ is satisfied. In this case, an approximation employed for the Jacobian matrix **J** need not be very accurate. This situation is analogous to employing the secant method for finding the root of a scalar equation using approximations to the derivative of the equation (Subsection 2.1.8). In some situations, the equation $\tilde{\mathbf{z}} = \mathbf{f}(\overline{\mathbf{x}})$ cannot be satisfied and convergence does not occur.

Gauss Solution — When the number of measurements *n* exceeds the number of unknown variables *p*, if the iterative solution process converges, the product $\mathbf{J}^T\,\mathbf{W}\,\boldsymbol{\delta z} = \left(\mathbf{W}^{½}\mathbf{J}\right)^T\left(\mathbf{W}^{½}\boldsymbol{\delta z}\right)$ must be a *p*-length null vector (Eq 360). Equivalently, the inner (dot) product of every column of $\mathbf{W}^{½}\mathbf{J}$ and the vector $\mathbf{W}^{½}\boldsymbol{\delta z}$ is the scalar zero. Thus, unlike the Newton solution: (a) $\boldsymbol{\delta z}$ is not

driven to the null vector, and (b) the choices for **W** and **J** may affect the solution. After convergence, the derivative of the cost function (Eq 354) satisfies

$$\frac{\partial C}{\partial \mathbf{x}} = -2\,\mathbf{J}^T\,\mathbf{W}\,\boldsymbol{\delta}\mathbf{z} = -2\left(\mathbf{W}^{½}\mathbf{J}\right)^T\left(\mathbf{W}^{½}\boldsymbol{\delta}\mathbf{z}\right) = 0 \qquad n > p\text{ , at convergence} \qquad \text{Eq 379}$$

The fact that the Newton and Gauss solutions satisfy different conditions can lead to an apparent contradiction. If one has error-free measurements and $n = p$, then the Newton solution will yield the exact aircraft location although an approximate Jacobian matrix is used. However, if additional error-free measurements are available, then the Gauss solution may be in error due to the use of an approximate Jacobian matrix.

Utilizing Perfect Measurements — The Newton estimator (Eq 362) does not take account of measurement errors, and can utilize measurements which are treated as perfect (i.e., have zero error) without modification. However, when redundant measurements are available, the optimal estimator (Eq 361) utilizes the inverse of measurement error covariance $\mathbf{R}^{-1}$ as the weighting matrix, and thus cannot utilize perfect measurements *per se*. There are several ways to address situations involving assumed-perfect measurements and $n > p$:

- Use the general estimator with a weight matrix **W** that has a positive diagonal element for the perfect measurement that is much larger than the other diagonal elements. Although inelegant, this method is simple to implement and is always available.
- Recast the minimization problem of Eq 358, treating the perfect measurement as a constraint that's handled using a Lagrange multiplier. This method requires slightly more effort to implement, and is described in Appendix Section 9.5. It is not often used in navigation or surveillance systems.
- Discard as many measurements as necessary to arrive at a situation where the number of measurements is equal to the number of variables. Presumably, the discarded measurements are less accurate and/or redundant relative to the measurements retained. Then use the Newton estimator. While not desirable, this method is always available.
- Choose a coordinate framework such that the perfectly measured quantity is one of the variables sought. The problem can be then be recast with that variable as a known parameter. This method is not always available, but is available for a common aviation situation — the aircraft's altimeter measurement is considered to be error-free. In such situations, the spherical earth framework is used.

While a measurement may be treated as error-free when computing the unknown variables, it need not be considered to be error-free when computing their estimation error covariance.

8.1.6 Advantages

Uses All Measurements — An important reason for employing the NLLS technique is to be

able to utilize all measurements — i.e., all types (see next two paragraphs) and a greater number than there are unknown variables. Using redundant equations has several advantages: (1) enables averaging of measurement errors, (2) usually eliminates ambiguous/extraneous solutions that can occur with the minimum required number of measurements, and (3) generally reduces the accuracy needed for the initial estimate in order to avoid divergence during the iteration process.

Utilizes Uninvertible Measurement Equations — While all of the measurement equations in Chapters 3-7 are analytically invertible (i.e., expressions exist for the unknown variables as functions of the known quantities), invertibility is not always possible. Thus, another important reason for utilizing the NLLS approach is its capability to utilize measurement equations that cannot be inverted. Such situations can arise because a set of analytic expression that accurately characterize the measurements is too complex to be inverted. But there are other reasons as well.

Utilize Measurements Lacking an Analytic Expression — The measurement equations — symbolized by $f_i(L_A, \lambda_A, h_A, t_X)$ in Eq 350 — are the most accurate available representation of the quantities that are measured. Since invertibility is not required, these 'equations' need not be analytic expressions. What is required is the capability to compute numerical values, for a given set of values for the independent variables, for each measured quantity (e.g., aircraft-station range or signal time-of-arrival). Combinations of complex analytic expressions, numerical algorithms (such as Vincenty's) and lookup tables have been used in measurement 'equations'.

Approximate Jacobians Are Useful — The elements of the Jacobian matrix (**J** in Eq 356) need not be precisely equal to the partial derivatives of the measurement equations (which may not even have analytic expressions for its derivatives). In navigation and surveillance applications, the natural sources of such approximations are the plane and spherical geometry and trigonometry that describes most measurements (Subsection 8.3.2). The analyst should be aware that, in the over-determined / Gauss situation ($n > p$), the choices for both the weight matrix **W** and the Jacobian matrix **J** may affect the solution — see Subsection 8.1.5 (Eq 379). However, use of the spherical earth approximation for the elements of **J**, when an ellipsoid earth model is used for the measurement equations, is common practice and appears to have a negligible effect on solution accuracy (Subsection 8.5.7).

Provides Accuracy/Error Estimates — An important characteristic of the NLLS technique is that it provides expressions for both (a) the unknown navigation variables and (b) the variance of the estimation error of those variable. These quantities are computed separately — one is not needed to find the other. The methods addressed in Chapters 3-7 do not provide characterizations of the sensitivity of their solutions to various parameters.

Estimates of aircraft position error sensitivity to aircraft location, station types/locations and

measurement error statistics are needed to understand a system's capabilities. They are often used in planning studies to assess the feasibility of a proposed new system or modification. Since measurement error statistics are usually not regarded as having the same precision as position solutions, characterizing the earth as an ellipsoid is usually not necessary in planning studies.

Useful/Proven Optimization Criterion — When there are more measurements than unknown variables, there is no single best way to combine the equations. In addition to the above-cited advantages, the case for the NLLS technique largely rests on four points: (1) it's logical to weight the equations in accordance with their expected accuracy; (2) the NLLS technique is analytically tractable, involving recursive solution of linear equations based on (possibly approximate) first derivatives of the measurement equations but not requiring their second derivatives; (3) when the number measurements and unknowns are equal, the NLLS technique reduces to Newton's method for finding the roots of a set of equations, a technique which is over 350 years old and still in common use; and (4) the Gauss method for utilizing redundant measurements has proven to be a useful in a wide variety of applications for over 200 years.

A case study of several optimization techniques (Ref. 50) concluded that — for a navigation application — the NLLS technique always yields a 'good', and often the 'best' solution for the techniques considered. Several important radio navigation systems have been deployed with the presumption that users would employ the NLLS technique or an evolved form of it (e.g., Kalman Filter) to convert a set of measurements to latitude/longitude coordinates. Examples include Loran-C, Omega and GPS.

8.1.7 Disadvantages

Lack of Physical Insight — The primary disadvantage of the Gauss-Newton NLLS technique is that it provides only limited insight into the properties/limitations of the problem involved, especially those that are related to the geometry. With the NLLS technique, the measurement equations are considered individually, while the solution methods addressed in previous chapters consider the measurements as a group. By inverting the measurement equations simultaneously, the properties of the solution can be ascertained. The most important of these are:

- Existence — Can a solution be found from the measurements available? For what parts of the area near the sensors does a solution exist/not exist?
- Uniqueness — Given a set of measurements, is there more than one solution? What parts of the area near the sensors has an ambiguous and/or extraneous solution?

These properties are illustrated in Figure 26 and Figure 31. Lack of problem insight does not imply that such properties are not a concern. (The Jacobian matrix and DoP matrix, which is a function of the Jacobian matrix, do provide some indication of the solution's behavior.) One

remedy to this disadvantage is to conduct a separate analysis using a method similar to those described in earlier chapters, which may require approximating the problem at hand. Another approach is to perform extensive simulations using the NLLS method, to understand its behavior.

Convergence Failure — For any iterative method, there are two concerns regarding convergence of the process:

- Divergence — failure to converge to any solution
- False convergence — settling on a different minimum than the one corresponding to the vehicle location.

Occurrence of these may be related to the lack of insight into the problem. For example: a solution may not exist for some combinations of measurement values, causing the iteration process to diverge. Alternatively, the iteration process may converge to an ambiguous solution of the measurement equations, rather than to the actual vehicle location.

General remedies to convergence failure are (1) prevention during the system design and (2) detection during real-time operation — either before or after the iteration process. By having insight into a problem, conditions that are conducive to divergence and false convergence may be prevented by the design. Example prevention measures include: (a) placement of sensors so that ambiguous locations are not in the service area; (b) providing redundant measurements, which generally reduce/eliminate problem areas; and (c) providing accurate values to initialize the iteration process. Subsection 8.5.1 contains examples of (b) and (c).

Examples of real-time measures include, checking the measurements for infeasible values before beginning the iteration process. This is particularly relevant when the minimum number of sensors is being used. Examples of are found in Subsections 6.3.2, 6.4.3, 6.5.3, 7.2.4, 7.7.1, 7.9.1, 7.10.1 and 7.12.1. However, not all non-convergent situations can be identified from the measurements. After the iteration process has converged, the solution can be compared with a previous solution or information from another sensor. Usually, the speed and direction of the correct and an ambiguous solution are quite different.

8.1.8 Remarks

Historical Credit — Ascribing the NLLS technique to Gauss and Newton is established practice (Ref. 58), if perhaps not totally accurate. The least-squares technique is usually credited to Carl Friedrich Gauss. However, a case has been made for Adrien-Marie Legendre (Ref. 56). Isaac Newton is usually credited with the technique for iterative solution of an equation whereby the independent variable is changed by the ratio of the dependent variable to its derivative. Reporedly, however, “his method differs substantially from the modern method” (Ref. 59).

Dilution of Precision (DoP) — When the measurement errors for individual stations are uncorrelated and have a common variance, then the accuracy of the solution for the navigation variables (Eq 368) is the product of: (a) a factor, $(\mathbf{J}^T\mathbf{J})^{-1}$, that depends only on the geometry of the aircraft and the stations; and (b) a factor, σ^2_{meas}, that depends largely on the electronic systems involved. Investigations centered on the geometry factor — termed the Dilution of Precision (DoP) — are an important aspect of planning studies (Section 8.4).

Sensitivity to Weight Matrix — Another type of planning study examines the effect of using a different error covariance matrix in measurement processing than is actually true. Eq 365, with **W** used for processing and **R** representing the true error, can be used for such studies.

Jacobian Rank — The necessity that the Jacobian matrix **J** be of full rank is an observability requirement. Essentially, in order for an unknown variable to be determined, a change from the assumed initial value must cause a unique signature in the available measurements.

Initial Estimate — The first iteration step requires that initial estimates be provided for the quantities sought. Potential sources for the initial estimates are: (1) a solution based on an assumed spherical-earth; (2) a previous estimate, possibly updated by changes from the previous solution (obtained from, e.g., a 'tracker' or dead-reckoning system); and (3) user-provided.

Qualitative Characteristics — While the ordinary least-squares and NLLS techniques have been applied to many fields, qualitative conclusions drawn in one field may not be valid in another. Although least-squares grew out of the fields of astronomy and geodesy, much of the modern literature involves its application to model parameter identification. Often parameter identification situations can be characterized as fitting an equation with a few unknown parameters and heuristically chosen functions to many (hundreds or thousands of) measurements[*] (e.g., Ref. 60). While this literature is mathematically relevant, care must be exercised before adopting qualitative conclusions to navigation and surveillance applications.

In contrast to parameter identification, navigation/surveillance applications usually involve: (a) at most, only a few more measurements than unknown variables; (b) a scientific basis for the functions being fitted; and (c) good initial estimates for the unknown variables. These factors mitigate most concerns in the parameter estimation field — e.g., that a solution will diverge or yield a local (rather than a global) minimum, and that generating a solution will require significant computational resources. Informally, one might characterize navigation and surveillance applications as 'Newton-like' (whereby the ratio of measurements to variables is close to one),

[*] Generally, providing real-time navigation or surveillance measurements requires costs for ground stations — real estate, equipment, installation and maintenance. These are often several orders of magnitude more than that of parameter identification measurements.

while parameter identification applications are 'Gauss-like' (whereby the ratio of measurements to variables is much greater than one).

Probabilistic Interpretation — Although not done herein, probability distributions can be assigned to the measurement errors. This enables generation of additional statistical metrics — e.g., hypothesis tests and confidence bounds (e.g., Ref. 61). Such analyses are most useful when there are many more measurements than there are unknown variables.

Jacobian Matrix Units — The unit of measure of element (*i*,*j*) of the Jacobian matrix is the ratio of the unit for measurement $\tilde{z}_i$ divided by the unit for variable x_j. In situations where angles are involved — as the measurement and/or the variable — it may be necessary to multiply or divide an expression by the radius of the earth R_e in order to achieve compatible units.

8.2 Equations for Systems Employing Cartesian Coordinates

8.2.1 Introduction

Application of the NLLS technique described in Section 8.1 only requires specification of the measurement equations (Eq 350) and weight matrix (Eq 354). Moreover, the latter is not needed in some situations. Among the most common least-squares applications are those involving 'range-type' measurements of the distance between an aircraft and a known location. These include:

- Actual slant-range measurements of the distance between an aircraft and a station — such as a radar or a DME transponder. Usually, these involve transmission and reception of signals by both the station and the aircraft (two-way ranging).
- Pseudo slant-range measurements of the distance, plus a range offset common to all stations, between an aircraft and one of set of stations with synchronized clocks — such as a multilateration remote unit or GPS satellite. Usually, these involve transmission of signals by one entity and reception by the other (one-way ranging).
- Altitude measurements of the distance between an aircraft and the center of the earth — usually performed by a barometric altimeter (see Appendix Section 9.1).

Range-type measurements can be processed/analyzed using any rectangular coordinate frame, since the form of Pythagoras's equation is the same in all frames. Thus the choice generally depends upon the application. (They can also be processed/analyzed in a spherical frame; this topic is addressed in Section 8.3.) One option, suitable for small areas, is a local tangent plane frame (Subsection 5.1.2). For larger areas, the earth-centered earth-fixed (ECEF) frame **e** introduced in Section 5.1.1 is more suitable, and is used in this section. If station **S** is has latitude L_S, longitude λ_S and altitude h_S, its ECEF coordinates are

$$\underline{\mathbf{r}}_S^{\mathbf{e}} = \begin{bmatrix} x_S \\ y_S \\ z_S \end{bmatrix} = \begin{bmatrix} \cos(L_S)\cos(\lambda_S) \\ \cos(L_S)\sin(\lambda_S) \\ \sin(L_S) \end{bmatrix} (R_e + h_S) \qquad \text{Eq 380}$$

Assuming that the aircraft **A** is has unknown latitude L_A, longitude λ_A and altitude h_A, then its unknown ECEF coordinates are

$$\underline{\mathbf{r}}_S^{\mathbf{e}} = \begin{bmatrix} x_A \\ y_A \\ z_A \end{bmatrix} = \begin{bmatrix} \cos(L_A)\cos(\lambda_A) \\ \cos(L_A)\sin(\lambda_A) \\ \sin(L_A) \end{bmatrix} (R_e + h_A) \qquad \text{Eq 381}$$

A caveat concerning notation: In this section, the scalar z denotes an axis in a rectangular coordinate frame, while in Section 8.1, the vector **z** denotes a generic measurement.

8.2.2 Measurement Equations

Range Measurement — The non-linear scalar measurement model, corresponding to Eq 350, for the slant-range d_{AS} between ranging station **S** and aircraft **A** is

$$\begin{gathered} \tilde{d}_{AS} = d_{AS} + v_{AS} \\ d_{AS} = \sqrt{(x_A - x_S)^2 + (y_A - y_S)^2 + (z_A - z_S)^2} \end{gathered} \qquad \text{Eq 382}$$

Here, x_S, y_S, z_S are the ECEF coordinates of **S**. The partial derivatives of d_{AS} with respect to the unknown aircraft position variables (corresponding to the partial derivatives in Eq 353) are

$$\frac{\partial d_{AS}}{\partial x_A} = \frac{x_A - x_S}{d_{AS}} \qquad \frac{\partial d_{AS}}{\partial y_A} = \frac{y_A - y_S}{d_{AS}} \qquad \frac{\partial d_{AS}}{\partial z_A} = \frac{z_A - z_S}{d_{AS}} \qquad \text{Eq 383}$$

Pseudo Slant-Range Measurement — The non-linear scalar measurement model, corresponding to Eq 350, for the pseudo slant-range p_{AS} between station **S** and aircraft **A** is

$$\begin{gathered} \tilde{p}_{AS} = p_{AS} + v_{AS} \\ p_{AS} = \sqrt{(x_A - x_S)^2 + (y_A - y_S)^2 + (z_A - z_S)^2} + ct_X \end{gathered} \qquad \text{Eq 384}$$

Here, x_S, y_S, z_S are the Cartesian coordinates of **S** and c is the known speed of propagation.

The partial derivatives of p_{AS} with respect to the unknown variables (corresponding to the partial derivatives in Eq 353) are, using d_{AS} defined in Eq 382

$$\frac{\partial p_{AS}}{\partial x_A} = \frac{x_A - x_S}{d_{AS}} \qquad \frac{\partial p_{AS}}{\partial y_A} = \frac{y_A - y_S}{d_{AS}} \qquad \frac{\partial p_{AS}}{\partial z_A} = \frac{z_A - z_S}{d_{AS}} \qquad \frac{\partial p_{AS}}{\partial t_X} = c \qquad \text{Eq 385}$$

Altitude Measurement — Let r_A be the distance from the aircraft **A** to the earth's center. Then the non-linear scalar measurement model, corresponding to Eq 350, for an altimeter measurement is

$$\tilde{r}_A = R_e + \tilde{h}_A = R_e + h_A + v_{alt}$$
$$r_A = R_e + h_A = \sqrt{(x_A)^2 + (y_A)^2 + (z_A)^2} \qquad \text{Eq 386}$$

The partial derivatives of r_A with respect to the unknown variables are

$$\frac{\partial r_A}{\partial x_A} = \frac{x_A}{r_A} \qquad \frac{\partial r_A}{\partial y_A} = \frac{y_A}{r_A} \qquad \frac{\partial r_A}{\partial z_A} = \frac{z_A}{r_A} \qquad \text{Eq 387}$$

Two-Dimensional Azimuth Measurement — Consider a two-dimensional Cartesian problem formulation where *x* denotes east and *y* denotes north. Then the azimuth angle $\psi_{A/S}$ of the aircraft **A** with respect to station **S** is

$$\tilde{\psi}_{A/S} = \psi_{A/S} + v_{AS}$$
$$\psi_{A/S} = \arctan\left(\frac{x_A - x_S}{y_A - y_S}\right) \qquad \text{Eq 388}$$

The partial derivatives of $\psi_{A/S}$ with respect to the unknown variables are

$$\frac{\partial \psi_{A/S}}{\partial x_A} = \frac{y_A - y_S}{(x_A - x_S)^2 + (y_A - y_S)^2} \qquad \frac{\partial \psi_{A/S}}{\partial y_A} = \frac{-(x_A - x_S)}{(x_A - x_S)^2 + (y_A - y_S)^2} \qquad \text{Eq 389}$$

8.2.3 Remarks

Multilateration Application — An airport surface is a small enough region that the earth can be treated as flat within its perimeter, and a tangent plane coordinate system can be used. Also, aircraft on the surface can be assumed to be at the same altitude. Thus the multilateration pseudo slant-range equations can be processed with two position variables. If low-altitude aircraft are involved, altitude information provided by aircraft can be employed for the vertical dimension, and combined with the multilateration horizontal solution.

GPS Application — GPS is at the opposite end of the size scale from airport multilateration. The 'ground stations' are satellites in orbit approximately 10,900 NM above the surface — about three times the earth's radius. At this scale, the ECEF frame is the natural setting.

Solution Option — When processing a set of pseudo slant-range measurements (Eq 384), one solution method is to subtract one pseudo slant-range from the others. Analytically, this reduces the number of measurement equations by one, eliminates t_X as an unknown variable and increases the measurement error per equation. The hyperbolic geometry associated with range differences can provide insights into regions where a set of stations provides (and does not provide) effective measurements (e.g., Section 7.3). However, knowing the clock offset and associated TDoP may be useful in some situations, and the additional computational cost is insignificant.

8.3 Equations for Systems Employing Spherical Coordinates

8.3.1 Introduction / Rationale

As shown in Chapter 7, Cartesian coordinates and range-type measurements result in simple measurement equations. However, in the context of much of aircraft navigation — involving station-aircraft distances of hundreds of miles — ECEF coordinates have important limitations:

- ECEF coordinates do not handle azimuth measurements well — e.g., the aircraft azimuth angle from a VOR or radar station
- Each of the unknown ECEF variables x_A, y_A, z_A is a function of the aircraft latitude, longitude and altitude, complicating the placing of restrictions on the latter, more natural set of unknown variables.

Another reason to utilize spherical coordinates in an NLLS solution is noted in Subsection 8.1.6, under the title "Approximate Jacobians Useful". Accurate solutions can be readily found when the Jacobian matrix elements are approximations to derivatives of the measurement equation. A spherical earth model often is often used to obtain sufficiently accurate representations of the Jacobian elements.

In this section, it is assumed that station **S** is has known latitude L_S, longitude λ_S and altitude h_S. It is similarly assumed that the aircraft **A** is has unknown latitude L_A and longitude λ_A and possibly unknown altitude h_A. It is further assumed that initial estimates for the unknown aircraft coordinates $\bar{L}_A, \bar{\lambda}_A, \bar{h}_A$ and the time of transmission $\bar{t}_X$ by **A** or **S** (if applicable) are available.

8.3.2 Measurement Equations

Slant-Range Measurement — The slant-range d_{AS} between station **S** and aircraft **A** can be expressed in terms of L_A, λ_A and h_A by substituting Eq 81 into Eq 212. Thus the nonlinear slant-range measurement model is:

$$\tilde{d}_{AS} = d_{AS} + v_{AS}$$

$$d_{AS} = \sqrt{4(R_e + h_A)(R_e + h_S)\sin^2\left(\tfrac{1}{2}\theta_{AS}\right) + (h_A - h_S)^2}$$

$$= \sqrt{\begin{array}{c} 4(R_e + h_A)(R_e + h_S)\left[\sin^2\left(\tfrac{1}{2}(L_A - L_S)\right) + \cos(L_A)\cos(L_S)\sin^2\left(\tfrac{1}{2}(\lambda_A - \lambda_S)\right)\right] \\ +(h_A - h_S)^2 \end{array}} \qquad \text{Eq 390}$$

The partial derivatives of d_{AS} with respect to the unknown aircraft position variables (corresponding to the partial derivatives in Eq 353) are

$$\frac{\partial d_{AS}}{\partial L_A} = \frac{(R_e + h_A)(R_e + h_S)}{d_{AS}}\left[\sin(L_A - L_S) - 2\sin(L_A)\cos(L_S)\sin^2\left(\tfrac{1}{2}(\lambda_A - \lambda_S)\right)\right]$$

$$\frac{\partial d_{AS}}{\partial \lambda_A} = \frac{(R_e + h_A)(R_e + h_S)}{d_{AS}}\cos(L_A)\cos(L_S)\sin(\lambda_A - \lambda_S) \qquad \text{Eq 391}$$

$$\frac{\partial d_{AS}}{\partial h_A} = \frac{2(R_e + h_S)}{d_{AS}}\left[\sin^2\left(\tfrac{1}{2}(L_A - L_S)\right) + \cos(L_A)\cos(L_S)\sin^2\left(\tfrac{1}{2}(\lambda_A - \lambda_S)\right)\right] + \frac{h_A - h_S}{d_{AS}}$$

Pseudo Slant-Range Measurement — The pseudo slant-range p_{AS} between station **S** and aircraft **A** can be expressed in terms of L_A, λ_A and h_A by modifying Eq 390 to include the clock synchronization offset Δt. Thus the nonlinear slant-range measurement model is:

$$\tilde{p}_{AS} = p_{AS} + v_{AS}$$
$$p_{AS} = d_{AS} + ct_X \qquad \text{Eq 392}$$

Here $\tilde{p}_{AS}$ denotes the error-corrupted measurement, p_{AS} denotes the error-free pseudo slant-range and v_{pS} denotes the measurement error.

The partial derivatives of p_{AS} with respect to the unknown variables (corresponding to the partial derivatives in Eq 353) are

$$\frac{\partial p_{AS}}{\partial L_A} = \frac{\partial d_{AS}}{\partial L_A} \qquad \frac{\partial p_{AS}}{\partial \lambda_A} = \frac{\partial d_{AS}}{\partial \lambda_A} \qquad \frac{\partial p_{AS}}{\partial h_A} = \frac{\partial d_{AS}}{\partial h_A} \qquad \frac{\partial p_{AS}}{\partial t_X} = c \qquad \text{Eq 393}$$

The measurement residual, corresponding to the left-hand side of Eq 353, is

$$\delta p_{AS} = \tilde{p}_{AS} - \bar{p}_{AS} \qquad \text{Eq 394}$$

Altitude Measurement — The measurement model for the altitude of the aircraft **A** is simply:

$$\tilde{h}_A = h_A + v_{alt} \qquad \text{Eq 395}$$

Here $\tilde{h}_A$ denotes the error-corrupted measurement, h_A denotes the error-free altitude and v_{alt} denotes the measurement error.

The partial derivatives of h_A with respect to the unknown variables (corresponding to the partial derivatives in Eq 353) are

$$\frac{\partial h_A}{\partial L_A} = 0 \qquad \frac{\partial h_A}{\partial \lambda_A} = 0 \qquad \frac{\partial h_A}{\partial h_A} = 1 \qquad \text{Eq 396}$$

Geocentric Angle (Spherical-Range) Measurement — The geocentric angle θ_{AS} (equivalent to spherical-range) between station **S** and aircraft **A** can be expressed in terms of L_A and λ_A using Eq 81. Thus the nonlinear slant-range measurement model is:

$$\tilde{\theta}_{AS} = \theta_{AS} + v_{\theta S}$$
$$\theta_{AS} = 2\arcsin\left(\sqrt{\sin^2\left(\tfrac{1}{2}(L_A - L_S)\right) + \cos(L_A)\cos(L_S)\sin^2\left(\tfrac{1}{2}(\lambda_A - \lambda_S)\right)}\right) \quad \text{Eq 397}$$

Here $\tilde{\theta}_{AS}$ denotes the error-corrupted measurement, θ_{AS} denotes the error-free geocentric angle and $v_{\theta S}$ denotes the measurement error.

The partial derivatives of θ_{AS} with respect to the unknown aircraft position variables (corresponding to the partial derivatives in Eq 353) are

$$\frac{\partial\theta_{AS}}{\partial L_A} = \frac{1}{\sin(\theta_{AS})}\left[\sin(L_A - L_S) - 2\sin(L_A)\cos(L_S)\sin^2\left(\tfrac{1}{2}(\lambda_A - \lambda_S)\right)\right]$$
$$\frac{\partial\theta_{AS}}{\partial\lambda_A} = \frac{1}{\sin(\theta_{AS})}\cos(L_A)\cos(L_S)\sin(\lambda_A - \lambda_S) \quad \text{Eq 398}$$
$$\frac{\partial\theta_{AS}}{\partial h_A} = 0$$

In Eq 398, the expression for $\sin(\theta_{AS})$ can be found using Eq 397 or Eq 142.

Azimuth Measurement, Station-to-Aircraft — The azimuth angle $\psi_{A/S}$ of aircraft **A** with respect to station **S** is expressed in terms of L_A and λ_A by Eq 87 (in a form compatible with the two-argument arc tangent function). Thus the nonlinear measurement model is:

$$\tilde{\psi}_{A/S} = \psi_{A/S} + v_{\psi S}$$
$$\psi_{A/S} = \arctan\left\{\frac{\cos(L_A)\sin(\lambda_A - \lambda_S)}{\sin(L_A)\cos(L_S) - \cos(L_A)\sin(L_S)\cos(\lambda_A - \lambda_S)}\right\} \quad \text{Eq 399}$$

Here $v_{\psi S}$ denotes the angle measurement error.

The partial derivatives of $\psi_{A/S}$ with respect to the unknown aircraft position variables L_A and λ_A (corresponding to the partial derivatives in Eq 353) are

$$\frac{\partial\psi_{A/S}}{\partial L_A} = -\frac{\mathrm{Den}\sin(L_A)\sin(\lambda_A - \lambda_S)}{\mathrm{Den}^2 + \mathrm{Num}^2} - \frac{\mathrm{Num}\left[\cos(L_A)\cos(L_S) + \sin(L_A)\sin(L_S)\cos(\lambda_A - \lambda_S)\right]}{\mathrm{Den}^2 + \mathrm{Num}^2} \quad \text{Eq 400}$$
$$\frac{\partial\psi_{A/S}}{\partial\lambda_A} = \frac{\mathrm{Den}\cos(L_A)\cos(\lambda_A - \lambda_S) - \mathrm{Num}\cos(L_A)\sin(L_S)\sin(\lambda_A - \lambda_S)}{\mathrm{Den}^2 + \mathrm{Num}^2}$$
$$\frac{\partial\psi_{A/S}}{\partial h_A} = 0$$
$$\mathrm{Num} = \cos(L_A)\sin(\lambda_A - \lambda_S)$$
$$\mathrm{Den} = \sin(L_A)\cos(L_S) - \cos(L_A)\sin(L_S)\cos(\lambda_A - \lambda_S)$$

Azimuth Measurement, Aircraft-to-Station — The azimuth angle $\psi_{S/A}$ of station **S** with respect to aircraft **A** is expressed in terms of L_A and λ_A by Eq 86 (in a form compatible with the two-argument arc tangent function). Thus the nonlinear measurement model is:

$$\tilde{\psi}_{S/A} = \psi_{S/A} + v_{\psi A}$$
$$\psi_{S/A} = \arctan\left\{\frac{\cos(L_S)\sin(\lambda_S - \lambda_A)}{\sin(L_S)\cos(L_A) - \cos(L_S)\sin(L_A)\cos(\lambda_S - \lambda_A)}\right\} \qquad \text{Eq 401}$$

Here $v_{\psi A}$ denotes the angle measurement error.

The partial derivatives of $\psi_{S/A}$ with respect to the unknown aircraft position variables L_A and λ_A (corresponding to the partial derivatives in Eq 353) are

$$\frac{\partial \psi_{S/A}}{\partial L_A} = \frac{\text{Num}\,[\sin(L_A)\sin(L_S) + \cos(L_A)\cos(L_S)\cos(\lambda_S - \lambda_A)]}{\text{Num}^2 + \text{Den}^2} \qquad \text{Eq 402}$$
$$\frac{\partial \psi_{S/A}}{\partial \lambda_A} = \frac{-\text{Den}\,[\cos(L_S)\cos(\lambda_S - \lambda_A)] + \text{Num}\,[\cos(L_S)\sin(L_A)\sin(\lambda_S - \lambda_A)]}{\text{Num}^2 + \text{Den}^2}$$
$$\frac{\partial \psi_{S/A}}{\partial h_A} = 0$$
$$\text{Num} = \cos(L_S)\sin(\lambda_S - \lambda_A)$$
$$\text{Den} = \sin(L_S)\cos(L_A) - \cos(L_S)\sin(L_A)\cos(\lambda_S - \lambda_A)$$

8.4 Solutions for Homogeneous Range-Type Measurements

8.4.1 Introduction / Rationale

Systems that employ a single type of range measurements are common. Examples are:

- True slant-ranges: DME/DME
- True spherical-ranges: Loran-C (experimental), star elevation*
- Pseudo slant-ranges: GPS, Galileo, WAM
- Pseudo spherical-ranges: Loran-C, Omega, Decca.

Slant- and spherical-ranges can be interchanged, provided that the station and aircraft altitudes are known (e.g., Eq 44 and Eq 54 and Subsection 3.2.2). Often the purpose of a slant-range system is to obtain aircraft latitude/longitude, so that conversion of their measurements to spherical-ranges can be useful.

* When a spherical earth model is employed, spherical-ranges and geocentric angles are interchangeable (differing only by the earth's radius as a scale factor). Then, a user's elevation angle of a star is equivalent to the spherical-range to the star subpoint. Since star elevation measurements are often not highly accurate, the spherical-earth approximation is sufficient for most applications. When high-accuracy measurements are available and an ellipsoidal earth model is used, stellar elevations and spherical-ranges should be treated as separate measurements types.

As noted in Section 7.1, systems that utilize pseudo ranges and those that utilize range differences are virtually identical at the analysis level (Subsection 8.4.5 contains a proof). The term pseudo range is used when receivers estimate the time of signal transmission. However, once a range-difference system found the location of both a transmitter and receiver, the time of transmission can be computed if it is needed.

8.4.2 Dilution of Precision (DoP)

When the measurements have common characteristics (e.g., involve different ground stations performing the same function and of the same design), it's frequently assumed that the measurement errors are uncorrelated and have the same variance σ_{meas}^2. This assumption is buttressed when there are different propagation paths involved. In such situations, the estimation error covariance for the unknown variables (Eq 368) can be expressed the product of the scalar σ_{meas}^2 and the matrix $\mathbf{(J}^T\mathbf{J)}^{-1}$. The matrix $\mathbf{(J}^T\mathbf{J)}^{-1}$ depends only on the measurement geometry, and can provide insight into advantageous locations for ground stations and/or aircraft operations.

DoP analysis can be applied to problems formulated in both Cartesian (e.g., examples in Sub-sections 8.5.1 and 8.5.2) and spherical (e.g., examples in Subsections 8.5.4 and 8.5.5) frameworks. An ellipsoidal earth model is almost never used for DoP calculations, as that level of precision is not needed for system characterization. DoP analysis is most often used in conjunction with slant- and spherical-range measurements, and their differences. However, DoP analysis can be used with angle-only systems.

The DoP matrix **M** is a dimensionless — and possibly scaled and/or rotated — version of $\mathbf{(J}^T\mathbf{J)}^{-1}$. The corresponding axes are orthogonal and 'commensurate' — i.e., one unit of change in each 'DoP variable' represents the same amount of physical distance. Although it's not required, very often the first three DoP axes correspond to the east, north and up directions. If it's appropriate, the fourth element corresponds the unknown time of transmission t_X. Thus

$$\mathbf{M} = \mathbf{C}\left(\mathbf{J}^T\mathbf{J}\right)^{-1}\mathbf{C}^T = \begin{bmatrix} m_{ee} & m_{en} & m_{eu} & m_{et} \\ m_{en} & m_{nn} & m_{nu} & m_{nt} \\ m_{eu} & m_{nu} & m_{uu} & m_{ut} \\ m_{et} & m_{nt} & m_{ut} & m_{tt} \end{bmatrix} \qquad \text{Eq 403}$$

Various scalar DoP quantities are computed from **M**, including Horizontal Dilution of Precision (HDoP), Vertical Dilution of Precision (VDoP), Time Dilution of Precision (TDoP) and Geometric Dilution of Precision (GDoP):

$$\begin{aligned} \text{HDoP} &= \sqrt{m_{ee} + m_{nn}} & \text{VDoP} &= \sqrt{m_{uu}} \\ \text{TDoP} &= \sqrt{m_{tt}} & \text{GDoP} &= \sqrt{m_{ee} + m_{nn} + m_{uu} + m_{tt}} \end{aligned} \qquad \text{Eq 404}$$

When the problem formulation utilizes the Cartesian ECEF frame, it's conventional to rotate the matrix $(\mathbf{J}^T\mathbf{J})^{-1}$ into the local-level frame at the estimated aircraft location using an expanded version of the direction cosine matrix of Eq 131:

$$\mathbf{C} = \begin{bmatrix} -\sin(\hat{\lambda}_A) & \cos(\hat{\lambda}_A) & 0 & 0 \\ \sin(-\hat{L}_A)\cos(\hat{\lambda}_A) & \sin(-\hat{L}_A)\sin(\hat{\lambda}_A) & \cos(-\hat{L}_A) & 0 \\ \cos(-\hat{L}_A)\cos(\hat{\lambda}_A) & \cos(-\hat{L}_A)\sin(\hat{\lambda}_A) & -\sin(-\hat{L}_A) & 0 \\ 0 & 0 & 0 & 1 \end{bmatrix} \quad \text{Eq 405}$$

When the problem formulation utilizes the spherical-earth framework, for DoP analysis the horizontal perturbation variables δL_A and $\delta\lambda_A$ are adjusted so that equal geocentric angles correspond to equal distances. Expressions are given later in this section.

8.4.3 Range Measurement Systems

Cartesian Coordinates / Slant-Range Measurements — For the case of problems formulated in Cartesian coordinates, the quantities sought are the aircraft coordinates $\mathbf{x}_c = (x_A, y_A, z_A)$. A nominal value for $\mathbf{x}_c$, denoted by $\bar{\mathbf{x}}_c$, is known. The difference between $\mathbf{x}_c$ and $\bar{\mathbf{x}}_c$, denoted by $\boldsymbol{\delta}\mathbf{x}_c$, is to be found

$$\boldsymbol{\delta}\mathbf{x}_c = [\delta x_A \quad \delta y_A \quad \delta z_A]^T \quad \text{Eq 406}$$

For slant-range measurements, the partial derivatives of the measurements with respect to the coordinates are given by Eq 383. This expression can be written as the unit vector pointing from ranging station **S***i* toward aircraft **A**. Thus each row of the Jacobian matrix is

$$\mathbf{u}_{c,ASi} = \begin{bmatrix} u_{c,ASi,x} & u_{c,ASi,y} & u_{c,ASi,z} \end{bmatrix} = \begin{bmatrix} \dfrac{x_A - x_{Si}}{d_{ASi}} & \dfrac{y_A - y_{Si}}{d_{ASi}} & \dfrac{z_A - z_{Si}}{d_{ASi}} \end{bmatrix} \quad \text{Eq 407}$$

$$d_{ASi} = \sqrt{(x_A - x_{Si})^2 + (y_A - y_{Si})^2 + (z_A - z_{Si})^2}$$

The Jacobian matrix for the aggregate of *n* measurements can be written

$$\mathbf{J} = \mathbf{U}_c = \begin{bmatrix} \mathbf{u}_{c,AS1} \\ \mathbf{u}_{c,AS2} \\ \vdots \\ \mathbf{u}_{c,ASn} \end{bmatrix} \quad \text{Eq 408}$$

The estimation problem to be solved is: find the value of $\boldsymbol{\delta}\mathbf{x}_c$ that best satisfies

$$\mathbf{U}_c\,\boldsymbol{\delta}\mathbf{x}_c \approx \boldsymbol{\delta}\mathbf{z} \quad \text{Eq 409}$$

Here $\boldsymbol{\delta}\mathbf{z}$ is the difference between the measured ranges and the computed ranges based on $\bar{\mathbf{x}}_c$. The errors in $\boldsymbol{\delta}\mathbf{z}$ are assumed to be independent and identically distributed.

From Eq 360, the estimate of the deviation of $\mathbf{x}_c$ from its nominal value $\bar{\mathbf{x}}_c$ is

$$\boldsymbol{\delta}\hat{\mathbf{x}}_c = [\mathbf{U}_c^T\mathbf{U}_c]^{-1}\mathbf{U}_c^T\boldsymbol{\delta}\mathbf{z} \qquad \text{Eq 410}$$

The covariance of the error in the estimate of $\boldsymbol{\delta}\mathbf{x}_c$ is given by (see Eq 368)

$$E(\boldsymbol{\delta}\hat{\mathbf{x}}_c - \boldsymbol{\delta}\mathbf{x})(\boldsymbol{\delta}\hat{\mathbf{x}}_c - \boldsymbol{\delta}\mathbf{x})^T = [\mathbf{U}_c^T\,\mathbf{U}_c]^{-1}\sigma_{RngMeas}^2 \qquad \text{Eq 411}$$

Here, $\sigma_{RngMeas}$ is the common standard deviation of the range measurements, expressed in linear units. The choice of $\mathbf{U}_c$ for the Jacobian matrix for a system utilizing only slant-range measurements alludes to the fact that its rows are dimensionless unit vectors. However, the properties of a unit vector are not used. It is also useful to have a separate symbol represent the Jacobian matrix elements for position variables alone.

For this case, the DoP matrix $\mathbf{M}_c$ is given by the three-variable version of Eq 403, where the matrix $\mathbf{C}$ may be needed to transform the results into a local-level coordinate frame at the aircraft location.

$$\mathbf{M}_c = \mathbf{C}(\mathbf{U}_c^T\,\mathbf{U}_c)^{-1}\mathbf{C}^T = \begin{bmatrix} m_{ee} & m_{en} & m_{eu} \\ m_{en} & m_{nn} & m_{nu} \\ m_{eu} & m_{nu} & m_{uu} \end{bmatrix} \qquad \text{Eq 412}$$

Spherical Coordinates / Slant-Range Measurements — For a problem formulated in spherical coordinates, the quantities sought are the aircraft coordinates $\mathbf{x}_s = (L_A, \lambda_A, h_A)$. Thus the perturbation quantities are

$$\boldsymbol{\delta}\mathbf{x}_s = [\delta L_A \quad \delta\lambda_A \quad \delta h_A\,]^T \qquad \text{Eq 413}$$

The elements of $\mathbf{x}_s$ and $\boldsymbol{\delta}\mathbf{x}_s$ are 'mixed' — there are two angular and one linear distance, and the two angular variable correspond to different geocentric angles.

For slant-range measurements, the partial derivatives of the measurements with respect to the coordinates are given by Eq 391. Thus the elements of the row $\mathbf{u}_{s,ASi}$ of the Jacobian corresponding to station **S***i* are

$$\begin{aligned}
u_{s,ASi,L} &= \frac{(R_e + h_A)(R_e + h_{Si})}{d_{ASi}}\left[\sin(L_A - L_{Si}) - 2\sin(L_A)\cos(L_{Si})\sin^2\left(\tfrac{1}{2}(\lambda_A - \lambda_{Si})\right)\right] \\
u_{s,ASi,\lambda} &= \frac{(R_e + h_A)(R_e + h_{Si})}{d_{ASi}}\cos(L_A)\cos(L_{Si})\sin(\lambda_A - \lambda_{Si}) \\
u_{s,ASi,h} &= \frac{2(R_e + h_{Si})}{d_{ASi}}\left[\sin^2\left(\tfrac{1}{2}(L_A - L_{Si})\right) + \cos(L_A)\cos(L_{Si})\sin^2\left(\tfrac{1}{2}(\lambda_A - \lambda_{Si})\right)\right] \\
&\quad + \frac{h_A - h_{Si}}{d_{ASi}}
\end{aligned} \qquad \text{Eq 414}$$

$$d_{ASi} = \sqrt{\begin{matrix} 4(R_e + h_A)(R_e + h_{Si}) \\ \left[\sin^2\left(\frac{1}{2}(L_A - L_{Si})\right) + \cos(L_A)\cos(L_{Si})\sin^2\left(\frac{1}{2}(\lambda_A - \lambda_{Si})\right)\right] \\ +(h_A - h_{Si})^2 \end{matrix}}$$

The components of $\mathbf{u}_{s,ASi}$ in Eq 414 are not dimensionless and do not constitute a unit vector.

If the subscript *c* (Cartesian formulation) is replaced by *s* (spherical formulation), the expressions for the Jacobian matrix (Eq 408), the perturbation vector (Eq 410) and its error covariance (Eq 411) also apply to those for a spherical problem formulation.

$$\mathbf{J} = \mathbf{U}_s = \begin{bmatrix} \mathbf{u}_{s,AS1} \\ \mathbf{u}_{s,AS2} \\ \vdots \\ \mathbf{u}_{s,ASn} \end{bmatrix} \quad \text{Eq 415}$$

$$\boldsymbol{\delta}\hat{\mathbf{x}}_s = [\mathbf{U}_s^T\mathbf{U}_s]^{-1}\mathbf{U}_s^T\boldsymbol{\delta}\mathbf{z}$$

$$E(\boldsymbol{\delta}\hat{\mathbf{x}}_s - \boldsymbol{\delta}\mathbf{x})(\boldsymbol{\delta}\hat{\mathbf{x}}_s - \boldsymbol{\delta}\mathbf{x})^T = [\mathbf{U}_s^T\,\mathbf{U}_s]^{-1}\sigma^2_{RngMeas}$$

Here the DoP variables are considered to be

$$\boldsymbol{\delta}\mathbf{x}'_s = [R_e\,\delta L_A \quad R_e\cos(L_A)\,\delta\lambda_A \quad \delta h_A\,]^T \quad \text{Eq 416}$$

The 3x3 DoP matrix for $\boldsymbol{\delta}\mathbf{x}'_s$ is given by

$$\mathbf{M}_s = \mathbf{C}(\mathbf{U}_s^T\,\mathbf{U}_s)^{-1}\mathbf{C}^T = \begin{bmatrix} m_{ee} & m_{en} & m_{eu} \\ m_{en} & m_{nn} & m_{nu} \\ m_{eu} & m_{nu} & m_{uu} \end{bmatrix} \quad \text{Eq 417}$$

$$\mathbf{C} = \mathrm{diag}(R_e, R_e\cos(L_A), 1) \quad \text{Eq 418}$$

Spherical Coordinates / Spherical-Range Measurements — Spherical ranges are inherently two-dimensional (latitude and longitude); altitude does not play a role. Thus the quantities sought are the aircraft coordinates $\mathbf{x}_a = (L_A, \lambda_A)$. Consequently the perturbation variables are:

$$\boldsymbol{\delta}\mathbf{x}_a = [\delta L_A \quad \delta\lambda_A\,]^T \quad \text{Eq 419}$$

The partial derivatives of geocentric angle measurements with respect to the above coordinates are given by Eq 398. Thus the elements of the row $\mathbf{u}_{a,ASi}$ of the Jacobian matrix corresponding to station **S***i* are

$$u_{a,ASi,L} = \frac{1}{\sin(\theta_{ASi})}\left[\sin(L_A - L_{Si}) - 2\sin(L_A)\cos(L_{Si})\sin^2\left(\frac{1}{2}(\lambda_A - \lambda_{Si})\right)\right]$$

$$u_{a,ASi,\lambda} = \frac{1}{\sin(\theta_{ASi})}\cos(L_A)\cos(L_{Si})\sin(\lambda_A - \lambda_{Si}) \quad \text{Eq 420}$$

$$\sin(\theta_{ASi}) = \sqrt{\begin{matrix}[\cos(L_{Si})\sin(\lambda_{Si}-\lambda_U)]^2 \\ +[\cos(L_U)\sin(L_{Si}) - \sin(L_U)\cos(L_{Si})\cos(\lambda_{Si}-\lambda_U)]^2\end{matrix}}$$

Provided the subscript *c* is replaced by *a*, the expressions for the Jacobian matrix (Eq 408), the estimate of the perturbation vector (Eq 410) and its error covariance (Eq 411) for a slant-range measurements and a Cartesian problem formulation also apply to those for spherical-range measurements and spherical coordinates.

$$\mathbf{J} = \mathbf{U}_a = \begin{bmatrix} \mathbf{u}_{a,AS1} \\ \mathbf{u}_{a,AS2} \\ \vdots \\ \mathbf{u}_{a,ASn} \end{bmatrix} \qquad \text{Eq 421}$$

$$\boldsymbol{\delta}\hat{\mathbf{x}}_a = [\mathbf{U}_a^T\mathbf{U}_a]^{-1}\mathbf{U}_a^T\boldsymbol{\delta}\mathbf{z}$$

$$E(\boldsymbol{\delta}\hat{\mathbf{x}}_a - \boldsymbol{\delta}\mathbf{x})(\boldsymbol{\delta}\hat{\mathbf{x}}_a - \boldsymbol{\delta}\mathbf{x})^T = [\mathbf{U}_a^T\mathbf{U}_a]^{-1}\sigma^2_{RngMeas}$$

Here the DoP variables are considered to be

$$\boldsymbol{\delta}\mathbf{x}'_a = [\delta L_A \;\; \cos(L_A)\,\delta\lambda_A\,]^T \qquad \text{Eq 422}$$

The 2x2 DoP matrix corresponding to $\boldsymbol{\delta}\mathbf{x}'_a$ is

$$\mathbf{M}_a = \mathbf{C}(\mathbf{U}_a^T\mathbf{U}_a)^{-1}\mathbf{C}^T = \begin{bmatrix} m_{ee} & m_{en} \\ m_{en} & m_{nn} \end{bmatrix} \qquad \text{Eq 423}$$

$$\mathbf{C} = \text{diag}(1, \cos(L_A))$$

8.4.4 Pseudo Range Measurement Systems: Lee's Method

Problem Formulation — Systems employing pseudo range measurements of either slant- or spherical-ranges, measure a set of 'ranges' that include an additive, common unknown offset (also called a bias). The common offset is an additional unknown variable, and the number of measurements must be at least one more than the number of position variables to be found.

Pseudo range versions of all of the cases considered in Subsection 8.4.3 have been deployed. For these systems, the perturbation vector* is

$$\boldsymbol{\delta}\mathbf{X}_k = [\boldsymbol{\delta}\mathbf{x}_k^T \;\; \delta b]^T \qquad \text{Eq 424}$$

Here, as in Subsection 8.4.3, subscript *k* designates the system type — i.e., *k* can be *c* (Cartesian coordinates / slant-range measurements, Eq 406), *s* (spherical coordinates / slant-range measurements, Eq 413) or *a* (spherical coordinates / spherical-range measurements, Eq 419). Also, δb

* For homogeneous range-type measurement systems involving a common time/range bias, the vector of all unknown variables is denoted using a capital **X** and the vector of unknown position variables by a lower case **x**.

denotes the unknown range offset/bias in distance units. If there are n pseudo range measurements, the Jacobian matrix is nx3 or nx4, depending upon the framework of the analysis. Thus,

$$\mathbf{J}_{k,PR} = [\mathbf{U}_k \;\; \mathbf{1}]$$
$$\mathbf{1} = [1 \;\; 1 \;\; \cdots \;\; 1]^T \qquad \text{Eq 425}$$

Analysis of this situation is similar to analysis of the 'with intercept' problem in linear regression theory. The estimation problem is: find the value of $\boldsymbol{\delta}\mathbf{X}_k$ that best satisfies

$$\mathbf{J}_{k,PR}\,\boldsymbol{\delta}\mathbf{X}_k \approx \boldsymbol{\delta}\mathbf{z} \qquad \text{Eq 426}$$

The errors in $\boldsymbol{\delta}\mathbf{z}$ are assumed to be independent and identically distributed, with zero mean and variance $\sigma^2_{RngMeas}$.

Estimation of the Common Bias — In analyzing pseudo range systems, it is possible to utilize both a whole value bias b and a bias perturbation δb, and to update b from δb at each iteration (as is done for position variables). Thus, during the estimation process, δb is driven to zero. However, since the common bias appears linearly in the measurement equations — b (equivalent to t_X) would be an additive term in each $f_i(L_A, \lambda_A, h_A, t_X)$ of Eq 350 — it is not necessary to utilize a whole value bias b. Instead, as is done herein, b can be ignored in finding a position solution. Then the iteration process drives δb is to value that is generally not zero. When the process has converged, the last estimate for the δb is taken to be the bias.

Lee's (or First Form of) Partitioned Matrix Solution — From the partitioning of $\mathbf{J}_{k,PR}$ in Eq 425, it follows that

$$\left(\mathbf{J}_{k,PR}\right)^T \mathbf{J}_{k,PR} = \begin{bmatrix}\mathbf{U}_k^T \\ \mathbf{1}^T\end{bmatrix}[\mathbf{U}_k \;\; \mathbf{1}] = \begin{bmatrix}\mathbf{U}_k^T\mathbf{U}_k & \mathbf{U}_k^T\mathbf{1} \\ \mathbf{1}^T\mathbf{U}_k & n\end{bmatrix} \qquad \text{Eq 427}$$

In the proof of the Matrix Inversion Lemma (Ref. 62), one form of the inverse of a 2x2 partitioned matrix has a simpler expression for the upper left-hand block. Applying that to the right-hand side of Eq 427 results in

$$\left(\left(\mathbf{J}_{k,PR}\right)^T \mathbf{J}_{k,PR}\right)^{-1} = \begin{bmatrix}\mathbf{M}^1_{k,PR} & \mathbf{b}^1_k \\ (\mathbf{b}^1_k)^T & m^1_{k,PR}\end{bmatrix} \qquad \text{Eq 428}$$

$$\mathbf{M}^1_{k,PR} = \left[\mathbf{U}_k^T\left(\mathbf{I} - \tfrac{1}{n}\mathbf{1}\mathbf{1}^T\right)\mathbf{U}_k\right]^{-1}$$
$$\mathbf{b}^1_k = -\frac{1}{n}\mathbf{M}^1_{k,PR}\mathbf{U}_k^T\mathbf{1}$$
$$m^1_{k,PR} = \frac{1}{n}\left(1 + \frac{1}{n}\mathbf{1}^T\mathbf{U}_k\mathbf{M}^1_{k,PR}\mathbf{U}_k^T\mathbf{1}\right) \qquad \text{Eq 429}$$
$$= \frac{1}{n}\left(1 + \frac{1}{n}\mathbf{1}^T\mathbf{U}_k\left[\mathbf{U}_k^T\left(\mathbf{I} - \tfrac{1}{n}\mathbf{1}\mathbf{1}^T\right)\mathbf{U}_k\right]^{-1}\mathbf{U}_k^T\mathbf{1}\right)$$

Here, $\mathbf{M}^1_{k,PR}$ is the p x p DoP matrix for the position estimation errors and $m^1_{k,PR}$ is the scalar DoP for the range offset estimation error. (The superscript '1' on the symbols in Eq 428 is a label designating the first form of the inverse of $\left(\mathbf{J}_{k,PR}\right)^T \mathbf{J}_{k,PR}$). The estimate for $\boldsymbol{\delta}\mathbf{X}_k$ is

$$\boldsymbol{\delta}\widehat{\mathbf{X}}_k = \left(\left(\mathbf{J}_{k,PR}\right)^T \mathbf{J}_{k,PR}\right)^{-1} \left(\mathbf{J}_{k,PR}\right)^T \boldsymbol{\delta}\mathbf{z} \qquad \text{Eq 430}$$

The solution for the components of $\boldsymbol{\delta}\widehat{\mathbf{X}}_k$, $\boldsymbol{\delta}\hat{\mathbf{x}}_k$ and $\delta\hat{b}$, are

$$\begin{aligned} \boldsymbol{\delta}\hat{\mathbf{x}}_k &= \mathbf{M}^1_{k,PR}\mathbf{U}_k^T\left(\mathbf{I} - \tfrac{1}{n}\mathbf{1}\mathbf{1}^T\right)\boldsymbol{\delta}\mathbf{z} \\ &= \left[\mathbf{U}_k^T\left(\mathbf{I} - \tfrac{1}{n}\mathbf{1}\mathbf{1}^T\right)\mathbf{U}_k\right]^{-1}\mathbf{U}_k^T\left(\mathbf{I} - \tfrac{1}{n}\mathbf{1}\mathbf{1}^T\right)\boldsymbol{\delta}\mathbf{z} \\ \delta\hat{b} &= \left(m^1_{k,PR}\,\mathbf{1}^T - \frac{1}{n}\mathbf{1}^T\mathbf{U}_k\mathbf{M}^1_{k,PR}\,\mathbf{U}_k^T\right)\boldsymbol{\delta}\mathbf{z} \\ &= \frac{1}{n}\left(\mathbf{1}^T - \mathbf{1}^T\,\mathbf{U}_k\left[\mathbf{U}_k^T\left(\mathbf{I} - \tfrac{1}{n}\mathbf{1}\mathbf{1}^T\right)\mathbf{U}_k\right]^{-1}\mathbf{U}_k^T\left(\mathbf{I} - \tfrac{1}{n}\mathbf{1}\mathbf{1}^T\right)\right)\boldsymbol{\delta}\mathbf{z} \end{aligned} \qquad \text{Eq 431}$$

The estimation error covariances/variances for the variables $\boldsymbol{\delta}\hat{\mathbf{x}}_k$ and $\delta\hat{b}$ are

$$\begin{aligned} E(\boldsymbol{\delta}\hat{\mathbf{x}}_k - \boldsymbol{\delta}\mathbf{x}_k)(\boldsymbol{\delta}\hat{\mathbf{x}}_k - \boldsymbol{\delta}\mathbf{x}_k)^T &= \mathbf{M}^1_{k,PR}\,\sigma^2_{RngMeas} \\ &= \left[\mathbf{U}_k^T\left(\mathbf{I} - \tfrac{1}{n}\mathbf{1}\mathbf{1}^T\right)\mathbf{U}_k\right]^{-1}\sigma^2_{RngMeas} \\ E\left(\delta\hat{b} - \delta b\right)^2 &= m^1_{k,PR}\,\sigma^2_{RngMeas} \\ &= \frac{1}{n}\left(1 + \frac{1}{n}\mathbf{1}^T\,\mathbf{U}_k\left[\mathbf{U}_k^T\left(\mathbf{I} - \tfrac{1}{n}\mathbf{1}\mathbf{1}^T\right)\mathbf{U}_k\right]^{-1}\mathbf{U}_k^T\,\mathbf{1}\right)\sigma^2_{RngMeas} \end{aligned} \qquad \text{Eq 432}$$

Second Form of Partitioned Matrix Solution — The proof of the Matrix Inversion Lemma involves a second form of the inverse of a 2x2 partitioned matrix whereby the inverse has a simpler expression for the lower right-hand block. Applying this form to Eq 427 yields:

$$\left(\left(\mathbf{J}_{k,PR}\right)^T \mathbf{J}_{k,PR}\right)^{-1} = \begin{bmatrix} \mathbf{M}^2_{k,PR} & \mathbf{b}^2_k \\ (\mathbf{b}^2_k)^T & m^2_{k,PR} \end{bmatrix} \qquad \text{Eq 433}$$

$$\begin{aligned} \mathbf{M}^2_{k,PR} &= (\mathbf{U}_k^T\,\mathbf{U}_k)^{-1} + m^2_{k,PR}\,(\mathbf{U}_k^T\,\mathbf{U}_k)^{-1}\mathbf{U}_k^T\mathbf{1}\mathbf{1}^T\mathbf{U}_k(\mathbf{U}_k^T\,\mathbf{U}_k)^{-1} \\ &= \left[(\mathbf{U}_k^T\,\mathbf{U}_k)^{-1} + \frac{(\mathbf{U}_k^T\,\mathbf{U}_k)^{-1}\mathbf{U}_k^T\mathbf{1}\mathbf{1}^T\mathbf{U}_k(\mathbf{U}_k^T\,\mathbf{U}_k)^{-1}}{n - \mathbf{1}^T\,\mathbf{U}_k(\mathbf{U}_k^T\,\mathbf{U}_k)^{-1}\mathbf{U}_k^T\,\mathbf{1}}\right] \\ \mathbf{b}^2_k &= -\,m^2_{k,PR}\,(\mathbf{U}_k^T\,\mathbf{U}_k)^{-1}\mathbf{U}_k^T\mathbf{1} \\ m^2_{k,PR} &= \frac{1}{n - \mathbf{1}^T\,\mathbf{U}_k\,(\mathbf{U}_k^T\,\mathbf{U}_k)^{-1}\,\mathbf{U}_k^T\,\mathbf{1}} \end{aligned} \qquad \text{Eq 434}$$

The superscript '2' on symbols in Eq 433 designates the second form of the inverse of $\left(\mathbf{J}_{k,PR}\right)^T \mathbf{J}_{k,PR}$. $\mathbf{M}^2_{k,PR}$ is a second form of the DoP matrix for the position estimation errors and $m^2_{k,PR}$ is a second form for the scalar DoP for the range offset estimation error.

The solution for the components of $\boldsymbol{\delta\hat{\mathbf{X}}}_k$, $\boldsymbol{\delta\hat{\mathbf{x}}}_k$ and $\delta\hat{b}$, are

$$\begin{aligned}\boldsymbol{\delta\hat{\mathbf{x}}}_k &= \left(\mathbf{M}^2_{k,PR}\,\mathbf{U}_k^T + \mathbf{b}_k^2\,\mathbf{1}^T\right)\boldsymbol{\delta\mathbf{z}} \\ &= \left[(\mathbf{U}_k^T\,\mathbf{U}_k)^{-1}\mathbf{U}_k^T - \frac{(\mathbf{U}_k^T\,\mathbf{U}_k)^{-1}\mathbf{U}_k^T\mathbf{1}\mathbf{1}^T}{n - \mathbf{1}^T\,\mathbf{U}_k(\mathbf{U}_k^T\,\mathbf{U}_k)^{-1}\mathbf{U}_k^T\,\mathbf{1}}\left[\mathbf{I} - \mathbf{U}_k(\mathbf{U}_k^T\,\mathbf{U}_k)^{-1}\mathbf{U}_k^T\right]\right]\boldsymbol{\delta\mathbf{z}} \\ \delta\hat{b} &= \left((\mathbf{b}_k^2)^T\mathbf{U}_k^T + m^2_{k,PR}\mathbf{1}^T\right)\boldsymbol{\delta\mathbf{z}} \\ &= \left[\frac{1}{n - \mathbf{1}^T\,\mathbf{U}_k\,(\mathbf{U}_k^T\,\mathbf{U}_k)^{-1}\,\mathbf{U}_k^T\,\mathbf{1}}\mathbf{1}^T\left[\mathbf{I} - \mathbf{U}_k(\mathbf{U}_k^T\,\mathbf{U}_k)^{-1}\mathbf{U}_k^T\right]\right]\boldsymbol{\delta\mathbf{z}}\end{aligned} \qquad \text{Eq 435}$$

The estimation error covariances/variances for the variables $\boldsymbol{\delta\hat{\mathbf{x}}}_k$ and $\delta\hat{b}$ are

$$\begin{aligned}E(\boldsymbol{\delta\hat{\mathbf{x}}}_k - \boldsymbol{\delta\mathbf{x}}_k)(\boldsymbol{\delta\hat{\mathbf{x}}}_k - \boldsymbol{\delta\mathbf{x}}_k)^T &= \mathbf{M}^2_{k,PR}\,\sigma^2_{RngMeas} \\ &= \left[(\mathbf{U}_k^T\,\mathbf{U}_k)^{-1} + \frac{(\mathbf{U}_k^T\,\mathbf{U}_k)^{-1}\mathbf{U}_k^T\mathbf{1}\mathbf{1}^T\mathbf{U}_k(\mathbf{U}_k^T\,\mathbf{U}_k)^{-1}}{n - \mathbf{1}^T\,\mathbf{U}_k(\mathbf{U}_k^T\,\mathbf{U}_k)^{-1}\mathbf{U}_k^T\,\mathbf{1}}\right]\sigma^2_{RngMeas} \\ E\left(\delta\hat{b} - \delta b\right)^2 &= m^2_{k,PR}\,\sigma^2_{RngMeas} \\ &= \frac{1}{n - \mathbf{1}^T\,\mathbf{U}_k\,(\mathbf{U}_k^T\,\mathbf{U}_k)^{-1}\,\mathbf{U}_k^T\,\mathbf{1}}\sigma^2_{RngMeas}\end{aligned} \qquad \text{Eq 436}$$

The first form of the solution yields a simpler expression for the position DoP matrix ($\mathbf{M}^1_{k,PR}$ in Eq 429) while the second form yields a simpler expression for the bias DoP ($m^2_{k,PR}$ in Eq 434).

Chain Solution for the Bias — When $\boldsymbol{\delta\hat{\mathbf{x}}}_k$ has been found, a solution for $\delta\hat{b}$ can be found from the Normal Equations (Eq 359 with **W** the identity matrix) when **J** is given by Eq 425

$$\begin{aligned}\mathbf{1}^T\,\mathbf{U}_k\,\boldsymbol{\delta\hat{\mathbf{x}}}_k + n\,\delta\hat{b} &= \mathbf{1}^T\boldsymbol{\delta\mathbf{z}} \\ \delta\hat{b} &= \frac{1}{n}\,\mathbf{1}^T(\boldsymbol{\delta\mathbf{z}} - \mathbf{U}_k\,\boldsymbol{\delta\hat{\mathbf{x}}}_k)\end{aligned} \qquad \text{Eq 437}$$

Alternative Derivation for the Estimator — From Eq 426 it follows that

$$\begin{aligned}\left(\mathbf{I} - \tfrac{1}{n}\mathbf{1}\mathbf{1}^T\right)\mathbf{J}_{k,PR}\,\boldsymbol{\delta\mathbf{X}}_k &\approx \left(\mathbf{I} - \tfrac{1}{n}\mathbf{1}\mathbf{1}^T\right)\boldsymbol{\delta\mathbf{z}} \\ \left(\mathbf{I} - \tfrac{1}{n}\mathbf{1}\mathbf{1}^T\right)\mathbf{U}_k\,\boldsymbol{\delta\mathbf{x}}_k &\approx \left(\mathbf{I} - \tfrac{1}{n}\mathbf{1}\mathbf{1}^T\right)\boldsymbol{\delta\mathbf{z}} \\ \mathbf{J}'_{k,PR}\,\boldsymbol{\delta\mathbf{x}}_k &\approx \boldsymbol{\delta\mathbf{z}}' \\ \mathbf{J}'_{k,PR} &= \left(\mathbf{I} - \tfrac{1}{n}\mathbf{1}\mathbf{1}^T\right)\mathbf{U}_k \\ \boldsymbol{\delta\mathbf{z}}' &= \left(\mathbf{I} - \tfrac{1}{n}\mathbf{1}\mathbf{1}^T\right)\boldsymbol{\delta\mathbf{z}} \\ \mathbf{R}' = E\,[\boldsymbol{\delta\mathbf{z}}'(\boldsymbol{\delta\mathbf{z}}')^T] &= \left(\mathbf{I} - \tfrac{1}{n}\mathbf{1}\mathbf{1}^T\right)\sigma^2_{RngMeas}\end{aligned} \qquad \text{Eq 438}$$

Pre-multiplying the left-hand side of Eq 426 by $\left(\mathbf{I} - \frac{1}{n}\mathbf{1}\mathbf{1}^T\right)$ eliminates the common bias as an unknown variable. Pre-multiplying the right-hand side by $\left(\mathbf{I} - \frac{1}{n}\mathbf{1}\mathbf{1}^T\right)$ eliminates the common bias from the measurements $\boldsymbol{\delta\mathbf{z}}'$. From $\mathbf{J}'_{k,PR}\,\boldsymbol{\delta\mathbf{x}}_k \approx \boldsymbol{\delta\mathbf{z}}'$, an estimate $\boldsymbol{\delta\hat{\mathbf{x}}}_k$ of the first line Eq 431

can be found using Eq 360 with the weight matrix **W** set to the identity matrix **I**.

$$\begin{aligned} \boldsymbol{\delta}\hat{\mathbf{x}}_k &= \left[\left(\mathbf{J}'_{k,PR}\right)^T \mathbf{J}'_{k,PR}\right]^{-1} \left(\mathbf{J}'_{k,PR}\right)^T \boldsymbol{\delta}\mathbf{z}' \\ E(\boldsymbol{\delta}\hat{\mathbf{x}}_k - \boldsymbol{\delta}\mathbf{x}_k)(\boldsymbol{\delta}\hat{\mathbf{x}}_k - \boldsymbol{\delta}\mathbf{x}_k)^T &= \left[\left(\mathbf{J}'_{k,PR}\right)^T \mathbf{J}'_{k,PR}\right]^{-1} \left(\mathbf{J}'_{k,PR}\right)^T \mathbf{R}' \, \mathbf{J}'_{k,PR} \left[\left(\mathbf{J}'_{k,PR}\right)^T \mathbf{J}'_{k,PR}\right]^{-1} \\ &= \left[\left(\mathbf{J}'_{k,PR}\right)^T \mathbf{J}'_{k,PR}\right]^{-1} \sigma^2_{RngMeas} \end{aligned} \qquad \text{Eq 439}$$

Since the errors for $\boldsymbol{\delta}\mathbf{z}'$ are correlated, the estimator of first line in Eq 439 may appear to be suboptimal. However, its error covariance, as found from Eq 365 and shown on the second line, is identical to the first line of Eq 432.

Role of Matrix $\left(\mathbf{I} - \frac{1}{n}\mathbf{1}\mathbf{1}^T\right)$ — The preceding equations demonstrate that the matrix $\left(\mathbf{I} - \frac{1}{n}\mathbf{1}\mathbf{1}^T\right)$ is central to Lee's method. It is a factor in both the Jacobian matrix $\mathbf{J}'_{k,PR}$ and in the measurement vector $\boldsymbol{\delta}\mathbf{z}'$. Matrix $\left(\mathbf{I} - \frac{1}{n}\mathbf{1}\mathbf{1}^T\right)$ is idempotent, and like all idempotent matrices (except for the identity matrix), it cannot be inverted. It is, however, its own pseudoinverse.

Newton Estimator — For Lee's Method, when the number of measurements *n* and unknown variables *p* (including the time/range bias) are equal, there is no 'pure Newton' estimator for the position variables that does not involve the common bias.* That is, $\left[\left(\mathbf{J}'_{k,PR}\right)^T \mathbf{J}'_{k,PR}\right]^{-1} \left(\mathbf{J}'_{k,PR}\right)^T$ does not reduce to a simpler form (as do Eq 360 and Eq 361), because $\mathbf{J}'_{k,PR}$ is not square. In such situations, there are three options: (1) employ the general Newton estimator of Eq 362, with Jacobian matrix given by Eq 425; (2) utilize the Gauss-Newton pseudo range system position-only estimators of the first lines of Eq 431 and Eq 435 (which apply to any number of measurements); and (3) use the station-difference position-only Newton estimator of Eq 451.

Condition for Singularities — Considering the second solution form, the denominators of both lines in Eq 435 involve the same difference of two positive numbers — the number of measurements *n* minus the sum of the elements of the projection matrix $\mathbf{P}_k = \mathbf{U}_k(\mathbf{U}_k^T \mathbf{U}_k)^{-1}\mathbf{U}_k^T$ for the associated true range measurement system (Eq 369). Since $\mathbf{P}_k$ is symmetric and a projection (therefore idempotent), the following bound is true.

$$\mathbf{1}^T \mathbf{U}_k(\mathbf{U}_k^T \mathbf{U}_k)^{-1}\mathbf{U}_k^T \mathbf{1} = \mathbf{1}^T \mathbf{P}_k \mathbf{1} = (\mathbf{P}_k \mathbf{1})^T(\mathbf{P}_k \mathbf{1}) = \|\mathbf{P}_k \mathbf{1}\|^2 \leq \|\mathbf{1}\|^2 = n \qquad \text{Eq 440}$$

The equality in Eq 440 only holds when $\mathbf{1}$ is in the column space of $\mathbf{U}_k$. That is, for a specific aircraft-station geometry, a solution only exists when $\mathbf{1}$ is not in the column space of $\mathbf{U}_k$.

Considering the first solution form, $\boldsymbol{\delta}\hat{\mathbf{x}}_k$ and $\delta\hat{b}$ can only be found when $\mathbf{U}_k^T\left(\mathbf{I} - \frac{1}{n}\mathbf{1}\mathbf{1}^T\right)\mathbf{U}_k$ is invertible, which is equivalent to $\left(\mathbf{I} - \frac{1}{n}\mathbf{1}\mathbf{1}^T\right)\mathbf{U}_k$ being full column rank. That is, when $\mathbf{1}$ is not in

* When *n* = *p* and pseudo slant-ranges are involved, Bancroft's algorithm (Chapter 7) provides non-iterative solutions for the unknown variables.

the column space of $\mathbf{U}_k$. This is the same requirement as that for the second form.

When $\mathbf{1}$ is in the column space of $\mathbf{U}_k$, then $\mathbf{J}_{k,PR}$ (Eq 425) is not full column rank. When this occurs, errors in a combination of pseudo range measurements are indistinguishable from the common range bias. One familiar such situation is, for a three-station system in a plane, when the aircraft is on a baseline extension (Figure 31). From the expression for $\mathbf{M}'_{k,PR}$ in Eq 434, a pseudo range system will inherit the singularities for the associated true range measurement system as well as have those caused by the use of pseudo range measurements.

DoP Matrix — DoPs for the position variables for a pseudo range system can be computed using the first line of Eq 429. This calculation is almost the same as is done range measurement systems — see Subsection 8.4.3 (Eq 412, Eq 418 and Eq 423) — except that $\mathbf{U}_k^T\,\mathbf{U}_k$ replaced by $\mathbf{U}_k^T\left(\mathbf{I}-\frac{1}{n}\mathbf{1}\mathbf{1}^T\right)\mathbf{U}_k$. Upon comparing $\mathbf{M}_{k,PR}^2$ of the first line of Eq 434 to $(\mathbf{U}_k^T\,\mathbf{U}_k)^{-1}$, which applies to true ranging systems, it is clear that — for an equal number of measurements and equal measurement errors — a system that utilizes true ranges will have smaller position errors. Thus, possibly after scaling $\mathbf{U}_k$ by the inverse of $\mathbf{C}$, the first line of Eq 434 is equivalent to

$$\mathbf{M}_{k,PR} = \mathbf{M}_{k,Rng} + \frac{\mathbf{M}_{k,Rng}\mathbf{C}^{-T}\mathbf{U}_k^T\,\mathbf{1}\mathbf{1}^T\mathbf{U}_k\mathbf{C}^{-1}\mathbf{M}_{k,Rng}}{n\;-\;\mathbf{1}^T\mathbf{U}_k\,\mathbf{C}^{-1}\mathbf{M}_{k,Rng}\,\mathbf{C}^{-T}\,\mathbf{U}_k^T\mathbf{1}} \qquad \text{Eq 441}$$

Here, $\mathbf{M}_{k,PR}$ is the DoP matrix for pseudo range measurements and $\mathbf{M}_{k,Rng}$ is the DoP matrix for the same set of ground stations when they provide true range measurements. The second term on the right-hand side of Eq 441 can be considered to be the 'penalty DoP' incurred for using pseudo ranges in lieu of true ranges. It is proportional to the range bias DoP.

Measurement Geometry Interpretation — It follows from Eq 438 that an *n*-station pseudo range system is equivalent to a fictitious *n*-station system with the characteristic that each station measures the difference between the aircraft range and the average of the ranges from all stations. The Jacobian matrix for this fictitious system is given by $\mathbf{J}'_{k,PR}$, which can be contrasted that for $\mathbf{J}_{k,PR}$ in Eq 425. Matrix $\frac{1}{n}\mathbf{1}\mathbf{1}^T$ projects the rows of any matrix onto the vector $\mathbf{1}$; matrix $\left(\mathbf{I}-\frac{1}{n}\mathbf{1}\mathbf{1}^T\right)$ projects any matrix onto the space orthogonal to the vector $\mathbf{1}$. Therefore, $\mathbf{J}'_{k,PR}$ is the projection of $\mathbf{U}_k$ onto the space which is orthogonal to vector $\mathbf{1}$. Computationally, each row of $\mathbf{J}'_{k,PR}$ is equal to the difference between the corresponding row of $\mathbf{U}_k$ and mean of all rows of $\mathbf{U}_k$.

For a true slant-range system, each row of the Jacobian matrix can be thought of as a unit vector along the line-of-sight between the aircraft and a station's location that terminates on (and points toward) the aircraft. For the equivalent fictitious system, the rows of $\mathbf{J}'_{k,PR}$ correspond to vectors connecting (a) the tails of the unit vectors for the true range systems with (b) the mean of all unit vector tail locations. This mean location has some characteristics of as a virtual aircraft location.

However, the rows of $\mathbf{J}'_{k,PR}$ do not lie along the lines connecting the virtual aircraft location and stations and are generally not unit vectors (they may have magnitudes greater or less than one). An example is presented in Subsection 8.5.2.

Situations where the actual aircraft location and the virtual aircraft location are close (much less than a unit vector) corresponds to favorable measurement geometry. If the aircraft is within the polygonal surface formed by the perimeter stations, the mean of the tail locations will generally be small, because the individual unit vectors point in many directions and tend to cancel. However, if the aircraft is outside the polygonal surface, the unit vectors will all point in the same general direction and tend to add, indicating unfavorable measurement geometry.

Projection Matrix — It follows from Eq 370 and Eq 438 that the projection matrix $\mathbf{P}'_{k,PR}$ for $\mathbf{J}'_{k,PR}$ is given by

$$\mathbf{P}'_{k,PR} = \left(\mathbf{I} - \tfrac{1}{n}\mathbf{1}\mathbf{1}^T\right)\mathbf{U}_k\left[\mathbf{U}_k^T\left(\mathbf{I} - \tfrac{1}{n}\mathbf{1}\mathbf{1}^T\right)\mathbf{U}_k\right]^{-1}\mathbf{U}_k^T\left(\mathbf{I} - \tfrac{1}{n}\mathbf{1}\mathbf{1}^T\right) \qquad \text{Eq 442}$$

Matrix $\mathbf{P}'_{k,PR}$ projects from $\Re^n$ into a subspace of $\Re^n$ orthogonal to $\mathbf{1}$ with dimension at most $p-1$ (the number of position variables). When $n > p$, it is not possible that $\mathbf{P}'_{k,PR} = \mathbf{I} - \frac{1}{n}\mathbf{1}\mathbf{1}^T$, because $\mathbf{I} - \frac{1}{n}\mathbf{1}\mathbf{1}^T$ projects into a subspace of $\Re^n$ that is orthogonal to $\mathbf{1}$ with dimension $n-1$. However, when $n = p$ and $\mathbf{J}_{k,PR}$ is invertible, it follows that $\mathbf{P}'_{k,PR} = \mathbf{I} - \frac{1}{n}\mathbf{1}\mathbf{1}^T$, because $\mathbf{P}'_{k,PR}$ then also projects onto the subspace orthogonal to $\mathbf{1}$ of dimension $n-1$. Also, $\left[\mathbf{I} - \mathbf{P}'_{k,PR}\right]\boldsymbol{\delta z} = \frac{1}{n}\mathbf{1}\mathbf{1}^T\boldsymbol{\delta z} = \left(\frac{1}{n}\mathbf{1}^T\boldsymbol{\delta z}\right)\mathbf{1}$. An example is provided in Subsection 8.5.2 (Eq 467).

Condition at Convergence — When $n > p$, at convergence (Eq 379),

$$\left(\mathbf{J}'_{k,PR}\right)^T\boldsymbol{\delta z} = \mathbf{U}_k^T\left(\mathbf{I} - \tfrac{1}{n}\mathbf{1}\mathbf{1}^T\right)\boldsymbol{\delta z} = \mathbf{0} \quad \Rightarrow \quad \mathbf{U}_k^T\boldsymbol{\delta z} = \mathbf{U}_k^T\mathbf{1}\left(\tfrac{1}{n}\mathbf{1}^T\boldsymbol{\delta z}\right) \qquad \text{Eq 443}$$

The right-hand side of Eq 443 relates the measurements and the aircraft-station geometry. The inner product of each column of $\mathbf{U}_k$ with $\boldsymbol{\delta z}$ is equal to the inner product of the same column of $\mathbf{U}_k$ with $\mathbf{1}$ when scaled by the average of the measurements.

8.4.5 Pseudo Range Measurement Systems: Station Difference Method

Introduction — The traditional/common method of analyzing pseudo range systems (systems whereby all range measurements have a common bias/offset) is to group and subtract the pseudo range measurements for the n stations in pairs. The unknown offset then cancels, and true range differences are formed. The number of differences must be at least equal to the number of position variables to be found; thus the number of pseudo ranges must be at least one more than the number of unknown position variables. Material in this subsection is based on Ref. 46.

Difference Matrix — Following Lee, define the $(n-1) \times n$ matrix of station measurement differences $\mathbf{D}$ is taken to be

$$\mathbf{D} = \begin{bmatrix} 1 & -1 & 0 & 0 & \cdots & 0 & 0 \\ 0 & 1 & -1 & 0 & \cdots & 0 & 0 \\ 0 & 0 & 1 & -1 & \cdots & 0 & 0 \\ \cdots & \cdots & \cdots & \cdots & \cdots & \cdots & \cdots \\ 0 & 0 & 0 & 0 & \cdots & 1 & -1 \end{bmatrix} \qquad \text{Eq 444}$$

An alternative form for **D**, commonly used in terrestrial radio navigation systems (e.g., Loran-C and Decca) is

$$\mathbf{D} = \begin{bmatrix} 1 & -1 & 0 & 0 & \cdots & 0 & 0 \\ 1 & 0 & -1 & 0 & \cdots & 0 & 0 \\ 1 & 0 & 0 & -1 & \cdots & 0 & 0 \\ \cdots & \cdots & \cdots & \cdots & \cdots & \cdots & \cdots \\ 1 & 0 & 0 & 0 & \cdots & 0 & -1 \end{bmatrix} \qquad \text{Eq 445}$$

The expressions developed below apply to both forms of **D**. Matrix **D** plays the same role for Station Difference Method that matrix $\left(\mathbf{I} - \frac{1}{n}\mathbf{1}\mathbf{1}^T\right)$ plays for Lee's Method.

Optimal Estimator — The estimation problem to be solved follows from Eq 409: find the value of $\boldsymbol{\delta x}_k$ that best satisfies

$$\mathbf{D}\mathbf{U}_k\,\boldsymbol{\delta x}_k \approx \mathbf{D}\,\boldsymbol{\delta z} \qquad \text{Eq 446}$$

The right-hand side of Eq 446 constitutes the measurements for this estimation problem. The vector $\mathbf{D}\,\boldsymbol{\delta z}$ has covariance matrix $(\mathbf{D}\mathbf{D}^T)\sigma^2_{RngMeas}$. Thus the optimal estimator (Eq 361) of $\boldsymbol{\delta x}_k$ utilizes the weight matrix $(\mathbf{D}\mathbf{D}^T)^{-1}$ and is

$$\boldsymbol{\delta \hat{x}}_k = [\mathbf{U}_k^T\mathbf{D}^T(\mathbf{D}\mathbf{D}^T)^{-1}\mathbf{D}\mathbf{U}_k]^{-1}\,\mathbf{U}_k^T\mathbf{D}^T(\mathbf{D}\mathbf{D}^T)^{-1}\mathbf{D}\,\boldsymbol{\delta z} \qquad \text{Eq 447}$$

Straightforward manipulation shows that

$$\mathbf{D}^T(\mathbf{D}\mathbf{D}^T)^{-1}\mathbf{D} = \mathbf{I}_n - \frac{1}{n}\mathbf{1}\mathbf{1}^T \qquad \text{Eq 448}$$

Consequently, the optimal estimator (Eq 447) can be written

$$\boldsymbol{\delta \hat{x}}_k = \left[\mathbf{U}_k^T\left(\mathbf{I} - \frac{1}{n}\mathbf{1}\mathbf{1}^T\right)\mathbf{U}_k\right]^{-1}\mathbf{U}_k^T\left(\mathbf{I} - \frac{1}{n}\mathbf{1}\mathbf{1}^T\right)\boldsymbol{\delta z} \qquad \text{Eq 449}$$

The optimal position estimators for the Station Difference Method (Eq 449) and for Lee's Method (first line of Eq 431) are identical, as they must be. If follows that the estimation error for a range-difference system is given by the first line of Eq 432, and can also be written

$$E(\boldsymbol{\delta \hat{x}}_k - \boldsymbol{\delta x}_k)(\boldsymbol{\delta \hat{x}}_k - \boldsymbol{\delta x}_k)^T = [(\mathbf{D}\mathbf{U}_k)^T(\mathbf{D}\mathbf{D}^T)^{-1}(\mathbf{D}\mathbf{U}_k)]^{-1}\sigma^2_{RngMeas} \qquad \text{Eq 450}$$

After the position estimate $\boldsymbol{\delta \hat{x}}_k$ is found, the common measurement bias can be computed from Eq 437.

Newton Estimator — For the special (but commonly occurring) case where the minimum number of measurement differences are available, $\mathbf{DU}_k$ is a square, invertible matrix. For this situation Eq 447 becomes

$$\boldsymbol{\delta}\hat{\mathbf{x}}_k = [\mathbf{DU}_k]^{-1}(\mathbf{D}\,\boldsymbol{\delta}\mathbf{z}) \qquad \dim(\mathbf{x}_k) = \dim(\mathbf{z}) - 1 \qquad \text{Eq 451}$$

The associated estimation error covariance is given by Eq 450. Eq 451 has the form of a Newton estimator (Eq 362), with Jacobian matrix $\mathbf{DU}_k$ and measurement vector $\mathbf{D}\,\boldsymbol{\delta}\mathbf{z}$.

General Estimator — A less accurate estimate for $\boldsymbol{\delta}\mathbf{x}_k$ can be generated by using a general weight $\mathbf{W}$ matrix in Eq 447, in lieu of $(\mathbf{DD}^T)^{-1}$

$$\boldsymbol{\delta}\hat{\mathbf{x}}_k = [(\mathbf{DU}_k)^T\mathbf{W}(\mathbf{DU}_k)]^{-1}(\mathbf{DU}_k)^T\mathbf{W}(\mathbf{D}\,\boldsymbol{\delta}\mathbf{z}) \qquad \text{Eq 452}$$

The associated estimation error is (from Eq 365)

$$\begin{aligned} &E(\boldsymbol{\delta}\hat{\mathbf{x}}_k - \boldsymbol{\delta}\mathbf{x}_k)(\boldsymbol{\delta}\hat{\mathbf{x}}_k - \boldsymbol{\delta}\mathbf{x}_k)^T \\ &= [(\mathbf{DU}_k)^T\mathbf{W}(\mathbf{DU}_k)]^{-1}(\mathbf{DU}_k)^T\mathbf{W}(\mathbf{DD}^T)\mathbf{W}(\mathbf{DU}_k)[(\mathbf{DU}_k)^T\mathbf{W}(\mathbf{DU}_k)]^{-1}\sigma^2_{RngMeas} \end{aligned} \qquad \text{Eq 453}$$

For the case where the minimum number of measurement differences are available ($n = p$) $\mathbf{DU}_k$ is a square, invertible matrix ($n-1$ x $n-1$) and Eq 452 reduces to the Newton estimator. A special case of the general estimator is $\mathbf{W} = \mathbf{I}$.

8.5 Example Applications and Interpretations

8.5.1 Example 8 Continued: Slant-Range Measurement Systems in Flatland

Introduction — This subsection continues the analysis, begun in Subsection 7.12.1, of surveillance or navigation systems in two dimensions ('Flatland'). The systems employ ground stations that are used to measure slant-ranges to an 'aircraft'. This subsection considers true slant-range measurements for two- and three-station configurations, with the stations being separated by one BLU.

The first topic addressed is a numerical Horizontal Dilution of Precision (HDoP) analysis using the methodology described in Subsections 8.4.2 and 8.4.3. Upon carrying out straightforward calculations (particularly involving Eq 412 with $\mathbf{C}$ equal to the identity matrix), HDoP contours are shown in Figure 42. The left-hand panel pertains to a two-station configuration and the right-hand panel to three stations. The calculations assume that each station's signal can be received up to 3.5 BLUs in range. For these figures, HDoPs for both configurations are symmetrical about a 'vertical' axis, and thus are truncated 'to the left'.

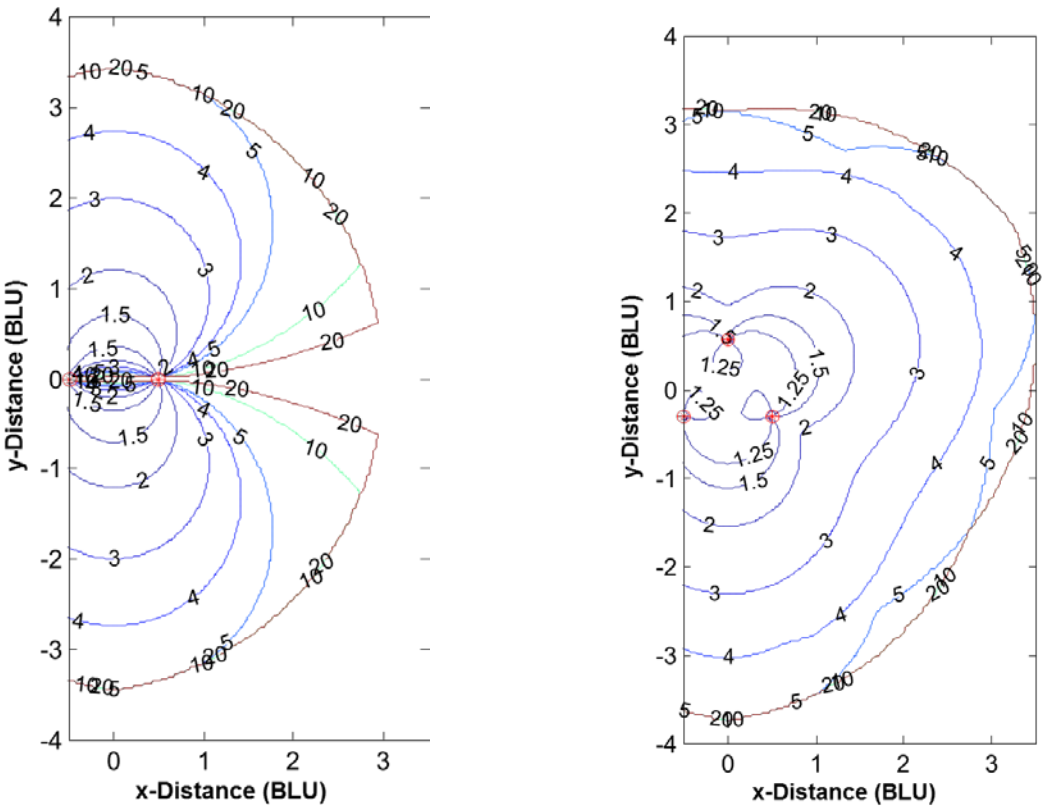

(a) Two Stations (b) Three Stations

Figure 42 HDoP Contours for True Slant-Range Measurement Systems in Flatland

Two Ground Stations

DoP Equations — In Figure 42(a), the HDoP pattern exhibits strong directionality. Coverage is best perpendicular to the baseline and is poor to non-existent along the station baseline and its extensions. A two-station configuration can be readily analyzed along the station bisector — see Figure 43, which has the station baseline turned 90 degrees from that in Figure 42(a).

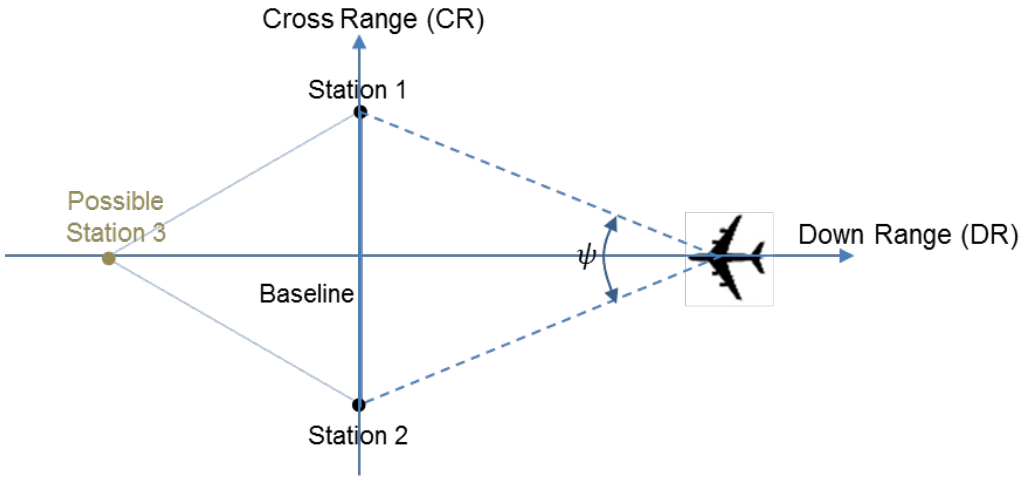

Figure 43 Aircraft on the Perpendicular Bisector of Two Stations in Flatland

From Figure 43, it is straightforward to calculate DoP values along the perpendicular bisector of the station baseline. For any point, the Jacobian matrix $\mathbf{U}_{c,Rng\text{-}2}$ (Eq 407 and Eq 408) is

$$\mathbf{U}_{c,Rng\text{-}2} = \begin{bmatrix} \cos(\frac{1}{2}\psi) & -\sin(\frac{1}{2}\psi) \\ \cos(\frac{1}{2}\psi) & \sin(\frac{1}{2}\psi) \end{bmatrix} \qquad \text{Eq 454}$$

In Eq 454, the first coordinate is down range (DR), the second is cross range (CR), and ψ is the angle at the aircraft subtended by vectors pointing toward the stations. Thus the DoP matrix is

$$\mathbf{M}_{c,Rng\text{-}2} = \left(\mathbf{U}_{c,Rng\text{-}2}^{T}\,\mathbf{U}_{c,Rng\text{-}2}\right)^{-1} = \begin{bmatrix} \dfrac{1}{2\cos^2(\frac{1}{2}\psi)} & 0 \\ 0 & \dfrac{1}{2\sin^2(\frac{1}{2}\psi)} \end{bmatrix} \qquad \text{Eq 455}$$

$$= \mathrm{diag}\left(\,\mathrm{DRDoP}_{c,Rng\text{-}2}^2, \mathrm{CRDoP}_{c,Rng\text{-}2}^2\,\right)$$

From Eq 455, the aircraft location estimation errors for the two axes are uncorrelated (for locations on the bisector). HDoP along the perpendicular bisector is

$$\mathrm{HDoP}_{c,Rng\text{-}2} = \sqrt{\mathrm{DRDoP}_{c,Rng\text{-}2}^2 + \mathrm{CRDoP}_{c,Rng\text{-}2}^2} = \frac{\sqrt{2}}{|\sin(\psi)|} \qquad \text{Eq 456}$$

The minimum value of $\mathrm{HDoP}_{c,Rng\text{-}2}$ is $\sqrt{2} \approx 1.414$. This occurs when the aircraft is one-half a baseline length from the baseline along the perpendicular bisector, where $\psi = \pi/2$. From that point, $\mathrm{HDoP}_{c,Rng\text{-}2}$ increases in both directions. Due to the down range component's behavior, $\mathrm{HDoP}_{c,Rng\text{-}2}$ is infinite at the baseline (where $\psi = \pi$). However, it has usable values close to the baseline — e.g., along the baseline perpendicular bisector, $\mathrm{HDoP}_{c,Rng\text{-}2}$ is less than 5 within one-tenth of the baseline length. Due to the cross range component's behavior, $\mathrm{HDoP}_{c,Rng\text{-}2}$ also grows with distance (as ψ approaches zero and 2π). However, along a baseline bisector,

$HDoP_{c,Rng\text{-}2}$ is less than 5 within 3.46 times the baseline length.

It's instructive to consider HDoP components separately. Both are symmetric about the baseline, ($\psi = \pi$). From Eq 455, it's evident that DRDoP improves with distance from the stations and approaches $1/\sqrt{2} \approx 0.707$, because the two range measurements are effectively averaged. Asymptotically, CRDoP$\sim \frac{\sqrt{2}\,DR}{B} = 1.4\frac{DR}{B}$ where *B* is the length of the baseline. Thus CRDoP degrades linearly with range, the same behavior as an angle measurement system.

Using HDoP equal to five as a criterion, the two-station service area may be approximated by a 7 BLU x 1 BLU rectangle which includes the baseline as a bisector, bordered by four right triangles with sides of 3 BLU and 1 BLU. Thus, except for a small set of locations adjacent to the baseline, the service area is roughly: (7 x 1) + 4 x (½ x 3 x 1) = 13 BLU^2.

Iteration Process Convergence — When a closed-form solution is available, there is no need to use an iterative method such as NLLS. However, a system involving two ranging ground stations illustrates the NLLS convergence issues raised in Subsection 8.1.7. As shown in Subsection 7.12.1, this measurement system imposes constraints on the measurement values (e.g., Eq 341); thus, when measurement errors occur, a solution may not exist. Also shown in Subsection 7.12.1 is that for every potential aircraft location, there is a second location on the opposite side of (and equal distance from) the station baseline that also satisfies the measurement equations. Thus, solution uniqueness can be an issue as well.

To illustrate NLLS convergence behavior, a Monte Carlo experiment was conducted for the station configuration shown in Figure 43. Using (DR, CR) coordinates and Base Line Units (BLUs) for distances, the station locations are $(0, \pm 0.5)$ while the true aircraft locations form a grid of all combinations of $DR = 0,1,2,3,4$ and $CR = 0,1,2,3$. The aircraft location estimates used to initialize the NLLS iteration process are the true locations plus a Gaussian random variable (in each axis) with zero-mean. The standard deviation of the initial estimate is either 0.2 BLU or 2 BLU. The former value characterizes continuous operation of a system (for a surveillance system, aircraft is being tracked); the latter value, 2 BLUs, is representative of a situation with poor initialization (for a surveillance system, aircraft is being acquired). The result of the iterative process are grouped into three categories: (a) converged to the correct aircraft location, (b) converged to the ambiguous aircraft location, or (c) failed to converge. The results of the experiment, using 1,000 trials for each aircraft location and each initialization error standard deviation are shown in Table 14 and Table 15.

Table 14 Convergence 'during Acquisition' (2 Ranging Stations)

	Result	DR=0	DR=1	DR=2	DR=3	DR=4
	Correct Converge	59.8%	68.4%	83.3%	92.3%	96.3%
CR=3	False Converge	0.0%	30.2%	13.6%	4.8%	2.3%
	Diverge	40.2%	1.4%	3.1%	2.9%	1.4%
	Correct Converge	66.4%	67.8%	83.4%	91.1%	97.3%
CR=2	False Converge	0.0%	26.7%	12.4%	5.8%	1.7%
	Diverge	33.6%	5.5%	4.2%	3.1%	1.0%
	Correct Converge	75.6%	59.7%	81.6%	92.8%	96.3%
CR=1	False Converge	0.0%	26.4%	11.5%	5.4%	3.1%
	Diverge	24.4%	13.9%	6.9%	1.8%	0.6%
	Correct Converge	2.5%	67.6%	84.9%	93.8%	98.2%
CR=0	False Converge	0.0%	27.3%	15.1%	6.2%	1.8%
	Diverge	97.5%	5.1%	0.0%	0.0%	0.0%

Table 15 Convergence 'while Tracking' (2 Ranging Stations)

	Result	DR=0	DR=1	DR=2	DR=3	DR=4
	Correct Converge	100.0%	100.0%	100.0%	100.0%	100.0%
CR=3	False Converge	0.0%	0.0%	0.0%	0.0%	0.0%
	Diverge	0.0%	0.0%	0.0%	0.0%	0.0%
	Correct Converge	99.9%	100.0%	100.0%	100.0%	100.0%
CR=2	False Converge	0.0%	0.0%	0.0%	0.0%	0.0%
	Diverge	0.1%	0%	0%	0%	0%
	Correct Converge	96.7%	100.0%	100.0%	100.0%	100.0%
CR=1	False Converge	0.0%	0.0%	0.0%	0.0%	0.0%
	Diverge	3.3%	0.0%	0.0%	0.0%	0.0%
	Correct Converge	92.1%	100.0%	100.0%	100.0%	100.0%
CR=0	False Converge	0.0%	0.0%	0.0%	0.0%	0.0%
	Diverge	7.9%	0.0%	0.0%	0.0%	0.0%

Table 14 and Table 15 demonstrate that initialization accuracy can strongly influence the iteration process's performance. For the 'acquisition' initialization, overall performance is: correct convergence, 78.0%; false convergence, 9.7%; divergence, 12.3%. Moreover, performance is poorer for locations closer to the baseline. For example, for aircraft 1 BLU from the baseline in the DR direction, the convergence rate for the true aircraft location averaged 65.9% and the false convergence rate is over 26% for all four locations. For many applications, this performance would be unacceptable. In contrast, for the 'tracking' initialization, overall performance is: correct convergence, 99.4%; false convergence, 0.0%; divergence, 0.6%. Only along the baseline connecting the stations, or its extensions, is the iteration process success rate less than 100%.

Three Ground Stations

DoP Equations — A similar DoP analysis can be performed for a three-station configuration. For

an arbitrary point along a baseline bisector

$$\mathbf{U}_{c,Rng\text{-}3} = \begin{bmatrix} \cos(\frac{1}{2}\psi) & -\sin(\frac{1}{2}\psi) \\ \cos(\frac{1}{2}\psi) & \sin(\frac{1}{2}\psi) \\ \pm 1 & 0 \end{bmatrix} \qquad \text{Eq 457}$$

In Eq 457, in the (3,2)-element, the upper sign pertains when the aircraft is 'to the right' of Station 3 in Figure 43, and the lower sign pertains when the aircraft is 'to the left' of Station 3. For either case, the DoP matrix is

$$\mathbf{M}_{c,Rng\text{-}3} = \left(\mathbf{U}_{c,Rng\text{-}3}^{T}\,\mathbf{U}_{c,Rng\text{-}3}\right)^{-1} = \begin{bmatrix} \dfrac{1}{1+2\cos^2(\frac{1}{2}\psi)} & 0 \\ 0 & \dfrac{1}{2\sin^2(\frac{1}{2}\psi)} \end{bmatrix} \qquad \text{Eq 458}$$
$$= \mathrm{diag}(\,\mathrm{DRDoP}_{c,Rng\text{-}3}^2\,,\mathrm{CRDoP}_{c,Rng\text{-}3}^2\,)$$

Again, the aircraft location estimation errors for the two axes are uncorrelated, and are symmetric about the baseline. Another point of interest is that $\mathrm{DRDoP}_{c,Rng\text{-}3}$ is continuous when an aircraft passes over Station 3. From Eq 458, it follows that HDoP for points on the bisector is

$$\mathrm{HDoP}_{c,Rng\text{-}3} = \sqrt{\mathrm{DRDoP}_{c,Rng\text{-}3}^2 + \mathrm{CRDoP}_{c,Rng\text{-}3}^2} = \frac{\sqrt{3}}{\sqrt{\sin^2(\psi) + 2\sin^2(\frac{1}{2}\psi)}} \qquad \text{Eq 459}$$

The minimum value for $\mathrm{HDoP}_{c,Rng\text{-}3}$ is $2/\sqrt{3} \approx 1.155$, which occurs at the center of the triangle formed by the stations ($\psi = 4\pi/3$), where $\mathrm{DRDoP}_{c,Rng\text{-}3} = \mathrm{CRDoP}_{c,Rng\text{-}3}$. At the midpoint of the baseline between Stations 1 and 2 ($\psi = \pi$), $\mathrm{HDoP}_{c,Rng\text{-}3}$ is $\sqrt{3/2} \approx 1.225$. At Station 3 ($\psi = 5\pi/3$), $\mathrm{HDoP}_{c,Rng\text{-}3}$ is $2\sqrt{3/5} \approx 1.549$. Along a baseline bisector, there is no advantage to being within the perimeter of the triangle joining the stations.

The DoP matrices in Eq 458 and Eq 455 are quite similar; the primary difference is that the (1,1)-term for the three-station configuration does not have unbounded solutions along the baseline which occur in the two-station case. For three stations, DoP along the bisector down-range axis approaches $1/\sqrt{3} \approx 0.577$ with distance in either direction, because three range measurements are effectively being averaged. CRDoP is identical to that for two stations.

The estimator matrix for this system is shown in Eq 460. It reflects the geometry and statistics of the measurement scenario. The cross range estimate is not affected by the Station 3 measurement — which is expected, since $\mathrm{CRDoP}_{c,Rng\text{-}3} = \mathrm{CRDoP}_{c,Rng\text{-}2}$. The associated projection matrix is shown in Eq 461.

$$\left(\mathbf{U}_{c,Rng\text{-}3}^{T}\mathbf{U}_{c,Rng\text{-}3}\right)^{-1}\mathbf{U}_{c,Rng\text{-}3}^{T}=\begin{bmatrix}\dfrac{\cos(\frac{1}{2}\psi)}{1+2\cos^2(\frac{1}{2}\psi)} & \dfrac{\cos(\frac{1}{2}\psi)}{1+2\cos^2(\frac{1}{2}\psi)} & \dfrac{\pm 1}{1+2\cos^2(\frac{1}{2}\psi)}\\ \dfrac{-1}{2\sin(\frac{1}{2}\psi)} & \dfrac{1}{2\sin(\frac{1}{2}\psi)} & 0\end{bmatrix} \quad \text{Eq 460}$$

$$\mathbf{P}_{c,Rng\text{-}3}=\mathbf{U}_{c,Rng\text{-}3}\left(\mathbf{U}_{c,Rng\text{-}3}^{T}\mathbf{U}_{c,Rng\text{-}3}\right)^{-1}\mathbf{U}_{c,Rng\text{-}3}^{T}$$

$$=\begin{bmatrix}\dfrac{\cos^2(\frac{1}{2}\psi)}{1+2\cos^2(\frac{1}{2}\psi)}+\dfrac{1}{2} & \dfrac{\cos^2(\frac{1}{2}\psi)}{1+2\cos^2(\frac{1}{2}\psi)}-\dfrac{1}{2} & \dfrac{\pm\cos(\frac{1}{2}\psi)}{1+2\cos^2(\frac{1}{2}\psi)}\\ \dfrac{\cos^2(\frac{1}{2}\psi)}{1+2\cos^2(\frac{1}{2}\psi)}-\dfrac{1}{2} & \dfrac{\cos^2(\frac{1}{2}\psi)}{1+2\cos^2(\frac{1}{2}\psi)}+\dfrac{1}{2} & \dfrac{\pm\cos(\frac{1}{2}\psi)}{1+2\cos^2(\frac{1}{2}\psi)}\\ \dfrac{\pm\cos(\frac{1}{2}\psi)}{1+2\cos^2(\frac{1}{2}\psi)} & \dfrac{\pm\cos(\frac{1}{2}\psi)}{1+2\cos^2(\frac{1}{2}\psi)} & \dfrac{1}{1+2\cos^2(\frac{1}{2}\psi)}\end{bmatrix} \quad \text{Eq 461}$$

For three stations there are six bisector radials extending outward from the station cluster (rather than two radials for the two-station case). As a result, the service area is roughly circular. The service area (for maximum HDoP equal to five) is approximately π 3.5 BLU x 3.5 BLU ≈ 36 BLU^2, or 12 BLU^2 per station (roughly twice the value for a two-station configuration).

Iteration Process Convergence — The Monte Carlo experiment performed for two ranging stations was repeated for three stations, using an initialization error standard deviation of 2 BLU that's characteristic of an 'acquisition' situation. Comparing Table 16 with Table 14 shows the dramatic improvement that a redundant station can provide. Here the overall performance is: correct convergence, 99.0%; false convergence, 0.0%; divergence, 1.0%. This performance is comparable to that of the two-station configuration with 'tracking' initialization. (Partly because NLLS initialization accuracy is significantly poorer during acquisition than tracking, some systems require use of a redundant sensor during acquisition.)

Table 16 Convergence 'during Acquisition' (3 Ranging Stations)

	Result	DR=0	DR=1	DR=2	DR=3	DR=4
	Correct Converge	99.2%	99.9%	99.9%	100.0%	100.0%
CR=3	False Converge	0.0%	0.0%	0.0%	0.0%	0.0%
	Diverge	0.8%	0.1%	0.1%	0.0%	0.0%
	Correct Converge	98.6%	100.0%	100.0%	100.0%	99.8%
CR=2	False Converge	0.0%	0.0%	0.0%	0.0%	0.0%
	Diverge	1.4%	0.0%	0.0%	0.0%	0.2%
	Correct Converge	93.2%	99.9%	99.2%	99.5%	99.7%
CR=1	False Converge	0.0%	0.0%	0.0%	0.0%	0.0%
	Diverge	6.8%	0.1%	0.8%	0.5%	0.3%
	Correct Converge	100.0%	99.9%	95.6%	97.4%	99.1%
CR=0	False Converge	0.0%	0.0%	0.0%	0.0%	0.0%
	Diverge	0.0%	0.1%	4.4%	2.6%	0.9%

8.5.2 Example 9 Continued: Pseudo Slant-Range Measurement Systems in Flatland

Introduction — This subsection continues analysis, begun in Subsection 7.12.2, of surveillance/navigation systems operating in Flatland. The systems employ ground stations that are used to measure the pseudo slant-range to an aircraft, and the stations are separated by one BLU. Similar to Subsection 8.5.1, this subsection emphasizes DoP behavior. The methodology employed is described in Subsection 8.4.4, but without the vertical component.

Three Stations' HDoP on a Baseline Extension — Subsection 7.7.3 contains a taxonomy of the solutions for a situation involving three pseudo range stations in Flatland. On a baseline extension, the governing equation (e.g., Eq 279) has a double root — i.e., an ambiguous or extraneous solution does not exist. Referring to Figure 43, for an aircraft along the CR axis with $CR > \frac{1}{2}B$

$$\mathbf{U}_{c,Rng\text{-}3} = \begin{bmatrix} 0 & 1 \\ 0 & 1 \\ \cos(\alpha) & \sin(\alpha) \end{bmatrix} \qquad \text{Eq 462}$$

Here, α is the angle between the unit vector from Station 3 to the aircraft and the DR axis. Eq 462 does not contain any of the sides or angles of stations in Figure 43. Thus an equation similar to Eq 462 applies to any three-station configuration when the stations are not collinear.

It follows from Eq 429 that the inverse of the HDoP matrix is

$$\begin{aligned} \left(\mathbf{M}^{1}_{c,PR\text{-}3}\right)^{-1} &= \mathbf{U}^{T}_{c,Rng\text{-}3}\left(\mathbf{I} - \tfrac{1}{n}\mathbf{1}\mathbf{1}^{T}\right)\mathbf{U}_{c,Rng\text{-}3} \\ &= \frac{2}{3}\begin{bmatrix} \cos^2(\alpha) & -\cos(\alpha)[1-\sin(\alpha)] \\ -\cos(\alpha)[1-\sin(\alpha)] & [1-\sin(\alpha)]^2 \end{bmatrix} \end{aligned} \qquad \text{Eq 463}$$

The matrix on the second line of Eq 463 is singular; thus, its inverse, the HDoP matrix, does not exist. It follows that, when an aircraft approaches any baseline extension (not including the nearest station), HDoP grows unboundedly large.

Three Stations' HDoP at a Station — When the aircraft location is the same as a station location, the governing equation also has a double root. However the situation is qualitatively different from that for a baseline extension, as the elements of $\mathbf{U}_{c,Rng\text{-}3}$ for the station involved have the indeterminate form 0/0. Thus matrix $\mathbf{U}_{c,Rng\text{-}3}$ is not defined. As is seen below, when an aircraft approaches a station (except along a baseline extension), HDoP approaches a finite limit; the limit value varies with the aircraft's direction.

Three Stations' DoP Along the Axis of Symmetry — As is done in Subsection 8.5.1, HDoP and its down-range and cross-range components are examined along the perpendicular bisector of the baseline joining Stations 1 and 2 in Figure 43. Substituting $\mathbf{U}_{c,Rng\text{-}3}$ from Eq 457 into $\mathbf{J}'_{k,PR} = \left(\mathbf{I} - \frac{1}{n}\mathbf{1}\mathbf{1}^{T}\right)\mathbf{U}_{k}$ yields the Jacobian matrix $\mathbf{J}'_{c,PR\text{-}3}$ (Eq 464) for an equivalent system having measurements involving the same stations. The DoP matrix $\mathbf{M}_{c,PR\text{-}3}$ and estimator matrix

then follow using Eq 439. Concerning the ambiguous signs in Eq 464 and Eq 465, the upper sign applies when the aircraft is 'to the right' of Station 3 in Figure 43, and the lower sign applies when the aircraft is 'to the left' of Station 3.

$$\mathbf{J}'_{c,PR\text{-}3} = \begin{bmatrix} \mp\frac{1}{3}\left[1 \mp \cos(\frac{1}{2}\psi)\right] & -\sin(\frac{1}{2}\psi) \\ \mp\frac{1}{3}\left[1 \mp \cos(\frac{1}{2}\psi)\right] & \sin(\frac{1}{2}\psi) \\ \pm\frac{2}{3}\left[1 \mp \cos(\frac{1}{2}\psi)\right] & 0 \end{bmatrix} \qquad \text{Eq 464}$$

$$\mathbf{M}_{c,PR\text{-}3} = \left(\left(\mathbf{J}'_{c,PR\text{-}3}\right)^T \mathbf{J}'_{c,PR\text{-}3}\right)^{-1} = \text{diag}(\,\text{DRDoP}^2_{c,PR\text{-}3}, \text{CRDoP}^2_{c,PR\text{-}3}\,) \qquad \text{Eq 465}$$

$$\text{DRDoP}_{c,PR\text{-}3} = \frac{\sqrt{3/2}}{1 \mp \cos(\frac{1}{2}\psi)} \qquad \text{CRDoP}_{c,PR\text{-}3} = \frac{\sqrt{1/2}}{\sin(\frac{1}{2}\psi)}$$

Along the perpendicular bisector of the baseline joining Stations 1 and 2 in Figure 43, $\text{CRDoP}_{c,PR\text{-}3}$ is identical to the cross-range DoPs for two and three true slant-range stations.

However, the behavior of $\text{DRDoP}_{c,PR\text{-}3}$ is different from that for true ranging systems in several ways. Notably, $\text{DRDoP}_{c,PR\text{-}3}$ is discontinuous at Station 3 (where $\psi = 5\pi/3$). When Station 3 is approached from inside the three station perimeter ('from the right' in Figure 43), $\text{DRDoP}_{c,PR\text{-}3}$ approaches 0.656; when Station 3 is approached 'from the left', $\text{DRDoP}_{c,PR\text{-}3}$ approaches 9.142 — a discontinuity of 8.486. Outside the perimeter enclosing the stations, $\text{DRDoP}_{c,PR\text{-}3}$ increases very rapidly. When $|DR| > \left(\frac{\sqrt{3}}{2}\right)B$, where B is the baseline length, $\text{DRDoP}_{c,PR\text{-}3}$ is symmetric and is asymptotically equal to $9.8\left(\frac{DR}{B}\right)^2$. Thus $\text{DRDoP}_{c,PR\text{-}3}$ increases quadraticly with range from the Station 1-2 baseline, whereas cross-range DoP increases linearly as $1.4\left(\frac{DR}{B}\right)$. Noting that $\text{HDoP}_{c,PR\text{-}3}$ is infinite along any baseline extension, the $\text{HDoP}_{c,PR\text{-}3}$ value of 9.250 when Station 3 is approached 'from the left' is the minimum $\text{HDoP}_{c,PR\text{-}3}$ in the V-shaped region bounded by two baseline extensions. This is part of the rationale for aircraft not operating in the regions bounded by the baseline extensions.

The minimum $\text{HDoP}_{c,PR\text{-}3}$ occurs at the center of the triangle formed by the stations ($\psi = 4\pi/3$). At that location, $\text{DRDoP}_{c,PR\text{-}3}$ and $\text{CRDoP}_{c,PR\text{-}3}$ have the same value, $1/\sqrt{3} \approx 0.577$ (and thus $\text{HDoP}_{c,PR\text{-}3} = 2/\sqrt{3} \approx 1.155$). These are the same values that a three-station true range system would have. At the midpoint of the baseline joining Stations 1 and 2 ($\psi = \pi$), $\text{DRDoP}_{c,PR\text{-}3} = \sqrt{3/2} \approx 1.225$ and $\text{CRDoP}_{c,PR\text{-}3} = 1/\sqrt{2} \approx 0.707$ (and thus $\text{HDoP}_{c,PR\text{-}3} = \sqrt{2} \approx 1.414$). The faster growth rate of $\text{DRDoP}_{c,PR\text{-}3}$ relative to $\text{CRDoP}_{c,PR\text{-}3}$ is evident. Continuing 'to the right' beyond the baseline joining Stations 1 and 2, $\text{HDoP}_{c,PR\text{-}3}$ is equal to 2 at approximately 18% of a baseline length outside the perimeter, and is equal to 5 at approximately 56% of a baseline length. HDoP is greater than 10 before the down-range distance equals 90% of a baseline.

Figure 44 shows down range and cross range DoPs along a baseline bisector for systems employing two and three-station true ranges and three-station pseudo ranges. DoP values are shown as a function of distance along the DR axis from the Station 1-2 baseline.

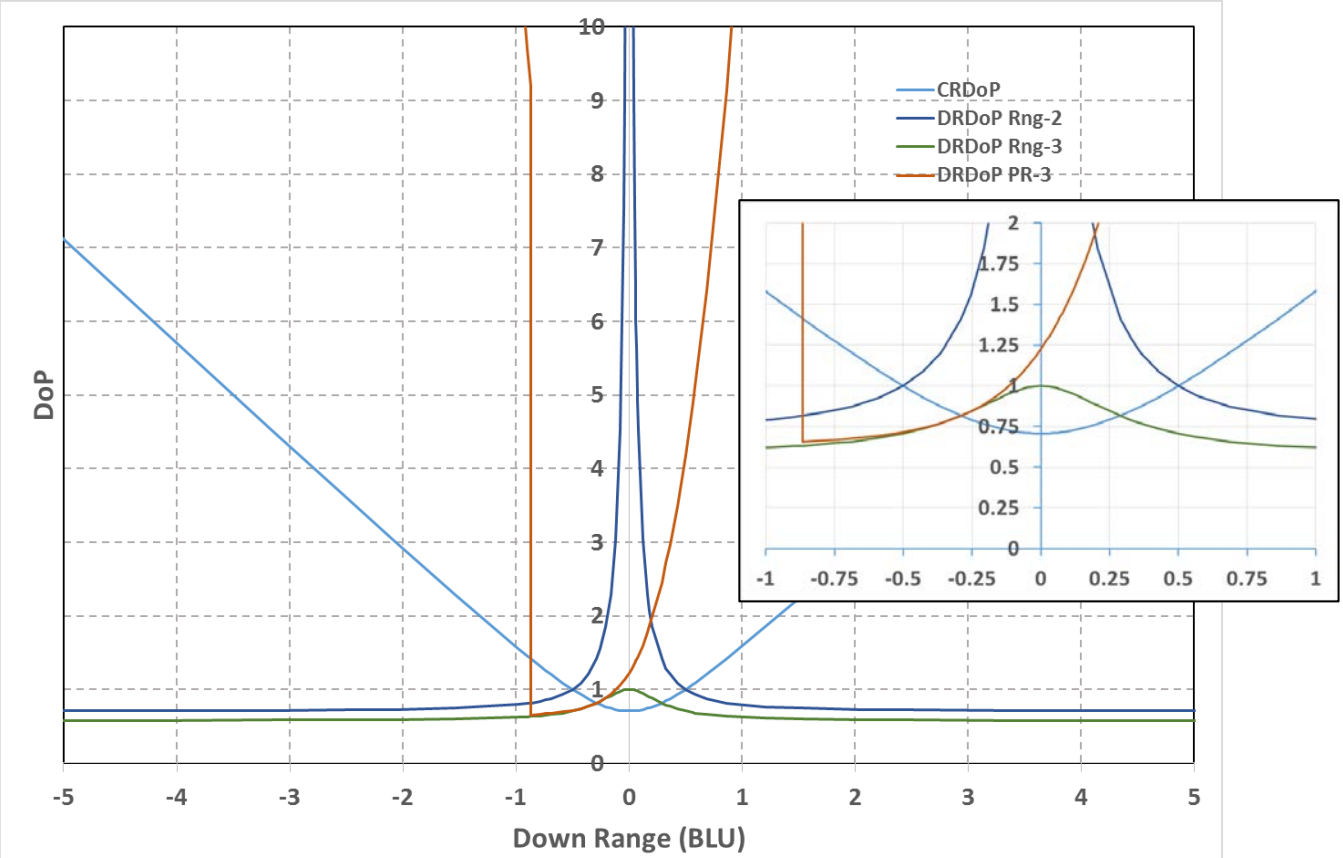

Figure 44 DoPs Along a Symmetry Axis for True and Pseudo Range Systems

Three Stations' Measurement Geometry Along the Axis of Symmetry — The estimator matrix for locations on the perpendicular bisector is shown in Eq 466. As expected, the estimator implicitly forms two differences from the three pseudo range measurements. The associated projection matrix (Eq 467) is equal to the idempotent matrix $\mathbf{I} - \frac{1}{3}\mathbf{1}\mathbf{1}^T$, which can occur when $n = p$ (Eq 442).

$$\left(\left(\mathbf{J}'_{c,PR\text{-}3}\right)^T \mathbf{J}'_{c,PR\text{-}3}\right)^{-1} \left(\mathbf{J}'_{c,PR\text{-}3}\right)^T = \begin{bmatrix} \frac{\mp 1}{2\left[1 \mp \cos\left(\frac{1}{2}\psi\right)\right]} & \frac{\mp 1}{2\left[1 \mp \cos\left(\frac{1}{2}\psi\right)\right]} & \frac{\pm 1}{1 \mp \cos\left(\frac{1}{2}\psi\right)} \\ \frac{-1}{2\sin\left(\frac{1}{2}\psi\right)} & \frac{1}{2\sin\left(\frac{1}{2}\psi\right)} & 0 \end{bmatrix} \quad \text{Eq 466}$$

$$\mathbf{P}'_{c,PR\text{-}3} = \mathbf{J}'_{c,PR\text{-}3}\left(\left(\mathbf{J}'_{c,PR\text{-}3}\right)^T \mathbf{J}'_{c,PR\text{-}3}\right)^{-1} \left(\mathbf{J}'_{c,PR\text{-}3}\right)^T = \begin{bmatrix} \frac{2}{3} & -\frac{1}{3} & -\frac{1}{3} \\ -\frac{1}{3} & \frac{2}{3} & -\frac{1}{3} \\ -\frac{1}{3} & -\frac{1}{3} & \frac{2}{3} \end{bmatrix} \quad \text{Eq 467}$$

Figure 45 provides a geometric interpretation of Lee's Method for the three-station pseudo range system shown in Figure 43. The solid blue lines are unit vectors along the lines-of-sight from the three stations to the aircraft. These unit vectors form the rows of the Jacobian matrix for true range system, and can be considered to terminate at the aircraft. The solid red lines are vectors from the tails of the blue unit vectors to the mean of the three unit vector tail locations. (The red lines for Station 3 vectors partially overlay the blue lines.) This mean location can be thought of as the virtual aircraft location for the pseudo range system employing the same stations.

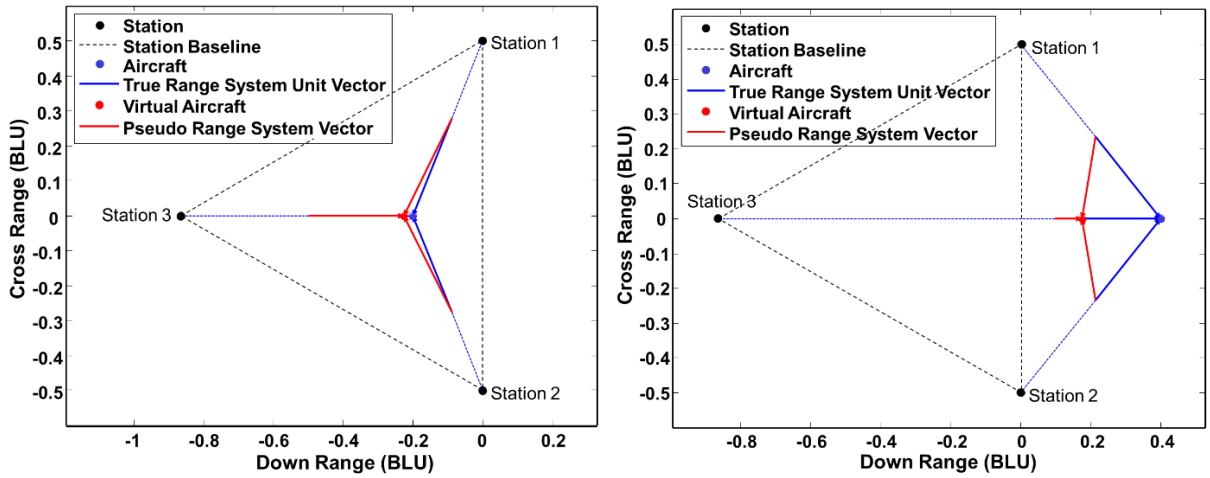

(a) Favorable Measurement Geometry (b) Unfavorable Measurement Geometry

Figure 45 Geometric Interpretation of Lee's Method for Three Stations

When the aircraft is within the perimeter formed by the stations, the locations of the tails of the blue unit vectors tend to cancel when forming their mean. Thus, the virtual aircraft location is close to the true aircraft location, and the pseudo range system vectors are similar in length and orientation to the unit vectors for the true ranging system — i.e., the measurement geometry is favorable.

In contrast, when the aircraft is outside the perimeter of the stations, the unit vectors point to only half the plane or volume involved; thus the mean of the vector tails reflects reinforcement as well as cancellation. Then the pseudo range system vectors are shorter (and have different orientations) than the unit vectors for the true ranging system — i.e., the measurement geometry is unfavorable. In particular, in Figure 45(b), the pseudo range system vector for Station 3 is much shorter than the Station-3 vector in Figure 45(a) — graphically indicating the inability of a pseudo range system to determine distance from the station cluster.

Three Stations' HDoP Along a Baseline — Consider a side of the triangle formed by the stations in Figure 43 — specifically, the CR axis. DoPs do not exist at a station and are infinite along a baseline extension, so attention is limited to $|CR| < \frac{1}{2}B$. Along this side, $\text{CRDoP}_{c,PR\text{-}3} =$

$1/\sqrt{2} \approx 0.707$ at every point. (This can be shown using geometric analysis similar to that in Figure 45.) Also, along this side, $DRDoP_{c,PR\text{-}3}$ has a minimum value of 1.225 at the center and approaches a maximum value of 1.472 as a station is approached. Thus, within the perimeter of the stations, including the baselines but not the stations themselves, the maximum value of $HDoP_{c,PR\text{-}3}$ is 1.633.

Three Stations' HDoP for Concentric Circles — For the three-station configuration in Figure 43, $HDoP_{c,PR\text{-}3}$ is computed for concentric circles centered on the stations' centroid — see Figure 46. Here, the angle is measured clockwise from the negative DR axis. Thus 0 deg corresponds to the direction of Station 3, 60 deg corresponds to the direction of the mid-point of the baseline connection Stations 1 and 3, and 120 deg corresponds to the direction of Station 1.

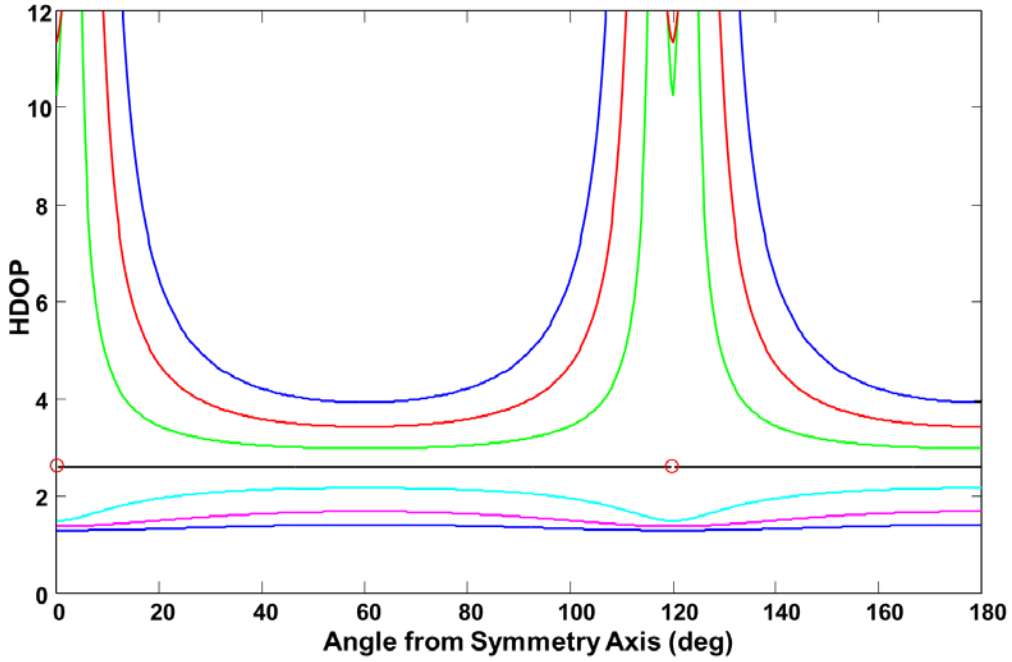

Figure 46 HDoPs for Three-Station Pseudo Range System on Concentric Circles

The circles used for Figure 46 are described in Table 17, listed from the smallest to largest radii. Radii and maximum perimeter penetrations are in BLUs.

Table 17 Concentric Circles Used to Characterize HDoP

Line Color	Circle Radius	Radius Description	Max. Perimeter Penetration*	HDoP at Max. Pen.*
Blue	0.289	Inscribed circle radius	0	1.414
Magenta	0.389	Inscribed circle radius + 10% of BLU	0.100	1.686
Cyan	0.505	Extraneous solution detectable†	0.217	2.174
Black	0.577	Circumscribed circle radius	0.289	2.582
Green	0.635	110% of Circumscribed circle radius	0.346	2.972
Red	0.693	120% of Circumscribed circle radius	0.401	3.421

Line Color	Circle Radius	Radius Description	Max. Perimeter Penetration*	HDoP at Max. Pen.*
Blue	0.751	130% of Circumscribed circle radius	0.462	3.930

* Along a radial from the centroid that is perpendicular to a baseline at its midpoint
† See Figure 31

Three Stations' HDoP Contours — Figure 47 shows $HDoP_{c,PR\text{-}3}$ contours for the station configuration shown in Figure 43. Because HDoP is infinite along the baseline extensions, contours for $HDoP_{c,PR\text{-}3} \geq 1.633$ (the maximum HDoP with the station perimeter) terminate at stations.

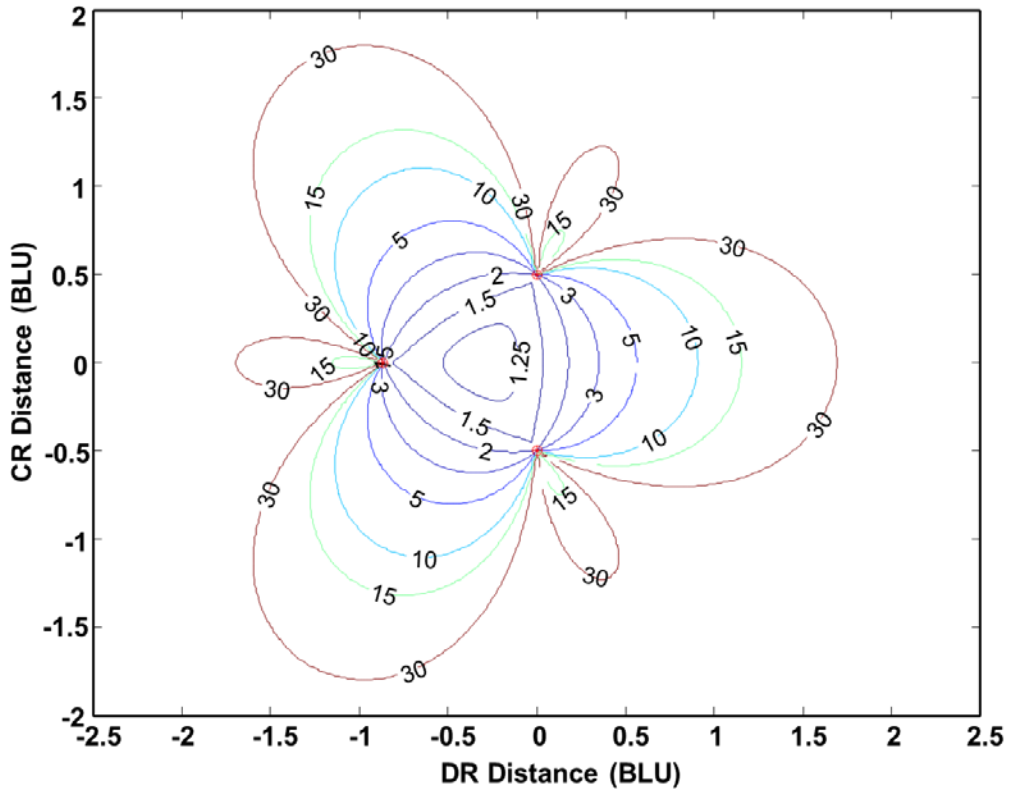

Figure 47 HDoP Contours for Three Pseudo Range Measurements in Flatland

Simple GPS Model — A three-station pseudo slant-range system provides a simple but useful model for GPS behavior. Thus, consider the situation shown in Figure 48, which assumes a spherical earth and circular satellite orbits. For these reasonable simplifications, the GPS satellites orbital radius is slightly greater than four Earth Radius Units (ERUs); the user and three satellites are in the same vertical plane; Satellites 1 and 2 have the same elevation angle α, while Satellite 3 is directly above the user. The constellation cross-range axis is the user's horizontal axis, and the constellation down-range axis is the user's vertical axis.

In Figure 48(a), the representative earth-based user is outside the perimeter of the satellite locations. However, the user is close, horizontally and vertically, to the center of the baseline

between Satellites 1 and 2. For α=5 deg (approximately the minimum usable value), the user's vertical distance to the baseline is 4.4% of the baseline. For α=10 deg (as in Figure 48(a)), the user-baseline distance is 8.9% of the baseline.

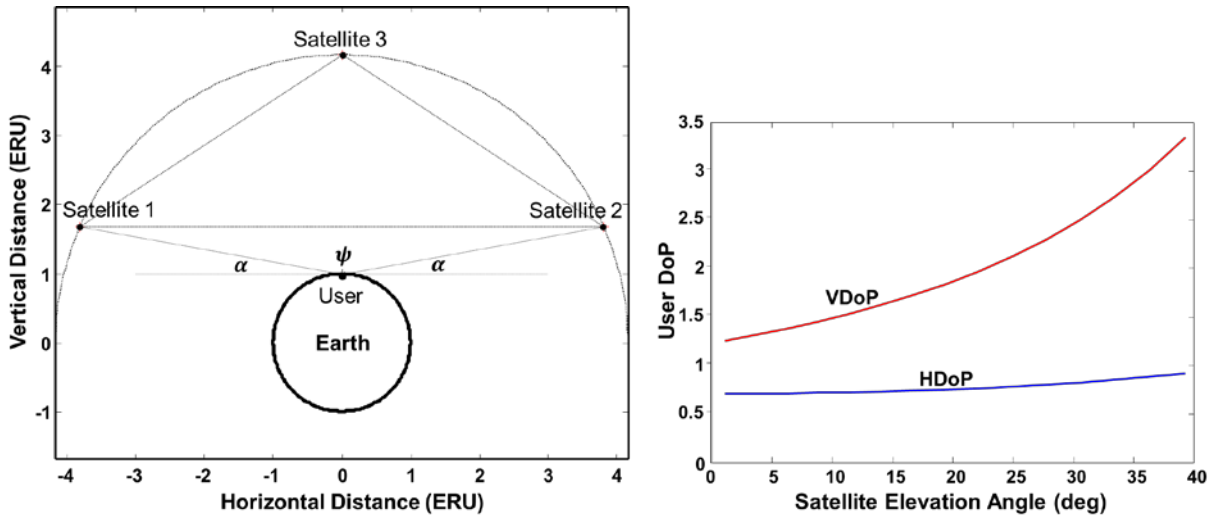

(a) Satellite-User Geometry (b) User HDoP and VDoP

Figure 48 Three-Satellite Vertical-Plane Model for GPS-User Geometry

The down-range distances involved can be related to Figure 44. Near a baseline, CRDoP (blue curve) is relatively flat, while $\text{DRDoP}_{c,PR\text{-}3}$ (orange curve) is rapidly increasing. HDoP and VDoP curves for the GPS model of Figure 48(a), shown in Figure 48(b), are consistent with Figure 44. They illustrate behavior that is contrary to that for true range systems — i.e., low-elevation GPS satellites are more important to VDoP than to HDoP.

Four Stations — Figure 49 shows $\text{HDoP}_{c,PR\text{-}4}$ contours for two four station pseudo range configurations. As is the case for true slant-range systems (Subsection 8.5.1), utilizing a redundant station eliminates the occurrence of infinite solutions — e.g., the infinite HDoPs along the baseline extensions of a three-station pseudo range configuration are eliminated. Evidence is that the $\text{HDoP}_{c,PR\text{-}4} = 20$ contour encircles the station cluster, whereas the $\text{HDoP}_{c,PR\text{-}3} = 20$ contours are blocked by the baseline extensions and terminate on stations. A redundant station also provides an increase in the service area. But the quadratic increase in $\text{HDoP}_{c,PR\text{-}4}$ with distance from the station cluster still limits the coverage area.

A square or rectangular station arrangement provides effective coverage within the perimeter of an area such as an airport (Figure 49(a)). However, other four-station configurations provide larger service areas. An alternative that is better suited to maximizing coverage is the four-station Wye configuration (Figure 49(b)). For this configuration, a BLU is defined as the distance from the center station to each of the three outlying stations.

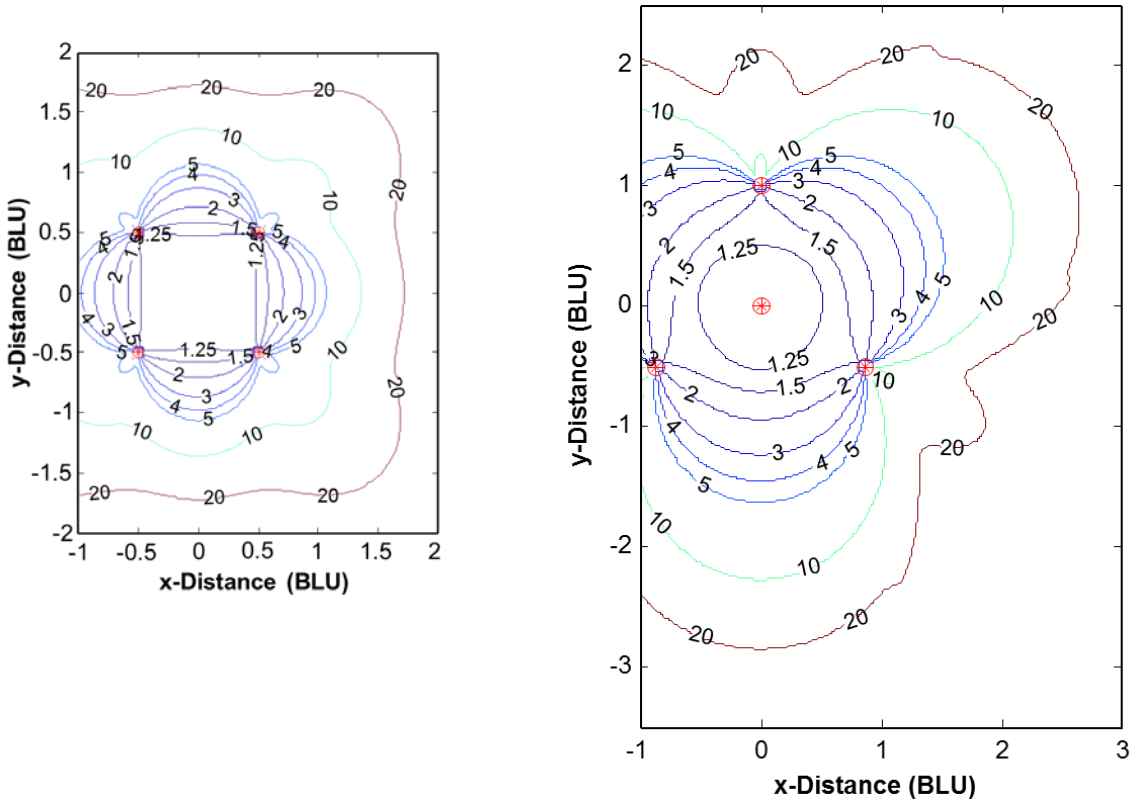

(a) Square Configuration (b) Wye Configuration

Figure 49 HDoP Contours for Two Four-Station Configurations

8.5.3 Interpretation: Pseudo vs. True Slant-Range Systems

Service Area Comparison — Figure 50 is a comparison of the service areas in which a given HDoP is achieved for the five system configurations addressed in Subsections 8.5.1 and 8.5.2, assuming a common baseline length. Since HDoP is used as a surrogate for accuracy, common range measurement error variances are implicitly assumed as well. Figure 50 indicates that, for HDoP = 5, a navigation or surveillance system utilizing true slant-range measurements can have a service area that is 10 times that of a system utilizing pseudo slant-range measurements with the same number of ground stations. For HDoP = 2, the coverage ratio is smaller, approximately 5. However, while convenient for analysis purposes, having equal or comparable baselines for different types of systems is not necessarily required for actual systems.

Siting Flexibility — A more useful conclusion that can be drawn is that true slant-range systems have greater station siting flexibility. Pseudo slant-range systems must have station locations that almost surround the service area, while true slant-range systems do not. Stated informally, true range systems can look outward from the station cluster, while pseudo range systems must look inward from the stations' perimeter or to locations a fraction of a baseline length outside the perimeter and near the center of a baseline. To address this limitation, pseudo slant-range

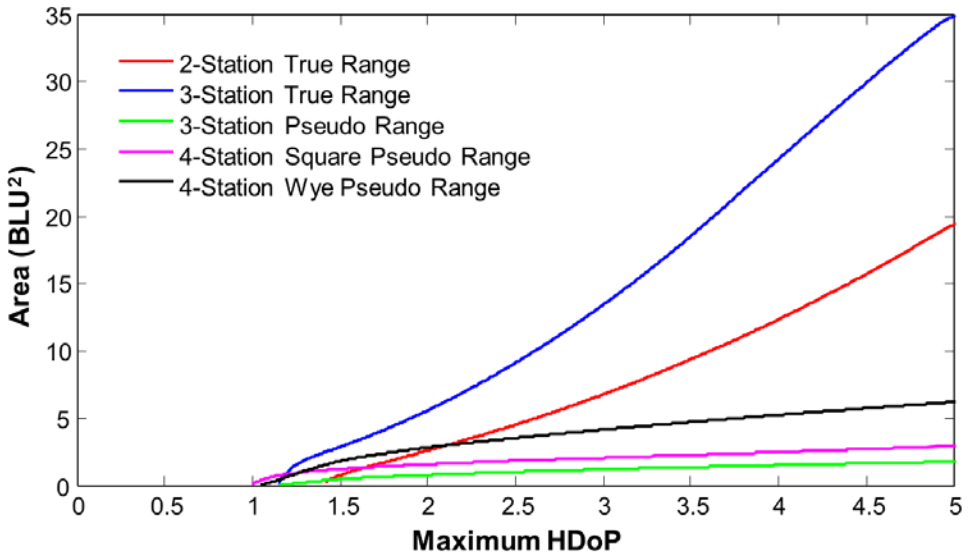

Figure 50 Coverage Area vs. HDoP for Five System Concepts

systems have been deployed with extremely long baselines. The ultimate in this regard are satellite navigation systems, which employ satellites as stations and thus have baseline lengths approaching eight earth radii.

LOPs for True and Pseudo Range Measurements — Figure 51 provides another explanation of why HDoPs for pseudo slant-range systems degrade much more rapidly with distance from the stations than do HDoPs for true slant-range systems.

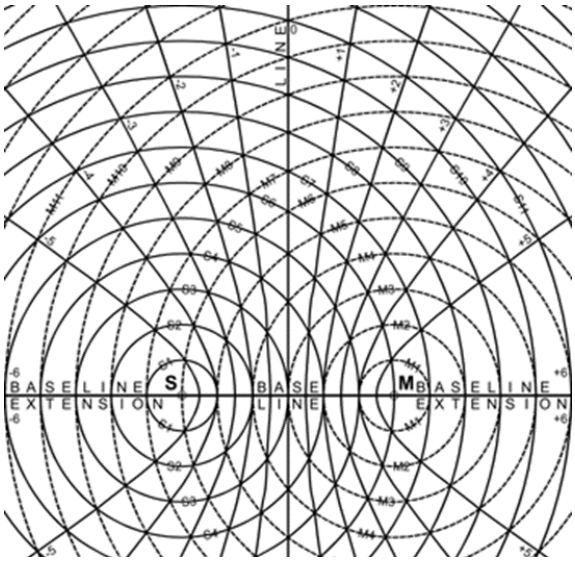

Figure 51 LOPs for True Slant-Range and Pseudo Slant-Range Systems

The figure shows two stations and the circular LOPs they would generate if the stations were used for true slant-range measurements. The circular LOP crossing angles starts at zero on the baseline, where the solution is unstable. Moving ‘outward’ along the baseline perpendicular

bisector, the crossing angle becomes useful within about one-tenth of the baseline length, and remains useful to about 3.5 baseline lengths (outside of the limits of the figure) where the crossing angle becomes too shallow. An important aspect in this system is that the separation between circular LOPs for each station remains constant with distance from the station — only the crossing angles cause degraded accuracy.

Figure 51 also shows a family of hyperbolic LOPs for the same pair of pseudo slant-range stations. If there were two pairs of stations, degradation in their crossing angles with distance from the stations would be evident (e.g., Figure 30). However, a second source of accuracy degradation is involved: for pseudo slant-range systems, the LOPs become further apart with distance from the stations (much as the LOPs for an angle measurement system do). The combination of divergence of the LOPs and degraded LOP crossing angles limits the service area of a pseudo slant-range system to, roughly, the region enclosed by the stations' perimeter.

8.5.4 Example 10 Continued: Three Pseudo Spherical-Range Stations

Introduction — This subsection continues the example, begun in Subsection 7.12.3, of an aircraft that utilizes three stations in the U.S. Northeast Loran-C chain (**M** Seneca, NY; **W** Caribou, ME; and **X** Nantucket, MA). Two topics are addressed that are relevant to material in this chapter: (1) Horizontal Dilution of Precision (HDoP), and (2) accounting for the earth's ellipticity.

HDoP Contours — While more frequently used in a rectangular framework, Horizontal Dilution of Precision (HDoP) is also applicable to spherical geometries — see Subsections 8.4.2 and 8.4.3. The approach here is based on the range-difference technique of Subsection 8.4.5 — specifically Eq 421-Eq 423 and Eq 450. Assuming that the stations are ordered as **M**, **W**, **X**, HDoP is given by

$$\mathbf{M}_{a,PR\text{-}3} = \mathbf{C}[(\mathbf{D}\mathbf{U}_a)^T(\mathbf{D}\mathbf{D}^T)^{-1}(\mathbf{D}\mathbf{U}_a)]^{-1}\mathbf{C}^T \qquad \text{Eq 468}$$

$$\mathbf{D} = \begin{bmatrix} 1 & -1 & 0 \\ 1 & 0 & -1 \end{bmatrix}$$

$$\mathbf{C} = \mathrm{diag}(1, \cos(L_A))$$

The elements of the matrix $\mathbf{U}_a$ (the Jacobian matrix for the position variables) are given in Eq 420. Then $\mathrm{HDoP}_{a,PR\text{-}3}$ is found from the diagonal elements of $\mathbf{M}_{a,PR\text{-}3}$

$$\mathrm{HDoP}_{a,PR\text{-}3} = \sqrt{\mathrm{LatDoP}^2_{a,PR\text{-}3} + \mathrm{LonDoP}^2_{a,PR\text{-}3}} \qquad \text{Eq 469}$$

Eq 468 and Eq 469 are evaluated for a grid of points, and $\mathrm{HDoP}_{a,PR\text{-}3}$ contours are draws — see Figure 52. Also shown is a potential flight path involving airports in/near the coverage area.

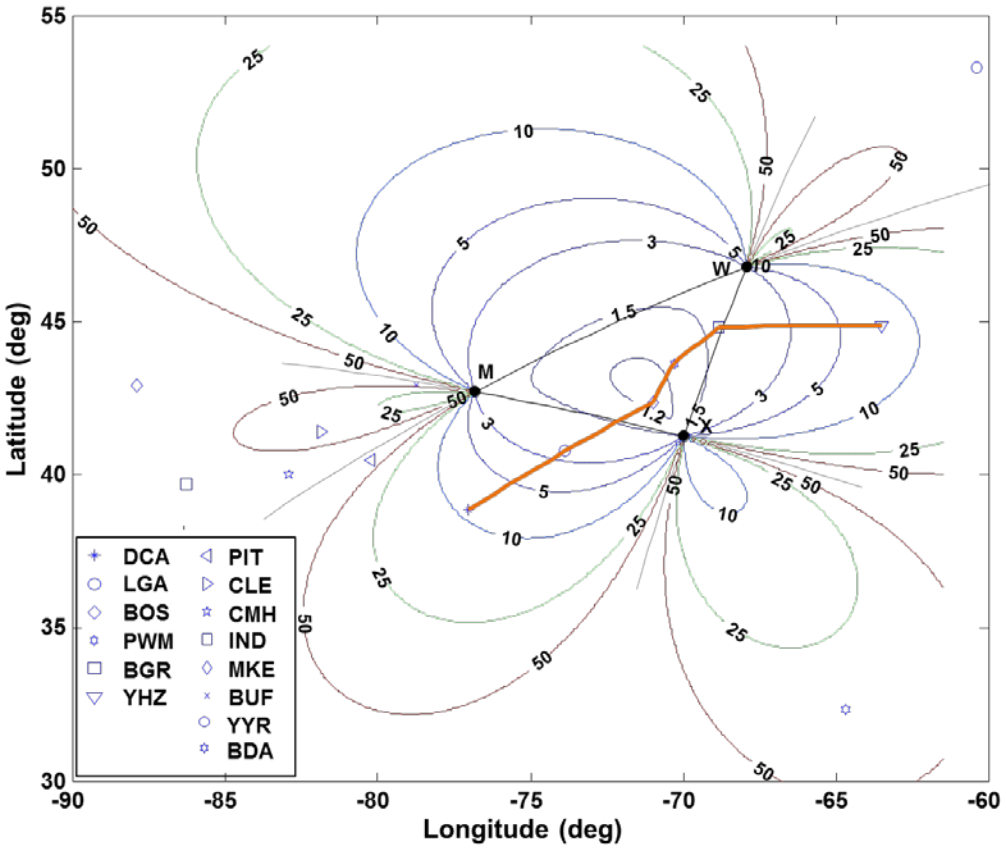

Figure 52 HDoP Contours for a Triad of Stations (Loran NE Chain)

Figure 52 is qualitatively similar to Figure 47(a), which applies to a two-dimensional Cartesian setting and pseudo slant-range measurements. For example: (a) the HDoP values are similar at comparable locations, both inside and outside the station perimeter; (b) HDoP is infinite along the baseline extensions, causing exterior contours to terminate at stations; and (c) HDoP is discontinuous when transitioning between the interior of the station perimeter and the interior of the adjacent region between two baselines. Material in Subsection 7.7.3 concerning extraneous and ambiguous solutions is relevant here as well. The area where $HDoP_{a,PR\text{-}3} \leq 5$ is approximately 233 thousand square nautical miles.

Accounting for Ellipsoidal Earth —If the earth were a sphere, Razin's algorithm, as described in Section 7.10, could be used without modification. However, the earth is better modeled as an ellipsoid of revolution (Section 2.2). Since ellipticity errors resulting from modeling the earth as a sphere tend to increase with distance, they can become important for accurate, long-range systems. For example, consider four airport locations: LaGuardia, NY (LGA); Boston, MA (BOS); Portland, ME (PWM); and Bangor, ME (BGR). The path lengths between the three ground stations and these airports vary from 81.0 NM (**X** and BOS) to 444.3 NM (**W** and LGA); the average is 233.5 NM. Based on (a) the distances involved, (b) the 'rule of thumb' for the spherical earth approximation that the distance error is roughly 0.3% of the distance, and (c) the

Coast Guard's Loran-C accuracy goal of 0.25 NM, the effect of mis-modeling the earth's shape should be addressed for some applications.

Table 18 shows the position error resulting from applying Razin's algorithm to range-differences generated using Vincenty's algorithm (Subsection 2.2.3), rather than those for a spherical earth (as assumed by the algorithm). The ellipticity error values, between 0.38 NM and 1.13 NM, are consistent with the 0.3% of distance 'rule of thumb'; all are greater than the goal of 0.25 NM.

Table 18 Example Ellipticity Errors for Razin's Algorithm

Airport	True Latitude (deg)	Lat Error* (deg)	True Longitude (deg)	Lon Error* (deg)	Distance Error (NM)
LGA	40.7772500	-0.0062000	-73.8726111	0.0011000	0.38
BOS	42.3629418	-0.0006300	-71.0063931	-0.0102000	0.45
PWM	43.6456435	0.0036400	-70.3086164	-0.0148100	0.68
BGR	44.8074444	0.0061100	-68.8281389	-0.0250500	1.13

* True minus estimated coordinate value

NLLS Methodology — The NLLS technique is used to improve the solution accuracy of Razin's algorithm. Specifically, the Newton form of the estimator for range differences is employed (Eq 451). Following Subsection 2.2.3, each true/measured spherical-range is computed using Vincenty's algorithm* for the distance s**(S,A)** along the surface of the ellipsoid between a station **S** at (L_S, λ_S) and aircraft **A** at (L_A, λ_A). The simulated measurement (Eq 350) is

$$\tilde{\mathbf{z}} = \begin{bmatrix} \tilde{z}_1 \\ \tilde{z}_2 \\ \tilde{z}_3 \end{bmatrix} = \begin{bmatrix} s(\mathbf{M},\mathbf{A}) \\ s(\mathbf{W},\mathbf{A}) \\ s(\mathbf{X},\mathbf{A}) \end{bmatrix} \qquad \text{Eq 470}$$

The equation for each calculated spherical-range also employs Vincenty's algorithm. Here, the aircraft location replaced by its current estimate $\bar{\mathbf{A}}$. Thus, in Eq 350

$$\mathbf{f} = \begin{bmatrix} f_1(\mathbf{M},\bar{\mathbf{A}}) \\ f_2(\mathbf{W},\bar{\mathbf{A}}) \\ f_3(\mathbf{X},\bar{\mathbf{A}}) \end{bmatrix} = \begin{bmatrix} s(\mathbf{M},\bar{\mathbf{A}}) \\ s(\mathbf{W},\bar{\mathbf{A}}) \\ s(\mathbf{X},\bar{\mathbf{A}}) \end{bmatrix} \qquad \text{Eq 471}$$

The measurement difference residual vector therefore is

$$\mathbf{D}\,\delta\mathbf{z} = \begin{bmatrix} 1 & -1 & 0 \\ 1 & 0 & -1 \end{bmatrix} \begin{bmatrix} \tilde{z}_1 - f_1 \\ \tilde{z}_2 - f_2 \\ \tilde{z}_3 - f_3 \end{bmatrix} = \begin{bmatrix} 1 & -1 & 0 \\ 1 & 0 & -1 \end{bmatrix} \begin{bmatrix} s(\mathbf{M},\mathbf{A}) - s(\mathbf{M},\bar{\mathbf{A}}) \\ s(\mathbf{W},\mathbf{A}) - s(\mathbf{W},\bar{\mathbf{A}}) \\ s(\mathbf{X},\mathbf{A}) - s(\mathbf{X},\bar{\mathbf{A}}) \end{bmatrix} \qquad \text{Eq 472}$$

The Jacobian matrix is composed of partial derivatives of the measurements with respect to the unknown position variables L_A and λ_A. The elements of the Jacobian used in computations need

* Vincenty's algorithm is seleced based on the availability of validated computer code. Other methods can be used.

not be exact derivatives of the measurement equation (Subsection 8.1.6). This is fortuitous, because Vincenty's technique is not an equation in the analytic sense, but a recursive procedure; expressions for its derivatives cannot be computed easily.

In place of the derivatives with respect to L_A and λ_A of the distance along the surface of an ellipse for Vincenty's algorithm, scaled derivatives of the geocentric angle θ_{SA} are used. Thus, the Jacobian is computed using Eq 420

$$\frac{\partial s(\mathbf{S},\mathbf{A})}{\partial L_A} = R_e \frac{\partial \theta_{SA}}{\partial L_A}\bigg|_{A=\bar{A}} \qquad \frac{\partial s(\mathbf{S},\mathbf{A})}{\partial \lambda_A} = R_e \frac{\partial \theta_{SA}}{\partial \lambda_A}\bigg|_{A=\bar{A}} \qquad \text{Eq 473}$$

In Eq 473, a reasonable value for R_e should be used, as a 1,000 ft change in R_e is equivalent to a 5x10^{-5} change in $\frac{\partial \theta_{SA}}{\partial L_A}$ or $\frac{\partial \theta_{SA}}{\partial \lambda_A}$. For calculations, the value for R_e following Eq 30 is employed here. The NLLS process is initialized using values for $\bar{L}_A$ and $\bar{\lambda}_A$ found using Razin's algorithm for a spherical earth. The perturbation corrections $\delta\hat{L}_A$ and $\delta\hat{\lambda}_A$ are found using Eq 451.

Jacobian Matrix Considerations — There are two differences in the Jacobian matrix used for computing DoP values and the matrix used for computing unknown variables. First, the Jacobian used for DoPs is taken from Eq 420 (for spherical-ranges), then scaled by the $\mathbf{C}$ matrix with the result that the elements of the product $\mathbf{U}_a\mathbf{C}^{-1}$ are dimensionless and the associated DoP variables are commensurate. In contrast, the Jacobian matrix used for computing an updated estimate of the unknown variables must be scaled so that Eq 357 is consistent. In this situation, where the measurement residual $\boldsymbol{\delta z}$ has units of linear distance, derivatives with respect to the geocentric angle found from Eq 420 must be scaled by the radius of the earth (e.g., Eq 473). Second, Jacobian matrices used for computing DoPs are evalued on a grid of assumed aircraft locations. In contrast, Jacobian matrices used to compute an update to the perturbation variables are evaluated at the current estimate of the aircraft location.

Calculation Results — Carrying out the NLLS process using Eq 451 yields a sequence of increasingly accurate position estimates for four airport locations. The associated residual errors are shown in Table 19. Convergence of the NLLS technique is rapid in this situation. Each of the first four iterations reduces the error by a minimum factor of 76; the average latitude or longitude error reduction by one iteration is a factor of 539. The fifth iteration appears to approach the limits of machine precision (calculations were done in double precision).

Table 19 NLLS Residual Error for Spherical-Range Differences (Stations **M**,**W**,**X**)

Iter-ation	LaGuardia (LGA)		Boston (BOS)	
	Lat Error* (deg)	Lon Error* (deg)	Lat Error* (deg)	Lon Error* (deg)
0	-0.006,204,297,044,61	0.001,098,559,038,59	-0.000,627,450,377,91	-0.010,195,811,988,10

1	-0.000,020,505,170,77	-0.000,001,816,926,14	-0.000,008,177,955,56	0.000,045,180,746,10
2	-0.000,000,027,423,43	0.000,000,018,116,62	-0.000,000,014,339,68	-0.000,000,157,274,01
3	-0.000,000,000,083,93	-0.000,000,000,062,20	-0.000,000,000,032,53	0.000,000,000,565,15
4	0.000,000,000,000,01	0.000,000,000,000,29	-0.000,000,000,000,04	-0.000,000,000,002,02
5	0.000,000,000,000,01	-0.000,000,000,000,01	0.000,000,000,000,01	0.000,000,000,000,03
Iter-ation	**Portland (PWM)**		**Bangor (BGR)**	
	Lat Error* (deg)	**Lon Error* (deg)**	**Lat Error* (deg)**	**Lon Error* (deg)**
0	0.003,642,517,508,14	-0.014,811,819,575,26	0.006,109,544,331,55	-0.025,054,253,476,51
1	0.000,001,297,312,66	0.000,072,399,332,72	0.000,018,565,242,40	0.000,160,340,474,51
2	-0.000,000,016,162,69	-0.000,000,244,802,54	-0.000,000,084,834,17	-0.000,000,437,980,97
3	0.000,000,000,041,82	0.000,000,000,817,39	0.000,000,000,213,29	0.000,000,001,148,99
4	-0.000,000,000,000,15	-0.000,000,000,002,72	-0.000,000,000,000,57	-0.000,000,000,003,05
5	0.000,000,000,000,01	0.000,000,000,000,04	-0.000,000,000,000,01	0.000,000,000,000,00

* True minus estimated coordinate value

Solution Precision — Aside from demonstrations such as this of the NLLS technique, in practice, when applied to Loran-C measurements, one or two iterations would generally be sufficient. Even with error-free measurements (as can be assumed during system analyses), there usually is no point in computing an aircraft's position to greater precision than that to which the ground stations are known. Loran-C station locations are published to 0.001 arc second, or approximately 0.1 ft, or 0.000,000,3 deg (Ref. 53), which is achieved with two iterations in the calculations employed here. For real-time operational use, if one optimistically takes the Loran-C measurement accuracy to be 10 ft (it has been quoted as "100 ft or better"), then computing the aircraft location to a precision of 0.000,03 deg would be sufficient.

Related Work — Razin's paper (Ref. 45) recognizes the need to modify the solution based on its derivation for an assumed spherical earth, and contains a technique to do so. References 52 and 53 do as well. The solution herein is closest to that in Ref. 52.

8.5.5 Example 11 Continued: Two Pairs of Pseudo Spherical-Range Stations

This subsection continues the example, begun in Subsection 7.12.4, concerning two distinct pairs of pseudo spherical-range navigation stations. For such a configuration, the solution algorithm for a spherical earth is described in Section 7.11. HDoP is utilized to obtain insight into this configuration's performance, both a distinct station pairs, and with 'cross chaining' as an additional capability. The methodology is similar to that employed in Subsection 8.5.4. The ellipticity error inherent in a solution that assumes a spherical earth can be corrected by the Gauss-Jordan NLLS technique. However, that topic is not pursued here.

For this situation, the Jacobian matrix and HDoP expressions follow directly from Subsection

8.5.4 — specifically, Eq 468 and Eq 469. The elements of matrix $\mathbf{U}_a$ (Jacobian matrix for angular-formulation position variables) are given in Eq 420. Matrix $\mathbf{U}_a$ has four rows, since there are four stations. Assuming that the order of the rows corresponds to stations at Seneca, Nantucket, Dana and Malone, the measurement difference matrix **D** is

$$\mathbf{D} = \begin{bmatrix} 1 & -1 & 0 & 0 \\ 0 & 0 & 1 & -1 \end{bmatrix} \qquad \text{Eq 474}$$

Figure 53 depicts HDoP contours for the four stations and seven airport shown in Figure 39. As expected, the solution becomes unstable along the extensions for the baselines connecting a same-chain station pair (Seneca-Nantucket and Dana-Malone). However, the solution is not unstable along the extensions for the paths connecting stations from different chains. For this example, there is a region where HDoP exceeds 50 close to the Dana-Seneca path, as the hyperbolic LOPs for the two chains are nearly parallel in this area.

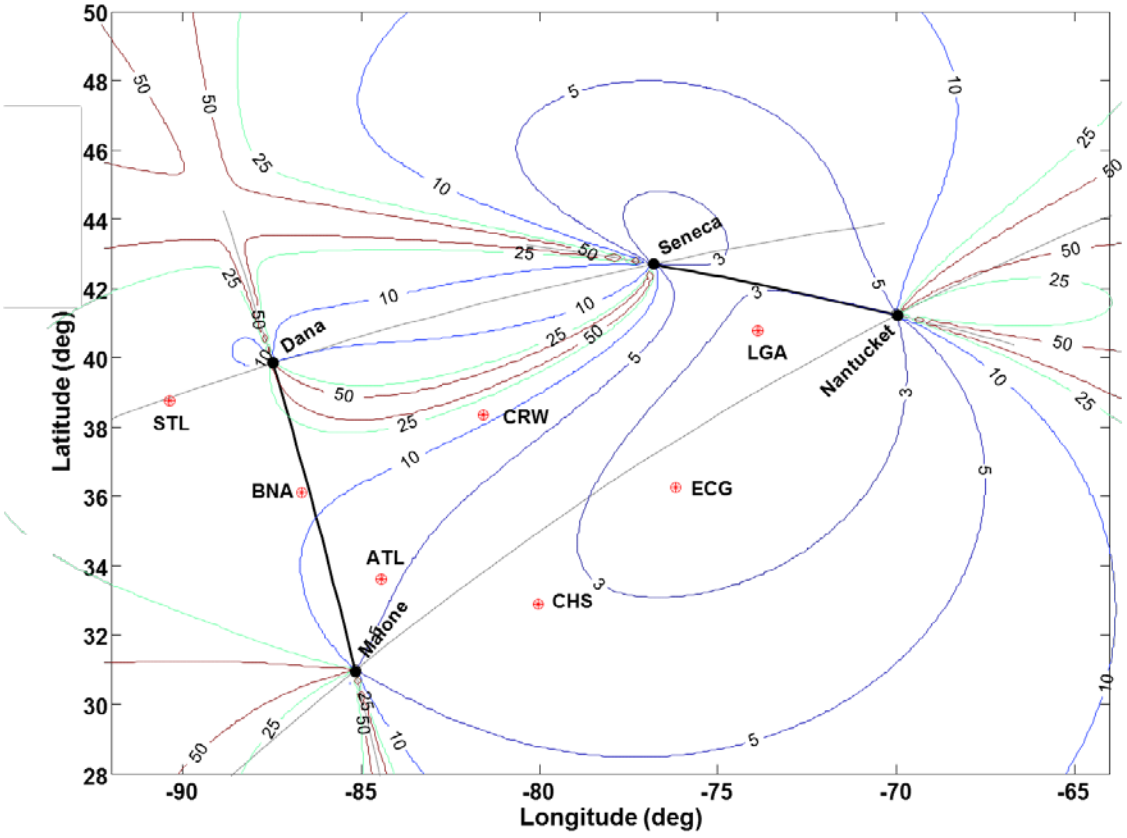

Figure 53 HDoP Contours for Two Pairs of Pseudo Spherical-Range Stations

As noted earlier, navigation and surveillance systems are developed/deployed to provide service in a defined area. In the case of the U.S. East Coast Loran-C Chain, the station at Carolina Beach, NC, was intended to support service in much of the U.S.Southeast. However, stations are

occasionally out-of-service. In such a circumstance, cross-chaining was an advanced capability that enabled operations to continue during a station outage (for appropriately equipped users).

A second advanced capability (relative to traditional Loran-C) was utilization of redundant stations to improve measurement geometry. The Dana station was in fact dual-rated: it was the master for the Great Lakes Chain and a secondary for the East Coast Chain. To determine the effect on HDoP of including the Seneca-Dana spherical-range difference, the analysis can be repeated with the **D** matrix modified to account for the additional range-difference measurement.

$$\mathbf{D} = \begin{bmatrix} 1 & -1 & 0 & 0 \\ 0 & 0 & 1 & -1 \\ 1 & 0 & -1 & 0 \end{bmatrix} \qquad \text{Eq 475}$$

Figure 54 depicts HDoP contours when measurements by the Seneca-Dana pair are included. HDoPs adjacent to the Seneca-Dana baseline are improved markedly (e.g., HDoPs less than 1.5 for six of the seven airports). HDoPs for the area further to the southeast are less improved.

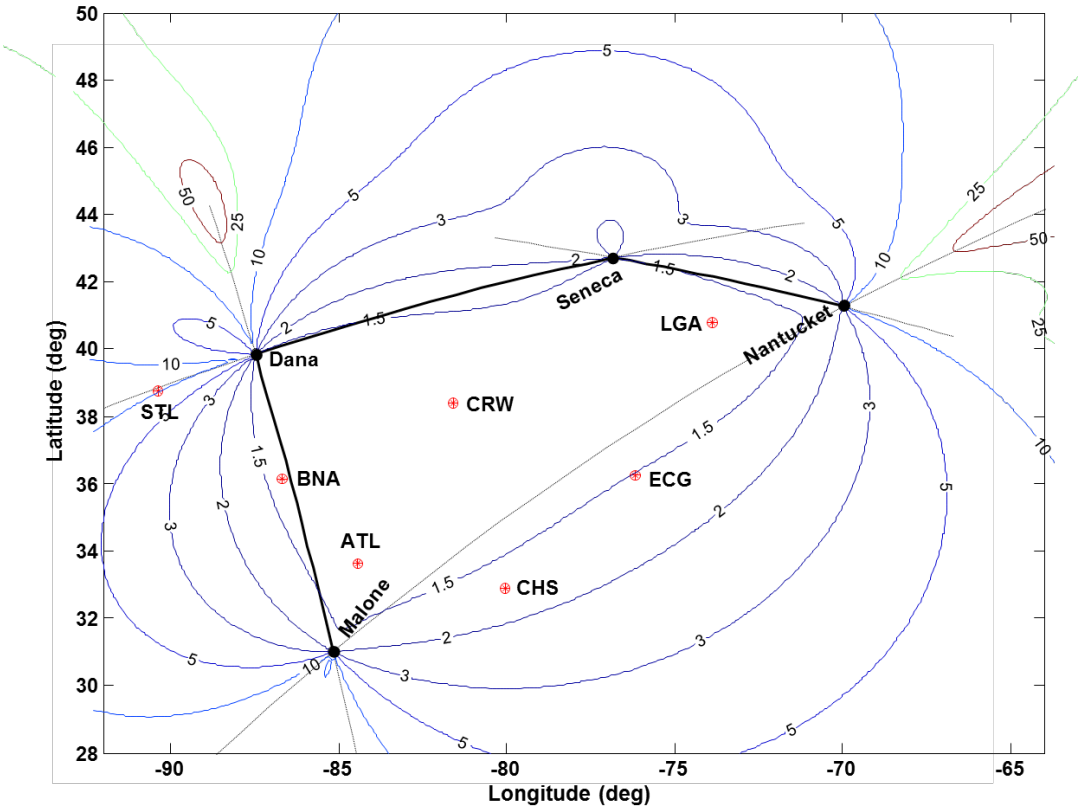

Figure 54 HDoP Contours for Three Pairs of Pseudo Spherical-Range Stations

The geographic size of service areas involved in Figure 53 and Figure 54 are large. For the two figures, HDoP is 5 or less for approximately 590 (Figure 53) and 1,050 (Figure 54) thousand square nautical miles, respectively. An important factor in achieving large coverage areas is use of long baselines — e.g., for Dana-Malone, approximately 544 NM; and for Seneca-Dana,

approximately 510 NM.

8.5.6 Example 12 Continued: Wide Area Multilateration (WAM)

Introduction — This subsection continues the example, begun in Subsection 7.12.5, of a WAM system that utilizes aircraft altitude reports and pseudo slant-range measurements from stations at three airports: Boston, MA (BOS); Manchester, NH (MHT); and Hartford, CT (BDL). The analysis in Subsection 7.12.5 assumes a spherical earth. This subsection accounts for the earth's ellipticity using the Gauss-Newton NLLS technique specialized to range difference systems (Subsection 8.4.5).

NLLS Methodology — Each slant-range difference measurement is computed using Appendix Section 9.3 (particularly Eq 500) for the slant-range $d(\mathbf{S},\mathbf{A})$ between a station **S** at coordinates (L_S, λ_S, h_S) and aircraft **A** at coordinates (L_A, λ_A, h_A). The simulated measurement (Eq 350) thus becomes

$$\tilde{\mathbf{z}} = \begin{bmatrix} \tilde{z}_1 \\ \tilde{z}_2 \\ \tilde{z}_3 \end{bmatrix} = \begin{bmatrix} d(\mathbf{BOS},\mathbf{A}) \\ d(\mathbf{MHT},\mathbf{A}) \\ d(\mathbf{BDL},\mathbf{A}) \end{bmatrix} \qquad \text{Eq 476}$$

In the measurement equation for each slant-range difference the aircraft location replaced by its current estimate $\bar{\mathbf{A}}$. Thus, in Eq 350

$$\mathbf{f} = \begin{bmatrix} f_1(\mathbf{BOS},\bar{\mathbf{A}}) \\ f_2(\mathbf{MHT},\bar{\mathbf{A}}) \\ f_3(\mathbf{BDL},\bar{\mathbf{A}}) \end{bmatrix} = \begin{bmatrix} d(\mathbf{BOS},\bar{\mathbf{A}}) \\ d(\mathbf{MHT},\bar{\mathbf{A}}) \\ d(\mathbf{BDL},\bar{\mathbf{A}}) \end{bmatrix} \qquad \text{Eq 477}$$

The measurement residual vector is $\boldsymbol{\delta}\mathbf{z} = \tilde{\mathbf{z}} - \mathbf{f}$ and the measurement difference matrix is

$$\mathbf{D} = \begin{bmatrix} 1 & -1 & 0 \\ 0 & 1 & -1 \end{bmatrix} \qquad \text{Eq 478}$$

The Jacobian matrix is composed of the partial derivatives of the measurements with respect to the unknown variables. In this case, only the position variables L_A and λ_A are relevant, since forming range differences eliminates the time variable. Because the NLLS technique is recursive, approximations of the derivatives of $d(\mathbf{S},\mathbf{A})$ are sufficient. Thus, the derivatives of slant-range with respect to L_A and λ_A are computed using the corresponding expressions for a spherical earth model ($\mathbf{u}_{s,ASi}$ found from Eq 414) and the current estimate of the aircraft location

$$\mathbf{U}_S = \begin{bmatrix} u_{s,\bar{A}\text{-}BOS,L} & u_{s,\bar{A}\text{-}BOS,\lambda} \\ u_{s,\bar{A}\text{-}MHT,L} & u_{s,\bar{A}\text{-}MHT,\lambda} \\ u_{s,\bar{A}\text{-}BDL,L} & u_{s,\bar{A}\text{-}BDL,\lambda} \end{bmatrix} \qquad \text{Eq 479}$$

The NLLS process is initialized using values for $\bar{L}_A$ and $\bar{\lambda}_A$ found using the spherical earth model

(Section 7.5 and Subsection 7.12.5). The perturbation corrections $\delta\hat{L}_A$ and $\delta\hat{\lambda}_A$ are found using the Newton estimator of Eq 451.

Calculation Results — Carrying out the NLLS process for five iterations for four airport locations yields a sequence of increasingly accurate position estimates. Their residual errors are shown in Table 20. 'Iteration 0' corresponds to the solution based on a spherical-earth model, which is used to initialize the iteration. For these four locations, the average ellipticity error is 1,204 ft; the maximum is 2,122 ft.

Table 20 NLLS Residual Error for WAM Slant-Range Difference Measurements

Iter-ation	Westfield-Barnes Regional (BAF)		Dillant-Hopkins, Keene (EEN)	
	Lat Error* (deg)	Lon Error* (deg)	Lat Error* (deg)	Lon Error* (deg)
0	-0.001,301,968,265,58	0.007,647,699,521,99	-0.001,104,331,349,71	0.003,587,102,019,89
1	-0.000,023,346,121,51	-0.000,083,388,490,38	0.000,003,508,767,16	-0.000,020,825,500,81
2	0.000,000,023,629,92	0.000,000,077,274,69	-0.000,000,013,518,20	0.000,000,091,899,49
3	-0.000,000,000,019,79	-0.000,000,000,082,41	0.000,000,000,068,21	-0.000,000,000,412,05
4	0.000,000,000,000,03	0.000,000,000,000,08	-0.000,000,000,000,27	0.000,000,000,001,82
5	0.000,000,000,000,01	0.000,000,000,000,00	0.000,000,000,000,00	-0.000,000,000,000,01
Iter-ation	**Lawrence Municipal (LWM)**		**Hanscom Field, Bedford (BED)**	
	Lat Error* (deg)	**Lon Error* (deg)**	**Lat Error* (deg)**	**Lon Error* (deg)**
0	-0.001,215,745,248,65	-0.003,554,998,523,51	-0.001,341,677,997,11	-0.001,310,031,212,80
1	0.000,003,288,339,05	0.000,029,318,295,92	-0.000,003,587,543,95	0.000,008,337,514,17
2	0.000,000,018,603,13	-0.000,000,113,464,86	-0.000,000,004,694,52	-0.000,000,028,663,83
3	0.000,000,000,023,39	0.000,000,000,519,98	-0.000,000,000,019,15	0.000,000,000,097,83
4	0.000,000,000,000,22	-0.000,000,000,002,11	-0.000,000,000,000,02	-0.000,000,000,000,33
5	0.000,000,000,000,00	0.000,000,000,000,01	-0.000,000,000,000,01	0.000,000,000,000,00

* True minus estimated coordinate value

In this example, convergence of the NLLS (actually, the Newton-Raphson) technique is rapid. Each of the first four iteration steps reduces the error by a minimum factor of 50; the average latitude or longitude error reduction by one iteration is a factor of 426. The fifth iteration appears to approach the limits of machine precision. This performance is consistent with that for pseudo spherical-range measurements addressed in Subsection 8.5.4.

Two iterations would be sufficient for virtually all real-world applications, as the survey error of most locations, including those of airports, exceeds 10^{-7} deg.

8.5.7 Example 13: Five Pseudo Spherical-Range Stations

Introduction — This subsection addresses an over-determined (Gauss-type) situation involving five stations in the U.S. Northeast Loran-C chain: **M** Seneca, NY; **W** Caribou, ME; **X** Nantucket,

MA; **Y** Carolina Beach, NC; and **Z** Dana, IN. Station coordinates are given in Ref. 53. Stations **M**, **W** and **X** are utilized in Example 10, which involves a fully-determined (Newton-type) situation. As was done previously, perfect measurements are assumed.

It's stated in Subsection 8.1.5 that, when a Gauss-type NLLS estimator converges, the derivative of the cost function with respect to the unknown variables **x** is zero (Eq 379). Equivalently, the the matrix product $\mathbf{J}^T\mathbf{W}\,\boldsymbol{\delta}\mathbf{z} = \left(\mathbf{W}^{½}\mathbf{J}\right)^T\left(\mathbf{W}^{½}\boldsymbol{\delta}\mathbf{z}\right)$ results in the zero vector. Consequently, if an approximation is employed for the Jacobian matrix **J**, the accuracy of the estimator $\hat{\mathbf{x}}$ may be affected. This example quantifies the effect of using spherical-earth Jacobian elements with ellipsoidal earth measurements.

NLLS Methodology — The methodology is similar to that used in Subsection 8.5.4. Each true/measured spherical-range is calculated using Vincenty's algorithm for the distance s**(S,A)** along the surface of the ellipsoid between a station **S** at (L_S, λ_S) and aircraft **A** at (L_A, λ_A).

$$\tilde{\mathbf{z}} = \begin{bmatrix}\tilde{z}_1\\ \tilde{z}_2\\ \tilde{z}_3\\ \tilde{z}_4\\ \tilde{z}_5\end{bmatrix} = \begin{bmatrix}s(\mathbf{M},\mathbf{A})\\ s(\mathbf{W},\mathbf{A})\\ s(\mathbf{X},\mathbf{A})\\ s(\mathbf{Y},\mathbf{A})\\ s(\mathbf{Z},\mathbf{A})\end{bmatrix} \qquad \text{Eq 480}$$

Similarly, each estimated spherical-range is calculated using Vincenty's algorithm; however, the current estimated aircraft location $\bar{\mathbf{A}}$ is employed.

$$\mathbf{f} = \begin{bmatrix}f_1(\mathbf{M},\bar{\mathbf{A}})\\ f_2(\mathbf{W},\bar{\mathbf{A}})\\ f_3(\mathbf{X},\bar{\mathbf{A}})\\ f_4(\mathbf{Y},\bar{\mathbf{A}})\\ f_5(\mathbf{Z},\bar{\mathbf{A}})\end{bmatrix} = \begin{bmatrix}s(\mathbf{M},\bar{\mathbf{A}})\\ s(\mathbf{W},\bar{\mathbf{A}})\\ s(\mathbf{X},\bar{\mathbf{A}})\\ s(\mathbf{Y},\bar{\mathbf{A}})\\ s(\mathbf{Z},\bar{\mathbf{A}})\end{bmatrix} \qquad \text{Eq 481}$$

The measurement difference residual vector is

$$\mathbf{D}\,\boldsymbol{\delta}\mathbf{z} = \begin{bmatrix}1 & -1 & 0 & 0 & 0\\ 1 & 0 & -1 & 0 & 0\\ 1 & 0 & 0 & -1 & 0\\ 1 & 0 & 0 & 0 & -1\end{bmatrix}\begin{bmatrix}\tilde{z}_1 - f_1\\ \tilde{z}_2 - f_2\\ \tilde{z}_3 - f_3\\ \tilde{z}_4 - f_4\\ \tilde{z}_5 - f_5\end{bmatrix} \qquad \text{Eq 482}$$

In computing the Jacobian matrix, in place of the derivatives with respect to L_A and λ_A of the distance along the surface of an ellipse, scaled derivatives of the geocentric angle θ_{SA} are used. Thus, the Jacobian is computed using (Eq 420)

$$\frac{\partial s(\mathbf{S},\mathbf{A})}{\partial L_A} = R_e\left.\frac{\partial \theta_{SA}}{\partial L_A}\right|_{A=\bar{A}} \qquad \frac{\partial s(\mathbf{S},\mathbf{A})}{\partial \lambda_A} = R_e\left.\frac{\partial \theta_{SA}}{\partial \lambda_A}\right|_{A=\bar{A}} \qquad \text{Eq 483}$$

The value of R_e given in Eq 31 is employed here. The NLLS process is initialized using values for $\bar{L}_A$ and $\bar{\lambda}_A$ found using Razin's algorithm for a spherical earth and stations **W**, **Y** and **Z**. The perturbation corrections $\delta\hat{L}_A$ and $\delta\hat{\lambda}_A$ are found using Eq 447.

Calculation Results — The NLLS process was carried out for ten airports within the perimeter enclosing the five Loran stations. Table 21 displays the residual errors for four airport locations, which are representative of those for all ten airports. Convergence of is rapid, and similar to that in Table 19. Two iterations reduce the position solution error to less than the Loran measurement error. Three iterations reduce the position solution error to less than the survey accuracy of the Loran stations. The solution error for the fifth iteration approaches the limits of machine precision. It's evident that use of a Jacobian matrix based on the spherical earth approximation does not significantly degrade solution accuracy or convergence rate.

Table 21 NLLS Residual Error for Spherical-Range Differences (Stations **M**,**W**,**X**,**Y**,**Z**)

Iteration	Washington Reagan (DCA)		Boston (BOS)	
	Lat Error* (deg)	Lon Error* (deg)	Lat Error* (deg)	Lon Error* (deg)
0	0.014,537,257,252,70	-0.018,604,127,029,66	0.026,547,737,503,24	-0.054,681,743,113,03
1	0.000,029,424,578,53	0.000,073,330,085,09	0.000,101,495,715,06	0.000,291,281,533,06
2	0.000,000,022,067,27	-0.000,000,198,214,65	0.000,000,077,282,17	-0.000,001,082,517,14
3	0.000,000,000,126,40	0.000,000,000,596,01	0.000,000,000,610,34	0.000,000,004,060,44
4	-0.000,000,000,000,03	-0.000,000,000,001,68	-0.000,000,000,000,46	-0.000,000,000,015,23
5	0.000,000,000,000,01	0.000,000,000,000,01	0.000,000,000,000,01	0.000,000,000,000,05
Iteration	**Pittsburgh (PIT)**		**Indianapolis (IND)**	
	Lat Error* (deg)	**Lon Error* (deg)**	**Lat Error* (deg)**	**Lon Error* (deg)**
0	0.018,908,798,526,81	-0.007,753,505,965,38	0.020,256,990,728,48	0.013,247,536,503,45
1	0.000,064,254,937,99	0.000,020,482,996,50	0.000,078,069,938,33	-0.000,204,926,202,17
2	0.000,000,145,432,17	-0.000,000,019,728,66	0.000,000,226,449,34	0.000,000,575,804,13
3	0.000,000,000,326,01	0.000,000,000,148,19	0.000,000,001,186,27	-0.000,000,001,696,70
4	0.000,000,000,000,74	-0.000,000,000,000,23	0.000,000,000,004,08	0.000,000,000,004,67
5	-0.000,000,000,000,01	-0.000,000,000,000,03	0.000,000,000,000,03	-0.000,000,000,000,03

* True minus estimated coordinate value

8.5.8 Example 14: Direction Finding From Aircraft

Introduction — This is a completely contrived example, intended to show how direction finding from an aircraft might be a useful emergency backup capability when other navigation systems are not available. It does not reflect current aircraft direction-finding capabilities. Currently, direction finding is done in conjunction with a single transmitter, in order to find the direction toward a location of interest, typically an airport. Currently the aircraft does not compute its latitude/longitude; for the application addressed herein, it would.

Here it is assumed that aircraft **A**, at an unknown location, measures the azimuth angles relative to geodetic north, $\psi_{1/A}$ and $\psi_{2/A}$, of known transmitters **1** and **2**. Typically, this requires that the aircraft have: (1) an antenna array that can measure the angle of arrival of a signal relative to the airframe; (2) a device, such as an Inertial Navigation System (INS), that measures the aircraft centerline azimuth relative to geodetic (true) north; and (3) the capability to compute the aircraft's location from these measurements.

Purposes — The functional purpose of this hypothetical system is to exhibit the analysis process for determining the latitude and longitude of aircraft **A** (L_A, λ_A) from knowledge of the latitude/ longitude of transmitters **1** (L_1, λ_1) and **2** (L_2, λ_2) and azimuth measurements $\psi_{1/A}$ and $\psi_{2/A}$.

A secondary purpose of this example is to illustrate the ability of the Gauss-Newton NLLS technique to address situations where a closed-form solution does not exist for the spherical-earth assumption. Azimuth measurements from an aircraft $\psi_{i/A}$ appear to be equivalent to azimuth measurements from ground sites $\psi_{A/i}$, which is addressed in Section 6.3; moreover their measurement equation is well-known (e.g., Eq 86 or Eq 87).

However, there is an analytic difference between ground-based and aircraft-based measurements of azimuth angles of two transmitters. For ground-based measurements, the aircraft location can be found by applying spherical trigonometry to triangle **A12** (as described in Section 6.3). For aircraft-based measurements, only two parts of triangle **A12** are known while three are needed. One can consider additional spherical triangles involving the north pole and derive two equations in two unknown variables. But closed-form solutions for those equations are not known.

NLLS Initialization — The initial estimate for the aircraft location is found using expressions for rhumb line navigation (Eq 505 and Eq 506), which are repeated here in current notation

$$\tan\left(\psi_{i/A}\right) = \frac{\lambda_i - \bar{\lambda}_A}{L'_i - \bar{L}'_A} \qquad i = 1{,}2 \qquad \text{Eq 484}$$

Here, L' denotes the 'stretched latitude' corresponding to actual latitude L. The expressions for converting between the two are:

$$L' \equiv \log\left(\tan\left(\tfrac{1}{2}L + \tfrac{1}{4}\pi\right)\right) \qquad L \equiv 2\arctan\left(e^{L'}\right) - \tfrac{1}{2}\pi \qquad \text{Eq 485}$$

Upon simultaneously solving Eq 484 for $i = 1{,}2$, the initial estimated aircraft location is:

$$\bar{L}'_A = \frac{(\lambda_2 - \lambda_1) + L'_1\tan\left(\psi_{1/A}\right) - L'_2\tan\left(\psi_{2/A}\right)}{\tan\left(\psi_{1/A}\right) - \tan\left(\psi_{2/A}\right)}$$

$$\bar{\lambda}_A = \frac{(L'_2 - L'_1)\tan\left(\psi_{1/A}\right)\tan\left(\psi_{2/A}\right) + \lambda_1\tan\left(\psi_{2/A}\right) - \lambda_2\tan\left(\psi_{1/A}\right)}{\tan\left(\psi_{2/A}\right) - \tan\left(\psi_{1/A}\right)} \qquad \text{Eq 486}$$

In Eq 486, for either/both expressions, the dependency on $\tan(\psi_{i/A})$ can be converted to a dependency on $\cot(\psi_{i/A})$ by multiplying the numerator and denominator by $\cot(\psi_{i/A})$. When using Eq 486 in conjunction with Eq 485, no constraints are placed on the computed values of $\bar{L}_A$ or $\bar{\lambda}_A$. It is possible for infeasible values to be found, particularly when the aircraft and stations are separated by large distances (e.g., thousands of miles).

Measurement Equation — The error-free measured azimuth angles $\psi_{1/A}$ and $\psi_{2/A}$ along the surface of the ellipsoid between stations **1** and **2** and aircraft **A** at its actual location are simulated using Vincenty's algorithm (Subsection 2.2.3). The measurement corresponding to Eq 350 is:

$$\tilde{\mathbf{z}} = \begin{bmatrix} \tilde{z}_1 \\ \tilde{z}_2 \end{bmatrix} = \begin{bmatrix} \psi_{1/A}(\mathbf{1},\mathbf{A}) \\ \psi_{2/A}(\mathbf{2},\mathbf{A}) \end{bmatrix} \qquad \text{Eq 487}$$

The equation for each calculated azimuth angle also employs Vincenty's algorithm. However, the actual aircraft location replaced by the current estimated location $\bar{\mathbf{A}}$. Thus,

$$\mathbf{f} = \begin{bmatrix} f_1(\mathbf{1},\bar{\mathbf{A}}) \\ f_2(\mathbf{2},\bar{\mathbf{A}}) \end{bmatrix} = \begin{bmatrix} \psi_{1/A}(\mathbf{1},\bar{\mathbf{A}}) \\ \psi_{2/A}(\mathbf{2},\bar{\mathbf{A}}) \end{bmatrix} \qquad \text{Eq 488}$$

The measurement residual vector corresponding to Eq 353 therefore is

$$\boldsymbol{\delta}\mathbf{z} = \begin{bmatrix} \tilde{z}_1 - f_1 \\ \tilde{z}_2 - f_2 \end{bmatrix} = \begin{bmatrix} \psi_{1/A}(\mathbf{1},\mathbf{A}) - \psi_{1/A}(\mathbf{1},\bar{\mathbf{A}}) \\ \psi_{2/A}(\mathbf{2},\mathbf{A}) - \psi_{2/A}(\mathbf{2},\bar{\mathbf{A}}) \end{bmatrix} \qquad \text{Eq 489}$$

Jacobian — The Jacobian matrix is composed of approximate partial derivatives of the measurements with respect to the unknown position variables L_A and λ_A. Here, the partial derivatives for azimuth measurements on a spherical earth are used (Eq 402); these are repeated here in current notation

$$\frac{\partial \psi_{i/A}}{\partial L_A} = \frac{\mathrm{Num}_i\,[\sin(L_A)\sin(L_i) + \cos(L_A)\cos(L_i)\cos(\lambda_i - \lambda_A)]}{(\mathrm{Num}_i)^2 + (\mathrm{Den}_i)^2} \qquad \text{Eq 490}$$

$$\frac{\partial \psi_{i/A}}{\partial \lambda_A} = \frac{-\mathrm{Den}_i\,[\cos(L_i)\cos(\lambda_i - \lambda_A)] + \mathrm{Num}_i\,[\cos(L_i)\sin(L_A)\sin(\lambda_i - \lambda_A)]}{(\mathrm{Num}_i)^2 + (\mathrm{Den}_i)^2}$$

$$\mathrm{Num}_i = \cos(L_i)\sin(\lambda_i - \lambda_A)$$

$$\mathrm{Den}_i = \sin(L_i)\cos(L_A) - \cos(L_i)\sin(L_A)\cos(\lambda_i - \lambda_A)$$

Numerical Examples — Two numerical examples are provided (Table 22). The first involves aircraft-transmitter ranges of dozens of miles, and demonstrates the capability to find an airport that does not have a radio beacon. The second example involves aircraft-transmitter ranges of hundreds of miles, showing that this method is not limited to short ranges. (In the second example, Lorsta is a Coast Guard term used for Loran Station; the Seneca, NY, and Caribou,

ME, stations were part of the U.S. East Coast Loran Chain.)

Table 22 Aircraft-Based Direction Finding Examples

	Short Range	Medium Range
Aircraft Location	Norwood Airport (OWD)	Logan Airport (BOS)
Transmitter Station 1	Logan Aiport VOR (BOS)	Lorsta Seneca
Aircraft-Station 1 Range	12.9 NM	258.9 NM
Transmitter Station 2	Gardner VOR (GDM)	Lorsta Caribou
Aircraft-Station 2 Range	44.8 NM	297.5 NM
Initial Position Error	1,025.160 ft	55,753.080 ft
Iteration 1 Position Error	1.450 ft	904.724 ft
Iteration 2 Position Error	0.002 ft	4.065 ft
Iteration 3 Position Error	0.000 ft	0.011 ft
Iteration 4 Position Error	———	0.000 ft

In Table 22, the initial position error is the error resulting from use of the rhumb line equations (Eq 486 in conjunction with Eq 485). The subsequent errors are for the Gauss-Newton NLLS algorithm. For these examples, convergence is rapid; sub-foot computational errors are achieved in two or three iterations.

Remark — The ability to compute a position solution from aircraft-based azimuth measurements is straightforward. However, the challenge of measuring the angle-of-arrival of a signal from a moving platform using a size-restricted antenna limits the accuracy of the measurements, and consequently the resulting position solution. Generally, the solution is is only useful as an emergency backup.

9. APPENDIX: RELATED SPECIALIZED TOPICS

9.1 Aircraft Altitude and Air Data Systems

9.1.1 Meanings of Altitude

This document is primarily mathematical, and — in Chapters 1-7 — the equations involve only one notion of altitude: geometric height above an assumed perfectly spherical earth, measured along a radial from the earth's center. However, when interpreting the results of calculations for applications, the analyst must be aware that there are multiple meanings of altitude. The differing meanings are of concern, because aircraft (a) utilize barometric altimeters, but (b) must also main a vertical geometric distance above terrain. Figure 55 illustrates several notions of vertical distance above the earth, or 'altitude':

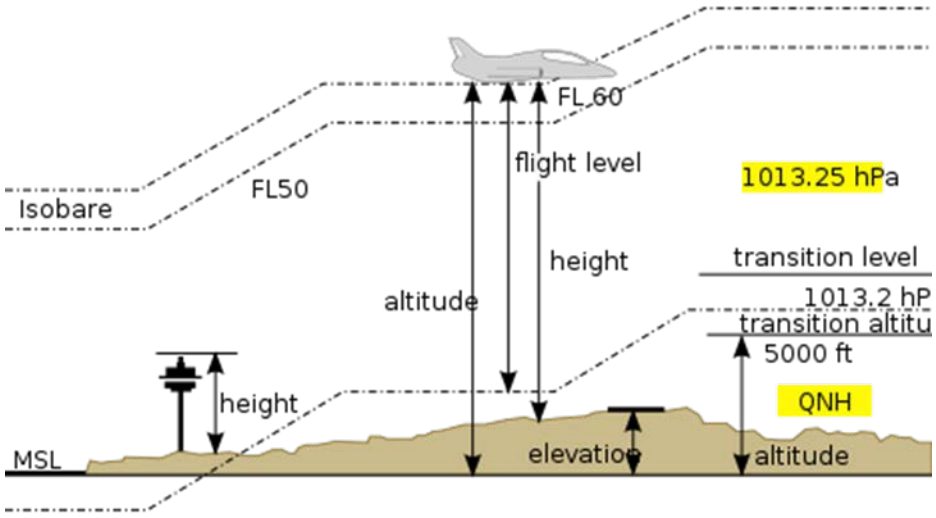

Figure 55 Different Notions of Altitude

- Height — or, better, Height Above Terrain (HAT) — is the vertical distance between an aircraft (or the top of a structure on the ground) and the terrain beneath it
- Altitude — or, better, Altitude MSL (above Mean Sea Level) — is the vertical distance between an aircraft and mean sea level. Generally, aircraft use altitude MSL in terminal areas/at low altitudes. To do so, the aircraft's altimeter is adjusted for the current local MSL pressure by applying the 'QNH' correction*, which is broadcast by a local airport.
- Flight Level — Vertical distance between an aircraft and the point below where the sea-level standard day pressure occurs (29.92 inches of mercury). In the U.S., flight

* QNH is not an acronym. It is one of a collection of standardized three-letter message encodings, all of which start with the letter "Q". They were initially developed for commercial radiotelegraph communication, and were later adopted by other radio services, especially amateur radio. Although created when radio used Morse code exclusively, Q-codes continued to be employed after the introduction of voice transmissions.

levels are used above the transition altitude of 18,000 ft.*

- Elevation — Height of the terrain above MSL.

These definitions are reasonably standard, but are not universally used. Documents related to aircraft procedures are particularly carefully to adhere to these definitions.

9.1.2 Aircraft Pitot-Static System

Aircraft certified under Federal Aviation Regulations† Parts 91, 121 and 135 are required to be equipped with a pitot-static system. A pitot-static system utilizes the static air pressure (collected at the static port), and the dynamic pressure due to the motion of the aircraft through the air (collected by the pitot tube) — illustrated in Figure 56, from Ref. 63. These combined pressures are utilized to provide the pilot with three indicators critical to operation of the aircraft:

- Airspeed indicator (ASI)
- Altimeter
- Vertical speed indicator (VSI).

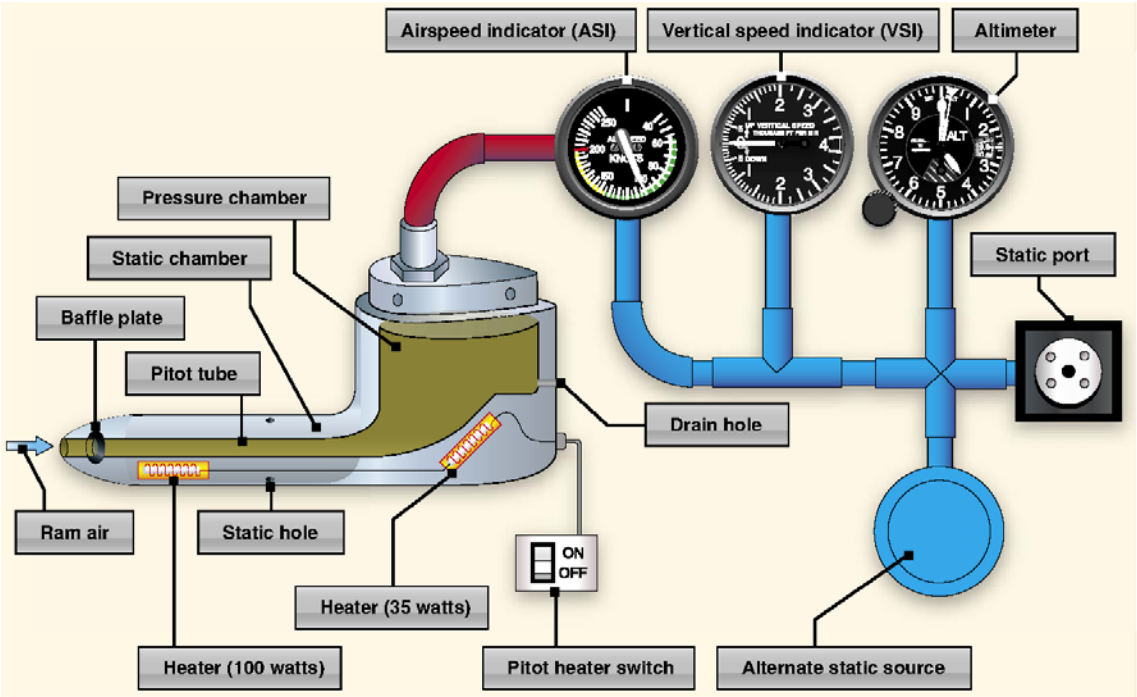

Figure 56 Basic Aircraft Pitot-Static System

* The figure, from Wikipedia, was drawn from a European perspective. It has (a) a lower transition altitude, and (b) the QNH quantified in hectopascals (hPa) rather than inches of mercury.

† The Federal Aviation Regulations, or FARs, are rules governing all aviation activities in the United States. The FARs are part of Title 14 of the Code of Federal Regulations (CFR).

9.1.3 Barometric Altimeter Temperature Sensitivity

The basic design of aircraft barometric altimeters does not provide a means for compensating for deviations from the assumed standard day sea level temperature of 15 °C (59 °F)*. Such a deviation results in an uncompensated altitude error that: (a) is the same for all aircraft at the same altitude, and (b) does not fluctuate. Temperatures that are less than the standard 15 °C cause the altimetry system to report a higher altitude than is true. Conversely, temperatures that are greater than the standard cause the altimetry system to report a lower altitude than is true (Figure 57).

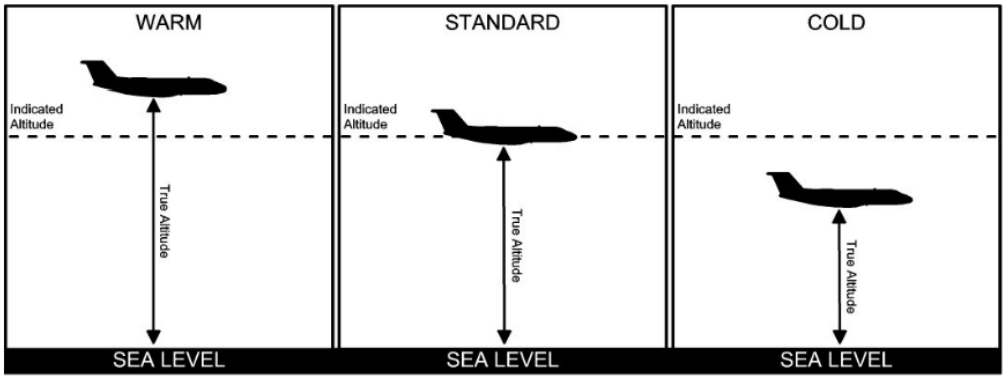

Figure 57 Effect of Non-Standard MSL Temperature on Barometric Altimeter Indication

Altitude errors due to uncompensated temperature deviations from the standard value are a particular concern for low-altitude operations. The amount is quantified by the ICAO Cold Temperature Error Table, which is reproduced in Ref. 64.

9.1.4 Vertical Speed Indicator Temperature Sensitivity

The Vertical Speed Indicator is subject to the same temperature sensitivity as the barometric altimeter. Most pertinent to VNAV approaches: Ref. 39 cautions: "Because of the pronounced effect of nonstandard temperature on baro-VNAV operations, VNAV approaches will contain a temperature restriction below which use of the approach is not authorized." For example, the RNAV (GPS) approach plate for Logan International Airport (BOS) runway 04R that was valid for 07 Feb 2013 to 07 March 2013 had this statement: "Uncompensated Baro-VNAV systems, LNAV/VNAV NA [Not Available] below -13 °C (9 °F) or above 43 °C (109 °F)".†

* The correction applied by a pilot in a terminal area, utilizing Automatic Terminal Information Service (ATIS) or Automated Weather Observation System (AWOS) information, only accounts for atmospheric deviations from the standard day pressure at sea level.

† The low-temperature restriction ensures that the actual vertical path flown is obstacle-free. The high-temperature restriction reduces the likelihood that at Decision Height, the aircraft will be above the minimum ceiling and/or have to execute a significant vertical flight correction.

The International Civil Aviation Organization (ICAO) has estimated the impact of temperature on VNAV approaches, and developed the following table (Ref. 65):

Table 23 Effect of Uncompensated Airport Temperature on VNAV Glide Path Angle

Airport Temperature	Actual Glide Path Angle
+30 ^{0}C (+86 ^{0}F)	3.2 deg
+15 ^{0}C (+59 ^{0}F)	3.0 deg
0 ^{0}C (+32 ^{0}F)	2.8 deg
-15 ^{0}C (+5 ^{0}F)	2.7 deg
-31 ^{0}C (-24 ^{0}F)	2.5 deg

For airport at MSL and a charted 3 deg glide path angle

Temperature compensation of the VNAV system is offered on many full-sized transport aircraft and some smaller aircraft, but is not often found in aircraft currently operating.

9.2 VNAV Constant Descent Angle Trajectory

9.2.1 Derivation of Equations

Barometric Vertical NAVigation (Baro VNAV) creates a descent path that is, absent instrumentation errors and incorrect assumptions concerning the atmosphere, similar to, but slightly different from, an ILS glide slope. Whereas ILS navigation involves flying a constant vertical angle α with respect to the plane of the runway, VNAV involves flying a constant vertical angle α' with respect to the horizontal plane at the current aircraft location, and is defined by

$$\tan(\alpha') = \frac{\text{vertical speed}}{\text{ground speed}} \qquad \text{Eq 491}$$

Generally, vertical speed is derived from the aircraft's pitot-static system, and ground speed is found from one of (a) the combination of airspeed and headwind, (b) a GPS receiver, or (c) range measurements to a DME ground station on the airport.

Employing the notation of Chapters 1-3, the differential equation governing a vertical trajectory involving a constant vertical descent angle α' with respect to the local horizontal plane is

$$dh = \tan(\alpha')\,(R_e + h)\,d\theta$$
$$\frac{dh}{R_e + h} = \tan(\alpha')\,d\theta \qquad \text{Eq 492}$$

Integrating both sides of Eq 492 from altitude h_U (the threshold crossing) to altitude h_S (the current aircraft location) yields the expression for the geocentric angle θ

$$\theta = \frac{\log\left(\frac{R_e + h_S}{R_e + h_U}\right)}{\tan(\alpha')} \qquad \text{Eq 493}$$

The natural logarithm is employed in Eq 493. This equation can be manipulated to find the altitude and descent angle as a function of the other two variables.

$$h = R_e\left[e^{\theta \tan(\alpha')} - 1\right]$$
$$= R_e\,\theta\tan(\alpha') + \frac{1}{2}R_e\,\theta^2\tan^2(\alpha') + \cdots \qquad \text{Eq 494}$$

$$\tan(\alpha') = \frac{\log\left(\frac{R_e + h}{R_e}\right)}{\theta}$$
$$= \frac{h}{\theta R_e} - \frac{h^2}{2\theta(R_e)^2} + \frac{h^3}{3\theta(R_e)^3} \pm \cdots \qquad \text{Eq 495}$$

The correspondence between the preceding three equations for VNAV approaches and those for an ILS glide slope approaches are: geocentric angle θ, Eq 493 ↔ Eq 40; altitude h, Eq 494 ↔ Eq 66; and vertical angles α' and α, Eq 495 ↔ Eq 48.

9.2.2 Typical Vertical Profiles

Figure 58 is a plot of aircraft altitude above MSL versus distance along the curved earth's surface from the runway threshold for (a) baro-VNAV guidance with a descent angle of 3.00 deg, (b) ILS guidance with a glide path angle of 3.00 deg, and (c) ILS guidance with a glide path angle of 2.90 deg. At the threshold, the baro-VNAV and ILS 3.00 deg curves coincide; at 5-7 NM from the threshold, the baro-VNAV curve is about halfway between the two curves for ILS guidance; at 14 NM, the baro-VNAV and ILS 2.90 deg curves essentially over lay each other.

9.2.3 Remarks

- References 2 and 3 specify the use of Eq 493 to Eq 495 in the design of VNAV approach procedures.
- Requirements for aircraft implementation of VNAV are found in FAA Advisory Circulars AC 90-105 (Ref. 39) and AC 20-138C (Ref. 40). These documents require the use of a flight director and vertical deviation indicator (VDI) and assume the use of a flight management system.

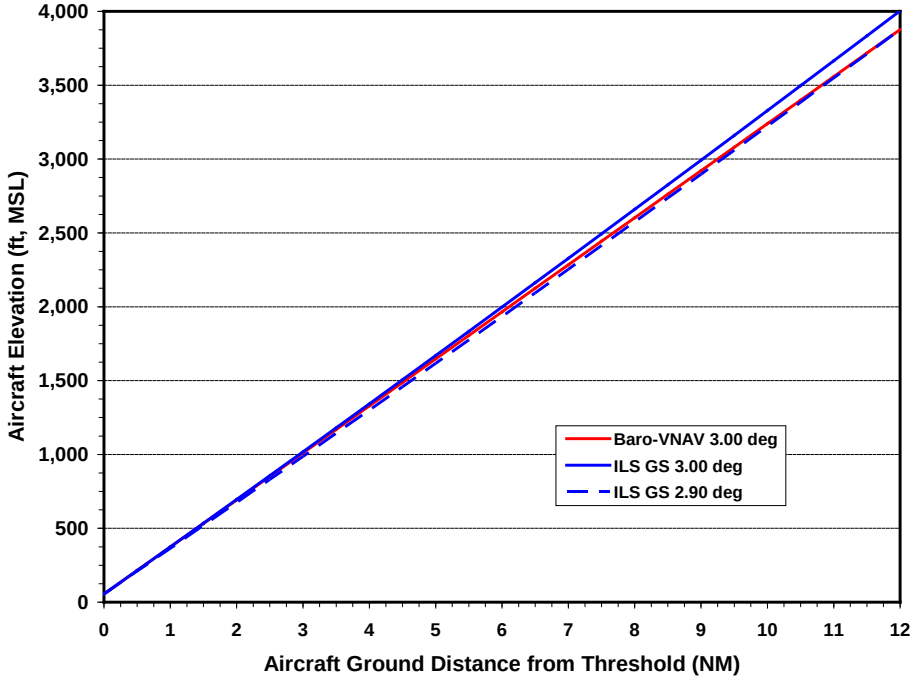

Figure 58 Aircraft Elevation vs. Distance along Ground, for Three Guidance Schemes

9.3 Ellipsoidal Earth Model and ECEF Coordinate Frame

This section presents coordinate frames and transformations associated with an ellipsoidal model for the earth. It draws on Section 2.2 (concerning ellipsoidal earth parameters) and Section 5.1 (concerning coordinate frames and transformations associated with a spherical earth model). In this document, the primary use of a model for an ellipsoidal relates to Chapter 8 — formulating analytic models for slant-range and slant-range difference measurements.

As in Section 5.1, the ellipsoidal earth-centered earth-fixed (ECEF) frame **e** is defined by:

- x^e-axis: lies in the plane of the equator and points toward the Greenwich meridian
- y^e-axis: completes the right-hand orthogonal system
- z^e-axis: lies along the earth's spin axis.

For these axis, the ellipsoid model for the earth's surface is

$$\frac{(x^e)^2}{a^2}+\frac{(y^e)^2}{a^2}+\frac{(z^e)^2}{b^2}=1 \qquad \text{Eq 496}$$

As in Section 2.2, in this section, a denotes the earth's equatorial radius and b its polar radius. The WGS-84 values for a and b are given in Section 2.2. Figure 25, depicting a spherical earth — with slight flattening at the poles — is relevant here, as well.

Figure 59 is depicts an ellipsoidal model of the earth, employing a plane passing through the spin axis. The coordinate quantities of greatest interest are:

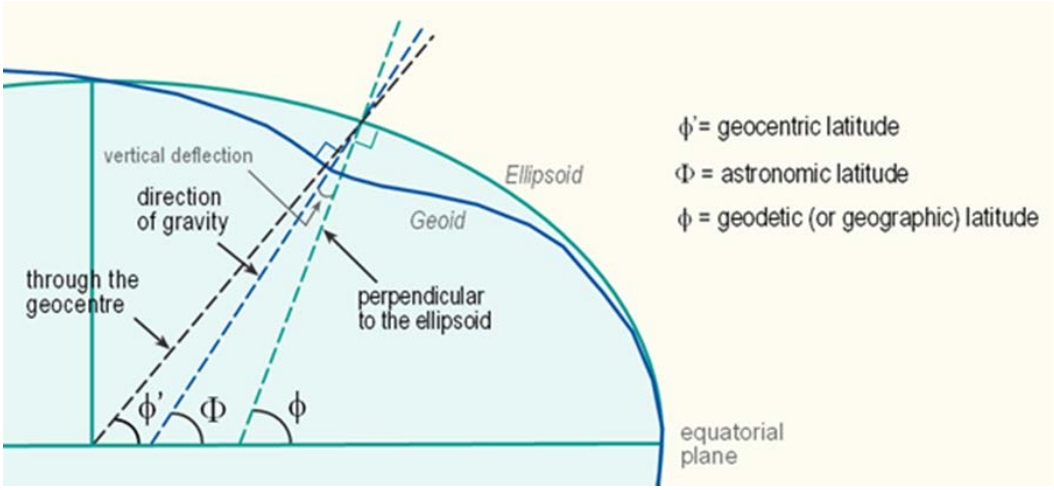

Figure 59 Ellipsoidal Earth Model for a Plane through the Spin Axis

- Geodetic latitude L (denoted by ϕ in Figure 59) — the angle that a normal to the ellipsoid surface makes with the plane of the equator. Geodetic latitude is generally used for navigation and surveying; other measures of latitude are used in mathematical analyses.
- Ellipsoid longitude λ — sometimes termed terrestrial longitude. Longitude for an ellipsoid earth model is conceptually the same as longitude for a spherical model.
- Several definitions of altitude are used. Height above the geoid, an equipotential gravitational surface that approximates mean sea level, is useful for some aspects of navigation. Height above the reference ellipsoid is more convenient for analysis. The two heights are related by the undulation of the geoid, which is published in the form of tables and/or formulas.

A user's height above the ellipsoid $h_{U,ellip}$, height above the geoid $h_{U,geoid}$ and undulation of the geoid at the user's location $\Delta h_{e-g}(L_U, \lambda_U)$ are related by

$$h_{U,ellip} = h_{U,geoid} + \Delta h_{e-g}(L_U, \lambda_U) \qquad \text{Eq 497}$$

Undulation of the geoid is usually computed as a harmonic expansion in latitude and longitude that's fit to measurements. Reference 66 is a source of data concerning undulation of the geoid relative to the WGS-84 reference ellipsoid. The order of the expansion used in Ref. 66 exceeds 2,000, which results in a resolution of 1 arc min. For the CONUS, the geoid is generally below the surface of the WGS-84 ellipsoid — more in the East and less in the West. For locations of interest — e.g., navigation and surveillance ground stations, runways, monuments, etc. — coordinates are generally provided in geodetic latitude and terrestrial longitude relative to the WGS-84 ellipsoid; their elevation is usually stated in relative to mean sea level.

To approximate an ellipsoidal earth at a location on its surface by a sphere, two radii of curvature (RoCs) are commonly defined —the RoC in the meridian (north-south orientation), R_{ns}, and the RoC in the prime vertical (east-west orientation), R_{ew}. These are given in Subsection 2.2.2 (Eq

27). The value for R_{ew} is repeated here, as it is needed below; again, e^2 denotes the earth's eccentricity.

$$R_{ew} = \frac{a}{[1 - e^2 \sin^2(L)]^{1/2}} = \frac{a^2}{[a^2 \cos^2(L) + b^2 \sin^2(L)]^{1/2}} \quad \text{Eq 498}$$

Given a user's geodetic latitude L_U, terrestrial longitude λ_U and height above the ellipsoid h_U, the location of the user **U** relative to the earth's center **O** in the *e*-frame is

$$\underline{\mathbf{r}}^{\mathbf{e}}_{\mathbf{OU}} = \begin{bmatrix} \underline{\mathrm{r}}^{\mathrm{e}}_{\mathrm{OU},x} \\ \underline{\mathrm{r}}^{\mathrm{e}}_{\mathrm{OU},y} \\ \underline{\mathrm{r}}^{\mathrm{e}}_{\mathrm{OU},z} \end{bmatrix} = \begin{bmatrix} (R_{ew} + h_U) \cos(L_U) \cos(\lambda_U) \\ (R_{ew} + h_U)\ \cos(L_U) \sin(\lambda_U) \\ [R_{ew}(1 - e^2) + h_U]\ \sin(L_U) \end{bmatrix} \quad \text{Eq 499}$$

It is evident from Eq 499 that R_{ew} is the distance along the normal between the ellipsoid surface and the earth's spin axis, while $R_{ew}(1 - e^2)$ is the distance between the ellipsoid surface and the equatorial plane.

Given the components of $\underline{\mathbf{r}}^{\mathbf{e}}_{\mathbf{OU}}$ and those of ground station $\underline{\mathbf{r}}^{\mathbf{e}}_{\mathbf{OS}}$, the slant-range between the user and station is

$$d_{US} = \sqrt{\left(\underline{\mathrm{r}}^{\mathrm{e}}_{\mathrm{OU},x} - \underline{\mathrm{r}}^{\mathrm{e}}_{\mathrm{OS},x}\right)^2 + \left(\underline{\mathrm{r}}^{\mathrm{e}}_{\mathrm{OU},y} - \underline{\mathrm{r}}^{\mathrm{e}}_{\mathrm{OS},y}\right)^2 + \left(\underline{\mathrm{r}}^{\mathrm{e}}_{\mathrm{OU},z} - \underline{\mathrm{r}}^{\mathrm{e}}_{\mathrm{OS},z}\right)^2} \quad \text{Eq 500}$$

Conversely, given the components of $\underline{\mathbf{r}}^{\mathbf{e}}_{\mathbf{OU}}$, the user's latitude, longitude and altitude can be found. User longitude is given by

$$\lambda_U = \arctan\left(\underline{\mathrm{r}}^{\mathrm{e}}_{\mathrm{OU},y}, \underline{\mathrm{r}}^{\mathrm{e}}_{\mathrm{OU},x}\right) \quad \text{Eq 501}$$

The expressions for user latitude L_U and elevation above the ellipsoid h_U in Eq 499 are not analytically invertible due to the dependence of R_{ew} on L_U. Thus a numerical solution is required. The three components of Eq 499 can be combined to eliminate elevation h_U, yielding

$$\frac{\sqrt{\left(\underline{\mathrm{r}}^{\mathrm{e}}_{\mathrm{OU},x}\right)^2 + \left(\underline{\mathrm{r}}^{\mathrm{e}}_{\mathrm{OU},y}\right)^2}}{\cos(L_U)} = \frac{\underline{\mathrm{r}}^{\mathrm{e}}_{\mathrm{OU},z}}{\sin(L_U)} + e^2 R_{ew}(L_U) \quad \text{Eq 502}$$

The geodetic latitude L_U can be found from Eq 502 by an iterative root-finding technique (Subsection 2.1.8), using the geocentric latitude as the initial value

$$L_{U,init} = \arctan\left(\frac{\underline{\mathrm{r}}^{\mathrm{e}}_{\mathrm{OU},z}}{\sqrt{\left(\underline{\mathrm{r}}^{\mathrm{e}}_{\mathrm{OU},x}\right)^2 + \left(\underline{\mathrm{r}}^{\mathrm{e}}_{\mathrm{OU},y}\right)^2}}\right) \quad \text{Eq 503}$$

Then h_U can be found from

$$h_U = \frac{\underline{r}^{e}_{OU,z}}{\sin(L_U)} - (1 - e^2)R_{ew}(L_U) \qquad \text{Eq 504}$$

Note that Eq 501 - Eq 504 are not needed when an ellipsoid earth model is employed in determining aircraft latitude, longitude and altitude by an iterative solution of the measurement equations.

9.4 Rhumb Line Navigation

9.4.1 Background

The defining characteristic of rhumb* line navigation is that the intended track over the ground has the same azimuth angle with respect to North at each location along the track. That is,

$$\psi = \arctan\left(\frac{\cos(L)\, d\lambda}{dL}\right) = \text{constant}$$
$$\tan(\psi) \int \frac{dL}{\cos(L)} = \int d\lambda \qquad \text{Eq 505}$$

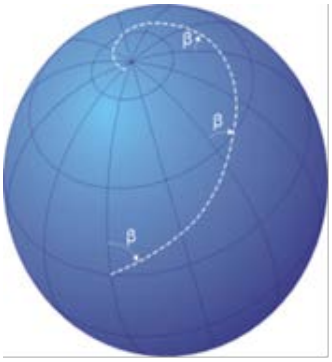

An example rhumb line course is shown to the right. Mathematically, such courses are loxodromes; they spiral toward, but do not reach, a pole. (The exception is a constant-latitude course; these are often treated separately.)

Rhumb line navigation has been used by mariners for hundreds of years.† The primary advantage of rhumb lines was that they simplified the helmsman's task in an era when only rudimentary tools were available. Even when a great circle route was being implemented, the path was approximated by a series of waypoints and rhumb line navigation was employed between waypoints.

Another important advantage of rhumb line navigation is that, for a Mercator projection, a rhumb line course is a straight line on a chart. This greatly simplifies the planning process, and likely contributed to the popularity of the Mercator projection.

Today, great circle navigation has largely replace rhumb line navigation, particularly for aviation, since it provides shorter paths and air routes are less restricted than marine routes. Rhumb line navigation is still in use for applications lacking a navigation computer..

Three factors cause great circle and rhumb line routes to be dissimilar:

* The word 'rhumb' apparently comes from Spanish/Portuguese *rumbo/rumo*, meaning course or direction (Wikipedia). An alternative term to rhumb line is 'loxodrome'.

† Rhumb lines were first discussed by the Portuguese mathematician Pedro Nunes in 1537, in (translated) *Treatise in Defense of the Marine Chart* (Wikipedia).

- Path length: The origin and destination (or end points of a navigation leg) are far apart (e.g., thousands of miles)
- Starting location: Route leg starts at mid- and/or high-latitude, and
- End location/route direction: The end point is at mid- and/or high-latitude on the same side of the equator.

Numerical examples illustrating the importance of these points are presented in Subsection 4.8.4.

Consistent with the intent of this document, the equations presented below are for rhumb line navigation with respect to a spherical earth (Refs. 28 and 67). More accurate equations applicable to an ellipsoidal earth may be found in Ref. 68.

9.4.2 Solution of the Indirect Problem

The Indirect problem of geodesy / navigation is defined in Section 1.2.2 and its solution for great circle navigation is given in Section 4.2. The known quantities are the latitude/longitude of the starting point **U** (L_U, λ_U) and end point **S** (L_S, λ_S). The quantities to be found are the distance D between **U** and **S**; and the azimuth angles $\psi_{S/U}$ at **U** and $\psi_{U/S}$ at **S** of the trajectory connecting **U** and **S**.

After integrating the second line of Eq 505 from **U** to **S**, the result is

$$\tan\left(\psi_{S/U}\right) = \frac{\lambda_S - \lambda_U}{\log\left(\dfrac{\tan\left(\frac{1}{2}L_S + \frac{1}{4}\pi\right)}{\tan\left(\frac{1}{2}L_U + \frac{1}{4}\pi\right)}\right)} = \frac{\lambda_S - \lambda_U}{L'_S - L'_U} \qquad \text{Eq 506}$$

The natural logarithm is used in Eq 506 and throughout this section. The quantity L', introduced in Eq 506 and defined in Eq 507, is sometimes termed the 'stretched latitude'. It's central to rhumb line navigation, and is plotted in Figure 60.

$$L' \equiv \log\left(\tan\left(\frac{1}{2}L + \frac{1}{4}\pi\right)\right)$$
$$L = 2\arctan\left(e^{L'}\right) - \frac{1}{2}\pi \qquad \text{Eq 507}$$

Since a constant azimuth angle is involved, it follows that

$$\psi_{U/S} = \psi_{S/U} \pm \pi \qquad \text{Eq 508}$$

Once the azimuth angle $\psi_{S/U}$ is known, the rhumb line distance along the earth's surface, D, between **U** and **S** can be found using

$$D = \frac{R_e}{\cos\left(\psi_{S/U}\right)}\int_{L_U}^{L_S} dL = \frac{R_e\left(L_S - L_U\right)}{\cos\left(\psi_{S/U}\right)} \qquad \text{when} \qquad L_S \neq L_U \qquad \text{Eq 509}$$

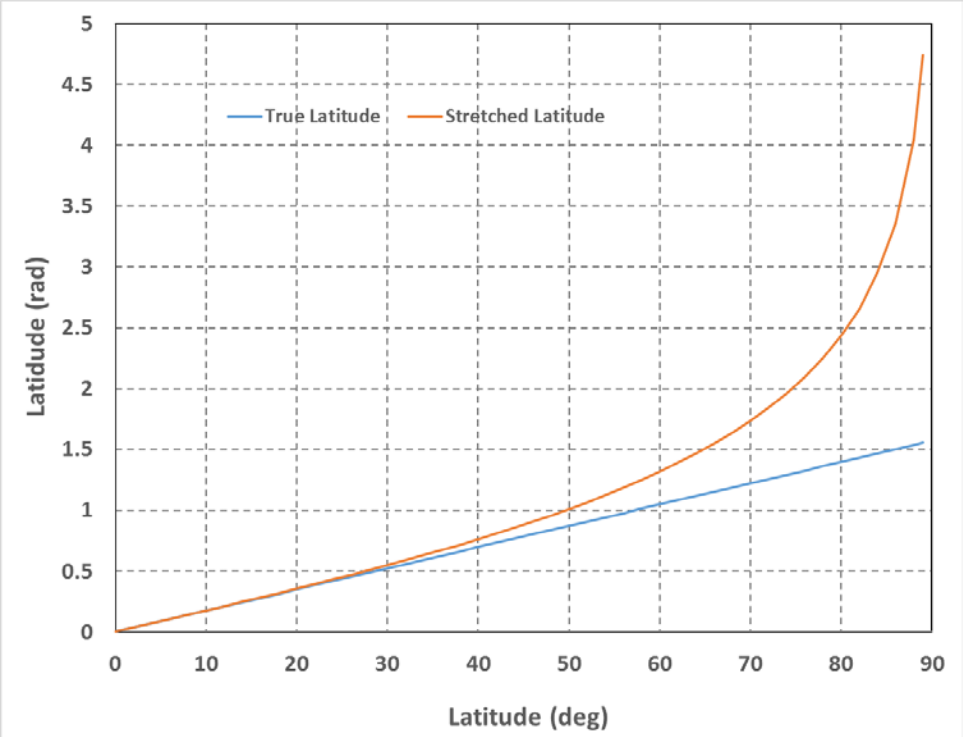

Figure 60 Comparision of Stretched and True Latitudes

This equation is correct when L_S is either larger or smaller than L_U, but fails when the angles are equal (i.e., for constant latitude paths). Then Eq 509 must be replaced by

$$D = R_e \cos(L_S)\,|\lambda_S - \lambda_U| = R_e \cos(L_U)\,|\lambda_S - \lambda_U| \qquad \text{when} \qquad L_S = L_U \qquad \text{Eq 510}$$

An equation for the distance D between **U** and **S** that does not depend on the solution for $\psi_{S/U}$ can be developed. For convenience, let

$$\Delta L_{US} = L_S - L_U \quad , \quad \Delta L'_{US} = L'_S - L'_U \quad , \quad \Delta\lambda_{US} = \lambda_S - \lambda_U \qquad \text{Eq 511}$$

From Eq 509 and Eq 506, it follows that

$$D\sin(\psi_{S/U}) = D\cos(\psi_{S/U})\tan(\psi_{S/U}) = R_e\,\Delta L_{US}\,\frac{\Delta\lambda_{US}}{\Delta L'_{US}} \qquad \text{Eq 512}$$

Then, from Eq 509 and Eq 512, the rhumb line distance D is given by

$$D = R_e\sqrt{(\Delta L_{US})^2 + \frac{(\Delta L_{US})^2}{(\Delta L'_{US})^2}(\Delta\lambda_{US})^2} \qquad \text{when} \qquad L_S \neq L_U \qquad \text{Eq 513}$$

9.4.3 Solution of the Direct Problem

The Direct problem of geodesy is defined in Section 1.2.2 and its solution for great circle navigation is given in Section 4.3. Here the known quantities are: the latitude/longitude, (L_U, λ_U), of the starting point **U**; the distance, *D*, between **U** and **S**; and the azimuth angle at **U**, $\psi_{S/U}$, of the trajectory connecting **U** and **S**. The quantities to be found are the latitude/longitude (L_S, λ_S), of the end point **S**.

From Eq 509 it follows that

$$L_S = L_U + \frac{D}{R_e}\cos(\psi_{S/U}) \qquad \text{Eq 514}$$

There does not appear to be a solution for λ_S that does not, at least implicitly, utilize the solution for L_S and then L'_S. One option is to manipulate Eq 506 to obtain

$$\lambda_S = \lambda_U + (L'_S - L'_U)\tan(\psi_{S/U}) \qquad \text{when} \qquad |\psi_{S/U}| \neq \tfrac{1}{2}\pi \qquad \text{Eq 515}$$

Alternative expressions for λ_S can be derived from Eq 512 and Eq 513

$$\begin{aligned} \lambda_S &= \lambda_U + \frac{D(L'_S - L'_U)}{R_e(L_S - L_U)}\sin(\psi_{S/U}) \\ &= \lambda_U + \frac{L'_S - L'_U}{L_S - L_U}\sqrt{\left(\frac{D}{R_e}\right)^2 - (L_S - L_U)^2} \qquad \text{when} \qquad |\psi_{S/U}| \neq \tfrac{1}{2}\pi \end{aligned} \qquad \text{Eq 516}$$

When $|\psi_{S/U}| = \frac{1}{2}\pi$, then

$$\lambda_S = \lambda_U + \operatorname{sgn}(\psi_{S/U})\frac{D}{R_e\cos(L_U)} \qquad \text{when} \qquad |\psi_{S/U}| = \tfrac{1}{2}\pi \qquad \text{Eq 517}$$

Finally, $\psi_{U/S}$ is found from Eq 508.

9.4.4 Remarks

There are many alternative expressions to Eq 507 for the stretched latitude, all of which can be derived by elementary manipulations. Examples include (Ref. 69):

$$\begin{aligned} L' &= \frac{1}{2}\log\left(\frac{1+\sin(L)}{1-\sin(L)}\right) = \log\left(\frac{1+\sin(L)}{\cos(L)}\right) = \log(\sec(L) + \tan(L)) \\ &= \tanh^{-1}(\sin(L)) = \sinh^{-1}(\tan(L)) = \cosh^{-1}(\sec(L)) \end{aligned} \qquad \text{Eq 518}$$

The Mercator map projection is essentially a plot using linear Cartesian coordinates with λ as the abscissa and L' as the ordinate.

9.5 NLLS Solution with a Measurement Constraint

9.5.1 Problem Formulation

This section revisits the topic of Section 8.1 — finding a solution to a set of redundant measurements. Here, an additional complication is introduced: there is a constraint on the unknown variables, often because it reflects a measurement that's considered to be error-free (or 'perfect'). It's assumed that the unconstrained measurement equations of Eq 350 - Eq 354 are applicable.

$$\tilde{\mathbf{z}} = \mathbf{f}(\mathbf{x}) + \mathbf{v} \qquad \dim(\mathbf{x}) \leq \dim(\tilde{\mathbf{z}}) \qquad \text{Eq 519}$$

For concreteness, it can be assumed that the navigation variables are $\mathbf{x} = [L_A \;\; \lambda_A \;\; h_A \;\; t_X]^T$, but other sets of unknowns are possible. Vector **v** represents errors in the unconstrained measurements.

It's assumed that the constraint (or additional, error-free measurement) is

$$y = g(\mathbf{x}) \qquad \text{Eq 520}$$

A set of nominal values for the unknown variables $\overline{\mathbf{x}}$ are assumed to be known. Thus $\mathbf{f}(\mathbf{x})$ and $g(\mathbf{x})$ can be linearlized about $\overline{\mathbf{x}}$ by setting $\mathbf{x} = \overline{\mathbf{x}} + \boldsymbol{\delta}\mathbf{x}$. Then, to first order

$$\boldsymbol{\delta}\mathbf{z} = \tilde{\mathbf{z}} - \mathbf{f}(\overline{\mathbf{x}}) = \mathbf{J}\,\boldsymbol{\delta}\mathbf{x} + \mathbf{v} \qquad \delta y = y - g(\overline{\mathbf{x}}) = (\nabla g)^T\,\boldsymbol{\delta}\mathbf{x} \qquad \text{Eq 521}$$

Here, the Jacobian matrix **J** is given by Eq 356 and the gradient vector ∇g by

$$(\nabla g)^T = \left[\frac{\partial g}{\partial x_1} \quad \frac{\partial g}{\partial x_2} \quad \cdots\right] \qquad \text{Eq 522}$$

The cost function to be minimized is

$$\min_{\boldsymbol{\delta}\mathbf{x},\mu} C = (\boldsymbol{\delta}\mathbf{z} - \mathbf{J}\,\boldsymbol{\delta}\mathbf{x})^T\,\mathbf{W}\,(\boldsymbol{\delta}\mathbf{z} - \mathbf{J}\,\boldsymbol{\delta}\mathbf{x}) + 2\mu(\delta y - (\nabla g)^T\,\boldsymbol{\delta}\mathbf{x}) \qquad \text{Eq 523}$$

In Eq 523, μ is a Largrange multiplier.

9.5.2 Problem Solution

General Solution — Taking the derivative of the right-hand side of Eq 523 with respect to **δx**, and setting the result equal to zero yields

$$\boldsymbol{\delta}\check{\mathbf{x}} = \left(\mathbf{J}^{\mathrm{T}}\mathbf{W}\,\mathbf{J}\right)^{-1}\mathbf{J}^T\mathbf{W}\,\boldsymbol{\delta}\mathbf{z} + \mu\nabla g = \boldsymbol{\delta}\hat{\mathbf{x}} + \mu\nabla g \qquad \text{Eq 524}$$

Here, $\boldsymbol{\delta}\hat{\mathbf{x}} = \left(\mathbf{J}^{\mathrm{T}}\mathbf{W}\,\mathbf{J}\right)^{-1}\mathbf{J}^T\mathbf{W}\,\boldsymbol{\delta}\mathbf{z}$ is the unconstrained general estimator (Eq 360).

Multiplying both sides of Eq 524 by $(\nabla g)^T$ and utilizing $\delta y = (\nabla g)^T\,\boldsymbol{\delta}\mathbf{x}$ yields

$$\mu = \frac{\delta y - (\nabla g)^T \left(\mathbf{J}^{\mathrm{T}} \mathbf{W}\, \mathbf{J}\right)^{-1} \mathbf{J}^T \mathbf{W}\, \boldsymbol{\delta z}}{(\nabla g)^T \nabla g} = \frac{\delta y - (\nabla g)^T \boldsymbol{\delta \hat{x}}}{(\nabla g)^T \nabla g} \qquad \text{Eq 525}$$

Substituting Eq 525 into Eq 524 yields

$$\boldsymbol{\delta \check{x}} = \left[\mathbf{I} - \frac{\nabla g\, (\nabla g)^T}{(\nabla g)^T \nabla g}\right] \boldsymbol{\delta \hat{x}} + \frac{\delta y}{(\nabla g)^T \nabla g} \nabla g \qquad \text{Eq 526}$$

Clearly Eq 526 satisfies $(\nabla g)^T\, \boldsymbol{\delta \check{x}} = \delta y$. The estimator of Eq 526 the sum of (a) the projection of the unconstrained estimator $\boldsymbol{\delta \hat{x}}$ onto the subspace of the unknown variables **x** that's orthogonal to the gradient ∇g, and (b) a Newton-Raphson-type of solution to the constraint equation.

Optimal Solution — The optimal solution is found by setting $\mathbf{W}=\mathbf{R}^{-1}$ in Eq 524 and Eq 525, or by using Eq 361 to compute the unconstrained estimator $\boldsymbol{\delta \hat{x}}$ in Eq 526.

Newton-Type Solution — When **J** is square, the expressions for μ (right-hand side of Eq 525) and $\boldsymbol{\delta \check{x}}$ (Eq 526) in terms of $\boldsymbol{\delta \hat{x}}$ remain valid. The expression for $\boldsymbol{\delta \hat{x}}$ is given by Eq 362.

Iterative Process — Using Eq 524 and Eq 525 or Eq 526, the updated values for the unknown variables are

$$\check{\mathbf{x}} = \bar{\mathbf{x}} + \boldsymbol{\delta \check{x}} \qquad \text{Eq 527}$$

After completing an iteration step (say, *k*), the process below is repeated for step *k*+1:

1. Compute the nominal values for the unknown variables from the updated values in the previous step *k* — i.e., set $\bar{\mathbf{x}} = \bar{\mathbf{x}}_{k+1} = \check{\mathbf{x}}_k$. For first step, the value for $\bar{\mathbf{x}}_0$ must be obtained by other means.
2. Evaluate the measurement residuals $\boldsymbol{\delta z}$ and δy using $\bar{\mathbf{x}}$ (Eq 521)
3. Optional: Evaluate δy for satisfaction of the constraint
4. Optional: Examine the components of $\boldsymbol{\delta z}$ for the presence of outliers
5. Optional: Compute the updated cost function *C* (Eq 523)
6. Compute the Jacobian matrix **J** (Eq 356) and gradient vector ∇g (Eq 522)
7. Compute the unconstrained perturbation vector estimate $\boldsymbol{\delta \hat{x}} = \boldsymbol{\delta \hat{x}}_{k+1}$ (Eq 360, Eq 361 or Eq 362)
8. Compute the Lagrange multiplier μ (right-most expression in Eq 525)
9. Compute the constrained perturbation estimate $\boldsymbol{\delta \check{x}}$ (right-most expression in Eq 524)
10. Compute the updated estimate of the variables sought $\check{\mathbf{x}} = \check{\mathbf{x}}_{k+1}$ (Eq 527)

A convergence check is performed at the beginning or end of each iteration step. At a minimum, this involves comparing the updated value of each element of $\check{\mathbf{x}}_{k+1}$ with its previous estimate $\check{\mathbf{x}}_k$, and comparing the value of $g(\check{\mathbf{x}}_{k+1})$ with the constraint y.

9.5.3 Solution Properties

Final Lagrange Multiplier — If/when convergence occurs, then the final Lagrange multiplier is (for the general case)

$$\mu = -\frac{(\nabla g)^T \left(\mathbf{J}^{\mathrm{T}}\mathbf{W}\,\mathbf{J}\right)^{-1}\mathbf{J}^T\mathbf{W}\,\boldsymbol{\delta}\mathbf{z}}{(\nabla g)^T\,\nabla g} = -\frac{(\nabla g)^T\,\boldsymbol{\delta}\hat{\mathbf{x}}}{(\nabla g)^T\,\nabla g} \qquad \text{Eq 528}$$

Thus the final Lagrange multiplier is the negative of the ratio of (a) the projection of the unconstrained estimator onto the gradient to the error-free measurement to (b) the square of the magnitude of the gradient.

Estimation Error — If the left-hand side of Eq 521 is substituted into Eq 526, the result is

$$\boldsymbol{\delta}\breve{\mathbf{x}} = \left[\mathbf{I} - \frac{\nabla g\,(\nabla g)^T}{(\nabla g)^T\,\nabla g}\right]\boldsymbol{\delta}\mathbf{x} + \left[\mathbf{I} - \frac{\nabla g\,(\nabla g)^T}{(\nabla g)^T\,\nabla g}\right]\left(\mathbf{J}^T\mathbf{W}\,\mathbf{J}\right)^{-1}\mathbf{J}^T\mathbf{W}\,\mathbf{v} + \frac{\delta y}{(\nabla g)^T\,\nabla g}\nabla g \qquad \text{Eq 529}$$

Thus, when convergence has occurred and $\delta y = 0$, the residual error in $\boldsymbol{\delta}\breve{\mathbf{x}}$ is the component of $\boldsymbol{\delta}\mathbf{x}$ that's orthogonal to the constraint gradient due to the associated measurement error.

General Estimator Error Covariance — Assume that the first and second moments of the measurement error $\mathbf{v}$ are given by

$$E(\mathbf{v}) = \mathbf{0} \qquad E(\mathbf{v}\mathbf{v}^T) = \mathbf{R} \qquad \text{Eq 530}$$

Then, from Eq 529, the covariance of the error for the general estimator is

$$\begin{aligned}\boldsymbol{\Sigma} &= E(\boldsymbol{\delta}\breve{\mathbf{x}} - \boldsymbol{\delta}\mathbf{x})(\boldsymbol{\delta}\breve{\mathbf{x}} - \boldsymbol{\delta}\mathbf{x})^T \\ &= \left[\mathbf{I} - \frac{\nabla g\,(\nabla g)^T}{(\nabla g)^T\,\nabla g}\right]\left(\mathbf{J}^T\mathbf{W}\mathbf{J}\right)^{-1}\mathbf{J}^T\mathbf{W}\mathbf{R}\mathbf{W}\mathbf{J}\left(\mathbf{J}^T\mathbf{W}\mathbf{J}\right)^{-1}\left[\mathbf{I} - \frac{\nabla g\,(\nabla g)^T}{(\nabla g)^T\,\nabla g}\right]\end{aligned} \qquad \text{Eq 531}$$

Optimal Estimator Error Covariance — If $\mathbf{W}=\mathbf{R}^{-1}$ then Eq 531 reduces to a modified version of the error covariance for the optimal estimator (Eq 366)

$$\boldsymbol{\Sigma} = E(\boldsymbol{\delta}\breve{\mathbf{x}} - \boldsymbol{\delta}\mathbf{x})(\boldsymbol{\delta}\breve{\mathbf{x}} - \boldsymbol{\delta}\mathbf{x})^T = \left[\mathbf{I} - \frac{\nabla g\,(\nabla g)^T}{(\nabla g)^T\,\nabla g}\right]\left(\mathbf{J}^T\mathbf{R}^{-1}\mathbf{J}\right)^{-1}\left[\mathbf{I} - \frac{\nabla g\,(\nabla g)^T}{(\nabla g)^T\,\nabla g}\right] \qquad \text{Eq 532}$$

For both expressions, the estimation error in the direction of the gradient is zero,

$$(\nabla g)^T\,\boldsymbol{\Sigma}\,\nabla g = 0 \qquad \text{Eq 533}$$

Newton Estimator Error Covariance — From Eq 529, the covariance of the error for the Newton estimator is

$$\boldsymbol{\Sigma} = E(\boldsymbol{\delta}\breve{\mathbf{x}} - \boldsymbol{\delta}\mathbf{x})(\boldsymbol{\delta}\breve{\mathbf{x}} - \boldsymbol{\delta}\mathbf{x})^T = \left[\mathbf{I} - \frac{\nabla g\,(\nabla g)^T}{(\nabla g)^T\,\nabla g}\right]\mathbf{J}^{-1}\mathbf{R}\,\mathbf{J}^{-T}\left[\mathbf{I} - \frac{\nabla g\,(\nabla g)^T}{(\nabla g)^T\,\nabla g}\right] \qquad \text{Eq 534}$$

Eq 533 also holds for this expression for $\mathbf{\Sigma}$.

Imperfect Perfect Measurement — While the measurement processing may assume that $y = g(\mathbf{x})$ without error (Eq 520), this may in fact not be true. Thus, assume that what is actually true is

$$\tilde{y} = y + v_y = g(\mathbf{x}) + v_y$$
$$E(v_y) = 0 \qquad E(v_y)^2 = \sigma_y^2 \qquad E(v_y \mathbf{v}) = \mathbf{0} \qquad \text{Eq 535}$$

In this situation, the constraint measurement residual actually is

$$\delta y = \tilde{y} - g(\bar{\mathbf{x}}) = (\nabla g)^T \, \boldsymbol{\delta}\mathbf{x} + v_y \qquad \text{Eq 536}$$

Thus, when $\delta y = 0$, $\boldsymbol{\delta}\mathbf{x}$ satisfies $(\nabla g)^T \, \boldsymbol{\delta}\mathbf{x} = -v_y$. Then, from Eq 525, the final value for μ is

$$\mu = \frac{v_y - (\nabla g)^T \left(\mathbf{J}^{\mathrm{T}} \mathbf{W} \mathbf{J}\right)^{-1} \mathbf{J}^T \mathbf{W} \mathbf{v}}{(\nabla g)^T \nabla g} \qquad \text{Eq 537}$$

If this expression is substituted into Eq 524, the result is

$$\boldsymbol{\delta}\check{\mathbf{x}} = \left[\mathbf{I} - \frac{\nabla g \, (\nabla g)^T}{(\nabla g)^T \nabla g}\right] \boldsymbol{\delta}\mathbf{x} + \left[\mathbf{I} - \frac{\nabla g \, (\nabla g)^T}{(\nabla g)^T \nabla g}\right] \left(\mathbf{J}^T \mathbf{W} \mathbf{J}\right)^{-1} \mathbf{J}^T \mathbf{W} \mathbf{v} + \frac{v_y}{(\nabla g)^T \nabla g} \nabla g \qquad \text{Eq 538}$$

Then the foregoing expressions for $\mathbf{\Sigma}$ can be modified to account for the imperfect 'perfect' measurement as follows

$$E\,(\boldsymbol{\delta}\check{\mathbf{x}} - \boldsymbol{\delta}\mathbf{x})(\boldsymbol{\delta}\check{\mathbf{x}} - \boldsymbol{\delta}\mathbf{x})^T = \mathbf{\Sigma} + \frac{\nabla g \, (\nabla g)^T}{[(\nabla g)^T \nabla g]^2} \sigma_y^2 \qquad \text{Eq 539}$$

Here, $\mathbf{\Sigma}$ is given by Eq 531, Eq 532 or Eq 534.

Approximation Fidelity — In forming the residuals $\boldsymbol{\delta}\mathbf{z}$ and δy in Eq 521, the most accurate information available is used for functions $\mathbf{f}$ and g. However, approximations can be used in forming their derivatives in Jacobian matrix $\mathbf{J}$ and gradient vector ∇g.

Multiple Constraints — When there are multiple constraints — say $y_i = g_i(\mathbf{x}), i = 1,2, \ldots$ — then the cost function of Eq 523 becomes

$$\min_{\boldsymbol{\delta}\mathbf{x}, \mu} C = (\boldsymbol{\delta}\mathbf{z} - \mathbf{J}\boldsymbol{\delta}\mathbf{x})^T \mathbf{W} (\boldsymbol{\delta}\mathbf{z} - \mathbf{J}\boldsymbol{\delta}\mathbf{x}) + 2 \sum_i \mu_i (\delta y_i - (\nabla g_i)^T \, \boldsymbol{\delta}\mathbf{x}) \qquad \text{Eq 540}$$

The solution then proceeds along the same lines as above.

10. REFERENCES

1. Nathaniel Bowditch: *The American Practical Navigator*; National Imagery and Mapping Agency; 2002.

2. FAA Order 8260.3B, Change 25: *United States Standard for Terminal Instrument Procedures (TERPS)*; Flight Standards Service; March 9, 2012.

3. FAA Order 8260.58: *United States Standard for Performance Based Navigation (PBN) Instrument Procedure Design*; Flight Standards Service; September 21, 2012.

4. Wikipedia: "Double-precision floating-point format"; retrieved April 14, 2016; https://en.wikipedia.org/wiki/Double-precision_floating-point_format

5. Wikipedia: "Inverse trigonometric functions"; retrieved November 1, 2014; http://en.wikipedia.org/wiki/Inverse_ trigonometric_functions.

6. Wikipedia: "Newton's method"; http://en.wikipedia.org/wiki/Newtons_method; retrieved November 1, 2014.

7. Christopher Jekeli; *Geometric Reference Systems in Geodesy*; Ohio State University; July 2006.

8. Friedrich Robert Helmert: *Die mathematischen und physikalischen Theorieen der höheren Geodäsie*; Part I, 1880; Part II, 1884.

9. Friedrich Robert Helmert: *Mathematical and Physical Theories of Higher Geodesy*; Translation into English of Parts I and II of previous reference; Aeronautical Chart and Information Center; St. Louis; 1964.

10. Marie Henri Andoyer: "Formule donnant la longueur de la géodésique, joignant 2 points de l'ellipsoide donnes par leurs coordonnées geographiques"; *Bulletin Geodsique*; No. 34, 77-81, 1932.

11. Paul D. Thomas: *Mathematical Models for Navigation Systems*; U.S. Naval Oceanographic Office; TR- 182; October 1965.

12. P.B. Morris, et al.: *Omega Navigation System Course Book*; TASC; July 1994.

13. Emanuel M. Sodano: "A rigorous non-iterative procedure for rapid inverse solution of very long geodesics"; *Bulletin Géodésique*; vol 47/48, pp 13-25; 1958.

14. Emanuel M. Sodano: "General non-iterative solution of the inverse and direct geodetic problems"; *Bulletin Géodésique*; vol 75, pp 69-89; 1965.

15. Emanuel M. Sodano: "Supplement to inverse solution of long geodesics"; *Bulletin Géodésique*; vol 85: 233-236; 1967.

16. Thaddeus Vincenty: "Direct and Inverse Solutions of Geodesics on the Ellipsoids with Applications of Nested Equations", *Survey Review*; XXIII, Number 176; April 1975.

17. C. M. Thomas and W. E. Featherstone: "Validation of Vincenty's Formulas for the Geodesic Using a New Fourth-Order Extension of Kivioja's Formula"; *Journal of Surveying Engineering*; American Society of Civil Engineers; February 2005.

18. Wikipedia: “Solution of triangles”; https://en.wikipedia.org/wiki/Solution_of_triangles; retrieved March 12, 2016.

19. Wikipedia: “Non-line-of-sight propagation”; http://en.wikipedia.org/wiki/Non-line-of-sight_propagation; retrieved November 1, 2014.

20. Armin W. Doerry: “Earth Curvature and Atmospheric Refraction Effects on Radar Signal Propagation”; Sandia National Laboratories; SAND2012-10690; January 2013.

21. Christian Wolff: “Cone of Silence”; http://www.radartutorial.eu/18.explanations/ex47.en.html; retrieved November 1, 2014.

22. Wikipedia: “History of trigonometry”; http://en.wikipedia.org/wiki/History_of_trigonometry; retrieved November 1, 2014.

23. Wikipedia: “Mathematics in medieval Islam”; retrieved November 1, 2014; http://en.wikipedia.org/wiki/Mathematics_ in_medieval_Islam.

24. I. Todhunter: *Spherical Trigonometry*; MacMillan; 5th edition, 1886.

25. W.M. Smart and R.M. Green: *Spherical Astronomy*; Cambridge University Press; Sixth Edition, 1977.

26. Wikipedia: “Spherical trigonometry”; http://en.wikipedia.org/wiki/Spherical_trigonometry; retrieved November 1, 2014.

27. Wolfram MathWorld: “Spherical Trigonometry”; retrieved November 1, 2014; http://mathworld.wolfram.com/ SphericalTrigonometry.html.

28. Ed Williams: “Aviation Formulary V1.46”; http://williams.best.vwh.net/avform.htm; retrieved November 1, 2014.

29. Kryss Katsiavriades and Talaat Qureshi: “Spherical Trigonometry”; retrieved November 1, 2014; http://www.krysstal.com/sphertrig.html.

30. Wikipedia: “Versine”; http://en.wikipedia.org/wiki/Versine; retrieved November 1, 2014.

31. Don Josef de Mendoza y Rios, F.R.S.: “Recherches sur les principaux Problemes de l'Astronomie Nautique”; *Proc. Royal Soc.*; Dec 22, 1796.

32. FAA, “National Flight Data Center (NFDC)”; retrieved April 13, 2016; https://nfdc.faa.gov/xwiki/bin/view/NFDC/WebHome.

33. AirNav.com: “Airport Information”; http://www.airnav.com/airport/KMCI; retrieved September 5, 2013.

34. FAA: “Welcome to the William J. Hughes Technical Center WAAS Test Team”; http://www.nstb.tc.faa.gov/index.htm; retrieved September 5, 2013.

35. M. Craymer; MathWorks; Geodetic Toolbox; retrieved April 13, 2016; http://www.craymer.com/software/matlab/geodetic/.

36. A.S. Lenart: “Solutions of Direct Geodetic Problem in Navigational Applications”; *International Journal on Marine Navigation and Safety of Sea Transportation*; vol. 5, no. 4; December 2011.

37. FAA Advisory Circular AC 90-100A: *U.S. Terminal and En Route Area Navigation (RNAV) Operations*; Flight Standards Service (AFS-400); March 1, 2007.

38. FAA Advisory Circular AC 120-108: *Continuous Descent Final Approach*; Flight Standards Service (AFS-400); January 20, 2011.

39. FAA Advisory Circular AC 90-105: *Approval Guidance for RNP Operations and Barometric Vertical Navigation in the U.S. National Airspace System*; Flight Standards Service (AFS-400); January 23, 2009.

40. FAA Advisory Circular AC 20-138C, *Airworthiness Approval of Positioning and Navigation Systems*; Aircraft Certification Service (AIR-130); May 8, 2012.

41. Hugh Dibley: *Action to Reduce Continuing CFIT Accidents by Defining & Training Constant Angle Approaches*; 16th Annual World Aviation Training Conference & Tradeshow; April 2013.

42. David Carbaugh and Bryan Wyness: "Hazards of Erroneous Glide Slope Indications"; *AeroMagazine*; Boeing; v21, January 2003. http://www.boeing.com/commercial/aeromagazine/

43. Mitch Narins: "The Global Loran / eLoran Infrastructure Evolution"; FAA; presentation before U.S. Space-Based PNT Advisory Board; June 3, 2014.

44. Bertrand T. Fang: "Simple Solutions for Hyperbolic and Related Position Fixes"; *IEEE Transactions on Aerospace and Electronic Systems*; September 1990, pp 748-753.

45. Sheldon Razin: "Explicit (Noniterative) Loran Solution"; *Navigation, Journal of the Institute of Navigation*; Vol. 14, No. 3, Fall 1967, pp. 265-269.

46. Harry Lee: "Accuracy Limitations of Hyperbolic Multilateration Systems"; Massachusetts Institute of Technology, Lincoln Laboratory; Technical Note 1973-11; March 22, 1973.

47. S. Bancroft: "An Algebraic Solution of the GPS Pseudorange Equations"; *IEEE Transactions on Aerospace and Electronic Systems*; AES-21, November 1985, pp 56-59.

48. Michael Geyer and Anastasios Daskalakis: "Solving Passive Multilateration Equations Using Bancroft's Algorithm"; *Digital Avionics Systems Conference (DASC)*; Seattle, WA; Oct. 31-Nov. 6, 1998.

49. Ming Yang and Kuo-Hwa Chen: "Performance Assessment of a Noniterative Algorithm for Global Positioning System (GPS) Absolute Positioning"; *Proc. Natl. Sci. Counc. ROC(A);* vol 25, no 2, pp 102-106; 2001.

50. Niilo Sirola: "Closed-form Algorithms in Mobile Positioning: Myths and Misconceptions"; *Proceedings of the 7th Workshop on Positioning, Navigation and Communication 2010 (WPNC'10)*; March 11, 2010.

51. Alfred Kleusberg: "Analytical GPS Navigation Solution"; *University of Stuttgart Research Compendium*; 1994.

52. Nicholas H.J. Stuifbergen: *Intersection of Hyperbolae on the Earth*; University of New Brunswick; Fredericton, New Brunswick, Canada; December 1980.

53. Paul Williams and David Last: "On Loran-C Time-Difference to Co-ordinate Converters"; *Proceedings - International Loran Association (ILA) - 32nd Annual Convention and Technical Symposium*; Boulder, Colorado; November 3-7, 2003.

54. Radio Technical Commission for Marine Services: *Minimum Performance Standards (MPS) Automatic Co-ordinate Conversion Systems*; Report of RTCM Special Committee No. 75; Washington, D.C; 1984.

55. Coast Guard Navigation Center: *POSAID2 ver 2.1a*.

56. Wikipedia: *Least Squares*; https://en.wikipedia.org/wiki/Least_squares; retrieved April 13, 2016.

57. Andrew Sage and James Melsa: *Estimation Theory with Applications to Communications and Control*; Robert Krieger Publishing Company; 1979.

58. Wikipedia: "Gauss–Newton algorithm"; retrieved April 22, 2016; https://en.wikipedia.org/wiki/Gauss%E2%80%93Newton_algorithm.

59. Wikipedia: "Newton's method"; retrieved April 22, 2016; https://en.wikipedia.org/wiki/Newton's_method.

60. Wikipedia: "Linear Least Squares (Mathematics)"; retrieved November 1, 2014; https://en.wikipedia.org/wiki/Linear_ least_squares_%28mathematics%29.

61. Shayle R. Searle: *Linear Models*; John Wiley and Sons; 1971.

62 Wikipedia: "Woodbury matrix identity"; retrieved February 12, 2016; https://en.wikipedia.org/wiki/Woodbury_matrix_identity.

63. FAA: *Pilot's Handbook of Aeronautical Knowledge*; Chapter 7, "Flight Instruments"; http://www.faa.gov/regulations_policies/handbooks_manuals/aviation/pilot_handbook/; retrieved May 14, 2014.

64. FAA: *Aeronautical Information Manual*; April 3, 2014.

65. ICAO Doc 8168: *Flight Procedures*: International Civil Aviation Organization; Procedures for Air Navigation Services – Aircraft Operations (PANS-OPS).

66. U.S. National Geospatial-Intelligence Agency (NGA): *Earth Gravitational Model EGM2008*; http://earth-info.nga.mil/GandG/wgs84/gravitymod/egm2008/egm08_wgs84.html; retrieved Sept. 15, 2014.

67. Henning Umland: *A Short Guide to Celestial Navigation*; March 8, 2004; http://www.titulosnauticos.net/astro/; retrieved Nov. 15, 2014.

68. G. G. Bennett, "Practical Rhumb Line Calculations on the Spheroid", *Journal of Navigation*; The Royal Institute of Navigation; Vol. 49, No. 01, pp 112-119: January 1996.

69. Wikipedia: "Mercator projection", https://en.wikipedia.org/wiki/Mercator_projection; retrieved April 5, 2016.